



HAL
open science

Electrochemical and photochemical studies of some remarkable ruthenium complexes

Denis Magero

► **To cite this version:**

Denis Magero. Electrochemical and photochemical studies of some remarkable ruthenium complexes. Theoretical and/or physical chemistry. Université Grenoble Alpes, 2017. English. NNT : 2017GREAV071 . tel-01712697

HAL Id: tel-01712697

<https://theses.hal.science/tel-01712697>

Submitted on 19 Feb 2018

HAL is a multi-disciplinary open access archive for the deposit and dissemination of scientific research documents, whether they are published or not. The documents may come from teaching and research institutions in France or abroad, or from public or private research centers.

L'archive ouverte pluridisciplinaire **HAL**, est destinée au dépôt et à la diffusion de documents scientifiques de niveau recherche, publiés ou non, émanant des établissements d'enseignement et de recherche français ou étrangers, des laboratoires publics ou privés.

THÈSE

Pour obtenir le grade de

DOCTEUR DE LA COMMUNITE UNIVERSITÉ GRENOBLE ALPES

Spécialité : **Chimie Physique Moléculaire et Structurale**

Arrêté ministériel : 25 mai 2016

Présentée par

Denis MAGERO

Thèse dirigée par **Mark Earl CASIDA**

préparée au sein du **Département de Chimie Moléculaire**

dans **l'école doctorale de Chimie et Sciences du Vivant**

Electrochemical and photochemical studies of some remarkable ruthenium complexes

Thèse soutenue publiquement le **14 December 2017**,
devant le jury composé de :

Prof. Frédérique LOISEAU

Département de Chimie Moléculaire, Université Grenoble Alpes, Présidente

Prof. Claude DAUL

Chemistry Department, University of Fribourg, Switzerland, Rapporteur

Prof. Liliana MAMMINO

Department of Chemistry, University of Venda, South Africa, Rapporteur

Prof. Chantal DANIEL

Directrice de Recherche CL CNRS/Laboratoire de Chimie Quantique, Université de Strasbourg, Examinatrice

Dr. Max Latévi LAWSON DAKU

Département de Chimie Physique, Université de Genève, Examineur

Prof. Mark Earl CASIDA

Département de Chimie Moléculaire, Université Grenoble Alpes, Directeur de thèse



Remerciements

I wish to sincerely thank Prof. Mark CASIDA for offering me an opportunity to work with him. Being a student from Africa, I understand how difficult it is to get an opportunity to study abroad, and even if you do, the chances of being accepted are very slim because you are not ‘known’. Mark took the risk and decided to give me the golden opportunity and I sincerely thank him. Thank you for inspiring the growth of Quantum Chemistry in Africa. You have planted a seed, a seed that will grow and produce other seeds, your legacy will for long be remembered in Africa.

This dream would not be a reality without the support of the French Embassy in Kenya. Thank you for the doctoral scholarship. In particular I would like to acknowledge all the people who were involved in planning for my stay in France. Thank you Sarah Ayito NGUEMA, for your concern and commitment towards ensuring that I had a comfortable stay in France as well as striving hard to ensure that we establish a collaboration. My gratitude also goes out to Matthew RENAUD, Pauline MOUTAUX and Marine GAZIKIAN for your support. To the staff and personnel at the École Doctorale Chimie et Science du Vivant and in particular Pourtier MAGALI, thank you for the assistance in all the administrative work. Thanks to Campus France and CROUS for organizing the stays and for financial administration. I wish to extend my gratitude to the people in France, for your kindness and warm welcome whenever I visited you and for making me confirm that ‘bureaucracy’ is truly a French word.

Thanks to the International Centre for Theoretical Physics (ICTP) for sponsoring a number of schools that I have attended. This has indeed con-

tributed greatly to my personal profile and academic growth.

My directors in Kenya, Dr. Nicholas MAKAU, Prof. George AMOLO and Prof. Lusweti KITUYI have been and continue to be a great inspiration. From my masters to Ph.D, you are honestly a blessing. Your constant calls of encouragements have been the much required fuel that has keep me going in this long journey. I may not have enough words to describe what I feel, but all I say is thank you very much.

Many thanks to my *comité de suivie de thèse*, Dr. Max Latévi LAWSON DAKU and Prof. Chantal DANIEL for taking their time to review my work, and for their support through exchange of ideas throughout my study. I am sincerely very thankful of that gesture. Thanks to my jury, for having accepted to read and examine this work.

To my lovely wife Rodah Cheruto SOY, thank you for being an inspiration. Your encouragement and support has brought me this far. For the time that I have been away studying, all the weekends that I have been spending in the lab, sleeping late and waking up early, literally, being absent during all this time, you have been patient with me and I thank you for that. To my daughter, the little ‘Professor’, Judith Aloo MAGERO, thank you for being a good time keeper, always waking me up at the right time of the night for me to go for study. We appreciate your presence in our life.

I wish to extend my gratitude to my dear parents, for the sacrifices that they made to bring me this far. It has been a journey that has not been easy, with roadblocks placed at every point, and preformed minds that we could not make it. Today, my heart is filled with a lot of gratitude because my parents can also stand tall and be counted, because I have gone through barriers that they never imagined. It has been a long journey, I remember many years ago, mum would pack for me some bread in the lunch box then dad would drop me to school with his ‘Zebra’ bicycle . My promise to you has been fulfilled, and wherever you are, I am sure that you must be very proud. To my brother Pius Gumo MAGERO, thank you for the efforts that you have put in. Your encouragement and support have made me to come this far.

I wish to thank the *Chimie théorique* group and especially my dear friend

Ala Aldin M. Hani M. DARGHOUTH for the support and encouragement throughout my study, and for being a true brother and colleague. Thank you Pierre GÉRARD for having solutions to my computing problems and for being there always to support. Thanks to Nicolas ALTOUNIAN, Rolf DAVID, Walid TOUWALI and Tarek MESTIRI. Thanks to Prof. Carlos PEREZ, for the encouragement and exchange of ideas. I wish to thank Prof. Anne MILET for the useful scientific discussions. I also acknowledge Prof. Hélène JAMET and Dr. Myneni HEMANADHAN for your useful scientific discussions and for the great brotherhood that you brought with the spicy food.

I owe an appreciation to Dr. Joseph CHAVUTIA, the my head of department at the Eldoret Polytechnic, for having a listening ear and being very understanding. It is because of your support that I was able to teach and study at the same time. I am truly very thankful for your gesture. I wish to thank my Kenyan family in Grenoble for the great company and guidance that you gave. Thanks to Carolyne MARTINS and Abdi FARAH and his family.

Members of the Computational Material Science Group in Kenya have been of invaluable help. Thanks to Victor MENGWA, Perpetual WANJIRU, Tolbert NGEYWO, Valid MWALUKUKU and Geoffrey ARUSEI. I also wish to give special thanks to Dr. Cleophas Muhavini WAWIRE for his great help in starting off this work.

I may not have acknowledged everyone in this writing, but I want to thank everybody that was involved in making this work a success.

*To my grandmother Marita Dienya and my grandfather Bill Masengeli
Walubengo. You passed on before seeing this come true, this is for you.*

Résumé

Cette thèse fait partie d'un projet franco-keyan dénommé *ELEPHOX* (**ELE**ctrochemical and **PHO**to Properties of Some Remarkable Ruthenium and Iron Comple**X**es). En particulier, notre focus est la continuation du travail de C. Muhavini Wawire, Damien Jouvenot, Frédérique Loiseau, Pablo Baudin, Sébastien Liatard, Lydia Njenga, Geoffrey Kamau, et Mark E. Casida, "Density-Functional Study of Luminescence in Polypyridine Ruthenium Complexes," *J. Photochem. and Photobiol. A* **276**, 8 (2014). Cet article a proposé une indice orbitalaire de temps de luminescence pour les complexes de ruthénium. Cependant cet article n'était limité qu'à quelques molécules. Afin d'avoir une théorie plus fiable et donc potentiellement plus utile, il faudra tester l'indice de luminescence sur beaucoup plus de molécules. Ayant établi le protocole, il était "évident" mais toujours un défi de le tester sur encore une centaine de molécules pour démontrer ou infirmer l'indice proposée. Pour ce faire, j'ai examiné les 98 pages de la Table I de A. Juris, V. Balzani, F. Bargelleti, S. Campagna, P. Belser, et A.V. Zelewsky, "*Ru(II) polypyridine complexes: Photophysics, photochemistry, electrochemistry, and chemiluminescence,*" *Chem. Rev.* **84**, 85 (1988) et j'ai extrait un nombre important de données susceptibles à comparaison avec les résultats des calculs de la théorie de la fonctionnelle de la densité (*DFT*) et la *DFT* dépendante du temps (*TD-DFT*). Comme les résultats étaient suffisamment encourageant, le modèle *DFT* était examiné de plus près avec la méthode d'une théorie de champs de ligands (*LFT*) à la base de la densité des états partielle (*PDOS*). Ainsi j'ai pu tester l'indice de luminescence proposée précédemment par la méthode *PDOS-LFT* et j'ai trouvé des difficultés avec l'indice initialement

proposée. Par contre, nous avons pu proposer une nouvelle indice de luminescence qui, à quelques exceptions près, a une corrélation linéaire avec une barrière énergétique moyenne pour l'état triplet excité dérivée à partir des données expérimentales. À l'avenir nous pouvons proposer une investigation plus directe de la barrière sur la surface triplet excité pour remplacer la valeur approximative déduite de l'expérience. Puis nous voulons voir si notre indice de luminescence s'appliquent aux cas des complexes d'iridium.

Mots-Clé: Chimie Quantique, Photochimie, État Excités, Complexes polypyridine ruthénium, Luminescence, Théorie de la Fonctionnelle de la Densité, Théorie de la Fonctionnelle de la Densité Dépendente du Temps, Densité d'état partielle, Surface d'énergie Potentielle pour un état Triplet, État de Transition.

Abstract

This thesis is part of the Franco-Kenyan project ELEPHOX (**EL**Electrochemical and **PHO**to Properties of Some Remarkable Ruthenium and Iron **Com**ple**X**es) project. In particular, it focused on the continuation of the work of C. Muhavini Wawire, Damien Jouvenot, Fréd erique Loiseau, Pablo Baudin, Sébastien Liatard, Lydia Njenga, Geoffrey Kamau, and Mark E. Casida, “Density-Functional Study of Luminescence in Polypyridine Ruthenium Complexes,” *J. Photochem. and Photobiol. A* **276**, 8 (2014). That paper proposed a luminescence index for estimating whether a ruthenium complex will luminesce or not. However that paper only tested the theory on a few molecules. In order for the theory to have a significant impact, it must be tested on many more molecules. Now that the protocol has been worked out, it was a straightforward but still quite challenging matter to do another 100 or so molecules to prove or disprove the theory. In order to do so, I went through the 98 pages of Table I of A. Juris, V. Balzani, F. Bרגelleti, S. Campagna, P. Belser, and A.V. Zelewsky, “Ru(II) polypyridine complexes: Photophysics, photochemistry, electrochemistry, and chemiluminescence,” *Chem. Rev.* **84**, 85 (1988) and extracted data suitable for comparing against density-functional theory (DFT) and time-dependent (TD-)DFT. Since the results were sufficiently encouraging, the DFT model was examined in the light of partial density of states ligand field theory (PDOS-LFT) and the previously proposed luminescence indices were tested. In fact, the originally proposed indices were not found to be very reliable but we were able to propose a new luminescence index based upon much more data and in analogy with frontier-molecular orbital ideas. Except for a few compounds, this

index provides a luminescence index with a good linear correlation with an experimentally-derived average excited-state activation energy barrier. Future work should be aimed at both explicit theoretical calculations of this barrier for ruthenium complexes and extension of the luminescence index idea to iridium complexes.

Keywords: Quantum Chemistry, Photochemistry, Excited States, Polypyridine ruthenium complexes, Luminescence, Density-functional theory, Time-dependent density-functional theory, Partial density of states, Triplet Surface, Transition State.

Table of Contents

Remerciements	i
Résumé	v
Abstract	vii
List of Tables	xiv
List of Figures	xvi
I Introduction	1
1 Introduction	2
1.1 Objectives	4
1.2 Structure and Organization	5
II Background Material	8
2 Transition Metal Complexes	9
2.1 Introduction	9
2.2 Definitions	10
2.2.1 Coordination number	10
2.2.2 Charge	11
2.2.3 Nomenclature	12

2.3	Transition Metal Structure and Properties	12
2.3.1	Geometries	12
2.3.2	Crystal Field Theory	13
2.3.2.1	Octahedral complexes	13
2.4	Ligand Field Theory	15
2.4.1	Molecular Orbitals	15
2.4.2	Molecular Orbital Formation	17
2.5	Photophysical Processes for Transition Metal Complexes	18
3	Schrödinger Equation	22
3.1	Ultraviolet Catastrophe	23
3.2	Photoelectric Effect	23
3.3	Quantization of Electronic Angular Momentum	24
3.4	Wave-Particle Duality	25
3.5	Time-Independent Schrödinger Equation	26
3.6	Time-Dependent Schrödinger Equation	29
3.7	Molecular Hamiltonian	30
3.8	Atomic Units	32
3.9	Born-Oppenheimer Approximation	34
4	Photophenomena and Luminescence	38
4.1	Introduction	38
4.2	Electronic Excitation	39
4.2.1	How does Electronic Excitation Occur?	40
4.2.2	Types of Electronic Transitions	40
4.3	State Energy Diagram	43
4.4	Excited State Deactivation	44
4.4.1	Introduction	44
4.4.2	Luminescence	44
4.4.2.1	Jablonski Diagram	45
4.4.3	Vibrational relaxation	46
4.4.4	Radiationless Deactivation	47
4.4.5	Radiative Deactivation	48

4.4.5.1	Fluorescence	48
4.4.5.2	Phosphorescence	49
4.5	Photochemical Processes on Potential Energy Surfaces	49
4.6	Excited State Lifetime	50
4.7	Quantum Yield	50
5	Hartree-Fock Approximation	53
5.1	The Hartree Product	54
5.2	Slater Determinant	55
5.3	The Electronic Hamiltonian	55
5.4	Coulomb and Exchange Integrals	56
5.5	Coulomb and Exchange Operators	59
5.6	Hartree-Fock Orbitals and Orbital energies	61
5.7	Koopmans' Theorem	63
5.8	Roothaan-Hall Equation	64
6	Density-Functional Theory	69
6.1	Hohenberg-Kohn Theorems	70
6.2	Thomas-Fermi Model	74
6.3	Kohn-Sham Approach	75
6.4	Exchange-Correlation Approximations (Jacob's Ladder)	79
6.4.1	Local Density Approximation(LDA)	79
6.4.2	Generalized Gradient Approximation (GGA)	80
6.4.3	Hybrid Functionals	81
6.4.4	Meta-Generalized Gradient Approximation (meta-GGA)	82
6.4.5	Double hybrid functionals	82
6.4.6	Jacob's Ladder of Density Functional Approximations	82
7	Basis Sets and Effective Core Potentials	87
7.1	Definition of a Basis Set	87
7.2	Types of Basis Functions (Atomic Orbitals)	88
7.2.1	Slater-Type Orbitals (STOs)	89
7.2.2	Gaussian-type orbitals (GTOs)	90
7.3	Classification of Basis Sets	92

7.3.1	Minimal Basis Sets (Single Zeta)	92
7.3.2	Double, Triple and Multi Zeta (ζ) Basis Sets and Split Valence Basis Sets	93
7.3.3	Polarization Function-Supplemented Basis Functions .	94
7.3.4	Diffuse-Function-Augmented Basis Functions	95
7.3.5	Effective Core Potential (ECP) Basis Functions (Pseu- dopotentials)	96
7.4	6-31G and 6-31G(d) Basis Sets	98
7.4.1	6-31G	98
7.4.2	6-31G(d)	98
7.5	Basis Set Superposition Error (BSSE)	99
7.5.1	Counterpoise Method	100
7.5.2	Chemical Hamiltonian Approach	100
7.5.3	Other Methods	100
8	Partial Density of States (PDOS)	106
9	Time-Dependent Density Functional Theory	109
9.1	Time-Dependent Schrödinger Equation	110
9.2	First Runge-Gross theorem	112
9.3	Second Runge-Gross theorem	113
9.4	Time-Dependent Kohn-Sham Equation	115
9.5	Exchange-Correlation Potentials	117
9.6	Linear Response Theory (LR)	118
9.7	Linear Response TD-DFT (LR TD-DFT)	118
9.7.1	Time-dependent linear density response	119
9.7.2	Kohn-Sham Linear Density Response	122
9.8	Casida Equations	124
9.9	‘Deadly Sins’ of TD-DFT	127
III	Original Research	131
10	DFT and TD-DFT for Ruthenium Complexes	132

10.1	Introduction	132
10.2	Computational Details	133
10.3	Results and Discussion	134
11	Partial Density of States Ligand Field Theory (PDOS-LFT): Recovering a LFT-Like Picture and Application to Photo- properties of Ruthenium(II) Polypyridine Complexes	140
11.1	Background Information on the Problem	141
12	Located a Transition State on the Excited-State Triplet Sur- face	165
12.1	Introduction	165
12.1.1	Background Information on the Problem	165
12.2	Computational Details	172
12.3	Results and Discussion	173
12.4	Conclusion	179
12.5	Acknowledgement	180
IV	Conclusion	185
13	Summary and Conclusion	186
A	Supplementary Material: Partial Density of States Ligand Field Theory (PDOS-LFT): Recovering a LFT-Like Picture and Application to the Photoproperties of Ruthenium Polypyri- dine Complexes	192
B	Curriculum Vitae	296
	Index	192

List of Tables

2.1	Table of the Werner complex colors.	14
3.1	Classical to quantum transformation of cartesian position and momentum operators.	30
3.2	Symbols used to show the interaction between nuclei electrons.	31
3.3	Atomic Units	33
4.1	Classification of different types of luminescence based upon the source of excitation energy.	45
7.1	Output of orbital functions for a 6-31G basis set from GAUSSIAN 09 for the carbon atom.	99
10.1	Comparison of parameters for geometries optimized at HF and DFT. Bond lengths are in (Å) and bond angles are in degrees.	135
10.2	Comparison of the position of spectral peaks calculated at different levels of theory; CIS, TD-HF and TD-DFT for 6-31G and 6-31G(d) basis sets. Wavelength is given in nm and the corresponding molar extinction coefficient is in parenthesis with units of $10^3 \text{ M}^{-1} \text{ cm}^{-1}$	137
12.1	Optimized structural bond lengths (Å) in acetonitrile for the three states for $[\text{Ru}(\text{bpy})_3]^{2+}$	173
12.2	Optimized structural bond lengths (Å) in acetonitrile for the three states for $[\text{Ru}(\text{mbpy})_3]^{2+}$	174

12.3 Optimized structural bond lengths (Å) in acetonitrile for the three states for $[\text{Ru}(\text{mphn})_3]^{2+}$	175
--	-----

List of Figures

1.1	World energy consumption [1].	3
2.1	Coordination complex.	10
2.2	The 2,2'-bipyridine molecule (bpy) showing the two nitrogen lone pairs which "bite" the central metal atom.	11
2.3	The hexacoordinate $[\text{Ru}(\text{bpy})_3]^{2+}$ complex. Hydrogen atoms have not been included for clarity purposes.	11
2.4	Splitting of the five d orbitals of a central metal ion in octahedral complexes.	14
2.5	Molecular orbital energy level diagram for an octahedral complex containing ligands that possess σ and π orbitals.	16
2.6	Molecular orbital diagram representing various types of electronic transitions in octahedral complexes.	18
3.1	xyz directions	31
3.2	Molecular Hamiltonian.	34
4.1	Potential energy diagrams with vertical transitions as in the Franck-Condon principle.	41
4.2	Singlet ground state to excited allowed singlet state.	41
4.3	Singlet ground state to excited forbidden triplet state.	42
4.4	Excited State Deactivation	44
4.5	Jablonski diagram.	46
4.6	Jablonski diagram showing the various processes. Original source [14].	47

5.1	SCF solution of the Hartree-Fock equation [14].	61
6.1	Jacob's ladder of Density Functional Approximations. Reproduced from (Ref. [25]) with permission of the PCCP Owner Societies.	83
7.1	Distortion of orbitals resulting from the inclusion of s and p orbitals.	94
7.2	Distortion of orbitals resulting from the inclusion of p and d orbitals.	94
9.1	Runge-Gross theorem: A pictorial illustration.	113
9.2	An illustration of the LR theory	118
10.1	ORTEP diagram showing the optimized structure of $[\text{Ru}(\text{trpy})_2]^{2+}$ with different measured bond lengths and angles. The ellipsoidal probability is at 70%.	135
10.2	Comparison of experimental with calculated absorption spectra at different levels of theory; CIS, TD-HF and TD-DFT for $[\text{Ru}(\text{trpy})_2]^{2+}$. Calculated spectra has been done with 100 singlet states and 6-31G basis set. Experimental spectra; measured at room temperature in acetonitrile [1].	136
10.3	Comparison of experimental with calculated absorption spectra at different levels of theory; CIS, TD-HF and TD-DFT for $[\text{Ru}(\text{trpy})_2]^{2+}$. Calculated spectra has been done with 100 singlet states and 6-31G(d) basis set. Experimental spectra; measured at room temperature in acetonitrile [1].	136
12.1	The diagram shows the principle potential energy curves in our model. The abscissa corresponds to a reaction pathway involving partial removal of a ligand while the ordinate represents the state energy. The dashed lines indicate diabatic states whose avoided crossing leads to the energetic barrier on the adiabatic surface between the ${}^3\text{MLCT}$ and ${}^3\text{MC}$ minima.	166

12.2 Pseudo-octahedral ligand field theory diagram for Ru complexes.	169
12.3 Spin density distribution of $^3\text{MLCT}$ state on $[\text{Ru}(\text{bpy})_3]^{2+}$ in acetonitrile.	176
12.4 Spin density distribution of $^3\text{MLCT}$ state on $[\text{Ru}(\text{mbpy})_3]^{2+}$ in acetonitrile.	177
12.5 Spin density distribution of $^3\text{MLCT}$ state on $[\text{Ru}(\text{mphen})_3]^{2+}$ in acetonitrile.	177
12.6 Spin density distribution of ^3MC state on $[\text{Ru}(\text{bpy})_3]^{2+}$ in acetonitrile.	178
12.7 Spin density distribution of ^3MC state on $[\text{Ru}(\text{mbpy})_3]^{2+}$ in acetonitrile.	178
12.8 Spin density distribution of ^3MC state on $[\text{Ru}(\text{mphen})_3]^{2+}$ in acetonitrile.	179
12.9 $^3\text{MLCT}$ to ^3MC state potential energy scan along the reaction coordinate of the axial distortion of the ^3MC state for $[\text{Ru}(\text{bpy})_3]^{2+}$	179

List of Acronyms and Abbreviations

$\hat{H}(t)$	TD Hamiltonian
ω	Fourier-transformed frequency domain
Φ	Quantum yield
AA	Adiabatic Approximation
BSSE	Basis Set Superposition Error
CFT	Crystal Field Theory
DFT	Density Functional Theory
DZ	Double Zeta
E_{xc}	Exchange-Correlation Potentials
EA	Electron Affinity
ECPs	Effective Core Potentials
GGA	Generalized Gradient Approximation
GTOs	Gaussian-type Orbitals
HAOs	Hydrogen-like Atomic Orbitals
HP	Hartree Product
IC	Internal Conversion

IE Ionization Energy
IP Ionization Potential
ISC Intersystem Crossing
KS Kohn-Sham
LCAO Linear Combination of Atomic Orbitals
LDA Local Density Approximation
LFT Ligand Field Theory
LR Linear Response Theory
LR TD-DFT Linear Response TD-DFT
mGGA Meta-Generalized Gradient Approximation
MO Molecular Orbital
PES Potential Energy Surfaces
QZ Quadruple Zeta
RG Runge-Gross theorem
STOs Slater-type orbitals
SV Split Valence
TD-DFT Time-Dependent Schrödinger Equation
TD-KS Time-Dependent Kohn-Sham Equation
TZ Triple Zeta
vr Vibrational relaxation
 $\chi_{\rho\rho}$ Generalized Susceptibility

Part I

Introduction

Chapter 1

Introduction

Problems that are facing the world today need an urgent solution from scientists. The world is facing a mirage of problems ranging from an ever increasing population, thus putting a strain on the already available limited resources. Most importantly, this increase implies an increase in demand in the consumption of everything, but fundamentally energy requirements increase significantly [1]. With such kinds of demands, the stain on the limited resources and their imminent depletion cannot be ignored. There are many other areas, not just energy that also face the same challenges.

One of the most fascinating natural processes is photosynthesis. It is fascinating because of the efficiency of the process [2]. The question that we ask ourselves here is, can we emulate this process artificially? This has been answered by many scientists. The main idea behind the process is that we need at least a donor atom, a spacer, and an acceptor. It is possible to artificially emulate a number of natural complex operations such as photosynthesis by building up or assembling smaller working molecular components into larger units which form nanodevices capable of carrying out similar functions. This strategy is known as bottom-up (small to big) and it involves the use of photochemical molecular devices (PMDs). PMDs can be defined as “structurally organized and functionally integrated systems capable of elaborating the energy and information input of photons to perform complex functions” [3]. Phototransistors, photocatalysts, photoactivated information storage and

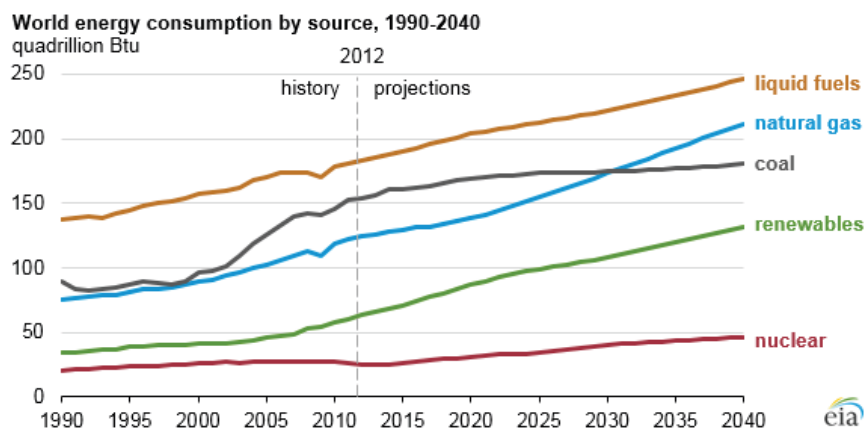


Figure 1.1 – World energy consumption [1].

retrieval, and solar cells are some of the examples of PMDs. These PMDs may be assembled together to come up with a single PMD which is also a nanodevice and capable of doing more complex functions.

Improving the performance of (PMDs) has been the focus of much research in the recent years. One of the approaches that has been considered is synthesizing molecular subunits with specific properties that are able to simulate the complex interactions of the subunits. It is a promising idea but it faces a number of challenges. The first challenge is that of quantum and atomistic effects at the nanoscale level. The second challenge is that not every molecule that has been modeled theoretically can be synthesized experimentally. This means that for the second challenge to be addressed, both experimentalists and theoreticians must work together.

A typical PMD configuration consists of the electron donor-spacer-pigment-spacer-acceptor, abbreviated as D-S-P-S-A. A good pigment (photosensitizer) has to fulfill important general requirements, irrespective of for which application it is aimed. Ru complexes fit particularly well in this description because of good chemical stability, redox properties, excited state reactivity, luminescence emission as well as excited state lifetimes which have attracted the attention of many researchers [4]. The main problem here is: How do

you tell which Ru complex will make a good pigment? Progress has been made on the prediction of what would make a good pigment before the lengthy project of working out its synthesis. To this end, [5] worked out some promising simple molecular-orbital (MO) based luminescence indices which may be helpful in estimating which compounds are likely to remain excited long enough to luminescence or transfer an electron or which may simply undergo unproductive radiationless deactivation back to the ground state. The two molecular orbital-based luminescence indices, both of which were based on the idea that luminescence quenching is the result of a low ${}^3\text{MLCT} \rightarrow {}^3\text{MC}$ barrier. One luminescence index proposes the difference between the e_g^* and the lowest energy π^* PDOS bands (ΔE) as an indicator. The second luminescence index is a product of the amount of π character in the t_{2g} band with the amount of ruthenium d character in the $1\pi^*$ band summarized as $d \times \pi$. The indices are proposed as qualitative luminescence predictors. Using the indices, which were tested on five compounds, they found that low values of ΔE and high values of $d \times \pi$ correlated with lack of luminescence while high values of ΔE and low values of $d \times \pi$ correlate well with luminescence. We work further on this indices by looking at more Ru complexes from [4].

The main objectives in this work are:

1.1 Objectives

A) *To test the robustness of molecular orbital (MO) luminescence indices that were proposed by [5] on a wider variety of compounds and, in the process, to perhaps identify additional luminescence indicators which can help in the design of new photochemical molecular devices (PMDs).*

Specifically, this entails,

- Optimization of crystal structures.
- Frequency calculation on each optimized structure.
- Time-dependent density functional theory calculations for each of the optimized structures.
- Single point calculation for each of the optimized structures.

- Extraction of partial density of states information using various in-house programs.
- B) *Study the Ru complex triplet excited transition state and find the size of the energy barrier.*

1.2 Structure and Organization

This thesis is divided into four major parts. The first part consists of one chapter, the introduction, that outlines what kind of problem is being tackled in the work as well as the objectives that are covered.

The second part is part two: background material consisting of eight chapters. The number of chapters contained in this particular part outlines the importance of understanding each and every process before the actual work is done.

Chapter two looks at transition metal complexes. This is actually what is being studied in this work. It outlines what they are and the various processes that they undergo. It is critical since it is the bare minimum with which one should familiarize oneself.

Chapter three introduces the Schrödinger equation. A good understanding of this equation provides a solid base for understanding photophenomena and luminescence.

Chapter four is the chapter on photophenomena and luminescence. The idea behind this chapter is that it looks at what happens in the excited state. This is important because we are dealing with excited state phenomena.

Chapters five to nine look at the wave function-based electronic structure theory. This is the method that is actually used in the work. In the various chapters, each of the methods, (all of which are important in this work) have been discussed exhaustively.

The third part is the part on original work. It is chapter 10, 11 and 12. This part is actually the core of this thesis. It is a detailed presentation of results that were achieved and gives the publications that resulted out of the work, both published and also work in progress.

The fourth part is a summary and conclusion. The chapter summarizes what we have accomplished and what could possibly be done to further improve the work. The other section consists of the appendices and gives supplementary information for the published paper and my curriculum vitae.

Bibliography

- [1] U.S. Energy Information Administration. <https://www.eia.gov/todayinenergy/detail.php?id=26212>. Accessed: 2017-07-30.
- [2] A. Silverstein, V. B. Silverstein, and L. S. Nunn. *Photosynthesis*. Science Concepts, Second Series. Twenty-First Century Books, 2007. ISBN 9780822567981.
- [3] J. P. Sauvage, J. P. Collin, J. C. Chambron, S. Guillerez, and C. Coudret. Ruthenium(II) and osmium(II) bis(terpyridine) complexes in covalently-linked multicomponent systems: Synthesis, electrochemical behavior, absorption spectra, and photochemical and photophysical properties. *Chem. Rev.*, 94:933, 1994.
- [4] A. Juris, V. Balzani, F. Barigelletti, S. Campagna, P. Belser, and A. Von Zelewsky. Ru(II) polypyridine complexes: Photophysics, photochemistry, electrochemistry, and chemiluminescence. *Coord. Chem. Rev.*, 84: 85, 1988.
- [5] C. M. Wawire, D. Jouvenot, F. Loiseau, P. Baudin, S. Liatard, L. Njenga, G. Kamau, and M. E. Casida. Density-functional study of luminescence in polypyridine ruthenium complexes. *J. Photochem. and Photobiol. A*, 276:8, 2014.

Part II

Background Material

Chapter 2

Transition Metal Complexes

‘The Nobel Prize in Chemistry 1913 was awarded to Alfred Werner “in recognition of his work on the linkage of atoms in molecules by which he has thrown new light on earlier investigations and opened up new fields of research especially in inorganic chemistry”. ’

http://www.nobelprize.org/nobel_prizes/chemistry/laureates/1913/14thOct, 2017

2.1 Introduction

Transition metal compounds form the core of the research in this thesis. They are also referred to as coordination compounds. In the field of photochemistry and photophysics, they form an important class of compounds essentially because of their extensive photophysical and photochemical properties [1]. In a coordination complex ML_n , there is typically a *central atom* which is a *d* metal or the cation of a *d* metal, M. The central atom is surrounded by anions (or cations in some cases such as nitroso (NO^+), cationic oniom ligands and hydrazinium ($H_2N-NH_3^+$) and its derivatives [2–5]) or molecules called *ligands*, L. A simple illustration of such a complex is shown in Fig. 2.1.

A coordination compound may also be defined as any compound that contains a coordination entity. A coordination entity is an ion or neutral

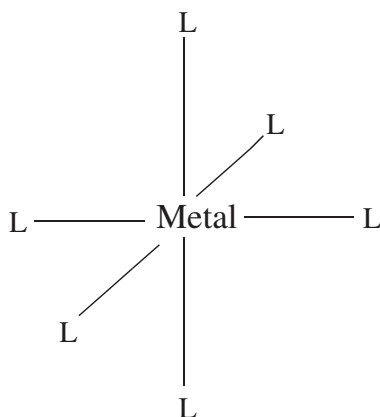


Figure 2.1 – Coordination complex.

molecule that is composed of a central atom, usually that of a metal, to which is attached a surrounding array of other atoms or groups of atoms, each of which is called a ligand [6]. Transition metal complexes have high symmetry, chemically significant oxidation states and often have an open-shell d orbital configuration. Coordination of the metal ion or atom in a non-spherically symmetric environment, that is, a ligand field, differentiates the energies of the d-orbitals [7]. There are several common terms that will be referred to in coordination chemistry, they have been reviewed in the next section.

2.2 Definitions

2.2.1 Coordination number

The coordination number is the number of ligands (donor atoms) bonded to the central atom [8]. Typical values of the coordination number are 2, 4 and 6. In the case of $[\text{Ru}(\text{bpy})_3]^{2+}$, the coordination number is 6. In this complex, each ligand “bites” the cation twice. This is why we speak of *monodentate* complexes because there is a single pair of “fangs” (that is lone pairs to form a coordinate bond). Certain have more than one lone pair that

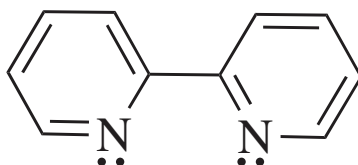


Figure 2.2 – The 2,2'-bipyridine molecule (bpy) showing the two nitrogen lone pairs which “bite” the central metal atom.

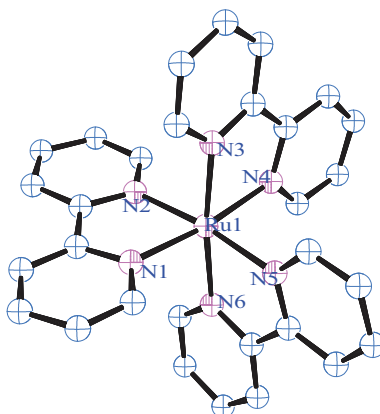


Figure 2.3 – The hexacoordinate $[\text{Ru}(\text{bpy})_3]^{2+}$ complex. Hydrogen atoms have not been included for clarity purposes.

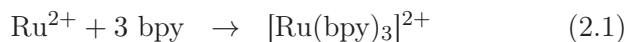
can “bite.” An example is the 2,2'-bipyridine (bpy) ligand (Fig. 2.2) which is *bidentate* (bites twice) because of the lone pairs on the nitrogen.

In Fig. 2.3, we see three bpy complexing with Ru^{2+} to form the $[\text{Ru}(\text{bpy})_3]^{2+}$ hexacoordinate complex. Especially in the case of polydentate ligands, we sometimes say that the ligands *chelate*. The word chelate comes from the Greek $\chi\eta\lambda\eta'$, which means “claw.” The ligands form a coordination sphere around the central atom.

2.2.2 Charge

According to charge conservation, the charge on the complex is simply the sum of the charge of the atom and the charges on the ligands.

Example:



2.2.3 Nomenclature

How do we name complexes? The naming of complexes follows the rules described in the IUPAC red book (https://www.iupac.org/cms/wp-content/uploads/2016/07/Red_Book_2005.pdf) under chapter IR-9 Coordination Compounds [6]. The reader is referred to this book if they wish to seek further details regarding the naming of coordination complexes.

2.3 Transition Metal Structure and Properties

Alfred Werner won the Nobel prize in chemistry in 1913. He had studied $[\text{Co}(\text{NH}_3)_n(\text{H}_2\text{O})_l\text{Cl}_m]\text{Cl}_{3-m}$ complexes with $n + l + m = 6$. Some of these complexes have the same empirical formula but different colors! Werner came up with the modern explanation of transition metal complexes while trying to figure out why this was so [9].

2.3.1 Geometries

Geometries of transition metal complexes can generally be classified into: (1) Octahedral ($n = 6$) where the central metal ion is surrounded by six ligands. It contains equatorial and axial positions. The equatorial position is the horizontal square planar arrangement in the xy-plane containing four ligands and the axial positions are the vertical positions along the z-axis. (2) Square planar ($n = 4$) where four ligands are attached to a central metal ion. It is considered to be an extremely z-out distorted octahedral complex because the ligands will be on the x- and y-axes. (3) Tetrahedral ($n = 4$) where four ligands are attached to a central metal ion. Its difference with the square planar geometry is that the four ligands approach the central metal ion in between the axes [10]. The three dimensionality of these structures means that there can be conformational (*cis/trans*) isomers and optical

isomers (enantiomers).

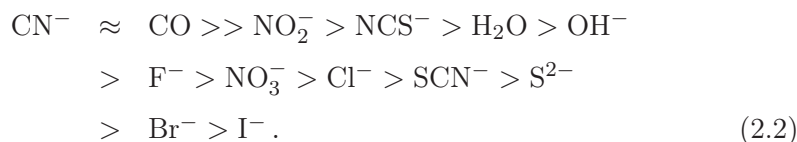
2.3.2 Crystal Field Theory

In this theory, the ligands are treated as negative point charges which set up an electrostatic field that repels electrons in the d orbitals of the central metal ion [11]. The interaction of the electrostatic field of the ligands with the d electrons results in splitting of the d orbitals into groups with different energies. In a gaseous transition-metal ion, the five d orbitals with different values of the magnetic quantum number (m) are degenerate (have the same energy). Symmetry plays a critical role in how the d orbitals split. In a complex with spherically symmetric ligand field, the five d orbitals end up in higher energy than the free ion because of the repulsion between the metal ion electron density and the spherical field of negative charge. This is an ideal case which never happens in reality. Practically, d orbitals are split according to the particular symmetry of the complex. Of particular interest is the octahedral symmetry where the central metal ion is surrounded by six ligands since the transition metals that are studied in this work have this symmetry. It should however be noted that, although most of the complexes studied have only pseudo-octahedral symmetry, octahedral symmetry is assumed as a first approximation in assigning orbitals.

2.3.2.1 Octahedral complexes

They are octahedral and highly symmetric. In the presence of an octahedral crystal field, the five d -orbitals interact differently with the surrounding ligands resulting in their splitting into a lower-energy triply degenerate set (t_{2g} composed of d_{xy} , d_{xz} and d_{yz}) and a higher-energy doubly degenerate set (e_g composed of d_{z^2} and $d_{x^2-y^2}$) separated by an energy, Δ_0 , known as ligand field splitting parameter [12]. The size of the ligand-field splitting Δ_0 of the d orbitals which results in the e_g and t_{2g} orbitals depends upon how strongly the ligands interact with the central atom. Those which interact more strongly with the central atom will result in a larger Δ_0 and are said to be “high field,” while small Δ_0 means only a small interaction and the

associated ligands are referred to as “low field.” This allows ligands to be arranged in a *spectrochemical series* according to the size of Δ_0 :



By varying the ligand, one can vary the ligand field splitting between the orbitals with sometimes spectacular consequences, notably for color and magnetic properties (but also for luminescence lifetimes.)

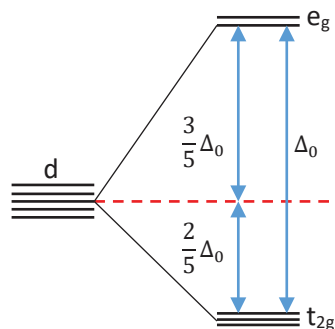


Figure 2.4 – Splitting of the five d orbitals of a central metal ion in octahedral complexes.

The optical properties also vary with the ligand-field strength. The size of Δ_0 is such that $d - d$ transitions are often in the visible. By varying Δ_0 through varying the ligand, we can vary the energy of the absorbed light and hence the color of the complex.

Table 2.1 – Table of the Werner complex colors.

$[\text{Co}(\text{NH}_3)_6\text{Cl}_3]$	yellow orange
$[\text{Co}(\text{NH}_3)_5(\text{H}_2\text{O})]\text{Cl}_3$	red
$[\text{Co}(\text{NH}_3)_5\text{Cl}]\text{Cl}_2$	purple
$[\text{Co}(\text{NH}_3)_4\text{Cl}_2]\text{Cl}$	green

As much as the crystal field theory (CFT) forms a good basis for studying magnetic, thermochemical and spectroscopic data by using empirical values

of Δ_0 , it faces a number of limitations. It does not take into account the overlap of ligand and metal atom orbitals because it treats ligands as point charges. As a consequence of this, it cannot account for the ligand spectrochemical series. The ligand field theory takes a broader look and addresses the weaknesses in the CFT. In the next section, we take a look at the ligand field theory.

2.4 Ligand Field Theory

Data from several experiments has shown that the metal-ligand bond in transition metal complexes is composed of some degree of covalency [12]. Ligand field theory (LFT)[13] is the theory that best accounts for the effects of covalent bonding as well as considering all the conceptual aspects of the simple crystal field theory (CFT). Ideally, LFT works in a similar manner as does CFT for the calculation of the energy level diagrams but it also considers spin-orbit coupling and inter-electronic repulsion when a free metal ion is converted to a complexed one. LFT is an application of molecular orbital theory that concentrates on the d orbitals of the central metal atom, thus providing a more substantial framework for understanding the origins of Δ_0 . Any chemist interested in the spectroscopy of metal complexes is obliged to use LFT.

2.4.1 Molecular Orbitals

The bonding and antibonding molecular orbitals for metal complexes are obtained by combining metal and ligand orbitals which have the same symmetry properties. Generally speaking, the formulation of a MO is [12],

$$\psi = a_M\varphi_M + a_L\varphi_L, \quad (2.3)$$

where φ_M and φ_L are metal and ligand orbital combinations and a_M and a_L are coefficients whose values are restricted by conditions of normalization and orthogonality.

Two types of bonding arise out of that combination, namely σ and π

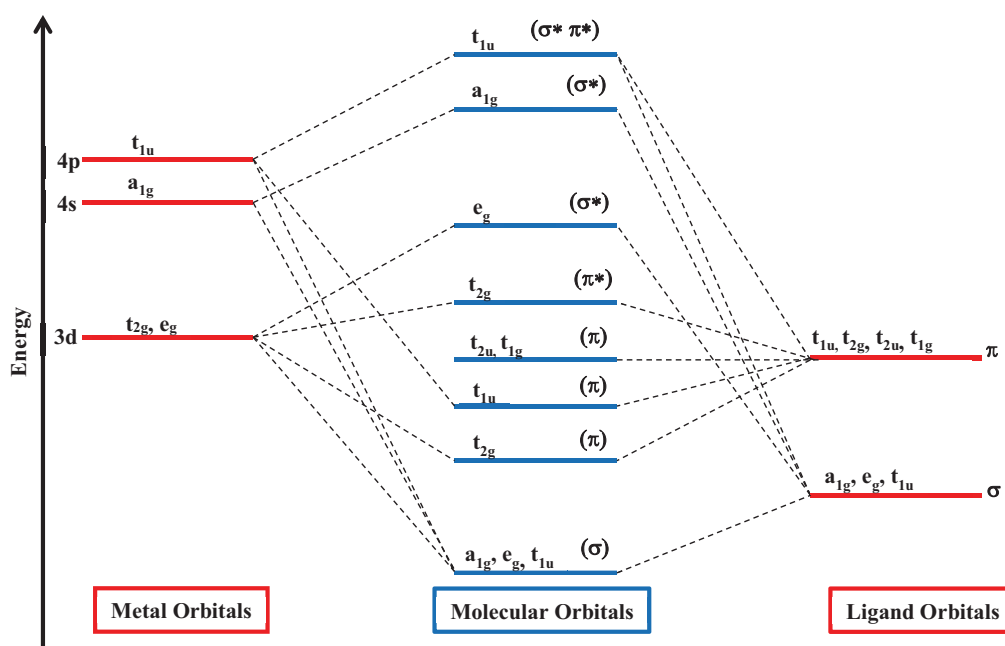


Figure 2.5 – Molecular orbital energy level diagram for an octahedral complex containing ligands that possess σ and π orbitals.

bonding. The σ and σ^* bonding arise from the direct overlap of a ligand lone-pair orbital with metal with the e_g orbitals in the wrong symmetry with t_{2g} . In this kind of bonding, the bonding orbitals (σ) are occupied by the electrons from the ligand and the antibonding orbitals (σ^*) levels are centered mainly on the metal. As described earlier, different ligands cause different Δ_0 between the t_{2g} and e_g sets.

The π bonding results from the interaction of ligand orbitals directed perpendicular to the metal-ligand axis interacting with the metal t_{2g} orbitals. Just as in the case of σ bonding, the nature of the ligand interacting with the metal ion determines what happens. Figure 2.5 shows the various kinds of molecular orbitals that arise owing to the different interactions between the ligand and the metal in an octahedral complex.

2.4.2 Molecular Orbital Formation

Several considerations must be made before the construction of the molecular orbitals of a complex, these include: shape determination and their relative energies. Symmetry plays an essential role in the construction of the MOs since it will give information of whether the overlap is non-zero or zero and hence the ability to predict whether an interaction can occur or not. To construct the molecular orbital, we consider orbitals from the metal ion as well as orbitals from the ligand [8].

i. Metal Orbitals

In the metal ion, nine valence shell orbitals are considered. The nine valence shell orbitals come from the 3d (5 atomic orbitals), 4s (1 atomic orbital) and 4p (3 atomic orbitals) orbitals. Owing to the fact that octahedral complexes are the most important to us, their symmetry in the O_h point group they may be classified according to symmetry as:

$$3d_z^2, 3d_x^2 - y^2; \quad e_g \quad (2.4)$$

$$3d_{xy}, 3d_{xz}, 3d_{yz} \quad t_{2g} \quad (2.5)$$

$$4s \quad a_{1g} \quad (2.6)$$

$$4p_x \quad t_{1u} \quad (2.7)$$

ii. Ligand Orbitals

Each of the ligand σ orbitals make up a total of six symmetry orbitals. By choosing the linear combinations of ligand σ orbitals that have the same symmetry properties as the various metal σ orbitals, MO construction is done in such a way that each of them overlaps with a particular one of the six metal ion orbitals that are suitable for σ bonding.

2.5 Photophysical Processes for Transition Metal Complexes

Figure 2.6 shows the various types of electronic transitions that are expected in octahedral complexes at relatively low energies [1, 12].

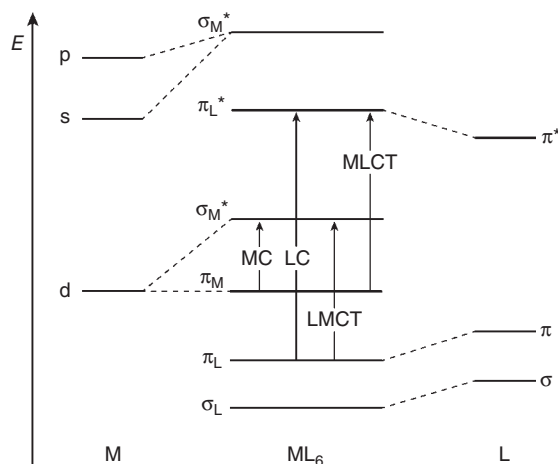


Figure 2.6 – Molecular orbital diagram representing various types of electronic transitions in octahedral complexes.

Based on the location of the MOs involved, these electronic transitions can be classified into three types:

i. **Transitions between MOs mainly localized on the central metal**

These MOs are mainly from metal d orbitals such as the $t_{2g}(\pi)$ and $e_g(\sigma^*)$. They are more commonly known as $d-d$ transitions or metal centered (MC) transitions. They are transitions from π_M orbitals to σ_M^* orbitals.

ii. **Transitions between MOs mainly localized on the ligands and MO's mainly localized on the central metal**

These transitions are known as charge-transfer (CT) or electron-transfer transitions. They include ligand-to-metal charge-transfer (LMCT) transitions such as of type $\pi_L \rightarrow \pi_M^*$ and the metal-to-ligand charge-transfer (MLCT) transitions such as of type $\pi_M \rightarrow \pi_L^*$.

iii. **Transitions between MOs mainly localized on the ligands**

They only involve ligand orbitals which are almost unaffected by coordination to the metal. These include ligand centered (LC) transitions of type $\pi_L \rightarrow \pi_L^*$.

Bibliography

- [1] P. S. Wagenknecht and P. C. Ford. Metal centered ligand field excited states: their roles in the design and performance of transition metal based photochemical molecular devices. *Coord. Chem. Rev.*, 255(5): 591–616, 2011.
- [2] V. L. Goedken, L. M. Vallarino, and J. V. Quagliano. Cationic ligands. coordination of the 1, 1, 1-trimethylhydrazinium cation to nickel (II). *Inorg. Chem.*, 10(12):2682–2685, 1971.
- [3] S. Govindarajan, K. C. Patil, H. Manohar, and P. Werner. Hydrazinium as a ligand: structural, thermal, spectroscopic, and magnetic studies of hydrazinium lanthanide di-sulphate monohydrates; crystal structure of the neodymium compound. *Dalton Trans.*, (1):119–123, 1986.
- [4] O. S. Bushuyev, F. A. Arguelles, P. Brown, B. L. Weeks, and L. J. Hope-Weeks. New energetic complexes of copper (II) and the acetone carbohydrazide schiff base as potential flame colorants for pyrotechnic mixtures. *Eur. J. Inorg. Chem.*, 2011(29):4622–4625, 2011.
- [5] A. D. McNaught and A. Wilkinson. *IUPAC. Compendium of Chemical Terminology, the “Gold Book”*, volume II. Blackwell Scientific Publications, Oxford, 1997.
- [6] N. G. Connelly, Royal Society of Chemistry (Great Britain), International Union of Pure, and Applied Chemistry. *Nomenclature of Inorganic Chemistry: IUPAC recommendations 2005*. Royal Society of Chemistry Publishing/IUPAC, 2005. ISBN 9780854044382.
- [7] P. C. Ford. The ligand field photosubstitution reactions of d^6 hexacoordinate metal complexes. *Coord. Chem. Rev.*, 44(1):61–82, 1982.
- [8] M. Gerloch and E. C. Constable. *Transition Metal Chemistry: The Valence Shell in d-Block Chemistry*. Wiley, 1994. ISBN 9783527292189.
- [9] F. A. Cotton and G. Wilkinson. *Advanced inorganic chemistry: a comprehensive text*. Interscience Publishers, 1972. ISBN 9780471175605.

-
- [10] K. Sridharan. *Spectral Methods in Transition Metal Complexes*. Elsevier Science, 2016. ISBN 9780128096543.
- [11] P. Atkins. *Shriver and Atkins' Inorganic Chemistry*. Oxford University Press, Oxford, United Kingdom, 2010. ISBN 9780199236176.
- [12] M. Montalti, A. Credi, L. Prodi, and M. T. Gandolfi. *Handbook of Photochemistry*. CRC Press, third edition, 2006. ISBN 9781420015195.
- [13] Figgis B. N. and M. A. Hitchman. *Ligand field theory and its applications*. Special topics in inorganic chemistry. Wiley-VCH, 2000. ISBN 9780471317760.

Chapter 3

Schrödinger Equation

It is by logic that we prove, but by intuition that we discover.

J. H. Poincaré, ca. 1900.

Introduction

In this chapter, an introductory review of elementary quantum mechanics is given. Advanced concepts of the density functional theory are built starting from the fundamental aspects of electronic structure theory using mathematical manipulation techniques to solve the fundamental equations. All these concepts lead to the build up of the Schrödinger equation, which is the ‘backbone’ of electronic structure and methods. Starting from the ultraviolet calamity and the photoelectric effect (ideas that spurred the improvement of quantum mechanics) a step by step approach is shown of how the Schrödinger equation builds up. Also discussed in this chapter is the Born-Oppenheimer approximation, which separates the motion of an electron from that of the nucleus. They are reviewed herein. This chapter has been written based on the following references [1–9]; among others cited in text.

3.1 Ultraviolet Catastrophe

This is also referred to as black-body radiation. A black-body is an idealized object which absorbs and emits all incident radiation without favouring particular frequencies [9]. The Rayleigh-Jeans law is an equation that describes the intensity of black-body radiation as a function of frequency for a fixed temperature. The law works for low frequencies but fails for high frequencies. This phenomenon is referred to as the ultraviolet catastrophe. Max Planck explained the black-body radiation by introducing the concept of quantization of energy using the Planck's constant (h) in his equation:

$$E = nh, \quad (3.1)$$

where h is the Planck's constant (6.626×10^{-27} J.s). Planck could not give a justification for his assumption of energy quantization. The idea was taken up further by Einstein who adopted Planck's assumption to explain the photoelectric effect.

3.2 Photoelectric Effect

Photoelectric effect is the ejection of electrons from a metal surface by light. The classical wave theory of light suggested that the intensity of the light determined the amplitude of the wave. Experiments however showed that the kinetic energy of the ejected electrons depends on the colour (which is a function of frequency) of the light. Einstein explained the observation by assuming that the light consisted of packets of energy (photons), with each photon having an energy [8, 10],

$$E_{\text{photon}} = h\nu, \quad (3.2)$$

where h is Planck's constant and ν is the frequency of the light.

Einstein went ahead to explain that for an electron to be ejected, the forces holding the electron in the metal must first be overcome [what is commonly referred to as the work function (Φ)] and then the extra energy that

remains is the one which removes the electron from the metal. Conservation of energy results in the equation for the photoelectric effect written as,

$$h\nu = E_{\text{photon}} = \Phi + KE_{\text{max}}, \quad (3.3)$$

where Φ is the minimum energy needed by an electron to escape the metal (metal's work function), and KE_{max} is the maximum kinetic energy of an emitted electron. The equation in essence tells us two things; first, increasing the light's frequency will increase the photon energy and therefore the kinetic energy of the emitted electron. Secondly, increasing light intensity at fixed frequency will increase the rate of emission of electrons, but has no effect on the kinetic energy of the emitted electron. Consequently, reaping from the fruits of his hard work, Einstein was awarded the Nobel prize [11] in physics in 1921 for his work. The photoelectric effect shows that light can exhibit both particle-and wavelike behaviour from diffraction experiments.

3.3 Quantization of Electronic Angular Momentum

The discussion about quantization of electronic angular momentum takes us back to the structure of matter. Various experiments in the 19th century such as the electric discharge tube and radioactivity led to the discovery of charged particles, electrons and protons. The important fact to any chemist is that chemical properties of atoms and molecules are determined by their electronic structure. This raises the question about the nature of the motions and energies of the electrons. To this extent, several atomic models were proposed to explain the above question. The specific models will not be dealt with in detail but the problem that is at hand is that classical physics could not explain what held the electron in position as it moved around the nucleus since it was expected to lose energy by radiation and therefore would spiral toward the nucleus.

Neil Bohr brought in the concept of quantization of energy for the hydrogen atom to solve the problem. According to Bohr, electrons orbit about the nucleus of an atom in stable allowed electronic orbits with a quantized

electronic angular momentum [12] of,

$$l = mvr = n\hbar, \text{ with } \hbar = \frac{h}{2\pi}. \quad (3.4)$$

A quantized angular momentum implies that the energy will in-turn be quantized. Bohr used the principle of quantization to explain the line spectrum of the hydrogen atom. A photon of light of frequency ν is absorbed or emitted with the transition of an electron from one allowed energy level to another.

$$E_{\text{upper}} - E_{\text{lower}} = h\nu. \quad (3.5)$$

Bohr's expression for the allowed energy levels worked perfectly for the hydrogen atom spectrum but failed in atoms with more than one electron. It did not account for chemical bonding in molecules also. This failure could be attributed to the use of classical mechanics for the description of the electronic motions in atoms. The main difference is that, in quantum mechanics, only certain energies of motion are allowed (i.e., energy is quantized) while in classical mechanics, a continuous range of energies is allowed. This prompted Louis de Broglie to introduce the wave aspect for electrons.

3.4 Wave-Particle Duality

The failure of Bohr to describe the electronic motion in atoms prompted de Broglie to suggest that the motion of electrons has a wave aspect. The wavelength (λ) of an electron of mass m and speed v is,

$$\lambda = \frac{h}{mv} = \frac{h}{p}, \quad (3.6)$$

where $\vec{p} = m\vec{v}$ is the particle momentum (whose magnitude is p) and m refers to the relativistic mass. The wave-particle duality of light was proven by the fact that light behaves as a wave since it can be diffracted, and as a particle because it contains packets of energy [8].

For an electron behaving as a wave, the wave completing the integral

number of wavelength for a stable electron orbit is,

$$2\pi r = n\lambda. \quad (3.7)$$

This can be rewritten as below with the inclusion of the de Broglie relation,

$$mvr = n\hbar. \quad (3.8)$$

The wave-particle duality leads to the Heisenberg's uncertainty principle. The question is, how can an electron be both a particle (localized) and a wave (non localized)? The Heisenberg's uncertainty principle states that the position and momentum of a particle cannot be known simultaneously at the same time.

$$\Delta x \Delta p \geq \frac{\hbar}{2}. \quad (3.9)$$

If the orbital radius of an electron in an atom is known exactly (position), then the angular momentum must be completely unknown. This principle set in a new quantum theory that was consistent with the uncertainty principle since the Bohr model specifies the exact radius and that the orbital angular momentum must be an integer hence a weakness. In general, the more precisely the position is measured, the less accurate is the determination of momentum because the act of measurement introduces an uncontrollable disturbance in the system being measured. Schrödinger replaced this idea with the probability of finding an electron in a particular position or volume of space.

3.5 Time-Independent Schrödinger Equation

The Schrödinger equation is classified under what is called 'modern quantum mechanics' [10] based on the Copenhagen interpretation. In his equation, Schrödinger replaced the wave in classical mechanics with a wave function $\psi(r) = \psi(x, y, z)$. There exist two forms of the Schrödinger equation, the time-dependent and the time-independent Schrödinger equation, distin-

guished by whether the wave is stationary or travelling. In the next section of the discussion, a heuristic justification of the Schrödinger equation is given starting from the basic idea of the wave equation.

The time-independent Schrödinger equation is mostly used because we are interested in atoms and molecules without the time-dependent interactions. Starting from the basic idea of the classical one-dimensional wave equation,

$$\frac{\partial^2 u}{\partial x^2} = \frac{1}{v^2} \frac{\partial^2 u}{\partial t^2}. \quad (3.10)$$

We can solve this wave equation by the separating the variables, by writing $u(x, t)$ as the product of a function of x and a harmonic function of time:

$$u(x, t) = \psi(x) \cos(\omega t), \quad (3.11)$$

where $\psi(x)$ is the spatial amplitude of the wave. Replacing Eq.(3.11) in Eq. (3.10) gives the equation for the spatial amplitude,

$$\frac{d^2 \psi}{dx^2} + \frac{\omega^2}{v^2} \psi(x) = 0, \quad (3.12)$$

but $\omega = 2\pi\nu$ and $\nu\lambda = v$ leading to,

$$\frac{d^2 \psi}{dx^2} + \frac{4\pi^2}{\lambda^2} \psi(x) = 0. \quad (3.13)$$

This is an ordinary differential equation describing the spatial amplitude of the matter wave as a function of position. From Eq. (3.13), the idea of de Broglie matter waves can be introduced. The total energy of a particle is the sum of its kinetic energy and its potential energy, given by the equation below,

$$E = \frac{p^2(x)}{2m} + V(x). \quad (3.14)$$

Solving for momentum, p , yields,

$$p(x) = \sqrt{2m[E - V(x)]}. \quad (3.15)$$

Using the de Broglie formula, an expression for the wavelength can be found as,

$$\lambda = \frac{h}{p} = \frac{h}{\sqrt{2m[E - V(x)]}}. \quad (3.16)$$

Substituting λ into Eq.(3.13),

$$\frac{d^2\psi}{dx^2} + \frac{2m}{\hbar^2}[E - V(x)]\psi(x) = 0, \quad (3.17)$$

which can be rewritten as,

$$-\frac{\hbar^2}{2m} \frac{d^2\psi(x)}{dx^2} + V(x)\psi(x) = E\psi(x). \quad (3.18)$$

In three dimensions, the single-particle one-dimensional equation can be extended to,

$$\begin{aligned} & -\frac{\hbar^2}{2m} \nabla^2 \psi(\vec{r}) + V(\vec{r})\psi(\vec{r}) = E\psi(\vec{r}) \\ \equiv & \left(-\frac{\hbar^2}{2m_e} \nabla^2 + V(\vec{r}) \right) \psi(\vec{r}) = E\psi(\vec{r}) \\ \equiv & \underbrace{\left(-\frac{\hbar^2}{8\pi^2 m_e} \nabla^2 + V(\vec{r}) \right)}_{\hat{H}} \psi(\vec{r}) = E\psi(\vec{r}) \\ \equiv & \hat{H}\psi(\vec{r}) = E\psi(\vec{r}). \end{aligned} \quad (3.19)$$

Here, \hat{H} is the Hamiltonian operator. Equation (3.19) is known as the time-independent (does not contain a time variable), non-relativistic (not valid when the velocities of particles approach the speed of light) Schrödinger equation. The $\psi(x)$ wavefunctions obtained from this equation are called stationary state wavefunctions and they describe a particle of mass (m_e)

∇^2 is the Laplacian or Laplace-operator, defined as the sum of differential operators (in cartesian coordinates). $\nabla^2 = \frac{\partial^2}{\partial x^2} + \frac{\partial^2}{\partial y^2} + \frac{\partial^2}{\partial z^2}$

moving in a potential field $V(x)$. From this equation, the energy and any other related properties of a molecule may be obtained by solving it. Solutions to Eq. (3.19) correspond to different stationary states of a particle and the one with the lowest energy is called the ground state.

3.6 Time-Dependent Schrödinger Equation

Although most of the problems of chemical interest can be described by the time-independent non-relativistic Schrödinger equation, the time-dependent Schrödinger equation is described herein for the purposes of distinction between the two of them. The time-dependent Schrödinger equation is given as a postulate of quantum mechanics, unlike the Schrödinger equation that can be derived starting from the classical wave equation. The “derivation” is only heuristic but not rigorous. The time-independent Schrödinger equation can be rigorously derived from the time-independent Schrödinger equation. From Eq. (3.13) the idea of de Broglie matter waves with the space and time variable $[\phi(x, t)]$ is introduced. The only difference between this equation and the time-independent Schrödinger equation is that the time variable has been introduced. The total energy of a particle is the sum of its kinetic energy and its potential energy, given by,

$$E = \frac{p^2(x)}{2m} + V(x, t). \quad (3.20)$$

The other steps have been omitted as they are similar to those for the time-independent equation,

$$\frac{\partial^2 \psi(x, t)}{\partial x^2} + \frac{2m}{\hbar^2} [i\hbar \frac{\partial}{\partial t} - V(x, t)] \psi(x, t) = 0, \quad (3.21)$$

Which can be rewritten as;

$$\left[\frac{-\hbar^2}{2m} \frac{\partial^2}{\partial x^2} + V(x, t) \right] \Psi(x, t) = i\hbar \frac{\partial}{\partial t} \Psi(x, t). \quad (3.22)$$

This is the time-dependent Schrödinger equation.

3.7 Molecular Hamiltonian

$$\hat{H}\psi(\vec{r}) = E\psi(\vec{r}), \quad (3.23)$$

\hat{H} is the Hamiltonian operator. This operator is constructed from the energy expression in classical mechanics. In classical mechanics, the classical energy is calculated as:

$$\begin{aligned} E &= \text{kinetic energy} + \text{potential energy} \\ &= \frac{1}{2}m_e v^2 - \frac{Ze^2}{4\pi\epsilon_0 r} \\ &= \frac{p^2}{2m_e} - \frac{Ze^2}{4\pi\epsilon_0 r} \end{aligned} \quad (3.24)$$

Replacing each cartesian and momentum coordinate by the corresponding operator in Table 3.1,

Table 3.1 – Classical to quantum transformation of cartesian position and momentum operators.

Position	Momentum
$x \rightarrow \hat{x}$	$p_x \rightarrow \hat{p}_x$
$y \rightarrow \hat{y}$	$p_y \rightarrow \hat{p}_y$
$z \rightarrow \hat{z}$	$p_z \rightarrow \hat{p}_z$

Results in:

$$\begin{aligned} \hat{H} &= \frac{1}{2m_e} (\hat{p}_x^2 + \hat{p}_y^2 + \hat{p}_z^2) \\ &= -\frac{\hbar^2}{2m_e} \left(\frac{\delta^2}{\delta x^2} + \frac{\delta^2}{\delta y^2} + \frac{\delta^2}{\delta z^2} \right) - \frac{Ze^2}{4\pi\epsilon_0 r} \\ &= \frac{\hbar^2}{2m_e} \nabla^2 - \frac{Ze^2}{4\pi\epsilon_0 r} \end{aligned} \quad (3.25)$$

In other words, \hat{H} is composed of the kinetic and potential energy operator,

$$\hat{H} = \hat{T} + \hat{V}. \quad (3.26)$$

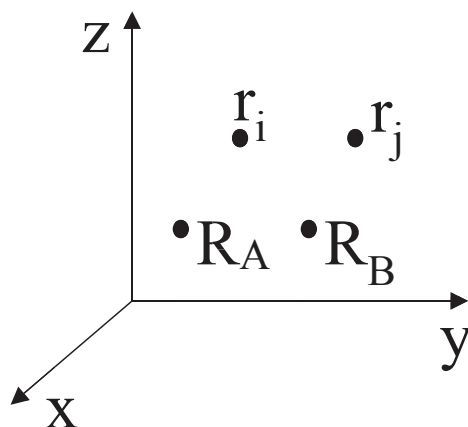


Figure 3.1 – xyz directions

Table 3.2 – Symbols used to show the interaction between nuclei electrons.

	Symbol	Indices	Position	Mass	Charge
Electrons	N	i, j	r_j	m_e	$-e$
Nuclei	M	A, B	R_A	M_A	$+eZ_A$

A molecular system consisting of M nuclei and N electrons is a complex many-body problem. A system with N electrons and M nuclei in the cartesian coordinates x, y and z may be depicted as Fig. 3.1.

The interaction between the nuclei and the electrons has been described using the symbols in Table 3.2.

A and B run over the M nuclei while i and j denote the N electrons in the system. The analogous time-independent, non-relativistic Schrödinger equation for the many body problem is,

$$\hat{H}\Psi_i(\vec{x}_1, \vec{x}_2, \dots, \vec{x}_N, \vec{R}_1, \vec{R}_2, \dots, \vec{R}_M) = E_i\Psi_i(\vec{x}_1, \vec{x}_2, \dots, \vec{x}_N, \vec{R}_1, \vec{R}_2, \dots, \vec{R}_M) \quad (3.27)$$

\hat{H} is the differential operator representing the total energy for the molecular system. We shall consider five contributions to the \hat{H} . The \hat{H} being considered here does not include the external electric and magnetic fields which will necessitate the inclusion of other terms in the \hat{H} such as the spin-orbit

coupling. The \hat{H} is given as,

$$\hat{H} = \hat{T}_e + \hat{T}_N + \hat{V}_{ee} + \hat{V}_{NN} + \hat{V}_{eN}, \quad (3.28)$$

where,

$$\begin{aligned} \hat{T}_e &= - \sum_i^N \frac{\hbar^2}{2m_e} \nabla_i^2 \\ \hat{T}_N &= - \sum_A^M \frac{\hbar^2}{2M_A} \nabla_A^2 \\ \hat{V}_{ee} &= \sum_{i<j}^N \frac{e^2}{4\pi\epsilon_0|r_i - r_j|} \\ \hat{V}_{NN} &= \sum_{A<B}^M \frac{e^2 Z_A Z_B}{4\pi\epsilon_0|R_A - R_B|} \\ \hat{V}_{eN} &= \sum_i^N \sum_A^M \frac{e^2 Z_A}{4\pi\epsilon_0|r_i - R_A|}. \end{aligned} \quad (3.29)$$

In SI units.

3.8 Atomic Units

The system of atomic units was developed to simplify mathematical equations by setting many fundamental constants equal to 1. Equations are expressed in a very compact form, without any fundamental physical constants. Consequently, atomic units remove units from equations. Physical quantities such as the mass of an electron, m_e , the modulus of its charge, $|e|$, Planck's constant h divided by 2π , the 2π times the permittivity of the vacuum, are all set to unity. A new set of units called the atomic units is defined; the atomic unit of energy is called a hartree and is denoted by E_h . The atomic units that have been adopted are shown in Table 3.3.

With the expression of the physical constants as unity, \hat{H} simplifies to,

Table 3.3 – Atomic Units

Quantity	Atomic Unit	SI units	Symbol
mass	mass of an electron	$9.1094 \times 10^{-31} \text{Kg}$	m_e
charge	elementary charge	$1.6022 \times 10^{-19} \text{C}$	e
action	$\frac{h}{2\pi}$	$1.0546 \times 10^{-34} \text{Js}$	\hbar
Length	$\frac{4\pi\epsilon_0\hbar}{m_e e^2}$	$5.2918 \times 10^{-11} \text{m}$	$a_0(\text{bohr})$
energy	$\frac{\hbar^2}{m_e a_0^2}$	$4.3547 \times 10^{-18} \text{J}$	$E_h(\text{hartree})$
		27.21138 eV	
		627.5095 kcal mol ⁻¹	
		219474.6 cm ⁻¹	
		$3.157 \times 10^5 \text{ K}$	

$$\hat{H} = -\frac{1}{2m_e} \sum_i^N \nabla_i^2 - \sum_A^M \frac{1}{2M_A} \nabla_A^2 + \sum_{i<j}^N \frac{1}{|r_i - r_j|} + \sum_{A<B}^M \frac{Z_A Z_B}{|R_A - R_B|} - \sum_i^N \sum_A^M \frac{1}{r_i - R_A}. \quad (3.30)$$

A quick look at the \hat{H} will give you the impression that it is an approximation since it does not include interaction with external electric and magnetic fields, spin-orbit coupling, orbit-orbit coupling and any relativistic correction of the kinetic energy. This is just to point out this fact, but it is not a big issue since it is always possible to add these factors to a calculation when they are needed.

The ultimate goal that we aim at is solving the Schrödinger equation. Looking at the problem that is at hand, it is mind boggling since it is a prodigious problem both conceptually and computationally. The question is, can this be solved?

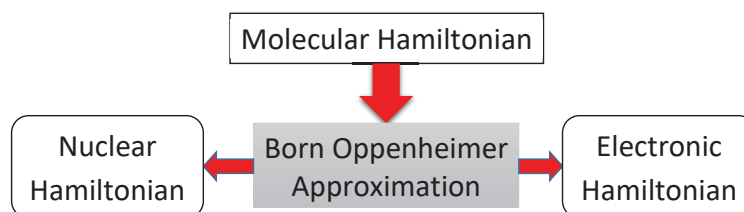


Figure 3.2 – Molecular Hamiltonian.

3.9 Born-Oppenheimer Approximation

The famous Born-Oppenheimer Approximation (clamped-nuclei approximation) simplifies the Schrödinger equation by taking advantage of the significant differences between the masses of nuclei and electrons [13]. The lightest nuclei (^1H) weights about 1800 times more than an electron, which implies that the electrons are much lighter than the nuclei and therefore move much faster.

I particularly like the explanation of this approximation using the comparison of a swarm of flies around a cow, and so I will not hesitate to state it here. The situation of the electrons and nuclei in a molecule can be compared to a swarm of flies around a herd of cows. The sound of the buzzing flies (electrons) does not make the cow (nuclei) to move but as the cow moves off to new pasture, the swarm of flies follow suit instantaneously. This in essence means that the movement of electrons around the nucleus does not make it to move appreciably but the movement of the nucleus triggers an immediate movement of the electrons along with it.

With the above explanation, you realize that the electrons move in a field of fixed nuclei. If the nuclei are fixed in space, they do not move and therefore their kinetic energy is zero and the potential energy due to nucleus-nucleus repulsion is a constant. Consequently, the complete Hamiltonian reduces to an electronic Hamiltonian. Simply put, the Born-Oppenheimer Approximation does what is depicted in Fig. 3.2.

$$\begin{aligned}
\hat{H}_{elec}(\mathbf{r}; \mathbf{R}) &= -\frac{1}{2} \sum_{i=1}^N \nabla_i^2 - \sum_{i=1}^N \sum_{A=1}^M \frac{Z_A}{r_{iA}} + \sum_{i=1}^N \sum_{i < j}^M \frac{1}{r_{ij}} \\
&= \hat{T}(\mathbf{r}) + \hat{V}_{Ne}(\mathbf{r}; \mathbf{R}) + \hat{V}_{ee}(\mathbf{r}).
\end{aligned} \tag{3.31}$$

$\underbrace{\mathbf{R}}_{\text{Matrix}} = (\underbrace{\vec{R}_1, \vec{R}_2, \dots, \vec{R}_M}_{\text{Vectors}})$ is a parameter in the above equation. In this case, the Schrödinger equation is solved for the electronic problem for a given set of fixed nuclear positions. If a new set of nuclear coordinates is generated, the electronic problem must be solved for this set also as it is an entirely new problem. The Schrödinger equation involving the electronic Hamiltonian is,

$$\hat{H}_e(\mathbf{r}; \mathbf{R}) \Psi_I^e(\mathbf{x}; \mathbf{R}) = E_I^e(\mathbf{R}) \Psi_I^e(\mathbf{x}; \mathbf{R}). \tag{3.32}$$

Solutions of the electronic Schrödinger equation for a large number of nuclear geometries and for electronic states are useful in constructing the molecular potential energy surface (PES),

$$V(\mathbf{R}) = V_{nn}(\mathbf{R}) + E_I^e(\mathbf{R}). \tag{3.33}$$

Bibliography

- [1] W. Koch and M. C. Holthausen. *A Chemist's Guide to Density Functional Theory*. Wiley-VCH, Germany, 2015. ISBN 9783527802814.
- [2] A. C. Phillips. *Introduction to Quantum Mechanics*. Manchester Physics Series. Wiley, 2013. ISBN 9781118723258.
- [3] K. I. Ramachandran, G. Deepa, and K. Namboori. *Computational Chemistry and Molecular Modeling: Principles and Applications*. Springer Berlin Heidelberg, 2008. ISBN 9783540773023.
- [4] D. B. Cook. *Handbook of Computational Quantum Chemistry*. Dover Books on Chemistry. Dover Publications, 2005. ISBN 9780486443072.
- [5] T. Tsuneda. *Density Functional Theory in Quantum Chemistry*. SpringerLink : Bücher. Springer, Japan, 2014. ISBN 9784431548256.
- [6] F. Jensen. *Introduction to Computational Chemistry*. Wiley, Great Britain, 1999. ISBN 9780471980858,0471980854,0471984256.
- [7] J. G. Lee. *Computational Materials Science: An Introduction, Second Edition*. CRC Press, 2016. ISBN 9781498749763.
- [8] I. N. Levine. *Quantum Chemistry*. Pearson Education, 2013. ISBN 9780321918185. pp. 3-6.
- [9] P. W. Atkins and R. S. Friedman. *Molecular Quantum Mechanics*. Oxford University Press, Oxford, 2011. ISBN 9780199541423.
- [10] D. A. McQuarrie. *Quantum Chemistry*. University Science Books, 2008. ISBN 9781891389504.
- [11] The nobel prize in physics 1921. http://www.nobelprize.org/nobel_prizes/physics/laureates/1921/einstein-facts.html, 2017. Accessed: 2017-02-14.

-
- [12] A. Szabo and N. S. Ostlund. *Modern Quantum Chemistry: Introduction to Advanced Electronic Structure Theory*. Macmillan Publishing Company, New York, 1982.
- [13] L. Piela. *Ideas of Quantum Chemistry*. Elsevier Science, 2006. ISBN 9780080466767.

Chapter 4

Photophenomena and Luminescence

‘And God said, “Let there be light,” and there was light. God saw that the light was good, and he separated the light from the darkness.’

Genesis 1:3-4

4.1 Introduction

Photochemistry can be viewed as the study of the interaction of light with matter [1]. It has been argued by some scientists, including my own Prof. Mark Casida that photochemistry came into action when God said: “Let there be light.”

Photochemistry has a wide range of uses and applications that include: photosynthetic processes in green plants, a type of photo-catalysis, accumulation of fossil fuels, vision, cancer treatment, water treatment, charge separation and energy migration which are key in applications of solar energy conversion and signal processing, luminescent sensors, optical brighteners, atmospheric photochemistry, electrochemiluminescent materials (light emitting diodes (LEDs), organic light emitting diodes (OLEDs), light-emitting electrochemical cells (LECs)), photodegradation, photostabilization, photolithography, and stereolithography. It also has applications in the fields

of biomaterials and tissue engineering specifically in oncology (treatment of cancer), molecular biology and biosurgery [2–6]. With such kinds of applications, the importance of photochemistry in changing and improving the life of mankind cannot be ignored and thus it remains an active area of research.

In photochemistry, we are specific about the kind of light that we are interested in: Typically, we deal with chemical reactions and physical changes that result from interactions between matter and visible (400-800 nm) or ultraviolet (200-400 nm) light of the electromagnetic spectrum [7]. When such interactions occur, photon energy is added to the ground state energy of the molecule resulting in an excited state. The energy can be transferred to the molecule by chemical reaction, intermolecular energy transfer or absorption of radiation. The excited state possesses more stored energy and thus will be different from its ground state precursor. Differences between the ground and excited state includes the geometry, vibrational and rotational energies and redox potentials. With the differences listed above, it is expected that ground and excited states will undergo different chemical reactions. In a chemical reaction, other reactions may also take place such as the thermal reactions that are induced by heat. One of the major challenges when dealing with photochemistry will be to identify products resulting from the primary photoprocess and those from thermal reactions.

4.2 Electronic Excitation

Molecular excitation results from the interaction of matter with a photon of suitable energy, chemical reaction, or intermolecular energy transfer. Of the three pathways of excitation, photochemistry remains the *de facto* alternative route to thermal reactions. This is because it offers the easiest mechanism to selectively populate an excited state. An electronic excited state arises from the interaction of matter with a photon of suitable energy as shown below.



This is made possible by the fact that energy of matter is quantized and only certain specific energies are allowed, that is why we are talking of ‘a photon of suitable energy’. The energy of the photon can be calculated from quantum theory as $E = h\nu$.

4.2.1 How does Electronic Excitation Occur?

Electronic transition from ground to excited state after the absorption of a photon of suitable energy is guided by the Franck-Condon principle [8]. It obeys this principle based on the fact that we are looking at the vertical excitation corresponding to an electronic excitation only, without change in the nuclear positions. This is because electronic transitions occur for a very short time that the nuclei do not change their positions during the transition [9] since electrons are much lighter than nuclei. This often results in an increase in the excited state bond length since transition from the ground to excited state often involves transfer of an electron from a bonding orbital into an anti-bonding orbital. Another reason is that the excited state electronic structure differs from that of the ground state and thus has a different energy profile.

The above can be shown by considering the contribution from the nuclear component. To show this, vibrational wave functions must be known. Let us consider a simple harmonic oscillator, whose vibrational energy levels are quantized and the potential energy well for internuclear distances is given by a parabolic curve as shown in Fig. 4.1.

4.2.2 Types of Electronic Transitions

The intensity of electronic transitions is guided by a number of rules (selection rules) based on the spin and symmetry [3]. We consider closed and open shell molecules in our discussion. The Laporte selection rule forbids transitions between states of the same parity. This rule requires that an electronic transition must be accompanied by a change in the orbital angular momentum quantum number. The spin selection rule, denoted as $\Delta S = 0$, requires that there should be no change in the spin multiplicity. Spin

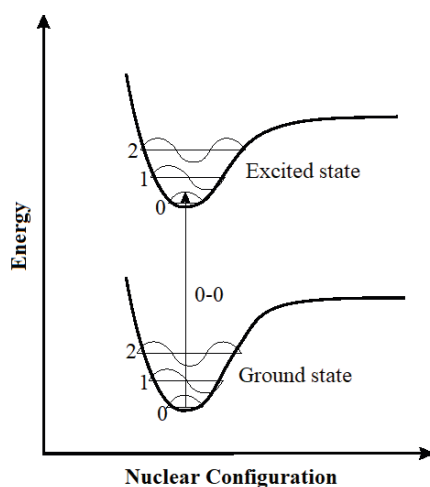


Figure 4.1 – Potential energy diagrams with vertical transitions as in the Franck-Condon principle.

multiplicity can be calculated from the equation $2S + 1$, where S is the total spin of all electron spins. It results in two kinds of electronic transitions; the allowed transition where there is no spin flip and the forbidden transition that involves spin flip. Now, the question is, what types of spin multiplicity exist? The first type of spin multiplicity is the singlet (S_0). It arises from the excitation of a single electron from its spin-paired singlet ground state to an excited state having electrons in two orbitals, each containing a single unpaired electron as shown in Fig. 4.2. Singlet ground state to singlet excited state is considered an allowed transition since it does not involve change in spin and it gives rise to intense bands in the absorption spectra characterized by large values of extinction coefficient ($\epsilon \approx 10^2 - 10^4 \text{ M}^{-1} \text{ cm}^{-1}$).



Figure 4.2 – Singlet ground state to excited allowed singlet state.

The second type of multiplicity is known as the triplet (T_0). It arises from the excitation of a single electron from its spin-paired singlet ground state to an excited state where the spins are in the same directions in the two orbitals as shown in Fig. 4.3. Transition from a spin-paired singlet ground state to a triplet excited state is considered a forbidden transition according to the spin selection rule, ($\Delta S = 0$) and it gives rise to bands that can hardly be observed in the absorption spectra characterized by small values of extinction coefficient ($\epsilon \approx 1 - 10^2 \text{ M}^{-1} \text{ cm}^{-1}$).



Figure 4.3 – Singlet ground state to excited forbidden triplet state.

The spin selection rule is however relaxed for electronic transitions involving heavy atoms such as actinides, lanthanides and complexes of second and third row transition metal complexes because of spin-orbit coupling [10]. This arises when the magnetic field produced by electrons in motion interacts with magnetic field due to the electron spin. Spin-orbit coupling is a heavy metal atom orbital effect that may lead to loss of distinction between singlet and triplet states because of the mixing of the states of different multiplicities. In essence, this is actually quite positive from an application point of view because the long-lived, low-energy triplet excited states are readily accessible enabling many applications. With increase in atomic number, spin-orbit coupling is more pronounced and there is reduction in the number of forbidden electronic transitions. In our calculations, we are dealing with the ruthenium atom which is considered as a heavy atom; however, spin-orbit effects have not been included in all the calculations.

4.3 State Energy Diagram

To further understand photochemistry, state energy diagrams are used to show the position of energy levels of the ground state, the excited singlet states and the excited triplet states of the molecule. One point to note is that an excited triplet state has a lower energy than that of the corresponding excited singlet state. This is justified by the requirement of Hund's rule [11]. Another factor that weighs in heavily for the position of the energy level is the type of transition that is taking place. Later on, we shall be able to define the different kinds of transitions that are likely to be encountered in transition metal complexes; but to make our point, transitions involving metal to ligand tend to have low energies while transitions of only ligand molecular orbitals are more energetic. Spin arrangement in the orbitals will be in such a way as maximizes their spatial separation, an effect commonly known as the spin correlation effect.

This further step explains what is expected in the molecular orbitals (MO). Bonding molecular orbitals form when atomic orbital wavefunctions enhance each other in the region between the nuclei ($\Psi_{xy} = \Psi_x + \Psi_y$) while the antibonding molecular orbitals are formed when the atomic orbital wavefunctions cancel each other in the region between the nuclei ($\Psi_{xy}^* = \Psi_x - \Psi_y$). Orbitals containing lone pairs of electrons that are neither bonding nor antibonding with no role in bonding are called nonbonding molecular orbitals (n). On addition of an electron to a molecule it goes into the lowest unoccupied molecular orbital (LUMO), if an electron is removed it is removed from the highest occupied molecular orbital (HOMO). In this case, the lowest electronic transition is from HOMO to LUMO.

The energies of electronic states form an important core of this work. It is the inspiration behind the development of the program PDOS.PY. This is because the presence of metal ions in the transition metal complexes have a large number of closely spaced orbitals that can interact with each other to give a multiplicity of states that are very similar to each other in energy which is further complicated by the presence of spin-orbit coupling. This makes it very complex to separate the states and the program PDOS.PY was

specifically designed to help solve this problem.

4.4 Excited State Deactivation

4.4.1 Introduction

The excited state that was formed by absorption of a photon of suitable energy is unstable with high energy and must undergo deactivation to be stable. There are several ways in which deactivation of an excited state (A^*) can occur; photochemical reaction, luminescence, radiationless deactivation, and the quenching process [12]. Figure 4.4 shows the possible pathways of deactivation of the excited state.

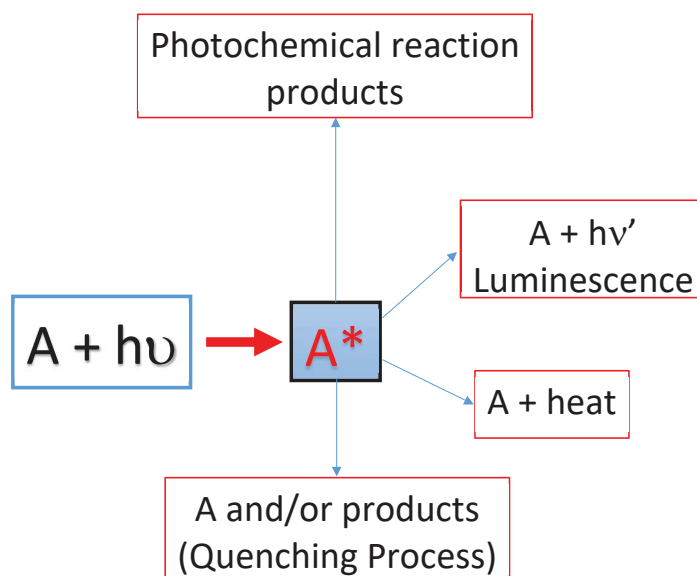


Figure 4.4 – Excited State Deactivation

It will be shown in detail how each of the above processes occurs.

4.4.2 Luminescence

Luminescence can be defined as the emission of ultraviolet, visible or infrared photons from an electronically excited species by cold light [13].

Conversely, incandescence involves hot light. There exist different types of luminescence depending on the mode of excitation. The different types of luminescence based upon the source of excitation energy are:

Table 4.1 – Classification of different types of luminescence based upon the source of excitation energy.

Type	Energy Source
Chemiluminescence	Chemical reaction
Triboluminescence	Mechanical e.g. frictional and electrostatic forces
Bioluminescence	Chemical reaction (within living organisms)
Thermoluminescence	Heat
Electroluminescence	Electric field
Radioluminescence	Ionizing radiation such as the X-rays, α
Cathodoluminescence	Cathode rays
Photoluminescence (fluorescence, phosphorescence)	Radiation (UV, Visible, IR)

In this work, the type of luminescence being studied is photoluminescence (fluorescence, phosphorescence) that involves absorption of light (photons).

4.4.2.1 Jablonski Diagram

The Jablonski diagram [7] is used to represent the properties of excited states and their relaxation processes. This is because de-activation can lead to heading back to the ground state (photophysical process) or with formation of other species (photochemical process). Photophysical processes are represented by the Jablonski diagram. There is a convention used to show this processes in the Jablonski diagram: It is assumed that the ground state is a singlet and electronic states are represented by thick horizontal lines arranged in vertical order while the states of different multiplicity are separated horizontally. Vibrational levels are represented by thin lines. Absorption or emission of a photon associated with radiative transitions are shown by straight arrows, while radiationless transitions (internal conversion and intersystem crossing) are shown by wavy arrows. Rotational levels are

not shown. Fig 4.5 is the Jablonski diagram being discussed.

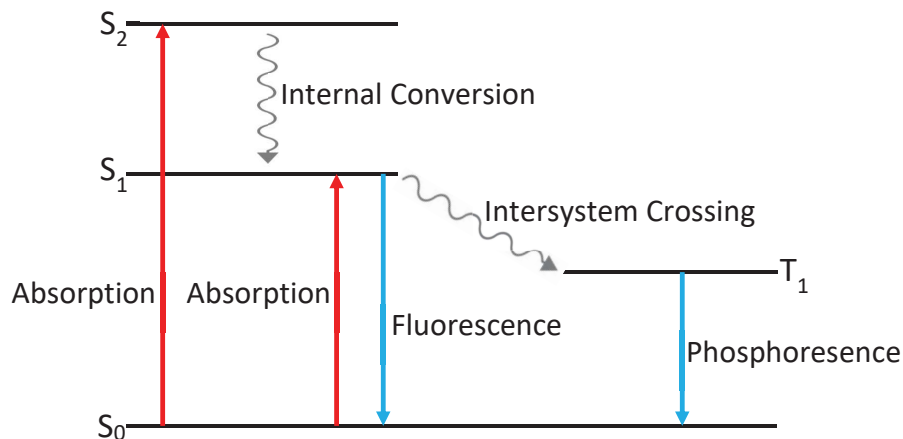


Figure 4.5 – Jablonski diagram.

A particularly impressive diagrammatic representation of this phenomena is from [14], which has been borrowed to illustrate the process.

In the next subsection, we discuss the various photophysical processes in the Jablonski diagram.

4.4.3 Vibrational relaxation

As mentioned earlier, an electronically excited state has excess electronic energy. In addition to this, it also possesses excess of vibrational energy [9]. Vibrational relaxation occurs when a transition between a vibrationally excited state ($v > 0$) and the vibrational ground state ($v = 0$) happens in a given electronic state due to collision of excited state molecules with other surrounding species. This is so since vibrational levels are associated with each electronic state. Excess vibrational energy is given as heat and the time scales range from $10^{-13} - 10^{-9}$ s. Typically, this is the fastest process taking place in the excited state.

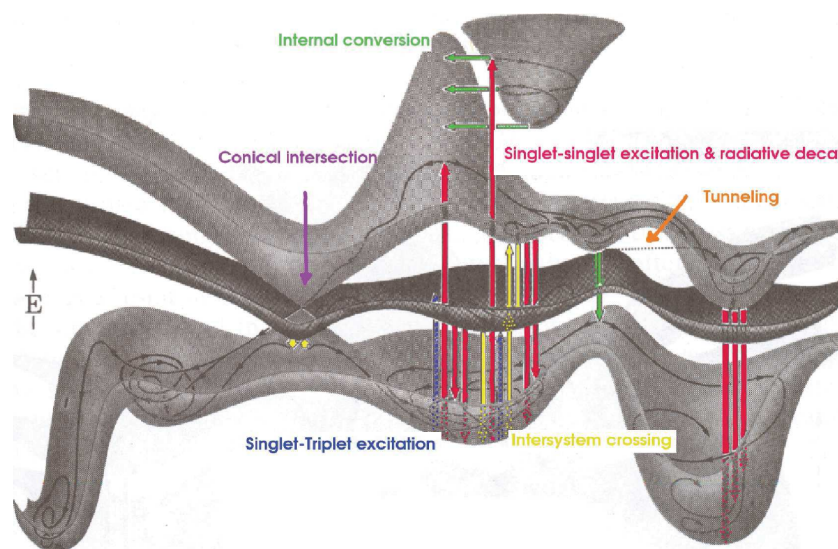


Figure 4.6 – Jablonski diagram showing the various processes. Original source [14].

4.4.4 Radiationless Deactivation

In the Jablonski diagram, radiationless deactivation is represented by a horizontal wavy line. It occurs between vibrational levels of the same energy of different electronic states. The mechanisms that fall under this class are the internal conversion (IC) and the intersystem crossing (ISC). Internal conversion is transition between two electronic states of the same spin multiplicity. Internal conversion involves transformation of electronic excitation into vibrational energy through nuclear tunneling [15].

Intersystem crossing is a spin-forbidden transition between two vibrational levels with the same energy in similar electronic states of different multiplicities for example $S_1 \rightarrow T_1$. Unlike IC, ISC involves concurrent change in spin. To compete with other deactivation processes, IC is fast and involves vibrational relaxation. Both IC and ISC are usually followed by vibrational relaxation (vr) to the lowest vibrational level of the new electronic state. With the complexity in the excited states due to the numerous states involved, it is assumed that IC within any one spin manifold is significantly

faster than direct deactivation to the ground state or ISC [3]. According to Kasha's rule[16], IC between excited states is more rapid than IC to ground state since emission occurs from the lowest excited-state of a given multiplicity.

4.4.5 Radiative Deactivation

These deactivation mechanisms obey the same selection rules as the ones for light absorption. The mechanisms here are understood in terms of the Pauli exclusion principle. Deactivation from S_1 is allowed, leading to a ground state with spin-paired electrons in one orbital hence a short-lived excited state (fluorescence). Forbidden de-excitation, such as that of a triplet excited state, violates the Pauli exclusion principle and has a long lived excited state (phosphorescence).

4.4.5.1 Fluorescence

Fluorescence is a spin allowed photon emission between states of the same multiplicity from the lowest vibrational level of the lowest excited singlet state, $S_1(v = 0)$ [7]. It occurs in timescales of $10^{-12} - 10^{-6}$ s. It can be expressed as,



The characteristics of fluorescence emission are independent of the excitation wavelength except for polarization and in cases where there is a small energy gap between the initial and final electronic states. The Franck-Condon principle plays an important role in determining the band shapes for radiative deactivation. At the 0-0 transition, the excited state is undistorted and a sharp line shaped emission band is expected. On the contrary, a distorted excited state (<0-0 energy) will result in a broad Gaussian-shaped emission band. The 0-0 transition is usually the same for absorption and fluorescence [13]. This is not however the case for energies higher than the 0-0 energy where the absorption and emission spectra for the same transition is shifted. This shift is called the Stokes shift. It is simply the difference in

wavelength between the maximum of the excitation spectrum (shorter wavelength, higher energy), and the maximum of the emission spectrum (longer wavelength, lower energy) [17]. It can be used to measure of the extent of distortion between the ground and the excited state. The larger the magnitude of Stokes shift the greater the structural or solvation differences between the two states.

4.4.5.2 Phosphorescence

Phosphorescence is defined as a spin forbidden transition between states of different multiplicity, normally from the lowest vibrational level of the lowest excited triplet state, $T_1(v = 0)$ [7]. It occurs in timescales of $10^{-3} - 10^2$ s. It can be expressed as,



There are two routes in which the triplet state may be populated; the first one is by direct absorption from the ground state, which is not very significant because it is a forbidden transition. The other alternative is by first excitation by an allowed transition from S_0 to S_1 then followed by an inter-system crossing from S_1 to T_1 . Phosphorescence can generally occur because of any of the two methods described above. Excited state lifetimes resulting from phosphorescence are long.

4.5 Photochemical Processes on Potential Energy Surfaces

Potential energy surface (PES) can be defined as a mathematical function that gives the energy of a molecule as a function of its geometry. Within the limits of the Born-Oppenheimer approximation, we can be able to show what happens on the PES when photochemical reactions occur. For more details on the Born-Oppenheimer approximation and PES, the reader is referred to section 3.9. Here, each electronic state of a molecule can be represented by a PES that describes the change in energy of the system on changing nuclear

coordinates [18]. How do we represent this processes on the PES? We begin the reaction coordinate once we have an excited state from photo-excitation then terminate it at the ground state [19].

4.6 Excited State Lifetime

The excited-state lifetime (τ) is the time taken for a given excited state to survive before decaying by radiative or nonradiative mechanisms to the ground state [7]. It can also be defined from a kinetic point of view as the rate of depopulation of the excited (singlet or triplet) states following an optical excitation from the ground state. From excited state dynamics, several intramolecular decay steps are involved and each one of them is characterized by its own rate constant and each excited state is characterized by its lifetime, given by,

$$\tau = \frac{1}{\sum_i k_i}, \quad (4.3)$$

where k_i is the first order rate constant for unimolecular or pseudo-unimolecular processes that causes the disappearance of the excited state [12].

Experimentally, it is possible to measure the excited state lifetime from a time-resolved experiment in which a very short pulse excitation is made, followed by measurement of the time-dependent intensity.

4.7 Quantum Yield

Quantum yield (Φ) can be defined as a measure of the efficiency of a photoreaction, that is, how efficient the process of absorption of light leads to the production of excited state molecules [7]. It is a measure of the number of moles of a species produced upon absorption of a mole of photons. Mathematically, it can be expressed as,

$$\Phi = \frac{\text{number of excited state molecules formed}}{\text{number of photons absorbed}}. \quad (4.4)$$

Bibliography

- [1] V. Balzani and S. Campagna. *Photochemistry and Photophysics of Coordination Compounds II*. Topics in Current Chemistry. Springer Berlin Heidelberg, 2007. ISBN 9783540733492.
- [2] B. P. Chan. Biomedical applications of photochemistry. *Tissue Eng. Part B-Re.*, 16(5):509–522, 2010.
- [3] P. S. Wagenknecht and P. C. Ford. Metal centered ligand field excited states: their roles in the design and performance of transition metal based photochemical molecular devices. *Coord. Chem. Rev.*, 255(5): 591–616, 2011.
- [4] V. Balzani, G. Bergamini, and P. Ceroni. Photochemistry and photocatalysis. *Rend. Fis. Acc. Lincei*, 28 (Suppl 1):S125–S142, 2017.
- [5] Q. Sun, S. Mosquera-Vazquez, Y. Suffren, J. Hankache, N. Amstutz, L. M. L. Daku, E. Vauthey, and A. Hauser. On the role of ligand-field states for the photophysical properties of ruthenium (II) polypyridyl complexes. *Coord. Chem. Rev.*, 282:87–99, 2015.
- [6] C. Daniel. Photochemistry and photophysics of transition metal complexes: Quantum chemistry. *Coord. Chem. Rev.*, 282-283:19, 2015.
- [7] B. Wardle. *Principles and Applications of Photochemistry*. Wiley, 2009. ISBN 9780470710135.
- [8] M. Nic, J. Jirat, Division of Chemical Nomenclature, Structure Representation International Union of Pure, Applied Chemistry, and B. Kosata. *IUPAC goldbook*. IUPAC, 2006.
- [9] D. M. Roundhill. *Photochemistry and Photophysics of Metal Complexes*. Modern Inorganic Chemistry. Springer US, 2013. ISBN 9781489914958.
- [10] K. K. Rohatgi-Mukherjee. *Fundamentals of Photochemistry*. A Halsted Press book. Wiley, 1978. ISBN 9780852267844.

- [11] M. Sauer, J. Hofkens, and J. Enderlein. *Handbook of Fluorescence Spectroscopy and Imaging: From Ensemble to Single Molecules*. Wiley, 2010. ISBN 9783527633524.
- [12] A. Juris, V. Balzani, F. Barigelletti, S. Campagna, P. Belser, and A. Von Zelewsky. Ru(II) polypyridine complexes: Photophysics, photochemistry, electrochemistry, and chemiluminescence. *Coord. Chem. Rev.*, 84: 85, 1988.
- [13] B. Valeur and M. N. Berberan-Santos. *Molecular Fluorescence: Principles and Applications*. Wiley, 2013. ISBN 9783527650026.
- [14] J. Michl and V. V. Bonačić-Koutecký. *Electronic aspects of organic photochemistry*. Wiley, 1990. ISBN 9780471896265.
- [15] Wawire C. *Theoretical Investigation of Ruthenium Photosensitizers*. PhD thesis, Université de Grenoble, 2012.
- [16] M. Kasha. Characterization of electronic transitions in complex molecules. *Discussions of the Faraday society*, 9:14–19, 1950.
- [17] D. Ganten and K. Ruckpaul. *Stokes Shift*, pages 1807–1807. Springer Berlin Heidelberg, 2006. ISBN 978-3-540-29623-2. doi: 10.1007/3-540-29623-9_8808.
- [18] V. Balzani, P. Ceroni, and A. Juris. *Photochemistry and Photophysics: Concepts, Research, Applications*. Wiley, 2014. ISBN 9783527671052.
- [19] M. A. Robb and M. Olivucci. Photochemical processes: potential energy surface topology and rationalization using VB arguments. *J. Photochem. and Photobiol. A*, 144(2):237–243, 2001.

Chapter 5

Hartree-Fock Approximation

“Let us, as nature directs, begin first with first principles.”

Aristotle, Poetics I.

Methods used for electronic structure calculations have a long history of development dating back to 1926 after the discovery of the Schrödinger equation. Starting from the initial methods that were not quite as accurate (no electron correlation) and could only allow for the calculation of compounds with few atoms to the current methods that are more accurate (includes electron correlation) and offer the possibility of calculating a greater number of atoms. This chapter looks back at the background and theory of electronic structure methods, starting with the most basic approximate methods used to solve the Schrödinger equation to advanced quantum chemical techniques which will be reviewed in later chapters. In the core of the development of these methods lies the Hartree-Fock approximation. This is quite an extensive topic that has been discussed here in detail but here are other references, in addition to what has been quoted in text; [1-8].

As the ultimate goal is to solve the many-electron Schrödinger equation, at the point that we are, it still poses an unsolved problem. Previous steps taken aimed towards solving this problem direct us to this step. The Hartree-Fock approximation comes in handy at this step. In a nut shell, it gives the simplest lowest energy variational solution of the Schrödinger equation. Using a single Slater determinant for the trial wave function, the

Hartree-Fock approximation optimizes molecular orbitals to give the lowest possible total energy. Worth mentioning is that this approximation does not include the effects of electron correlation. These effects will be included much latter when looking at the more accurate methods. The Hartree-Fock approximation is based on two major assumptions [9],

- i.) The wave function can be written as one Slater determinant.
- ii.) Each electron interacts with an average charge distribution due to the other electrons.

In the next steps, it will be shown how this is achieved using mathematical and chemical principles.

5.1 The Hartree Product

Picking up from the Born-Oppenheimer approximation, the most appropriate place to begin is to use the orbital approximation that satisfies the Pauli exclusion principle. The wave function is given by a simple product,

$$\Psi(\mathbf{x}) = \psi_1(\vec{x}_1)\psi_2(\vec{x}_2)\dots\psi_n(\vec{x}_n), \quad (5.1)$$

the Hartree product, which does not satisfy the principle of indistinguishability, because it is not an eigenstate of permutation operators. In other words, the wave function should be antisymmetric with respect to the interchange of any set of space-spin coordinates. The implication is that in addition to the three spatial degrees of freedom that the electron possess, it also has an intrinsic spin coordinate, either spin up α , or spin down β [10]. The generic (α or β) spin coordinate is referred to as ω and the set of spin coordinates is $\vec{\mathbf{x}} = \{\vec{r}, \omega\} \equiv \{\vec{r}, \alpha \text{ or } \beta\}$. The notation for the orbitals now changes from $\psi(\vec{r})$, a spatial orbital, to $\chi(\vec{\mathbf{x}})$, a spin orbital. The Hartree product is now written as:

$$\Psi_{\text{HP}}(\vec{\mathbf{x}}_1, \vec{\mathbf{x}}_2, \dots, \vec{\mathbf{x}}_N) = \chi_1(\vec{\mathbf{x}}_1)\chi_2(\vec{\mathbf{x}}_2)\dots\chi_N(\vec{\mathbf{x}}_N). \quad (5.2)$$

5.2 Slater Determinant

Ψ_{HP} in Eq.(5.2) still does not satisfy the antisymmetry principle. It is however possible to build an antisymmetric solution by introducing the Slater determinant [11, 12] built from orthonormal spin orbitals, $\chi_i(\vec{x})$. This is the trial wave function.

$$\Psi(\underline{\mathbf{x}}) = \frac{1}{\sqrt{N!}} \begin{vmatrix} \chi_1(\vec{x}_1) & \chi_2(\vec{x}_1) & \chi_3(\vec{x}_1) & \cdots & \chi_N(\vec{x}_1) \\ \chi_1(\vec{x}_2) & \chi_2(\vec{x}_2) & \chi_3(\vec{x}_2) & \cdots & \chi_N(\vec{x}_2) \\ \chi_1(\vec{x}_3) & \chi_2(\vec{x}_3) & \chi_3(\vec{x}_3) & \cdots & \chi_N(\vec{x}_3) \\ \vdots & \vdots & \vdots & \ddots & \vdots \\ \chi_1(\vec{x}_N) & \chi_2(\vec{x}_N) & \chi_3(\vec{x}_N) & \cdots & \chi_N(\vec{x}_N) \end{vmatrix} \quad (5.3)$$

With the Slater determinant, each electron is associated with every orbital and therefore the electrons are indistinguishable. Notice that if we try to put two electrons in the same orbital at the same time, that is, set $\chi_1 = \chi_2$, then $\Psi(\vec{x}_1, \vec{x}_2) = 0$. A keen observation will tell you that this is the Pauli exclusion principle stated in a more sophisticated manner, which is a consequence of the antisymmetry principle.

A more compact notation is introduced for simplicity [9]. Occupied orbitals $\{\chi_i(\mathbf{x}), \chi_j(\mathbf{x}), \dots, \chi_k(\mathbf{x})\}$ can be expressed in shorthand in ket symbol as $|\chi_i\chi_j\dots\chi_k\rangle$ or simply as $|ij\dots k\rangle$.

5.3 The Electronic Hamiltonian

To find the variationally best Slater determinant, there is need to work with the electronic Hamiltonian, which is given as the sum of N one-electron terms and $N(N - 1)/2$ two-electron terms:

$$\hat{H}_{el} = \sum_i^N h(i) + \sum_{i<j}^N v(i, j) + V_{NN}. \quad (5.4)$$

V_{NN} is a constant for a fixed set of nuclear coordinates $\{R_I\}$ and therefore is ignored. The one-electron operator $h(i)$ is,

$$h(i) = -\frac{1}{2}\nabla_i^2 - \sum_M \frac{Z_M}{r_{iM}}, \quad (5.5)$$

and

$$v(i, j) = \frac{1}{r_{ij}}. \quad (5.6)$$

5.4 Coulomb and Exchange Integrals

Assuming that the wave function is normalized, $E_{el} = \langle \Psi | \hat{H}_{el} | \Psi \rangle$, the variational principle can be used to minimize the energy within the given functional space to obtain the optimal Hartree-Fock energy (E_{HF}) and wave function.

$$E_{\text{HF}} = \min_{\Psi_{\text{SD}} \rightarrow N} E[\Psi_{\text{SD}}], \quad (5.7)$$

and also subject to the constraint that the orbitals be orthonormal. Here, we see that $E[\Psi_{\text{SD}}]$ is in square brackets. This is known as a functional. A functional is a function whose argument is itself a function. It is normally denoted by the use of a square bracket for its argument $F[f]$ to distinguish it from an ordinary function $f(\vec{r})$. There are thus two conditions that must be fulfilled. Starting with the first condition of minimization with the variational principle, the expectation value of the Hamiltonian operator with a Slater determinant is sought. This is done by expanding the determinant and constructing the individual terms. The electronic Hamiltonian [Eq. (5.4)] can be inserted in the energy expression $E_{\text{SD}} = \int \Psi_{\text{SD}} \hat{H}_{elec} \Psi_{\text{SD}} d\vec{x}$ to calculate the energy of the Slater determinant. This leads to:

$$E_{\text{SD}} = \int \Psi \left\{ \sum_{i=1}^N h(i) \right\} \Psi d\vec{x} + \int \Psi \left\{ \sum_{i<j}^N \frac{1}{r_{ij}} \right\} \Psi d\vec{x}. \quad (5.8)$$

We can rewrite the integrals of sums as sums of integrals, that is,

$$E_{\text{SD}} = \sum_{i=1}^N \left\{ \int \Psi^* h(i) \Psi d\vec{x}(i) \right\} + \sum_{i<j}^N \left\{ \int \Psi^* \frac{1}{r_{ij}} \Psi d\vec{x}(i) d\vec{x}(j) \right\}. \quad (5.9)$$

The first term of Eq.(5.9) is simply the sum of the one-electron energies $h_{i,i}$ of each orbital since each one-electron operator h acts on a very small part of the wave function. It simplifies to,

$$\sum_{i=1}^N \left\{ \int \Psi^* h(i) \Psi d\vec{x}(i) \right\} = \sum_{i=1}^N \left\{ \int \chi_i^* h \chi_i dr d\omega \right\} = \sum_{i=1}^N h_{i,i}. \quad (5.10)$$

The one-electron operator h includes both the electron's kinetic and potential energy created by the attractive Coulombic interaction with the nuclei. The second term of Eq.(5.9) is the two-electron terms (two-electron integrals). The solution to the two-electron integrals is more complicated because of the antisymmetrisation of the wave function. Each term in the two-electron integral is,

$$\frac{\iint \left\{ \chi_i^*(\vec{x}_1) \chi_j^*(\vec{x}_2) - \chi_i^*(\vec{x}_2) \chi_j^*(\vec{x}_1) \right\} \frac{1}{r_{12}} \left\{ \chi_i(\vec{x}_1) \chi_j(\vec{x}_2) - \chi_i(\vec{x}_2) \chi_j(\vec{x}_1) \right\} d\vec{x}_1 d\vec{x}_2}{\iint \left\{ \chi_i^*(\vec{x}_1) \chi_j^*(\vec{x}_2) - \chi_i^*(\vec{x}_2) \chi_j^*(\vec{x}_1) \right\} \frac{1}{r_{12}} \left\{ \chi_i(\vec{x}_1) \chi_j(\vec{x}_2) - \chi_i(\vec{x}_2) \chi_j(\vec{x}_1) \right\} d\vec{x}_1 d\vec{x}_2}. \quad (5.11)$$

Equation (5.11) can be multiplied out to give,

$$\begin{aligned} & \iint \chi_i^*(\vec{x}_1) \chi_j^*(\vec{x}_2) \frac{1}{r_{12}} \chi_i(\vec{x}_1) \chi_j(\vec{x}_2) d\vec{x}_1 d\vec{x}_2 \\ & - \iint \chi_i^*(\vec{x}_1) \chi_j^*(\vec{x}_2) \frac{1}{r_{12}} \chi_i(\vec{x}_2) \chi_j(\vec{x}_1) d\vec{x}_1 d\vec{x}_2 \\ & - \iint \chi_i^*(\vec{x}_2) \chi_j^*(\vec{x}_1) \frac{1}{r_{12}} \chi_i(\vec{x}_1) \chi_j(\vec{x}_2) d\vec{x}_1 d\vec{x}_2 \\ & + \iint \chi_i^*(\vec{x}_2) \chi_j^*(\vec{x}_1) \frac{1}{r_{12}} \chi_i(\vec{x}_2) \chi_j(\vec{x}_1) d\vec{x}_1 d\vec{x}_2 \\ & = 2 \iint \chi_i^*(\vec{x}_1) \chi_j^*(\vec{x}_2) \frac{1}{r_{12}} \chi_i(\vec{x}_1) \chi_j(\vec{x}_2) d\vec{x}_1 d\vec{x}_2 \\ & - 2 \iint \chi_i^*(\vec{x}_1) \chi_j^*(\vec{x}_2) \frac{1}{r_{12}} \chi_j(\vec{x}_1) \chi_i(\vec{x}_2) d\vec{x}_1 d\vec{x}_2 \end{aligned} \quad (5.12)$$

Considering that the first and fourth, as well as the second and third terms are identical two by two, the equation can be rewritten in terms of the spatial orbitals and coordinates as,

$$\iint |\psi_i^2|(r_1) \frac{1}{r_{12}} |\psi_j^2|(r_2) dr_1 dr_2. \quad (5.13)$$

Equation (5.13) is known as the Coulombic integral. It is the energy of the Coulombic interaction between an electron in orbital i with an electron in orbital j . Its shorthand notation is J_{ij} . J_{ij} contributes positive energy (destabilization) since both ψ_i^2 and $1/r$ are always positive. ψ_i^2 is the probability of finding an electron at a given point in space. The other integrals in Eq.(5.12) become,

$$- \iint \psi_i^*(r_1) \psi_j^*(r_2) \frac{1}{r_{12}} \psi_i(r_2) \psi_j(r_1) dr_1 dr_2. \quad (5.14)$$

Equation (5.14) is known as the exchange integral, K_{ij} . It "corrects" J_{ij} to account for the antisymmetry of the wave function and also removes the self-interaction error because $J_{ii} = K_{ii}$, thus, $J_{ii} - K_{ii} = 0$. The HF energy, E_{HF} , is given by the sum of the integrals discussed above.

$$\begin{aligned} E_{\text{HF}} &= \langle \Psi | \hat{H}_{el} | \Psi \rangle \\ &= \sum_{i=1}^N h_{i,i} + \sum_{i,j=1,N}^{i<j} (J_{i,j} - K_{i,j}) \\ &= \sum_{i=1}^N h_{i,i} + \frac{1}{2} \sum_{i,j=1,N} (J_{i,j} - K_{i,j}) \equiv \sum_{i=1}^N \langle i | h | i \rangle + \frac{1}{2} \sum_{i,j=1,N} ([ii|jj] - [ij|ji]), \end{aligned} \quad (5.15)$$

which is the expectation value of the non-relativistic electronic Hamiltonian, \hat{H} , with respect to the N-electron Slater determinant of orthonormal spin-orbitals. The one electron integral is,

$$\langle i | \hat{h} | j \rangle = \int d\mathbf{x}_1 \chi_i^*(\mathbf{x}_1) \hat{h}(r_1) \chi_j(\mathbf{x}_1), \quad (5.16)$$

and the two-electron integral (Mulliken charge cloud notation)[9] is,

$$[ij|kl] = \int d\mathbf{x}_1 d\mathbf{x}_2 \chi_i^*(\mathbf{x}_1) \chi_j(\mathbf{x}_1) \frac{1}{r_{12}} \chi_k^*(\mathbf{x}_2) \chi_l(\mathbf{x}_2). \quad (5.17)$$

5.5 Coulomb and Exchange Operators

It can be seen that E_{HF} , [Eq.(5.15)], is a functional of the spin orbitals, $E_{\text{HF}} = E[\{\chi_i\}]$. The next step is to determine the set of spin orbitals which give the best single determinant. This is done by minimizing Eq.(5.15), E_{HF} , with respect to the constraint that the spin-orbitals are orthonormal, and what better way to do it than to use the Lagrange method of undetermined multipliers,

$$\mathcal{L}[\{\chi_i\}] = E_{\text{HF}}[\{\chi_i\}] - \sum_{ij} \epsilon_{ij} (\langle i|j \rangle - \delta_{ij}). \quad (5.18)$$

Here the ϵ_{ij} are the Lagrange multipliers and $\langle i|j \rangle$ is the overlap between spin orbitals i and j . δ_{ij} is the constraint that the orbitals must be orthonormal, that is, $\langle \chi_i | \chi_j \rangle = \delta_{ij}$. And the solution, which is the equation for the best Hartree-Fock spin orbitals is,

$$\begin{aligned} \hat{h}(\vec{x}_1) \chi_i(\vec{x}_1) + \sum_{j \neq i} \left[\int d\mathbf{x}_2 |\chi_j(\vec{x}_2)|^2 r_{12}^{-1} \right] \chi_i(\vec{x}_1) - \sum_{j \neq i} \left[\int d\mathbf{x}_2 \chi_j^*(\vec{x}_2) \chi_i(\vec{x}_2) r_{12}^{-1} \right] \chi_j(\vec{x}_1) \\ = \epsilon_i \chi_i(\vec{x}_1), \end{aligned} \quad (5.19)$$

where ϵ_i is the energy eigenvalue (orbital energy) associated with spin orbital χ_i . The term,

$$\sum_{j \neq i} \left[\int d\mathbf{x}_2 |\chi_j(\vec{x}_2)|^2 r_{12}^{-1} \right] \chi_i(\vec{x}_1), \quad (5.20)$$

in Eq. (5.19) is known as the *Coulomb term*. It is the Coulomb interaction of an electron in spin orbital χ_i with the average charge distribution of the other electrons. It shows that the first electron χ_i experiences a one-electron Coulomb potential. The Coulomb term contains a self-interaction error which must be removed since an electron cannot interact with itself. The corresponding Coulomb operator is,

$$\hat{\mathcal{J}}_j(\vec{x}_1) = \int dx_2 |\chi_j(\vec{x}_2)|^2 r_{12}^{-1}, \quad (5.21)$$

and

$$\hat{\mathcal{K}}_j(\vec{x}_1)\chi_i(\vec{x}_1) = \left[\int dx_2 \chi_j^*(\vec{x}_2)\chi_i(\vec{x}_2)r_{12}^{-1} \right] \chi_j(\vec{x}_1), \quad (5.22)$$

is called the exchange term and it arises from the antisymmetric nature of the wave function since it exchanges spin orbitals χ_i and χ_j . The Hartree-Fock equations can be expressed in terms of the Coulomb and exchange operators in a more compact form as,

$$\left[\hat{h}(\vec{x}_1) + \sum_{j \neq i} \hat{\mathcal{J}}_j(\vec{x}_1) - \sum_{j \neq i} \hat{\mathcal{K}}_j(\vec{x}_1) \right] \chi_i(\vec{x}_1) = \epsilon_i \chi_i(\vec{x}_1). \quad (5.23)$$

A keen inspection of the above equation tells us that it is an eigenvalue equation and the exchange operators serves to remove the self-interaction error in the Coulomb energy since,

$$\hat{\mathcal{J}}_i(\vec{x}_1)\chi_i(\vec{x}_1) = \hat{\mathcal{K}}_i(\vec{x}_1)\chi_i(\vec{x}_1). \quad (5.24)$$

This implies that the restriction $i \neq j$ can be removed making \hat{f}_i orbital independent. It also shows that obeying the Pauli exclusion principle keeps the electrons apart in space and therefore reduces the total electron repulsion energy. The new operator, known as the Fock operator is,

$$\hat{f}(\vec{x}_1) = \hat{h}(\vec{x}_1) + \sum_j \left(\hat{\mathcal{J}}_j(\vec{x}_1) - \hat{\mathcal{K}}_j(\vec{x}_1) \right). \quad (5.25)$$

The canonical Hartree-Fock (molecular orbital) equation is:

$$\hat{f}(\vec{x}_1)\chi_i(\vec{x}_1) = \epsilon_i \chi_i(\vec{x}_1), \quad (5.26)$$

where ϵ_i is the orbital energy of χ_i . The next step involves finding spin orbitals that are eigenfunctions of the Fock operator. In this regard, there

are two ways in which the Hartree-Fock equation can be solved; either numerically (exact Hartree-Fock) or by a set of basis functions (Hartree-Fock-Roothan equations). Each of the above solutions depends on orbitals.

5.6 Hartree-Fock Orbitals and Orbital energies

The question here is, how does one determine those spin-orbitals which are eigenfunctions of the Fock operator? Both the numerical and basis functions solution of the Hartree-Fock equation depend on the orbitals since the Fock operator has a functional dependence on the occupied spin orbitals. Once the occupied spin orbitals are known (of course at this point they are unknown) the Fock operator becomes a well-defined Hermitian operator, which will have an infinite number of eigenfunctions [9]. To determine a specific Fock orbital, all the other occupied orbitals must be known. This means that some initial orbitals must be guessed (in this case occupied orbitals) and the guesses refined iteratively in what is known as the self-consistent field (SCF) approach [13]. Figure 5.1 shows how the process takes place.

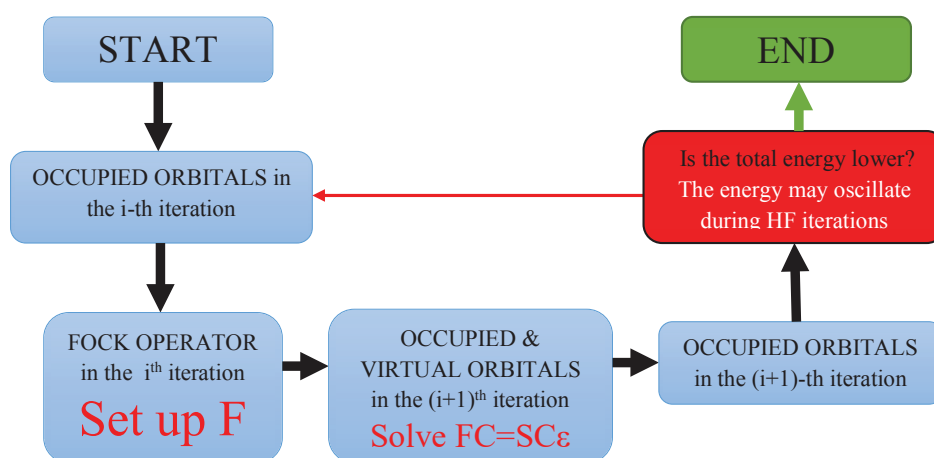


Figure 5.1 – SCF solution of the Hartree-Fock equation [14].

The index convention a, b, c, d, e, f, h (virtual), i, j, k, l, m, n (occupied) and $p, q, r, s, t, u, v, w, x, y, z$ has been adopted for the various orbital energies. The Fock matrix is diagonal in the basis of the canonical orbitals,

$$F_{i,j} = \langle \chi_i | \hat{h} | \chi_j \rangle = \epsilon_i \langle \chi_i | \chi_i \rangle = \epsilon_j \delta_{i,j}. \quad (5.27)$$

We can express the orbital energies as,

$$\begin{aligned} \epsilon_i &= F_{i,i} \\ &= \langle \chi_i | \hat{h} | \chi_i \rangle + \sum_k \langle \chi_i | (J_k - K_k) | \chi_i \rangle \\ &= \langle \chi_i | \hat{h} | \chi_i \rangle + \sum_k \left(\langle \chi_i | J_k | \chi_i \rangle - \sum_k \langle \chi_i | K_k | \chi_i \rangle \right) \\ &= \epsilon_i^{(0)} + \sum_k ((ii||kk) - (ik||ki)). \end{aligned} \quad (5.28)$$

Considering the index convention that was adopted above, the occupied orbitals can be expressed as,

$$\begin{aligned} \epsilon_i &= \epsilon_i^{(0)} + \sum_j ((ii||jj) - (ij||ji)) \\ &= \epsilon_i^{(0)} + \sum_{j \neq i} ((ii||jj) - (ij||ji)), \end{aligned} \quad (5.29)$$

and virtual orbitals,

$$\epsilon_a = \epsilon_a^{(0)} + \sum_k ((aa||kk) - (ak||ka)). \quad (5.30)$$

From Eq.(5.29), it can be seen that ϵ_i is the energy of occupied spin orbital (χ_i). It includes $\epsilon_i^{(0)}$ which is the attraction to the nuclei and kinetic energy. It also includes Coulomb and exchange interactions with each of the remaining electrons ($N - 1$). The unoccupied orbital energy ϵ_a , shown in Eq.(5.30), includes the Coulomb and exchange interactions with N electrons of the Hartree-Fock ground state. Adding up the orbital energies of the occupied states results in,

$$\sum_{i=1,N} \epsilon_i = \sum_{i=1,N} \epsilon_i^{(0)} + \sum_{j,k=1,N} ([jj||kk] - [kj||jk]). \quad (5.31)$$

A comparison of Eq.(5.31), the total energies of the occupied states and the total Hartree-Fock energy Eq.(5.15) can be written as,

$$E_{\text{HF}} = \sum_{i=1}^N \langle i|h|i \rangle + \frac{1}{2} \sum_{i,j=1,N} ([ii|jj] - [ij|ji]), \quad (5.32)$$

which shows that,

$$E_{\text{HF}} \neq \sum_{i=1,N} \epsilon_i. \quad (5.33)$$

This can be justified by the fact that ϵ_i includes exchange and Coulomb interactions between an electron in a spin orbital χ_i and electrons in all other occupied spin orbitals χ_j . Similarly, ϵ_j includes exchange and Coulomb interactions between an electron in χ_j and electrons in all other occupied spin orbitals χ_i . The sum of orbital energies thus includes the electron-electron interactions twice because addition of ϵ_i and ϵ_j includes electron-electron interactions between an electron in χ_i and χ_j twice. To account for this error, a factor of $\frac{1}{2}$ is included in the energy expression for the total energy.

5.7 Koopmans' Theorem

To attach physical meaning to the orbital energies ϵ_i and ϵ_a shown in the previous section, we use the Koopmans' theorem. It states that given an N -electron Hartree-Fock single determinant Ψ_N with occupied and virtual χ energies ϵ_i and ϵ_a , then the ionization potential to produce an $(N - 1)$ electron single determinant $\Psi_{N-1} = \hat{a}_i \Psi$ with identical spin orbitals, obtained by removing an electron from spin orbital χ_a , and the electron affinity to produce an $(N + 1)$ electron single determinant $\Psi^a = \hat{a}_a^\dagger \Psi$ with identical spin orbitals, obtained by adding an electron to spin orbital χ_r are just $-\epsilon_i$ and $-\epsilon_a$ respectively. Let us consider the energy of a system with one electron removed from orbital number k , and assume that the molecular orbitals are identical for the two systems.

$$\begin{aligned}
 E_N &= \sum_{i=1}^N h_{i,i} + \frac{1}{2} \sum_{i,j=1,N} (J_{i,j} - K_{i,j}) + V_{nn} \\
 E_{N-1}^k &= \sum_{i=1}^{N-1} h_{i,i} + \frac{1}{2} \sum_{i,j=1,N-1} (J_{i,j} - K_{i,j}) + V_{nn}.
 \end{aligned}
 \tag{5.34}$$

Subtracting the two energies,

$$E_N - E_{N-1}^k = h_k + \sum_{i,j=1,N} (J_{k,i} - K_{k,i}) = \epsilon_k.
 \tag{5.35}$$

The energy obtained in eq.(5.35), ϵ_k is seen to be exactly the same as the orbital energy obtained in eq.(5.28), ϵ_i . As a result of the Koopmans' theorem, the ionization energy (I.E) within the frozen molecular orbital approximation is given simply as the orbital energy. Similarly, the electron affinity (EA) of a neutral molecule is given as the orbital energy of the corresponding anion or as the energy of the k^{th} unoccupied orbital energy in the neutral species. Mathematically,

$$E_{N+1}^k - E_N = \epsilon_k.
 \tag{5.36}$$

In a nutshell, the Koopmans' theorem gives us a way of calculating approximate ionization potentials (IP) and electron affinities (EA). Koopmans' IPs are reasonable first approximations to experimental IPs. Electron affinities from Koopmans' theory are badly reproduced because correlation and relaxation effects do not cancel.

5.8 Roothaan-Hall Equation

The Hartree-Fock equation can be solved in two ways; either numerically [15] (exact Hartree-Fock, that is, by mapping the orbitals on a set of grid points) or by a set of basis functions (Hartree-Fock-Roothan equations). Numerical methods are more applicable in small highly symmetric systems, like atoms and diatomic molecules. Most if not all calculations use a basis set expansion which expresses the unknown molecular orbitals in terms of a set

of known functions. A basis function may be a Gaussian, exponential, plane wave or polynomial. This study has adopted the finite basis set of Gaussian-type orbitals (GTOs) which is preferred by most quantum chemists. All our calculations include scalar relativistic effects of core electrons for the ruthenium atom.

Introducing a basis set (linear combination of atomic orbitals (LCAO), MO=LCAO) transforms the Hartree-Fock equations into the Roothaan equations [16]. Each MO is expanded as a linear combination of three dimensional one electron functions, known as atomic orbitals¹. Typically, these atomic orbitals are called Slater-type orbitals. Denoting the atomic orbital basis functions as χ_μ ,

$$\chi_i(\vec{\mathbf{x}}) = \sum_{\mu=1}^K \chi_\mu C_{\mu i}(\vec{\mathbf{x}}), \quad (5.37)$$

for each spin orbital i . K is an integer relating to the size of the basis set which is typically larger than the number of electrons in the system. A matrix equation can be obtained for the set of molecular orbital expansion coefficients ($C_{\mu i}$) by substituting the linear expansion Eq.(7.1) into Eq.(5.26)² Using the index ν leads to,

$$f(\vec{\mathbf{x}}_1) \sum_{\nu} C_{\nu i} \chi_{\nu}(\vec{\mathbf{x}}_1) = \epsilon_i \sum_{\nu} C_{\nu i} \chi_{\nu}(\vec{\mathbf{x}}_1). \quad (5.38)$$

Multiplying from the left by a specific basis function $\chi_{\mu}^*(\vec{\mathbf{x}}_1)$ and integrating gives a matrix equation,

$$\sum_{\nu} C_{\nu i} \int d\mathbf{x}_1 \chi_{\mu}^*(\vec{\mathbf{x}}_1) \hat{f}(\vec{\mathbf{x}}_1) \chi_{\nu}(\vec{\mathbf{x}}_1) = \epsilon_i \sum_{\nu} C_{\nu i} \int d\mathbf{x}_1 \chi_{\mu}^*(\vec{\mathbf{x}}_1) \chi_{\nu}(\vec{\mathbf{x}}_1). \quad (5.39)$$

Introducing the matrix element notation,

-
1. They are not solutions to the atomic HF problem.
 2. The idea behind this is that the problem of calculating the Hartree-Fock molecular orbitals reduces to the problem of calculating the set of expansion coefficients $C_{\mu i}$ variationally.

$$S_{\mu\nu} = \int d\mathbf{x}_1 \chi_\mu^*(\vec{\mathbf{x}}_1) \chi_\nu(\vec{\mathbf{x}}_1) \equiv \langle \chi_\mu | \chi_\nu \rangle, \quad (5.40)$$

$$F_{\mu\nu} = \int d\mathbf{x}_1 \chi_\mu^*(\vec{\mathbf{x}}_1) \hat{f}(\vec{\mathbf{x}}_1) \chi_\nu(\vec{\mathbf{x}}_1) \equiv \langle \chi_\mu | F | \chi_\nu \rangle. \quad (5.41)$$

simplifies the Hartree-Fock-Roothaan equations [16] which can be written in matrix form as,

$$\sum_\nu F_{\mu\nu} C_{\nu i} = \epsilon_i \sum_\nu S_{\mu\nu} C_{\nu i}, \quad (5.42)$$

or simply as matrices in the form,

$$\mathbf{FC} = \mathbf{SC}\epsilon, \quad (5.43)$$

where ϵ is a diagonal matrix of the orbital energies ϵ_i . To determine the unknown MO coefficients, $C_{\mu i}$, the Fock matrix must be diagonalized³. Equation (5.43) is therefore solved self consistently [17].

3. The Fock matrix is only known if all the MO coefficients are known.

Bibliography

- [1] J. C. Slater. A simplification of the Hartree-Fock method. *Phys. Rev.*, 81(3):385, 1951.
- [2] T. Tsuneda. *Density Functional Theory in Quantum Chemistry*. SpringerLink : Bücher. Springer, Japan, 2014. ISBN 9784431548256.
- [3] D. B. Cook. *Handbook of Computational Quantum Chemistry*. Dover Books on Chemistry. Dover Publications, 2005. ISBN 9780486443072.
- [4] K. I. Ramachandran, G. Deepa, and K. Namboori. *Computational Chemistry and Molecular Modeling: Principles and Applications*. Springer Berlin Heidelberg, 2008. ISBN 9783540773023.
- [5] T. Helgaker, P. Jorgensen, and J. Olsen. *Molecular Electronic-Structure Theory*. Wiley, 2014. ISBN 9781119019558.
- [6] R. F. Nalewajski. *Perspectives in Electronic Structure Theory*. Springer Berlin Heidelberg, 2012. ISBN 9783642201806.
- [7] G. Giuliani and G. Vignale. *Quantum Theory of the Electron Liquid*. Masters Series in Physics and Astronomy. Cambridge University Press, 2005. ISBN 9780521821124.
- [8] E. K. U. Gross, E. Runge, and O. Heinonen. *Many-Particle Theory*. Taylor & Francis, 1991. ISBN 9780750301558.
- [9] A. Szabo and N. S. Ostlund. *Modern Quantum Chemistry: Introduction to Advanced Electronic Structure Theory*. Macmillan Publishing Company, New York, 1982.
- [10] W. Koch and M. C. Holthausen. *A Chemist's Guide to Density Functional Theory*. Wiley-VCH, Germany, 2015. ISBN 9783527802814.
- [11] J. C. Slater. The theory of complex spectra. *Phys. Rev.*, 34:1293–1322, Nov 1929. doi: 10.1103/PhysRev.34.1293.
- [12] J. C. Slater. Note on Hartree's method. *Phys. Rev.*, 35(2):210, 1930.

-
- [13] F. Jensen. *Introduction to Computational Chemistry*. Wiley, Great Britain, 1999. ISBN 9780471980858,0471980854,0471984256.
- [14] L. Piela. *Ideas of Quantum Chemistry*. Elsevier Science, Netherlands, 2013.
- [15] J. Kobus. Diatomic molecules: Exact solutions of HF equations. *Adv. Quantum Chem.*, 28:1–14, 1997.
- [16] C. C. J. Roothaan. New developments in molecular orbital theory. *Rev. Mod. Phys.*, 23(2):69, 1951.
- [17] Cramer C. J. *Essentials of Computational Chemistry Theories and Models*. Wiley, Great Britain, 2nd edition, 2004.

Chapter 6

Density-Functional Theory

“At the moment I am struggling with a new atomic theory. I am very optimistic about this thing and expect that if I can only solve it, it will be very beautiful.”

Erwin Schrödinger.

In the study of electronic structure methods, the Hartree-Fock approximation was introduced in the previous chapter. It was noted that the Hartree-Fock approximation does not include electron correlation. In this chapter, the density functional theory (DFT) method which includes the electron correlation is discussed.

DFT [1, 2] is presently the most promising and successful approach to computing the electronic structure of matter having a wide range of applications including, but not limited to atoms, molecules and solids, and quantum fluids. DFT is based on the idea of replacing the wave function $\Psi(\vec{x}_1, \vec{x}_2, \dots, \vec{x}_N)$, which is a complicated function of $3N$ spatial coordinates and N spin coordinates, with the spin density $\rho(\vec{r})$, which is a simpler object which depends only upon the three coordinates (x, y, z) and the spin σ . In DFT, there is a shift from the use of wave functions (which are considered to be complicated and computationally expensive in terms of solving the many-electron problem) to a functional of the electronic density with an electron density $\rho(\vec{r})$. (A functional is a function of a function. Square brackets [] are used to distinguish a functional from a simple function). Ideally, DFT re-

places the interacting many-electron problem with an effective single-particle problem that can be solved much more quickly. The electron density $\rho(\vec{r})$ represents the number of electrons per unit volume at some position \vec{r} in a molecule or in an atom. Its formula in terms of Ψ is given by:

$$\rho(\vec{r}) = N \int \dots \int |\Psi(\vec{x}_1, \vec{x}_2, \dots, \vec{x}_N)|^2 d\sigma_1 d\vec{x}_2 \dots d\vec{x}_N. \quad (6.1)$$

The above quantity is a non-negative simple function of three variables x , y and z , integrating to the total number of electrons.

$$\int \rho(\vec{r}) d(\vec{r}) = N. \quad (6.2)$$

Initially, the thought of replacing Ψ by ρ seemed to mean losing large amounts of information needed for practical calculations. It was however realized that $\rho(\vec{r})$ could be exploited in the study of ground-state properties of an atom or a molecule and a lot of research was done towards achieving this objective. The following sections outline the various theorems that have been used to develop DFT.

6.1 Hohenberg-Kohn Theorems

This section tries to answer the question which is at the very heart of DFT: Can we possibly replace the complicated N -electron wave function with its dependence on $3N$ spatial plus N spin variables by a simpler quantity, such as the electron density?

The Hohenberg-Kohn theorems [3] in DFT show that the ground-state energy (E_0) may be determined, in principle, by minimizing a functional of the density, which is a simpler object than Ψ . They answer the question, “Can we eliminate Ψ ?” These two theorems are the basis of modern DFT, and they formally answer the question asked in the first paragraph with the following theorems.

Theorem 1 (Existence Theorem) *It states: The external potential $v_{ext}(\vec{r})$ of a nondegenerate system of N interacting electrons is determined, within a*

trivial additive constant, by the ground-state electron density $\rho_0(\vec{r})$. Since ρ determines the number of electrons, it follows that $\rho(\vec{r})$ also determines the ground-state Ψ up to a trivial phase factor and all other electronic properties of the system.

It legitimizes the use of $\rho(\vec{r})$ as basic variable. The proof is based upon the variational principle and the Hamiltonian,

$$\hat{H} = \underbrace{-\frac{1}{2} \sum_{i=1,N} \nabla_i^2}_{\hat{T}} + \underbrace{\sum_{i=1,N} v_{ext}(\vec{r}_i)}_{V_{ext}} + \underbrace{\sum_{i,j=1,N}^{(i<j)} \frac{1}{r_{ij}}}_{V_{ee}}, \quad (6.3)$$

where \hat{T} is the electron kinetic energy, V_{ext} is the nuclear attraction and/or interaction with an applied electric field and V_{ee} is the electron repulsion.

This implies that it is possible from $\rho_0(\vec{r})$ to determine other properties of the ground-state such as the kinetic energy, the potential energy as well as the total energy in addition to N and $v_{ext}(\vec{r})$. This theorem can be proven by considering the minimum-energy principle for the ground-state. It is a proof by contradiction. If there are two systems, with the same charge density, but different potentials, the variational principle then requires that the two systems must have different $v_{ext}(\vec{r})$.

$$\begin{aligned} v_{ext}^{(1)} &\rightarrow \Psi_1 \rightarrow \rho \\ v_{ext}^{(2)} &\rightarrow \Psi_2 \rightarrow \rho \\ v_{ext}^{(1)} - v_{ext}^{(2)} &\neq \text{constant}. \end{aligned} \quad (6.4)$$

This can be proved by contradiction;

$$\Psi_1 \neq \Psi_2 \quad (6.5)$$

since,

$$v_{ext}^{(1)} - v_{ext}^{(2)} \neq \text{constant}. \quad (6.6)$$

What has been presented in Eq.(6.5) and Eq.(6.6) requires proof:

$$\begin{aligned}
\hat{H}_1 &= E_1 \Psi \\
\hat{H}_2 &= E_2 \Psi \\
(\hat{H}_1 - \hat{H}_2) \Psi &= (\hat{V}_{ext}^1 - \hat{V}_{ext}^2) \Psi = (E_1 - E_2) \Psi \\
\Rightarrow \hat{V}_{ext}^1 - \hat{V}_{ext}^2 &= E_1 - E_2 \text{ except possibly where } \Psi = 0. \\
(\text{In fact, you can make violations when } \Psi \neq 0 \text{ is separated by regions where } & \\
\Psi = 0.) &
\end{aligned} \tag{6.7}$$

Using the variational principle;

$$\begin{aligned}
E_1 &= \langle \Psi_1 | \hat{T} | \Psi_1 \rangle + \int v_{ext}^{(1)}(\vec{r}) \rho(\vec{r}) d\vec{r} \\
&< \langle \Psi_2 | \hat{T} | \Psi_2 \rangle + \int v_{ext}^{(1)}(\vec{r}) \rho(\vec{r}) d\vec{r} \\
E_2 &= \langle \Psi_2 | \hat{T} | \Psi_2 \rangle + \int v_{ext}^{(2)}(\vec{r}) \rho(\vec{r}) d\vec{r} \\
&< \langle \Psi_1 | \hat{T} | \Psi_1 \rangle + \int v_{ext}^{(2)}(\vec{r}) \rho(\vec{r}) d\vec{r}.
\end{aligned} \tag{6.8}$$

Equation 6.8 attests to the fact that the system is nondegenerate. It results to,

$$\begin{aligned}
\langle \Psi_1 | \hat{T} + \hat{V}_{ee} | \Psi_1 \rangle &< \langle \Psi_2 | \hat{T} + \hat{V}_{ee} | \Psi_2 \rangle \\
\langle \Psi_2 | \hat{T} + \hat{V}_{ee} | \Psi_2 \rangle &< \langle \Psi_1 | \hat{T} + \hat{V}_{ee} | \Psi_1 \rangle.
\end{aligned} \tag{6.9}$$

This is a contradiction and so we may conclude that there cannot be two different $v_{ext}(\vec{r})$ that give the same ρ for their ground-states. Thus, ρ determines N and v and hence all properties of the ground-state.

Looking at it keenly, there will be some problems associated with degenerate wave functions since the theorem assumes that the wave functions are non-degenerate, this brings about a problem known as v -representability. The v -representability raises the question, given a function, how do you know that the density is a ground state density of a local potential $v(\vec{r})$, that is, "Is the wave function universal?" The Levy-Lieb [4, 5] constrained-search approach addresses this issue by giving a route to the exact ground-state

wave function Ψ_0 from the ground-state density ρ_0 . It shows that the v -representability in an interacting system is not required for the proof of the HK theorem. From the variational principle,

$$E_0 = \min_{\Psi} \langle \Psi | \hat{H} | \Psi \rangle, \quad (6.10)$$

$$E_0 = \min_{\Psi} \langle \Psi | \hat{T} + \hat{V}_{ee} + \hat{V}_{ext} | \Psi \rangle, \quad (6.11)$$

The allowed antisymmetric N -electron wave function is searched for and the one that yields the lowest expectation value of the Hamilton operator is the ground-state wave function.

The kinetic (\hat{T}) and electron-electron repulsion (\hat{V}_{ee}) are separated from the energy because the external potential is determined by the density and is independent of the wave function generating that density.

$$E_0 = \min_{\rho} \left[\underbrace{\left(\min_{\Psi \rightarrow \rho} \langle \Psi | \hat{T} + \hat{V}_{ee} | \Psi \rangle \right)}_{F_{HK}[\rho]} + \int V_{ext}(\vec{r}) \rho(\vec{r}) d(\vec{r}) \right], \quad (6.12)$$

The term $F_{HK}[\rho]$ is universal since it does not depend on the external field $v(\vec{r})$ thus has no v -representability problem hence no degeneracy problem.

Theorem 2 (Variational Principle) *It states that $F_{HK}[\rho]$, the universal functional (that is; independent of V_{ext}) that delivers the ground-state energy of the system, delivers the lowest energy if and only if the input density is the true ground-state density, ρ_0 . In other words, the electronic energy satisfies the variational condition for the ground-state energy.*

$$E_{v_{ext}}[\rho] = T[\rho] + V_{ne}[\rho] + V_{ee}[\rho] = \int \rho(\vec{r}) v_{ext}(\vec{r}) d\vec{r} + F_{HK}[\rho]. \quad (6.13)$$

$F_{HK}[\rho]$ is minimal at the exact ground-state density $\rho_0(\vec{r})$, and its minimum gives the exact ground-state energy, E_0 , of the system. $F_{HK}[\rho]$ is defined independently of v_{ext} and therefore it is a universal functional of $\rho(\vec{r})$. For a

trial density $\tilde{\rho}(r)$, such that $\tilde{\rho}(r) \geq 0$ and $\int \tilde{\rho}(r) dr = N$,

$$E_0 \leq E_{v_{ext}}[\tilde{\rho}]. \quad (6.14)$$

There is a problem here. The problem is; how does one know that the trial density $\tilde{\rho}(r)$ is a density arising from an antisymmetric N -body wave function $\Psi(\vec{\mathbf{x}}_1, \vec{\mathbf{x}}_2, \dots, \vec{\mathbf{x}}_N)$? This is known as the N -representability problem. This problem has been solved for the single-particle density whereby any nonnegative function can be written in terms of some antisymmetric $\Psi(\vec{\mathbf{x}}_1, \vec{\mathbf{x}}_2, \dots, \vec{\mathbf{x}}_N)$. According to (pg. 55 of Ref.[2]), $\rho(\vec{r})$ is N -representable if it can be obtained from an antisymmetric wave function,

$$\rho(\vec{r}) \geq 0 \quad \int \rho(\vec{r}) dr = N \quad \text{and} \quad \int |\nabla \rho(\vec{r})^{1/2}|^2 dr < \infty. \quad (6.15)$$

Using the variational principle, and applying the second HK theorem, to the HK energy functional, the Euler-Lagrange equation is obtained:

$$\mu = \frac{\delta E_{v_{ext}}[\rho]}{\delta \rho(\vec{r})} = v_{ext}(\vec{r}) + \frac{\delta F_{HK}[\rho]}{\delta \rho(\vec{r})}, \quad (6.16)$$

where μ is the chemical potential. Equation (6.16) is the basic working equation of DFT. If the $F_{HK}[\rho]$ is known, this method can be applied to any system. It is however not easy to determine the $F_{HK}[\rho]$ accurately and so approximations of the functional must be used.

6.2 Thomas-Fermi Model

The Thomas-Fermi model [6] is a quantum statistical model of electrons which, takes into account only the kinetic energy while treating the nuclear-electron and electron-electron contributions in a completely classical way. It is based on the uniform electron gas, a fictitious model system of constant electron density in which the electron density is the key variable in atomic calculations. The local density approximation for the kinetic energy of a

slowly varying electron gas is,

$$T_{\text{TF}}[\rho] = \frac{3}{10}(3\pi^2)^{2/3} \int \rho^{5/3}(\vec{r}) d\vec{r}. \quad (6.17)$$

Combining Eq. (6.17) with the classical expression for the nuclear-electron attractive potential and the electron-electron repulsive potential gives the Thomas-Fermi expression for the energy of an atom,

$$E_{\text{TF}}[\rho] = C_F \int \rho^{5/3}(\vec{r}) d\vec{r} - Z \int \frac{\rho(\vec{r})}{r} d\vec{r} + \frac{1}{2} \iint \frac{\rho(\vec{r}_1)\rho(\vec{r}_2)}{r_{12}} d\vec{r}_1 d\vec{r}_2, \quad (6.18)$$

where $C_F = \frac{3}{10}(3\pi^2)^{2/3}$. Equation (6.18) gives the energy completely in terms of the electron density $\rho(\vec{r})$ and is a very coarse approximation to the true kinetic energy, and exchange and correlation effects are completely neglected. However, it is the first example of a genuine density functional for the energy. Using Eq. (6.18), $\rho(\vec{r})$ can be mapped onto an energy E without any additional information. That is, it is a functional expressing the energy in terms of the density. In the Thomas-Fermi approximation, no molecular system is stable against dissociation [7]. This means that molecules are not bound because the kinetic energy is not well-enough approximated [8].

6.3 Kohn-Sham Approach

Kohn and Sham [9] proposed a different unknown universal functional. This was after the realization that most of the problems with direct density functionals like the Thomas-Fermi method were connected with the way the kinetic energy was determined. Kohn and Sham introduced the concept of a reference system of non-interacting electrons which behave as uncharged fermions and therefore do not interact with each other via Coulomb repulsion. The advantage of this reference system is that the major part of the kinetic energy can be computed to good accuracy. By this method, as much information as possible is computed exactly, leaving only a small part of

the total energy to be determined by an approximate functional (pg. 41-42 of Ref. [1]). This results in a system of N noninteracting electrons moving in a local potential \hat{v}_s whose ground-state density is assumed to be exactly the same as the ground-state density of the real interacting system of N electrons. The ground-state kinetic energy can be computed as,

$$T_s = -\frac{1}{2} \sum_{i=1}^N n_i \langle \psi_i | \nabla^2 | \psi_i \rangle, \quad (6.19)$$

where, ψ_i and n_i are the Kohn-Sham spin orbitals and their occupation numbers respectively. The ψ_i are orthonormal, $\langle \psi_i | \psi_j \rangle = \delta_{ij}$, $\rho(\vec{r}) = \sum_i n_i |\psi_i(\vec{r})|^2$, and the Pauli principle requires that $0 \leq n_i \leq 1$. Kohn and Sham invoked this non-interacting reference system, with the one electron Hamiltonian,

$$\hat{H}_s = -\frac{1}{2} \sum_i^N \nabla_i^2 + \sum_i^N v_s(\vec{r}_i), \quad (6.20)$$

where there are no electron-electron repulsion terms since it is a one electron Hamiltonian, and the ground-state electron density is exactly ρ . For such a system there will be an exact determinantal ground-state wave function given by,

$$\Psi_s = \frac{1}{\sqrt{N!}} \det[\psi_1 \psi_2 \dots \psi_N], \quad (6.21)$$

where the ψ_i are the N lowest eigenstates of the one-electron Hamiltonian or a linear combination of determinants with the same energy and $\psi_1, \psi_2 \dots \psi_N$,

$$\det[\psi_1, \psi_2 \dots \psi_N] = \begin{vmatrix} \psi_1(\vec{x}_1) & \psi_1(\vec{x}_1) & \dots & \psi_N(\vec{x}_1) \\ \psi_1(\vec{x}_2) & \psi_2(\vec{x}_2) & & \psi_N(\vec{x}_2) \\ \vdots & \vdots & & \vdots \\ \psi_1(\vec{x}_N) & \psi_2(\vec{x}_N) & \dots & \psi_N(\vec{x}_N) \end{vmatrix}. \quad (6.22)$$

The functional of density, $T_s[\rho]$ is not the exact kinetic-energy functional. To get $T_s[\rho]$ as the exact kinetic-energy component, Kohn and Sham separated out $T_s[\rho]$ as the kinetic energy component,

$$F[\rho] = T_s[\rho] + J[\rho] + E_{xc}[\rho], \quad (6.23)$$

where,

$$E_{xc}[\rho] = T[\rho] - T_s[\rho] + V_{ee}[\rho] - J[\rho]. \quad (6.24)$$

The quantity $E_{xc}[\rho]$ is called the exchange-correlation energy. It contains the difference between T and T_s i.e., the kinetic energy difference between the true interacting and fictitious non-interacting system and the nonclassical part of $V_{ee}[\rho]$.

Lagrange multipliers ϵ_{ij} for the orthonormalization conditions on ψ_i and ψ_j are applied to satisfy the necessary conditions that the N orbitals must satisfy to be the minimizing orbitals. The reason for this is that for minimization, the orbitals must be orthonormal.

$$0 = \frac{\delta \mathcal{L}}{\delta \psi_i^*(\vec{r})} = \hat{h}\psi_i(\vec{r}) - \sum_j \epsilon_{i,j} \psi_j(\vec{r}), \quad (6.25)$$

$$\mathcal{L} = E - \sum_{i,j} \epsilon_{i,j} (\langle \psi_i | \psi_j \rangle - \delta_{ij}), \quad (6.26)$$

which can also be expressed (after diagonalization of the matrix of Lagrange multipliers) as the Kohn-Sham orbital equation,

$$\hat{h}_s \psi_i(\vec{r}) = \epsilon_i \psi_i(\vec{r}).$$

From Eq.(6.25), the Coulomb potential is given as,

$$v_H[\rho](\vec{r}_1) = \int \frac{\rho(\vec{r}_2)}{r_{12}} d\vec{r}_2, \quad (6.27)$$

and the xc potential is given as,

$$v_{xc}[\rho](\vec{r}) = \frac{\delta E_{xc}[\rho]}{\delta \rho(\vec{r})}. \quad (6.28)$$

From the above equation, it is very important to realize that if the exact forms of E_{xc} and v_{xc} were known, the Kohn-Sham strategy would lead to the

exact energy, that is, the correct eigenvalue of the Hamiltonian operator \hat{H} of the Schrödinger equation. This is unfortunately not the case here. This means that the only way forward is to work with approximations. This has been the goal of modern density functional theory; finding better and better approximations to these two quantities, the $E_{xc}[\rho]$. The Kohn-Sham equation approached this problem by applying it to a system of non-interacting electrons moving in the external potential $v_s(\vec{r}) = v_{eff}(\vec{r})$. For a given $v_{eff}(\vec{r})$, one obtains the $\rho(\vec{r})$ that satisfies the corresponding Euler equation by solving the N one-electron equations,

$$\left[-\frac{1}{2}\nabla^2 + v_s(\vec{r}) \right] \psi_i = \epsilon_i \psi_i. \quad (6.29)$$

and setting,

$$\rho(\vec{r}) = \sum_i^N \sum_s |\psi_i(\vec{r}, s)|^2. \quad (6.30)$$

v_{eff} depends on $\rho(\vec{r})$ thus the calculations are solved self-consistently. We begin with a guessed $\rho(\vec{r})$, construct $v_{eff}(\vec{r})$ and then find a new $\rho(\vec{r})$.

Expressing E_{xc} in terms of Eq. (6.24), the Euler equation is expressed as,

$$\mu = v_s(\vec{r}) + \frac{\delta T_s[\rho]}{\delta \rho(\vec{r})}, \quad (6.31)$$

where the KS effective potential is defined by,

$$v_s(\vec{r}) = v_{ext}(\vec{r}) + \frac{\delta J[\rho]}{\delta \rho(\vec{r})} + \frac{\delta E_{xc}[\rho]}{\delta \rho(\vec{r})} = V_{ext}(\vec{r}) \int \frac{\rho(\vec{r}')}{|\vec{r} - \vec{r}'|} d\vec{r}' + v_{xc}(\vec{r}), \quad (6.32)$$

with the exchange-correlation potential being given as,

$$v_{xc}(\vec{r}) = \frac{\delta E_{xc}[\rho]}{\delta \rho(\vec{r})}. \quad (6.33)$$

6.4 Exchange-Correlation Approximations (Jacob's Ladder)

In the previous section, it has been shown that the Kohn-Sham formalism allows an exact treatment of most of the contributions to the electronic energy of an atomic or molecular system, including the major fraction of the kinetic energy. The remaining unknown parts are summed into the exchange-correlation functional $E_{xc}[\rho]$. The exact form of this functional is not known and an approximate description is used instead. The quality of the density functional approach depends solely on the accuracy of the chosen approximation to E_{xc} . The following sections outline some of the E_{xc} functionals that have been developed over time. Ideally, these functionals can be classified into two major classes, those that are based on the electronic wave function (generalized Kohn-Sham theory) and those that are based on the electron density (pure density functionals).

6.4.1 Local Density Approximation(LDA)

In summary, the E_{xc} employs only the local density at each point. The exchange-correlation functionals are guided by studies of the hypothetical uniform electron gas because it is the only system for which the form of the exchange and correlation energy functionals is known exactly or at least to very high accuracy. LDA assumes that the density $\rho(\vec{r})$ can be treated locally as an uniform electron gas (UEG); the exchange-correlation density at each point in the system is the same as that of an uniform electron gas of the same density. E_{xc} is given as,

$$E_{xc}^{LDA} = \int \epsilon_{xc}^{UEG}(\rho(\vec{r}))\rho(\vec{r})d\vec{r}, \quad (6.34)$$

where ϵ_{xc}^{UEG} is the exchange-correlation energy per particle of a uniform electron gas of density $\rho(\vec{r})$. The energy per particle is weighted with the probability $\rho(\vec{r})$ that there is an electron at this position in space. $\epsilon_{xc}^{UEG}(\rho(\vec{r}))$

can be further divided into exchange and correlation contributions,

$$\epsilon_{xc}(\rho(\vec{r})) = \epsilon_x(\rho(\vec{r})) + \epsilon_c(\rho(\vec{r})). \quad (6.35)$$

The $\epsilon_x(\rho(\vec{r}))$ is known and it is given by the Hartree Fock exchange for the homogeneous electron gas,

$$\epsilon_x(\rho(\vec{r})) = -\frac{3}{4} \left(\frac{3}{\pi} \rho(\vec{r}) \right)^{1/3}. \quad (6.36)$$

Replacing the above in Eq. (6.34) gives the $\rho^{4/3}(\vec{r})$ of the exchange energy. For the correlation part, $\epsilon_c(\rho(\vec{r}))$ such an explicit expression is not known. For the $\epsilon_x(\rho(\vec{r}))$, accurate values can be obtained courtesy of quantum Monte-Carlo calculations of the homogeneous electron gas by Ceperly and Alder [10, 11]. Based on results from the explicit calculations, authors have come up with an approximate analytic expression for ϵ_c . Some of the ϵ_c expressions include that by Vosko, Wilk, and Nusair [12], Perdew and Wang [13] and Perdew, Burke and Ernzerhof [14]. The LDA has an advantage of producing many experimentally relevant physical properties to a good level of accuracy in strongly bound systems. It however tends to overestimate bonding energies as well as underestimating bond lengths.

6.4.2 Generalized Gradient Approximation (GGA)

The accuracy that was achieved by using the LDA was not sufficient for most applications in chemistry. This is because LDA used only the information about the density $\rho(\vec{r})$ at a particular point \vec{r} . What the GGA does is to bring in information about the gradient of the charge density, $\vec{\nabla}\rho(\vec{r})$ to account for the true in-homogeneous electron density. The local density approximation is interpreted as the first term of a Taylor expansion of the uniform density, resulting in,

$$E_{xc}^{GGA}[\rho] = \int \epsilon_{xc}^{UEG}(\rho)\rho(\vec{r})d\vec{r} + \int C_{xc}(\rho(\vec{r}))x(\vec{r})d\vec{r}, \quad (6.37)$$

where the reduced gradient is given by,

$$x(\vec{r}) = \frac{|\vec{\nabla}\rho(\vec{r})|}{\rho^{4/3}(\vec{r})}. \quad (6.38)$$

Equation (6.37) is known as the gradient expansion approximation (GEA). The GEA did not however perform to the required expectations in that there was no improved accuracy and it often performed even worse than the simple local density approximation. The generalized gradient approximation, GGA, was the more successful approach,

$$E_{xc}^{GGA} = \int \epsilon_{xc}(\rho(\vec{r}), x(\vec{r}))\rho(\vec{r})d\vec{r}. \quad (6.39)$$

Different versions of the GGA include the Perdew and Wang (PW91) [15], Perdew, Burke, and Enzerhof (PBE) [14] and Beeke-Lee-Yang-Parr (BLYP) [16, 17].

6.4.3 Hybrid Functionals

These functionals mix a fraction of exact exchange (Hartree-Fock exchange) with GGA exchange and correlation [18, 19]. The simplest hybrid functional takes the form,

$$E_{xc}^{hyb} = aE_{xc}^{exact} + (1 - a)E_x^{GGA} + E_c^{GGA}, \quad (6.40)$$

where the constant $a \approx 1/4$ for molecules from empirical or theoretical estimations [20].

All the calculations in this work utilized the B3LYP (Becke, three-parameter, Lee-Yang-Parr) hybrid functional [12, 17, 18, 21]. It takes the form,

$$E_{xc}^{B3LYP} = (1 - a)E_x^{LDA} + aE_{xc}^{LDA} + bE_x^{B88} + cE_c^{LYP} + (1 - c)E_c^{LDA}. \quad (6.41)$$

where $a = 0.20$, $b = 0.72$, and $c = 0.81$ from the B3P functional [18], LDA is the local density approximation, B88 is Becke's 1988 generalized gradient approximation (GGA) for exchange, and LYP is the Lee, Yang, and Parr's 1988 GGA for correlation. At this point in time, it is important to note that with the improvements, these functionals are perhaps the most accurate

density functionals in use for quantum chemical calculations having been used for many calculations in the recent years and currently.

6.4.4 Meta-Generalized Gradient Approximation (meta-GGA)

Meta-GGAs (mGGAs) [22], in addition to the local density and the first gradient as input, also requires the orbital kinetic energy density. The correlation energy in this functional is free of self-interaction error. Meta-GGAs significantly improve the molecular atomization energies and metal surface energies compared to GGA while the lattice constants are changed slightly. The general form [23] of the mGGA is,

$$E_{XC}[\rho] = \int e_{xc}(\rho(\vec{r}), \nabla\rho(\vec{r}), \tau(\vec{r}))\rho(\vec{r}) d\vec{r}, \quad (6.42)$$

where the kinetic-energy density is given by;

$$\tau(\vec{r}) = \frac{1}{2} \sum_i \underbrace{\left[\vec{\nabla}\psi_i(\vec{r}) \right] \cdot \left[\vec{\nabla}\psi_i(\vec{r}) \right]}_{|\vec{\nabla}\psi_i(\vec{r})|^2}. \quad (6.43)$$

6.4.5 Double hybrid functionals

Double hybrid functionals [24] include a certain amount of HF exchange with semilocal exchange density functional and second-order Møller-Plesset (MP2) correlation with a semilocal correlation density functional. This functional includes unoccupied KS orbitals in the calculation.

6.4.6 Jacob's Ladder of Density Functional Approximations

Jacob's ladder of density functional approximations [26] gives the line of development of density functionals for the exchange-correlation energy. It suggests moving from the Hartree world up to the Heaven of chemical accuracy. As shown in Fig. 6.1, the ladder has five rungs, each corresponding to the increase in complexity of choices for the ingredients of the energy density. At the lowest rung of the ladder, rung 1, the dependence is on the local density only (LDA), followed by rung 2 where there is an explicit

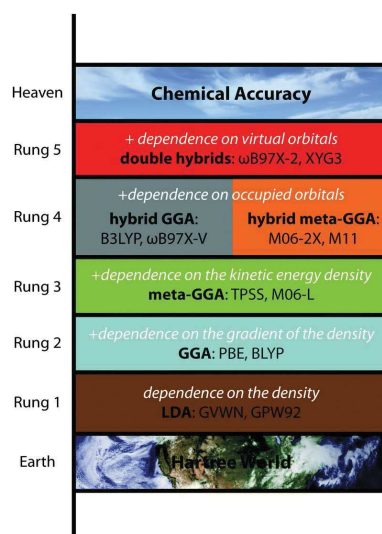


Figure 6.1 – Jacob's ladder of Density Functional Approximations. Reproduced from (Ref. [25]) with permission of the PCCP Owner Societies.

dependence on gradients of the density (GGA). In rung 3, there is an explicit dependence on the kinetic energy density (meta-GGAs). Rung 4 has an explicit dependence on occupied orbitals (hybrid functionals), while rung 5 has an explicit dependence on unoccupied orbitals (fully nonlocal).

This particular ladder was very well described by Casida [27], "According to the Bible, Jacob had a dream in which he saw a ladder descending from Heaven to Earth and angels climbing and descending the ladder. In John Perdew's dream, the angels are users of DFT who climb the ladder to gain greater precision (at greater cost), but who also need to be able to descend the ladder depending upon their needs."

Bibliography

- [1] W.Koch and M.C. Holthausen. *A Chemist's Guide to Density Functional Theory*. Wiley/VCH, Weinheim, 2001.
- [2] R. G. Parr and W. Yang. *Density Functional Theory of Atoms and Molecules*. Oxford University Press, New York, 1989.
- [3] P. Hohenberg and W. Kohn. Inhomogeneous electron gas. *Phys. Rev.*, 136(3B):B864, 1964.
- [4] Mel Levy. Universal variational functionals of electron densities, first-order density matrices, and natural spin-orbitals and solution of the v -representability problem. *P. Nat. Acad. Sci.*, 76(12):6062–6065, 1979.
- [5] Elliott H. Lieb, R. M. Dreizler, and J da Providencia. Density functional methods in physics. *Nato Asi Series B*, 123, 1985.
- [6] L. H. Thomas. The calculation of atomic fields. In *Mathematical Proceedings of the Cambridge Philosophical Society*, volume 23, pages 542–548. Cambridge Univ Press, 1927.
- [7] E. Teller. On the stability of molecules in the Thomas-Fermi theory. *Rev. Mod. Phys.*, 34:627–631, Oct 1962. doi: 10.1103/RevModPhys.34.627. URL <https://link.aps.org/doi/10.1103/RevModPhys.34.627>.
- [8] E. H. Lieb. Thomas-Fermi and related theories of atoms and molecules. *Rev. Mod. Phys.*, 53(4):603, 1981.
- [9] W. Kohn and L. J. Sham. Self-consistent equations including exchange and correlation effects. *Phys. Rev.*, 140:A1133, 1965.
- [10] D. M. Ceperley and B. J. Alder. Ground state of the electron gas by a stochastic method. *Phys. Rev. Lett.*, 45(7):566, 1980.
- [11] G. Ortiz and P. Ballone. Correlation energy, structure factor, radial distribution function, and momentum distribution of the spin-polarized uniform electron gas. *Phys. Rev. B*, 50(3):1391, 1994.

-
- [12] S. H. Vosko, L. Wilk, and M. Nusair. Accurate spin-dependent electron liquid correlation energies for local spin density calculations: A critical analysis. *Can. J. Phys.*, 58(8):1200–1211, 1980.
- [13] J. Perdew and Y. Wang. Accurate and simple analytic representation of the electron-gas correlation energy. *Phys. Rev. B*, 45(23):13244, 1992.
- [14] J. P. Perdew, K. Burke, and M. Ernzerhof. Generalized gradient approximation made simple. *Phys. Rev. Lett.*, 77(18):3865, 1996.
- [15] J. P. Perdew, J. A. Chevary, S. H. Vosko, K. A. Jackson, M. R. Pederson, D. J. Singh, and C. Fiolhais. Atoms, molecules, solids, and surfaces: Applications of the generalized gradient approximation for exchange and correlation. *Phys. Rev.*, B 46:6671, 1993.
- [16] A. D. Becke. Density-functional exchange-energy approximation with correct asymptotic behavior. *Phys. Rev. A*, 38(6):3098, 1988.
- [17] C. Lee, W. Yang, and R. G. Parr. Development of the Colle-Salvetti correlation energy formula into a functional of the electron density. *Phys. Rev. B*, 37:785, 1988.
- [18] A. D. Becke. Density-functional thermochemistry. III. The role of exact exchange. *J. Chem. Phys.*, 98:5648, 1993.
- [19] A. D. Becke. A new mixing of Hartree-Fock and local density-functional theories. *J. Chem. Phys.*, 98(2):1372–1377, 1993.
- [20] J. P. Perdew, M. Ernzerhof, and K. Burke. Rationale for mixing exact exchange with density functional approximations. *J. Chem. Phys.*, 105(22):9982–9985, 1996.
- [21] P. J. Stephens, F. J. Devlin, C. F. Chabalowski, and M. J. Frisch. Ab initio calculation of vibrational absorption and circular dichroism spectra using density functional force fields. *J. Phys. Chem.*, 98(45):11623–11627, 1994.

- [22] J. P. Perdew, S. Kurth, A. Zupan, and P. Blaha. Accurate density functional with correct formal properties: A step beyond the generalized gradient approximation. *Phys. Rev. Lett.*, 82(12):2544, 1999.
- [23] F. Zahariev, S. S. Leang, and M. S. Gordon. Functional derivatives of meta-generalized gradient approximation (meta-GGA) type exchange-correlation density functional. *J. Chem. Phys.*, 138(24):244108, 2013.
- [24] Y. Zhao, B. J. Lynch, and D. G. Truhlar. Doubly hybrid meta DFT: New multi-coefficient correlation and density functional methods for thermochemistry and thermochemical kinetics. *J. Phys. Chem. A*, 108(21):4786–4791, 2004.
- [25] N. Mardirossian and M. Head-Gordon. ω B97X-V: A 10-parameter, range-separated hybrid, generalized gradient approximation density functional with nonlocal correlation, designed by a survival-of-the-fittest strategy. *Phys. Chem. Chem. Phys.*, 16(21):9904–9924, 2014.
- [26] J. P. Perdew and K. Schmidt. Jacob’s ladder of density functional approximations for the exchange-correlation energy. In *AIP Conference Proceedings*, pages 1–20. IOP Institute of Physics Publishing Limited, 2001.
- [27] M. E. Casida. John perdew’s Jacob’s ladder. <https://sites.google.com/site/markcasida/dft>, 2015. online; accessed 27th August, 2015.

Chapter 7

Basis Sets and Effective Core Potentials

Basis sets form the core of quantum mechanical calculations since they are used to provide the best representation of the unknown molecular orbitals. To solve the Hartree-Fock equation, there is need to choose a numerical method. A basis set comes in handy for this purpose, either the Gaussian-type orbitals (GTOs) or Slater-type orbitals (STOs). In this chapter, the description of what a basis set is, how it works, and different types is given. In this work, ruthenium polypyridine complexes have been studied extensively. Ruthenium is classified as a heavy atom and this explains why there is also a review of the effective core potentials (ECPs) which are used to include scalar relativistic effects of core electrons.

7.1 Definition of a Basis Set

A basis set is a mathematical description of orbitals of a system, which is used for the purpose of approximate theoretical calculations [1]. As mentioned earlier on, introducing a basis set which ideally is a linear combination of atomic orbitals (LCAO, MO=LCAO) transforms the Hartree-Fock equations into the Roothaan equations [2]. Each unknown MO is expanded as a linear combination of three dimensional one electron functions, known as

atomic orbitals. Denoting the atomic orbital basis functions as χ_μ , for each spin orbital i ,

$$\psi_i(\vec{r}) = \sum_{\mu=1}^K \chi_\mu(\vec{r}) C_{\mu i} \quad (7.1)$$

where K is an integer relating to the size of the basis set larger than the number of electrons in the system.

Any wave function may be expanded as a linear combination of a complete set of basis functions, hence not an approximation. This kind of a basis set requires that an infinite number of functions must be used, which is normally impossible in actual calculations. Use of a finite basis set usually implies that the MO is approximate [3]. Keeping the total number of basis functions to a minimum is computationally attractive but it is more useful to choose basis set functional forms that permit the various integrals appearing in the HF equations to be evaluated in a computationally efficient fashion. The basis functions must be chosen to have a form that is useful in a chemical sense in that the functions should have large amplitude in regions of space where the electron probability density is also large and small amplitudes where the probability density is small.

7.2 Types of Basis Functions (Atomic Orbitals)

The types of basis sets used in atomistic modelling is extremely diverse. Atomistic calculations often use spherical symmetry to reduce the Schrödinger equation to a one-dimensional problem which may be solved by numerical integration. A similar approach is possible for diatomics. Some polyatomic quantum chemistry programs use tabulated numerical atomic orbitals as basis functions, however by far the most popular choice in molecular calculations has been the use of analytic basis functions. These may be divided into two types according to whether their decay with the radial variable r is exponential [Slater-type orbitals (STOs)($e^{-\zeta r}$)] [4] or Gaussian [Gaussian-type orbitals (GTOs)($e^{-\alpha r^2}$)].

7.2.1 Slater-Type Orbitals (STOs)

STOs closely resemble hydrogenic atomic orbitals to a very large extent. The hydrogen atom (one electron atom) is of great interest in this context because it is one of the few quantum mechanical problems with an analytic solution [5]. For the hydrogen atom and other one electron ions, the solution of the Schrödinger equation gives atomic orbitals which are a product of a radial function that depends on the distance of the electron from the nucleus and a spherical harmonic. The hydrogen-like atomic orbitals (HAOs) have the form,

$$\psi_{n,l,m}(r, \theta, \varphi) = R_{n,l}(r)Y_{n,l}(\theta, \varphi), \quad (7.2)$$

where $Y_{n,l}(\theta, \varphi)$ are complex-valued spherical harmonics [whose real and imaginary parts give atomic orbitals their characteristic shapes (s, p, d, f)] and the radial dependence $R_n(r)$ is given as,

$$R_{n,l}(r) = L_{n,l}(r)e^{-r/a_0}. \quad (7.3)$$

The complex form of the HAOs simultaneously satisfy the three eigenvalue equations:

$$\begin{aligned} \hat{H}\psi_{nlm} &= E_n\psi_{nlm} & n &= 1, 2, 3 \\ \hat{L}^2\psi_{nlm} &= l(l+1)\psi_{nlm} & l &= 0, 1, 2, 3, \dots, (n-1) \\ \hat{L}_z\psi_{nlm} &= m\psi_{nlm} & m &= 0, \pm 1, \pm 2, \pm 3, \dots, \pm l. \end{aligned} \quad (7.4)$$

Each eigenvalue is characterized by one quantum number (n). n is the principal quantum number which typifies the total electron energy, l is the orbital quantum number that describes square of the angular momentum and m is the magnetic number which gives the z-component of the angular momentum. Orbitals, which are eigenfunctions that are specified by the quantum numbers are essential in understanding the behaviour of electrons in atoms. The analytic solution influences greatly how basis sets are constructed [6].

Having looked at the analytic solution of the HAOs, it is now easier to

link STOs to hydrogenic atomic orbitals. STOs have the form,

$$Y_{l,m}(\theta, \varphi)r^{n-1}e^{-\zeta r} \quad \text{or} \quad x^n y^m z^l e^{-\zeta r} \\ \text{or} \quad \left[\frac{\zeta^3}{\pi} \right]^{0.5} e^{-\zeta r} \text{ (Simplified equation for hydrogen-like systems).} \quad (7.5)$$

The distance between the nucleus and electron has an exponential dependence that mirrors the exact orbitals for the hydrogen atom. STOs differ from HAOs in the radial part $R_n(r)$, which is independent of l . One obvious implication of this difference is that STOs do not possess radial nodes like a real atomic orbital because of the wrong behaviour of the ns functions when $n > 1$ resulting in some loss of orthogonality. By making LCAO of STOs, the radial nodes can be introduced (Schmidt orthogonalization) [7]. Owing to the large number of the integrals needed for computation, STOs face a problem in the analytical calculation of integrals centered on three or four different atoms. This limits their utility in molecular systems of any significant size because of the difficulty in calculation of integrals which is computationally very expensive. It is still possible to use STOs for atomic and diatomic calculations where such restrictions do not exist [3, 8, 9]. STOs exhibit correct short and long range behaviour. One of the commercial codes that use the STOs even for polyatomic molecules is the AMSTERDAM DENSITY FUNCTIONAL CODE, (ADF)[10].

7.2.2 Gaussian-type orbitals (GTOs)

GTOs come in as a solution to the problem of STOs, which is, the difficulty of calculating certain matrix elements in the Fock matrix. GTOs which contain the exponential ($e^{-\alpha r^2}$), replace the STOs ($e^{-\zeta r}$) with functions that look like STOs but in which the matrix elements can be calculated in an easier way. The aspect of simplification arises from the fact that the product of two GTOs at two different positions can be rewritten as a GTO centered between these two positions. GTOs have the form,

$$Y_{l,m}(\theta, \varphi)r^{n-1}e^{-\alpha r^2} \quad \text{or} \quad x^n y^m z^l e^{-\alpha r^2} \quad (7.6)$$

One major difference between STOs and GTOs is that the r -factor of the exponential in GTO is squared. Although GTOs are convenient to use from a computational point of view, the exponential difference leads to two obvious problems arising from their use: first, faster decay at larger r , consequently leading to poor approximation of the true radial function in the outer region and secondly, lack of cusps (discontinuous derivative) at $r = 0$ compared to real HAOs that have a cusp hence improper representation of the behaviour near the nucleus. Both the STOs (gives proper radial shape) and GTOs (computational efficiency) have attractive features that any computational chemist would love to combine for purposes of computational efficiency and accuracy. The question is, how can we do this? It is possible by linearly combining several GTOs (primitive Gaussians) with fixed coefficients to form the contracted GTO. One would expect that with contracted GTOs there will be lack of accuracy, but this is not the case because the core orbitals are insensitive to the molecular environment hence making linear combination possible. Primitive Gaussians are the original GTOs centered on the same nucleus. They have a standardized form and some examples corresponding to s , p , d , and f atomic orbitals are represented as:

$$\begin{aligned}
 s \text{ function} & : e^{-\alpha r^2}, \\
 p \text{ function} & : (x, y, z)e^{-\alpha r^2}, \\
 d \text{ function} & : (x^2, y^2, z^2, xy, yz, zx)e^{-\alpha r^2}, \\
 f \text{ function} & : (x^3, y^3, z^3, x^2y, x^2z, xy^2, y^2z, yz^2, xz^2, xyz)e^{-\alpha r^2},
 \end{aligned} \tag{7.7}$$

Mathematically, a contracted GTO with three Gaussians (3G) can be defined as,

$$e^{(-\alpha r)} \approx c_1 e^{-\alpha_1 r^2} + c_2 e^{-\alpha_2 r^2} + c_3 e^{-\alpha_3 r^2} \tag{7.8}$$

There are 6 cartesian d functions. This is a consequence of the fact that the $x^2 + y^2 + z^2 = r^2$ combination is really an s function. Similar remark for the f functions times the appropriate angular part $x^n + y^m + z^l$. There are various types of functions for contracted GTOs; these will be discussed later

on in this chapter. In quantum chemistry, GTOs dominate for molecular computation owing to the large number of integrals that must be computed.

7.3 Classification of Basis Sets

7.3.1 Minimal Basis Sets (Single Zeta)

An AO is described by one STO (or STO-like) basis function. In this basis set, a minimal number of functions are used to represent all the electrons of the ground state atoms and any empty valence orbitals. To explain this further, specific examples of H ($1s^1$) and C ($1s^2 2s^2 2p^2$) atoms are considered. The minimal basis set for hydrogen is one “1s” orbital and “1s” orbital, “2s” orbital and the full set of three “2p” orbitals for the carbon atom respectively. For the methane molecule, the total number of basis sets can be calculated as; $4 \times (1s) + 1s + 2s + 2p_x, 2p_y, 2p_z = 9$ basis functions [11]. There are several minimal basis sets that are used in computation. The STO- n G [12–15] basis sets approximating STOs akin to AOs with n primitive functions is the most common. It is a linear combination of n GTOs fitted to each STO. Some examples include STO-3G, STO-4G, STO-6G. The STO-3G basis set implies that each basis function is a contraction of three primitive Gaussians. Its radial part can be written as;

$$\text{STO-3G} = c_1 e^{-\alpha_1 r^2} + c_2 e^{-\alpha_2 r^2} + c_3 e^{-\alpha_3 r^2}. \quad (7.9)$$

Another example of the minimal basis set is the MINI sets of Huzinaga and co-workers [13] such as the MINI-1, MINI-2. The difference comes in from the number of primitives used for different kinds of functions. Minimal basis sets are unsuitable in calculations including electron correlation. They provide poor results for molecules owing to their inadequacy at describing the process of bond formation and deviation from the spherical symmetry [12]. Another weakness is that energies and wave functions from minimal basis set are not very close to the HF limits. For more accurate calculations, more extensive basis sets must be used. The next basis set involves improvement of the minimal basis set.

7.3.2 Double, Triple and Multi Zeta (ζ) Basis Sets and Split Valence Basis Sets

Each AO is described by two basis functions for the double zeta (DZ), three basis functions for the triple zeta (TZ) and four basis functions for the quadruple zeta (QZ) basis sets. A DZ basis set uses two s-functions for 1s (1s and 1s'), four s-functions for 1s and 2s (1s, 1s', 2s and 2s') and two sets of p-functions (2p and 2p') for first row elements. DZ basis sets make better descriptions of bond formation because they describe bonding in different directions uniquely [12]. Increasing the size of the basis functions has an advantage of inching closer and closer to the HF limit. Chemical intuition helps in deciding which AOs to add. The most significant observation is that core orbitals hardly participate in chemical bonding while valence orbitals mainly contribute to chemical bonding. This chemical consequence ideally means that flexibility in the valence basis functions is more beneficial than in the core; therefore, many basis functions should be used for valence orbitals to calculate electronic states accurately. If, for instance, we look at atoms bonded to more electropositive elements, they will take on partial negative charge from loss of valence electrons, thus affecting the density distribution of the remaining electrons [16]. This particular observation brought in the development of the 'split valence' or 'valence-multiple- ζ ' basis sets.

Split valence (SV) basis functions split each valence orbital into two parts, an inner shell and an outer shell. One type of contracted Gaussian-type function is used for core orbitals and multiple contracted functions for valence orbitals. Some examples of SV basis sets developed by Pople [17] are 3-21G, 6-21G, 4-31G, 6-31G and 6-311G. It is easy to identify the contraction method used in the SV basis set from its naming. The number of primitives used in the contracted core functions is indicated by the first number. Preceding numbers after the hyphen show the numbers of primitives used in the valence functions. Two such numbers indicate that it is a valence-double- ζ basis and three numbers, valence-triple- ζ . To illustrate this, for the 6-31G basis set, '6' means 6 primitive functions for core orbitals and '31' means the use of doubly-split basis functions combining contracted basis functions of 3

primitive functions with one uncontracted basis function for valence orbitals. The 6-311G makes use of triply split basis functions for valence orbitals. Examples of the SV basis set is the Dunning Huzinaga basis function described as DZ for the doubly split, TZ for the triply split and QZ for the quadruply split functions for valence orbitals. The DZV, TZV, and QZV belong to the Ahlrichs-type. So far, the basis sets described, beginning from the minimal basis sets to DZ, TZ, QZ and split valence basis sets do not consider possible contributions from basis functions in which the quantum number l is larger than the maximum value present in the ground state of the atom. When the value of l is large, it will have an effect on the adjacent atoms through polarization. The following basis sets takes this into consideration.

7.3.3 Polarization Function-Supplemented Basis Functions

Bonding in molecules leads to significant polarization or distortion of atomic orbitals by neighbouring atoms.

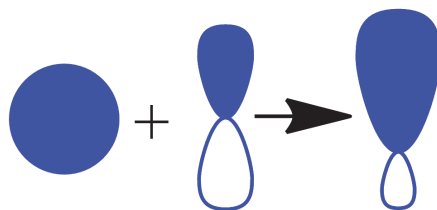


Figure 7.1 – Distortion of orbitals resulting from the inclusion of s and p orbitals.

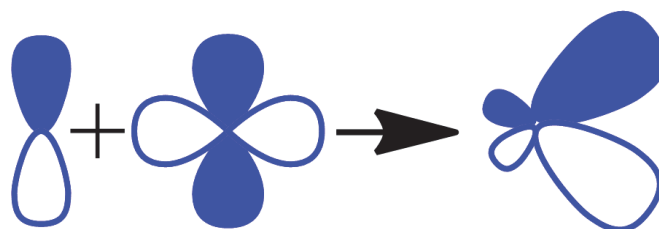


Figure 7.2 – Distortion of orbitals resulting from the inclusion of p and d orbitals.

To take this into consideration, basis functions with high values of l must be included [18]. Essentially, polarization allows for change in shape of orbitals in the sense that the molecular wave-function has the flexibility to distort away from spherical symmetry in the surrounding of each atom. Addition of polarization functions incorporates an elaborate electron distribution; for instance, the distortion of the s orbital is accounted for by inclusion of p -type basis function while that of p orbitals by inclusion of d -type functions and d orbitals by inclusion of f -type functions. The resulting basis set is referred to as the DZ plus polarization (DZP) or the SV plus polarization (SVP) basis. Examples of the DZP basis set is the (6-31G* or 6-31G(d)) which adds of one polarization function (d type functions) for all non-hydrogen atoms and the (6-31G** or 6-31G(d,p)) that adds one p orbital function to each hydrogen atom in the Pople type function [1]. Exception of polarization function on the hydrogen atoms in the (6-31G* or 6-31G(d)) basis is for the reason that mostly, hydrogen atoms sit at the end of the bonds. In addition, the large number of hydrogen atoms means that adding functions to hydrogen will cause the basis set to grow very quickly. Polarization functions for hydrogen atoms must be included if they play a significant role in the property of interest. Addition of two sets of polarization functions to a TZ basis set results in a triple zeta plus double polarization (TZ2P) type basis.

The significance of polarization functions at different levels of calculations cannot be ignored. Correlated methods require more polarization functions and higher angular momentum to get the same convergence as the HF level. For the HF level however, the difference noticed is not much with the expansion of the basis set beyond TZ2P [3].

The use of polarization function-supplemented basis functions considerably improves the description of molecular geometries and molecular relative energies.

7.3.4 Diffuse-Function-Augmented Basis Functions

For systems in which the highest energy MOs are spatially more diffuse such as anions, loose supermolecular complexes, molecules with lone pairs

(notably hydrogen-bonding N, O and F atoms) and highly excited electronic states than standard valence size functions, diffuse basis functions are used to allow the weakly bound electrons to localize far from the remaining electron density. This means that the orbitals are able to occupy a larger region of space [16]. Addition of a diffuse function is shown by a plus (+) in Pople-type basis functions. Examples include the 6-31+G(d) basis set in which one s and one set of p functions have been added to the heavy atoms. 6-31++G(d), adds diffuse functions to the H atoms too. Addition of diffuse functions on hydrogen atoms often makes a noticeable change in accuracy. Other examples are in the MIDI! and MIDIY basis sets in which diffuse sp sets have augmented leading to MIDIX+ and MIDIY+. The ‘aug’ prefix is used to indicate the presence of diffuse functions for the correlation consistent basis sets cc-pVnZ. Examples under this family are aug-cc-pVTZ which has diffuse *f*, *d*, *p*, and *s* functions on heavy atoms and diffuse *d*, *p*, and *s* functions on H and He.

Diffuse-function-augmented basis functions produce better results for the calculation of acidities and electron affinities.

7.3.5 Effective Core Potential (ECP) Basis Functions (Pseudopotentials)

The previous types of basis sets discussed mainly deal with the first and second row elements of the periodic table. As we move towards the third row elements and beyond (heavy elements), there is an increase in the number of electrons and this poses several challenges to a computational chemist. The first challenge is that with the increase in the number of electrons and orbitals, a large number of basis functions are required to describe them. Since most of these electrons are core, there is a challenge to represent them adequately. The second challenge is that the core electrons in heavy elements reach velocities sufficiently close speed of light that they show relativistic effects. Relativistic effects have an effect on geometries, energies and other properties. It is impossible for a non-relativistic Hamiltonian operator to account for such effects. The third challenge is reduction in the speed of *ab*-

initio calculations due to the large number of two-electron repulsion integrals involved. These problems can be circumvented by using an ECP [19].

An ECP or pseudo-potential adds to the Fock operator a one-electron operator which treats core electrons as an imaginary sphere of dense charge distribution providing a highly repulsive potential and preventing the valence electrons from collapsing into the inner orbital [1]. In the N electron HF Roothan-Hall equations, the core electrons are replaced by an effective potential function instead of being counted explicitly. ECPs drastically reduce the number of basis functions, incorporate the relativistic effects of the core electrons and speed up calculations by reducing the scope of the electronic structure problem for heavy elements. ECPs obey the Pauli exclusion principle.

The construction of ECPs is dependent on the number of electrons to be included in the core. Based on this, ECPs can largely be classified into two; ‘large-core’ ECPs which include everything except the outermost (valence) shell and ‘small-core’ ECPs which scale back to the next lower shell. For calculations involving heavier metals, the small-core ECPs that include the sub valence shell are preferred because polarization of the sub shell has some chemical consequences. Examples of ECP basis functions are LanL2DZ, of Los Alamos National Laboratory (DZ means double-*zeta*) and the Stuttgart relativistic small core (STRSC) and large core (STRLC) ECP basis functions (Germany).

Calculations on transition metal molecules rely heavily on the use of ECPs. Specifically, this work studies ruthenium (Ru) transition metal complexes and an ECP is used for the Ru atom. Ru ($Z=44$) is a fifth row atom with an atomic configuration of $[\text{Kr}]4d^75s^1$ which justifies the use of an ECP since it is a heavy element. The double- ζ quality LanL2DZ basis set for ruthenium along with the corresponding ECP was used. Since Ru is a heavy element, the core electrons are not chemically important because they are not actively involved in chemical bonding. The ECP also serves to account for the relativistic effects. Ru is a heavy metal and the small-core ECP that includes the subvalence shell is used. The ECP is composed of 28 core electrons ($[\text{Ar}]3d^{10}$) and the double- ζ basis set treats the remaining

$(4s^2 4p^6 4d^7 5s^1, 16 \text{ electrons})$.

7.4 6-31G and 6-31G(d) Basis Sets

These two basis sets were used for all calculations with the atoms C, N, O, and Cl. This explains the reason why they are reviewed here in more detail.

7.4.1 6-31G

This is a Pople-type split valence basis set. For each atom (except H) in the molecule, the 6-31G basis, consists of one contracted Gaussian composed of six primitives for each core orbital and two functions for each valence-shell orbital, a contracted Gaussian of three primitives and a single uncontracted primitive. An example of the carbon atom using this basis set means that the core orbital, ($1s$) is represented by six primitives and the four valence orbitals ($2s, 2p_x, 2p_y, 2p_z$) are represented by two contracted orbitals. Each contracted orbital contains four primitives comprised of three contracted and one uncontracted orbital. The total number of primitives required to represent the C atom is 6 (inner) + 4×4 (valence electrons) = 22 . Below is an output of orbital functions for a 6-31G basis set from GAUSSIAN 09 for the carbon atom which relates to what had been discussed previously.

Similarly, N and O will have the same number of orbital functions as C because they share the core and the valence electron orbitals.

7.4.2 6-31G(d)

This basis set was used in order to study the effect of adding the polarization function on the results. It is exactly the same as the 6-31G with the difference coming in due to the addition of six d-type polarization functions for each non-hydrogen atom.

Table 7.1 – Output of orbital functions for a 6-31G basis set from GAUSSIAN 09 for the carbon atom.

	2	0			
S	6	1.00	0.000000000000		
			0.4173511460D+04	0.1834772160D-02	
			0.6274579110D+03	0.1399462700D-01	
			0.1429020930D+03	0.6858655181D-01	
			0.4023432930D+02	0.2322408730D+00	
			0.1282021290D+02	0.4690699481D+00	
			0.4390437010D+01	0.3604551991D+00	
SP	3	1.00	0.000000000000		
			0.1162636186D+02	-0.1149611817D+00	0.6757974388D-01
			0.2716279807D+01	-0.1691174786D+00	0.3239072959D+00
			0.7722183966D+00	0.1145851947D+01	0.7408951398D+00
SP	1	1.00	0.000000000000		
			0.2120314975D+00	0.1000000000D+01	0.1000000000D+01

7.5 Basis Set Superposition Error (BSSE)

Gaussian basis sets remain the choice of many in representing molecular orbitals in electronic structure calculations [20–23]. The use of finite basis sets (basis sets that are far from the basis set limit) often introduces systematic errors in the results. BSSE is an error that arises from the use of finite basis sets. It results from calculations of the interaction energy of two weakly bound systems leading to an overestimation of the attractive interaction [24]. To understand the BSSE, we look at two basis sets for different systems, one combined and the other isolated. Pooled basis sets of two fragments in the system is closer to the basis set limit i.e., (complete basis) than is the fragment basis set in the isolated systems. The interaction energy between two molecules or atoms (monomers) close enough to form a dimer is calculated as the energy difference between the product complex AB (dimer) and its components A and B (monomers),

$$E_{int} = E(AB, r_c) - E(A, r_e) - E(B, r_e), \quad (7.10)$$

where r_c is the distance between A and B in the dimer AB and r_e is the size of the separate reactants (monomers). E_{int} is often too large, thus overestimating the stability of the complex. Several methods have been used to minimize the BSSE; they are discussed below.

7.5.1 Counterpoise Method

The counterpoise method (CP)[25] is an approximate method for estimating the size of the BSSE. In this method, the energies of the monomer are calculated by using the same (combined) basis set as the dimer. The CP corrected interaction energy is calculated as,

$$E_{int}(CP) = E(AB, r_c)^{AB} - E(A, r_e)^{AB} - E(B, r_e)^{AB}. \quad (7.11)$$

Superscripts AB indicate that the complex and the separate components are calculated in the same (combined) basis. This method tends to overestimate the BSSE effect. The overestimation can be attributed to the fact that the full basis set is used for the monomer calculations.

7.5.2 Chemical Hamiltonian Approach

The chemical Hamiltonian approach (CHA) [26] eliminates the BSSE in the conventional Hamiltonian with a new one designed to prevent basis set mixing. This is done by removing all the projector-containing terms which would allow basis set extension removing the terms of the Hamiltonian making BSSE.

7.5.3 Other Methods

Other methods [24] used to reduce the BSSE include; The same number of optimized parameters (SNOOP) method. In this method, there is an identical number of wave function parameters in the monomer and dimer calculations at both the HF and correlated levels of theory. The LSDALTON

2016 program [27] has been used to do these calculations. The restricted localized orbital (RLO) has been used to estimate intramolecular BSSE.

Bibliography

- [1] K. I. Ramachandran, G. Deepa, and K. Namboori. *Computational Chemistry and Molecular Modeling: Principles and Applications*. Springer Berlin Heidelberg, 2008. ISBN 9783540773023.
- [2] C. C. J. Roothaan. New developments in molecular orbital theory. *Rev. Mod. Phys.*, 23(2):69, 1951.
- [3] F. Jensen. *Introduction to Computational Chemistry*. Wiley, Great Britain, 1999. ISBN 9780471980858,0471980854,0471984256.
- [4] J. C. Slater. Atomic shielding constants. *Phys. Rev.*, 36(1):57, 1930.
- [5] X. L. Yang, S. H. Guo, F. T. Chan, K. W. Wong, and W. Y. Ching. Analytic solution of a two-dimensional hydrogen atom. I. Nonrelativistic theory. *Phys. Rev. A*, 43(3):1186, 1991.
- [6] Valerio Magnasco. *Methods of Molecular Quantum Mechanics : An Introduction to Electronic Molecular Structure*. John Wiley and Sons, 2009.
- [7] G. B. Arfken and H. J. Weber. *Mathematical Methods for Physicists*. Elsevier Science, Netherlands, 2013. ISBN 9781483288062.
- [8] I. Ema, D. L. V. Garcia, G. Ramírez, R. López, R. J. Fernández, H. Meissner, and J. Paldus. Polarized basis sets of Slater-type orbitals: H to Ne atoms. *J. Comp. Chem.*, 24(7):859–868, 2003.
- [9] M. Springborg. *Methods of Electronic-Structure Calculations - from Molecules to Solids*. Wiley-VCH, New York, 2000.
- [10] Evert Jan Baerends, Tom Ziegler, A. J. Atkins, Jochen Autschbach, Donald Bashford, O. Baseggio, A. Bérces, F. Matthias Bickelhaupt, C. Bo, P. M. Boerritger, Luigi Cavallo, C. Daul, D. P. Chong, D. V. Chulhai, L. Deng, R. M. Dickson, J. M. Dieterich, D. E. Ellis, M. van Faassen, A. Ghysels, A. Giammona, Stan J. A. van Gisbergen, A. Goez,

- A. W. Götz, S. Gusarov, F. E. Harris, P. van den Hoek, Z. Hu, Christoph R. Jacob, H. Jacobsen, L. Jensen, L. Joubert, J. W. Kaminski, G. van Kessel, C. König, F. Kootstra, A. Kovalenko, Mykhaylo Krykunov, Erik van Lenthe, D. A. McCormack, A. Michalak, M. Mitoraj, S. M. Morton, Johannes Neugebauer, V. P. Nicu, Louis Noodleman, V. P. Osinga, S. Patchkovskii, Michele Pavanello, C. A. Peeples, Pierre Herman Theodoor Philipsen, D. Post, Cory C. Pye, H. Ramanantoanina, P. Ramos, W. Ravenek, J. I. Rodríguez, P. Ros, R. Rüger, P. R. T. Schipper, D. Schlüns, H. van Schoot, G. Schreckenbach, J. S. Seldenthuis, Mike Seth, Jaap G. Snijders, Miquel Solà, Stener M., M. Swart, D. Swerhone, G. te Velde, V. Tognetti, P. Vernooijs, L. Versluis, Lucas Visscher, O. Visser, Fan Wang, T. A. Wesolowski, E. M. van Wezenbeek, G. Wiesenekker, S. K. Wolff, T. K. Woo, and A. L. Yakovlev. ADF2017, SCM, Theoretical Chemistry, Vrije Universiteit, Amsterdam, The Netherlands, <https://www.scm.com>.
- [11] R. Poirier, R. Kari, and I. G. Csizmadia. *Handbook of Gaussian basis sets: A compendium for ab-initio molecular orbital calculations*, volume 24 of *Physical Sciences Data*. Elsevier, 1985. ISBN 9780444424938.
- [12] F. Jensen. Atomic orbital basis sets. *WIREs Comput. Mol. Sci.*, 3(3): 273–295, 2013.
- [13] W. J. Pietro and W. J. Hehre. Molecular orbital theory of the properties of inorganic and organometallic compounds. 3. STO-3G basis sets for first- and second-row transition metals. *J. Comp. Chem.*, 4(2):241–251, 1983.
- [14] W. J. Hehre, R. F. Stewart, and J. A. Pople. Self-consistent molecular-orbital methods. I. Use of gaussian expansions of Slater-type atomic orbitals. *J. Chem. Phys.*, 51(6):2657–2664, 1969.
- [15] J. B. Collins, P. R. Schleyer, J. S. Binkley, and J. A. Pople. Self-consistent molecular orbital methods. XVII. geometries and binding energies of second-row molecules. a comparison of three basis sets. *J. Chem. Phys.*, 64(12):5142–5151, 1976.

- [16] Cramer C. J. *Essentials of Computational Chemistry Theories and Models*. Wiley, Great Britain, 2nd edition, 2004.
- [17] R. Krishnan, M. J. Frisch, and J. A. Pople. Contribution of triple substitutions to the electron correlation energy in fourth order perturbation theory. *J. Chem. Phys.*, 72(7):4244–4245, 1980.
- [18] P. W. Atkins and R. S. Friedman. *Molecular Quantum Mechanics*. Oxford University Press, Oxford, 2011. ISBN 9780199541423.
- [19] T. R. Cundari, M. T. Benson, M. L. Lutz, and S. O. Sommerer. *Effective Core Potential Approaches to the Chemistry of the Heavier Elements*, pages 145–202. John Wiley and Sons, Inc., 2007. ISBN 9780470125854. doi: 10.1002/9780470125854.ch3.
- [20] C. M. Wawire, D. Jouvenot, F. Loiseau, P. Baudin, S. Liatard, L. Njenga, G. Kamau, and M. E. Casida. Density-functional study of luminescence in polypyridine ruthenium complexes. *J. Photochem. and Photobiol. A*, 276:8, 2014.
- [21] Q. Sun, B. Dereka, E. Vauthey, L. M. Lawson-Daku, and A. Hauser. Ultrafast transient IR spectroscopy and DFT calculations of ruthenium (II) polypyridyl complexes. *Chem. Sci.*, 8(1):223–230, 2017.
- [22] N. Yoshikawa, S. Yamabe, S. Sakaki, N. Kanehisa, T. Inoue, and H. Takashima. Transition states of the $^3\text{MLCT}$ to ^3MC conversion in $[\text{Ru}(\text{bpy})_2(\text{phen derivative})]^{2+}$ complexes. *J. Mol. Struct.*, 1094: 98–108, 2015.
- [23] C. Daniel. Photochemistry and photophysics of transition metal complexes: Quantum chemistry. *Coord. Chem. Rev.*, 282-283:19, 2015.
- [24] F. Jensen. Using valence bond methods to estimate intramolecular basis set superposition errors. *J. Chem. Phys.*, 146(18):184109, 2017.
- [25] F. Jensen. An atomic counterpoise method for estimating inter and intramolecular basis set superposition errors. *J. Chem. Theory Comput.*, 6(1):100–106, 2009.

- [26] B. I. Mayer. BSSE-free second-order intermolecular perturbation theory. *Mol. Phys.*, 92(3):503–510, 1997.
- [27] Kęstutis Aidas, Celestino Angeli, Keld L. Bak, Vebjørn Bakken, Radovan Bast, Linus Boman, Ove Christiansen, Renzo Cimiraglia, Sonia Coriani, Pål Dahle, Erik K. Dalskov, Ulf Ekström, Thomas Enevoldsen, Janus J. Eriksen, Patrick Ettenhuber, Berta Fernández, Lara Ferrighi, Heike Fliegl, Luca Frediani, Kasper Hald, Asger Halkier, Christof Hättig, Hanne Heiberg, Trygve Helgaker, Alf Christian Hennum, Hinne Hettema, Eirik Hjertenæs, Stinne Høst, Ida-Marie Høyvik, Maria Francesca Iozzi, Branislav Jansík, Hans Jørgen Aa. Jensen, Dan Jonsson, Poul Jørgensen, Joanna Kauczor, Sheela Kirpekar, Thomas Kjærgaard, Wim Klopper, Stefan Knecht, Rika Kobayashi, Henrik Koch, Jacob Kongsted, Andreas Krapp, Kasper Kristensen, Andrea Ligabue, Ola B Lutnæs, Juan I. Melo, Kurt V. Mikkelsen, Rolf H. Myhre, Christian Neiss, Christian B. Nielsen, Patrick Norman, Jeppe Olsen, Jógvan Magnus H. Olsen, Anders Osted, Martin J. Packer, Filip Pawłowski, Thomas B. Pedersen, Patricio F. Provasi, Simen Reine, Zilvinas Rinkevicius, Torgeir A. Ruden, Kenneth Ruud, Vladimir V. Rybkin, Pawel Sałek, Claire C. M. Samson, Alfredo Sánchez de Merás, Trond Saue, Stephan P. A. Sauer, Bernd Schimmelpfennig, Kristian Sneskov, Arnfinn H. Steindal, Kristian O. Sylvester-Hvid, Peter R. Taylor, Andrew M. Teale, Erik I. Tellgren, David P. Tew, Andreas J. Thorvaldsen, Lea Thøgersen, Olav Vahtras, Mark A. Watson, David J. D. Wilson, Marcin Ziolkowski, and Hans Ågren. The Dalton quantum chemistry program system. *WIREs Comput. Mol. Sci.*, 4(3):269–284, 2014. doi: 10.1002/wcms.1172.

Chapter 8

Partial Density of States (PDOS)

Partial density of states (PDOS) analysis is a well-established procedure in condensed matter theory, though there are several variants of the PDOS procedure to be found in the literature. The variant we use is essentially the same as the one proposed by Roald Hoffmann and sketched on pp. 32-36 of Ref. [1]. For concreteness, we give here a brief description of our PDOS analysis.

The density of states (DOS) function is given by,

$$\text{DOS}(\epsilon) = \sum_i g(\epsilon - \epsilon_i), \quad (8.1)$$

where g is a normalized gaussian,

$$\int g(\epsilon) d\epsilon = 1, \quad (8.2)$$

with fixed full-width-at-half-maximum (FWHM, chosen to be 1 eV in the present study) and ϵ_i is the energy of the i th molecular orbital (MO). The formula for the PDOS for the μ th atomic orbital (AO) is,

$$\text{PDOS}_\mu(\epsilon) = \sum_i q_{\mu,i} g(\epsilon - \epsilon_i), \quad (8.3)$$

where $q_{\mu,i}$ is the Mulliken charge of the μ th AO in the i th MO. It is calculated as,

$$q_{\mu,i} = \sum_{\nu} S_{\mu,\nu} P_{\mu,\nu}, \quad (8.4)$$

where,

$$S_{\mu,\nu} = \langle \mu | \nu \rangle, \quad (8.5)$$

is the AO overlap matrix and,

$$P_{\mu,\nu}^{(i)} = C_{\nu,i} C_{\mu,i}, \quad (8.6)$$

is the i th MO density matrix calculated from the MO coefficient matrix, \mathbf{C} . Normally we are interested in the PDOS for a group of orbitals (such as all the d orbitals on the ruthenium atom). In that case, the appropriate PDOS is obtained as a sum over the PDOS of all relevant orbitals,

$$\text{PDOS}(\epsilon) = \sum_{\mu} \text{PDOS}_{\mu}(\epsilon). \quad (8.7)$$

These equations were implemented in our own in-house PYTHON program PDOS.PY. PDOS.PY has the same functionality as the PYTHON program GAUSSSUM (<http://gausssum.sourceforge.net/>) and against which it has been checked.

An advantage of PDOS.PY is that multiple PDOS as well as the total DOS may be plotted on the same graph. We needed this for the present work and it does not seem to be very easy to do with GAUSSSUM. All of the PDOS figures presented in the main article and in this supplementary material were prepared using PDOS.PY.

Users of GAUSSSUM should note that GAUSSSUM and PDOS.PY differ in their definitions of the gaussian convolution. In GAUSSSUM, the gaussians always have unit height. In PDOS.PY, the gaussians always have unit area. This latter choice seems more logical to us. This means that the ratio of

peak heights calculated with GAUSSSUM to that of PDOS.PY is,

$$\frac{\text{GAUSSSUM}}{\text{PDOS.PY}} = \sqrt{\frac{\pi}{\log 2}} \frac{\text{FWHM}}{2}. \quad (8.8)$$

Bibliography

- [1] R. Hoffmann. *Solids and Surfaces: A Chemist's View of Bonding in Extended Structures*. VCH Publishers, New York, 1988.

Chapter 9

Time-Dependent Density Functional Theory

*“DFT and TD-DFT are like identical twins who are born at the same time
but change with time and separation.”*

MAGERO Denis.

Among the other references quoted in text, this chapter is also based on references [1–15].

The Hohenberg-Kohn-Sham DFT makes exclusive use of the ground-state electron density ($\rho(\vec{r})$) to completely describe the N -electron system, thus, it is limited to ground-state time-independent problems. As chemists, we are also interested in phenomena occurring in electronic excited-states and those may be derived from an aspect of time evolution. For instance in our case, we need to look at the excited-state spectra which is just one among the many excited-state phenomena of interest in chemistry. Time-dependent density-functional theory (TD-DFT) has been specifically tailored to address excited-state problems. It is not surprising at all if we compare DFT and TD-DFT to identical twins who are born at the same time but changes come in with time and separation. This is because both methods have a similar idea of replacing the wave function Ψ with the spin density ρ , which is a simpler object. In TD-DFT, the complicated many-body time-dependent

Schrödinger equation is replaced by a set of time-dependent single-particle equations whose orbitals result in the same time-dependent density $\rho(\vec{r}, t)$. The time-dependent density $\rho(\vec{r}, t)$ is simply a function of how electrons are distributed in the system at a given time.

The next sections describe the formalism of TD-DFT starting from the Runge-Gross theorem [16], time-dependent generalization of the Hohenberg-Kohn theorem [17], Kohn-Sham construction [18], exchange-correlation (xc) functionals and ending with the Casida equation.

9.1 Time-Dependent Schrödinger Equation

We start by considering an N -electron system with coordinates $r = (\vec{r}_1, \dots, \vec{r}_N)$ described by the non-relativistic time-dependent Schrödinger equation and moving in an explicitly time-dependent external scalar potential $v(\vec{r}, t)$,

$$\hat{H}(t)\Psi(t) = i\frac{\partial}{\partial t}\Psi(t) = i\frac{\partial\Psi(t)}{\partial t}. \quad (9.1)$$

Using Eq. (9.1), we can calculate the Ψ at any other time t provided that the state of the system at an initial time t_0 is known. It describes what is known as an initial value problem. This means that if you have $\Psi_0 = \Psi(t_0)$, you can obtain $\Psi(t)$ by propagating the wave function forward in time:

$$\begin{array}{c} \Psi(t_0) \\ \downarrow \\ \hat{H}\Psi(t_0) \\ \downarrow \\ i\hbar\left(\frac{\delta\Psi}{\delta t}\right)_{t=t_0} \\ \downarrow \\ \Psi(t_0 + dt) = \Psi(t_0) - \frac{i}{\hbar}\hat{H}\Psi dt. \end{array} \quad (9.2)$$

The implication is that Ψ at time t is a functional of the wave function at time t_0 , $\Psi[\Psi_0](t)$. The Hamiltonian is given as,

$$H(t) = \hat{T} + \hat{W} + \hat{V}_{ext}(t). \quad (9.3)$$

The first term is the kinetic energy expressed as,

$$\hat{T} = -\frac{1}{2} \sum_{i=1}^N \nabla_i^2, \quad (9.4)$$

the second term is the electron-electron interaction,

$$\hat{W} = \frac{1}{2} \sum_{i < j}^N \frac{1}{|\vec{r}_i - \vec{r}_j|}, \quad (9.5)$$

and the last term is the time-dependent potential operator,

$$\hat{V}_{ext}(t) = \sum_{i=1}^N v_{ext}(\vec{r}_i, t). \quad (9.6)$$

As one moves from time, $t = t_0$ to $t = t_n$, the system also evolves in time from an initial state at $t = t_0$ to some state at $t = t_n$ and changes in density also come with the evolution. The electron density can be calculated as,

$$\rho(\vec{r}, t) = N \int d^3\vec{r}_2 \dots \int d^3\vec{r}_N |\Psi(\vec{r}, \vec{r}_2, \dots, \vec{r}_N, t)|^2, \quad (9.7)$$

where $\rho(\vec{r}, t)d^3\vec{r}$ is the probability of finding an electron in a region $d^3\vec{r}$ at time t . The density is normalized to the number of electrons:

$$\int d^3\vec{r} \rho(\vec{r}, t) = N. \quad (9.8)$$

From Eq. (9.1), the associated value of a physical observable, \hat{O} is obtained from the expectation value,

$$\langle O \rangle(t) = \langle \Psi(t) | \hat{O} | \Psi(t) \rangle \quad (9.9)$$

From the above equation, the current density \vec{j} can be expressed. Since the formal TD-DFT is ultimately based upon \vec{j} , it is only logical to show that O are functionals of the time-dependent charge density. Ideally, the TD density

gives all the information that is needed about the electronic problem. The Runge-Gross theorem shows this logic.

9.2 First Runge-Gross theorem

TD-DFT [19] has been improving over the years with new developments being incorporated. The basic mathematical foundations of TD-DFT are presented in the Runge-Gross theorem [20]. It formalizes the TD generalization of the Hohenberg-Kohn theorem as well its construction.

The Runge-Gross theorem is thus a proof that two spatially-different external potentials cannot induce the same time-dependent densities. It deals with the quantum states arising from a fixed initial state. This is because the TD Schrödinger equation is a first-order differential equation in the time coordinate.

Theorem 3 (Existence Theorem) *In other words, the densities $\rho(\vec{r}, t)$ and $\rho'(\vec{r}, t)$ evolving from a common initial state Ψ_0 under the influence of two potentials $v(\vec{r}, t)$ and $v'(\vec{r}, t)$ both Taylor-expandable around t_0 are always different provided that the potentials differ by more than a purely time-dependent function $c(t)$. The external potential is assumed to be time-independent for $t < t_0$ and the time-dependent field comes on exactly at time t_0 . That is,*

$$v(\vec{r}, t) \neq v'(\vec{r}, t) + c(t) \Rightarrow \rho(\vec{r}, t) \neq \rho'(\vec{r}, t). \quad (9.10)$$

Figure 9.1 is an illustration of the Runge-Gross theorem.

This theorem is analogous to the first Hohenberg-Kohn theorem of DFT. There is a one-to-one correspondence between the external potential and the density and the TD potential is a functional of the TD density unique up to a time-dependent phase $\alpha(t)$.

$$\Psi(t) = \Psi[\rho, \Psi_0](t)e^{i\alpha(t)}, \quad (9.11)$$

For a system is in its ground-state,

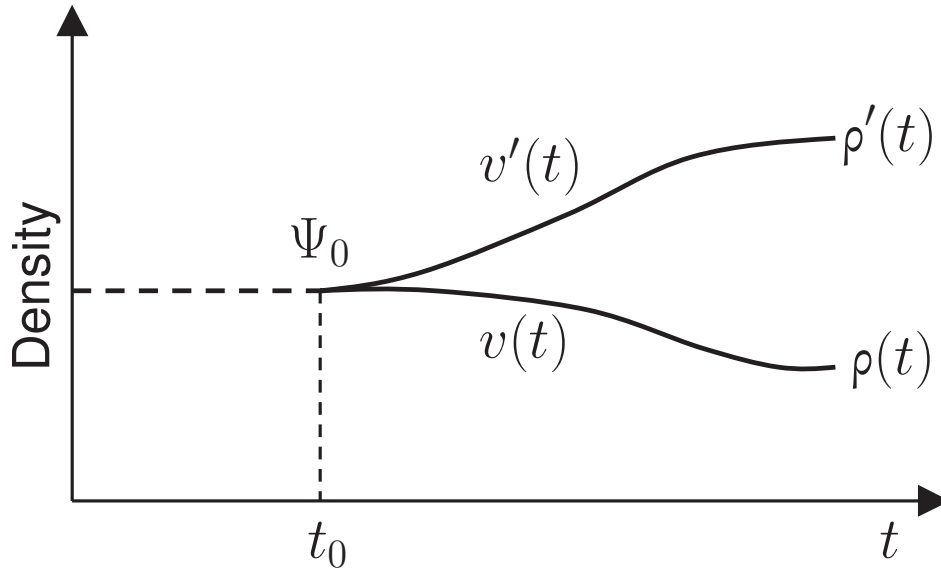


Figure 9.1 – Runge-Gross theorem: A pictorial illustration.

$$\Psi(t) = \Psi[\rho](t)e^{i\alpha(t)}. \quad (9.12)$$

The above theorem can be proven by showing that two potentials differing by more than a function of time ($v \neq v' + c(t)$) produce different current densities, \vec{j} and \vec{j}' generated by v and v' . More details about the proof can be found in Ref. [21].

9.3 Second Runge-Gross theorem

At this point, one would expect that this section would be second Hohenberg-Kohn theorem since in static quantum mechanics, the ground-state of the system can be determined through the minimization of the total energy functional, $E[\Psi] = \langle \Psi | \hat{H} | \Psi \rangle$, analogous to the Rayleigh-Ritz variational principle. That is not the case however! This is because in TD systems, there is no variational principle on the basis of the total energy for it is not a conserved quantity. For the TD systems, time evolution is derived from

stationary-action (variational) principle. What is used here is the; ***Frenkel-Dirac variational principle*** which involves finding the stationary points of the action,

$$A = \int_{t_0}^{t_1} dt \langle \Psi(t) | i \frac{\partial}{\partial t} - \hat{H}(t) | \Psi(t) \rangle, \quad (9.13)$$

subject to the condition that $\delta\Psi(t_0) = \delta\Psi(t_1) = 0$ yields the time-dependent Schrödinger equation.

$$\hat{H}(t)\Psi(t) = -i \frac{\partial}{\partial t} \Psi(t). \quad (9.14)$$

It however faces the limitation that the density must be v -representable. This is a disadvantage in itself because it is difficult to develop the exact formalism since the condition limits the range of possible variations with the unexpected result that $A = 0$ will have other solutions besides the exact $\rho(t)$. This problem will be discussed under the TD Kohn-Sham equation.

The time-dependent Schrödinger equation can be solved by calculating the stationary point of the functional $A[\rho]$ because the action, A , is a density functional. It then follows that its solution can be obtained by the function $\Psi(t)$ that makes the functional stationary. $A[\rho]$ is stationary at the exact density of the system, that is,

$$\frac{\delta A}{\delta \rho(\vec{r}, t)} = 0 = \int_{t_0}^{t_1} dt' \langle \frac{\delta \Psi(t')}{\delta \rho(\vec{r}, t)} | i \frac{\partial}{\partial t'} - \hat{H}(t') | \Psi(t') \rangle + c.c., \quad (9.15)$$

From this equation, it can be seen that the phase factor simply contributes an additive constant, $A = A[\rho] + \text{constant}$. The additive constant is rendered immaterial with the application of the variational condition, Eq. (9.13) and this provides the analogue of the second HK theorem for TD-DFT. The action functional is now written as,

$$A[\rho] = S[\rho] - \int_{t_0}^{t_1} \int \rho(\vec{r}, t) v_{ext}(\vec{r}, t) dt d\vec{r}, \quad (9.16)$$

which defines $S[\rho]$. $S[\rho]$ is a universal functional independent of the external

potential v defined as,

$$S[\rho] = \sum_i f_i \int_{t_0}^{t_1} \left\langle \psi_i(t) \left| i \frac{\partial}{\partial t} - \frac{1}{2} \nabla^2 \right| \psi_i(t) \right\rangle dt - \frac{1}{2} \int_{t_0}^{t_1} \iint \frac{\rho(\vec{r}_1, t) \rho(\vec{r}_2, t)}{\vec{r}_1 \vec{r}_2} d\vec{r}_1 d\vec{r}_2 dt - A_{xc}[\rho], \quad (9.17)$$

where $\rho(\vec{r}, t) = \sum_i f_i |\psi_i(\vec{r}, t)|^2$. The assumption here is that there is a similar dependence for $\rho(\vec{r}, t)$ and $v_{ext}(\vec{r}, t)$. Given a trial function such as one of single-determinantal form, the Frenkel-Dirac variational principle can be used to derive an approximate time-dependent equation.

9.4 Time-Dependent Kohn-Sham Equation

The Runge-Gross theorem tells us that ideally, all observables can be calculated with the knowledge of the one-body density. The problem however has always been: how do you calculate the one-body density? This problem was however addressed thanks to the Kohn and Sham idea of using an auxiliary system of non-interacting KS electrons subject to an external local potential (v_{KS}) to solve the interacting Schrödinger equation [22]. KS equations for TD systems can be derived by assuming the existence of a potential, $v_{\text{eff}}(\vec{r}, t)$ whose orbitals $\psi_i(\vec{r}, t)$ yield the same charge density $\rho(\vec{r}, t)$ as the interacting system, the same way that it is done for the time independent case. The minimization of the action [Eq. (9.16)] leads to the TD Kohn-Sham equation,

$$i \frac{\partial}{\partial t} \Psi(\vec{r}, t) = \left[-\frac{1}{2} \nabla^2 + v_{KS}(\vec{r}, t) \right] \Psi(\vec{r}, t). \quad (9.18)$$

The KS electrons obey this equation. Since the KS system does not interact, its wave function is simply a Slater determinant of N occupied single-particle orbitals and the density of the non-interacting system is obtained from the TD KS orbitals according to,

$$\rho(\vec{r}, t) = \sum_i^{occ} |\psi(\vec{r}, t)|^2. \quad (9.19)$$

The solution of Eq. (9.18) yields the true density $\rho(\vec{r}, t)$ of the interacting system without the need to calculate the many-body wave function. The next step involves applying the RG theorem to the non-interacting system of electrons in the KS potential v_{KS} , in a manner analogous to what was done for the interacting electrons. The implication is a one-to-one correspondence between a given density $\rho(\vec{r}, t)$ and the KS potential that yields that density given that the initial KS Slater determinant is fixed:

$$\rho(\vec{r}, t) \leftrightarrow v_{KS}(\vec{r}, t). \quad (9.20)$$

Thus, v_{KS} is a unique functional of the density and initial state,

$$v_{KS}(\vec{r}, t) \equiv v_{KS}[\rho, \Psi_0](\vec{r}, t). \quad (9.21)$$

The KS potential, v_{KS} (TD effective potential) can be decomposed into,

$$v_{KS}(\vec{r}, t) = v_{ext}(\vec{r}, t) + v_{Hartree}(\vec{r}, t) + v_{xc}(\vec{r}, t), \quad (9.22)$$

where $v_{ext}(\vec{r}, t)$ is the external potential, $v_{Hartree}(\vec{r}, t)$ is the Hartree potential $= \int d^3r' \frac{\rho(\vec{r}, t)}{|\vec{r}-\vec{r}'|}$ that depends on the instantaneous TD density only and $v_{xc}(\vec{r}, t)$ is the exchange correlation (xc) potential. In ground-state DFT, v_{xc} is written as a functional derivative of the xc energy. However, the extension of this formulation to the TD case is not straightforward because of a problem related to causality [23]. This problem arises because time propagation in TD means that $\psi(t_0)$ actually determines $\psi(t_1)$. Van Leeuwen solved the problem by using the Keldish formalism to define a new action functional \tilde{A} [23]. The TD exchange-correlation potential, v_{xc} can be expressed in terms of the new exchange correlation action functional as [23],

$$v_{xc}(\vec{r}, t) = \frac{\delta \tilde{A}_{xc}[\rho]}{\delta \rho(\vec{r}, t)}. \quad (9.23)$$

However, the exact TD exchange correlation action functional (xc kernel) is unknown and approximations must be used in practical implementations of TD-DFT. The next section deals with v_{xc} approximations used in TD-DFT.

9.5 Exchange-Correlation Potentials

The exact TD-DFT v_{xc} is unknown and hence must be approximated. The exact exchange-correlation potential depends on the entire history of the density.

The Adiabatic Approximation (AA) is the simplest and most successful TD xc-approximation. It ignores all dependence on the history and allows only a dependence on the instantaneous density. In other words, the AA is said to be a local approximation in time. It is written as,

$$\begin{aligned} v_{xc}^{adia}[\rho](\vec{r}, t) &= \frac{\delta A_{xc}[\rho]}{\delta \rho(\vec{r}, t)}, \\ &\cong \frac{\delta E_{xc}[\rho(t)]}{\delta \rho(\vec{r}; t)}, \\ &= v_{xc}^{approx}[\rho(t)](\vec{r}), \end{aligned} \quad (9.24)$$

where,

$$A_{xc} = \int_{t_0}^{t_1} E_{xc}[\rho(t)]. \quad (9.25)$$

E_{xc} is the exchange correlation functional of TD Kohn Sham theory, $\rho(t)$ is the density ρ at time, t . $v_{xc}^{adia}[\rho](\vec{r}, t)$ is a function of four variables (x, y, z, t) and the spin while $\rho(\vec{r}; t)$ is a function of x, y , and z since t is regarded as a fixed parameter. The flexibility of this variable makes it possible to use all the approximate functionals E_{xc} from ground-state DFT in TD-DFT. The AA approximation has been remarkably successful in calculating optical spectra and effectively defines conventional TD-DFT.

9.6 Linear Response Theory (LR)

The ultimate goal of many, if not all chemists is to study excited-state properties. Time-dependent density functional theory forms the basis used to calculate excitation energies and optical spectra because it captures the essential dynamical nature of an excitation process. In particular, the linear response theory (LR) [24] is used when considering response of a molecular property (dynamic polarizability) to a weak time-dependent external perturbation of the unperturbed molecule. It is a way of describing how matter interacts with the electromagnetic field. The weak perturbation may be compared with a spectroscopy experiment. The LR of a system will contain all the information about its excitation spectrum. It determines single excitation energies of molecules from first principles. Simply put, the response theory figures out how a system reacts to outside influences. Linear response theory can be depicted schematically as in Fig. 9.2.



Figure 9.2 – An illustration of the LR theory

9.7 Linear Response TD-DFT (LR TD-DFT)

In this section a discussion of the Fourier-transformed frequency domain (ω) is done. Spectral information about the system can be obtained from the KS orbitals since they reproduce the exact density in frequency-space, and

via a Fourier-transform of the KS orbitals in a similar manner as in Sec. 9.4. In a consistent step by step manner, it will be shown how LR TD-DFT can be used to extract linear absorption spectra by inducing small perturbations to the KS orbitals [25].

9.7.1 Time-dependent linear density response

Three components will be key in describing the TD linear response density, the Hamiltonian, $\hat{H}(t)$, Eq. (9.3), TD external perturbation $\delta v_{ext}(\vec{r}, t)$ and the external potential $v_{ext}(\vec{r})$ at $t < t_0$, the ground-state (Ψ_0) and at $t > t_0$ where there is time evolution. For convenience, bra ($\langle |$) ket ($| \rangle$) [26] notation has been used. Thus, the ground-state (Ψ_0) at $t < t_0$ can be expressed as $|\Psi_0\rangle$. A small perturbation, $\delta v_{ext}(\vec{r}, t)$, is slowly introduced in the KS Hamiltonian at $t = t_0$. Considering the two variables of time at $t < t_0$ and $t > t_0$, $v_{ext}(\vec{r}, t)$ is given as,

$$t < t_0, \quad v_{ext}(\vec{r}, t) = v_{ext}(\vec{r}) \quad \text{and}, \quad (9.26)$$

$$t > t_0, \quad v_{ext}(\vec{r}, t) = v_{ext}(\vec{r}) + \delta v_{ext}(\vec{r}, t). \quad (9.27)$$

This means that at $t < t_0$, the density evolution is simply the ground-state density $\rho_0(\vec{r})$ and the density at $t > t_0$ is time-dependent starting from the ground-state density as shown below,

$$t < t_0, \quad \rho(\vec{r}, t) = \rho_0(\vec{r}) \quad \text{and}, \quad (9.28)$$

$$t > t_0, \quad \rho(\vec{r}, t) = \rho_0(\vec{r}) + \delta\rho(\vec{r}, t). \quad (9.29)$$

$\rho(\vec{r}, t)$ can be expanded in powers of the potential as,

$$\rho(\vec{r}, t) = \rho_0(\vec{r}) + \delta\rho(\vec{r}, t) + \dots, \quad (9.30)$$

Since we are interested in the density evolution with time, we keep the first order term, $\delta\rho(\vec{r}, t)$. It is possible to relate $\delta\rho(\vec{r}, t)$ and $\delta v_{ext}(\vec{r}, t)$ mathematically as,

$$\delta\rho(\vec{r}, t) = \int d^3r' \int dt' \chi_{\rho\rho}(\vec{r}, \vec{r}'; t - t') \delta v_{ext}(\vec{r}', t'). \quad (9.31)$$

This is known as the linear density response, $\delta\rho(\vec{r}, t)$ to the perturbation $\delta v_{ext}(\vec{r}, t)$. The density-density response function or generalized susceptibility, $\chi_{\rho\rho}(\vec{r}, \vec{r}'; t - t')$ can be expressed in terms functionals as,

$$\chi_{\rho\rho}(\vec{r}, \vec{r}'; t - t') = \left. \frac{\delta\rho[v_{ext}](\vec{r}, t)}{\delta v_{ext}(\vec{r}', t')} \right|_{v_{ext}[\rho_0]},$$

or

$$\chi_{\rho\rho}(\vec{r}, \vec{r}'; t - t') = -i\Theta(t - t') \langle \Psi_0 | [\hat{\rho}(\vec{r}, t - t'), \hat{\rho}(\vec{r}')] | \Psi_0 \rangle, \quad (9.32)$$

where

$$\hat{\rho}(\vec{r}) = \sum_r \Psi_r(\vec{r}) \Psi_r^*(\vec{r}) \hat{a}_r^\dagger \hat{a}_r \quad (2^{\text{nd}} \text{ quantization}),$$

where $\Theta(t - t')$ is known as the Heaviside step function that takes care of causality. A Fourier transform of Eq. (9.32) gives spectral information about the system, that is, $\chi_{\rho\rho}(\vec{r}, \vec{r}'; t - t')$ becomes $\chi_{\rho\rho}(\vec{r}, \vec{r}'; \omega)$. The Lehmann representation of the density density response function given as,

$$\chi_{\rho\rho}(\vec{r}, \vec{r}', \omega) = \sum_n \left[\frac{\langle \Psi_0 | \hat{\rho}(\vec{r}) | \Psi_n \rangle \langle \Psi_n | \hat{\rho}(\vec{r}') | \Psi_0 \rangle}{\omega - \omega_{n0} + i\eta} - \frac{\langle \Psi_0 | \hat{\rho}(\vec{r}') | \Psi_n \rangle \langle \Psi_n | \hat{\rho}(\vec{r}) | \Psi_0 \rangle}{\omega + \omega_{n0} + i\eta} \right]. \quad (9.33)$$

Equation (9.33) forms the core of LR theory since it shows explicitly how a frequency-dependent perturbation couples to the excitation spectrum of a system. Excitation energies lie at the poles of $\chi_{\rho\rho}$ and oscillator strengths are obtained from the residues. We can also get the absorption spectrum by taking the imaginary part of Eq. (9.33). We wish to show how the spectral

function,

$$S(\omega) = \sum_I f_I [\delta(\omega - \omega_I) + \delta(\omega + \omega_I)] , \quad (9.34)$$

may be calculated from the dynamic polarizability,

$$\alpha(\omega) = \sum_I \frac{f_I}{\omega_I^2 - \omega^2} , \quad (9.35)$$

as

$$S(\omega) = \frac{2\omega}{\pi} \lim_{\eta \rightarrow 0} \alpha(\omega + i\eta) . \quad (9.36)$$

We do this by noticing that

$$\alpha(\omega) = \sum_I \left(\frac{f_I}{2\omega} \right) \left(\frac{1}{\omega_I - \omega} - \frac{1}{\omega_I + \omega} \right) , \quad (9.37)$$

so that,

$$\begin{aligned} \frac{2\omega}{\pi} \alpha(\omega + i\eta) &= \sum_I \frac{f_I}{\pi} \left(\frac{1}{\omega_I - \omega - i\eta} - \frac{1}{\omega_I + \omega + i\eta} \right) \\ &= \sum_I \frac{f_I}{\pi} \left[\frac{\omega_I - \omega + i\eta}{(\omega_I - \omega - i\eta)(\omega_I - \omega + i\eta)} \right] \\ &\quad - \sum_I \frac{f_I}{\pi} \left[\frac{\omega_I + \omega - i\eta}{(\omega_I + \omega + i\eta)(\omega_I + \omega - i\eta)} \right] \\ &= \sum_I \frac{f_I}{\pi} \left[\frac{\omega_I - \omega + i\eta}{(\omega_I - \omega)^2 + \eta^2} - \frac{\omega_I + \omega - i\eta}{(\omega_I + \omega)^2 + \eta^2} \right] \\ &= \sum_I \frac{f_I}{\pi} \left[\frac{\omega_I - \omega}{(\omega_I - \omega)^2 + \eta^2} - \frac{\omega_I + \omega}{(\omega_I + \omega)^2 + \eta^2} \right] \\ &\quad + i \sum_I \frac{f_I}{\pi} \left[\frac{\eta}{(\omega_I - \omega)^2 + \eta^2} + \frac{\eta}{(\omega_I + \omega)^2 + \eta^2} \right] . \end{aligned} \quad (9.38)$$

$$+ i \sum_I \frac{f_I}{\pi} \left[\frac{\eta}{(\omega_I - \omega)^2 + \eta^2} + \frac{\eta}{(\omega_I + \omega)^2 + \eta^2} \right] . \quad (9.39)$$

It is now easy to separate the real and imaginary parts:

$$\begin{aligned}\frac{2\omega}{\pi}\Re\alpha(\omega + i\eta) &= \sum_I \frac{f_I}{\pi} \left[\frac{\omega_I - \omega}{(\omega_I - \omega)^2 + \eta^2} - \frac{\omega_I + \omega}{(\omega_I + \omega)^2 + \eta^2} \right] \\ \frac{2\omega}{\pi}\Im\alpha(\omega + i\eta) &= \sum_I \frac{f_I}{\pi} \left[\frac{\eta}{(\omega_I - \omega)^2 + \eta^2} + \frac{\eta}{(\omega_I + \omega)^2 + \eta^2} \right].\end{aligned}\quad (9.40)$$

Since the Lorentzian representation of the Dirac delta function is

$$\delta(x) = \frac{1}{\pi} \lim_{\eta \rightarrow 0} \frac{\eta}{x^2 + \eta^2}, \quad (9.41)$$

it follows that so that,

$$\frac{2\omega}{\pi} \lim_{\eta \rightarrow 0} \Im\alpha(\omega + i\eta) = \sum_I f_I [\delta(\omega_I - \omega) + \delta(\omega_I + \omega)] \quad (9.42)$$

which is just the spectral function of Eq. (9.34) because the Dirac delta function is an even function [$\delta(x) = -\delta(x)$]. Interestingly, if η is small but finite, not taking the limit simply corresponds to Lorentzian broadening of the spectral function.

9.7.2 Kohn-Sham Linear Density Response

In Sec. 9.7.1, a discussion has been made of how to extract the various quantities from the density-density response. However, the practicality of the equations discussed in Sec. 9.7.1 remains limited because it is an interacting system of electrons and thus requires an input of many-body eigenstates and eigenenergies. To make the equations more practical, we consider a fictitious system of non-interacting KS electrons that produces the same density response as the interacting system. The only difference between this section and the previous section is that here, we are considering a system of non-interacting electrons and thus utilize the KS orbitals, ϕ_i . The initial equations that share similarities have been skipped and we start from the dressed KS potential which is given as,

$$\delta v_{\text{KS}}[\rho, \Psi_0, \Phi_0](\vec{r}, t) = \delta v_{\text{ext}}[\rho](\vec{r}, t) + \int d^3\vec{r}' \frac{\delta\rho(\vec{r}', t)}{|\vec{r} - \vec{r}'|} + \delta v_{xc}[\rho, \Psi_0, \Phi_0](\vec{r}, t). \quad (9.43)$$

(but both $\Psi_0[\rho], \Phi_0[\rho]$ are eliminated if you begin from the ground-state.)
The density response is related to the KS potential by,

$$\delta\rho(\vec{r}, t) = \int d^3\vec{r}' \int dt' \chi_{\rho\rho}^{\text{KS}}(\vec{r}, \vec{r}'; t - t') \delta v_{\text{KS}}(\vec{r}', t'), \quad (9.44)$$

and the Lehmann spectral representation for the KS system is,

$$\chi_{\rho\rho}^{\text{KS}}(\vec{r}, \vec{r}'; \omega) = \sum_n \left[\frac{\langle \Phi_0 | \hat{\rho}(\vec{r}) | \Phi_n \rangle \langle \Phi_n | \hat{\rho}(\vec{r}') | \Phi_0 \rangle}{\omega - \omega_{n0}^{\text{KS}} + i\eta} - \frac{\langle \Phi_0 | \hat{\rho}(\vec{r}') | \Phi_n \rangle \langle \Phi_n | \hat{\rho}(\vec{r}) | \Phi_0 \rangle}{\omega + \omega_{n0}^{\text{KS}} + i\eta} \right], \quad (9.45)$$

where Φ_n is the excited KS determinant of the ground-state KS potential and ω_{n0}^{KS} is the corresponding KS excitation frequency. Equation (9.45) can further simplify to the sum over KS single excitations to be,

$$\chi_{\rho\rho}^{\text{KS}}(\vec{r}, \vec{r}'; \omega) = \sum_{k=0}^N \sum_{j=N+1}^{\infty} \left[\frac{\phi_j(\vec{r}) \phi_k^*(\vec{r}) \phi_j^*(\vec{r}') \phi_k(\vec{r}')}{\omega - (\epsilon_j - \epsilon_k) + i\eta} - \frac{\phi_k(\vec{r}) \phi_j^*(\vec{r}) \phi_k^*(\vec{r}') \phi_j(\vec{r}')}{\omega + (\epsilon_j - \epsilon_k) + i\eta} \right]. \quad (9.46)$$

As mentioned earlier, the $\chi_{\rho\rho}^{\text{KS}}$ results from KS single excitations and thus does not contain double and higher multiple KS excitations hence not a true representation of excitations from the interacting system. To get a true picture, there is need to relate the interacting, $\chi_{\rho\rho}$, and KS density-density response functions $\chi_{\rho\rho}^{\text{KS}}$. The equation is,

$$\begin{aligned} \chi_{\rho\rho}(\vec{r}, \vec{r}'; t - t') = & \chi_{\rho\rho}^{\text{KS}}(\vec{r}, \vec{r}'; t - t') + \int d^3x \int d\tau \int d^3x' \int d\tau' \chi_{\rho\rho}^{\text{KS}}(\vec{r}, \mathbf{x}, t - \tau) \\ & \times \left\{ \frac{\delta(\tau - \tau')}{|\mathbf{x}' - \mathbf{x}|} + f_{xc}[\rho_0](\mathbf{x}, \mathbf{x}', \tau - \tau') \right\} \chi_{\rho\rho}(\mathbf{x}', \mathbf{r}', \tau' - t'), \end{aligned} \quad (9.47)$$

where $f_{xc}[\rho_0](\vec{r}, \vec{r}', t - t')$ is the TD xc kernel defined as,

$$f_{xc}[\rho_0](\vec{r}, \vec{r}', t - t') = \left. \frac{\delta v_{xc}(\vec{r}, t)}{\delta \rho(\vec{r}', t')} \right|_{\rho(\vec{r}', t') = \rho_0}. \quad (9.48)$$

The role of f_{xc} is to bring in the missing double and higher multiple excitations that were missing in the $\chi_{\rho\rho}^{\text{KS}}$. To obtain accurate spectra in TD-DFT, accurate approximations to f_{xc} must be constructed. Doing a Fourier-transform on Eq. (9.47) gives the frequency domain equation,

$$\begin{aligned} \chi_{\rho\rho}(\vec{r}, \vec{r}'; \omega) = & \chi_{\rho\rho}^{\text{KS}}(\vec{r}, \vec{r}'; \omega) + \int d^3\vec{x} \int d^3x' \chi_{\rho\rho}^{\text{KS}}(\vec{r}, \vec{x}, \omega) \\ & \times \left\{ \frac{1}{|\vec{x}' - \vec{x}|} + f_{xc}[\rho_0](\vec{x}, \vec{x}', \omega) \right\} \chi_{\rho\rho}(\vec{x}', \vec{r}', \omega). \end{aligned} \quad (9.49)$$

From the Eq. (9.49), we can see that two situations arise, one ideal and the other of practical. Looking at the ideal situation: from the ground-state DFT, the $\chi_{\rho\rho}^{\text{KS}}$ can be constructed and $\chi_{\rho\rho}$ solved self-consistently. Practically, as will be seen in the next section under the Casida equations, it has to be rewritten as a non-linear eigenvalue problem in terms of matrices represented in a basis set of molecular orbitals.

9.8 Casida Equations

As mentioned earlier, we are interested in the response of a system initially in a stationary state (ground-state), Ψ_0 , to a weak external perturbation. Typically, we can obtain the dynamic response of the charge density

from TD-DFT. There are several methods that can be used to extract excitations from TD-DFT: A case in point is the absorption spectrum obtained from the poles of the excitation energies, ω_I and the oscillator strengths, f_I . The biggest challenge has been how to compute the said quantities accurately. This challenge was overcome in 1995 by Casida, [27], by using the Casida equations that efficiently convert the search for poles of response functions into a large eigenvalue problem. He provided a procedure of how to calculate the said quantities using knowledge from the linear density response of the system by reformulating the linear response time-dependent density functional response theory to resemble the standard implementation of LR-TDHF. The dynamic polarizability, $\alpha(\omega)$, that describes the response of the dipole moment to a TD electric field can be calculated from the response of the charge density obtained from TD-DFT. With such information, the electronic excitation spectrum in the usual dipole approximation can be determined.

We can derive the Casida equation by considering an N -electron system initially in its ground stationary state, Ψ_0 , exposed to a TD perturbation turned on adiabatically at time, $t = -\infty$. The equation for the dynamic response of the KS density matrix is,

$$\left\{ \omega \begin{bmatrix} \mathbf{1} & \mathbf{0} \\ \mathbf{0} & -\mathbf{1} \end{bmatrix} - \begin{bmatrix} \mathbf{A} & \mathbf{B} \\ \mathbf{B}^* & \mathbf{A}^* \end{bmatrix} \right\} \begin{pmatrix} \delta \vec{P}(\omega) \\ \delta \vec{P}^*(\omega) \end{pmatrix} = \begin{pmatrix} \vec{v}_{appl}(\omega) \\ \vec{v}_{appl}^*(\omega) \end{pmatrix}. \quad (9.50)$$

Rearranging this expression to the form of dynamic polarizability according to the sum-over-states (SOS) relation,

$$\alpha(\omega) = \sum_{I \neq 0} \frac{f_I}{\omega_I^2 - \omega^2} \quad (9.51)$$

we can extract the excitation energies and oscillator strengths. In Eq. (9.51), f_I is given as,

$$f_I = \frac{2}{3} \omega_I (|\langle \Psi_0 | \hat{x} | \Psi_I \rangle|^2 + |\langle \Psi_0 | \hat{y} | \Psi_I \rangle|^2 + |\langle \Psi_0 | \hat{z} | \Psi_I \rangle|^2), \quad (9.52)$$

related with the excitation energy,

$$\omega_I = E_I - E_0. \quad (9.53)$$

The excitation energies, ω_I are determined by the poles of the dynamic polarizability and f_I determines the equivalent oscillator strengths. It is worth mentioning when the exciting frequency hits a resonance capable of exciting an electron, the dynamic response of the density matrix, $\vec{v}_{appl}(\omega)$, should be infinite even for a small perturbation. Considering other factors, such as the impact of the frequencies described in the previous statement to the equation for the dynamic response of the KS density matrix, Eq. (9.50), takes the form $\chi(+\infty) = 0$. It results in the matrix pseudo-eigenvalue problem that is simply an expression of the dynamic polarizability in the basis of unperturbed MOs.

$$\begin{bmatrix} \mathbf{A} & \mathbf{B} \\ \mathbf{B}^* & \mathbf{A}^* \end{bmatrix} \begin{pmatrix} \vec{X}_I \\ \vec{Y}_I \end{pmatrix} = \omega_I \begin{bmatrix} \mathbf{1} & \mathbf{0} \\ \mathbf{0} & -\mathbf{1} \end{bmatrix} \begin{pmatrix} \vec{X}_I \\ \vec{Y}_I \end{pmatrix}. \quad (9.54)$$

The pseudo-eigenvalue problem has both an excitation ($\omega_I > 0$) and de-excitation ($\omega_I < 0$) both of which are paired and whose solution can be found and only differ at the interchange of X and Y .

$$\begin{pmatrix} \vec{X}_I \\ \vec{Y}_I \end{pmatrix} \leftrightarrow \omega_I = E_I - E_0 = -\omega_I \leftrightarrow \begin{pmatrix} \vec{Y}_I \\ \vec{X}_I \end{pmatrix}. \quad (9.55)$$

Equation (9.54) can be solved in a simpler manner by introducing the Tamm-Dancoff approximation (TDA) [28]. With this approximation, the $\underline{\underline{B}}$ matrices are ignored and the solution to the following equation is sought,

$$\mathbf{A}\vec{X}_I = \omega_I\vec{X}_I. \quad (9.56)$$

The exact Eq. (9.54) can be reduced to a matrix equation similar to the TDA equation but without making approximations within the local density approximation (LDA) and generalized gradient approximation (GGA). It can be rewritten as,

$$\mathbf{\Omega}\vec{F}_I = \omega_I\vec{F}_I, \quad (9.57)$$

where,

$$\begin{aligned} \mathbf{\Omega} &= (\mathbf{A} - \mathbf{B})^{+1/2}(\mathbf{A} + \mathbf{B})(\mathbf{A} - \mathbf{B})^{+1/2} \\ \vec{F}_I &= (\mathbf{A} - \mathbf{B})^{-1/2}(\vec{X}_I + \vec{Y}_I). \end{aligned} \quad (9.58)$$

The excitation energies of the system can be obtained from the eigenvalues of Eq. (9.57) while the eigenvectors $(\vec{X}_I, \vec{Y}_I)^\dagger$ give the spectroscopic oscillator strengths and to assign the symmetry of each transition, although in practice, the symmetry of the excited-state is many times already reflected in \vec{F}_I . To solve the Casida’s equations, one is needed to diagonalize the ground-state Hamiltonian in order to get a number of the empty KS states.

9.9 ‘Deadly Sins’ of TD-DFT

‘Deadly Sins’ of TD-DFT are simply the possible sources of errors when doing calculations with TD-DFT. If one commits any of this ‘sins’, then one is likely not to go to Heaven (get accurate TD-DFT results) [29]. According to [29], there are four of them:

- Errors can arise from ground-state DFT calculation. If one begins with wrong KS orbital energies, TD-DFT calculations cannot produce accurate results. This is known as *The sin of the ground-state*.
- Errors arising from local approximations to an adiabatic $f_{xc}(r, r')$, that is properties that require nonlocality are known as *The sin of locality*.
- *The sin of forgetfulness* arises from phenomena missing when the adiabatic approximation is made, that is, properties that require nonlocality in time, and finally,
- *The sin of the wave function* arises from the difference between the true wave function and the KS wave function.

Bibliography

- [1] D. G. Tempel. *Time-Dependent Density Functional Theory for Open Quantum Systems and Quantum Computation*. PhD thesis, Harvard University, 2012.
- [2] D. Presti. *Quantum computational methodologies for the study of molecular crystals*. PhD thesis, Université Pierre et Marie Curie - Paris VI, 2015.
- [3] Fundamentals of time-dependent density functional theory. Lecture Notes in Physics. Springer Berlin Heidelberg, 2012. ISBN 9783642235177.
- [4] M. Marques. Time-dependent density functional theory. Lecture Notes in Physics. Springer, 2006. ISBN 9783540354222.
- [5] C. Fiolhais, F. Nogueira, and M. A. L. Marques. *A Primer in Density Functional Theory*. Lecture Notes in Physics. Springer Berlin Heidelberg, 2008. ISBN 9783540370727.
- [6] R. Van Leeuwen. Key concepts in time-dependent density-functional theory. *International Journal of Modern Physics B*, 15(14):1969–2023, 2001.
- [7] E. K. U. Gross, C. A. Ullrich, and U. J. Gossmann. Density functional theory of time-dependent systems. In *Density Functional Theory*, pages 149–171. Springer, 1995.
- [8] R. E. Stratmann, G. E. Scuseria, and M. J. Frisch. An efficient implementation of time-dependent density-functional theory for the calculation of excitation energies of large molecules. *J. Chem. Phys.*, 109(19): 8218–8224, 1998.
- [9] P. Elliott, F. Furche, and K. Burke. Excited states from time-dependent density functional theory. *Rev. Comp. Chem.*, 26:91, 2009.

-
- [10] M. E. Casida and M. Huix-Rotllant. Progress in time-dependent density-functional theory. *Ann. Rev. Phys. Chem.*, 63:287–323, 2012.
- [11] M. A. L. Marques and E. K. Gross. Time-dependent density functional theory. *Annu. Rev. Phys. Chem.*, 55:427–455, 2004.
- [12] M. E. Casida. Time-dependent density-functional theory for the calculation of molecular electronic excited states 2nd year masters, theoretical chemistry. <https://sites.google.com/site/markcasida/tddft>, January 2009. online; accessed 1st July, 2017.
- [13] R. F. Nalewajski. *Perspectives in Electronic Structure Theory*. Springer Berlin Heidelberg, 2012. ISBN 9783642201806.
- [14] N. Ferré, M. Filatov, and M. Huix-Rotllant. *Density-Functional Methods for Excited States*. Topics in Current Chemistry. Springer International Publishing, 2015. ISBN 9783319220819.
- [15] X. Gonze. Adiabatic density-functional perturbation theory. *Phys. Rev. A*, 52(2):1096, 1995.
- [16] E. Runge and E. K. U. Gross. Density-functional theory for time-dependent systems. *Phys. Rev. Lett.*, 52:997, 1984.
- [17] P. Hohenberg and W. Kohn. Inhomogeneous electron gas. *Phys. Rev.*, 136(3B):B864, 1964.
- [18] W. Kohn and L. J. Sham. Self-consistent equations including exchange and correlation effects. *Phys. Rev.*, 140:A1133, 1965.
- [19] E. K. U. Gross and W. Kohn. Time-dependent density functional theory. *Adv. Quant. Chem*, 21:255–291, 1990.
- [20] E. K. U. Gross and W. Kohn. Local density-functional theory of frequency-dependent linear response. *Phys. Rev. Lett.*, 55(26):2850, 1985.

- [21] C. Ullrich. *Time-Dependent Density-Functional Theory: Concepts and Applications*. Oxford Graduate Texts. Oxford University Press, Oxford, 2012. ISBN 9780199563029.
- [22] E. K. U. Gross, J. F. Dobson, and M. Petersilka. Density functional theory of time-dependent phenomena. In *Density functional theory II*, pages 81–172. Springer, 1996.
- [23] R. Van Leeuwen. Causality and symmetry in time-dependent density-functional theory. *Phys. Rev. Lett.*, 80(6):1280, 1998.
- [24] M. E. Casida. Time-dependent density functional response theory of molecular systems: Theory, computational methods, and functionals. *Theo. Comput. Chem.*, 4:391 – 439, 1996. ISSN 1380-7323. doi: [http://dx.doi.org/10.1016/S1380-7323\(96\)80093-8](http://dx.doi.org/10.1016/S1380-7323(96)80093-8).
- [25] M. Petersilka, U. J. Gossmann, and E. K. U. Gross. Excitation energies from time-dependent density-functional theory. *Phys. Rev. Lett.*, 76: 1212, 1996.
- [26] A. Szabo and N. S. Ostlund. *Modern Quantum Chemistry: Introduction to Advanced Electronic Structure Theory*. Macmillan Publishing Company, New York, 1982.
- [27] M. E. Casida. Time-dependent density-functional response theory for molecules. In D. P. Chong, editor, *Recent Advances in Density Functional Methods, Part I*, page 155. World Scientific, Singapore, 1995.
- [28] S. Hirata and M. Head-Gordon. Time-dependent density functional theory within the Tamm-Dancoff approximation. *Chem. Phys. Lett.*, 314:291, 1999.
- [29] K. Burke, J. Werschnik, and E. K. U. Gross. Time-dependent density functional theory: Past, present, and future. *J. Chem. Phys.*, 123(6): 062206, 2005.

Part III

Original Research

Chapter 10

DFT and TD-DFT for Ruthenium Complexes

This chapter is my contribution to a projected review article,
“Challenge of time-dependent density-functional theory for photochemistry”
by Mark E. Casida, Myneni Hemanadhan, Ala M. H. H. Aldin
Darghouth, and Denis Magero.

It gives a good basic introduction to how well (TD-)DFT works for ruthenium complexes. The next chapter will then go into this subject in much more detail.

10.1 Introduction

Ruthenium complexes have attracted intense research in the recent years and also in the past. This is because ruthenium complexes have a wide range of applications in every day life such as the organic solar cells, light emitting diodes and photo-molecular chemical devices just to mention but a few[1]. To make its application a reality, the excited state properties of the compound must be studied. This have been done experimentally in various ways but there is also need to develop theoretical methods that can accurately predict the excited state properties so as to compliment experimental data and vice

versa. To this date, there are several methods that can be used to study excited state properties theoretically. Some of the methods that can be used include the time-dependent density-functional theory (TD-DFT), time-dependent Hartree Fock (TD-HF), and the configuration interaction (CI) among many others. This work compares the three methods to find out which one is able to predict excited state properties accurately by comparing with experimental spectra.

10.2 Computational Details

Ground state optimization was done with density functional theory (DFT) and Hartree Fock. The DFT calculations were performed by using the GAUSSIAN09[2] (version D.01) program package. Calculated gas phase absorption spectra for the compound was done using different methods for excited state calculations including the time dependent (TD) density-functional theory (TD-DFT)[3], time-dependent Hartree Fock (TD-HF) and configuration interaction (CI) levels of theory. All the calculations were done with the Becke three parameters hybrid exchange and the Lee-Yang-Parr correlation functionals (B3LYP)[4, 5]. All-electron 6-31G and 6-31G(d)[6–12] basis set was used for C, H and N atoms while a double- ζ quality basis set LANL2DZ and the corresponding effective core potential (ECP) was used for Ru[13].

X-ray crystallographic data for the compound was obtained from the Cambridge crystallographic data centre (CCDC) with reference code BEN-HUZ. Ground state optimization was done by starting with the crystallographic data. The minima was tested by calculating vibrational frequencies and checking out for the presence or absence of imaginary frequencies. The absence of imaginary frequencies gave an indication that the geometry was at the minima. Excited state calculations used the optimized ground state geometries with the same basis sets and functionals. Calculations were done at different levels of theory including the CI, TD-DFT and TD-HF. The number of excited states for all the calculations was 100 singlet states. Results obtained from theoretical calculations are obtained as spectral functions. The oscillator strength can be obtained from the spectral function which is given

by,

$$S(\omega) = \sum_I f_I \delta(\omega - \omega_I), \quad (10.1)$$

where f_I is the oscillator strength and ω_I is the electronic excitation energy obtained as $E_I - E_0$.

To compare calculated gas phase absorption spectra with experimental spectra, the spectral function from theoretical calculations is converted to the molar extinction coefficient. This was done by the use of an in house build program, SPECTRUM.PY, which converts the spectral function into molar extinction coefficient so that calculated gas phase absorption spectra and experimental spectra can be compared directly on the same graph. SPECTRUM.PY was used to plot the gas phase absorption spectra as well as the experimental spectra. It has the advantage of being usable for different units (i.e., nm, cm^{-1} and eV). It is also possible to have several plots of both calculated and experimental curves on the same graph at a single go using this programme. Comparison of experimental and calculated absorption spectra that has been done with SPECTRUM.PY is shown in Fig.10.2 and Fig.10.3.

All the gas phase absorption calculations were Gaussian broadened with a full-width-at-half-maximum (FWHM) of 4000 cm^{-1} , which is accounted for by SPECTRUM.PY, to account for spectral broadening due to vibrational structure, solvent effects, and finite experimental resolution. It is of importance therefore to note that FWHM is the only empirical parameter involved in the comparison of theoretical and measured spectra.

10.3 Results and Discussion

Optimized Geometry Figure 10.1 shows an optimized structure of $[\text{Ru}(\text{trpy})_2]^{2+}$. Table 10.1 gives a comparison of selected geometries parameters calculated at different levels of theory with experimental data.

Table 10.1 gives a comparison of calculated bond lengths and angles with HF and DFT with experimental data and results from other works.

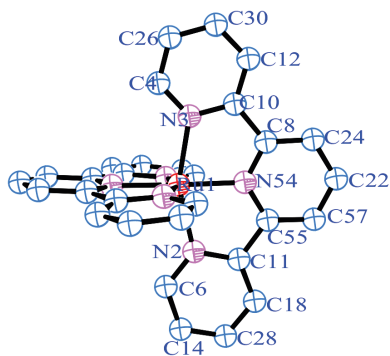


Figure 10.1 – ORTEP diagram showing the optimized structure of $[\text{Ru}(\text{trpy})_2]^{2+}$ with different measured bond lengths and angles. The ellipsoidal probability is at 70%.

Table 10.1 – Comparison of parameters for geometries optimized at HF and DFT. Bond lengths are in (\AA) and bond angles are in degrees.

	HF	DFT	Exp.[14]	Other Works ¹
RuN ₂	2.21	2.122	2.074	2.11
RuN ₅₄	2.086	2.018	1.984	2.011
RuN ₃	2.21	2.122		
N ₅₄ C ₅₅	1.336	1.365	1.345	1.36
N ₂ C ₁₁	1.353	1.382	1.374	1.38
C ₁₁ C ₅₅	1.489	1.474	1.466	1.47
N ₂ C ₆	1.33	1.354	1.35	1.36
RuN ₅₄ C ₅₅	118.132	118.784	119.4	118.8
RuN ₂ C ₁₁	112.473	113.477	113.4	113.8
RuN ₂ C ₆	127.502	127.336	127.5	126.6
N ₅₄ RuN ₂	77.002	78.456	78.6	78.9

Spectra Figure 10.2 shows a comparison of the different absorption spectra at different levels of theory compared with experimental data for 6-31G basis set. Figure 10.3 shows the same calculations with 6-31G(d) basis set.

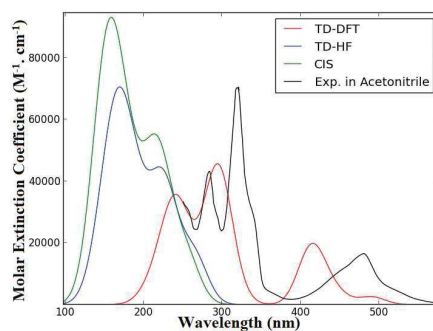


Figure 10.2 – Comparison of experimental with calculated absorption spectra at different levels of theory; CIS, TD-HF and TD-DFT for $[\text{Ru}(\text{trpy})_2]^{2+}$. Calculated spectra has been done with 100 singlet states and 6-31G basis set. Experimental spectra; measured at room temperature in acetonitrile [1].

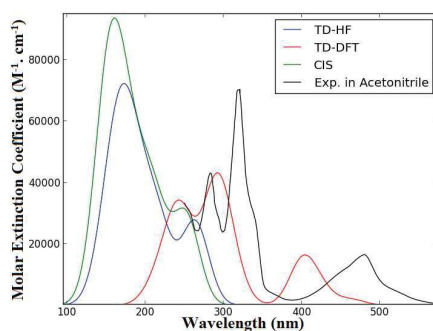


Figure 10.3 – Comparison of experimental with calculated absorption spectra at different levels of theory; CIS, TD-HF and TD-DFT for $[\text{Ru}(\text{trpy})_2]^{2+}$. Calculated spectra has been done with 100 singlet states and 6-31G(d) basis set. Experimental spectra; measured at room temperature in acetonitrile [1].

Table 10.2 compares the calculated absorption peaks obtained from three different levels of calculations with experimental data.

In both the ground state optimization and the excited state calculations with different methods, TD-DFT gives the best representation of experimental spectra.

Table 10.2 – Comparison of the position of spectral peaks calculated at different levels of theory; CIS, TD-HF and TD-DFT for 6-31G and 6-31G(d) basis sets. Wavelength is given in nm and the corresponding molar extinction coefficient is in parenthesis with units of $10^3 \text{ M}^{-1} \cdot \text{cm}^{-1}$.

	CIS	TD-HF	TD-DFT	Exp. (λ_{max}) ²
6-31G	158[93.19]	169[70.61]	240[35.78]	
	213[55.40]	220[44.68]	293[45.73]	
			415[19.90]	476[17.70]
6-31G(d)	160[93.77]	172[72.42]	242[34.38]	
	245[32.03]	262[27.93]	292[43.22]	
			403[16.47]	476[17.70]

Bibliography

- [1] J. P. Sauvage, J. P. Collin, J. C. Chambron, S. Guillerez, and C. Coudret. Ruthenium(II) and osmium(II) bis(terpyridine) complexes in covalently-linked multicomponent systems: Synthesis, electrochemical behavior, absorption spectra, and photochemical and photophysical properties. *Chem. Rev.*, 94:933, 1994.
- [2] M. J. Frisch, G. W. Trucks, H. B. Schlegel, G. E. Scuseria, M. A. Robb, J. R. Cheeseman, G. Scalmani, V. Barone, B. Mennucci, G. A. Petersson, H. Nakatsuji, M. Caricato, X. Li, H. P. Hratchian, A. F. Izmaylov, J. Bloino, G. Zheng, J. L. Sonnenberg, M. Hada, M. Ehara, K. Toyota, R. Fukuda, J. Hasegawa, M. Ishida, T. Nakajima, Y. Honda, O. Kitao, H. Nakai, T. Vreven, J. A. Montgomery, Jr., J. E. Peralta, F. Ogliaro, M. Bearpark, J. J. Heyd, E. Brothers, K. N. Kudin, V. N. Staroverov, R. Kobayashi, J. Normand, K. Raghavachari, A. Rendell, J. C. Burant, S. S. Iyengar, J. Tomasi, M. Cossi, N. Rega, J. M. Millam, M. Klene, J. E. Knox, J. B. Cross, V. Bakken, C. Adamo, J. Jaramillo, R. Gomperts, R. E. Stratmann, O. Yazyev, A. J. Austin, R. Cammi, C. Pomelli, J. W. Ochterski, R. L. Martin, K. Morokuma, V. G. Zakrzewski, G. A. Voth, P. Salvador, J. J. Dannenberg, S. Dapprich, A. D. Daniels, Å. Farkas, J. B. Foresman, J. V. Ortiz, J. Cioslowski, and D. J. Fox. Gaussian 09 Revision D.01. Gaussian Inc. Wallingford CT 2009.

- [3] M. E. Casida. Time-dependent density-functional theory for molecules and molecular solids. *J. Molec. Struct.: THEOCHEM*, 914(1):3, 2009.
- [4] A. D. Becke. Density-functional thermochemistry. III. The role of exact exchange. *J. Chem. Phys.*, 98:5648, 1993.
- [5] C. Lee, W. Yang, and R. G. Parr. Development of the Colle-Salvetti correlation energy formula into a functional of the electron density. *Phys. Rev. B*, 37:785, 1988.
- [6] R. Ditchfield, W. J. Hehre, and J. A. Pople. Self-consistent molecular-orbital methods. IX. An extended Gaussian-type basis for molecular-orbital studies of organic molecules. *J. Chem. Phys.*, 54(2):724–728, 1971.
- [7] W. J. Hehre, R. Ditchfield, and J. A. Pople. Self-consistent molecular orbital methods. XII. Further extensions of Gaussian-type basis sets for use in molecular orbital studies of organic molecules. *J. Chem. Phys.*, 56(5):2257–2261, 1972.
- [8] P. C. Hariharan and J. A. Pople. The influence of polarization functions on molecular orbital hydrogenation energies. *Theor. Chim. Acta*, 28(3): 213–222, 1973.
- [9] P. C. Hariharan and J. A. Pople. Accuracy of AH_n equilibrium geometries by single determinant molecular orbital theory. *Mol. Phys.*, 27(1): 209–214, 1974.
- [10] M. M. Francl, W. J. Pietro, W. J. Hehre, J. S. Binkley, M. S. Gordon, D. J. DeFrees, and J. A. Pople. Self-consistent molecular orbital methods. XXIII. A polarization-type basis set for second-row elements. *J. Chem. Phys.*, 77(7):3654–3665, 1982.
- [11] V. A. Rassolov, M. A. Ratner, J. A. Pople, P. C. Redfern, and L. A. Curtiss. 6-31G* basis set for third-row atoms. *J. Comp. Chem.*, 22(9): 976–984, 2001.

-
- [12] G. A. Petersson and M. A. Al-Laham. A complete basis set model chemistry. II. Open-shell systems and the total energies of the first-row atoms. *J. Chem. Phys.*, 94(9):6081–6090, 1991.
- [13] P. J. Hay and W. R. Wadt. Ab initio effective core potentials for molecular calculations. potentials for K to Au including the outermost core orbitals. *J. Chem. Phys.*, 82:299, 1985.
- [14] M. Kozłowska, P. Rodziewicz, D. M. Brus, J. Breczko, and K. Brzezinski. Bis (2, 2': 6', 2''-terpyridine) ruthenium (II) bis (perchlorate) hemihydrate. *Acta. Crystallogr. E*, 68(11):1414–1415, 2012.
- [15] X. Zhou, A. Ren, and J. Feng. Theoretical studies on the ground states in (M= Fe, Ru, Os) and excited states in using density functional theory. *J. Organomet. Chem.*, 690(2):338–347, 2005.

Chapter 11

Partial Density of States Ligand Field Theory (PDOS-LFT): Recovering a LFT-Like Picture and Application to Photoproperties of Ruthenium(II) Polypyridine Complexes

Introduction

This chapter forms the core part of my thesis. The work that was done and the contribution towards scientific knowledge is divided into two sections. In the first section, the MO indices that were proposed by [1] are validated by applying them to a bigger number of compounds that were carefully selected from [2] which contains data about hundreds of Ru complexes based on the length of the excited state lifetime both at room temperature and

at liquid nitrogen temperature. In particular, the work involved modelling using GAUSSVIEW or using the X-ray crystal structures of 112 Ru complexes. Optimization of the ground state structures and frequency calculations were also done. All the optimized complexes that did not have imaginary frequencies were considered as the probable global minimum. Excited state calculations and TD-DFT calculations were done also.

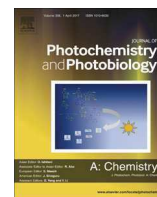
11.1 Background Information on the Problem

Ru complexes have a wide range of applications as light harvesting antennas or photocatalytic centers in photochemical molecular devices (PMDs) such as phosphorescent dyes for display applications (commonly referred to as the organic light emitting diode OLED), photomolecular photoswitch, sensitizers of solar energy conversion and photocatalysis.[3–13]. This has attracted a lot of research in these complexes owing to their wide range of applications. For these complexes to have meaningful applications that have been listed above, they must have a long lived excited state lifetime (atleast 1 μ s) that is able to facilitate electron transfer. It is therefore paramount that the excited state lifetime must be well understood. This understanding is in terms of the deactivation mechanisms and what leads to the long or short excited state lifetime. This work looks at how to estimate the excited state lifetimes of Ru complexes using quantum chemical calculations. Quantum chemical calculations have been used many times before to study the structural and electronic properties of these complexes [14]. The article resulting from this work is given below.



Contents lists available at ScienceDirect

Journal of Photochemistry and Photobiology A: Chemistry

journal homepage: www.elsevier.com/locate/jphotochem

Partial density of states ligand field theory (PDOS-LFT): Recovering a LFT-like picture and application to photoproperties of ruthenium(II) polypyridine complexes



Denis Magero^a, Mark E. Casida^{a,*}, George Amolo^b, Nicholas Makau^c, Lusweti Kituyi^d

^a Département de Chimie Moléculaire (DCM, UMR CNRS/UGA 5250), Institut de Chimie Moléculaire de Grenoble (ICMG, FR2607), Université Grenoble-Alpes, 301 rue de la Chimie, BP 53, F-38041 Grenoble Cedex 9, France

^b Department of Physics and Space Science, The Technical University of Kenya, PO Box 52428-00200, Nairobi, Kenya

^c Computational Materials Science Group, Department of Physics, University of Eldoret, PO Box 1125-30100, Eldoret, Kenya

^d Department of Chemistry and Biochemistry, University of Eldoret, PO Box 1125-30100, Eldoret, Kenya

ARTICLE INFO

Article history:

Received 13 June 2017

Received in revised form 27 July 2017

Accepted 27 July 2017

Available online 31 August 2017

Keywords:

Polypyridine ruthenium complexes

Luminescence

Density-functional theory

Time-dependent density-functional theory

Partial density of states

ABSTRACT

Gas phase density-functional theory (DFT) and time-dependent DFT (TD-DFT) calculations are reported for a data base of 98 ruthenium(II) polypyridine complexes. Comparison with X-ray crystal geometries and with experimental absorption spectra measured in solution show an excellent linear correlation with the results of the gas phase calculations. Comparing this with the usual chemical understanding based upon ligand field theory (LFT) is complicated by the large number of molecular orbitals present and especially by the heavy mixing of the antibonding metal e_g^* orbitals with ligand orbitals. Nevertheless, we show that a deeper understanding can be obtained by a partial density-of-states (PDOS) analysis which allows us to extract approximate metal t_{2g} and e_g^* and ligand π^* orbital energies in a well-defined way, thus providing a PDOS analogue of LFT (PDOS-LFT). Not only do PDOS-LFT energies generate a spectrochemical series for the ligands, but orbital energy differences provide good estimates of TD-DFT absorption energies. Encouraged by this success, we use frontier-molecular-orbital-theory-like reasoning to construct a model which allows us in most, but not all, of the cases studied to use PDOS-LFT energies to provide a semiquantitative relationship between luminescence lifetimes at room temperature and liquid nitrogen temperature.

© 2017 Elsevier B.V. All rights reserved.

1. Introduction

Karl Ernst Claus had the highly unhealthy habit of tasting his chemicals, but (though it made him seriously sick on more than one occasion) it did help him to discover ruthenium in 1884, in part, by following the taste from one solution to another as he successively purified his samples [1]. At first this newcomer to the group of platinum metals seemed to have few applications. The situation soon changed, first with the discovery of important applications in catalysis, and now because of the rich photochemistry of ruthenium compounds [2–13]. In particular, ruthenium complexes may be used as pigments to capture light for drug delivery, photocatalysis, solar cells, or display applications [2,3]. Many of these applications rely on optical excitation leading to an

excited state with a long enough lifetime (typically about 1 μ s) to lead to charge transfer. This paper concerns a relatively simple model and its use to help us to understand and predict the photophenomena of ruthenium complexes.

The ideal model would be both quantitative and simple. In previous work [3], it was shown for five complexes that gas-phase density-functional theory (DFT) and time-dependent DFT (TD-DFT) provide quantitative tools for predicting ruthenium complex crystal geometries and solution absorption spectra. Equally importantly, the results were reduced to a ligand-field theory (LFT) [14] like framework that can be easily related back to the usual interpretive tool used by transition-metal-complex chemists. This was done via the use of the concepts of the density-of-states (DOS) and partial DOS (PDOS) of DFT molecular orbitals (MOs) to identify the energy range of the antibonding ruthenium e_g^* orbitals whose mixing with ligand orbitals otherwise makes them notoriously difficult to locate, unlike the much easier case of the nonbonding ruthenium t_{2g} orbitals. Luminescence indices

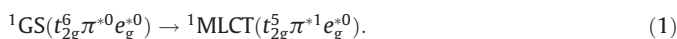
* Corresponding author.

E-mail addresses: magerode@gmail.com (D. Magero), denis.magero@ujf-grenoble.fr (M.E. Casida), magerod@yahoo.com (G. Amolo).

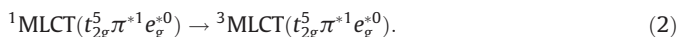
were also suggested based upon this PDOS-LFT to try to say something about relative luminescence lifetimes of different ruthenium complexes. However a theory based upon only five compounds can hardly be taken as proven. (Another approach to extracting LFT from DFT is ligand field DFT [15]. PDOS-LFT offers a complementary but simpler approach.)

Here we extend the earlier study to the large number of complexes whose photoproperties are tabulated in the excellent, if dated, review article of Balzini, Barigelletti, Capagna, Belser, and Von Zelewsky [16]. Our understanding is deepened by confronting calculations for on the order of 100 pseudo-octahedral ruthenium complexes with experimental data. In particular, we are able to obtain a roughly linear correlation (albeit with some exceptions) between a function of PDOS-LFT energies and an average activation energy describing nonradiative relaxation of the luminescent excited state.

The problem of ruthenium complex luminescence lifetimes has been well studied in the literature [18,5,16,2,6–9,19,20,10–13]. Even so, no universal detailed theory of luminescence lifetimes has emerged because of a diversity of ligand-dependent de-excitation mechanisms. Nevertheless there is a commonly accepted “generic mechanism” [16] based upon the pseudo-octahedral symmetry LFT diagram shown in Fig. 1. An initial singlet metal-ligand charge transfer state ${}^1\text{MLCT}(t_{2g}^5\pi^*e_g^0)$ is formed either directly by exciting the ground state [${}^1\text{GS}(t_{2g}^6\pi^0e_g^0)$] or by exciting another state and subsequent radiationless relaxation (see the caption of Fig. 1 for the definition of GS, MLCT, and MC):



Ruthenium complex spin-orbit coupling then leads to rapid intersystem crossing to form the corresponding triplet ${}^3\text{MLCT}(t_{2g}^5\pi^*e_g^0)$,



This ${}^3\text{MLCT}$ can phosphoresce back to the ${}^1\text{GS}$ or it can go over an excited-state transition state barrier to a triplet metal center state

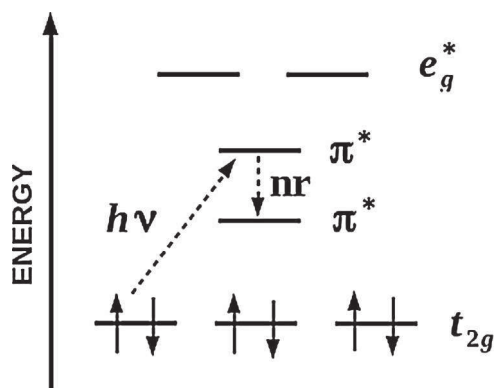


Fig. 1. Generic ligand field theory diagram for octahedral ruthenium(II) polypyridyl complexes. Note that ligand π^* orbital energy levels intercalate between ruthenium t_{2g} and e_g^* LFT states. The number of π^* levels varies depending upon the ligands (only two are shown here). Photon absorption leads to a $t_{2g} \rightarrow \pi^*$ transition from the ground state (GS) to a metal-to-ligand charge transfer (MLCT) state. As $d \rightarrow d$ transitions are symmetry forbidden by the $\Delta l = \pm 1$ selection rule in the atom, the creation of a MLCT excited state is favored over the formation of a metal-centered (MC) state. Kasha's rule [17] tells us that nonradiative (“nr” in the figure) transitions will take place until the dominant luminescence is from the lowest π^* orbital back to the t_{2g} orbital to reform the GS.

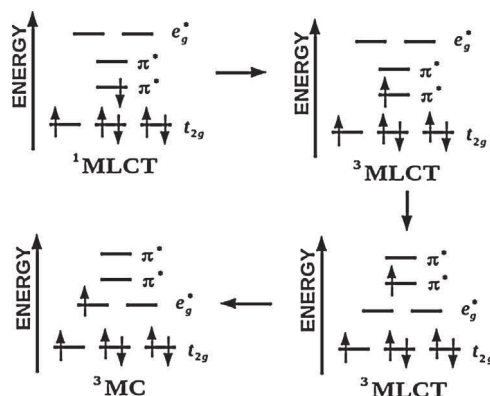
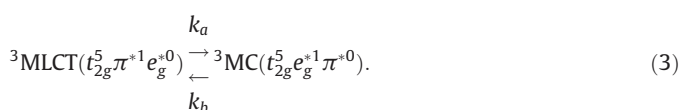
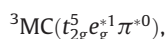
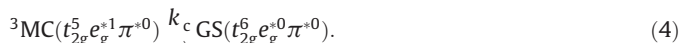


Fig. 2. Orbital diagrams for the electronic GS and the most relevant excited states for pseudo-octahedral ruthenium(II) polypyridyl complexes.



Notice how the MC e_g^* MO has now presumably become lower than the ligand-centered (LC) π^* MO (Fig. 2). This is possible because of geometric relaxation as illustrated in the state diagram shown in Fig. 3. The resultant state can then go through a photochemical funnel with intersystem crossing to return to the groundstate,



This is presumed to involve ligands coming partially or completely off and/or being replaced by solvent molecules. The rate constants k_a , k_b , and k_c are the same as those defined in Ref. [21]. Fig. 2 provides a summary in the form of orbitals and Fig. 3 in the form of potential energy curves for different states. A key assumption is that the main luminescence quenching at room temperature is due to the barrier crossing [Eq. (3)] followed by a rapid return to the ground state [Eq. (4)]. For this reason, we will focus on this barrier in seeking a PDOS-LFT explanation for relative luminescence lifetimes, but let us admit in advance that our answer, though general and useful, is unlikely to be universal. For one thing, a mixture of different types of ligands or of different types of metal-ligand bonds, means that there is likely to be more than one path for luminescence quenching. Still other mechanisms might come

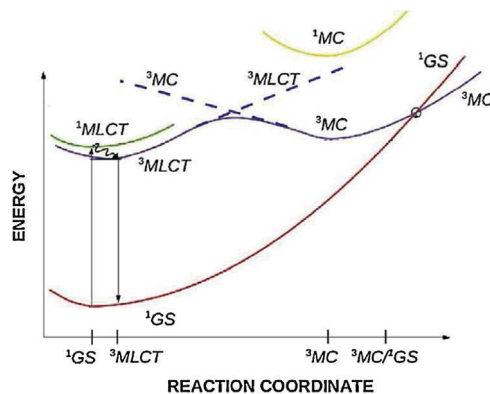


Fig. 3. The diagram shows the principle potential energy curves in our model. The abscissa corresponds to a reaction pathway involving partial removal of a ligand while the ordinate represents the state energy. The dashed lines indicate diabatic states whose avoided crossing leads to the energetic barrier on the adiabatic surface between the ${}^3\text{MLCT}$ and ${}^3\text{MC}$ minima. Figure from Ref. [3] based upon Ref. [22].

involving, say, unforeseen intermediate dark states. And, as we shall see in Section 3, the barrier crossing [Eq. (3)] is unlikely to be the only influence on the luminescence lifetime at room temperature. Nevertheless we shall be happy with a semi-quantitative PDOS-LFT-based theory of luminescence which works most of the time.

The rest of the paper is organized as follows: The next section discusses our choice of molecules, theoretical methods, and computational details. This is followed by a results section in which evidence is first given for the ability of DFT to give reasonably good geometries and of TD-DFT to give reasonably good absorption spectra. Secondly PDOS-LFT energy levels are discussed and shown to be useful for predicting photoproperties. And thirdly a model is presented which allows us to say something about luminescence lifetimes from PDOS-LFT energy levels. Section 4 concludes. PDOS and TD-DFT spectra are presented in a separate document as supporting information.

2. Data base, theoretical method, and computational details

2.1. Data base

Our theoretical calculations are based upon an old but unusually extensive list of the photoproperties of ruthenium complexes. In particular, our calculations are based upon the photoproperties of about 300 mononuclear ruthenium complexes reported in Table 1 of the 1988 review article of Juris, Balzini, Barigelletti, Capagna, Belser, and Von Zelewsky [16]. Of these, the 111 complexes shown in Tables 1–4 have luminescence data either

Table 1

Numbering of the compounds investigated in this paper. With a few exceptions (listed but unnumbered compounds), these are the mononuclear complexes with 77 K experimental luminescence lifetimes taken in their order of occurrence from Table 1 of Ref. [16]. An asterisk has been added if the original table also contained some information about room temperature lifetimes.

Number	Name
(1)*	[Ru(bpy)(CN) ₄] ²⁻
(2)	[Ru(bpy) ₂ Cl ₂]
(3)*	[Ru(bpy) ₂ (CN) ₂]
(4)*	[Ru(bpy) ₂ (en)] ²⁺
(5)	[Ru(bpy) ₂ (ox)]
(6)*	[Ru(bpy) ₃] ²⁺
(7)*	[Ru(bpy) ₂ (4-n-bpy)] ²⁺
(8)*	[Ru(bpy) ₂ (3,3'-dm-bpy)] ²⁺
(9)*	[Ru(bpy) ₂ (4,4'-dm-bpy)] ²⁺
(10)*	[Ru(bpy) ₂ (4,4'-dCl-bpy)] ²⁺
(11)	[Ru(bpy) ₂ (4,4'-dn-bpy)] ²⁺
(12)*	[Ru(bpy) ₂ (4,4'-dph-bpy)] ²⁺
(13)*	[Ru(bpy) ₂ (4,4'-DTB-bpy)] ²⁺
(14)*	<i>cis</i> -[Ru(bpy) ₂ (m-4,4'-bpy)] ⁴⁺
(15)*	[Ru(bpy) ₂ (bpz)] ²⁺
(16)*	[Ru(bpy) ₂ (phen)] ²⁺
(17)	[Ru(bpy) ₂ (4,7-dm-phen)] ²⁺
(18)*	[Ru(bpy) ₂ (4,7-Ph ₂ -phen)] ²⁺
(19)*	[Ru(bpy) ₂ (4,7-dhy-phen)] ²⁺
(20)	[Ru(bpy) ₂ (5,6-dm-phen)] ²⁺
(21)	[Ru(bpy) ₂ (DIAF)] ²⁺
(22)*	[Ru(bpy) ₂ (DIAFO)] ²⁺
(23)*	[Ru(bpy) ₂ (taphen)] ²⁺
(24)	<i>cis</i> -[Ru(bpy) ₂ (py) ₂] ²⁺
(25)	<i>trans</i> -[Ru(bpy) ₂ (py) ₂] ²⁺
(26)	[Ru(bpy) ₂ (pic) ₂] ²⁺
(27)	[Ru(bpy) ₂ (DPM)] ²⁺
(28)	[Ru(bpy) ₂ (DPE)] ²⁺
(29)*	[Ru(bpy) ₂ (PimH)] ²⁺
(30)*	[Ru(bpy) ₂ (PBzimH)] ²⁺
(31)*	[Ru(bpy) ₂ (biimH ₂)] ²⁺
(32)*	[Ru(bpy) ₂ (BiBzimH ₂)] ²⁺
(33)	[Ru(bpy) ₂ (NPP)] ⁺
(34)	[Ru(bpy) ₂ (piq)] ²⁺
(35)	[Ru(bpy) ₂ (hpiq)] ²⁺

Table 2

Numbering of the compounds investigated in this paper. With a few exceptions (listed but unnumbered compounds), these are the mononuclear complexes with 77 K experimental luminescence lifetimes taken in their order of occurrence from Table 1 of Ref. [16]. An asterisk has been added if the original table also contained some information about room temperature lifetimes.

Number	Name
(36)	[Ru(bpy) ₂ (pq)] ²⁺
(37)*	[Ru(bpy) ₂ (DMCH)] ²⁺
(38)	[Ru(bpy) ₂ (OMCH)] ²⁺
(39)*	[Ru(bpy) ₂ (biq)] ²⁺
(40)*	[Ru(bpy) ₂ (i-biq)] ²⁺
(41)*	[Ru(bpy) ₂ (BL4)] ²⁺
(42)*	[Ru(bpy) ₂ (BL5)] ²⁺
(43)*	[Ru(bpy) ₂ (BL6)] ²⁺
(44)*	[Ru(bpy) ₂ (BL7)] ²⁺
(45)*	[Ru(bpy) ₂ (3,3'-dm-bpy)] ²⁺
(46)*	[Ru(bpy) ₂ (4,4'-DTB-bpy)] ²⁺
(47)	[Ru(bpy)(h-phen)] ²⁺
(48)*	[Ru(bpy)(phen)] ²⁺
(49)	<i>cis</i> -[Ru(bpy)(phen)(py)] ²⁺
(50)	<i>trans</i> -[Ru(bpy)(phen)(py)] ²⁺
(51)	[Ru(bpy)(DIAFO)] ²⁺
(52)*	[Ru(bpy)(taphen)] ²⁺
(53)	[Ru(bpy)(py) ₂ (en)] ²⁺
(54)	[Ru(bpy)(py) ₃ Cl] ⁺
(55)	[Ru(bpy)(py) ₄] ²⁺
(56)	[Ru(bpy)(py) ₂ (PMA)] ²⁺
(57)	[Ru(bpy)(py) ₂ (2-AEP)] ²⁺
(58)	[Ru(bpy)(PMA)] ²⁺
(59)	[Ru(bpy)(pq)] ²⁺
(60)*	[Ru(bpy)(DMCH)] ²⁺
(61)*	[Ru(bpy)(biq)] ²⁺
(62)*	[Ru(bpy)(i-biq)] ²⁺
(63)*	[Ru(bpy)(trpy)Cl] ⁺
(64)*	[Ru(bpy)(trpy)(CN)] ⁺
(65)*	[Ru(4-n-bpy) ₃] ²⁺
(66)	[Ru(6-m-bpy)] ²⁺
(67)*	[Ru(3,3'-dm-bpy)] ²⁺
(68)	[Ru(3,3'-dm-bpy) ₂ (phen)] ²⁺
(69)	[Ru(3,3'-dm-bpy)(phen)] ²⁺
(70)*	[Ru(4,4'-dm-bpy) ₃] ²⁺

at room temperature (RT) or at the boiling point of liquid nitrogen (77 K). For convenience we have numbered them in the same order as they appear in Table 1 of review article [16]. Note that this luminescence data was not necessarily measured in the same solvent for different compounds, or even for any given compound, and that the reported precision of the measurements vary. The ligand abbreviations are given in Appendix B. With a few exceptions (CN⁻, Cl⁻, ox, NPP, NA, bt, en), the ligands are pyridine and polypyridine N-type ligands, many of are found in common lists of the well-known spectrochemical series governing the ligand field splitting Δ ,

$$\Delta : \text{Cl}^- < \text{py} < \text{en} < \text{bpy} < \text{phen} < \text{CN}^- \quad (5)$$

Calculations have been carried out on 98 of these 111 complexes, with 13 left untreated either because of lack of a good initial guess for the complex structure, convergence difficulties, or simple lack of time. Not every calculation is necessarily useful as some needed to be discarded for theoretical reasons (an unbound e_g^* orbital) and not every property could be calculated for every compound. Furthermore we were not able to find comparison data for every property of every complex but we think that the extensiveness of our calculations and of the comparison with experiment for a broad range of complexes and properties should be highly useful.

2.2. Computational methods and details

The calculations reported in this paper are very similar to those reported in Ref. [3]. Version B.05 of the GAUSSIAN 03 [23] quantum chemistry package was used in Ref. [3]. Here we use version D.01 of

Table 3

Numbering of the compounds investigated in this paper. With a few exceptions (listed but unnumbered compounds), these are the mononuclear complexes with 77 K experimental luminescence lifetimes taken in their order of occurrence from Table 1 of Ref. [16]. An asterisk has been added if the original table also contained some information about room temperature lifetimes.

Number	Name
(71)*	[Ru(4,4'-dm-bpy) ₂ (4,7-dhy-phen)] ²⁺
(72)*	[Ru(4,4'-dCl-bpy) ₃] ²⁺
(73)*	[Ru(4,4'-dph-bpy) ₃] ²⁺
(74)*	[Ru(4,4'-DTB-bpy) ₃] ²⁺
(75)	[Ru(6,6'-dm-bpy) ₃] ²⁺
(76)	[Ru(h-phen) ₃] ²⁺
(77)*	[Ru(phen) ₃] ²⁺
(78)*	[Ru(phen) ₂ (4,7-dhy-phen)] ²⁺
(79)	[Ru(phen) ₂ (pq)] ²⁺
(80)	[Ru(phen) ₂ (DMCH)] ²⁺
(81)	[Ru(phen) ₂ (biq)] ²⁺
(82)	[Ru(phen)(pq) ₂] ²⁺
(83)	[Ru(phen)(biq) ₂] ²⁺
(84)	[Ru(2-m-phen) ₃] ²⁺
(85)	[Ru(2,9-dm-phen) ₃] ²⁺
(86)*	[Ru(4,7-Ph ₂ -phen) ₃] ²⁺
(87)*	[Ru(4,7-dhy-phen)(tm1-phen) ₂] ²⁺
(88)	[Ru(DPA) ₃] ⁻
(89)	[Ru(DPA)(DPAH) ₂] ⁺
(90)	[Ru(DPAH) ₃] ²⁺
(91)	[Ru(Azpy) ₃] ²⁺
(92)	[Ru(NA) ₃] ²⁺
(93)	[Ru(hpiq) ₃] ²⁺
(94)	[Ru(pq) ₃] ²⁺
(95)	[Ru(pq) ₂ (biq)] ²⁺
(96)	[Ru(pq)(biq) ₂] ²⁺
(97)	[Ru(pynapy) ₃] ²⁺
(98)*	[Ru(DMCH) ₂ Cl ₂]
(99)*	[Ru(DMCH) ₂ (CN) ₂]
(100)	[Ru(DMCH) ₃] ²⁺
(101)	[Ru(dinapy) ₃] ²⁺
(102)	[Ru(biq) ₂ Cl ₂]
(103)*	[Ru(biq) ₂ (CN) ₂]
(104)	[Ru(biq) ₃] ²⁺
(105)	[Ru(i-biq) ₂ Cl ₂]

Table 4

Numbering of the compounds investigated in this paper. With a few exceptions (listed but unnumbered compounds), these are the mononuclear complexes with 77 K experimental luminescence lifetimes taken in their order of occurrence from Table 1 of Ref. [16]. An asterisk has been added if the original table also contained some information about room temperature lifetimes.

Number	Name
(106)*	[Ru(i-biq) ₂ (CN) ₂]
(107)*	[Ru(i-biq) ₃] ²⁺
(108)*	[Ru(trpy) ₂] ²⁺
(109)	[Ru(tro) ₂] ²⁺
(110)	[Ru(tsite) ₂] ²⁺
(111)	[Ru(dqp) ₂] ²⁺

GAUSSIAN 09 [24]. Density-functional theory (DFT) and time-dependent (TD-)DFT calculations were carried out using the same B3LYP functional. This is a three-parameter hybrid functional using Hartree–Fock (HF) exchange, the usual analytical form of the local density approximation (LDA) for exchange [25], Becke's 1988 generalized gradient approximation (GGA) exchange B88x [26], the Vosko–Wilk–Nusair parameterization of the LDA correlation (LDAc) [27], and Lee, Yang, and Parr's GGA for correlation (LYP88c) [28],

$$E_{xc}^{B3LYP} = (1 - a_0)E_x^{LDA} + a_0E_x^{HF} + a_xE_x^{B88x} + a_cE_c^{LYP88c} + (1 - a_c)E_c^{VWN80c}, \quad (6)$$

where $a_0 = 0.20$, $a_x = 0.72$, and $a_c = 0.81$ are taken from Becke's B3P functional [29].

These calculations require us to choose a Gaussian-type basis set. As in Ref. [3], we used the double-zeta quality LANL2DZ basis set for ruthenium along with the corresponding effective core potential (ECP) [30,31]. All-electron 6-31G and 6-31G(d) basis sets [32–38] were used for all the elements in the first three periods of the periodic table. Note that Ref. [3] only used the smaller 6-31G basis set, while the present work is able to verify basis set convergence by also reporting results with the larger 6-31G(d) compounds. However, due to the very large number of calculations carried out and the size of the molecules, calculations with still larger basis sets were judged to fall outside of the scope of the present study. Unless otherwise mentioned, extensive use of program defaults was used for many of the computational parameters. Neither explicit nor dielectric cavity models were used in our calculations, so that all calculations reported in this article are technically for gas-phase molecules.

It should be emphasized that, while a simple Web of Science [39] search shows that the B3LYP functional has been by far the most used functional for DFT calculations on ruthenium(II) polypyridine complexes, the B3LYP functional is gradually losing popularity to other functionals as shown, for example, by the results of the annual DFT popularity poll [40] which shows the B3LYP functional falling from second place (after PBE0) in 2010–2011 to third place (after PBE and PBE0) in 2012–2016. This, of course, is just what it says it is – namely a measure of the popularity of different functionals among users of DFT. Tspis reviews the scientific information assessing the performance of different functionals for coordination chemistry and indicates that the B3LYP functional is still an excellent choice [41]. Nevertheless Ref. [42] reports that the B3LYP functional tends to overestimate metal-ligand bond lengths and Ref. [43] reports better TD-DFT spectra when the B3PW91 functional is used. The choice of the B3LYP functional for this work was somewhat arbitrarily based upon its use in Ref. [3]. A few TD-B3PW91/6-31G calculations at B3LYP/6-31G optimized geometries have been added to give an idea of how these compare with TD-B3LYP calculations at the same geometries. The notation used here is method/basis and is occasionally extended to method A/basis A//method B/basis B where a calculation with method A and basis A has been carried out at geometries optimized using method B and basis B.

The geometries of all the complexes were optimized and (local) minima were confirmed by the absence of imaginary vibrational frequencies. Whenever possible, the geometry optimizations began from X-ray crystal structural data obtained from the Cambridge Crystallographic Data Centre (CCDC) [106,44]. This was the case for the compounds listed in Table 5. Start geometries indicated with an asterisk in Table 5 were constructed from the CCDC data of a related compound. Otherwise crystal coordinates were generated from the GAUSSVIEW program [107], taking into account specific symmetries and crystallographic volumes. The threshold for optimization was set to ultrafine with self consistent field (SCF) convergence being set to very tight.

Time-dependent DFT [108,109] gas-phase absorption spectra were calculated at the optimized ground-state geometries using the same functional and basis sets as for the ground-state calculation. In all cases, at least 100 singlet states were included in calculations of spectra. As in Ref. [3], a theoretical molar extinction spectrum is calculated via,

$$\varepsilon(\omega) = \frac{\pi N_A e^2}{2\varepsilon_0 m_e c \ln(10)} S(\omega), \quad (7)$$

from the corresponding spectral function,

$$S(\omega) = \sum_I f_I \delta(\omega - \omega_I), \quad (8)$$

Table 5

List of 39 compounds with crystal structures. An asterisk indicates that the CCDC structure was modified.

Number	CCDC [44] reference code	Citation
(2)	AHEHIF	Ref. [45,46]
(3)	LESLEB	Ref. [47]
(4)	SAXCIE	Ref. [48]
(5)	YAQJOP	Ref. [49]
(6)	BPYRUF	Ref. [50]
(7)	DIXVEL	Ref. [51]
(9)	JUQHEI	Ref. [52,53]
(10)	BAQYEV	Ref. [54,55]
(14)*	OBITIC01	Ref. [56,57]
(16)	TIXFOV	Ref. [58]
(17)	XOFQEO	Ref. [59,60]
(20)	IBAGAU	Ref. [61,62]
(21)	COMVIJ	Ref. [63]
(22)	YAGJAR10	Ref. [64]
(24)	GEBHEA	Ref. [65]
(25)	QUBRIO	Ref. [66,67]
(26)	MESWUC	Ref. [68,69]
(31)	KEWQOT	Ref. [70,71]
(32)	NUYKIC	Ref. [72,73]
(33)	XOCXIW	Ref. [74]
(36)	HUWGEL	Ref. [75,76]
(46)	QOMYEX	Ref. [77,78]
(48)	JEMWAA	Ref. [79,80]
(51)*	YAGJAR10	Ref. [64]
(62)*	PATLAX	Ref. [81]
(63)	WAKRUX	Ref. [82,83]
(64)	NAMFOY	Ref. [84,85]
(66)	FINREA	Ref. [86,87]
(74)	NOFPII	Ref. [88,89]
(75)	FINRIE	Ref. [90,87]
(77)	ZIFCAU	Ref. [91,92]
(81)	IFAXUI	Ref. [93,94]
(83)	GEYZOB	Ref. [95,96]
(84)	FINRAW	Ref. [97,87]
(91)	MARVAD	Ref. [98,99]
(94)	VAJLUO	Ref. [100,101]
(107)	PATLAX	Ref. [81]
(108)	BENHUZ	Ref. [102,103]
(109)	BOFGEJ	Ref. [104,105]

using an in-house python program `SPECTRUM.PY` [110]. The result is a theoretical spectrum with the same units and the same order of magnitude as the experimentally-measured absorption spectrum, thereby allowing easy comparison of theory and experiment, albeit at the expense of introducing a single empirical parameter which accounts for spectral broadening due to vibrational structure, solvent broadening (but not solvent shifts), and finite experimental resolution. This is the full width at half maximum (FWHM) which has been set to 40 nm throughout.

Density-of-states (DOS) and partial DOS (PDOS) were obtained using another in-house python program called `Pdos.PY` [111] previously described in the supplementary data associated with Ref. [3]. This allows us to identify the positions of ligand-field theory (LFT) like ruthenium *d* states as well as ligand π states after suitable broadening. At a practical level, using `Pdos.PY` involves carrying out another single point calculation with the option (`pop=full ginput iop(6/7=3,3/33=1,3/36=-1)`), thereby causing `GAUSSIAN` to output the number of basis functions `Nbasis`, the overlap matrix, the eigenvalues, and the MO coefficients. `Pdos.PY` then takes this information from the `GAUSSIAN` output files and calculates the (P)DOS. We used a FWHM of 0.25 eV with 40,000 points for graphing.

3. Results

The results of our calculations are divided into three subsections. In the first subsection (Section 3.1), we validate the

ability of DFT to be able to determine ground-state structures and the ability of TD-DFT to be able to simulate experimental absorption spectra. Section 3.2 extracts t_{2g} , e_g^* , and π^* energies from PDOS-LFT and shows that these correlate with peaks in measured absorption spectra. Section 3.3 discusses the extent to which PDOS-LFT can be used to predict which compounds may have long luminescence lifetimes.

3.1. Structure and properties

3.1.1. Geometries

We first test whether our DFT calculations are consistent with observed X-ray crystallography geometries by seeing how much typical bond lengths and bond angles change when the geometry is re-optimized in gas phase using the X-ray geometries as start geometries. Naturally we expect some expansion of the molecule as there are fewer constraints in the gas phase than in the solid phase but, nevertheless, we expect gas-phase and solid-state geometries to be correlated.

The need to judge correlation requires us to make a short review of linear regression as some of the concepts that we use are expected to be unfamiliar to even expert readers. Linear regression is just a least squares fit of $N(x_i, y_i)$ data points to the familiar equation,

$$y = mx + b. \quad (9)$$

Minimizing the error

$$\mathcal{E} = \sum_{i=1,N} (y_i - mx_i - b)^2, \quad (10)$$

gives the usual formulae for the slope and intercept,

$$m = \frac{\langle xy \rangle - \langle x \rangle \langle y \rangle}{\langle x^2 \rangle - \langle x \rangle^2} \quad (11)$$

$$b = \frac{\langle y \rangle \langle xy \rangle - \langle x \rangle \langle xy \rangle}{\langle x^2 \rangle - \langle x \rangle^2},$$

where we have introduced the notation,

$$\langle f(x, y) \rangle = \frac{1}{N} \sum_{i=1,N} f(x_i, y_i). \quad (12)$$

for the average of the $Nf(x_i, y_i)$ values. The goodness of fit is usually judged by the correlation coefficient defined as,

$$R^2 = \frac{(\langle xy \rangle - \langle x \rangle \langle y \rangle)^2}{(\langle x^2 \rangle - \langle x \rangle^2)(\langle y^2 \rangle - \langle y \rangle^2)}, \quad (13)$$

which is close to unity for a good fit. Up to this point, everything corresponds to the standard formulae implemented in typical spreadsheet programs.

However, we need to go a little further because the correlation coefficient is *not* a good measure of the error in the sense that the correlation coefficient calculated over a small range of x_i values may be very different from the correlation coefficient obtained when all the data is taken into consideration. That is why it is often better to calculate the standard error which is defined as the standard deviation of the y_i values from those obtained from the fit. It may be calculated as,

$$\Delta y = \sqrt{\left(\frac{N}{N-2}\right)(\langle y^2 \rangle - \langle y \rangle^2)(1 - R^2)}, \quad (14)$$

which also shows the relation of the standard error to the correlation coefficient. Furthermore, following Ref. [112], it is often

more interesting to invert the fit so that,

$$x = \frac{y}{m} - \frac{b}{m}. \quad (15)$$

The predictability,

$$\Delta x = \frac{\Delta y}{|m|}, \quad (16)$$

then represents the expected error in predicting the experimental results using our theoretical model. In reporting the results of our fits, we will give the slope m , the intercept b , the correlation coefficient R , and the predictability Δx .

In order to see how they are correlated, theoretical and experimental bond distances and angles were compared for 35 of the 39 complexes in Table 5. Complexes (14) and (62) are excluded because their start geometries were a modified version of the original X-ray crystal structures. Complexes (33) and (51) are excluded because we were unable to converge the gas-phase geometry optimizations.

Fig. 4 shows how calculated gas-phase bond lengths compare with X-ray crystal structure geometries. Only ligand-metal bond lengths have been considered. As expected the calculated gas-phase bond lengths are typically longer than those in the X-ray crystal structures. However Table 6 shows that the correlation is actually excellent with a predictability of 0.0251 Å for the 6-31G basis set and 0.0262 Å for the 6-31G(d) basis set. This may be compared with the typical error of 0.005 Å obtained for 20 organic molecules with the same functional and the 6-31G(d) basis set (p.

Table 6
Least squares fit parameters.

Basis set	m	b	R^2	Δx
Bond length/Å				
6-31G	1.04387	-0.04195	0.90450	0.02505
6-31G(d)	1.02988	-0.00602	0.89674	0.02617
Bond angles/degrees				
6-31G	1.07230	-6.39743	0.93055	1.10263
6-31G(d)	1.07424	-6.79970	0.92682	1.13407
λ/nm				
6-31G	0.78134	81.20545	0.47982	33.6319
6-31G(d)	0.77617	67.65579	0.40762	53.5672

124 of Ref. [113]). Note, however, that the comparison made there is against gas phase data and that predicting the geometries of transition metal complexes is in general more challenging than predicting the geometries of purely organic molecules. It is interesting to note that geometries predicted using the 6-31G basis set are better correlated with experimental X-ray geometries obtained using the seemingly better 6-31G(d) basis set. However the differences in the results obtained with the two basis sets are not really significant.

Fig. 5 shows how calculated gas-phase bond angles compare with X-ray crystal structure geometries. Only ligand-metal-ligand

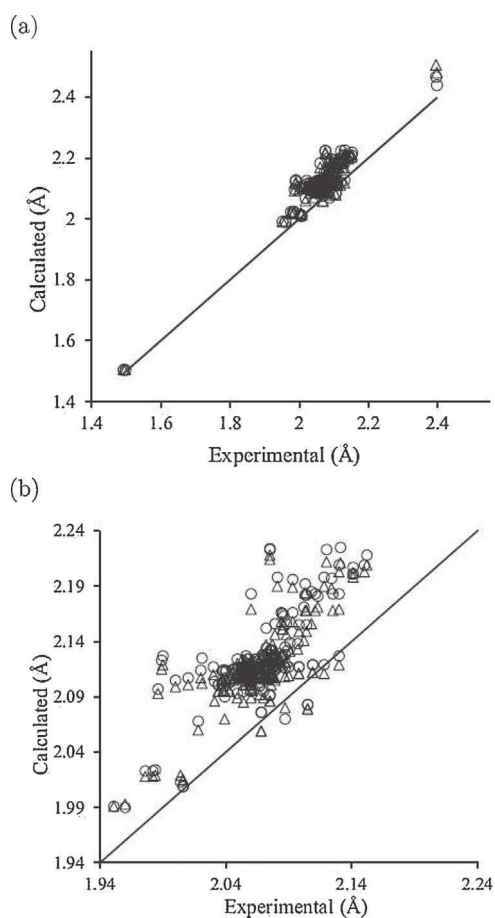


Fig. 4. (a) Correlation graph between calculated DFT bond lengths for the 6-31G (Δ) and 6-31G(d) (\circ) and 184 measured X-ray crystallographic bond lengths. (b) Enlargement. The 45° line indicates perfect agreement with experiment.

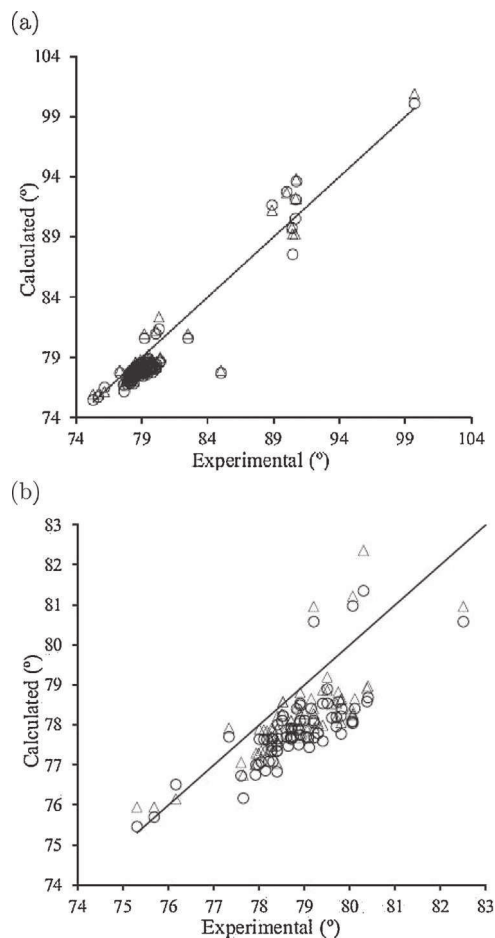


Fig. 5. (a) Correlation graph between calculated DFT bond angles for the 6-31G (Δ) and 6-31G(d) (\circ) and 85 measured X-ray crystallographic bond angles. (b) Enlargement. The 45° line indicates perfect agreement with experiment.

angles near 90° have been considered. The calculated bond angles tend to be smaller than the X-ray crystal structure bond angles. Table 6 shows that the correlation is actually excellent with a predictability of 1.103° for the 6-31G basis set and 1.134° for the 6-31G(d) basis set. This may be compared with the typical error quoted as being on the order of a few tenths of a degree obtained for 20 organic molecules with the same functional and the 6-31G (d) basis set (p. 124 of Ref. [113]). Of course, once again, this is not unexpected because the comparison is against gas phase data and that predicting the geometries of transition metal complexes is in general more challenging than predicting the geometries of purely organic molecules. It is also interesting to notice that, the 6-31G(d) basis set results correlated slightly less well with experiment than do the 6-31G basis set results, but the difference is not really significant.

3.1.2. Absorption spectra

We now wish to see if (TD-)DFT is able to give absorption spectra in reasonable agreement with experiment. Some example comparisons of spectra are given in Fig. 6. Many other TD-DFT spectra are given in the Supplementary Information. Note that no adjustable parameters have been used other than the FWHM (Section 2). Such spectra are expected to be accurate to about 0.2 eV, which is not extremely accurate but which is often adequate for qualitative assignments of spectral features. Typical complexes show two to four peaks, where some of the peaks are only visible as shoulders. Other spectra are given in the Supplementary Information. We have noticed that the lowest energy 6-31G(d) peak is often blue-shifted with respect to the corresponding 6-31G peak, with much less differences between the basis sets for higher-energy features in the TD-B3LYP spectra. We assume that this is due to error cancellation.

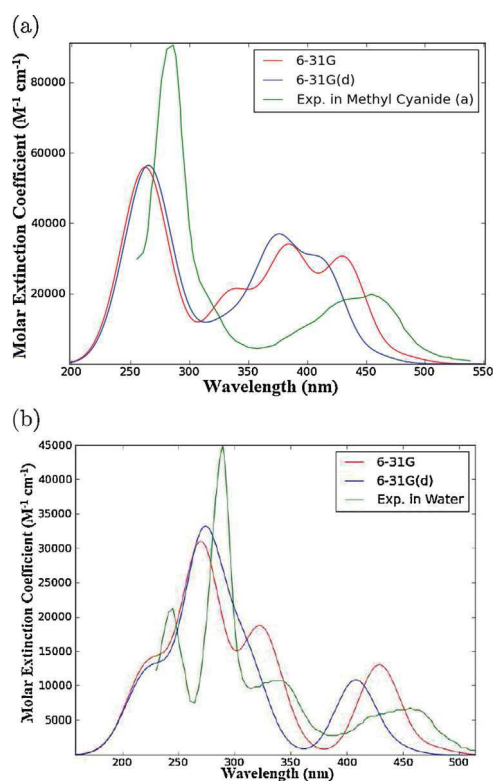


Fig. 6. Comparison of calculated gas-phase absorption spectra (6-31G, red; 6-31G (d) blue) with an experimental spectrum: (a) complex (18), experimental spectrum in acetonitrile from Ref. [114]; (b) complex (24), experimental spectrum in water from Ref. [115]. (For interpretation of the references to color in this figure legend, the reader is referred to the web version of the article.)

In order to compare theory and experiment for several molecules, it is useful to focus on the lowest energy transition. Data for this has been collected from several references and is conveniently provided in Table 1 of Ref. [16] for several solvents. Since the lowest energy transition is expected to be of $t_{2g} \rightarrow \pi^*$ charge-transfer type, we can anticipate some solvent dependence, though it is often relatively small. We have tried to minimize solvent effects by estimating a best value in acetonitrile, a common solvent for polypyridinal ruthenium complexes. As discussed in Ref. [116], there are several ways to estimate solvent shifts in spectra and all involve approximations. The one we chose consists of seeking the best linear relationship between the inverse wavelength and the orientation polarizability,

$$\Delta f(\epsilon, n) = \frac{\epsilon - 1}{2\epsilon + 1} - \frac{n^2 - 1}{2n^2 + 1}, \quad (17)$$

which comes out of Onsager's reaction field theory. Here ϵ is the solvent dielectric constant and n is the solvent refractive index. Note that this is only valid for a given transition weakly interacting with a dielectric medium. An example plot is shown in Fig. 7 for complex (3) where the solvent shift is particularly marked and there are two experimental values for the absorption in acetonitrile. The value from the linear plot for this compound and best estimates in acetonitrile where they could be extracted are shown in Table 7.

Fig. 8 shows how our TD-DFT spectra compare with experimental spectra for the placement of the lowest energy absorption maximum. The calculated predictability shown in Table 6 corresponds to 0.17 eV for the 6-31G basis set and to 0.27 eV for the 6-31G (d) basis set at 500 nm. This is the sort of accuracy we normally expect from TD-DFT in the absence of any particular problems such as, say, strong density relaxation upon excitation. [TD-B3LPW91/6-31G calculations at the B3LYP/6-31G optimized geometries have also been included in Fig. 8 (see Section 2), but no significant differences have been observed compared with the TD-B3LYP/6-31G results at the same geometries.] We conclude that our DFT model is a reasonably good descriptor of the experimental situation.

3.2. PDOS-LFT

We now come to the heart of this paper, namely the partial density-of-states (PDOS) technique for extracting ligand field theory (LFT) like information from DFT calculations. This is needed by chemists as it is their traditional tool for thinking about and discussing spectra (e.g., Fig. 6) and other photoprocesses in transition metal complexes. It is also nontrivial because the usual pseudo-octahedral orbitals t_{2g} and e_g^* do not emerge automatically from DFT calculations. This statement is less true of the nonbonding t_{2g} which can often be identified by direct visualization of DFT molecular orbitals, but it is very true of the antibonding

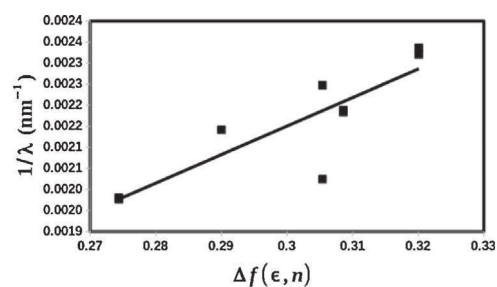


Fig. 7. Inverse of the wavelength of the lowest energy absorption plotted against the orientational polarization for complex (3) and various solvents listed in Table 1 of Ref. [16], except for chloroform which did not fit the trend established by the other solvents. Note that $\Delta f(\epsilon, n) = 0.3054$ for acetonitrile.

Table 7

Best estimates of the lowest energy absorption maximum in acetonitrile based upon data from Table 1 of Ref. [16].

Number	Wavelength (nm)	Number	Wavelength (nm)
(1)	431.2	(53)	476.0
(2)	524.0	(56)	465.0
(3)	457.2	(57)	455.0
(6)	451.5	(58)	478.0
(7)	493.0	(59)	479.1
(8)	448.0	(60)	559.0
(9)	445.0	(61)	547.0
(10)	448.0	(62)	450.0
(11)	514.0	(63)	506.0
(12)	458.0	(64)	487.3
(13)	450.0	(65)	480.0
(14)	450.0	(66)	448.0
(15)	472.7	(67)	456.0
(22)	440.0	(70)	456.0
(23)	440.0	(72)	462.0
(24)	450.0	(73)	474.0
(25)	474.0	(74)	456.0
(29)	460.0	(76)	453.0
(30)	458.0	(77)	467.4
(31)	473.0	(79)	483.0
(32)	463.0	(80)	522.0
(34)	483.0	(81)	522.0
(35)	480.0	(90)	375.0
(36)	478.0	(92)	505.0
(37)	528.0	(93)	494.0
(38)	562.0	(94)	483.5
(39)	526.0	(97)	526.0
(40)	540.0	(99)	605.1
(45)	453.0	(100)	540.0
(46)	454.0	(101)	585.0
(47)	450.0	(103)	605.1
(48)	442.0	(104)	524.0
(49)	448.0	(105)	436.0
(50)	476.0	(106)	414.8
(51)	446.0	(107)	392.0
(52)	438.0	(108)	473.1

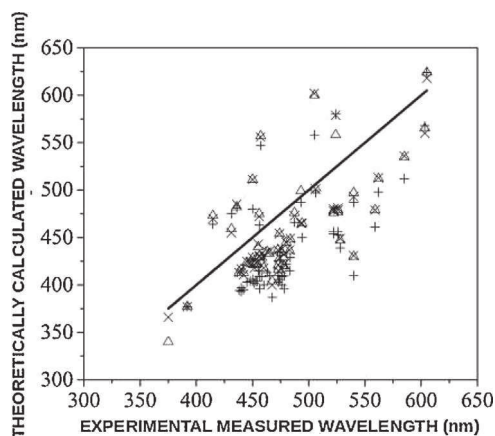


Fig. 8. Correlation graph between calculated lowest energy absorption wavelengths for the TD-B3LYP/6-31G//B3LYP/6-31G (Δ), TD-B3LYP/6-31G(d)//B3LYP/6-31G (+), and TD-B3PW91/6-31G//B3LYP/6-31G (\times) for 57 best estimates for the best estimate of the experimental lowest energy absorption wavelengths in acetonitrile. (The 45° line indicates perfect agreement with experiment.)

e_g^* orbitals which (because they are antibonding) mix heavily with ligand orbitals, making it impossible to identify individual e_g^* orbitals among the DFT molecular orbitals in the absence of special tools. The tool we have used here is the very simple one used in Ref. [3], namely a PDOS analysis based upon Mulliken charges. Other (P)DOS graphs may be found in the Supplementary Information.

The concept of the density-of-states (DOS) is borrowed from solid-state physics. The idea is to replace the orbital energy levels, which have become too dense for convenient interpretation, with a Gaussian-broadened stick spectrum,

$$\text{DOS}(\varepsilon) = \sum_i g(\varepsilon - \varepsilon_i), \quad (18)$$

where the gaussian,

$$g(\varepsilon) = \sqrt{\frac{\alpha}{\pi}} e^{-\alpha x^2}, \quad (19)$$

is normalized to unity. The parameter α is fixed by the FWHM according to the relation,

$$\text{FWHM} = 2\sqrt{\frac{\ln 2}{\alpha}}. \quad (20)$$

We loose the concept of individual orbital energy levels when using the DOS. Nevertheless an isolated DOS peak of unit area corresponds to a single underlying orbital energy level, a DOS peak integrating to an area of two corresponds to two closely spaced underlying orbital energy levels, etc. Fig. 9 provides an example of the DOS of two complexes. Note that each peak represents one to several underlying molecular orbital levels.

The partial density-of-states (PDOS) goes a step further by introducing an atomic orbital decomposition of the DOS. Thus the PDOS for the μ th atomic orbital is,

$$\text{PDOS}_\mu(\varepsilon) = \sum_i q_{\mu,i} g(\varepsilon - \varepsilon_i). \quad (21)$$

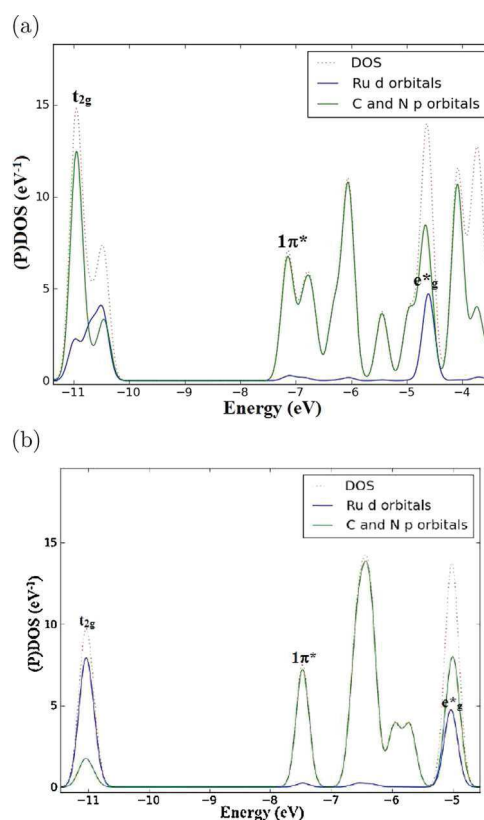


Fig. 9. B3LYP/6-31G (P)DOS calculated for (a) complex (18) and (b) complex (24). Note that the corresponding highest-occupied molecular orbital energies are -10.43 eV for complex (18) and -10.95 eV for complex (24). (For interpretation of the references to color in this figure legend, the reader is referred to the web version of the article.)

Here the quantity $q_{\mu,i}$ is the Mulliken atomic charge of atomic orbital μ in molecular orbital i . We obtain the ruthenium d PDOS by summing PDOS_{μ} over all d -type atomic orbitals on ruthenium. Similarly we obtain the π PDOS by summing PDOS_{μ} over all the p -type atomic orbitals on the heavy atoms (e.g., on C, N, and O) on the ligands. As seen in Fig. 9, the approximate energies of the t_{2g} and e_g^* orbitals on the ruthenium clearly emerge for complex (24) with the expected peak height ratio of 3:2. We also see a loss of t_{2g} degeneracy for complex (18) due to breaking of perfect octahedral symmetry in this complex as well as some small seemingly random d -orbital density contributing to molecular orbitals at other energies.

It should be noted that the PDOS analysis, while highly useful, also contains a degree of arbitrariness. In the first place, the precise picture will vary as the FWHM is varied. This is why it is best to use a fixed value of the FWHM as we do in this paper. Also, the PDOS shares the basis-dependence of the Mulliken analysis. This is illustrated in Fig. 10 where the e_g^* peak shifts slightly relative to the π^* peaks when going from the 6-31G to the 6-31G(d) basis set. Many other examples allowing the comparison of the PDOS calculated with the two different basis sets for a wide variety of complexes may be found in the Supplementary Information and provide further evidence for slight basis-set dependent shifts in the PDOS. However an important exception is in the case of unbound (i.e., positive energy) orbitals where a finite basis set is trying to describe a continuum. These cases are marked with an asterisk (*) in the Supplementary Information and can show very great differences between the position and character of the t_{2g} and e_g^* PDOS peaks in going from the 6-31G to the 6-31G(d) basis sets, such as is the case for complex (7)* where there is a simple t_{2g} peak

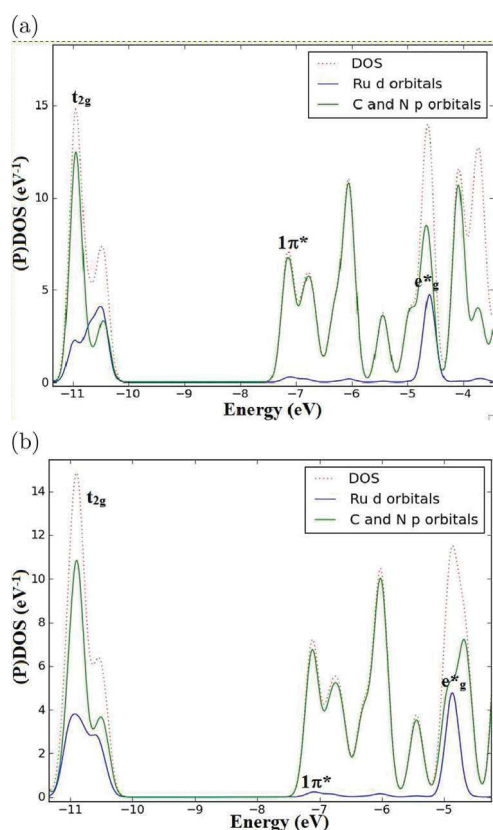


Fig. 10. B3LYP (P)DOS calculated for complex (18): (a) 6-31G basis and (b) 6-31G(d) basis. (For interpretation of the references to color in this figure legend, the reader is referred to the web version of the article.)

Table 8
 $\Delta_{\text{PDOS-LFT}}$ (cm^{-1}) for complexes with simple t_{2g} and e_g^* peaks.

Number	6-31G6-31G	6-31G(d)
(6)	49,300.	48,200.
(8)	48,800.	48,100.
(9)	48,900.	48,000.
(11)	49,300.	47,800.
(13)	49,100.	47,900.
(14)	47,800.	46,900.
(15)	49,500.	48,300.
(16)	48,800.	47,800.
(17)	48,300.	47,400.
(19)	47,800.	46,500.
(20)	48,800.	47,400.
(23)	48,400.	47,400.
(24)	48,400.	47,300.
(25)	48,400.	47,100.
(26)	48,300.	47,200.
(27)	48,000.	46,800.
(28)	47,700.	46,700.
(29)	48,700.	47,500.
(30)	48,500.	47,500.
(31)	48,500.	47,000.
(32)	48,000.	46,700.
(34)	49,000.	47,900.
(40)	48,700.	47,400.
(41)	48,900.	47,700.
(42)	48,800.	48,000.
(46)	48,900.	47,700.
(47)	48,800.	47,600.
(48)	48,700.	47,200.
(50)	48,300.	47,100.

in the PDOS calculated with the 6-31G basis set and a triple t_{2g} peak in the PDOS calculated with the 6-31G(d) basis set.

We thus have a ligand-field theory (LFT) like PDOS-LFT picture. However it is *not* LFT as the PDOS-LFT splitting $\Delta_{\text{PDOS-LFT}}$ calculated as the energy difference between the e_g^* and t_{2g} PDOS peaks is not the same as the Δ_{LFT} expected from LFT. We can see this by comparing numbers for the much studied complex (6). According to our calculations, $\Delta_{\text{PDOS-LFT}} = 49,300 \text{ cm}^{-1}$ calculated with the 6-31G basis set and $48,200 \text{ cm}^{-1}$ calculated with the 6-31G(d) basis set. This can be compared with the value $\Delta_{\text{PDOS-LFT}} = 48,000 \text{ cm}^{-1}$ and with $\Delta_{\text{LFT}} = 28,600 \text{ cm}^{-1}$ reported previously [3]. Clearly $\Delta_{\text{PDOS-LFT}}$ is much larger than Δ_{LFT} so that PDOS-LFT is different from the usual LFT.

Table 9
 $\Delta_{\text{PDOS-LFT}}$ (cm^{-1}) for complexes with simple t_{2g} and e_g^* peaks.

Number	6-31G6-31G	6-31G(d)
(52)	48,100.	46,800.
(53)	47,400.	46,700.
(55)	47,100.	45,700.
(56)	47,700.	46,600.
(57)	47,300.	46,300.
(58)	47,600.	46,400.
(70)	48,300.	47,500.
(71)	47,800.	46,600.
(75)	45,400.	44,700.
(76)	48,400.	47,600.
(77)	48,300.	47,300.
(78)	47,800.	46,600.
(85)	43,800.	43,400.
(87)	47,700.	46,300.
(90)	47,400.	45,700.
(93)	47,500.	46,600.
(94)	46,100.	44,700.
(96)	43,600.	42,500.
(97)	48,500.	47,100.
(104)	43,000.	42,200.
(107)	48,000.	47,400.

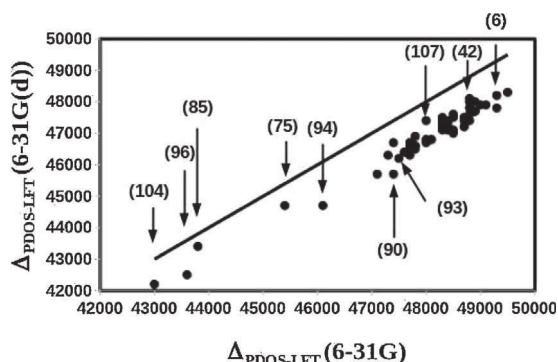


Fig. 11. Correlation plot between $\Delta_{\text{PDOS-LFT}}$ calculated in cm^{-1} with the 6-31G and 6-31G(d) basis sets for 55 complexes. The diagonal line indicates where points should lie in the event of hypothetical perfect agreement between the two sets of results. A least squares fit to the calculated points gives the equation $\Delta_{\text{PDOS-LFT}}(6-31\text{G}(d)) = 0.940 \Delta_{\text{PDOS-LFT}}(6-31\text{G}) + 1740 \text{ cm}^{-1}$. Complexes whose data points are marked: **(6)** [Ru(bpy)₃]²⁺, **(42)** [Ru(bpy)₂(BL5)]²⁺, **(107)** [Ru(i-biq)₂(BL5)]²⁺, **(93)** [Ru(hpiq)₃]²⁺, **(75)** [Ru(6,6'-dm-bpy)₃]²⁺, **(85)** [Ru(2,9-dm-phen)₃]²⁺, **(96)** [Ru(pq)(biq)₂]²⁺, and **(104)** [Ru(biq)₃]²⁺.

Tables 8 and 9 show the values of $\Delta_{\text{PDOS-LFT}}$ for complexes sufficiently close to octahedral symmetry to show simple t_{2g} and e_g^* PDOS peaks, excluding complexes where the e_g^* peak is unbound. Fig. 11 provides a graphical comparison of how $\Delta_{\text{PDOS-LFT}}$ changes in going from the 6-31G to the 6-31G(d) basis set. The correlation is linear up to some residual scatter which can be explained by the precision of the graphical measurement of the distance between peaks. In general, the $\Delta_{\text{PDOS-LFT}}$ splitting closes a bit when the larger basis set is used compared to the smaller basis set. Although $\Delta_{\text{PDOS-LFT}} \neq \Delta_{\text{LFT}}$, we do expect them to have the same trends and so to be able to establish spectrochemical series. Thus from Fig. 11 we may, for example, deduce the following relationship for ligand field strength:

Δ : bpy > i – biq > hpiq > DPAH > pq

> 6,6' – dm – bpy > 2,9 – dm – phen > biq.

Ligand abbreviations are defined in Appendix B.

Since the usual LFT splitting Δ_{LFT} is extracted from absorption spectra [14], it is interesting to see to what extent energy differences between PDOS-LFT peaks correlate with the position of TD-DFT absorption spectra peaks. Often times, TD-DFT results may be analyzed within the two-orbital two-electron model (TOTEM) (See, e.g., the review Ref. [109]). Let us consider a simpler hybrid functional,

$$E_{xc}^{\text{Hybrid}} = (1 - a_0)E_x^{\text{GGA}} + a_0E_x^{\text{HF}} + E_c^{\text{GGA}}, \quad (23)$$

$$\begin{aligned} \omega_S^{\text{Hybrid}} &= \varepsilon_a - \varepsilon_i + 2(i|f_H|ai) \\ &\quad - a_0(ii|f_H|aa) + (1 - a_0)(i|f_x^{\alpha,\alpha}|ai) \\ &\quad + a_c(i|f_c^{\alpha,\alpha} + f_c^{\alpha,\beta}|ai) \\ \omega_T^{\text{Hybrid}} &= \varepsilon_a - \varepsilon_i \\ &\quad + (1 - a_0)(i|f_x^{\alpha,\alpha}|ai) \\ &\quad + (1 - a_0)(i|f_x^{\alpha,\alpha}|ai) \end{aligned} \quad (24)$$

than the B3LYP functional [Eq. (6)] as it already captures all the essential features which are of interest to us here. In the Tamm-Dancoff approximation (See, e.g., the review Ref. [109]), the TOTEM model gives the following formulae for the singlet ω_S and triplet ω_T excitation energies: where we follow the notation of Ref. [109]. If the two-electron integrals are (or their sum is) sufficiently small, then we may expect that excitation energies may be approximated,

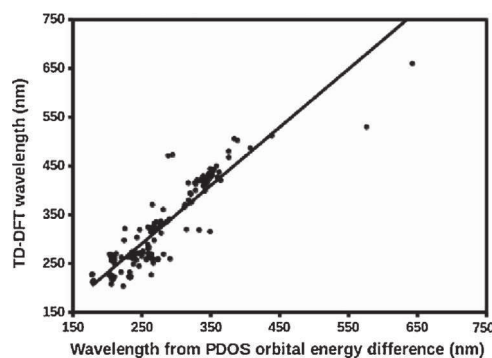


Fig. 12. Correlation plot between $t_{2g} \rightarrow \pi^*$ PDOS orbital energy differences calculated using the 6-31G basis set and TD-B3LYP(6-31G) absorption spectra peaks. A least squares fit to the 161 data points gives the line indicated on the graph whose equation is $\lambda(\omega_S) = 1.19\lambda(\varepsilon_{\pi^*} - \varepsilon_{t_{2g}}) - 7.63 \text{ nm}$.

albeit rather roughly, as orbital energy differences:

$$\omega \approx \varepsilon_a - \varepsilon_i. \quad (25)$$

This was checked by taking the same complexes treated in Fig. 11 and comparing the wavelength corresponding to the $\varepsilon_{t_{2g}} \rightarrow \varepsilon_{\pi^*}$ transitions with the wavelength of the corresponding peaks in the TD-B3LYP absorption spectra in Fig. 12. A least squares fit indicates quite a good correlation in the sense that the slope is only slightly greater than unity and the intercept is small. However there is a large scatter of the data points around the fit line which may be due to neglect of two-electron integrals but may equally well be due to difficulty assigning the precise positions of PDOS peaks and of peaks (and particularly of shoulders) in the TD-B3LYP spectra. Nevertheless we find the figure to be quite encouraging in that the figure suggests that a PDOS-LFT orbital model may provide useful insight into the behavior of excited states.

Table 10

Compounds with both room temperature (RT) and liquid nitrogen temperature (77 K) data from Table 1 of Ref. [16]. An asterisk has been added if the PDOS e_g^* orbital is unbound. Luminescence times are averages over different measurements in different solvents. See text for the definition of ΔE_{ave} .

Number	$\tau(77 \text{ K})$ μs	$\tau(\text{RT})$ μs	ΔE_{ave} cm^{-1}
(1)*	3.7	0.043	321.
(3)*	3.7	0.30	181.
(4)	0.84	0.070	179.
(6)	5.23	0.845	132.
(7)*	3.1	0.78	100.
(8)	5.25	0.533	165.
(9)	5.2	0.48	172.
(12)	5.6	1.92	77.
(13)	4.6	1.17	99.
(14)	7.59	0.454	203.
(15)	3.4	0.378	158.
(16)	6.6	0.497	186.
(18)	9.4	1.591	128.
(19)	3.9	0.628	132.
(21)	5.9	0.00007	818.
(22)	5.1	0.137	261.
(23)	1.8	0.05	259.
(29)	4.450	0.192	227.
(30)	4.240	0.340	182.
(31)	3.25	0.121	237.
(32)	3.000	0.115	235.
(37)	1.5	0.38	99.
(39)	1.65	0.27	131.
(40)	4.7	1.1	105.

Table 11

Compounds with both room temperature (RT) and liquid nitrogen temperature (77 K) data from Table 1 of Ref. [16]. An asterisk has been added if the PDOS e_g^* orbital is unbound. Luminescence times are averages over different measurements in different solvents. See text for the definition of ΔE_{ave} .

Number	$\tau(77K)$ μs	$\tau(RT)$ μs	ΔE_{ave} cm^{-1}
(41)	4.560	0.356	184.
(42)	4.090	0.390	170.
(43)	4.020	0.389	169.
(44)	4.070	0.360	175.
(46)	4.8	1.07	108.
(48)	12.45	0.784	200.
(52)	2.0	0.13	197.
(60)	1.9	0.39	114.
(61)	1.95	0.20	164.
(64)*	5.0	0.001	615.
(67)*	6.4	0.21	632.
(70)	4.6	0.525	157.
(71)	10.50	0.475	223.
(73)	4.79	1.31	94.
(74)	5.3	1.15	110.
(77)	9.93	0.673	194.
(78)	3.0	1.675	42.
(86)	9.58	4.796	50.
(87)	11.0	1.750	132.
(99)*	1.17	0.167	115.
(103)*	0.88	0.147	129.
(106)*	177.	0.237	477.
(107)	96.0	0.1475	467.
(108)	10.7	0.0037	575.

3.3. Luminescence lifetimes

Since gas-phase B3LYP geometries are a good indicator of ruthenium complex crystal geometries, gas-phase TD-B3LYP absorption spectra are a reasonable indicator of ruthenium complex absorption spectra in solution, and PDOS-LFT energies provide a first approximation to absorption spectra energies, then we may also hope to be able to say something about ruthenium complex luminescence lifetimes on the basis of PDOS-LFT information. Indeed this was the reasoning given in the seminal paper [3] where PDOS-LFT luminescence indices were proposed upon the basis of the idea that the room temperature (RT) luminescence lifetime should increase with the height of the $^3MLCT \rightarrow ^3MC$ barrier shown in Fig. 3. This barrier-height dependence would also imply a strong temperature dependence which is indeed seen in the 48 liquid nitrogen (77 K) and room temperature (RT) values in Tables 10 and 11 and the 46 points in Fig. 13.

In order to see where PDOS-LFT-derived luminescence indices may be able to say something about luminescence lifetimes, we need first to understand the various contributions to luminescence lifetimes. Luminescence lifetime experiments measure the decay rate of the intensity of light luminescing at a particular wavelength

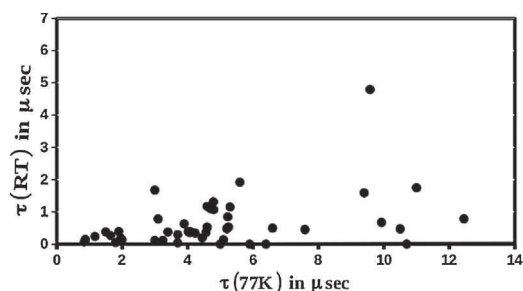


Fig. 13. Correlation between luminescence lifetimes at room temperature (RT) and at liquid nitrogen temperature (77 K).

as a function of time. This gives a temperature (T) dependent decay constant $k(T)$ which is related to the decay lifetime $\tau(T)$ by,

$$k(T) = \frac{1}{\tau(T)}. \quad (26)$$

The luminescence lifetime determined from the decay rate of measured intensity is a measure of the rate of disappearance of the luminescent species – in this case, the phosphorescent 3MLCT state. In addition to phosphorescence, other physical phenomena are also included in the decay lifetime $\tau(T)$ which generally depend upon the temperature T . The decay rate constant may be separated,

$$k(T) = k_0 + k_b^{nr}(T), \quad (27)$$

into a temperature-independent part,

$$k_0 = k^r + k_a^{nr}, \quad (28)$$

where the superscript “r” refers to “radiative” and the superscript “nr” refers to “nonradiative” [117]. The temperature-independent part describes processes which continue to be operational even at very low temperatures. (k_0 is assumed to be equal to $k(T)$ at $T = 84$ K in Ref. [118].) The temperature-dependent part may be further separated as [16],

$$k_b^{nr}(T) = k_{melt}(T) + k_{equilib}(T) + k_{barrier}(T), \quad (29)$$

where,

$$k_{melt}(T) = \frac{B}{1 + \exp\left[C\left(\frac{1}{T} - \frac{1}{T_B}\right)\right]} \quad (30)$$

describes the melting of the solid matrix of the solution at low temperature, where $k_{melt}(T) = \text{constant } B$ for $T \rightarrow \infty$ and $k_{melt}(T) = 0$ for $T \rightarrow 0$. T_B is the temperature at which $k_{melt}(T) = B/2$ and C is a temperature related to the viscosity effect;

$$k_{equilib}(T) = A_1 e^{-\Delta E_1/RT}, \quad (31)$$

describes thermal equilibrium with higher energy states of the same electronic nature (e.g., states with the same symmetry in an octahedral complex according to LFT but which are split with ligands giving only pseudo-octahedral symmetry), and

$$k_{barrier}(T) = A_2 e^{-\Delta E_2/RT}, \quad (32)$$

is an Arrhenius term describing crossing of the $^3MLCT \rightarrow ^3MC$ barrier prior to subsequent de-activation to 1GS . As pointed out in Ref. [21], ΔE_2 is only the $^3MLCT \rightarrow ^3MC$ activation energy barrier when $k_c \gg k_b$ [see Eqs. (3) and (4)], but the situation becomes more complicated if (for example) $k_b \gg k_c$. Putting it altogether results in,

Table 12

Parameters describing the temperature dependence of the luminescence decay rate of $[Ru(bpy)_3]^{2+}$ in propionitrile/buyronitrile (4:5 v/v) from p. 108 of Ref. [16], except: C and T_B were determined by variation within the recommended range until we obtained results similar to those in Fig. 6 of Ref. [118]. A_{ave} and ΔE_{ave} are calculated as explained in the text.

Parameter	Value
k_0	$2 \times 10^5 s^{-1}$
B	$2.1 \times 10^5 s^{-1}$
C	1900
T_B	125 K
A_1	$5.6 \times 10^5 s^{-1}$
ΔE_1	$90 cm^{-1}$
A_2	$1.3 \times 10^{14} s^{-1}$
ΔE_2	$3960 cm^{-1}$
A_{ave}	$2.707 \times 10^6 s^{-1}$
ΔE_{ave}	$159.98 cm^{-1}$

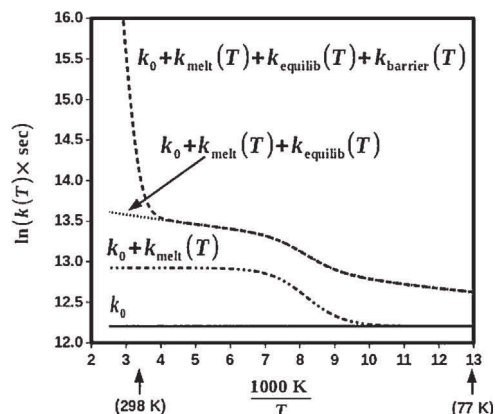


Fig. 14. Plot of $\ln(k)$ versus $1/T$ for luminescence decay rates for $[\text{Ru}(\text{bpy})_3]^{2+}$ in propionitrile/butyronitrile (4:5 v/v).

$$\begin{aligned}
 k &= k_0 + k_{\text{melt}}(T) + k_{\text{equilib}}(T) + k_{\text{barrier}}(T) \\
 &= k_0 + \frac{B}{1 + \exp\left[C\left(\frac{1}{T} - \frac{1}{T_B}\right)\right]} \\
 &\quad + A_1 e^{-\Delta E_1/RT} + A_2 e^{-\Delta E_2/RT}.
 \end{aligned} \quad (33)$$

The barrier term is commonly believed to dominate over the other terms at high-enough temperatures. If so, then we may hope to be able to relate ΔE_2 to the features of the PDOS-LFT theory.

But how high a temperature is high-enough to make this hope reasonable? We can get some idea of the answer to this question by examination of the relative importance of the different terms in Eq. (29) for $[\text{Ru}(\text{bpy})_3]^{2+}$ in propionitrile/butyronitrile (4:5 v/v) using the parameters given in Table 12. Data is often plotted as $\ln(k)$ versus $1/T$ as shown in Fig. 14. A look at the different contributions on the excited state lifetimes is also shown on the same plot. It looks very different on different scales as different physical effects come into play in different temperature regimes. Only k_0 is important below about 30 K. From about 30 K to 100 K, k_{equilib} becomes important. The melting term k_{melt} switches on from about 100 K to about 250 K. After 250 K, k_{barrier} rapidly begins to dominate. Unfortunately k_{barrier} is not the single overwhelmingly dominant term at RT (298 K).

This means that it is very difficult to extract an accurate value of the triplet barrier energy ΔE_2 from only the luminescence decay constants at 77 K and at RT. We have tried various ways to do so, but all of them suffer from some sort of numerical instability resulting from trying to get a relatively small number from taking the difference of two large numbers. Improved computational precision would not solve this problem because the accuracy of the two large numbers is limited by experimental precision. We therefore choose a different route and simply assume that RT is a high-enough temperature to neglect all but the barrier term. Fig. 14 shows that this is only a very rough approximation at best. However we have little alternative but to make this approximation given the nature of the primary readily available data. That is, the best that can be done if the only data available is the luminescence decay constants at 77 K and at RT, is to fit to the very simple equation,

$$k(T) = A_{\text{ave}} e^{-\Delta E_{\text{ave}}/RT}. \quad (34)$$

This may also be regarded as an alternative (overly simplistic) model. If we can use this model to explain how ΔE_{ave} may be estimated from PDOS-LFT, then we will nevertheless have access to

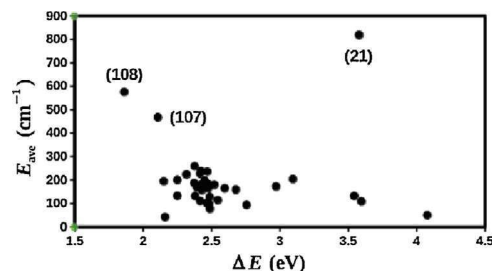


Fig. 15. Correlation between ΔE and E_{ave} .

information about the interrelationship of luminescence lifetimes at 77 K and at RT. With this caveat, we will confine subsequent discussion to luminescence indices for predicting ΔE_{ave} .

Let us now turn to the challenge posed in Ref. [3], namely that of coming up with MO-based indices (or, more exactly, PDOS-LFT-based indices) for predicting luminescence lifetimes. The argument was made that the ΔE_{ave} should be smallest when the ${}^3\text{MC}-{}^3\text{MLCT}$ state energy difference is smallest. In LFT-PDOS terms, this corresponds to ΔE_{ave} being smallest when the MO energy difference,

$$\Delta E = \varepsilon_{e_g^*} - \varepsilon_{\pi^*}, \quad (35)$$

is smallest. We can check this using the PDOS corresponding to the complexes listed in Tables 10 and 11. A few complexes have to be eliminated when the known underbinding of DFT has led to unbound e_g^* orbitals. Nevertheless, this still leaves 36 data points. The correlation between ΔE and E_{ave} is shown in Fig. 15. The correlation is surprisingly bad.

We are thus led to think more deeply about the avoided crossing of two states with diabatic energies E_1 and E_2 and coupling matrix element W . The adiabatic energies may be found by diagonalizing the two-state hamiltonian matrix,

$$\mathbf{H} = \begin{bmatrix} E_1 & W \\ W & E_2 \end{bmatrix}. \quad (36)$$

The exact and perturbative solutions are,

$$\begin{aligned}
 E_+ &= \bar{E} + \frac{1}{2} \sqrt{(\Delta E)^2 + 4W^2} \\
 &\approx E_2 - \frac{W^2}{\Delta E} \\
 E_- &= \bar{E} - \frac{1}{2} \sqrt{(\Delta E)^2 + 4W^2} \\
 &\approx E_1 + \frac{W^2}{\Delta E},
 \end{aligned} \quad (37)$$

where

$$\bar{E} = \frac{E_1 + E_2}{2}. \quad (38)$$

is the average of the diagonal elements. Following ideas very similar to those found in frontier MO theory (FMOT) [119,120], we will adapt the perturbative formulae evaluated at the ground state geometry,

$$E_- - E_1 \approx \frac{W^2}{\Delta E}. \quad (39)$$

as the estimate of the triplet state energy barrier. More exactly, the slope of the potential energy curve for the excited state at the ground-state equilibrium geometry provides a rough indication of trends in the height of the excited-state energy barrier.

Although we are not actually doing FMOT, but rather presenting something which we suppose to be novel, it should be born in mind that our theory resembles FMOT and so is subject to criticism similar to that which Dewar so reasonably leveled at FMOT [121]. Nevertheless FMOT continues to be used and indeed was honored by the 1981 Nobel Prize in Chemistry because, occasional failures set aside, FMOT frequently provides a simple explanation of chemical reactivity. Likewise we seek a simple explanation of luminescence lifetimes but expect there to be occasional exceptions. Eq. (39) suggests that E_{ave} should correlate better with $1/\Delta E$ than with ΔE . This hypothesis is tested in Fig. 16. Fig. 16 does indeed seem more linear than does Fig. 15, but the line in Fig. 16 seems to take the form of an upperbound to a scatter of E_{ave} values.

A clue as to how to further improve our theory is to notice that while E_{ave} has units of energy, $1/\Delta E$ has units of inverse energy. This should be corrected by the quantity W which also has units of energy, but which is not obviously related to the PDOS-LFT picture from which we seek to extract clues about luminescence lifetimes. Again, we take our lead from Roald Hoffmann (one of the fathers of FMOT), and estimate W by the Wolfberg–Helmholtz-like formula [122],

$$W = S\bar{E}, \quad (40)$$

where \bar{E} was defined in Eq. (38) and S is some sort of overlap matrix element. Let us assume that $S \approx$ constant, and so compare E_{ave} against $\bar{E}^2/\Delta E$ which both have the energy units. The result is shown in Fig. 17. Except for a few complexes [(14), (21), (107), (108), and possibly ((78))], the result is finally a reasonably good linear correlation. Indeed a least squares fit [$E_{ave} = (9.348 \text{ cm}^{-1}/\text{eV})(\bar{E}^2/\Delta E) + 50.764 \text{ cm}^{-1}$] indicates that

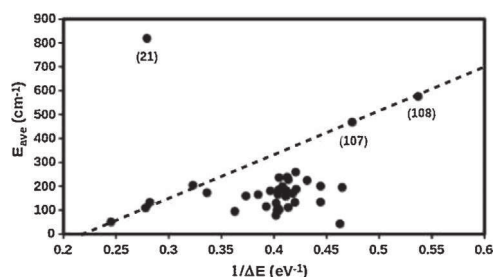


Fig. 16. Correlation between $1/\Delta E$ and E_{ave} . The dashed line is only a guide to the eye.

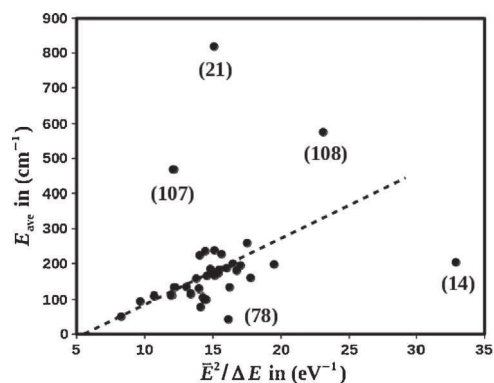


Fig. 17. Correlation between $\bar{E}^2/\Delta E$ and E_{ave} . The dashed line is only a guide to the eye.

the line passes pretty nearly through the origin as might be expected from our simple FMOT-like theory.

In principle we might be able to do better by being able to provide some suitable estimate of the overlap S . One suggestion was given in Ref. [3] which involved the percentage of d contribution to the π^* peak times the percentage of π contribution to the t_{2g} peak. We have tried this and several other similar ideas as a way to construct an estimate of S and have found no way to improve upon $\bar{E}^2/\Delta E$ as the best estimator of E_{ave} . We therefore conclude that this is the best we are going to obtain. The outliers in Fig. 17 (i.e., those far from the line correlating E_{ave} with $\bar{E}^2/\Delta E$ might easily be accounted for by such things as the roughness of the estimates of luminescence lifetimes which, on the one hand, are not always reported very accurately and which, on the other hand, have been averaged over different values in different solvents. It is also possible that not all ruthenium complexes have the same type of decay mechanism — and varying the ligands is an excellent way to increase the number of ways a ligand can come off and go on again, leading us back to the ground state. Indeed, as explained above, we do not even expect our FMOT-like approach to work 100% of the time and so are happy that it works as well as it seems to work.

4. Conclusion

We have shown that gas-phase DFT and TD-DFT calculations give results that correlate well with crystal geometries and with solution absorption spectra of ruthenium complex spectra. This is not really a surprise. It has been noticed before and has even been treated in review articles focusing on the spectra of transition metal complexes [123–125]. However quantifying this relationship for a very large group of ruthenium(II) polypyridine complexes is already useful.

Also important for present purposes, we have shown that PDOS-LFT provides an interpretational tool, different from, but similar to traditional LFT. It allows a semiquantitative prediction of trends in absorption spectra and it allows us to generate spectrochemical series based upon calculated $t_{2g}-e_g^*$ energy differences. This is far from easy to do by other means because TD-DFT calculations provide more information than is otherwise easily mapped onto LFT concepts. In particular, while the nonbonding t_{2g} orbitals may often be identified by visualization of specific individual molecular orbitals of the metal complex, the antibonding e_g^* orbitals mix too heavily with ligand orbitals to extract their energies by direct visualization of metal complex orbitals. On the other hand, approximate e_g^* orbital energies may be obtained in a well-defined manner using the PDOS technique.

This led us to believe that we might be able to develop a simple PDOS-LFT model which could be useful for understanding and hence for helping to design ligands to tailor specific photochemical properties of the ligands of ruthenium(II) polypyridine complexes. Indeed we were able to use ideas reminiscent of frontier molecular orbital theory to build a simple model which provides a linear correlation in many, but not all cases, between an average triplet state transition barrier energy and the square of the average of the e_g^* and lowest π^* PDOS-LFT energies divided by their difference. Exceptions might be due to insufficiently precise experimental data, approximations inherent in a FMOT-like approach, or real differences in the luminescence decay mechanisms of different complexes.

Our simple PDOS-LFT model will not replace more elaborate modeling, but it provides a relatively quick and easy way to relate luminescence lifetimes at room temperature and liquid nitrogen temperature. In so doing, it becomes possible to explore many

more complexes than would be possible with a more detailed model.

Some groups have successfully rationalized the trends in luminescence properties of some ruthenium(II) polypyridine complexes [126–128] and iridium(III) complexes [129] by the DFT-optimized $^3\text{MLCT} \rightarrow ^3\text{MC}$ energy barrier. In the future, we also plan to calculate triplet state energy barriers from explicit searches of TD-DFT excited-state potential energy surfaces for at least a few ruthenium(II) polypyridine complexes and compare them with our PDOS-LFT model.

Authors' contribution

Calculations were carried out by Denis Magero under the direction of Mark E. Casida (50%), George Amolo (16.67%), Nicholas Makau (16.67%), and Lusweti Kituyi (16.67%). The writing of the manuscript is the result of a joint effort based upon detailed progress reports by Denis Magero, commented by all the authors, and amalgamated into the present form by Mark E. Casida. All authors have read and approved the final manuscript.

Conflicts of interest

The authors declare no conflict of interest.

Acknowledgements

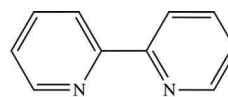
This work is part of the Franco-Kenyan ELEPHOX (ELEctrochemical and PHOtochemical Properties of Some Remarkable Ruthenium and Iron CompleXes) project. DM thanks the French Embassy in Kenya for his doctoral scholarship. DM and MEC would also like to acknowledge useful training and exchanges made possible through the African School on Electronic Structure Methods and Applications (ASESMA, <https://asesma.ictp.it/>). We would like to thank Pierre Girard, Sébastien Morin, and Denis Charapoff for technical support in the context of the Grenoble *Centre d'Expérimentation du Calcul Intensif en Chimie (CECIC)* computers used for the calculations reported here. DM acknowledges the Computational Material Science Group (CMSG) lab facilities, <http://www.uoeld.ac.ke/cmsg/>. DM and MEC acknowledge useful conversations with Cleophas Muhavini Wawire, Latévi Max Lawson Daku, Chantal Daniel, Qingchao Sun, Andreas Hauser, and Xiuwen Zhou. MEC acknowledges useful discussions with Frédérique Loiseau and with Damien Jouvenot.

Appendix A. Some common abbreviations

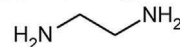
This paper contains a large number of abbreviations in order to keep the text from becoming too cumbersome. For the reader's convenience, we summarize some of these abbreviations in this appendix. Ligand abbreviations are given in the next appendix. Common solvent abbreviations are:

- acetonitrile, CH_3CN .
- heavy water, $^2\text{H}_2\text{O}$.
- dimethylformamide, $(\text{CH}_3)_2\text{N-CHO}$.
- ethyleneglycol, $\text{HOCH}_2\text{CH}_2\text{OH}$.
- ethylenediamine, $\text{H}_2\text{NCH}_2\text{CH}_2\text{NH}_2$.
- ether/*iso*-pentane/ethanol (5:5:2).
- ethanol, $\text{CH}_3\text{CH}_2\text{OH}$.
- water, H_2O .
- methanol, CH_3OH .
- propylene carbonate,

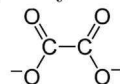
Some other abbreviations used in the text are:



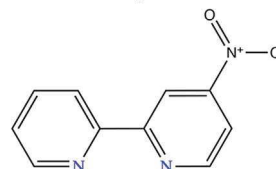
bpy: 2,2'-bipyridine



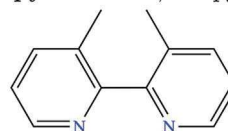
en: 1,2-ethylenediamine



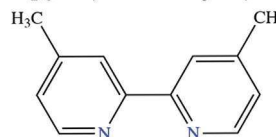
ox: oxalate ion



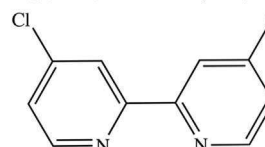
4-n-bpy: 4-nitro-2,2'-bipyridine



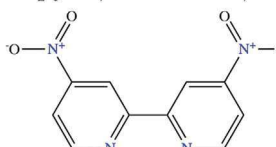
3,3'-dm-bpy: 3,3'-dimethyl-2,2'-bipyridine



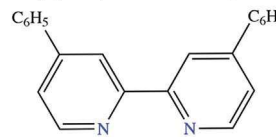
4,4'-dm-bpy: 4,4'-dimethyl-2,2'-bipyridine



4,4'-dCl-bpy: 4,4'-dichloro-2,2'-bipyridine



4,4'-dn-bpy: 4,4'-dinitro-2,2'-bipyridine



4,4'-dph-bpy: 4,4'-diphenyl-2,2'-bipyridine

Fig. 18. Ligand list (part I).

- atomic orbital.
- three-parameter hybrid Becke exchange plus Lee–Yang–Parr correlation density functional.
- density-functional theory.
- density-of-states.
- effective core potential.
- frontier molecular orbital theory.
- ground state.
- Ligand field theory.
- metal centered.
- metal-ligand charge transfer.
- molecular orbital.
- partial density of states.
- room temperature.
- self-consistent field.
- time dependent.
- volume to volume.

Appendix B. List of ligand abbreviations

The ligand abbreviations used in this paper are the same as those used in Ref. [16]. For the readers convenience, these ligands are shown in Figs. 18–26 and in order of their appearance in the Tables 1–4.

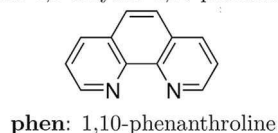
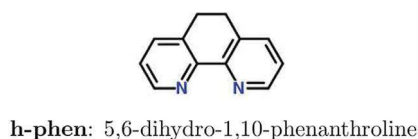
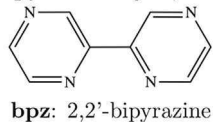
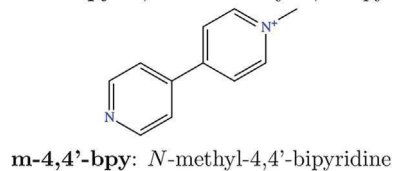
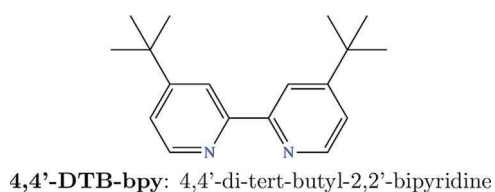


Fig. 19. Ligand list (part II).

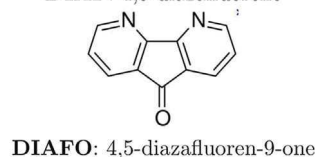
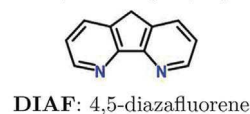
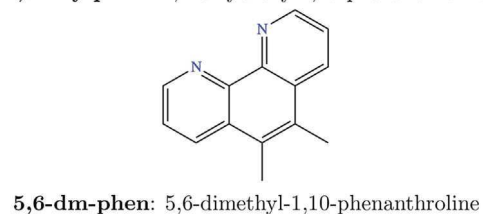
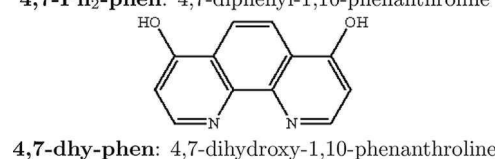
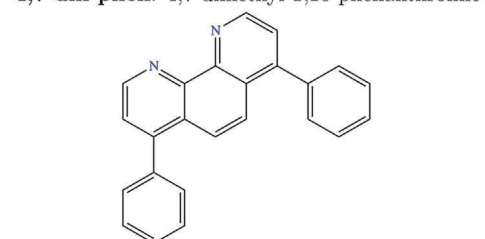
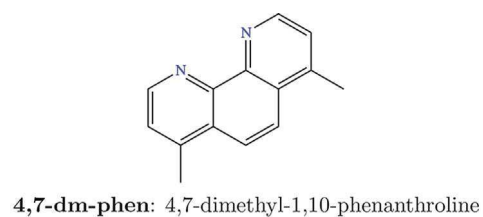


Fig. 20. Ligand list (part III).

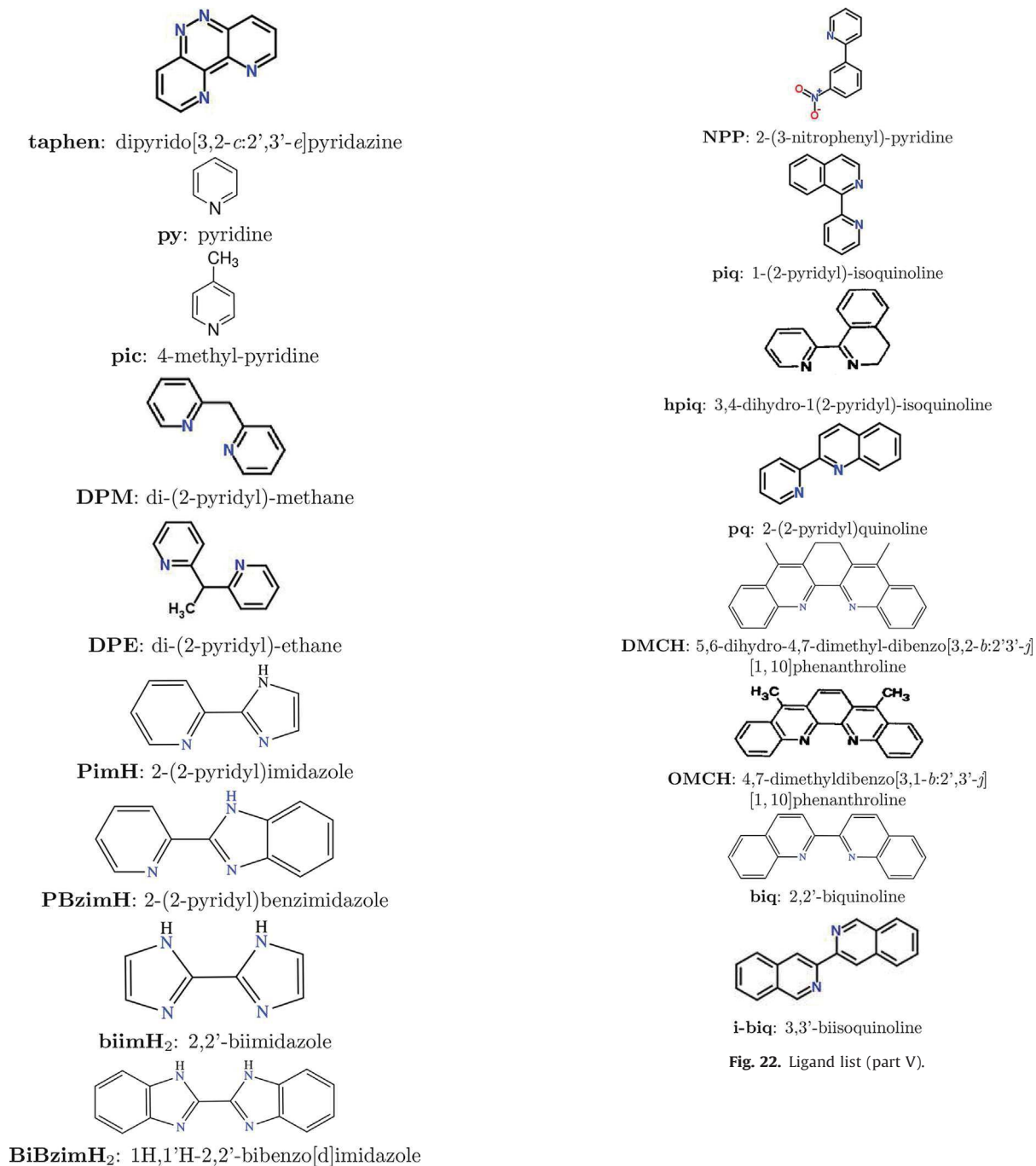


Fig. 22. Ligand list (part V).

Fig. 21. Ligand list (part IV).

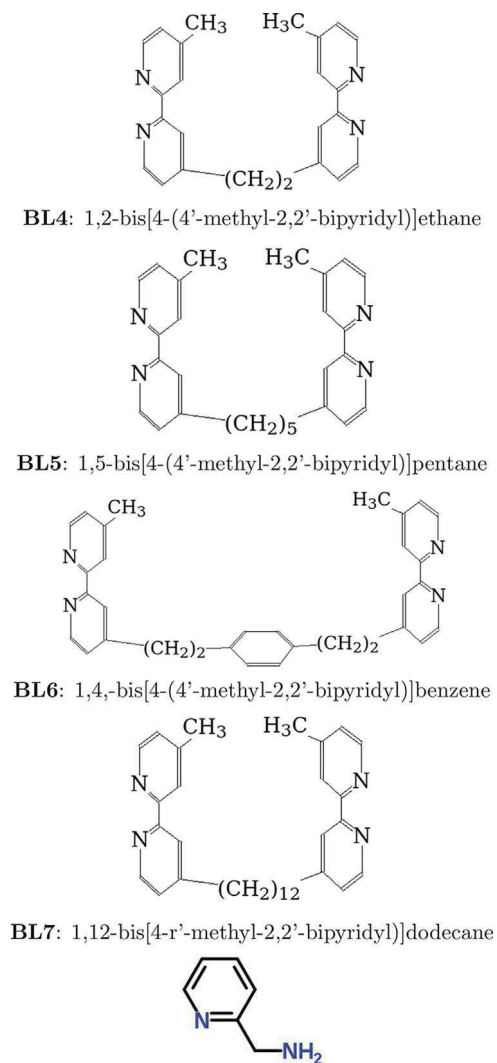


Fig. 23. Ligand list (part VI).

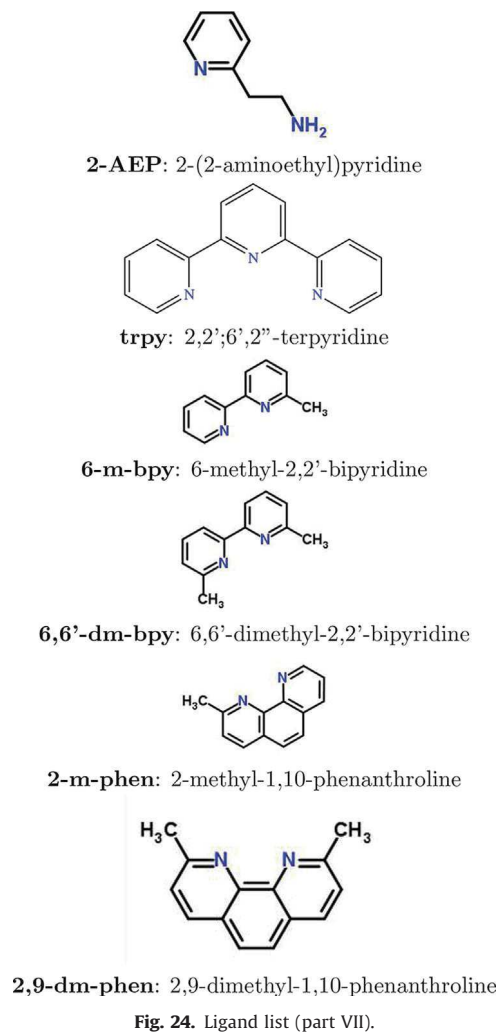
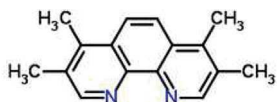
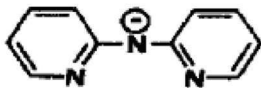


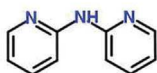
Fig. 24. Ligand list (part VII).



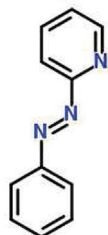
tm1-phen: 3,4,7,8-tetramethyl-1,10-phenanthroline



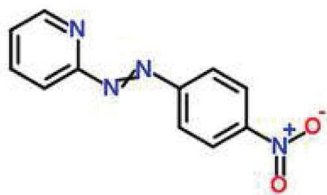
DPA: di-2-pyridylamine anion



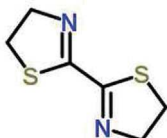
DPAH: di-2-pyridylamine



Azpy: 2-(phenylazo)pyridine

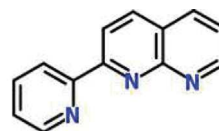


NA: 2-((4-nitrophenyl)azo)pyridine

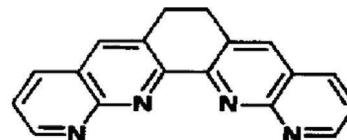


bt: 2,2'-bi-2-thiazoline

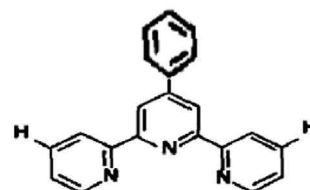
Fig. 25. Ligand list (part VIII).



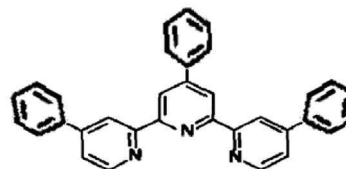
pynapy: 2-(2-pyridyl)-1,8-naphthyridine



dinapy: 5,6-dihydro-dipyrido[3,2-*b*:2',3'-*j*][1,10]phenanthroline



tro: 4'-phenyl-2,2',2''-tripyrindine



tsite: 4,4',4''-triphenyl-2,2',2''-tripyrindine



dqp: 2,6-di-(2'-quinolyl)pyridine

Fig. 26. Ligand list (part IX).

Appendix C. Supplementary data

Supplementary data associated with this article can be found, in the online version, at <http://dx.doi.org/10.1016/j.jphotochem.2017.07.037>.

References

- [1] D.E. Lewis, Klaus at Kazon is a place name (<https://en.wikipedia.org/wiki/Kazon>) and so should be capitalized. *Bull. Hist. Chem.* 41 (2016) 3.
- [2] J. Sauvage, et al., Ruthenium(II) and Osmium(II) bis(terpyridine) complexes in covalently-linked multicomponent systems: synthesis, electrochemical behavior, absorption spectra, and photochemical and photophysical properties, *Chem. Rev.* 94 (1994) 993.
- [3] C.M. Wawire, et al., Density-functional study of luminescence in polypyridine ruthenium complexes, *J. Photochem. Photobiol. A* 276 (2014) 8.
- [4] V. Balzani, A. Juris, Photochemistry and photophysics of Ru(II) polypyridine complexes in the Bologna group. From early studies to recent developments, *Coord. Chem. Rev.* 211 (2001) 97.
- [5] K. Nakamaru, Synthesis, luminescence quantum yields, and lifetimes of trischelated ruthenium(II) mixed-ligand complexes including 3,3'-dimethyl-2,2'-bipyridyl, *Bull. Chem. Soc. Jpn.* 55 (1982) 2697.
- [6] G. Liebsch, I. Klimant, O.S. Wolfbeis, Luminescence lifetime temperature sensing based on sol-gels and poly(acrylonitrile)s dyed with ruthenium metal-ligand complexes, *Adv. Mater.* 11 (1999) 1296.
- [7] A. Harriman, A. Khatyr, R. Ziessel, Extending the luminescence lifetime of ruthenium(II) poly(pyridine) complexes in solution at ambient temperature, *Dalton Trans.* 10 (2003) 2061.
- [8] M. Duati, et al., Enhancement of luminescence lifetimes of mononuclear ruthenium(II)-terpyridine complexes by manipulation of the σ -donor strength of ligands, *J. Inorg. Chem.* 42 (2003) 8377.
- [9] E.A. Medlycott, G.S. Hanan, Designing tridentate ligands for ruthenium(II) complexes with prolonged room temperature luminescence lifetimes, *Chem. Soc. Rev.* 34 (2005) 133.
- [10] K.J. Morris, M.S. Roach, W. Xu, J.N. Demas, B.A. DeGraff, Luminescence lifetime standards for the nanosecond to microsecond range and oxygen quenching of ruthenium(II) compounds, *Anal. Chem.* 79 (2007) 9310.
- [11] L.J. Nurkkala, et al., The effects of pendant vs. fused thiophene attachment upon the luminescence lifetimes and electrochemistry of tris(2,2'-bipyridine)ruthenium(II) complexes, *Eur. J. Inorg. Chem.* 26 (2008) 4101.
- [12] R.O. Steen, et al., The role of isometric effects on the luminescence lifetimes and electrochemistry of oligothiophenyl-bridged dinuclear tris(2,2'-bipyridine) ruthenium(II) complexes, *Eur. J. Inorg. Chem.* 11 (2008) 1784.
- [13] S. Ji, et al., Tuning the luminescence lifetimes of ruthenium(II) polypyridine complexes and its application in luminescent oxygen sensing, *J. Mater. Chem.* 20 (2010) 1953.
- [14] B.N. Figgis, M.A. Hitchman, *Ligand Field Theory and Its Applications*, Wiley-VCH, New York, 2000.
- [15] H. Ramanantoanina, W. Urland, A. García-Fuente, F. Cimpoesu, C. Daul, Ligand field density functional theory for the prediction of future domestic lighting, *Phys. Chem. Chem. Phys.* 28 (2014) 14625.
- [16] A. Juris, et al., Ru(II) polypyridine complexes: photophysics, photochemistry, electrochemistry, and chemiluminescence, *Coord. Chem. Rev.* 84 (1988) 85.
- [17] M. Kasha, Characterization of electronic transitions in complex molecules, *Discuss. Faraday Soc.* 9 (1950) 14.
- [18] G.A. Crosby, Spectroscopic investigations of excited states of transition-metal complexes, *Acc. Chem. Res.* 8 (1975) 231.
- [19] V. Balzani, S. Campagna (Eds.), *Photochemistry and Photophysics of Coordination Compounds. I*, Vol. 280 of *Top. Curr. Chem.*, Springer, Heidelberg, 2007.
- [20] V. Balzani, S. Campagna (Eds.), *Photochemistry and Photophysics of Coordination Compounds. II*, Vol. 281 of *Top. Curr. Chem.*, Springer, Heidelberg, 2007.
- [21] F. Barigelli, A. Juris, V. Balzani, P. Belser, A. von Zelewsky, Temperature dependence of the Ru(bpy)₂(CN)₂ and Ru(bpy)₂(i-biq)²⁺ luminescence, *J. Phys. Chem.* 91 (1987) 1095.
- [22] J. Heully, F. Alaray, M. Boggio-Pasqua, Spin-orbit effects on the photophysical properties of [Ru(bpy)₃]²⁺, *J. Chem. Phys.* 131 (2009) 184308.
- [23] M.J. Frisch, et al., Gaussian 03, Revision B. 05, Gaussian, Inc., Pittsburgh, PA, 2003.
- [24] M.J. Frisch, et al., Gaussian 09 Revision D.01, (2009).
- [25] W. Kohn, L.J. Sham, Self-consistent equations including exchange and correlation effects, *Phys. Rev.* 140 (1965) A1133.
- [26] A.D. Becke, Density-functional exchange-energy approximation with correct asymptotic behavior, *Phys. Rev. A* 38 (1988) 3098.
- [27] S.H. Vosko, L. Wilk, M. Nusair, Accurate spin-dependent electron liquid correlation energies for local spin density calculations: a critical analysis, *Can. J. Phys.* 58 (1980) 1200.
- [28] C. Lee, W. Yang, R.G. Parr, Development of the Colle-Salvetti correlation-energy formula into a functional of the electron density, *Phys. Rev. B* 37 (1988) 785.
- [29] A.D. Becke, Density-functional thermochemistry. III. The role of exact exchange, *J. Chem. Phys.* 98 (1993) 5648.
- [30] P.J. Hay, W.R. Wadt, *Ab initio* effective core potentials for molecular calculations. potentials for K to Au including the outermost core orbitals, *J. Chem. Phys.* 82 (1985) 299.
- [31] P.J. Hay, W.R. Wadt, *Ab initio* effective core potentials for molecular calculations. Potentials for the transition metal atoms Sc to Hg, *J. Chem. Phys.* 82 (1985) 270.
- [32] R. Ditchfield, W. Hehre, J.A. Pople, Self-consistent molecular-orbital methods. IX. An extended Gaussian-type basis for molecular-orbital studies of organic molecules, *J. Chem. Phys.* 54 (1971) 724.
- [33] W.J. Hehre, R. Ditchfield, J.A. Pople, Self-consistent molecular orbital methods. XII. Further extensions of Gaussian-type basis sets for use in molecular orbital studies of organic molecules, *J. Chem. Phys.* 56 (1972) 2257.
- [34] P. Hariharan, J.A. Pople, The influence of polarization functions on molecular orbital hydrogenation energies, *Theor. Chim. Acta* 28 (1973) 213.
- [35] P.C. Hariharan, J.A. Pople, Accuracy of AH_n equilibrium geometries by single determinant molecular orbital theory, *Mol. Phys.* 27 (1974) 209.
- [36] M.M. Francl, et al., Self-consistent molecular orbital methods. XXIII. A polarization-type basis set for second-row elements, *J. Chem. Phys.* 77 (1982) 3654.
- [37] V.A. Rassolov, M.A. Ratner, J.A. Pople, P.C. Redfern, L.A. Curtiss, 6-31G* basis set for third-row atoms, *J. Comp. Chem.* 22 (2001) 976.
- [38] G.A. Petersson, M.A. Al-Laham, A complete basis set model chemistry. II. Open-shell systems and the total energies of the first-row atoms, *J. Chem. Phys.* 94 (1991) 6081.
- [39] The Web of Science may be found at <https://pcs.webofknowledge.com> (accessed 16.07.17).
- [40] The annual Density Functional Theory popularity poll is organized by Marcel Swart, Matthias Bickelhaupt, and Miquel Duran and its results may be found at <http://www.marcelswart.eu/dft-poll/> (accessed 16.07.17).
- [41] A.C. Tsipis, DFT flavor of coordination chemistry, *Coord. Chem. Rev.* 272 (2014) 1.
- [42] R.K. Hocking, R.J. Deeth, T.W. Hambley, DFT study of the systematic variations in metal-ligand bond lengths of coordination complexes: the crucial role of the condensed phase, *Inorg. Chem.* 46 (2007) 8238.
- [43] C. Latouche, A. Balardi, V. Barone, Virtual eyes designed for quantitative spectroscopy of inorganic complexes: Vibronic signatures in the phosphorescence spectra of terpyridine derivatives, *J. Phys. Chem. B* 119 (2015) 7253.
- [44] The Cambridge Crystallographic Data Centre (CCDC), <https://www.ccdc.cam.ac.uk/> (accessed 06.02.16).
- [45] R. Prajapati, V.K. Yadav, S.K. Dubey, B. Durham, L. Mishra, CCDC 667743: Experimental Crystal Structure Determination, (2007), doi:<http://dx.doi.org/10.5517/ccqdv31>.
- [46] R. Prajapati, V.K. Yadav, S.K. Dubey, B. Durham, L. Mishra, Reactivity of metal (Zn^{II}, Ru^{II})-2,2'-bipyridyl with some bifunctional ligands, *Indian J. Chem. Sect. A* 47 (2008) 1780.
- [47] O.S. Odongo, J.F. Endicott, M.J. Heeg, CCDC 613874: Experimental Crystal Structure Determination, (2006), doi:<http://dx.doi.org/10.5517/cnlsdd>.
- [48] F.R. Fronczek, CCDC 287967: Experimental Crystal Structure Determination, (2005), doi:<http://dx.doi.org/10.5517/cc9nn8v>.
- [49] H. Shen, et al., A new three-dimensional ruthenium(II) complex via hydrogen bonds: Ru(bpy)₂(ox)·4H₂O (bpy = 2,2'-bipyridine, ox = oxalate ion), *Inorg. Chem. Commun.* 2 (1999) 615.
- [50] D.P. Rillema, D.S. Jones, H.A. Levy, Structure of tris(2,2'-bipyridyl)ruthenium (II) hexafluorophosphate, [Ru(bipy)₃][PF₆]₂: X-ray crystallographic determination, *J. Chem. Soc. Chem. Commun.* 1979 (1979) 849.
- [51] P. Reveco, R.H. Schmehl, W.R. Cherry, F.R. Froczeck, J. Selbin, Cyclometalated complexes of ruthenium. 2. Spectral and electrochemical properties and X-ray structure of bis(2,2'-bipyridine)(4-nitro-2-(2-pyridyl)phenyl)ruthenium (II), *Inorg. Chem.* 24 (1985) 4078.
- [52] D. Heseck, et al., CCDC 116354: Experimental Crystal Structure Determination, (1999), doi:<http://dx.doi.org/10.5517/cc3x2cf>.
- [53] D. Heseck, et al., Conversion of a new chiral reagent Δ -[Ru(bpy)₂(dmsO)Cl]PF₆ to (dmbpy = 4,4'-dimethyl-2,2'-bipyridine), *Chem. Commun.* 5 (1999) 403.
- [54] L.E. Hansen, et al., CCDC 212499: Experimental Crystal Structure Determination, (2003), doi:<http://dx.doi.org/10.5517/cc743t8>.
- [55] L.E. Hansen, et al., Syntheses and characterization of some chloro, methoxy, and mercapto derivatives of [Ru(η^2 -2,2'-bipyridine)₂]²⁺PF₆⁻: crystal and molecular structures of [Ru(η^2 -2,2'-bipyridine)₂(η^2 -4,4'-(X)₂-2,2'-bipyridine)]²⁺2PF₆⁻ (X=Cl, OCH₃), *Inorg. Chim. Acta* 348 (2003) 91.
- [56] M. Du, X. Ge, H. Liu, X. Bu, CCDC 169415: Experimental Crystal Structure Determination, (2001), doi:<http://dx.doi.org/10.5517/cc5p904>.
- [57] M. Du, X. Ge, H. Liu, X. Bu, Synthesis, spectra, and crystal structures of two Ru^{II} complexes with polypyridyl ligands: cis-[Ru(pby)₂(4,4'-bpy)Cl](PF₆)₂·H₂O and cis-[Ru(phen)₂(CH₃CN)₂](PF₆)₂, *J. Mol. Struct.* 610 (2002) 207.
- [58] B. Ye, X. Chen, T. Zeng, L. Ji, syntheses, spectra and crystal structures of ruthenium(II) complexes with polypyridyl:[Ru(bipy)₂(phen)](ClO₄)₂·H₂O and [Ru(bipy)₂(Me-phen)](ClO₄)₂, *Inorg. Chim. Acta* 240 (1995) 5.
- [59] V.W. Yam, B. Li, N. Zhu, CCDC 182310: Experimental Crystal Structure Determination, (2002), doi:<http://dx.doi.org/10.5517/cc63pzy>.
- [60] V.W. Yam, B. Li, N. Zhu, Synthesis of mesoporous silicates with controllable pore size using surfactant ruthenium(II) complexes as templates, *Adv. Mater.* 14 (2002) 719.
- [61] C.M. Kepert, et al., CCDC 230551: Experimental Crystal Structure Determination, (2004), doi:<http://dx.doi.org/10.5517/cc7qx4z>.

- [62] C.M. Kepert, et al., The synthesis and structure of heteroleptic tris(diimine) ruthenium(II) complexes, *Dalton Trans.* (2004) 1766.
- [63] L.J. Henderson Jr., F.R. Fronczek, W.R. Chery, Selective perturbation of ligand field excited states in polypyridine ruthenium(II) complexes, *J. Am. Chem. Soc.* 106 (1984) 5876.
- [64] Y. Wang, D.C. Jackman, C. Woods, D.P. Rillema, Crystal structure, physical, and photophysical properties of a ruthenium (II) bipyridine diazafluorenone complex, *J. Chem. Crystallogr.* 25 (1995) 549.
- [65] P.B. Hitchcock, et al., *Cis*-bis(2,2'-bipyridine)bis(pyridine)ruthenium(II), *J. Chem. Soc. Dalton Trans.* 1988 (1988) 1837.
- [66] B. Klop, H. Viebrock, A. von Zelewsky, D. Abeln, CCDC 162056: Experimental Crystal Structure Determination, (2001), doi:<http://dx.doi.org/10.5517/cc5fmmt>.
- [67] B. Klop, H. Viebrock, A. von Zelewsky, D. Abeln, Crystal structure analysis and chiral recognition study of Δ -[Ru(bpy)₂(py)₂][(+)-O,O'-dibenzoyl-D-tartrate]·12H₂O and Λ -[Ru(bpy)₂(py)₂][(-)-O,O'-dibenzoyl-L-tartrate]·12H₂O, *Inorg. Chem.* 40 (2001) 1196.
- [68] A.H. Velders, et al., CCDC 143552: Experimental Crystal Structure Determination, (2000), doi:<http://dx.doi.org/10.5517/cc4tcq0>.
- [69] A.H. Velders, et al., A simple example of the fluxional behaviour of ruthenium-coordinated C₂-symmetric monodentate ligands – synthesis ¹H NMR spectroscopic study and crystal structure of *cis*-[Ru(bpy)₂(4Pic)₂](PF₆)₂, *Eur. J. Inorg. Chem.* 2002 (2002) 193.
- [70] S. Derossi, H. Adams, M.D. Ward, CCDC 622792: Experimental Crystal Structure Determination, (2006), doi:<http://dx.doi.org/10.5517/ccnx22p>.
- [71] S. Derossi, H. Adams, M.D. Ward, Hydrogen-bonded assemblies of ruthenium (II)-biimidazole complex cations and cyanometallate anions: structures and photophysics, *Dalton Trans.* 2007 (2007) 33.
- [72] N. Rockstroh, et al., CCDC 760286: Experimental Crystal Structure Determination, (2010), doi:<http://dx.doi.org/10.5517/cctj4ct>.
- [73] N. Rockstroh, et al., Structural properties of ruthenium biimidazole complexes determining the stability of their supramolecular aggregates, *Z. Nat. B: Chem. Sci.* 65 (2010) 281.
- [74] P. Wang, et al., Structure and properties of diastereoisomers of a ruthenium (II) complex having a pyridylpyrazoline derivative as a ligand, *Chem. Lett.* 30 (2001) 940.
- [75] A.A. Farah, D.V. Stynes, W.J. Pietro, CCDC 140838: Experimental Crystal Structure Determination, (2000), doi:<http://dx.doi.org/10.5517/cc4qk5k>.
- [76] A.A. Farah, D.V. Stynes, W.J. Pietro, Syntheses, characterization and structures of 2-(2-pyridyl)-4-methylcarboxyquinoline ligand and bis(2,2-bipyridine)-2-(2-pyridyl)-4-methylcarboxyquinoline ruthenium(II) hexafluorophosphate, *Inorg. Chim. Acta* 343 (2003) 295.
- [77] S. Rau, et al., CCDC 236778: Experimental Crystal Structure Determination, (2004), doi:<http://dx.doi.org/10.5517/cc7yd0k>.
- [78] S. Rau, et al., Efficient synthesis of ruthenium complexes of the type (R-bpy)₂RuCl₂ and [(R-bpy)₂Ru(L-L)]Cl₂ by microwave-activated reactions (R: H, Me, *tert*-But) (L-L: substituted bibenzimidazoles, bipyrimidine, and phenanthroline), *Inorg. Chim. Acta* 357 (2004) 4496.
- [79] P.U. Maheswari, V. Rajendiran, M. Palaniandavar, R. Thomas, G.U. Kulkarni, CCDC 623203: Experimental Crystal Structure Determination, (2006), doi:<http://dx.doi.org/10.5517/ccnxhbc>.
- [80] P.U. Maheswari, V. Rajendiran, M. Palaniandavar, R. Thomas, G.U. Kulkarni, Mixed ligand ruthenium(II) complexes of 5,6-dimethyl-1,10-phenanthroline: the role of ligand hydrophobicity on DNA binding of the complexes, *Inorg. Chim. Acta* 359 (2006) 4601.
- [81] M. Kato, K. Sasano, M. Kimura, S. Yamauchi, Solid state effect on the phosphorescence spectrum of a tris(3,3'-biisoquinoline)ruthenium(II) salt, *Chem. Lett.* 21 (1992) 1887.
- [82] A. Taketoshi, T. Koizumi, T. Kanbara, CCDC 789502: Experimental Crystal Structure Determination, (2010), doi:<http://dx.doi.org/10.5517/ccvhjtn>.
- [83] A. Taketoshi, T. Koizumi, T. Kanbara, Aerobic oxidative dehydrogenation of benzylamines catalyzed by cyclometalated ruthenium complex, *Tetrahedron Lett.* 51 (2010) 6457.
- [84] C. Tsai, et al., Characterization of low energy charge transfer transitions in (terpyridine)(bipyridine)ruthenium(II) complexes and their cyanide-bridge bi- and tri-metallic analogues, *Inorg. Chem.* 50 (2011) 11965.
- [85] C. Tsai, et al., CCDC: 868664: Experimental Crystal Structure Determination, (2012), doi:<http://dx.doi.org/10.5517/ccy4xfd>.
- [86] D. Onggo, M.L. Scudder, D.C. Craig, H.A. Goodwin, CCDC: 222020: Experimental Crystal Structure Determination, (2003), doi:<http://dx.doi.org/10.5517/cc7g0ym>.
- [87] D. Onggo, M.L. Scudder, D.C. Craig, H.A. Goodwin, The influence of ortho-substitution within the ligand on the geometry of the tris(2,2'-bipyridine) ruthenium(II) and tris(1,10-phenanthroline)ruthenium(II) ions, *J. Mol. Struct.* 738 (2005) 129.
- [88] M. Schwalbe, et al., CCDC 614185: Experimental Crystal Structure Determination, (2006), doi:<http://dx.doi.org/10.5517/ccnm3fs>.
- [89] M. Schwalbe, et al., Synthesis and characterisation of poly(bipyridine) ruthenium complexes as building blocks for heterosupramolecular arrays, *Eur. J. Inorg. Chem.* 2008 (2008) 3310.
- [90] D. Onggo, M.L. Scudder, D.C. Craig, H.A. Goodwin, CCDC 222021: Experimental Crystal Structure Determination, (2003), doi:<http://dx.doi.org/10.5517/cc7g0zn>.
- [91] J. Gao, et al., CCDC 900121: Experimental Crystal Structure Determination, (2012), doi:<http://dx.doi.org/10.5517/ccz6n5z>.
- [92] J. Gao, et al., Molecule-based water-oxidation catalysts (WOCs): cluster-size-dependent dye-sensitized polyoxometalates for visible-light-driven O₂ evolution, *Sci. Rep.* 3 (2013) 1853.
- [93] E. Baranoff, et al., CCDC 182680: Experimental Crystal Structure Determination, (2002), doi:<http://dx.doi.org/10.5517/cc642x9>.
- [94] E. Baranoff, et al., Photochemical or thermal chelate exchange in the ruthenium coordination sphere of complexes of the Ru(phen)₂L family (L = diimine or dinitrile ligands), *Inorg. Chem.* 41 (2002) 1215.
- [95] E. Wachter, D.K. Heidary, B.S. Howerton, S. Parkin, E.C. Glazer, CCDC 881148: Experimental Crystal Structure Determination, (2012), doi:<http://dx.doi.org/10.5517/ccy4x4j>.
- [96] E. Wachter, D.K. Heidary, B.S. Howerton, S. Parkin, E.C. Glazer, Light-activated ruthenium complexes photo bind DNA and are cytotoxic in the photodynamic therapy window, *Chem. Commun.* 48 (2012) 9649.
- [97] D. Onggo, M.L. Scudder, D.C. Craig, H.A. Goodwin, CCDC 222019: Experimental Crystal Structure Determination, (2003), doi:<http://dx.doi.org/10.5517/cc7g0xl>.
- [98] A.C.G. Hotze, et al., CCDC 251699: Experimental Crystal Structure Determination, (2004), doi:<http://dx.doi.org/10.5517/cc8fxbx>.
- [99] A.C.G. Hotze, et al., Characterization by NMR Spectroscopy, X-ray Analysis and Cytotoxic Activity of the Ruthenium(II) Compounds [RuL₂](PF₆)₂ (L = 2-Phenylazopyridine or o-Tolylazopyridine) and [RuL'L']₂(PF₆)₂ (L, L' = 2-Phenylazopyridine, 2,2'-Bipyridine), *Eur. J. Inorg. Chem.* 2005 (2005) 2648.
- [100] A.A. Farah, W.J. Pietro, CCDC 199681: Experimental Crystal Structure Determination, (2002), doi:<http://dx.doi.org/10.5517/cc6psbz>.
- [101] A.A. Farah, W.J. Pietro, Synthesis, structure and electrochemical properties of tris(2-(2-pyridyl)-4-methylcarbonylquinoline)ruthenium(II) hexafluorophosphate, *Inorg. Chem. Comm.* 6 (2003) 662.
- [102] M. Kozłowska, P. Rodziewicz, D.M. Brus, J. Brezcko, K. Brzezinski, CCDC 909756: Experimental Crystal Structure Determination, (2012), doi:<http://dx.doi.org/10.5517/cczjnz3>.
- [103] M. Kozłowska, P. Rodziewicz, D.M. Brus, J. Brezcko, K. Brzezinski, Bis(2, 2': 6', 2"-terpyridine) ruthenium (II) bis (perchlorate) hemihydrate, *Acta Crystallogr. Sect. E: Struct.* 68 (2012) 1414.
- [104] E.C. Constable, et al., CCDC 676373: Experimental Crystal Structure Determination, (2008), doi:<http://dx.doi.org/10.5517/ccq9pht>.
- [105] E.C. Constable, et al., Bis(4'-phenyl-2,2':6',2"-terpyridine)ruthenium(II): Holding the [Ru(tpy)₂]²⁺ embraces at bay, *Inorg. Chem. Commun.* 11 (2008) 805.
- [106] F.H. Allen, The Cambridge structural database: a quarter of a million crystal structures and rising, *Acta Crystallogr. B* 58 (2002) 380.
- [107] R. Dennington, T. Keith, J. Millam, GaussView Version 5, Semichem Inc., Shawnee Mission, KS, 2009.
- [108] M.E. Casida, Time-dependent density-functional theory for molecules and molecular solids, *J. Mol. Struct.: THEOCHEM* 914 (2009) 3.
- [109] M.E. Casida, M. Huix-Rotllant, Progress in time-dependent density-functional theory, *Annu. Rev. Phys. Chem.* 63 (2012) 287.
- [110] The program SPECTRUM_V3.PY may be downloaded from <https://sites.google.com/site/markcasida/tddft>. Documentation (Project_Analyse_Numerique.pdf, in French) and sample input files *nm_exp.txt* and *nm_theo.txt* are also available from the same site (accessed 15.07.15).
- [111] The PDOS.PY program is described in the supplementary data associated with Ref. [3]. The current version of the program PABLO_BAUDIN_PDOS.PY and documentation *Pablo_Baudin_User_Guide.txt* may be downloaded from <https://sites.google.com/site/markcasida/stages> (accessed 15.07.15).
- [112] A.A.M.H.M. Darghouth, et al., Assessment of density-functional tight-binding ionization potentials and electron affinities of molecules of interest for organic solar cells against first-principles GW calculations, *Computation* 3 (2015) 616.
- [113] W. Koch, M.C. Holtzhausen, A Chemist's Guide to Density Functional Theory, Wiley-VCH, New York, 2000.
- [114] N. Yoshikawa, et al., Transition states of the ³MLCT to ³MC conversion in Ru (bpy)₂(phen derivative)²⁺ complexes, *J. Mol. Struct.* 1094 (2015) 98.
- [115] E. Borfecchia, et al., X-ray transient absorption structural characterization of the ³MLCT triplet excited state of *cis*-[Ru(bpy)₂(py)₂]²⁺, *Dalton Trans.* 42 (2013) 6564.
- [116] J.Y. Choi, E.J. Park, S.H. Chang, T.J. Kang, Solvent effects on the solvatochromism of 7-aminocoumarin derivatives in neat and binary solvent mixtures: correlation of the electronic transition energies with the solvent polarity parameters, *Bull. Korean Chem. Soc.* 30 (2009) 1452.
- [117] M. Maestri, N. Armaroli, V. Blazani, E.C. Constable, A.M.W.C. Thompson, Complexes of the Ruthenium(II)-2,2';6',2"-terpyridine Family. Effect of electron-accepting and donating substituents on the photophysical and electrochemical properties, *Inorg. Chem.* 34 (1995) 2759.
- [118] F. Barigelletti, P. Belsler, A. von Zelewsky, A. Juris, V. Balzani, Luminescence of mixed-ligand polypyridine-ruthenium(II) complexes in the temperature range 84–250 K. Interligand interactions and viscosity effects on radiationless processes, *J. Phys. Chem.* 89 (1985) 3680.
- [119] I. Fleming, *Frontier Orbitals and Organic Chemical Reactions*, John Wiley and Sons, New York, 1976.
- [120] N.T. Anh, *Frontier Orbitals: A Practical Manual*, John Wiley and Sons, The Atrium, Southern Gate, Chichester, West Sussex PO19 8SQ, England, 2007.
- [121] M.J.S. Dewar, A critique of frontier orbital theory, *THEOCHEM* 200 (1989) 301.
- [122] M. Wolfsberg, L. Helmholz, The spectra and electronic structure of the tetrahedral ions MnO Mn O₄⁻, CrO Cr O₄, and Cr O₄, *J. Chem. Phys.* 20 (1952) 837.

- [123] C. Daniel, Electronic spectroscopy and photoreactivity in transition metal complexes, *Coord. Chem. Rev.* 238–239 (2003) 143.
- [124] A. Rosa, G. Ricciardi, O. Gritsenko, E.J. Baerends, Excitation energies of metal complexes with time-dependent density functional theory, *Stuct. Bond.* 112 (2004) 49.
- [125] A.V.S. Záliš Jr., Modeling of charge-transfer transitions and excited states in d^6 transition metal complexes by DFT techniques, *Coord. Chem. Rev.* 251 (2007) 258.
- [126] E. Lebon, et al., Can a functionalized phosphine ligand promote room temperature luminescence of the $[\text{Ru}(\text{bpy})(\text{tpy})]^{2+}$ core? *Chem. Commun.* 48 (2012) 741.
- [127] E. Lebon, et al., Phosphoryl Group as a strong σ -donor anionic phosphine-type ligand: a combined experimental and theoretical study on long-lived room temperature luminescence of the $[\text{Ru}(\text{tpy})(\text{bpy})(\text{Ph}_2\text{PO})]^+$ Complex, *Inorg. Chem.* 53 (2014) 1946.
- [128] Q. Sun, B. Dereka, E. Vauthey, L.M. Lawson Daku, A. Hauser, Ultrafast transient IR spectroscopy and DFT calculations of ruthenium(II) polypyridyl complexes, *Chem. Sci.* 8 (2016) 223.
- [129] X. Zhou, P.L. Burn, B.J. Powell, Bond fission and non-radiative decay in iridium(III) complexes, *Inorg. Chem.* 55 (2016) 5266.

Bibliography

- [1] C. M. Wawire, D. Jouvenot, F. Loiseau, P. Baudin, S. Liatard, L. Njenga, G. Kamau, and M. E. Casida. Density-functional study of luminescence in polypyridine ruthenium complexes. *J. Photochem. and Photobiol. A*, 276:8, 2014.
- [2] A. Juris, V. Balzani, F. Barigelletti, S. Campagna, P. Belser, and A. Von Zelewsky. Ru(II) polypyridine complexes: Photophysics, photochemistry, electrochemistry, and chemiluminescence. *Coord. Chem. Rev.*, 84: 85, 1988.
- [3] J. P. Sauvage, J. P. Collin, J. C. Chambron, S. Guillerez, and C. Coudret. Ruthenium(II) and osmium(II) bis(terpyridine) complexes in covalently-linked multicomponent systems: Synthesis, electrochemical behavior, absorption spectra, and photochemical and photophysical properties. *Chem. Rev.*, 94:933, 1994.
- [4] V. Balzani and A. Juris. Photochemistry and photophysics of Ru(II) polypyridine complexes in the Bologna group. From early studies to recent developments. *Coordin. Chem. Rev.*, 211(1):97–115, 2001.
- [5] K. Nakamaru. Synthesis, luminescence quantum yields, and lifetimes of trischelated ruthenium (II) mixed-ligand complexes including 3, 3'-dimethyl-2, 2'-bipyridyl. *B. Chem. Soc. Jpn*, 55(9):2697–2705, 1982.
- [6] G. Liebsch, I. Klimant, and O. S. Wolfbeis. Luminescence lifetime temperature sensing based on sol-gels and poly(acrylonitrile)s dyed with ruthenium metal-ligand complexes. *Adv. Mat.*, 11:1296, 1999.
- [7] A. Harriman, A. Khatyr, and R. Ziessel. Extending the luminescence lifetime of ruthenium(II) poly(pyridine) complexes in solution at ambient temperature. *Dalton Trans.*, 10:2061, 2003.
- [8] M. Duati, S. Tasca, F. C. Lynch, H. Bohlen, J. G. Vos, S. Stagni, and M. D. Ward. Enhancement of luminescence lifetimes of mononuclear

- ruthenium(II)-terpyridine complexes by manipulation of the σ -donor strength of ligands. *J. Inorg. Chem.*, 42:8377, 2003.
- [9] E. A. Medlycott and G. S. Hanan. Designing tridentate ligands for ruthenium(II) complexes with prolonged room temperature luminescence lifetimes. *Chem. Soc. Rev.*, 34:133, 2005.
- [10] K. J. Morris, M. S. Roach, W. Xu, J. N. Demas, and B. A. DeGraff. Luminescence lifetime standards for the nanosecond to microsecond range and oxygen quenching of ruthenium(II) compounds. *Anal. Chem.*, 79:9310, 2007.
- [11] L. J. Nurkkala, R. O. Steen, H. K. J. Friberg, J. A. Häggström, P. V. Bernhardt, M. J. Riley, and S. J. Dunne. The effects of pendant vs. fused thiophene attachment upon the luminescence lifetimes and electrochemistry of tris(2,2'-bipyridine)ruthenium(II) complexes. *Eur. J. Inorg. Chem.*, 26:4101, 2008.
- [12] R. O. Steen, L. J. Nurkkala, S. J. Angus-Dunne, C. X. Schmitt, E. C. Constable, M. J. Riley, P. V. Bernhardt, and S. J. Dunne. The role of isometric effects on the luminescence lifetimes and electrochemistry of oligothiophenyl-bridged dinuclear tris(2,2'-bipyridine)ruthenium(II) complexes. *Eur. J. Inorg. Chem.*, 11:1784, 2008.
- [13] S. Ji, W. Wu, W. Wu, P. Song, K. Han, Z. Wang, S. Liu, H. Guo, and J. Zhao. Tuning the luminescence lifetimes of ruthenium(II) polypyridine complexes and its application in luminescent oxygen sensing. *J. Mater. Chem.*, 20:1953, 2010.
- [14] C. J. Cramer and D. G. Truhlar. Density functional theory for transition metals and transition metal chemistry. *Phys. Chem. Chem. Phys.*, 11(46):10757–10816, 2009.

Chapter 12

Located a Transition State on the Excited-State Triplet Surface

This is preliminary work aimed at finding the nature and height of the barrier on the lowest triplet excited-state surface.

12.1 Introduction

12.1.1 Background Information on the Problem

Ruthenium complexes continue to illicit immense interest owing to their wide range of applications ranging from photochemical molecular devices (PMDs), biological sensors, organic light emitting diodes (OLEDS) and biomedical applications just to mention but a few; and which has been the subject of many studies [1–11]. When talking about these complexes, the idea that comes into mind is the excited state lifetime. Study of the excited state lifetime demands that the working of the complexes must be understood in terms of the deactivation mechanisms and what leads to the long or short excited state lifetime. However, in this work we do not focus on how to modify the complex to have a long or short excited state lifetime, our focus

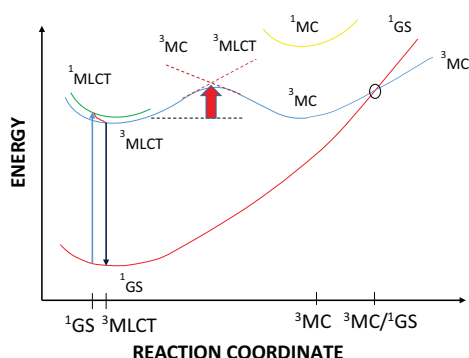


Figure 12.1 – The diagram shows the principle potential energy curves in our model. The abscissa corresponds to a reaction pathway involving partial removal of a ligand while the ordinate represents the state energy. The dashed lines indicate diabatic states whose avoided crossing leads to the energetic barrier on the adiabatic surface between the $^3\text{MLCT}$ and ^3MC minima.

is on how to estimate the excited state lifetimes of the complexes using the quantum chemical calculations. Quantum chemical calculations have been used before and many times to study the structural and electronic properties of these complexes [12].

Generally, there are two ways to look/understand the deactivation mechanisms of the ruthenium complexes, namely, the state based and the molecular orbital based way. We shall explain the two of them in detail and explain why one model is chosen over the other.

1. State based model

The process starts by the absorption of a photon in the ground state (S_0) which is then excited to the singlet metal to ligand charge transfer state ($^1\text{MLCT}$) that is quickly transformed to the triplet metal to ligand charge transfer ($^3\text{MLCT}$) through ultrafast intersystem crossing (ISC). The triplet states are excited states, which means that they are unstable and they must undergo a deactivation to be stabilized. Some of the methods in which the deactivation can occur include: i) A photochemical reaction where the original molecule disappears ii)

luminescence iii) radiationless deactivation and iv) quenching process [13]. The luminescent $^3\text{MLCT}$ can be depopulated in two ways, either through a radiative (emission) or non-radiative pathway. The major deactivation route at room temperature is believed to be to the $^3\text{MLCT}$ to the metal centered, ^3MC state. It is possible to determine the emission quantum yields and the excited state lifetimes from the individual rate constants. Experimentally, excited state lifetime is measured as a decay rate of the intensity of light luminescing at a particular wave as a function of time. Temperature, the decay constant $k(T)$ and decay lifetime $\tau(T)$ are related by,

$$k(T) = \frac{1}{\tau(T)}. \quad (12.1)$$

The decay lifetime $\tau(T)$ is temperature dependent and the decay rate constant can be separated into the temperature dependent and independent parts. The temperature independent processes are those that continue to occur even at very low temperatures.

$$k(T) = k_0 + k_b^{nr}(T), \quad (12.2)$$

where k_0 is the temperature dependent part and $k_b^{nr}(T)$ is the temperature independent part. The temperature dependent term is associated with;

- (a) Activated surface crossing to another excited state. For our case, we shall assume that this is the $^3\text{MLCT}$ to ^3MC surface crossing. This particular term will be studied more exhaustively later on.
- (b) Onset of vibrational modes that do not occur at low temperatures because of the frozen environment. Vibrational modes can favour radiationless decay.

The temperature dependent term may further be further expressed as,

$$k_b^{nr}(T) = k_{melt}(T) + k_{equilib}(T) + k_{barrier}(T), \quad (12.3)$$

where,

$$k_{melt}(T) = \frac{B}{1 + \exp \left[C \left(\frac{1}{T} - \frac{1}{T_B} \right) \right]}. \quad (12.4)$$

T_B is the temperature at which $k_{melt}(T)=B/2$ and C is a temperature related to the viscosity effect. This equation describes the behaviour of a system in the transition from glass to fluid of a solvent.

$$k_{equilib}(T) = A_1 e^{-\Delta E_1/RT}, \quad (12.5)$$

describes thermal equilibrium with higher energy states of the same electronic nature (e.g., states with the same symmetry in an octahedral complex according to LFT but which are split with ligands giving only pseudo-octahedral symmetry), and

$$k_{barrier}(T) = A_2 e^{-\Delta E_2/RT}, \quad (12.6)$$

is an Arrhenius term describing the temperature dependence of the luminescence lifetime at high temperatures ($T > 250$ K) and which as mentioned earlier is related to the activated surface crossing to another excited state. In this case, it is associated with the crossing of the ${}^3\text{MLCT} \rightarrow {}^3\text{MC}$ barrier prior to subsequent de-activation to ${}^1\text{GS}$.

Putting it altogether results in,

$$\begin{aligned} k &= k_0 + k_{melt}(T) + k_{equilib}(T) + k_{barrier}(T) \\ &= k_0 + \frac{B}{1 + C \left(\frac{1}{T} - \frac{1}{T_B} \right)} \\ &\quad + A_1 e^{-\Delta E_1/RT} + A_2 e^{-\Delta E_2/RT}. \end{aligned} \quad (12.7)$$

The barrier term is commonly believed to dominate over the other terms at high-enough temperatures. The assumption made is that barrier crossing followed by a rapid return to the ground state is the main reason for phosphorescence quenching.

The energy barrier for the surface crossing (${}^3\text{MLCT} \rightarrow {}^3\text{MC}$) is re-

lated to the energy gap between the two states and thus it can give an idea about the excited state lifetime of the complexes. Using the state based model, it is possible to estimate the excited state lifetime of d^6 complexes. The problem with the state based model is that the unoccupied states are heavily mixed and is difficult to recover the conventional mechanism from theoretical calculations. Using the next model that will be discussed, we will explain how this problem was overcome.

2. Molecular Orbital based model The orbital picture suggests that all the information needed to understand the state based model is already in the ground state molecular orbitals (MOs) of the complex. With this in mind, we now focus of the molecular orbitals, testing whether this hypothesis is true or false. Figure 12.2 gives the ‘pseudo-octahedral’ ligand field theory (LFT) picture that was recovered in Ref. [14] and the two MO based indices that were developed.

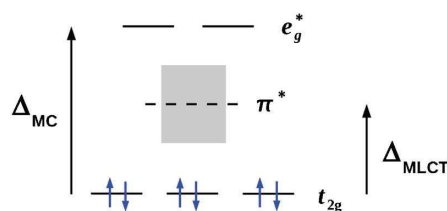


Figure 12.2 – Pseudo-octahedral ligand field theory diagram for Ru complexes.

The problem of mixing of the states in the unoccupied states was overcome[14] by the use of the projected density of states (PDOS). Based on the PDOS derived LFT-like picture. The authors proposed two molecular orbital-based luminescence indices, both of which were based on the idea that luminescence quenching is as a result of a low ${}^3\text{MLCT} \rightarrow {}^3\text{MC}$ barrier. One luminescence index proposes the difference between the e_g^* and the lowest energy π^* PDOS bands as an indicator of ΔE . The second luminescence index is a product of the amount of π character in the t_{2g} band with the amount of ruthenium d

character in the $1\pi^*$ band summarized as $d \times \pi$. The frontier molecular orbital theory that we recently looked at also looks at the activation barriers to estimate the excited state lifetime but it relies on the experimental activation barrier.

Using the above information, work was done on more than 90 complexes so as to validate the molecular orbital indices that were developed by [14]. In this work, a quantitative structure activity relationship (QSPR) was developed by identifying the target molecules that had a long excited state lifetime (those that are likely to remain excited long enough to luminescence or transfer an electron), and comparing against all the other complexes. The complexes studied were identified from [13] based on the length of their excited state lifetime. If a complex was within the parameter space, it was likely to have a long excited state lifetime, but if it did not lie within the parameter space, then it was not worth synthesising since it will not be very useful practically. But there was a gap in terms of just how much information could be extracted. In particular, the data about the lifetimes at room temperature and the activation barrier was not easy to come by, and this prompted the extension of this study to find how big or small the activation barrier is. This is because with this information, it is possible, using the luminescence indices to get exactly which complexes are going to have a long excited state lifetime or not since the height of the activation barrier is related to the length of the excited state lifetime. In this work, we seek to get the activation barriers theoretically. Indeed, we are not delving into a completely new world but each complex comes with its own challenges especially in the excited state. Recent work has shown that it is possible to calculate the activation energy from $^3\text{MLCT}$ to ^3MC [15]. The transition states of the $^3(\text{MLCT} \rightarrow \text{MC})$ conversion was determined as well as the energy barriers of the conversion. Those in complexes containing bpy and terpyridine ligands were reported to have small activation energies (less than 5 kcal/mol). The study employed DFT method with the Lee-Yang-Parr correlation functionals (B3YPP) [16, 17] and a double-zeta quality SDD basis set

for the ruthenium atom and the other atoms were described by a split valence Pople basis plus one polarization function (6-311G*). Calculations were done in acetonitrile solvent using the PCM method.

In Ref. [18], ultrafast transient infrared spectroscopy and DFT calculations of ruthenium(II) polypyridyl complexes has been used to characterize the transition from $^3(\text{MLCT} \rightarrow \text{MC})$. It has been shown from the potential energy curves that for $[\text{Ru}(\text{bpy})_3]^{2+}$, the triplet manifold along the metal-ligand distance for the ^3dd state is at a higher energy than the $^3\text{MLCT}$ state and that there is a substantial barrier between the two minima. The study makes use of the GAUSSIAN 09 program package with the mPW1PW91 functional, D95V basis set for H, C and N atoms and the LANL2DZ basis set for ruthenium. Calculations were performed in the gas phase and with the PCM method in order to take solvent effects into account.

In this work, the height of the activation barrier from $^3\text{MLCT}$ to ^3MC is the main interest. For this to be done, the relevant excited states must be identified so that a plot of the potential energy surface (PES) and the energies obtained can be used to calculate the height of the barrier. The $^3\text{MLCT}$ and ^3MC excited states must be correctly identified and the energies calculated as the transition occurs from one excited state to the other. The question is, how do we do this theoretically?

Mulliken spin density analysis has been used as an important tool to identify the nature of the excited electronic state. This method has been used previously [15, 18, 19, 19–21] for the same purpose. A unity net spin on ruthenium was associated with the $^3\text{MLCT}$ state while a net spin of 2 on ruthenium was identified as the ^3MC state. Jahn Teller effect [22] is used as the key principle to help in differentiating the different kinds of excited states. As the transition occurs from the $^3\text{MLCT}$ to ^3MC , there is lowering of the symmetry and therefore the axial bond lengths are distorted by the population of the e_g orbital. The two bond lengths are expected to be significantly longer compared to the other bonds in the molecule. The location of the ^3MC involves

the distortion of the structures to get a good starting guess for the triplet optimization. The reasoning behind this distortion is as follows; displacing ligands away from the ruthenium core will lower the energy of the unoccupied d orbitals, to a point at which the (d_{z^2} or $d_{x^2-y^2}$) become occupied. Therefore, by the elongation of the Ru-N bonds in the xy plane, the energy of the unoccupied orbitals decreases, hence populating the $d_{x^2-y^2}$ orbital, leading to the ^3MC state [23].

The Mulliken population analysis has been used in this work to characterize the nature of the triplet states in this work, the ultimate goal being the calculation of the size of the activation barrier.

12.2 Computational Details

All calculations have been done with the GAUSSIAN09 [24] code (version D.01). The first step involved the ground state optimization of all the three complexes in gas phase. The $^3\text{MLCT}$ and ^3dd states were also optimized both in gas phase and in acetonitrile using the PCM model to account for the solvent effects. A double- ζ quality basis set LANL2DZ and the corresponding effective core potential (ECP) [25] was used to characterize Ru. H, N and C atoms were described by the D95V basis set [26]. Frequency calculations were performed on the optimized geometries so as to check whether they were the true minima (with no imaginary frequencies). The MPW1PW91 exchange-correlation hybrid functional [27] was used. For all the calculations, (pop=full) was set to full so as to extract all the information. A density value of 0.004 was used in GAUSSVIEW to generate the spin density diagrams from cube files. $^3\text{MLCT}$ was obtained by optimizing the optimized ground state with the triplet spin, first in gas phase and then in solvent. The ^3MC excited state was obtained by elongating the two axial bond lengths to 2.4000 Å and then optimizing first in gas phase and then in solvent. All the optimized excited states converged to the true minima as an analysis of the frequencies did not show any negative frequencies. The potential energy scan was obtained by increasing the bond length of the two axial bonds in steps of 0.002 Å and fixing those particular parameters during an optimization.

12.3 Results and Discussion

Table 12.1,12.2,12.3 gives the optimized bond lengths, charge and spin density on ruthenium in acetonitrile for the ground state singlet state and the two triplet excited states for $[\text{Ru}(\text{bpy})_3]^{2+}$, $[\text{Ru}(\text{mbpy})_3]^{2+}$ and $[\text{Ru}(\text{mphen})_3]^{2+}$ respectively.

Table 12.1 – Optimized structural bond lengths (Å) in acetonitrile for the three states for $[\text{Ru}(\text{bpy})_3]^{2+}$.

	S_0	$^3\text{MLCT}$	^3MC
Spin(Ru)		0.993	1.874
Charge(Ru)		1.143	1.044
Bond lengths (Å) (This Work)			
Ru-N			
2	2.07249	2.07430	2.39994
3	2.07286	2.09534	2.12902
4	2.07270	2.07430	2.40019
5	2.07257	2.09534	2.12909
6	2.07328	2.04889	2.08448
7	2.07256	2.04890	2.08449
Other Works [18]			
Ru-N			
2	2.07266	2.07433	2.40638
3	2.07299	2.09533	2.13187
4	2.07278	2.07434	2.40647
5	2.07230	2.09533	2.13182
6	2.07252	2.04891	2.08578
7	2.07242	2.04892	2.08579

So far, the calculated bond lengths, charge and spin show excellent agreement with other works [18] on the same.

Figures 12.3, 12.4, 12.5 and 12.6, 12.7, 12.8 show the spin density distribution of the $^3\text{MLCT}$ and ^3MC of $[\text{Ru}(\text{bpy})_3]^{2+}$, $[\text{Ru}(\text{mbpy})_3]^{2+}$ and $[\text{Ru}(\text{mphen})_3]^{2+}$ respectively. For the $^3\text{MLCT}$ spin density, the excited state electron is localized on one of the three ligands as shown in Figs. 12.3, 12.4, and 12.5. This state gives a spin density on Ru of 0.993 which is essentially

Table 12.2 – Optimized structural bond lengths (Å) in acetonitrile for the three states for $[\text{Ru}(\text{mbpy})_3]^{2+}$.

	S_0	${}^3\text{MLCT}$	${}^3\text{MC}$
Spin(Ru)		1.011473	1.916306
Charge(Ru)		1.072959	0.964987
Bond lengths (Å)		(This Work)	
Ru-N			
2	2.0646903	2.0386164	2.1380399
3	2.1417344	2.1084160	2.4861674
18	2.0844091	2.0886892	2.0728442
19	2.1582617	2.1725408	2.1633806
34	2.1424503	2.1633302	2.4950329
35	2.0733401	2.0755988	2.1253608
Other Works [18]			
Ru-N			
2	2.06168		2.12842
3	2.13532		2.50581
18	2.08114		2.07758
19	2.15151		2.15821
34	2.13675		2.48641
35	2.06983		2.13332

Table 12.3 – Optimized structural bond lengths (Å) in acetonitrile for the three states for $[\text{Ru}(\text{mphen})_3]^{2+}$.

	S_0	${}^3\text{MLCT}$	${}^3\text{MC}$
Spin(Ru)		0.966200	1.934650
Charge(Ru)		1.098457	0.985159
Bond lengths (Å)		(This Work)	
Ru-N			
2		2.0245337	2.1308085
3		2.1247346	2.4985064
16		2.1019110	2.0827714
17		2.1759625	2.1708665
30		2.1515958	2.5123456
31		2.0682720	2.1268998
Other Works [18]			
Ru-N			
2	2.06548	2.02447	2.12839
3	2.14538	2.12483	2.51246
16	2.08095	2.10190	2.08142
17	2.15374	2.17611	2.16979
30	2.13737	2.15169	2.50153
31	2.07366	2.06829	2.12679

unity and the charge is 1.143. A comparison of the Ru-N bond lengths for this state and the ground state are not significantly different. In the ^3MC state, one electron is transferred to ruthenium and the spin density changes from unity to 1.874 which is approximately 2 and a charge of 1.044. The geometry of ^3MC is significantly different from that of the ground state and the coordination octahedron is strongly distorted due to Jahn-Teller effect [22]. There is elongation of the two axial bond lengths in the coordination octahedron; this can be observed from Tables 12.1, 12.2, and 12.3 where the Ru-N_2 (2.07433 Å) and Ru-N_4 (2.07434 Å) in the $^3\text{MLCT}$ state changes to Ru-N_2 (2.39994 Å) and Ru-N_4 (2.40019 Å) in the ^3MC state. This is a change of about 0.332 Å in the two axial bond lengths for the transition from $^3\text{MLCT}$ to ^3MC state. The other four bond lengths show minimal bond elongation ranging from 0.03559 to 0.03368 Å.

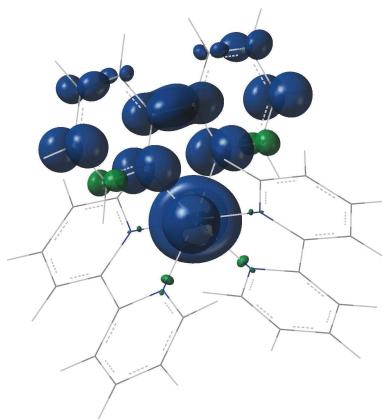


Figure 12.3 – Spin density distribution of $^3\text{MLCT}$ state on $[\text{Ru}(\text{bpy})_3]^{2+}$ in acetonitrile.

The PES scan of the transition from $^3\text{MLCT}$ to ^3MC state of $[\text{Ru}(\text{bpy})_3]^{2+}$ is shown in Fig. 12.9. This was traced by linearly elongating the two Ru-N bonds in steps of 0.002 Å from $^3\text{MLCT}$ to ^3MC and optimizing all the other structural parameters. Efforts to trace the PES scan for $[\text{Ru}(\text{mbpy})_3]^{2+}$ and $[\text{Ru}(\text{mphen})_3]^{2+}$ failed after running several calculations. The results obtained showed that the energy kept on increasing with the transition from $^3\text{MLCT}$ to ^3MC . This is not correct since a barrier is expected, however small

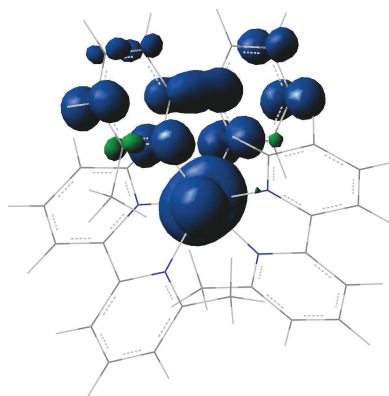


Figure 12.4 – Spin density distribution of $^3\text{MLCT}$ state on $[\text{Ru}(\text{mbpy})_3]^{2+}$ in acetonitrile.

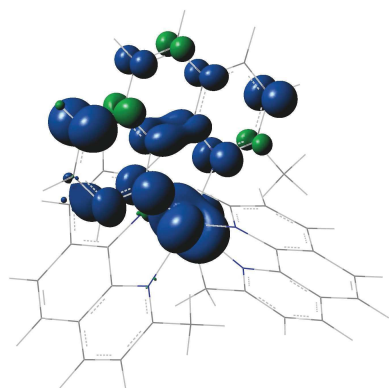


Figure 12.5 – Spin density distribution of $^3\text{MLCT}$ state on $[\text{Ru}(\text{mphen})_3]^{2+}$ in acetonitrile.

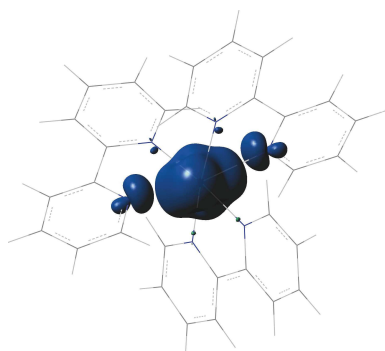


Figure 12.6 – Spin density distribution of ^3MC state on $[\text{Ru}(\text{bpy})_3]^{2+}$ in acetonitrile.

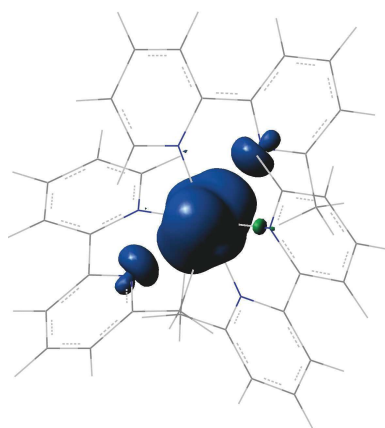


Figure 12.7 – Spin density distribution of ^3MC state on $[\text{Ru}(\text{mbpy})_3]^{2+}$ in acetonitrile.

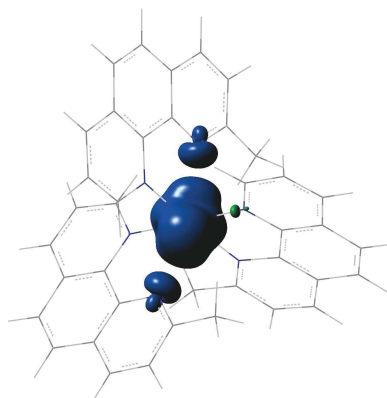


Figure 12.8 – Spin density distribution of ^3MC state on $[\text{Ru}(\text{mphen})_3]^{2+}$ in acetonitrile.

when this kind of transition is taking place. Other calculations on the same complexes will be done in the coming days to establish where the problem is.

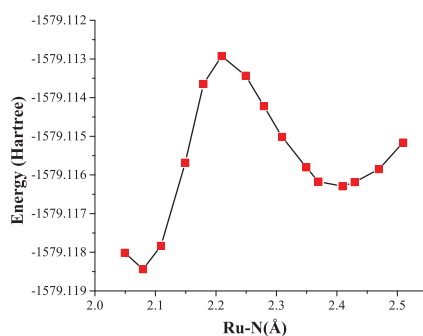


Figure 12.9 – $^3\text{MLCT}$ to ^3MC state potential energy scan along the reaction coordinate of the axial distortion of the ^3MC state for $[\text{Ru}(\text{bpy})_3]^{2+}$.

12.4 Conclusion

The main aim of this work was to learn how to do the excited state calculations, and eventually to be able to calculate the height of the activation barrier.

Information about the height of the activation barrier would be useful in terms of predicting the excited state lifetimes more directly. So far, this has been achieved to some extent as the excited state calculations for $[\text{Ru}(\text{bpy})_3]^{2+}$ have been done. Calculations for two other complexes, $[\text{Ru}(\text{mbpy})_3]^{2+}$ and $[\text{Ru}(\text{mphen})_3]^{2+}$ were not successful for reasons that have not yet been established since the $^3\text{MLCT}$ and ^3MC states were successfully identified. It is worthy mentioning that excited state dynamics are not the same for every ruthenium complex [18, 28, 29]. This is based on the fact that each complex may have different ligands as well as other factors that have a significant influence on the excited state dynamics that come into play such as the solvent effects. Results obtained for $[\text{Ru}(\text{bpy})_3]^{2+}$ are encouraging since with this information the activation barrier can be calculated directly. Most of the efforts will be directed towards the study of the activation barrier of homoleptic transition metal complexes.

12.5 Acknowledgement

The author thanks Anne MILET and Xiuwen ZHOU for the useful discussions regarding ruthenium complexes and particularly in helping in the calculations regarding the location of the triplet states.

Bibliography

- [1] J. P. Sauvage, J. P. Collin, J. C. Chambron, S. Guillerez, and C. Coudret. Ruthenium(II) and osmium(II) bis(terpyridine) complexes in covalently-linked multicomponent systems: Synthesis, electrochemical behavior, absorption spectra, and photochemical and photophysical properties. *Chem. Rev.*, 94:933, 1994.
- [2] V. Balzani and A. Juris. Photochemistry and photophysics of Ru(II) polypyridine complexes in the Bologna group. From early studies to recent developments. *Coordin. Chem. Rev.*, 211(1):97–115, 2001.
- [3] K. Nakamaru. Synthesis, luminescence quantum yields, and lifetimes of trischelated ruthenium (II) mixed-ligand complexes including 3, 3'-dimethyl-2, 2'-bipyridyl. *B. Chem. Soc. Jpn.*, 55(9):2697–2705, 1982.
- [4] G. Liebsch, I. Klimant, and O. S. Wolfbeis. Luminescence lifetime temperature sensing based on sol-gels and poly(acrylonitrile)s dyed with ruthenium metal-ligand complexes. *Adv. Mat.*, 11:1296, 1999.
- [5] A. Harriman, A. Khatyr, and R. Ziessel. Extending the luminescence lifetime of ruthenium(II) poly(pyridine) complexes in solution at ambient temperature. *Dalton Trans.*, 10:2061, 2003.
- [6] M. Duati, S. Tasca, F. C. Lynch, H. Bohlen, J. G. Vos, S. Stagni, and M. D. Ward. Enhancement of luminescence lifetimes of mononuclear ruthenium(II)-terpyridine complexes by manipulation of the σ -donor strength of ligands. *J. Inorg. Chem.*, 42:8377, 2003.
- [7] E. A. Medlycott and G. S. Hanan. Designing tridentate ligands for ruthenium(II) complexes with prolonged room temperature luminescence lifetimes. *Chem. Soc. Rev.*, 34:133, 2005.
- [8] K. J. Morris, M. S. Roach, W. Xu, J. N. Demas, and B. A. DeGraff. Luminescence lifetime standards for the nanosecond to microsecond range and oxygen quenching of ruthenium(II) compounds. *Anal. Chem.*, 79:9310, 2007.

- [9] L. J. Nurkkala, R. O. Steen, H. K. J. Friberg, J. A. Häggström, P. V. Bernhardt, M. J. Riley, and S. J. Dunne. The effects of pendant vs. fused thiophene attachment upon the luminescence lifetimes and electrochemistry of tris(2,2'-bipyridine)ruthenium(II) complexes. *Eur. J. Inorg. Chem.*, 26:4101, 2008.
- [10] R. O. Steen, L. J. Nurkkala, S. J. Angus-Dunne, C. X. Schmitt, E. C. Constable, M. J. Riley, P. V. Bernhardt, and S. J. Dunne. The role of isometric effects on the luminescence lifetimes and electrochemistry of oligothieryl-bridged dinuclear tris(2,2'-bipyridine)ruthenium(II) complexes. *Eur. J. Inorg. Chem.*, 11:1784, 2008.
- [11] S. Ji, W. Wu, W. Wu, P. Song, K. Han, Z. Wang, S. Liu, H. Guo, and J. Zhao. Tuning the luminescence lifetimes of ruthenium(II) polypyridine complexes and its application in luminescent oxygen sensing. *J. Mater. Chem.*, 20:1953, 2010.
- [12] C. J. Cramer and D. G. Truhlar. Density functional theory for transition metals and transition metal chemistry. *Phys. Chem. Chem. Phys.*, 11(46):10757–10816, 2009.
- [13] A. Juris, V. Balzani, F. Barigelletti, S. Campagna, P. Belser, and A. Von Zelewsky. Ru(II) polypyridine complexes: Photophysics, photochemistry, electrochemistry, and chemiluminescence. *Coord. Chem. Rev.*, 84: 85, 1988.
- [14] C. M. Wawire, D. Jouvenot, F. Loiseau, P. Baudin, S. Liatard, L. Njenga, G. Kamau, and M. E. Casida. Density-functional study of luminescence in polypyridine ruthenium complexes. *J. Photochem. and Photobiol. A*, 276:8, 2014.
- [15] N. Yoshikawa, S. Yamabe, S. Sakaki, N. Kanehisa, T. Inoue, and H. Takashima. Transition states of the $^3\text{MLCT}$ to ^3MC conversion in $[\text{Ru}(\text{bpy})_2(\text{phen derivative})]^{2+}$ complexes. *J. Mol. Struct.*, 1094: 98–108, 2015.

- [16] A. D. Becke. Density-functional thermochemistry. III. The role of exact exchange. *J. Chem. Phys.*, 98:5648, 1993.
- [17] C. Lee, W. Yang, and R. G. Parr. Development of the Colle-Salvetti correlation energy formula into a functional of the electron density. *Phys. Rev. B*, 37:785, 1988.
- [18] Q. Sun, B. Dereka, E. Vauthey, L. M. Lawson-Daku, and A. Hauser. Ultrafast transient IR spectroscopy and DFT calculations of ruthenium (II) polypyridyl complexes. *Chem. Sci.*, 8(1):223–230, 2017.
- [19] O. A. Borg, S. S. Godinho, M. J. Lundqvist, S. Lunell, and P. Persson. Computational study of the lowest triplet state of ruthenium polypyridyl complexes used in artificial photosynthesis. *J. Phys. Chem. A*, 112(19):4470–4476, 2008.
- [20] E. Ruiz, J. Cirera, and S. Alvarez. Spin density distribution in transition metal complexes. *Coord. Chem. Rev.*, 249(23):2649–2660, 2005.
- [21] Q. Sun, S. Mosquera-Vazquez, Y. Suffren, J. Hankache, N. Amstutz, L. M. L. Daku, E. Vauthey, and A. Hauser. On the role of ligand-field states for the photophysical properties of ruthenium (II) polypyridyl complexes. *Coord. Chem. Rev.*, 282:87–99, 2015.
- [22] F. Alary, M. Boggio-Pasqua, J. Heully, C. J. Marsden, and P. Vicendo. Theoretical characterization of the lowest triplet excited states of the tris- (1, 4, 5, 8-tetraazaphenanthrene) ruthenium dication complex. *Inorg. Chem.*, 47(12):5259–5266, 2008.
- [23] A. Maria, M. J. Lundqvist, H. Wolpher, O. Johansson, L. Eriksson, J. Bergquist, T. Rasmussen, H. Becker, L. Hammarström, and P. Norrby. Steric influence on the excited-state lifetimes of ruthenium complexes with bipyridyl-alkanylene-pyridyl ligands. *Inorg. chem.*, 47(9): 3540–3548, 2008.
- [24] M. J. Frisch, G. W. Trucks, H. B. Schlegel, G. E. Scuseria, M. A. Robb, J. R. Cheeseman, G. Scalmani, V. Barone, B. Mennucci, G. A. Peters-

- son, H. Nakatsuji, M. Caricato, X. Li, H. P. Hratchian, A. F. Izmaylov, J. Bloino, G. Zheng, J. L. Sonnenberg, M. Hada, M. Ehara, K. Toyota, R. Fukuda, J. Hasegawa, M. Ishida, T. Nakajima, Y. Honda, O. Kitao, H. Nakai, T. Vreven, J. A. Montgomery, Jr., J. E. Peralta, F. Ogliaro, M. Bearpark, J. J. Heyd, E. Brothers, K. N. Kudin, V. N. Staroverov, R. Kobayashi, J. Normand, K. Raghavachari, A. Rendell, J. C. Burant, S. S. Iyengar, J. Tomasi, M. Cossi, N. Rega, J. M. Millam, M. Klene, J. E. Knox, J. B. Cross, V. Bakken, C. Adamo, J. Jaramillo, R. Gomperts, R. E. Stratmann, O. Yazyev, A. J. Austin, R. Cammi, C. Pomelli, J. W. Ochterski, R. L. Martin, K. Morokuma, V. G. Zakrzewski, G. A. Voth, P. Salvador, J. J. Dannenberg, S. Dapprich, A. D. Daniels, \ddot{A} ř. Farkas, J. B. Foresman, J. V. Ortiz, J. Cioslowski, and D. J. Fox. Gaussian[®]09 Revision D.01. Gaussian Inc. Wallingford CT 2009.
- [25] P. J. Hay and W. R. Wadt. Ab initio effective core potentials for molecular calculations. potentials for K to Au including the outermost core orbitals. *J. Chem. Phys.*, 82:299, 1985.
- [26] T. H. Dunning and P. J. Hay. *Applications of Electronic Structure Theory*, volume 3. Springer, New York, 1976. ISBN 9781468485417.
- [27] C. Adamo and V. Barone. Exchange functionals with improved long-range behavior and adiabatic connection methods without adjustable parameters: The mPW and mPW1PW models. *J. Chem. Phys.*, 108(2):664–675, 1998.
- [28] M. Schwalbe, B. Schäfer, H. Görls, S. Rau, S. Tschierlei, M. Schmitt, J. Popp, G. Vaughan, W. Henry, and J. G. Vos. Synthesis and characterisation of poly(bipyridine)ruthenium complexes as building blocks for heterosupramolecular arrays. *Eur. J. Inorg. Chem.*, 2008(21):3310–3319, 2008. ISSN 1099-0682.
- [29] F. Alary, J. L. Heully, L. Bijeire, and P. Vicendo. Is the ³MLCT the only photoreactive state of polypyridyl complexes? *Inorg. chem.*, 46(8): 3154–3165, 2007.

Part IV

Conclusion

Chapter 13

Summary and Conclusion

Transition metal complexes and ruthenium and iridium complexes in particular have found an important role in electronic devices, including solar cells and organic light emitting diodes. One reason for this is the presence of a long-lived triplet excited state which is accessible via singlet excitation followed by intersystem crossing due to strong spin-orbit coupling. Such devices and the experiments needed to develop new materials for new devices can be expected to benefit from improved understanding through better theoretical modeling. However realistic modeling of these complexes, while increasingly possible, is complicated and compute intensive, hence limiting the number of complexes which can be treated. That is why a much simpler approach has been taken in this thesis, namely to see how much information about luminescence lifetimes may be obtained just by looking at gas-phase optimized geometries of ruthenium complexes and their orbital energies. On the order of 100 ruthenium complexes were studied and it was shown that the gas-phase DFT geometries are reasonably close to experimentally-measured crystal geometries. Furthermore TD-DFT spectra correlate reasonably well with solution spectra corrected for solvent effects. This authorizes us to use (TD-)DFT as a model for further investigation of the underlying physical chemical reasons why some complexes have longer lifetimes than other lifetimes. We immediately faced two difficulties.

The first difficulty is that it is difficult to overcome is to find a way to

relate the calculated DFT orbital energies with LFT energies. This is important because, not only do experimentalists rely highly upon LFT to explain their results and to plan experiments, but LFT brings out common features between related but different compounds. We were able to do this by taking advantage of earlier results from the Franco-Kenyan collaboration, namely the use of partial density of states (PDOS) analysis. In particular, while the nonbonding ruthenium t_{2g} orbitals are often identifiable by visualizing DFT orbitals, this is no longer true of the antibonding e_g^* orbitals which mix with the ligand orbitals in such a way that their density is split over many DFT energy levels. The PDOS approach takes this splitting specifically into account and allows us to find approximate e_g^* energy levels even when the e_g^* density has been split over many DFT orbitals. This provides an LFT-like picture which is *not* LFT but which resembles it enough to be able to use similar reasoning.

Another difficulty that had to be overcome is that the most common theory for ruthenium complex luminescence lifetimes is based upon estimations of the height of the transition state barrier on the triplet excited state curve. However this transition energy is rarely available experimentally. We were able to overcome this in the first instance by looking at an average luminescence lifetime calculated from experimentally available room temperature and liquid nitrogen lifetimes.

We were then able to check the value of luminescence indices proposed in earlier work from our Franco-Kenyan collaboration and found them to be less than optimal. However frontier-molecular orbital ideas led us to a new proposal for luminescence indices which, except for a few points, provides a reasonably linear correlation with the average luminescence lifetime. The few exceptions observed may be due to qualitatively different relaxation pathways, to the need for more or better experimental data in these cases, or, perhaps, still other as yet unimaginable reasons.

One approach for improving this study would be to cut out the need for experimentally-determined average barriers by direct calculation of theoretical activation energies for de-excitation of the triple excited state. We have included a chapter in this thesis where we have begun to explore this ap-

proach. It is indeed more difficult than the orbital-based approach but it is worthwhile. Though time did not allow us to finish this part of the project, it is envisaged that the work will continue after finishing the PhD.

Another avenue, and one suggested by a referee for our published paper, is that the study be extended to iridium compounds. This is also on our list of future “to-dos.”

Index

- 'Deadly Sins' of TD-DFT, 127
- 6-31G, 98
- 6-31G and 6-31G(d) basis sets, 98
- 6-31G(d), 98

- Adiabatic approximation, 117
- Atomic units, 32

- Basis set, 87
- Basis set superposition error (BSSE), 99
- Basis sets and effective core potentials, 87
- Born-Oppenheimer approximation, 34

- Casida equations, 124
- Chemical hamiltonian approach (CHA), 100
- Coulomb and exchange integrals, 56
- Coulomb and exchange operators, 59
- Counterpoise method (CP), 100
- Crystal field theory, 13

- Diffuse-function-augmented basis functions, 95
- Double hybrid functionals, 82
- Double, triple and multi zeta (ζ) basis sets and split valence basis sets, 93

- Effective core potential (ECP) basis functions (pseudopotentials), 96
- Effective core potentials, 87
- Electronic excitation, 39
- Electronic hamiltonian, 55
- Electronic transition, 40
- Exchange-correlation approximations, 79
- Exchange-correlation potentials, 117
- Excited state deactivation, 44
- Existence theorem, 70, 112

- First Runge-Gross theorem, 112
- Fluorescence, 48
- Forbidden electronic transitions, 42

-
- Franck-Condon principle, 40
 - Frenkel-Dirac variational principle, 114
 - Gaussian-type orbitals, 87
 - Gaussian-type orbitals (GTOs), 90
 - Generalized gradient approximation (GGA), 80
 - Generalized susceptibility, 120
 - Hartree product, 54
 - Hartree-Fock approximation, 53
 - Hartree-Fock orbitals and orbital energies, 61
 - Highest occupied molecular orbital (HOMO), 43
 - Hohenberg-Kohn theorems, 70
 - Hybrid functionals, 81
 - Incandescence, 45
 - Internal conversion, 47
 - Intersystem crossing, 47
 - Introduction, 2
 - Jablonski diagram, 45
 - Jacob's ladder, 79, 82
 - Kohn-Sham approach, 75
 - Kohn-Sham linear density response, 122
 - Koopmans' theorem, 63
 - Laporte selection rule, 40
 - Ligand field theory, 15
 - Linear combination of atomic orbitals, 87
 - Linear response TD-DFT, 118
 - Linear response theory, 118
 - Local density approximation(LDA), 79
 - Lowest unoccupied molecular orbital (LUMO), 43
 - Luminescence, 44
 - Meta-generalized gradient approximation (meta-GGA), 82
 - Minimal basis sets (single zeta), 92
 - Molecular hamiltonian, 30
 - Molecular orbitals, 43
 - Partial density of states (PDOS), 106
 - Phosphorescence, 49
 - Photochemical process, 45
 - Photoelectric effect, 23
 - Photophenomena and luminescence, 38
 - Photophysical processes, 45
 - Polarization function-supplemented basis functions, 94
 - Potential energy surfaces, 49
 - Quantization of electronic angular momentum, 24

-
- Quantum yield, 50
- Radiationless deactivation, 47
- Radiative deactivation, 48
- Restricted localized orbital (RLO), 101
- Second Runge-Gross theorem, 113
- Singlet, 41
- Slater determinant, 55
- Slater-type Orbitals, 87
- Slater-type orbitals, 89
- SNOOP, 100
- Spin selection rule, 40
- Spin-orbit coupling, 42
- State energy diagram, 43
- STO-3G, 92
- Tamm-Dancoff approximation (TDA), 126
- Thomas-Fermi model, 74
- Time-dependent density functional theory (TD-DFT), 109
- Time-dependent Kohn-Sham equation, 115
- Time-dependent linear density response, 119
- Time-dependent Schrödinger equation, 110
- Time-dependent Schrödinger equation, 29
- Time-independent Schrödinger equation, 26
- Triplet, 42
- Types of basis functions (Atomic orbitals), 88
- Types of electronic transitions, 40
- Ultraviolet catastrophe, 23
- Variational principle, 73
- Vibrational relaxation, 46, 47
- Wave-particle duality, 25

Appendix A

Supplementary Material: Partial Density of States Ligand Field Theory (PDOS-LFT): Recovering a LFT-Like Picture and Application to the Photoproperties of Ruthenium Polypyridine Complexes

Supplementary Material: Partial Density of States Ligand Field Theory (PDOS-LFT): Recovering a LFT-Like Picture and Application to the Photoproperties of Ruthenium Polypyridine Complexes

by Denis Magero, Mark E. Casida, Nicholas Makau, George Amolo, and Lusweti Kituyi
Last update: June 11, 2017

This supplementary material consists of a systematic collection of our calculated partial density of states (PDOS) and time-dependent B3LYP (TD-B3LYP) spectra for the complexes treated in the main paper.

B3LYP highest-occupied molecular orbital (HOMO) energies, taken directly from the GAUSSIAN outputs, are also given. These provide an indication of the start of the HOMO-LUMO (lowest unoccupied molecular orbital) gap. The corresponding notion in solid-state physics is the Fermi energy (roughly equal to the average of the HOMO and LUMO energies) which is an alternative way to indicate the position of the HOMO-LUMO gap.

Complexes indicated with an asterisk (*) have unbound (i.e., positive energy) e_g^* orbitals in their PDOS. Some complexes could not be included because of difficulty optimizing their geometries. The PDOS could not always be calculated because of current program limitations. Complexes with only TD-B3LYP spectra are indicated with a dagger (†).

Contents

1	Complex (1)*: $[\text{Ru}(\text{bpy})(\text{CN})_4]^{2-}$	5
2	Complex (2)†: $[\text{Ru}(\text{bpy})_2\text{Cl}_2]$	6
3	Complex (3)*: $[\text{Ru}(\text{bpy})_2(\text{CN})_2]$	7
4	Complex (4): $[\text{Ru}(\text{bpy})_2(\text{en})]$	8
5	Complex (5)*: $[\text{Ru}(\text{bpy})_2(\text{ox})]$	9
6	Complex (6): $[\text{Ru}(\text{bpy})_3]^{2+}$	10
7	Complex (7)*: $[\text{Ru}(\text{bpy})_2(4\text{-n-bpy})]^{2+}$	11
8	Complex (8): $[\text{Ru}(\text{bpy})_2(3,3'\text{-dm-bpy})]^{2+}$	12
9	Complex (9): $[\text{Ru}(\text{bpy})_2(4,4'\text{-dm-bpy})]^{2+}$	13
10	Complex (11): $[\text{Ru}(\text{bpy})_2(4,4'\text{-dn-bpy})]^{2+}$	14
11	Complex (12): $[\text{Ru}(\text{bpy})_2(4,4'\text{-dph-bpy})]^{2+}$	15
12	Complex (13): $[\text{Ru}(\text{bpy})_2(4,4'\text{-DTB-bpy})]^{2+}$	16
13	Complex (14): <i>cis</i> - $[\text{Ru}(\text{bpy})_2(\text{m-4,4'-bpy})_2]^{4+}$	17
14	Complex (15): $[\text{Ru}(\text{bpy})_2(\text{bpz})]^{2+}$	18
15	Complex (16): $[\text{Ru}(\text{bpy})_2(\text{phen})]^{2+}$	19
16	Complex (17): $[\text{Ru}(\text{bpy})_2(4,7\text{-dm-phen})]^{2+}$	20
17	Complex (18): $[\text{Ru}(\text{bpy})_2(4,7\text{-Ph}_2\text{-phen})]^{2+}$	21

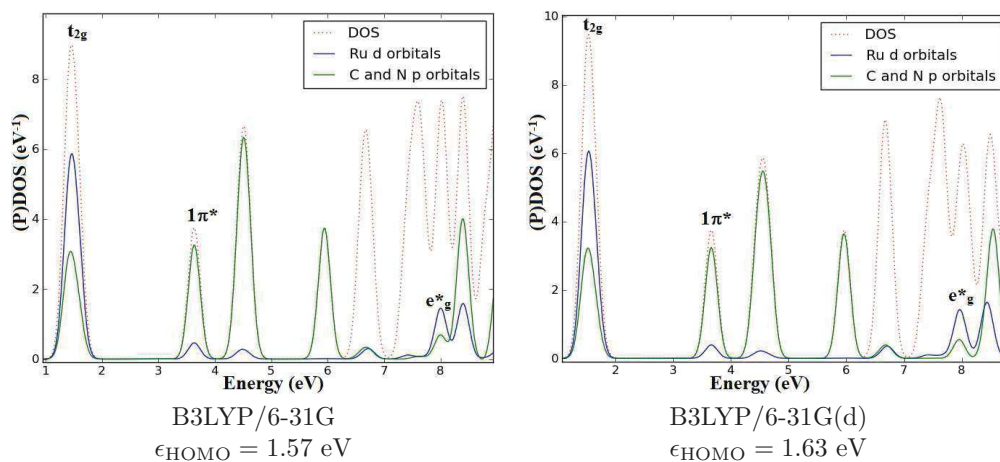
18 Complex (19): [Ru(bpy) ₂ (4,7-dhy-phen)] ²⁺	22
19 Complex (20): [Ru(bpy) ₂ (5,6-dm-phen)] ²⁺	23
20 Complex (21): [Ru(bpy) ₂ (DIAF)] ²⁺	24
21 Complex (22) [†] : [Ru(bpy) ₂ (DIAFO)] ²⁺	25
22 Complex (23): [Ru(bpy) ₂ (taphen)] ²⁺	26
23 Complex (24): <i>cis</i> -[Ru(bpy) ₂ (py) ₂] ²⁺	27
24 Complex (25): <i>trans</i> -[Ru(bpy) ₂ (py) ₂] ²⁺	28
25 Complex (26): [Ru(bpy) ₂ (pic) ₂] ²⁺	29
26 Complex (27): [Ru(bpy) ₂ (DPM)] ²⁺	30
27 Complex (28): [Ru(bpy) ₂ (DPE)] ²⁺	31
28 Complex (29): [Ru(bpy) ₂ (PimH)] ²⁺	32
29 Complex (30): [Ru(bpy) ₂ (PBzimH)] ²⁺	33
30 Complex (31): [Ru(bpy) ₂ (biimH ₂)] ²⁺	34
31 Complex (32): [Ru(bpy) ₂ (BiBzimH ₂)] ²⁺	35
32 Complex (34): [Ru(bpy) ₂ (piq)] ²⁺	36
33 Complex (35): [Ru(bpy) ₂ (hpiq)] ²⁺	37
34 Complex (36): [Ru(bpy) ₂ (pq)] ²⁺	38
35 Complex (37): [Ru(bpy) ₂ (DMCH)] ²⁺	39
36 Complex (38) [†] : [Ru(bpy) ₂ (OMCH)] ²⁺	40
37 Complex (39) [†] : [Ru(bpy) ₂ (biq)] ²⁺	41
38 Complex (40): [Ru(bpy) ₂ (i-biq)] ²⁺	42
39 Complex (41): [Ru(bpy) ₂ (BL4)] ²⁺	43
40 Complex (42): [Ru(bpy) ₂ (BL5)] ²⁺	44
41 Complex (46): [Ru(bpy)(4,4'-DTB-bpy) ₂] ²⁺	45
42 Complex (47): [Ru(bpy)(h-phen)] ²⁺	46
43 Complex (48): [Ru(bpy)(phen) ₂] ²⁺	47
44 Complex (50): <i>trans</i> -[Ru(bpy)(phen)(py) ₂] ²⁺	48
45 Complex (52): [Ru(bpy)(taphen) ₂] ²⁺	49

46 Complex (53): [Ru(bpy)(py) ₂ (en)] ²⁺	50
47 Complex (55): [Ru(bpy)(py) ₄] ²⁺	51
48 Complex (56): [Ru(bpy)(py) ₂ (PMA)] ²⁺	52
49 Complex (57): [Ru(bpy)(py) ₂ (2-AEP)] ²⁺	53
50 Complex (58): [Ru(bpy)(PMA) ₂] ²⁺	54
51 Complex (60): [Ru(bpy)(DMCH) ₂] ²⁺	55
52 Complex (61): [Ru(bpy)(biq) ₂] ²⁺	56
53 Complex (63) [†] : [Ru(bpy)(trpy)Cl] ⁺	57
54 Complex (64)*: [Ru(bpy)(trpy)(CN)] ⁺	58
55 Complex (66)*: [Ru(6-m-bpy) ₃] ²⁺	59
56 Complex (67)*: [Ru(3,3'-dm-bpy) ₃] ²⁺	60
57 Complex (69): [Ru(3,3'-dm-bpy)(phen) ₂] ²⁺	61
58 Complex (70): [Ru(4,4'-dm-bpy) ₃] ²⁺	62
59 Complex (71): [Ru(4,4'-dm-bpy) ₂ (4,7-dhy-phen)] ²⁺	63
60 Complex (73): [Ru(4,4'-dph-bpy) ₃] ²⁺	64
61 Complex (74): [Ru(4,4'-DTB-bpy) ₃] ²⁺	65
62 Complex (75): [Ru(6,6'-dm-bpy) ₃] ²⁺	66
63 Complex (76): [Ru(h-phen) ₃] ²⁺	67
64 Complex (77): [Ru(phen) ₃] ²⁺	68
65 Complex (78): [Ru(phen) ₂ (4,7-dhy-phen)] ²⁺	69
66 Complex (79): [Ru(phen) ₂ (pq)] ²⁺	70
67 Complex (80): [Ru(phen) ₂ (DMCH)] ²⁺	71
68 Complex (81): [Ru(phen) ₂ (biq)] ²⁺	72
69 Complex (82): [Ru(phen)(pq) ₂] ²⁺	73
70 Complex (83): [Ru(phen)(biq) ₂] ²⁺	74
71 Complex (84): [Ru(2-m-phen) ₃] ²⁺	75
72 Complex (85): [Ru(2,9-dm-phen) ₃] ²⁺	76
73 Complex (86): [Ru(4,7-Ph ₂ -phen) ₃] ²⁺	77

74 Complex (87): [Ru(4,7-dhy-phen)(tm1-phen) ₂] ²⁺	78
75 Complex (88)*: [Ru(DPA) ₃] ⁻	79
76 Complex (89): [Ru(DPA)(DPAH) ₂] ⁺	80
77 Complex (90): [Ru(DPAH) ₃] ²⁺	81
78 Complex (91): [Ru(Azpy) ₃] ²⁺	82
79 Complex (92): [Ru(NA) ₃] ²⁺	83
80 Complex (93): [Ru(hpiq) ₃] ²⁺	84
81 Complex (94): [Ru(pq) ₃] ²⁺	85
82 Complex (95): [Ru(pq) ₂ (biq)] ²⁺	86
83 Complex (96): [Ru(pq)(biq) ₂] ²⁺	87
84 Complex (97): [Ru(pynapy) ₃] ²⁺	88
85 Complex (98) [†] : [Ru(DMCH) ₂ Cl ₂]	89
86 Complex (99)*: [Ru(DMCH) ₂ (CN) ₂]	90
87 Complex (100): [Ru(DMCH) ₃] ²⁺	91
88 Complex (101): [Ru(dinapy) ₃] ²⁺	92
89 Complex (102) [†] : [Ru(biq) ₂ Cl ₂]	93
90 Complex (103)*: [Ru(biq) ₂ (CN) ₂]	94
91 Complex (104): [Ru(biq) ₃] ²⁺	95
92 Complex (105) [†] : [Ru(i-biq) ₂ Cl ₂]	96
93 Complex (106)*: [Ru(i-biq) ₂ (CN) ₂]	97
94 Complex (107): [Ru(i-biq) ₃] ²⁺	98
95 Complex (108): [Ru(trpy) ₂] ²⁺	99
96 Complex (109): [Ru(tro) ₂] ²⁺	100
97 Complex (110): [Ru(tsite) ₂] ²⁺	101
98 Complex (111)*: [Ru(dqp) ₂] ²⁺	102

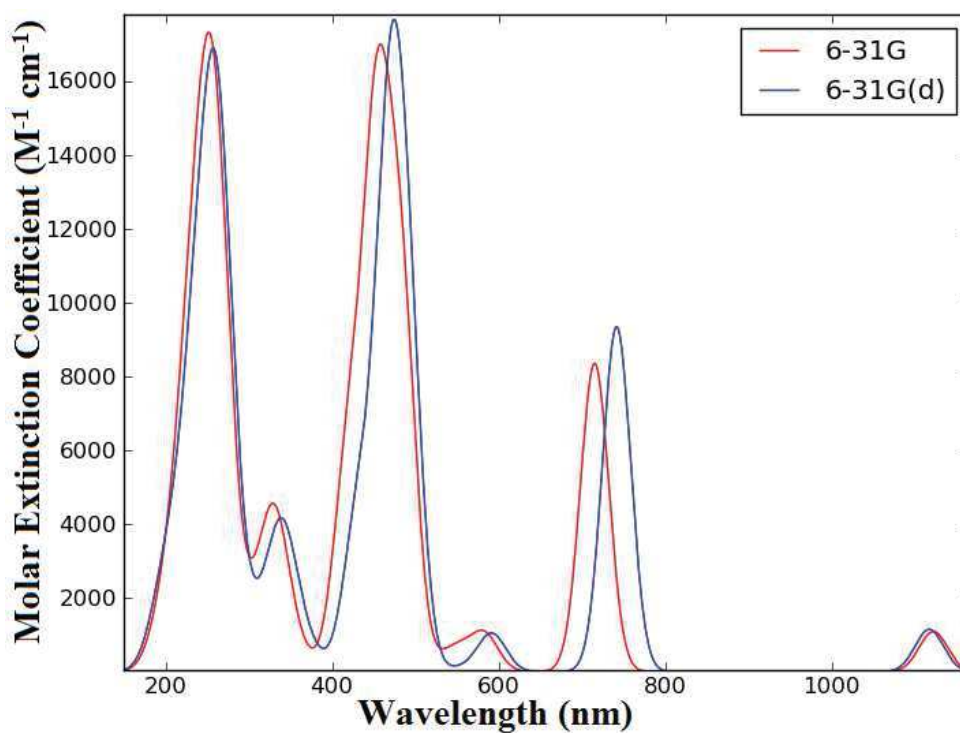
1. Complex (1)*: $[\text{Ru}(\text{bpy})(\text{CN})_4]^{2-}$

PDOS



Total and partial density of states of $[\text{Ru}(\text{bpy})(\text{CN})_4]^{2-}$ partitioned over Ru d orbitals and ligand C and N p orbitals.

Absorption Spectrum

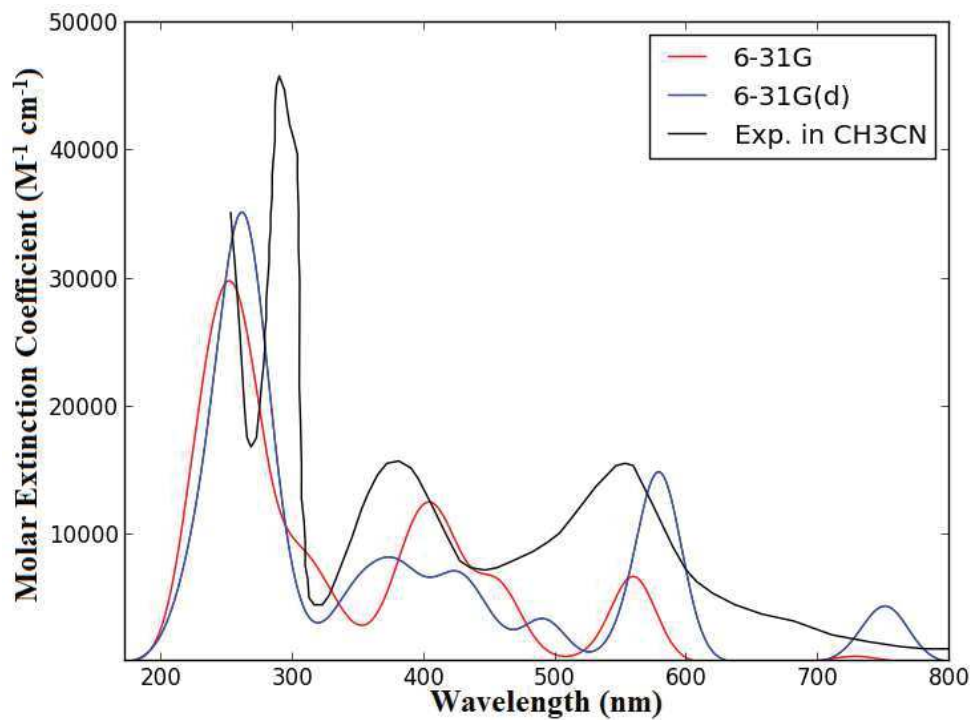


$[\text{Ru}(\text{bpy})(\text{CN})_4]^{2-}$ TD-B3LYP/6-31G and TD-B3LYP/6-31G(d) spectra.

2. Complex (2)[†]: [Ru(bpy)₂Cl₂]

B3LYP/6-31G B3LYP/6-31G(d)
 $\epsilon_{\text{HOMO}} = -4.52 \text{ eV}$ $\epsilon_{\text{HOMO}} = -4.47 \text{ eV}$

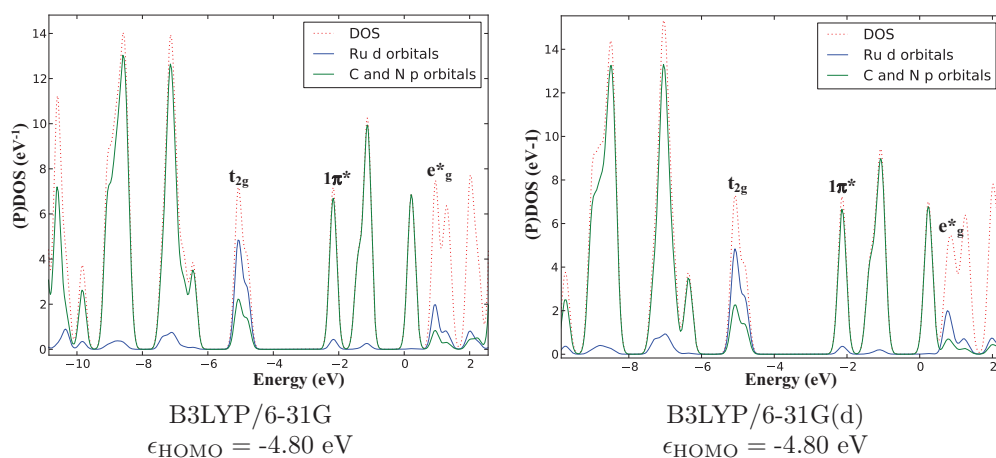
Absorption Spectrum



[Ru(bpy)₂Cl₂] TD-B3LYP/6-31G, TD-B3LYP/6-31G(d), and experimental spectra. Experimental curve measured at room temperature in acetonitrile [1].

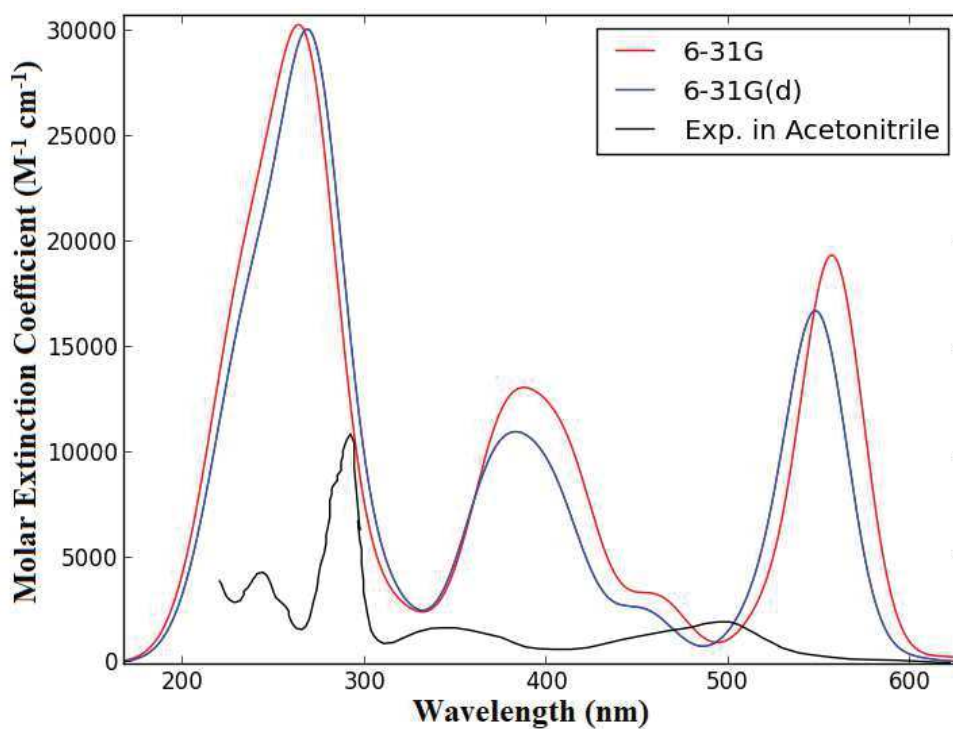
3. Complex (3)*: [Ru(bpy)₂(CN)₂]

PDOS



Total and partial density of states of [Ru(bpy)₂(CN)₂] partitioned over Ru d orbitals and ligand C and N p orbitals.

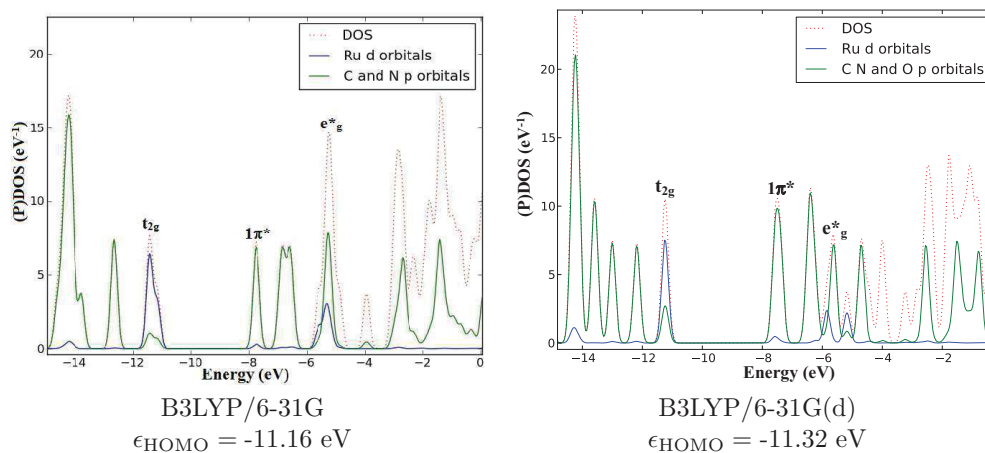
Absorption Spectrum



[Ru(bpy)₂(CN)₂] TD-B3LYP/6-31G, TD-B3LYP/6-31G(d), and experimental spectra. Experimental curve measured at room temperature in acetonitrile [2].

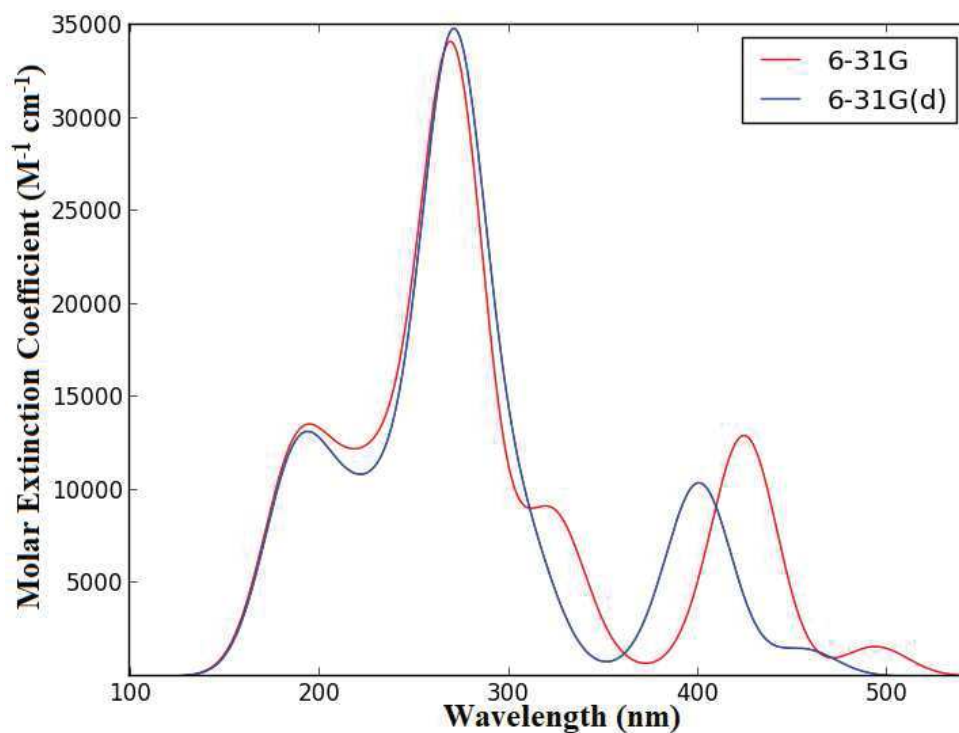
4. Complex (4): [Ru(bpy)₂(en)]

PDOS



Total and partial density of states of [Ru(bpy)₂(en)]²⁺ partitioned over Ru d orbitals and ligand C and N p orbitals.

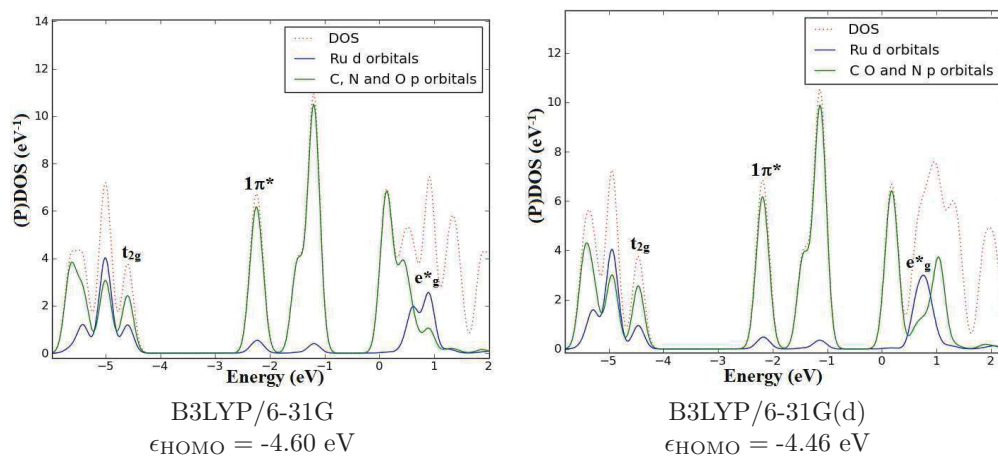
Absorption Spectrum



[Ru(bpy)₂(en)]²⁺ TD-B3LYP/6-31G and TD-B3LYP/6-31G(d) spectra.

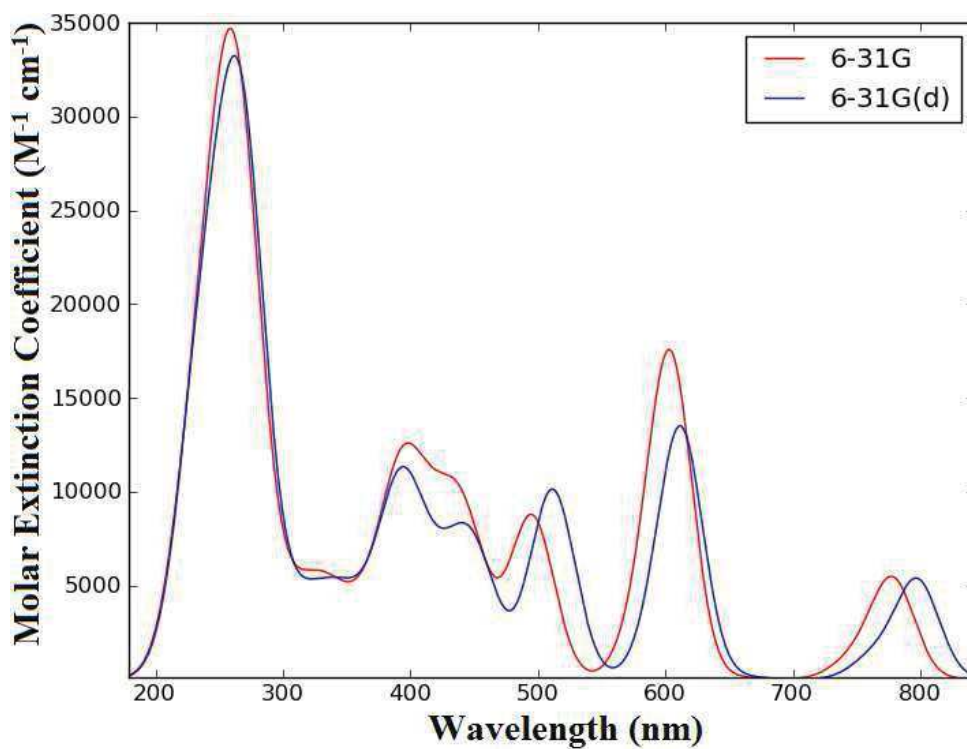
5. Complex (5)*: [Ru(bpy)₂(ox)]

PDOS



Total and partial density of states of [Ru(bpy)₂(ox)] partitioned over Ru d orbitals and ligand C, O and N p orbitals.

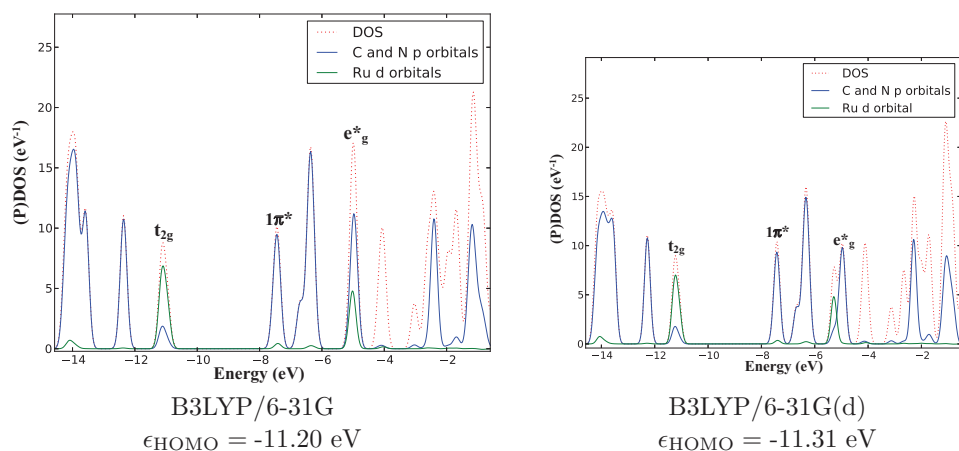
Absorption Spectrum



[Ru(bpy)₂(ox)] TD-B3LYP/6-31G and TD-B3LYP/6-31G(d) spectra.

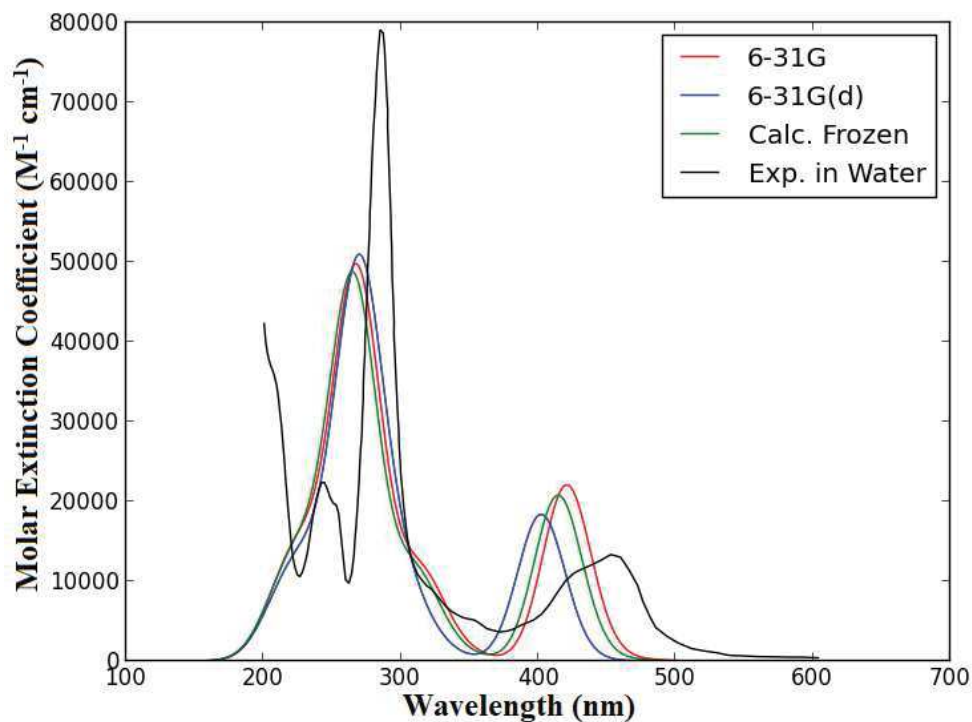
6. Complex (6): $[\text{Ru}(\text{bpy})_3]^{2+}$

PDOS



Total and partial density of states of $[\text{Ru}(\text{bpy})_3]^{2+}$ partitioned over Ru d orbitals and ligand C and N p orbitals.

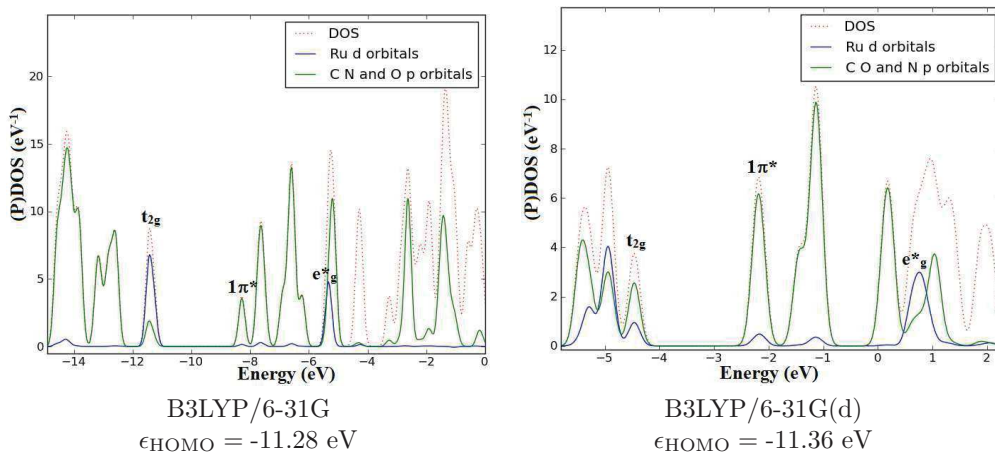
Absorption Spectrum



$[\text{Ru}(\text{bpy})_3]^{2+}$ TD-B3LYP/6-31G, TD-B3LYP/6-31G(d), and experimental spectra. “Frozen” means a calculation at the X-ray crystallography geometry without further optimization. Experimental curve measured at room temperature in water [3].

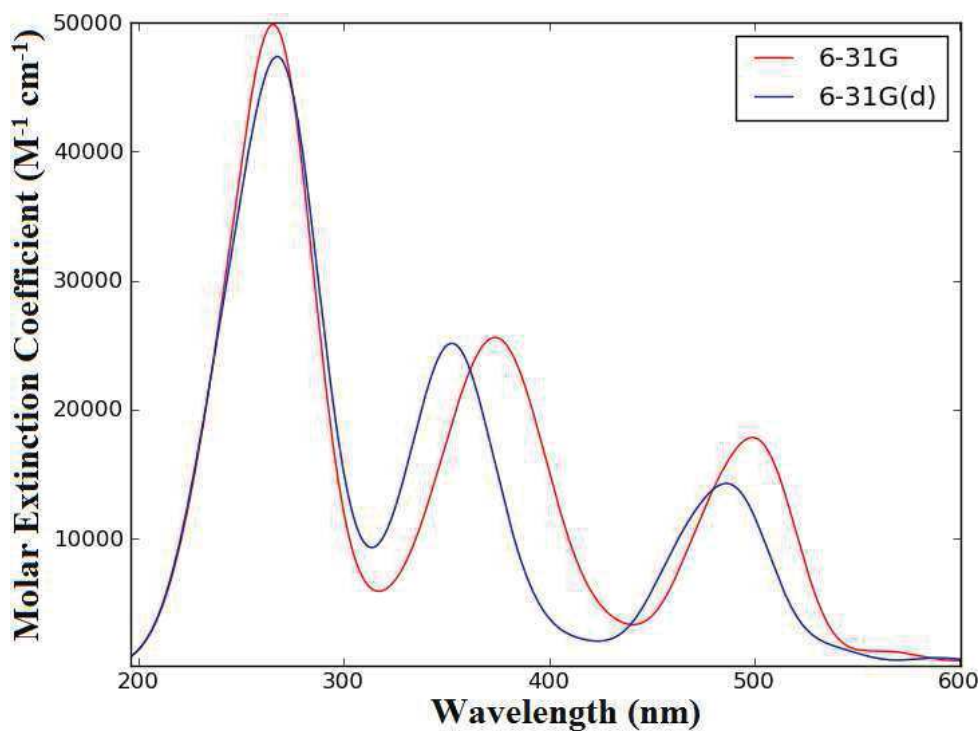
7. Complex (7)*: $[\text{Ru}(\text{bpy})_2(4\text{-n-bpy})]^{2+}$

PDOS



Total and partial density of states of $[\text{Ru}(\text{bpy})_2(4\text{-n-bpy})]^{2+}$ partitioned over Ru d orbitals and ligand C, O and N p orbitals.

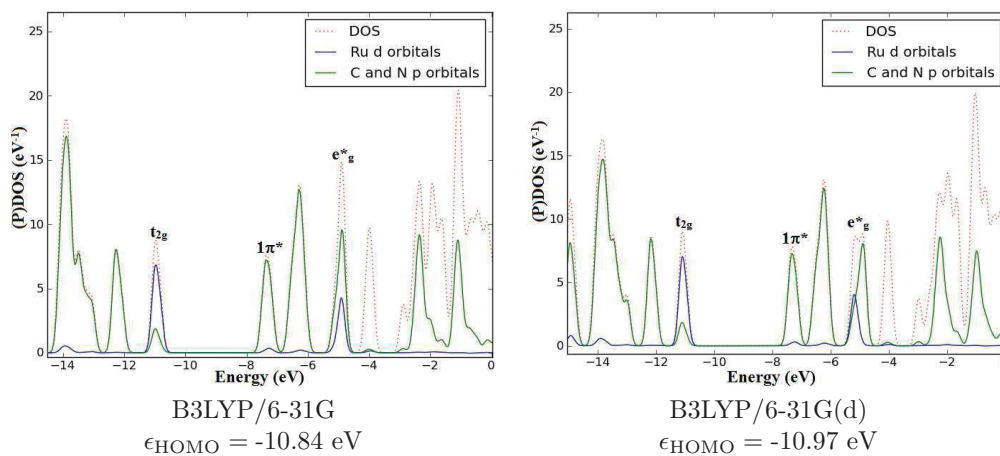
Absorption Spectrum



$[\text{Ru}(\text{bpy})_2(4\text{-n-bpy})]^{2+}$ TD-B3LYP/6-31G and TD-B3LYP/6-31G(d) spectra.

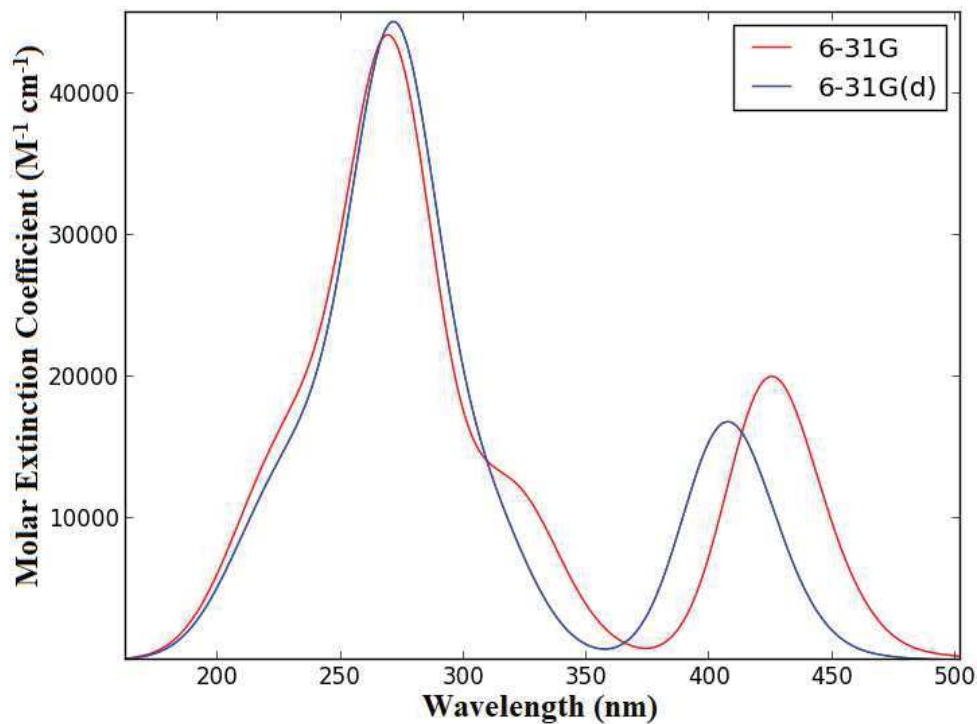
8. Complex (8): $[\text{Ru}(\text{bpy})_2(3,3'\text{-dm-bpy})]^{2+}$

PDOS



Total and partial density of states of $[\text{Ru}(\text{bpy})_2(3,3'\text{-dm-bpy})]^{2+}$ partitioned over Ru d orbitals and ligand C and N p orbitals.

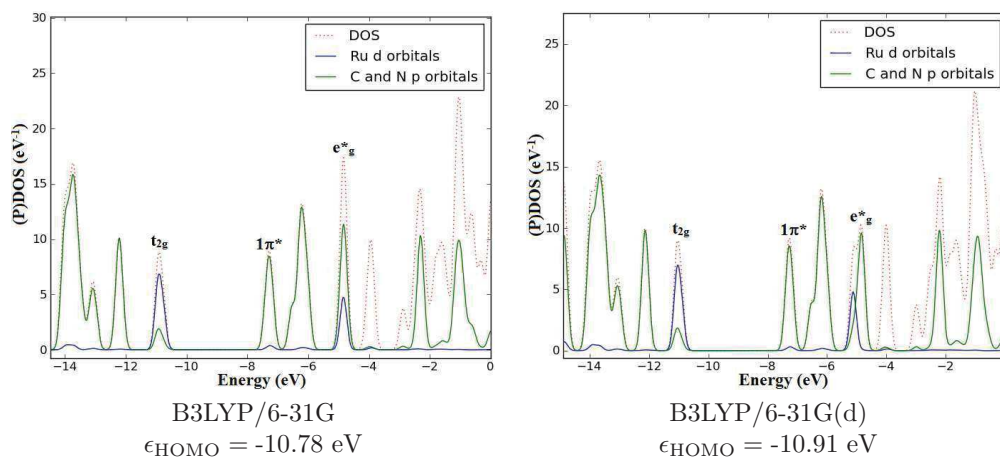
Absorption Spectrum



$[\text{Ru}(\text{bpy})_2(3,3'\text{-dm-bpy})]^{2+}$ TD-B3LYP/6-31G and TD-B3LYP/6-31G(d) spectra.

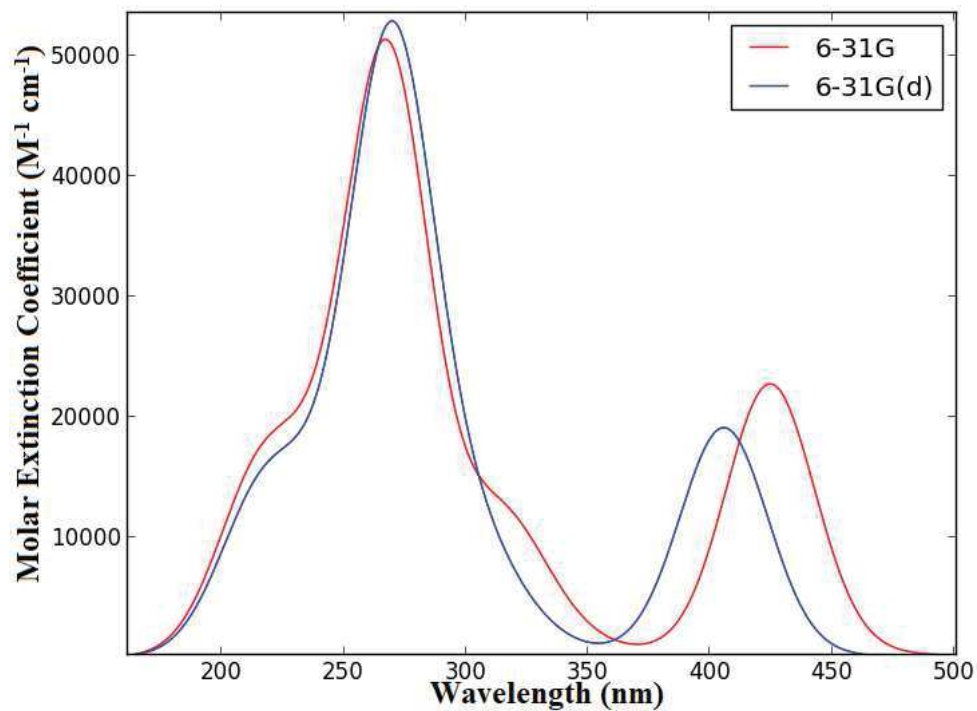
9. Complex (9): $[\text{Ru}(\text{bpy})_2(4,4'\text{-dm-bpy})]^{2+}$

PDOS



Total and partial density of states of $[\text{Ru}(\text{bpy})_2(4,4'\text{-dm-bpy})]^{2+}$ partitioned over Ru d orbitals and ligand C and N p orbitals.

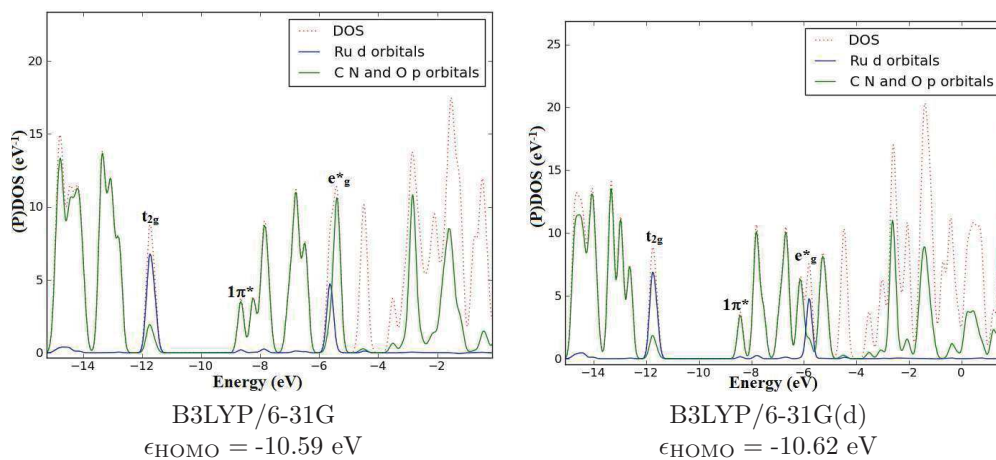
Absorption Spectrum



$[\text{Ru}(\text{bpy})_2(4,4'\text{-dm-bpy})]^{2+}$ TD-B3LYP/6-31G and TD-B3LYP/6-31G(d) spectra.

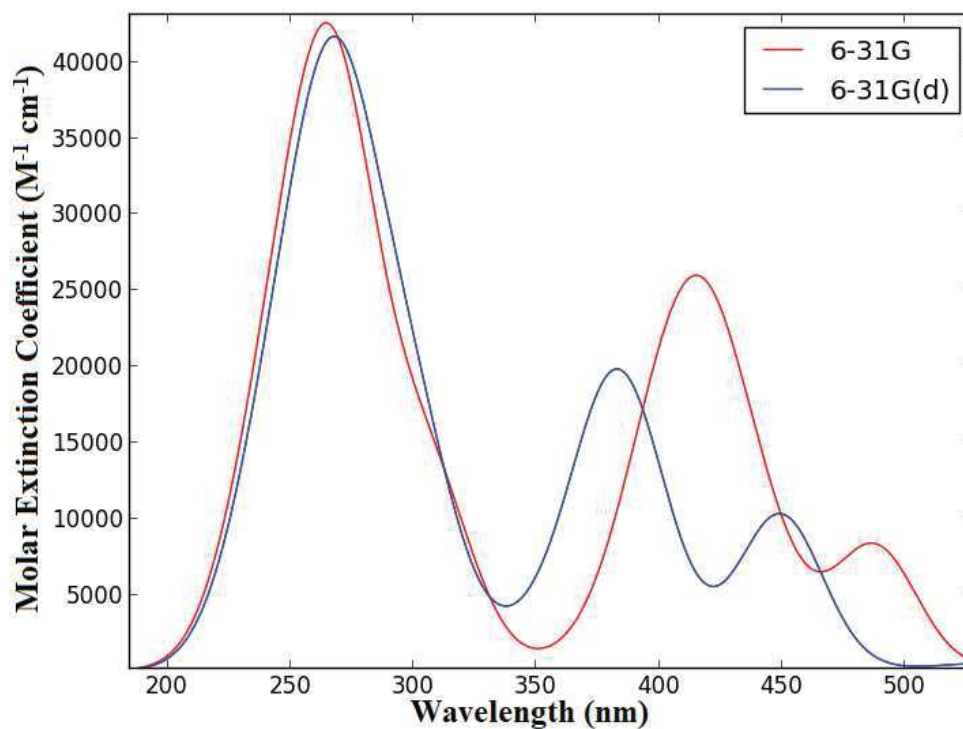
10. Complex (11): $[\text{Ru}(\text{bpy})_2(4,4'\text{-dn-bpy})]^{2+}$

PDOS



Total and partial density of states of $[\text{Ru}(\text{bpy})_2(4,4'\text{-dn-bpy})]^{2+}$ partitioned over Ru d orbitals and ligand C, O and N p orbitals.

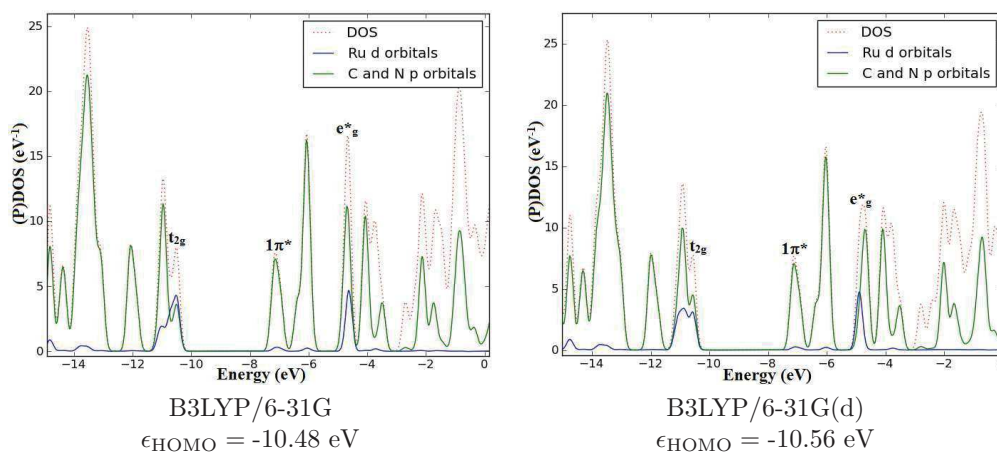
Absorption Spectrum



$[\text{Ru}(\text{bpy})_2(4,4'\text{-dn-bpy})]^{2+}$ TD-B3LYP/6-31G and TD-B3LYP/6-31G(d) spectra.

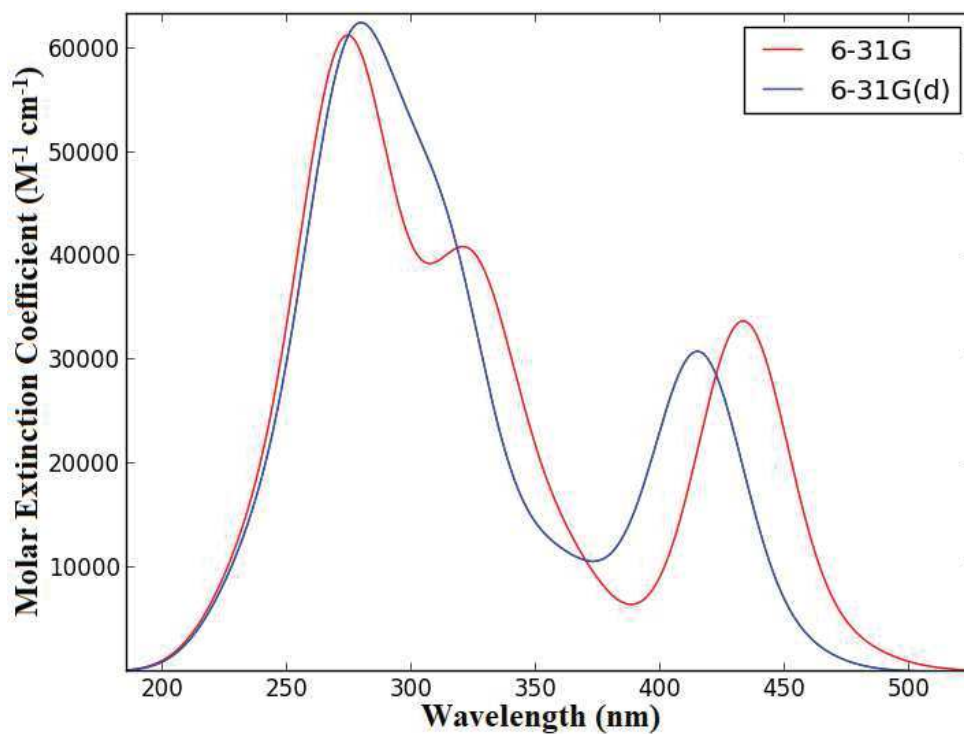
11. Complex (12): $[\text{Ru}(\text{bpy})_2(4,4'\text{-dph-bpy})]^{2+}$

PDOS



Total and partial density of states of $[\text{Ru}(\text{bpy})_2(4,4'\text{-dph-bpy})]^{2+}$ partitioned over Ru d orbitals and ligand C and N p orbitals.

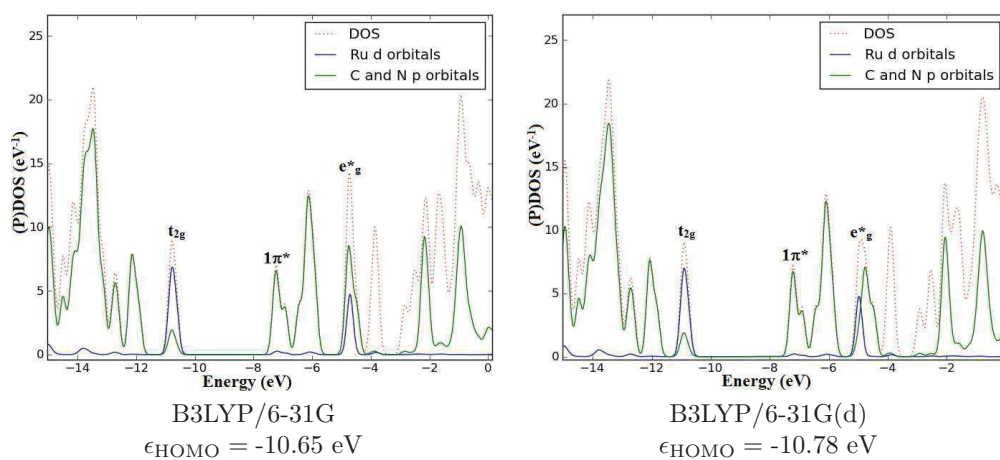
Absorption Spectrum



$[\text{Ru}(\text{bpy})_2(4,4'\text{-dph-bpy})]^{2+}$ TD-B3LYP/6-31G and TD-B3LYP/6-31G(d) spectra.

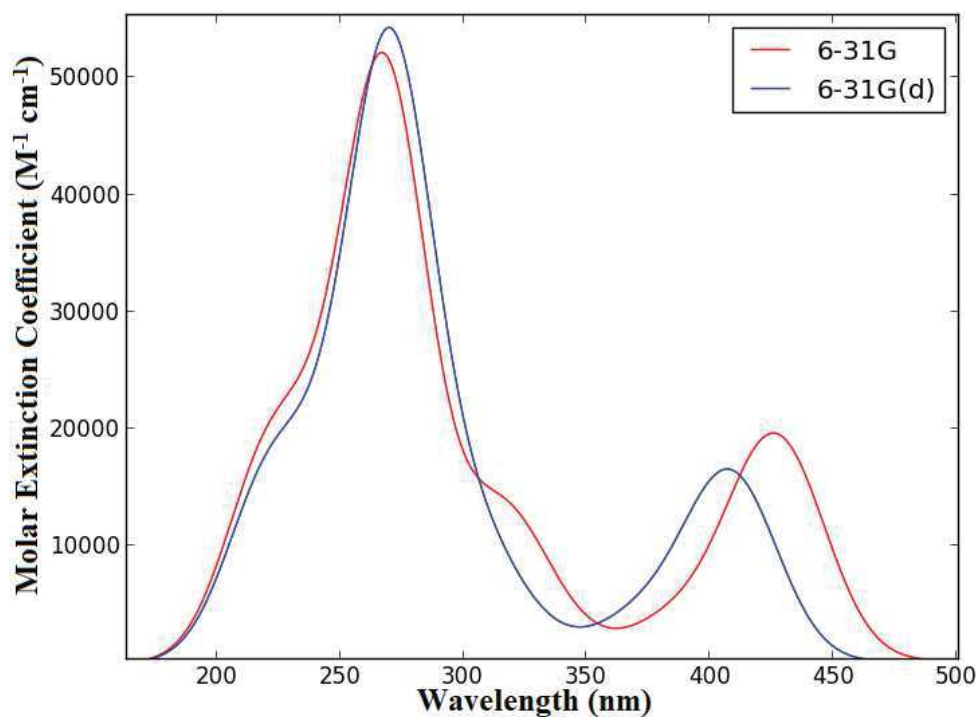
12. Complex (13): $[\text{Ru}(\text{bpy})_2(4,4'\text{-DTB-bpy})]^{2+}$

PDOS



Total and partial density of states of $[\text{Ru}(\text{bpy})_2(4,4'\text{-DTB-bpy})]^{2+}$ partitioned over Ru d orbitals and ligand C and N p orbitals.

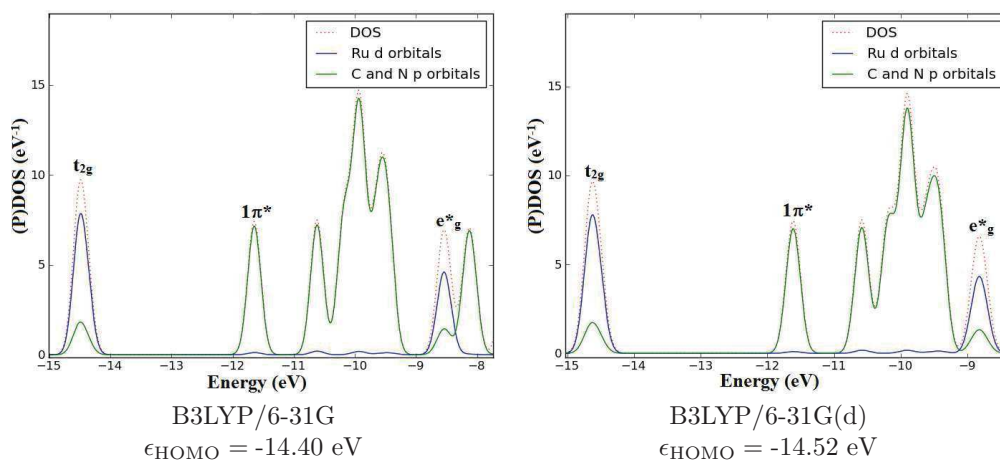
Absorption Spectrum



$[\text{Ru}(\text{bpy})_2(4,4'\text{-DTB-bpy})]^{2+}$ TD-B3LYP/6-31G and TD-B3LYP/6-31G(d) spectra.

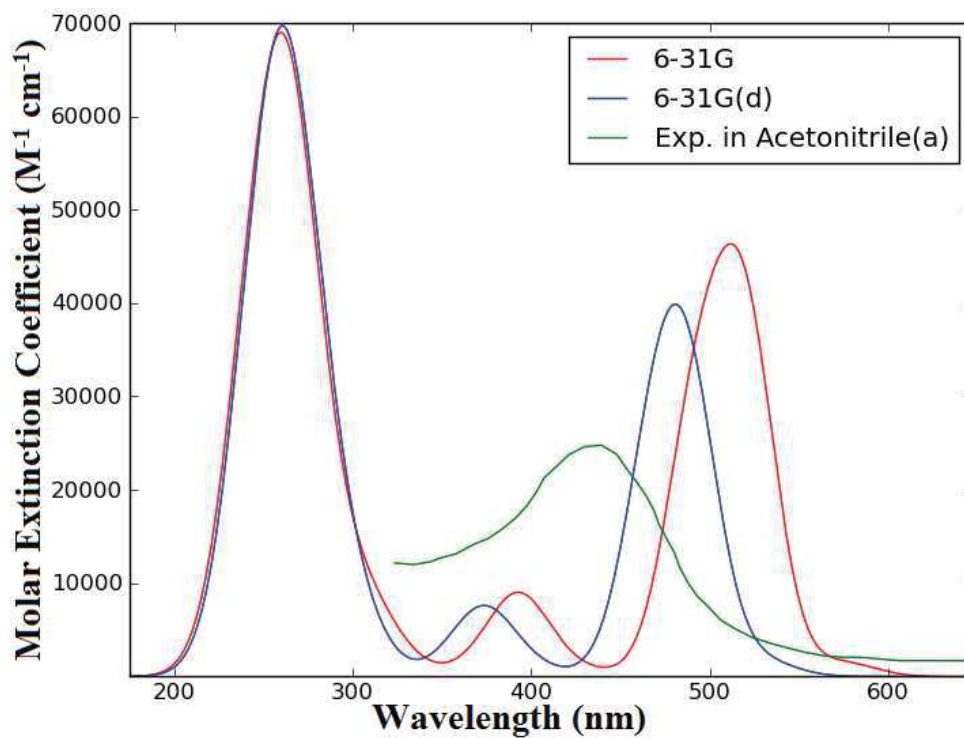
13. Complex (14): cis -[Ru(bpy)₂(m-4,4'-bpy)₂]⁴⁺

PDOS



Total and partial density of states of cis -[Ru(bpy)₂(m-4,4'-bpy)₂]⁴⁺ partitioned over Ru d orbitals and ligand C and N p orbitals.

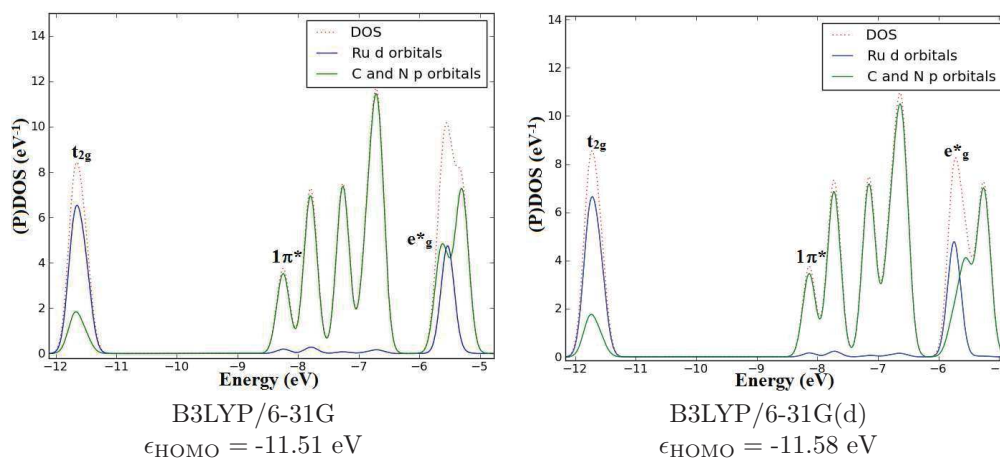
Absorption Spectrum



cis -[Ru(bpy)₂(m-4,4'-bpy)₂]⁴⁺ TD-B3LYP/6-31G, TD-B3LYP/6-31G(d), and experimental spectra. Experimental curve at 25°C in acetonitrile[4].

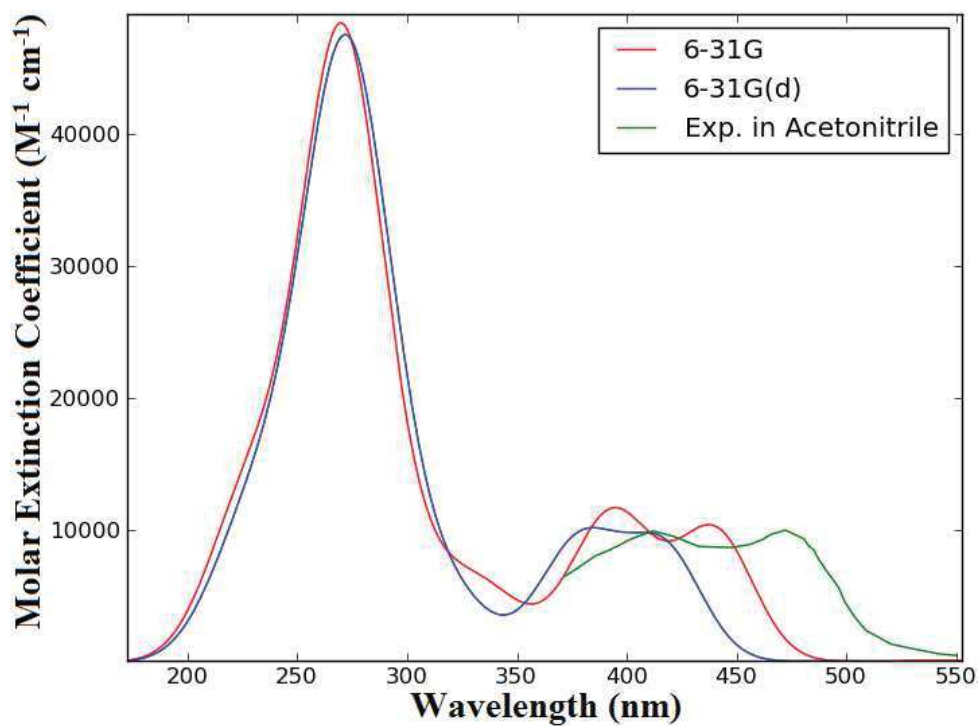
14. Complex (15): $[\text{Ru}(\text{bpy})_2(\text{bpz})]^{2+}$

PDOS



Total and partial density of states of $[\text{Ru}(\text{bpy})_2(\text{bpz})]^{2+}$ partitioned over Ru d orbitals and ligand C and N p orbitals.

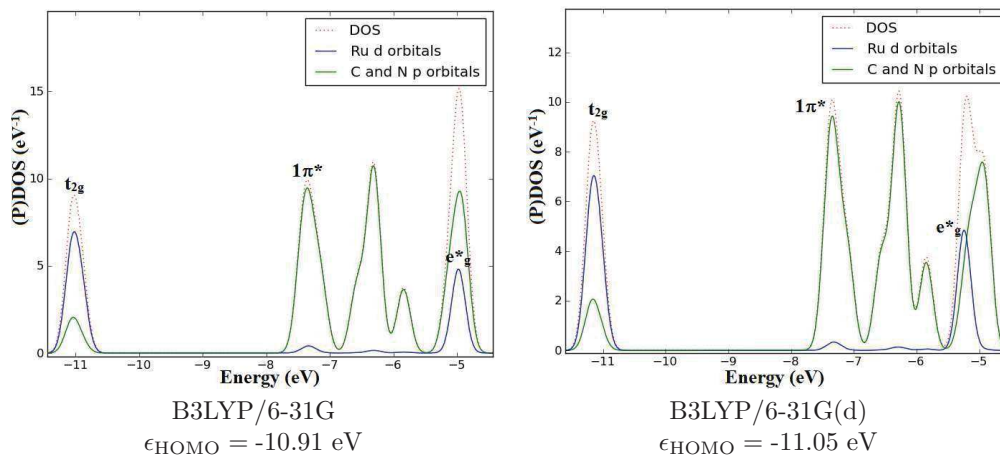
Absorption Spectrum



$[\text{Ru}(\text{bpy})_2(\text{bpz})]^{2+}$ TD-B3LYP/6-31G, TD-B3LYP/6-31G(d), and experimental spectra. Experimental curve from [5].

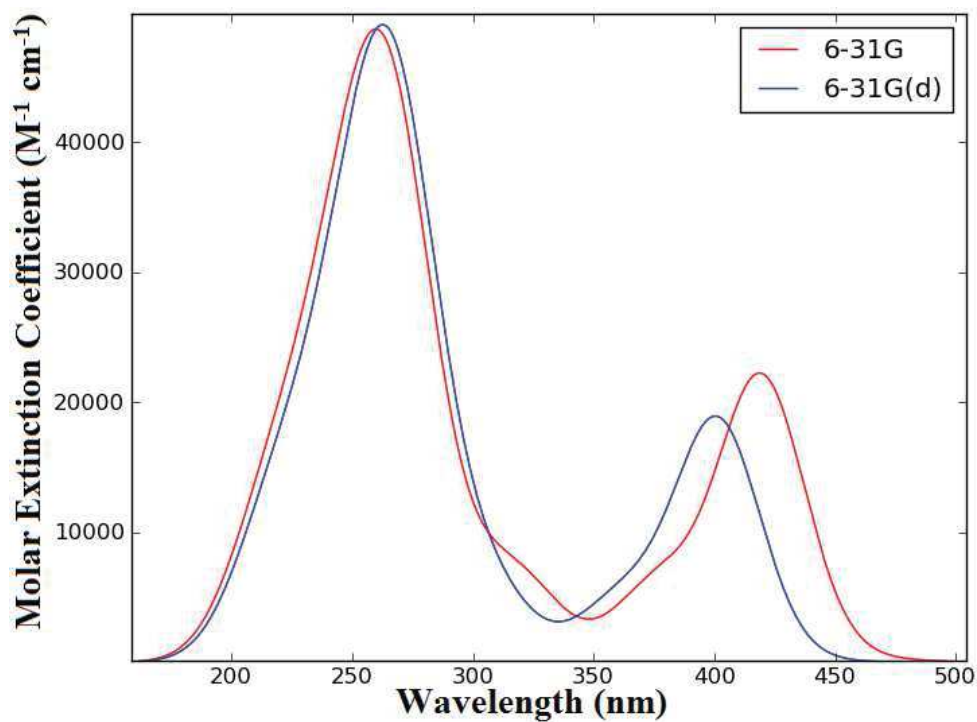
15. Complex (16): $[\text{Ru}(\text{bpy})_2(\text{phen})]^{2+}$

PDOS



Total and partial density of states of $[\text{Ru}(\text{bpy})_2(\text{phen})]^{2+}$ partitioned over Ru d orbitals and ligand C and N p orbitals.

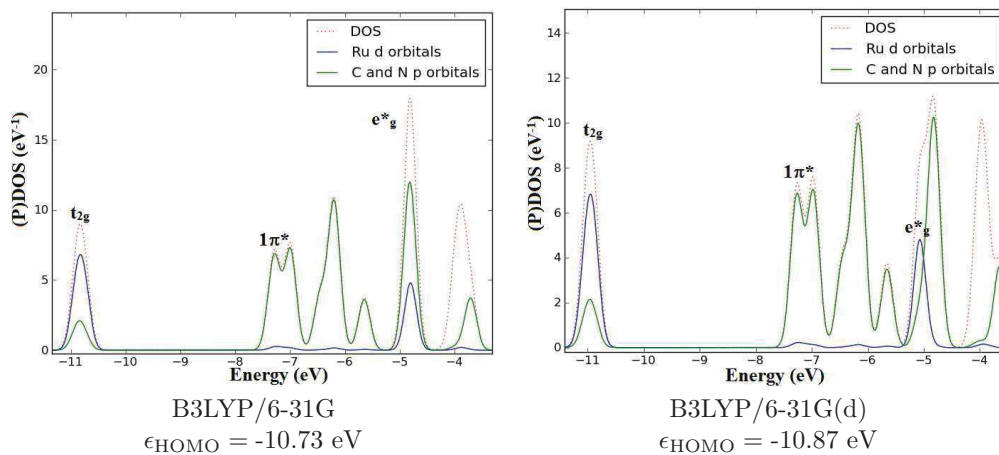
Absorption Spectrum



$[\text{Ru}(\text{bpy})_2(\text{phen})]^{2+}$ TD-B3LYP/6-31G and TD-B3LYP/6-31G(d) spectra.

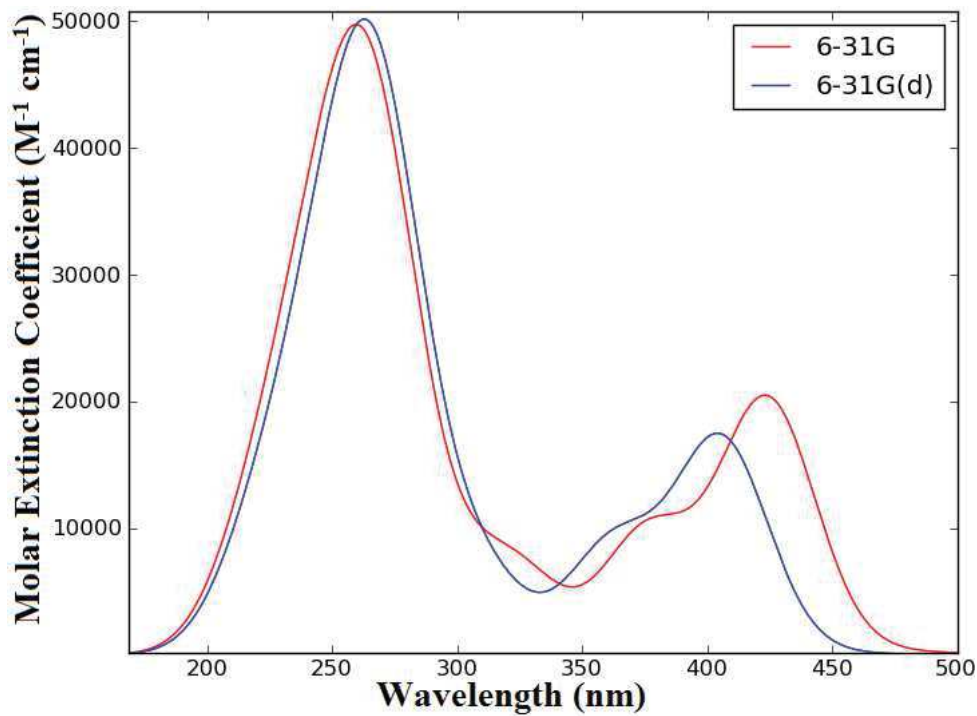
16. Complex (17): $[\text{Ru}(\text{bpy})_2(4,7\text{-dm-phen})]^{2+}$

PDOS



Total and partial density of states of $[\text{Ru}(\text{bpy})_2(4,7\text{-dm-phen})]^{2+}$ partitioned over Ru d orbitals and ligand C and N p orbitals.

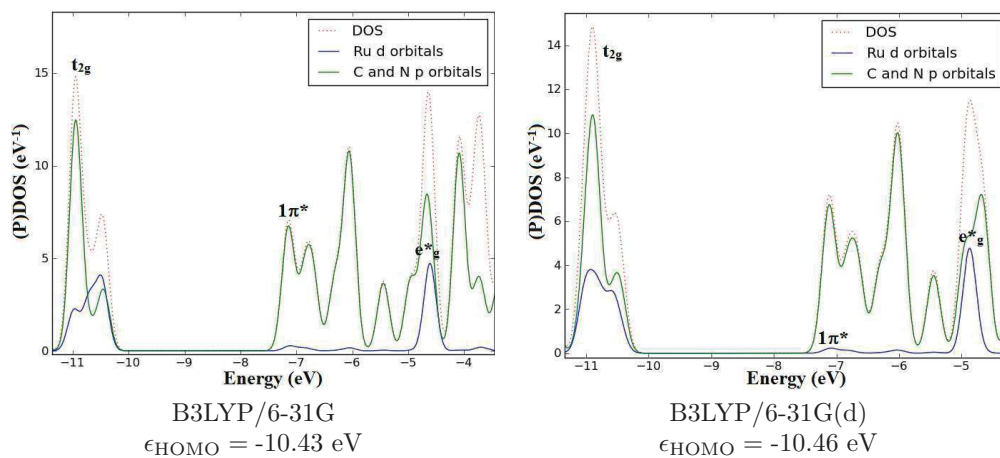
Absorption Spectrum



$[\text{Ru}(\text{bpy})_2(4,7\text{-dm-phen})]^{2+}$ TD-B3LYP/6-31G and TD-B3LYP/6-31G(d) spectra.

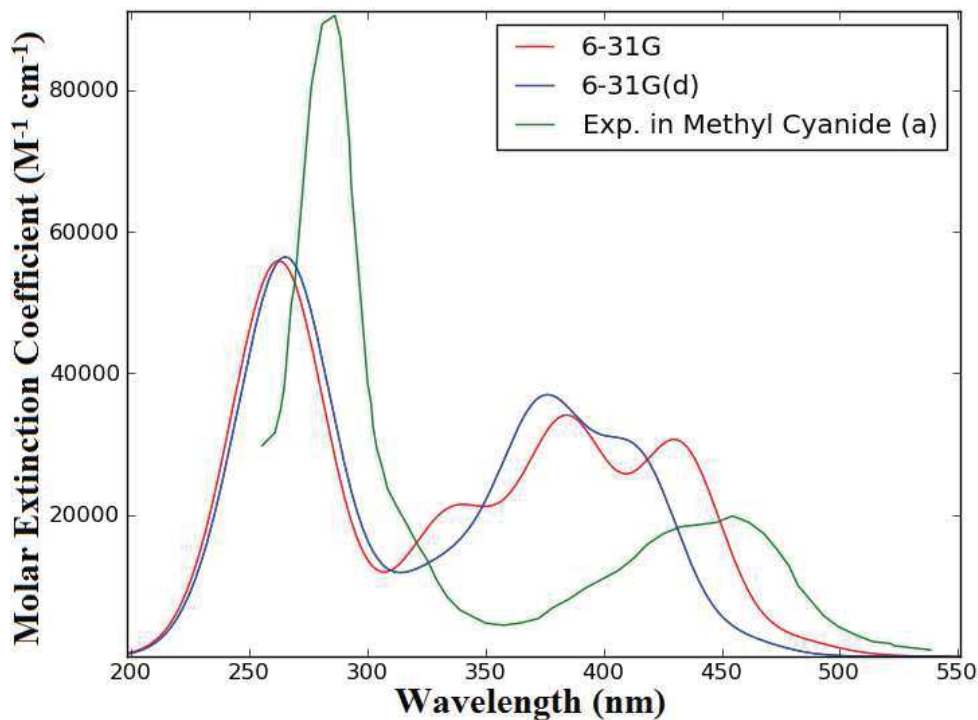
17. Complex (18): $[\text{Ru}(\text{bpy})_2(4,7\text{-Ph}_2\text{-phen})]^{2+}$

PDOS



Total and partial density of states of $[\text{Ru}(\text{bpy})_2(4,7\text{-Ph}_2\text{-phen})]^{2+}$ partitioned over Ru d orbitals and ligand C and N p orbitals.

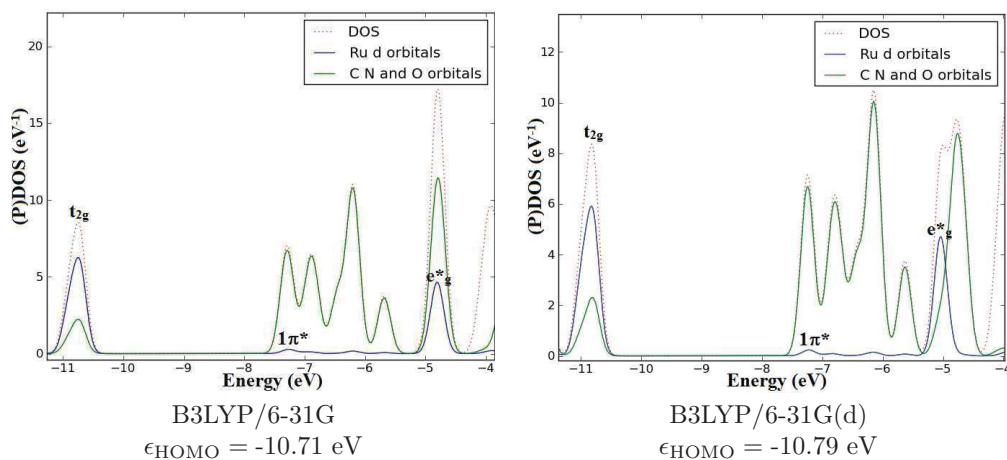
Absorption Spectrum



$[\text{Ru}(\text{bpy})_2(4,7\text{-Ph}_2\text{-phen})]^{2+}$ TD-B3LYP/6-31G, TD-B3LYP/6-31G(d), and experimental spectra. Experimental spectrum measured in acetonitrile [6].

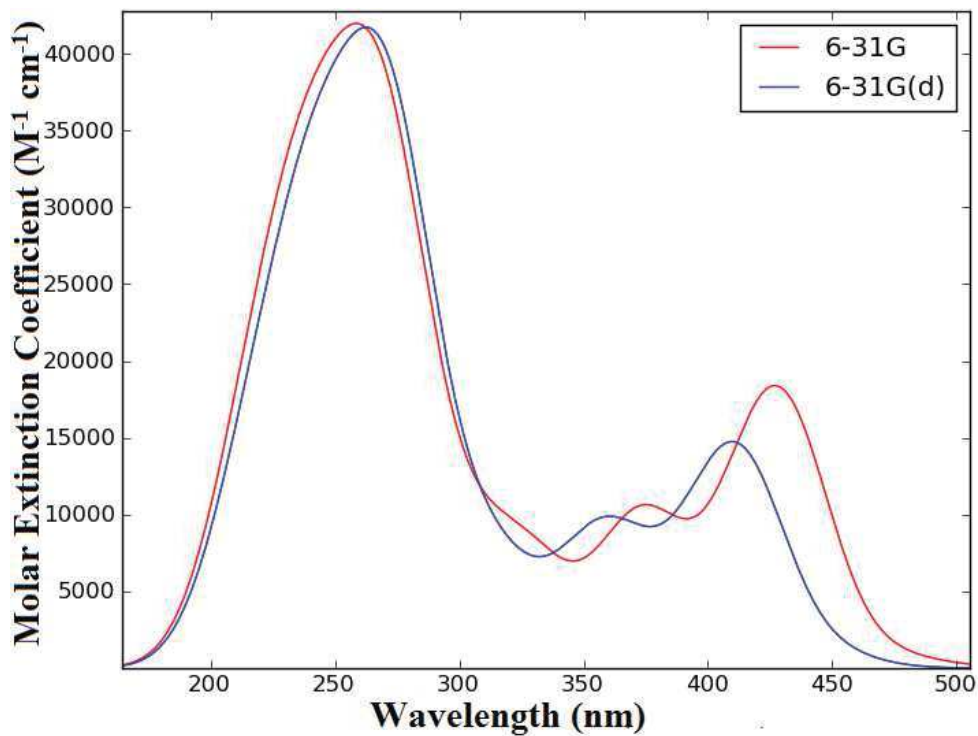
18. Complex (19): $[\text{Ru}(\text{bpy})_2(4,7\text{-dhy-phen})]^{2+}$

PDOS



Total and partial density of states of $[\text{Ru}(\text{bpy})_2(4,7\text{-dhy-phen})]^{2+}$ partitioned over Ru d orbitals and ligand C, O, and N p orbitals.

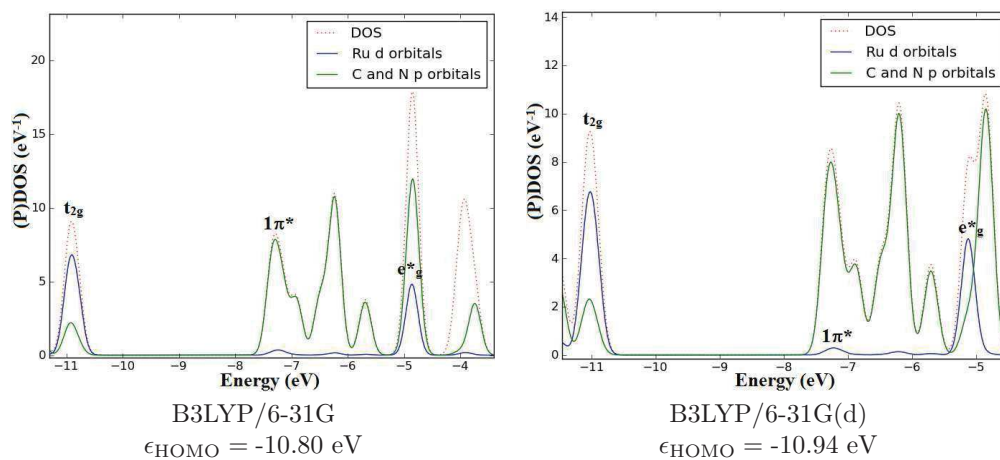
Absorption Spectrum



$[\text{Ru}(\text{bpy})_2(4,7\text{-dhy-phen})]^{2+}$ TD-B3LYP/6-31G and TD-B3LYP/6-31G(d) spectra.

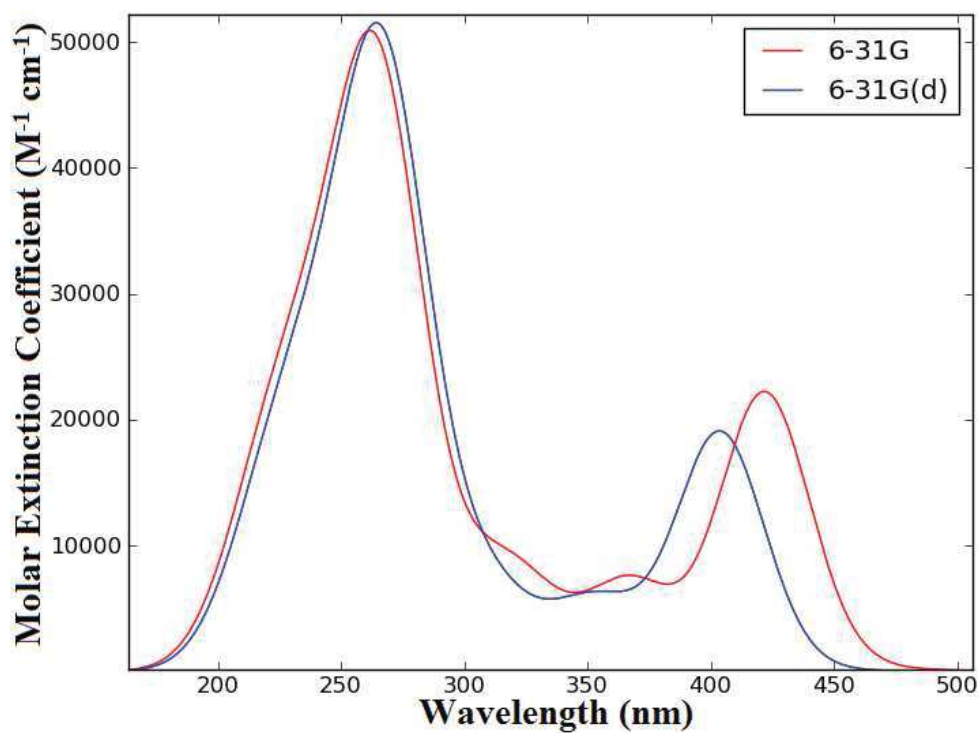
19. Complex (20): $[\text{Ru}(\text{bpy})_2(5,6\text{-dm-phen})]^{2+}$

PDOS



Total and partial density of states of $[\text{Ru}(\text{bpy})_2(5,6\text{-dm-phen})]^{2+}$ partitioned over Ru d orbitals and ligand C and N p orbitals.

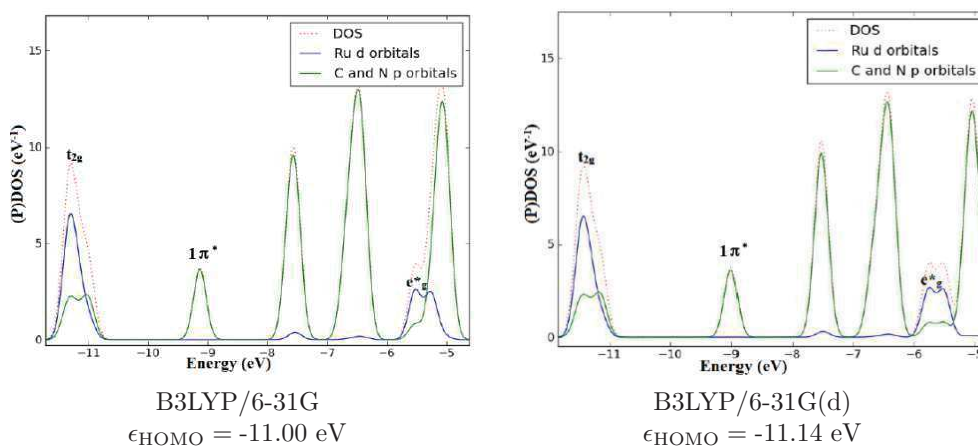
Absorption Spectrum



$[\text{Ru}(\text{bpy})_2(5,6\text{-dm-phen})]^{2+}$ TD-B3LYP/6-31G and TD-B3LYP/6-31G(d) spectra.

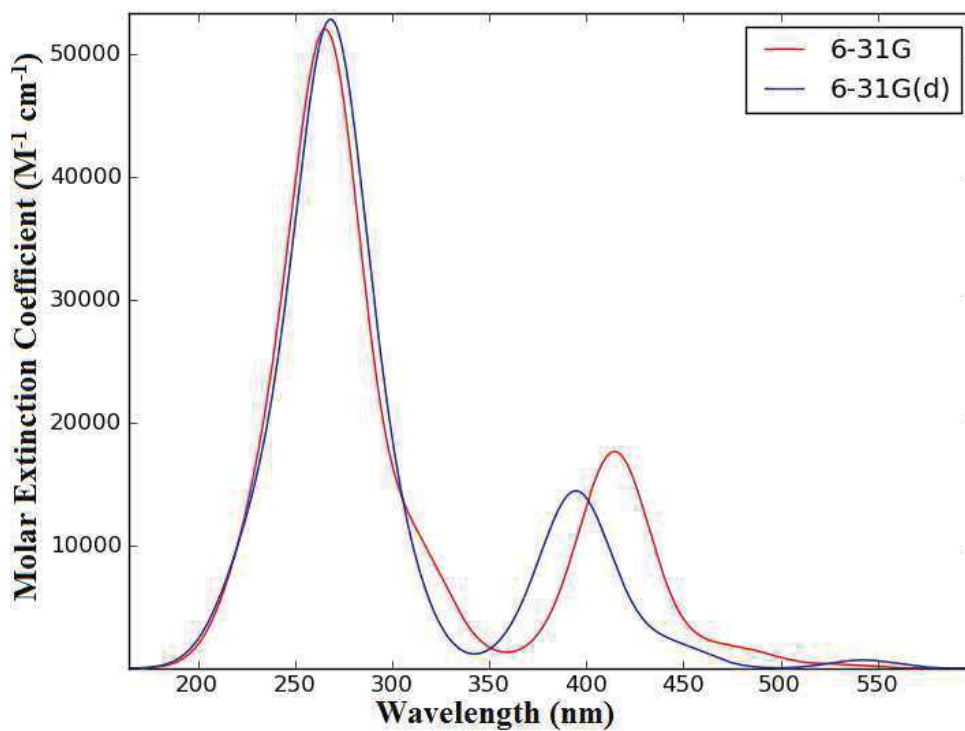
20. Complex (21): $[\text{Ru}(\text{bpy})_2(\text{DIAF})]^{2+}$

PDOS



Total and partial density of states of $[\text{Ru}(\text{bpy})_2(\text{DIAF})]^{2+}$ partitioned over Ru d orbitals and ligand C and N p orbitals.

Absorption Spectrum

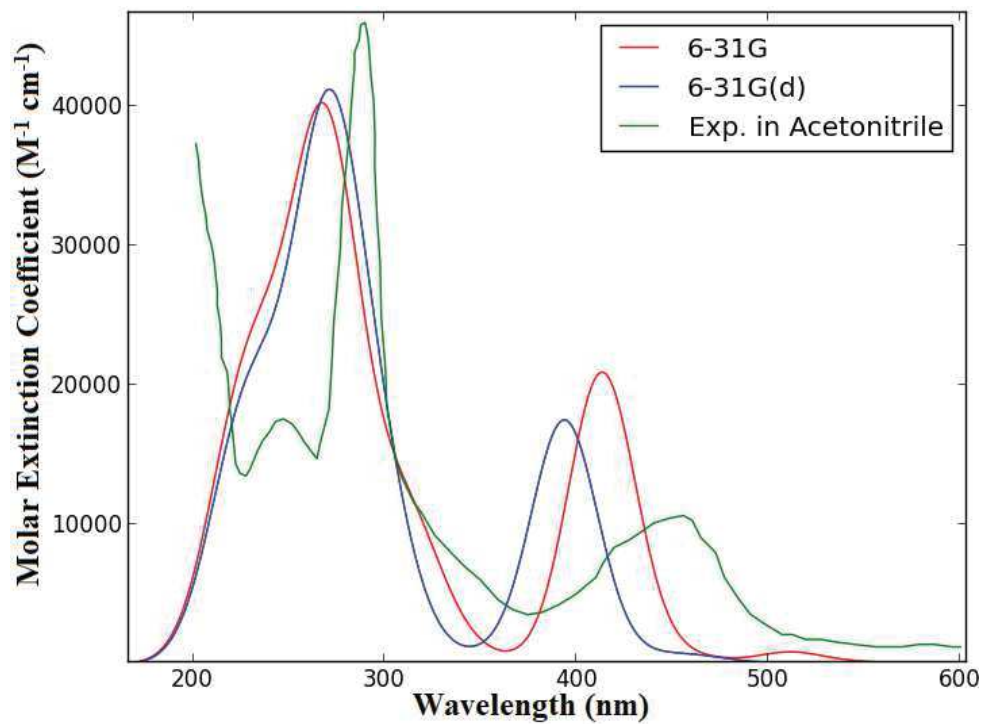


$[\text{Ru}(\text{bpy})_2(\text{DIAF})]^{2+}$ TD-B3LYP/6-31G and TD-B3LYP/6-31G(d) spectra.

21. Complex (22)[†]: [Ru(bpy)₂(DIAFO)]²⁺

B3LYP/6-31G B3LYP/6-31G(d)
 $\epsilon_{\text{HOMO}} = -11.17 \text{ eV}$ $\epsilon_{\text{HOMO}} = -11.30 \text{ eV}$

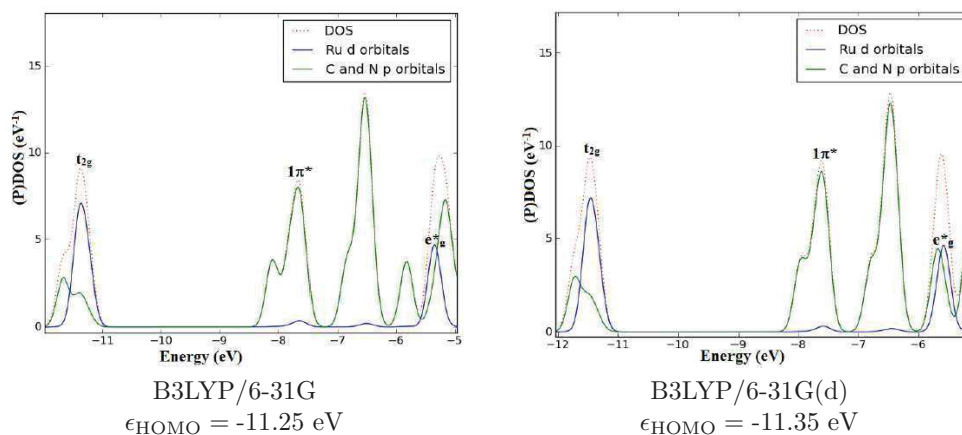
Absorption Spectrum



[Ru(bpy)₂(DIAFO)]²⁺ TD-B3LYP/6-31G, TD-B3LYP/6-31G(d), and experimental spectra. Experimental spectrum measured at room temperature in acetonitrile [7].

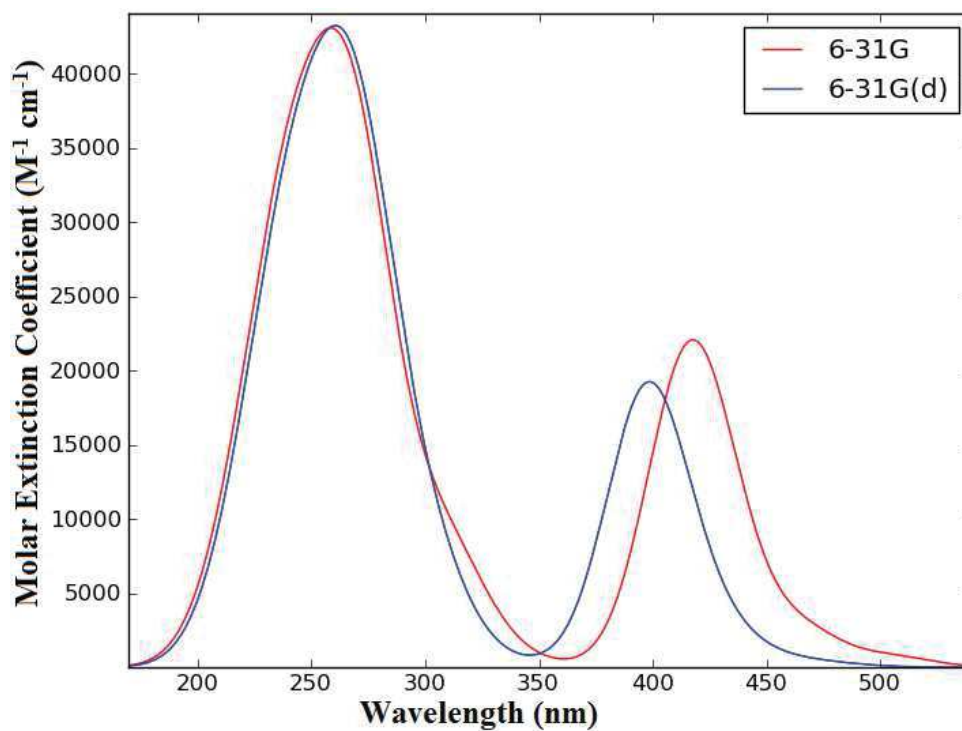
22. Complex (23): $[\text{Ru}(\text{bpy})_2(\text{taphen})]^{2+}$

PDOS



Total and partial density of states of $[\text{Ru}(\text{bpy})_2(\text{taphen})]^{2+}$ partitioned over Ru d orbitals and ligand C and N p orbitals.

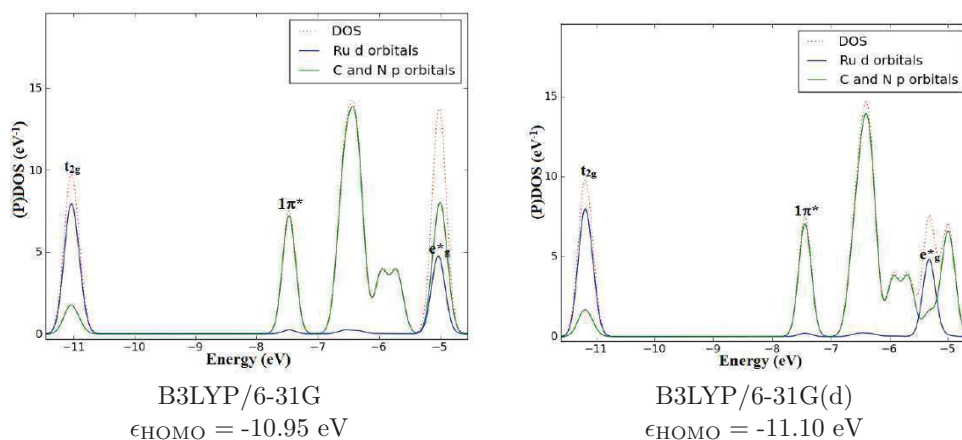
Absorption Spectrum



$[\text{Ru}(\text{bpy})_2(\text{taphen})]^{2+}$ TD-B3LYP/6-31G and TD-B3LYP/6-31G(d) spectra.

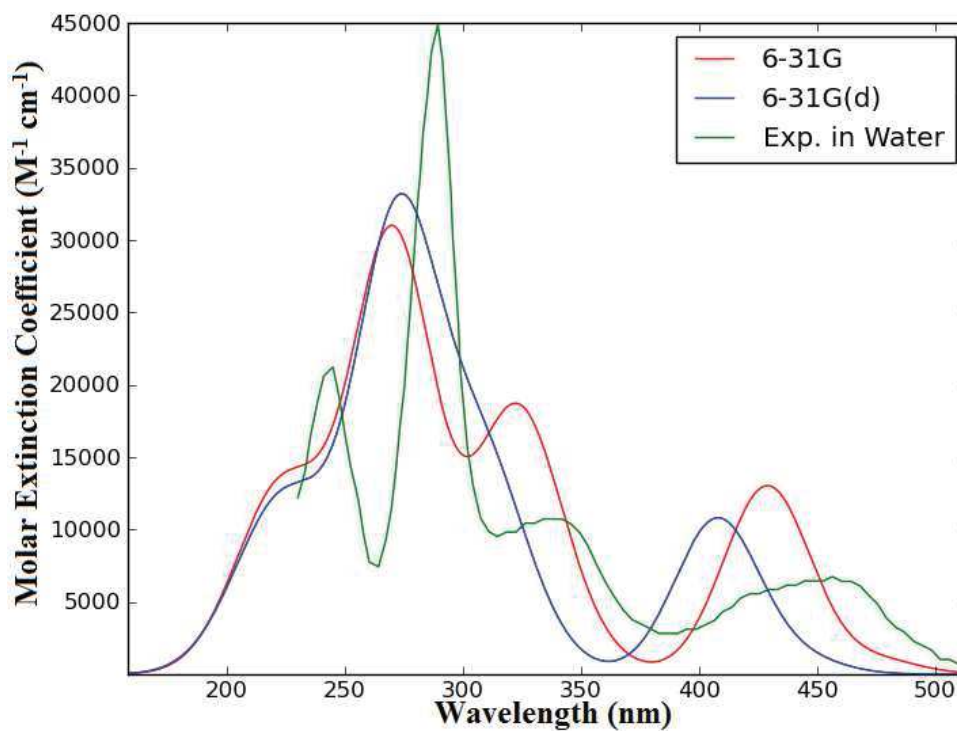
23. Complex (24): $cis\text{-}[\text{Ru}(\text{bpy})_2(\text{py})_2]^{2+}$

PDOS



Total and partial density of states of $cis\text{-}[\text{Ru}(\text{bpy})_2(\text{py})_2]^{2+}$ partitioned over Ru d orbitals and ligand C and N p orbitals.

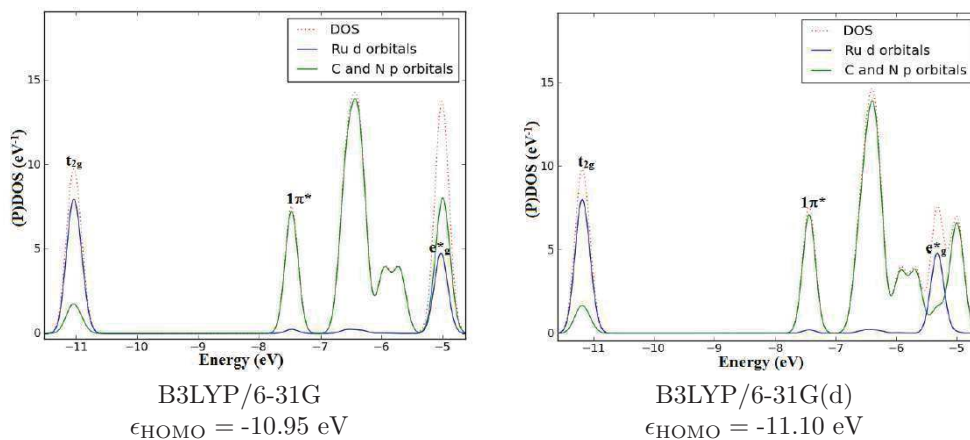
Absorption Spectrum



$Cis\text{-}[\text{Ru}(\text{bpy})_2(\text{py})_2]^{2+}$ TD-B3LYP/6-31G, TD-B3LYP/6-31G(d), and experimental spectra. Experimental spectrum measured in water [8].

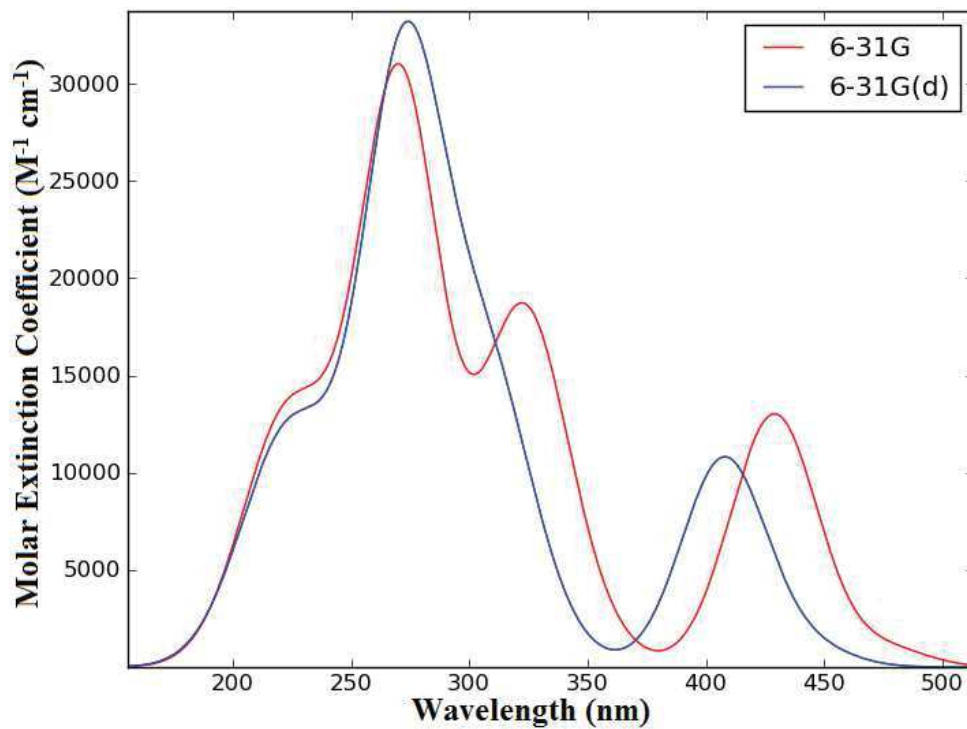
24. Complex (25): $trans\text{-}[\text{Ru}(\text{bpy})_2(\text{py})_2]^{2+}$

PDOS



Total and partial density of states of $trans\text{-}[\text{Ru}(\text{bpy})_2(\text{py})_2]^{2+}$ partitioned over Ru d orbitals and ligand C and N p orbitals.

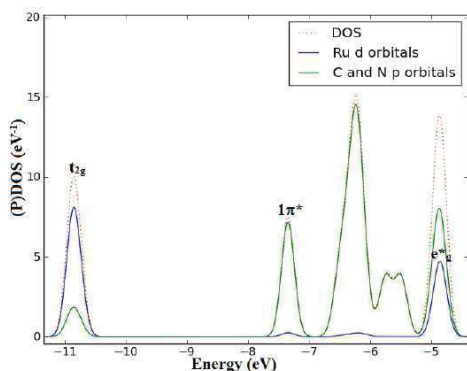
Absorption Spectrum



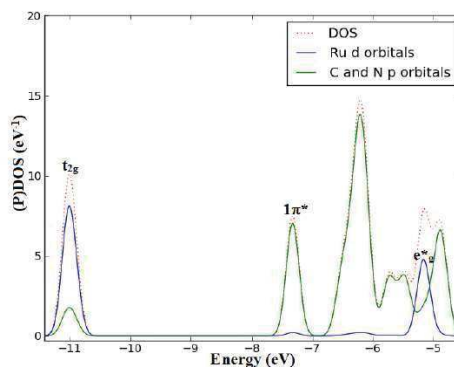
$Trans\text{-}[\text{Ru}(\text{bpy})_2(\text{py})_2]^{2+}$ TD-B3LYP/6-31G and TD-B3LYP/6-31G(d) spectra.

25. Complex (26): $[\text{Ru}(\text{bpy})_2(\text{pic})_2]^{2+}$

PDOS



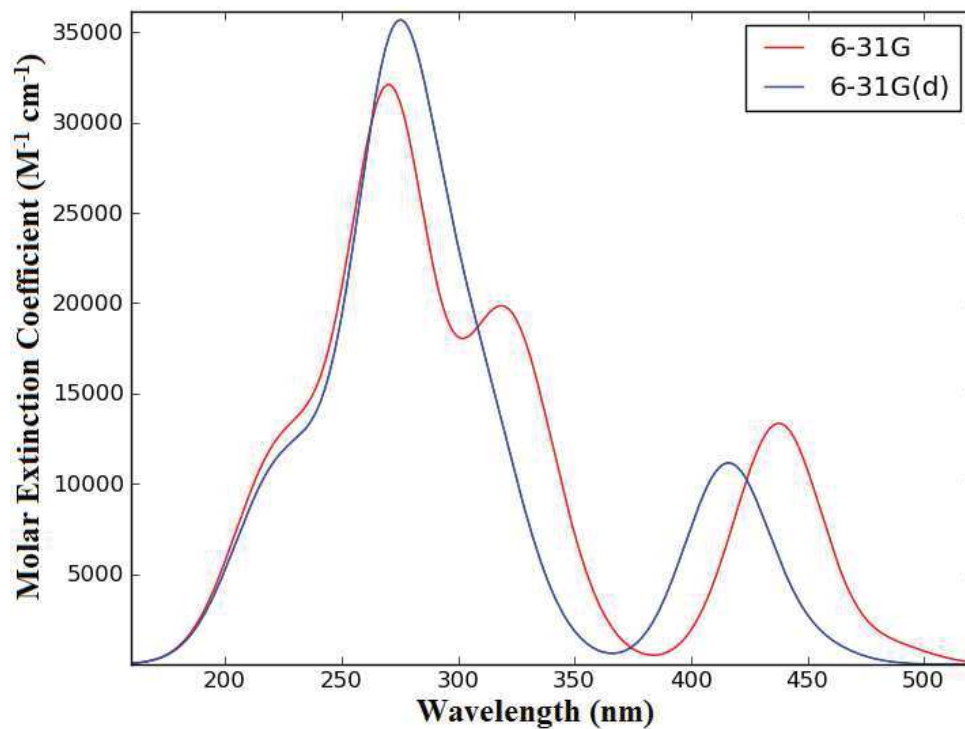
B3LYP/6-31G
 $\epsilon_{\text{HOMO}} = -10.78 \text{ eV}$



B3LYP/6-31G(d)
 $\epsilon_{\text{HOMO}} = -10.93 \text{ eV}$

Total and partial density of states of $[\text{Ru}(\text{bpy})_2(\text{pic})_2]^{2+}$ partitioned over Ru d orbitals and ligand C and N p orbitals.

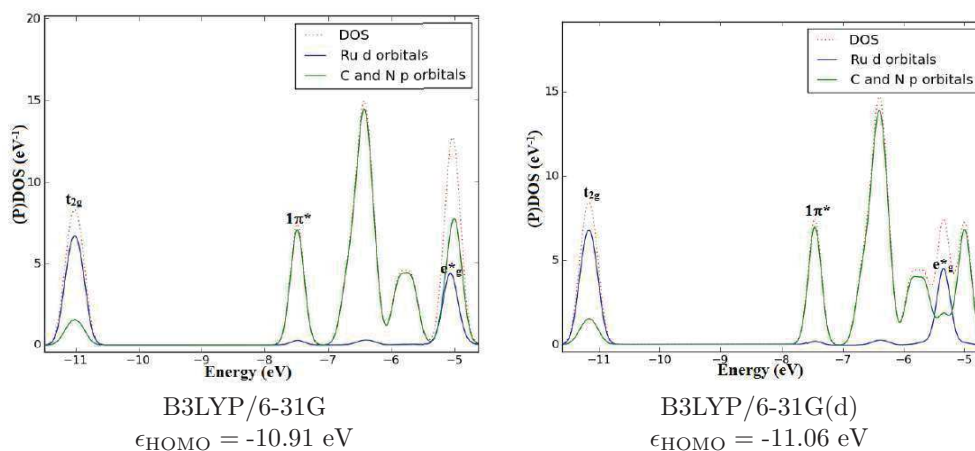
Absorption Spectrum



$[\text{Ru}(\text{bpy})_2(\text{pic})_2]^{2+}$ TD-B3LYP/6-31G and TD-B3LYP/6-31G(d) spectra.

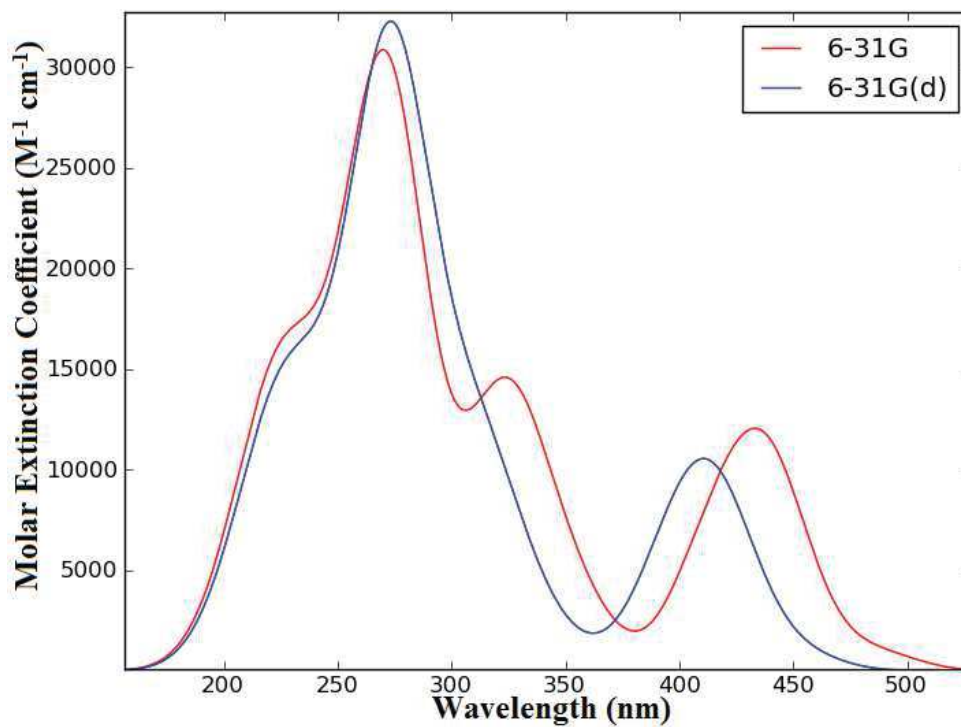
26. Complex (27): $[\text{Ru}(\text{bpy})_2(\text{DPM})]^{2+}$

PDOS



Total and partial density of states of $[\text{Ru}(\text{bpy})_2(\text{DPM})]^{2+}$ partitioned over Ru d orbitals and ligand C and N p orbitals.

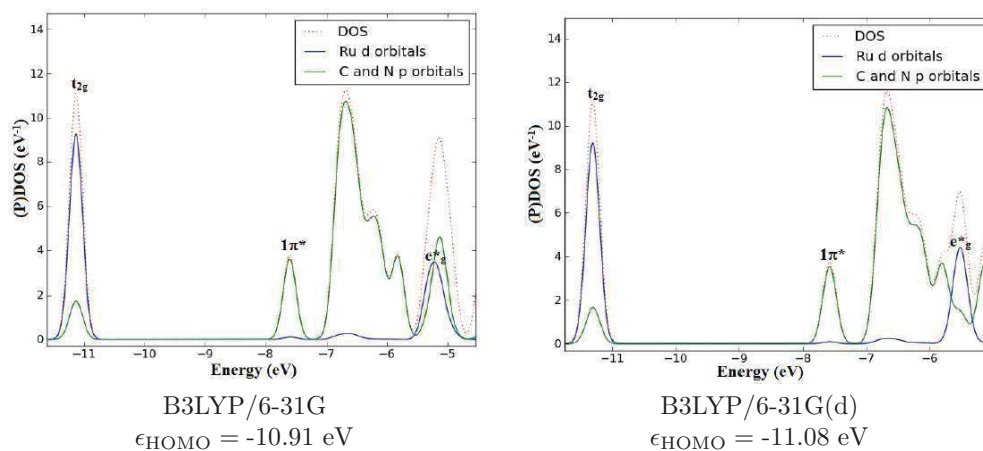
Absorption Spectrum



$[\text{Ru}(\text{bpy})_2(\text{DPM})]^{2+}$ TD-B3LYP/6-31G and TD-B3LYP/6-31G(d) spectra.

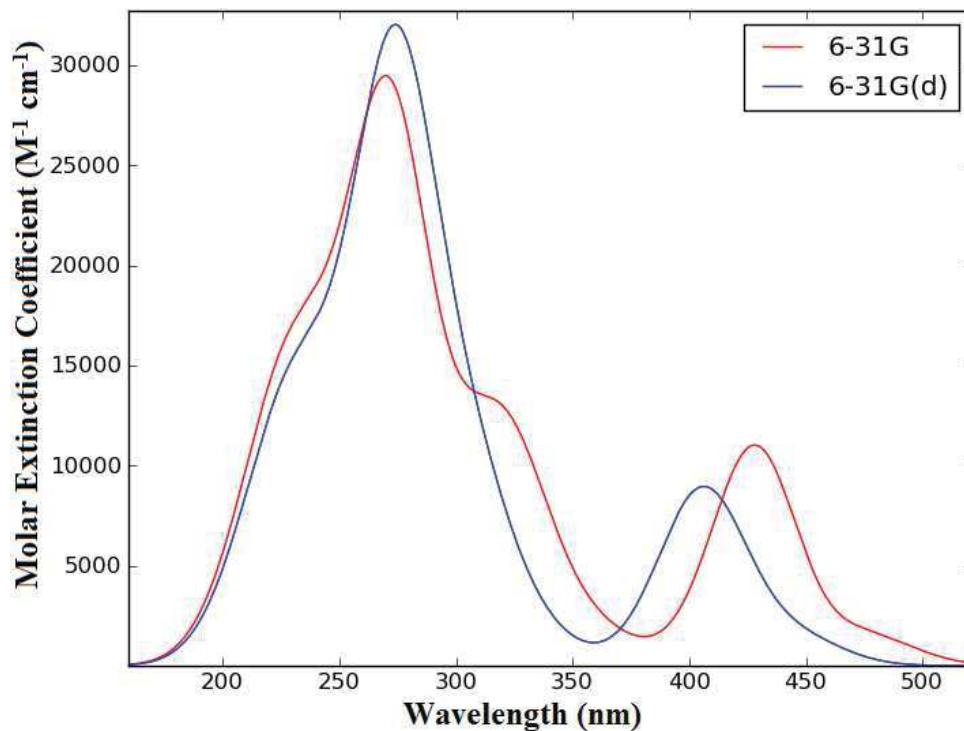
27. Complex (28): $[\text{Ru}(\text{bpy})_2(\text{DPE})]^{2+}$

PDOS



Total and partial density of states of $[\text{Ru}(\text{bpy})_2(\text{DPE})]^{2+}$ partitioned over Ru d orbitals and ligand C and N p orbitals.

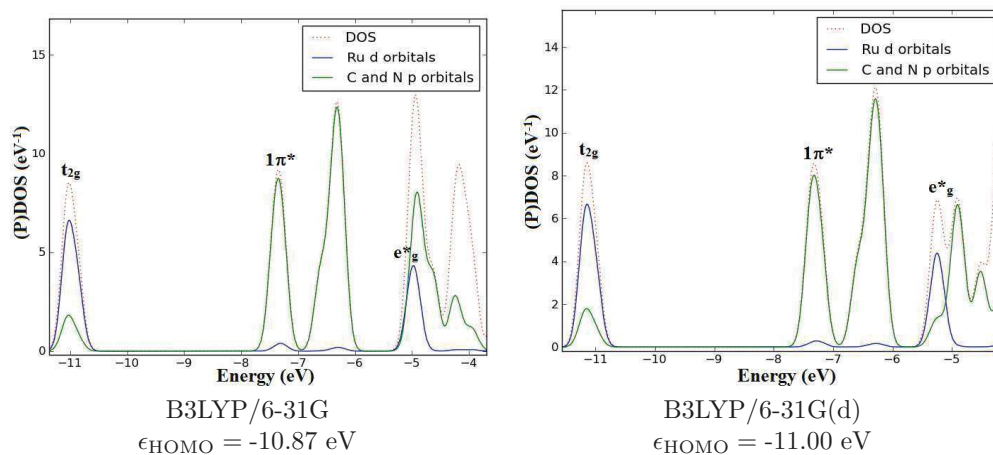
Absorption Spectrum



$[\text{Ru}(\text{bpy})_2(\text{DPE})]^{2+}$ TD-B3LYP/6-31G and TD-B3LYP/6-31G(d) spectra.

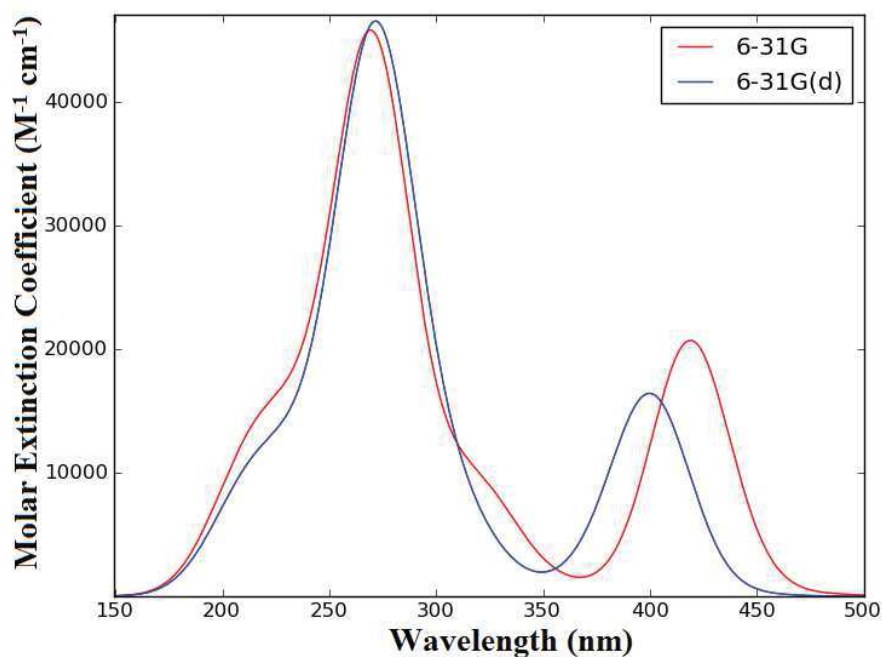
28. Complex (29): $[\text{Ru}(\text{bpy})_2(\text{PimH})]^{2+}$

PDOS



Total and partial density of states of $[\text{Ru}(\text{bpy})_2(\text{PimH})]^{2+}$ partitioned over Ru d orbitals and ligand C and N p orbitals.

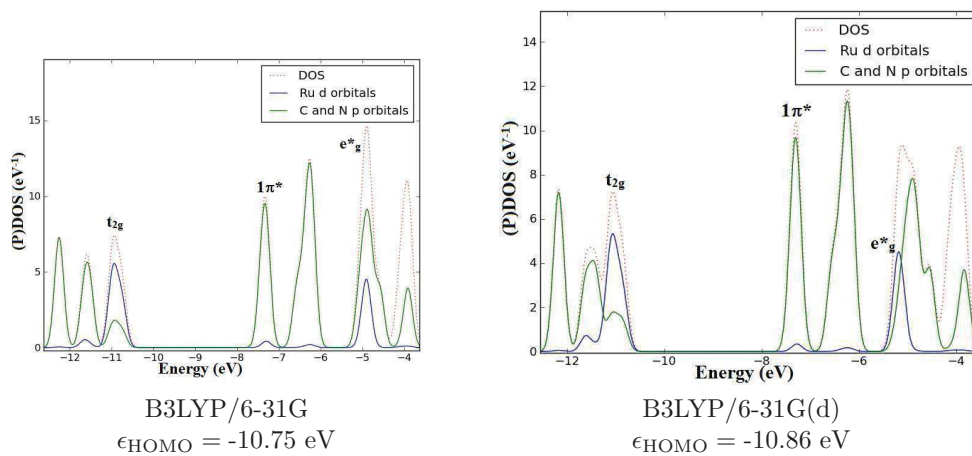
Absorption Spectrum



$[\text{Ru}(\text{bpy})_2(\text{PimH})]^{2+}$ TD-B3LYP/6-31G and TD-B3LYP/6-31G(d) spectra.

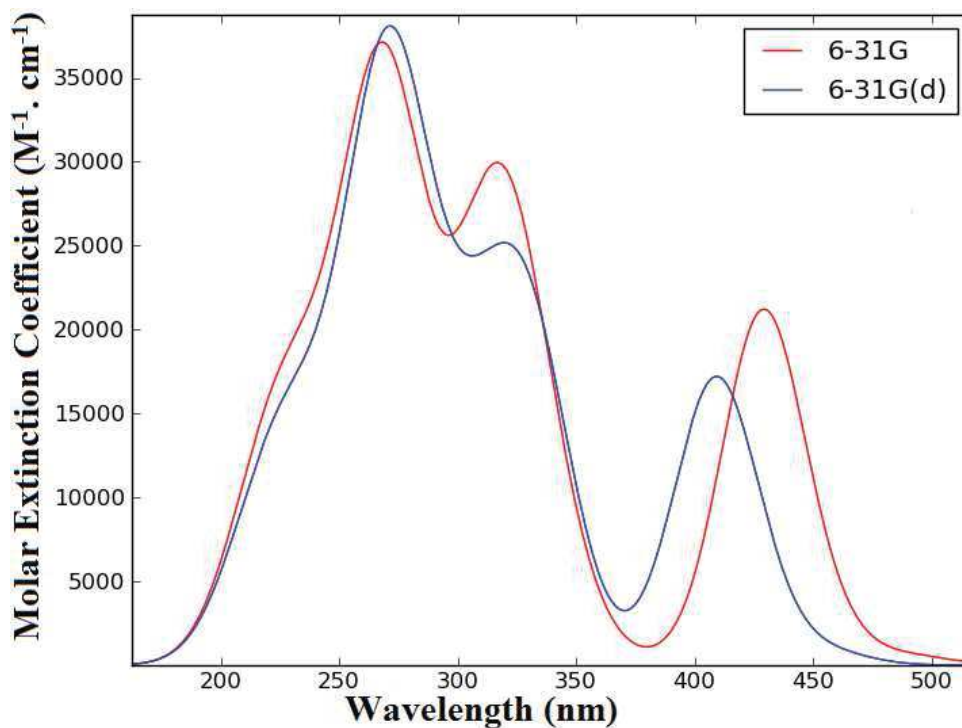
29. Complex (30): $[\text{Ru}(\text{bpy})_2(\text{PBzimH})]^{2+}$

PDOS



Total and partial density of states of $[\text{Ru}(\text{bpy})_2(\text{PBzimH})]^{2+}$ partitioned over Ru d orbitals and ligand C and N p orbitals.

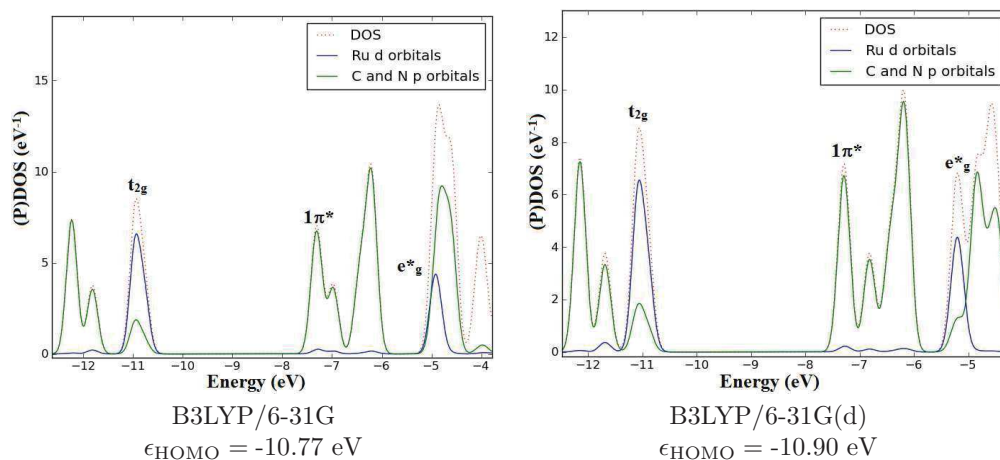
Absorption Spectrum



$[\text{Ru}(\text{bpy})_2(\text{PBzimH})]^{2+}$ TD-B3LYP/6-31G and TD-B3LYP/6-31G(d) spectra.

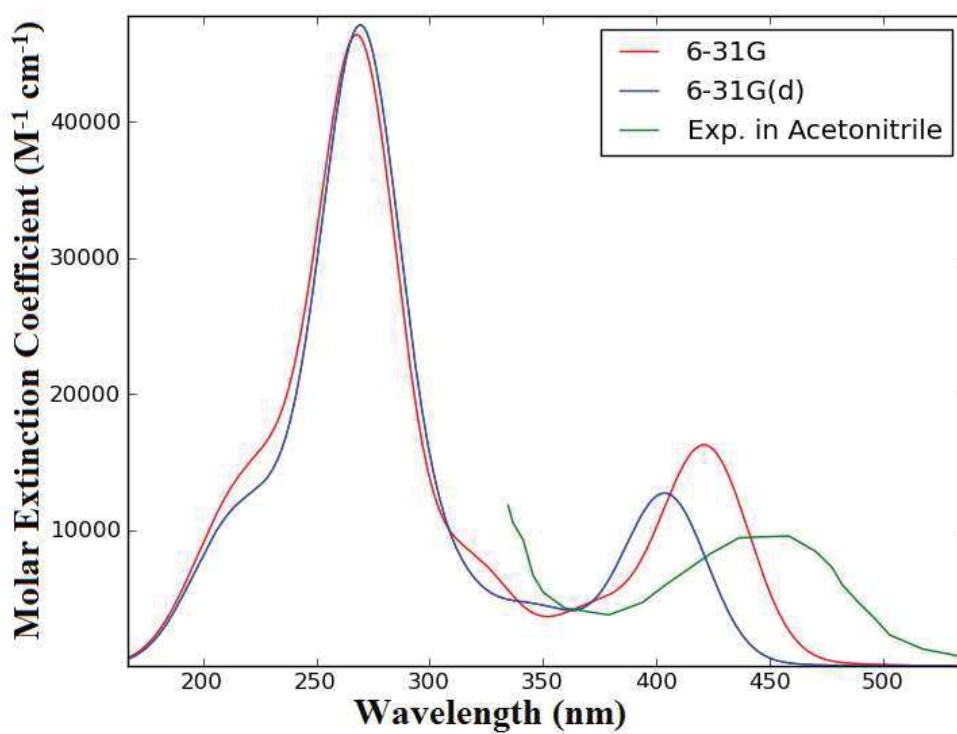
30. Complex (31): $[\text{Ru}(\text{bpy})_2(\text{biimH}_2)]^{2+}$

PDOS



Total and partial density of states of $[\text{Ru}(\text{bpy})_2(\text{biimH}_2)]^{2+}$ partitioned over Ru d orbitals and ligand C and N p orbitals.

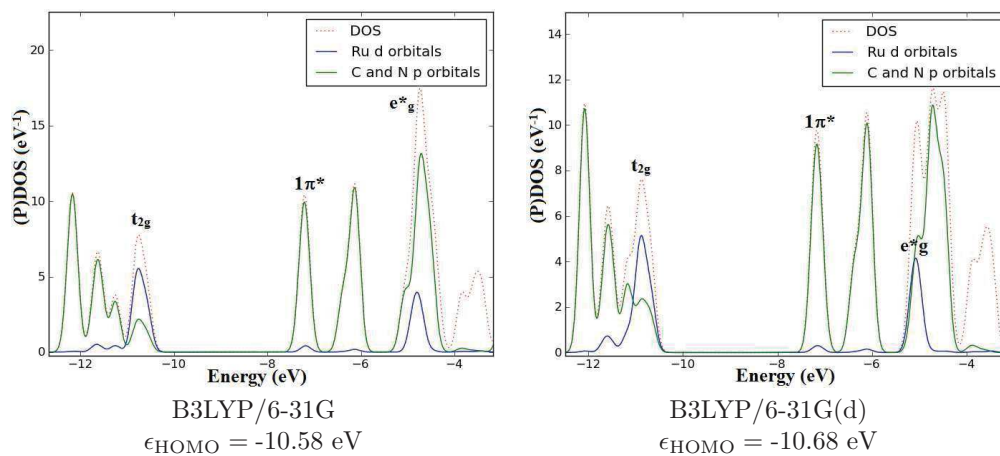
Absorption Spectrum



$[\text{Ru}(\text{bpy})_2(\text{biimH}_2)]^{2+}$ TD-B3LYP/6-31G and TD-B3LYP/6-31G(d) spectra.

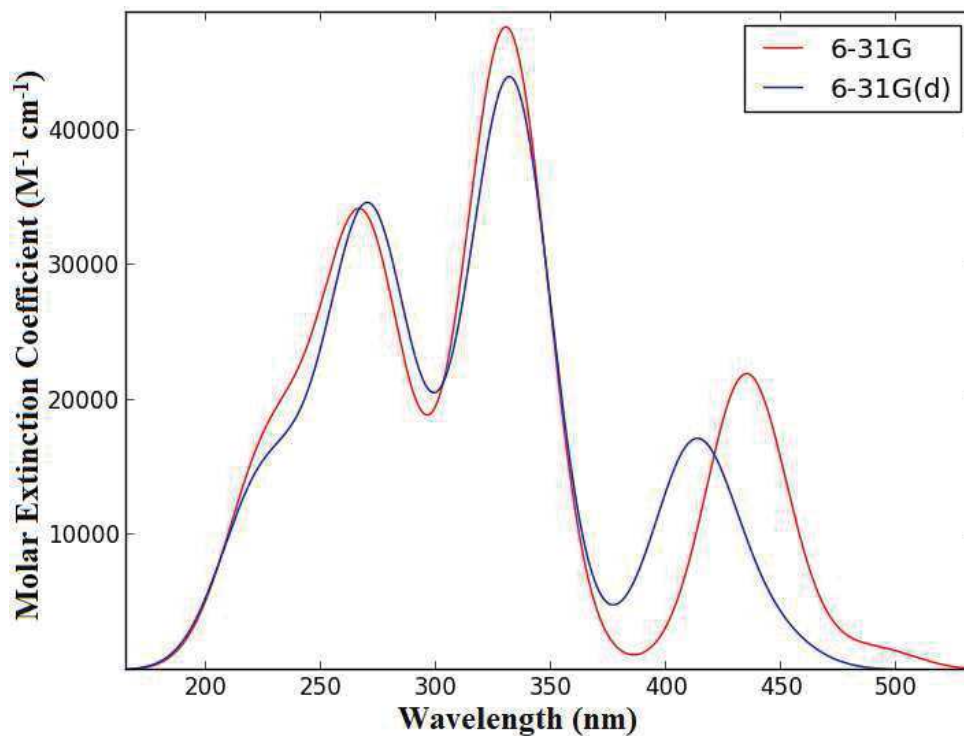
31. Complex (32): $[\text{Ru}(\text{bpy})_2(\text{BiBzimH}_2)]^{2+}$

PDOS



Total and partial density of states of $[\text{Ru}(\text{bpy})_2(\text{BiBzimH}_2)]^{2+}$ partitioned over Ru d orbitals and ligand C and N p orbitals.

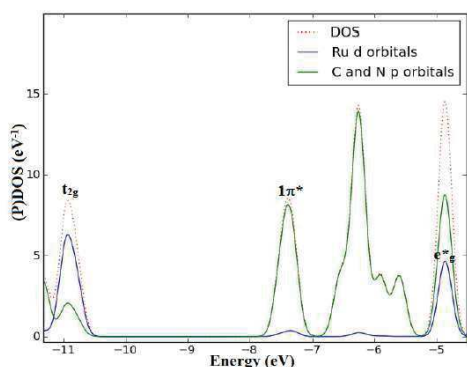
Absorption Spectrum



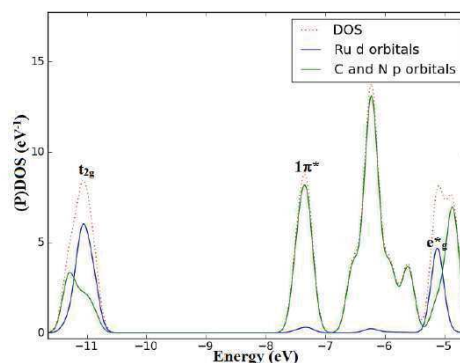
$[\text{Ru}(\text{bpy})_2(\text{BiBzimH}_2)]^{2+}$ TD-B3LYP/6-31G, TD-B3LYP/6-31G(d), and experimental spectra. Experimental curve measured at room temperature in acetonitrile[9].

32. Complex (34): $[\text{Ru}(\text{bpy})_2(\text{piq})]^{2+}$

PDOS



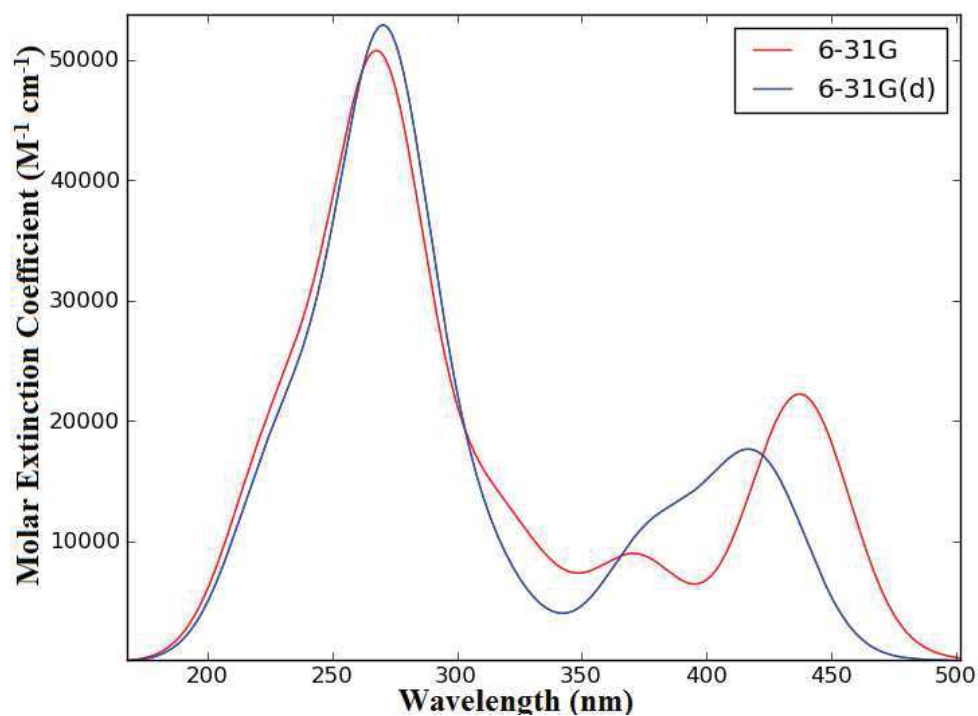
B3LYP/6-31G
 $\epsilon_{\text{HOMO}} = -10.79 \text{ eV}$



B3LYP/6-31G(d)
 $\epsilon_{\text{HOMO}} = -10.89 \text{ eV}$

Total and partial density of states of $[\text{Ru}(\text{bpy})_2(\text{piq})]^{2+}$ partitioned over Ru d orbitals and ligand C and N p orbitals.

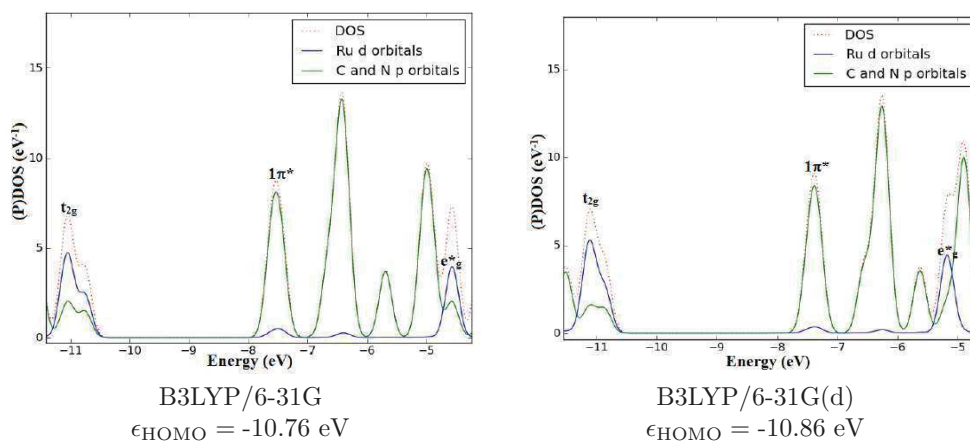
Absorption Spectrum



$[\text{Ru}(\text{bpy})_2(\text{piq})]^{2+}$ TD-B3LYP/6-31G and TD-B3LYP/6-31G(d) spectra.

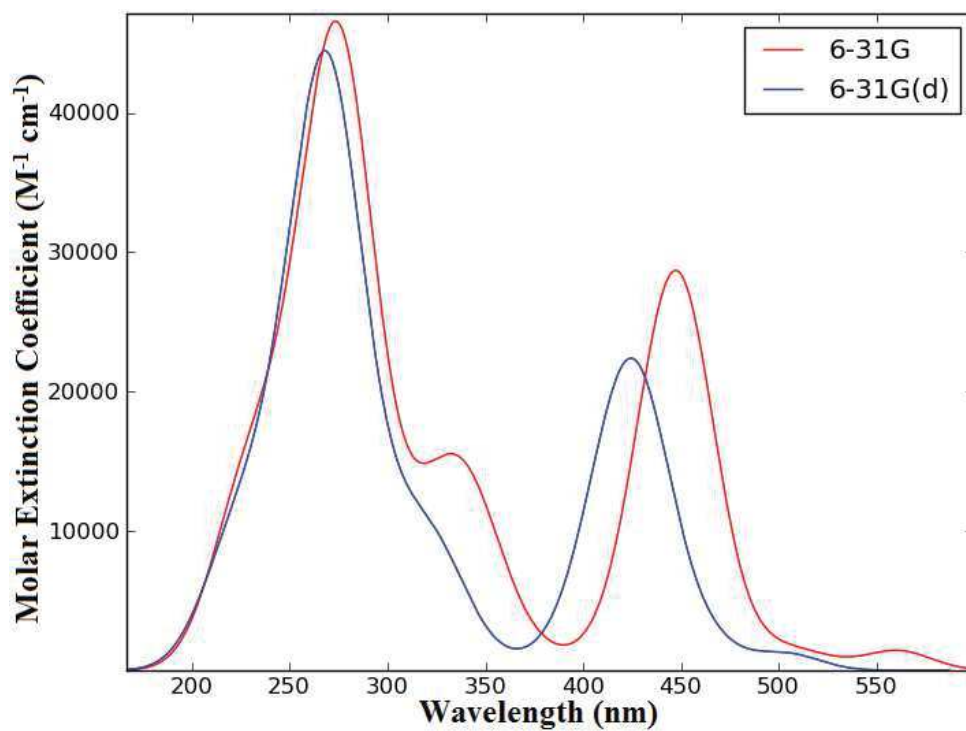
33. Complex (35): $[\text{Ru}(\text{bpy})_2(\text{hpiq})]^{2+}$

PDOS



Total and partial density of states of $[\text{Ru}(\text{bpy})_2(\text{hpiq})]^{2+}$ partitioned over Ru d orbitals and ligand C and N p orbitals.

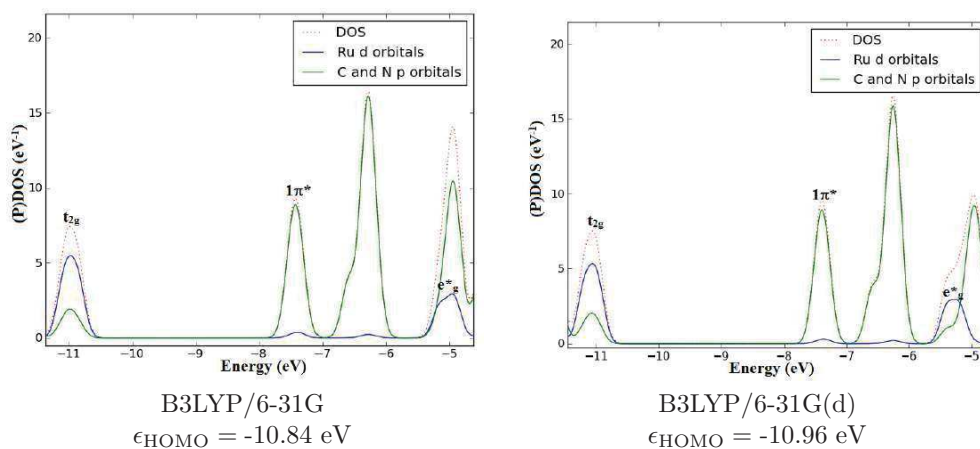
Absorption Spectrum



$[\text{Ru}(\text{bpy})_2(\text{hpiq})]^{2+}$ TD-B3LYP/6-31G and TD-B3LYP/6-31G(d) spectra.

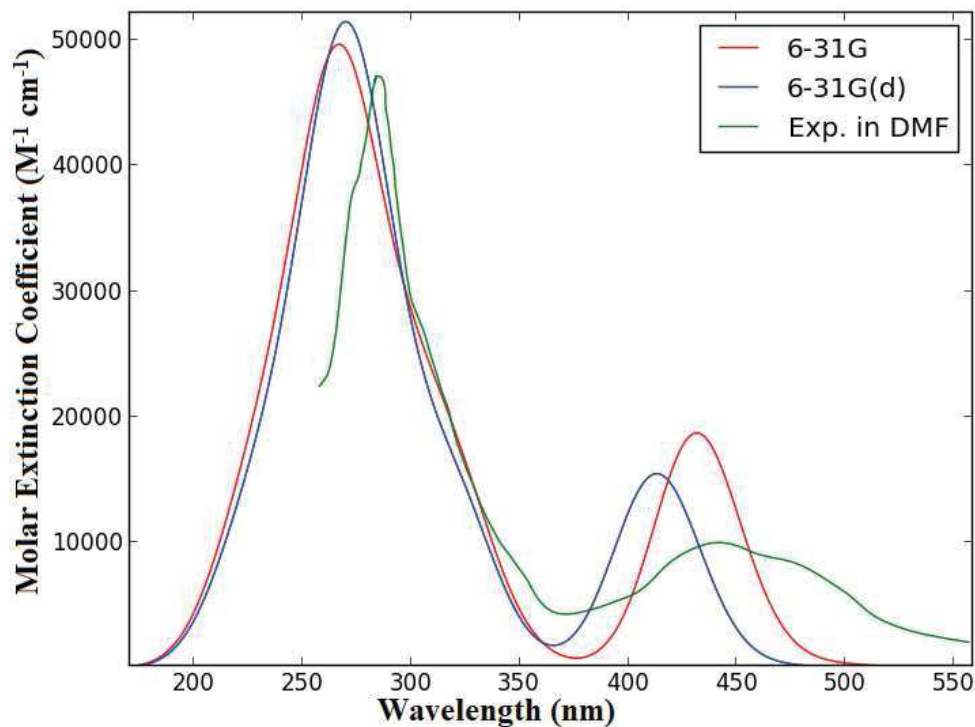
34. Complex (36): $[\text{Ru}(\text{bpy})_2(\text{pq})]^{2+}$

PDOS



Total and partial density of states of $[\text{Ru}(\text{bpy})_2(\text{pq})]^{2+}$ partitioned over Ru d orbitals and ligand C and N p orbitals.

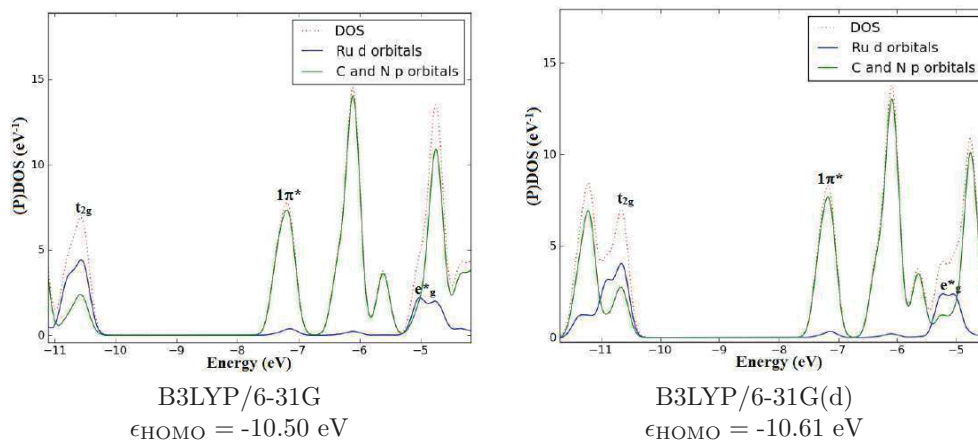
Absorption Spectrum



$[\text{Ru}(\text{bpy})_2(\text{pq})]^{2+}$ TD-B3LYP/6-31G, TD-B3LYP/6-31G(d), and experimental spectra. Experimental curve measured in DMF [10].

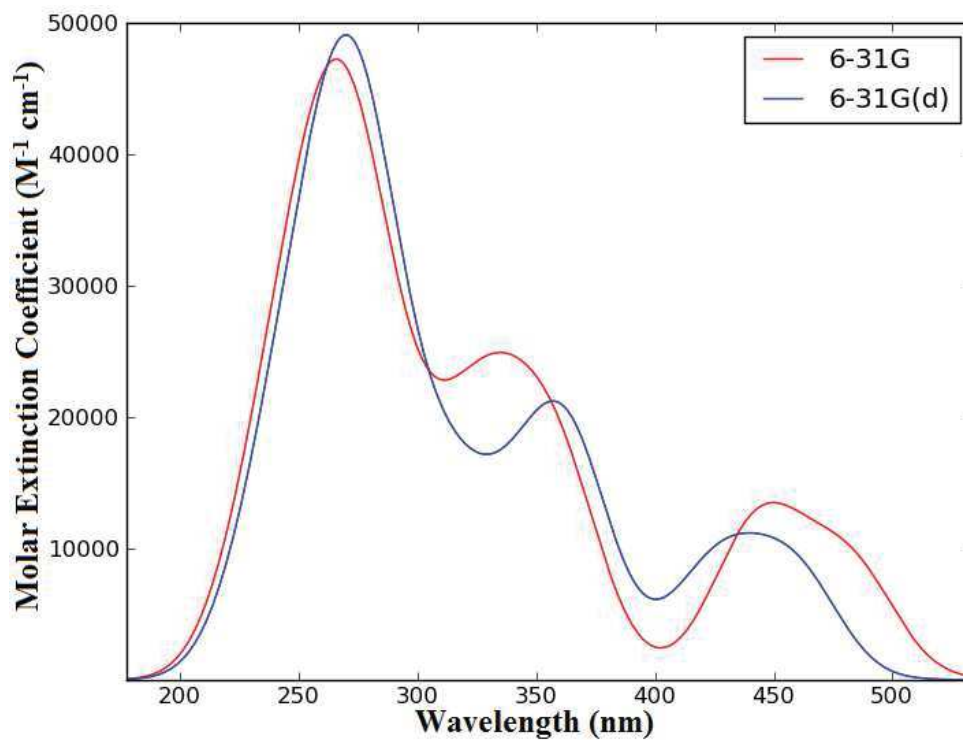
35. Complex (37): $[\text{Ru}(\text{bpy})_2(\text{DMCH})]^{2+}$

PDOS



Total and partial density of states of $[\text{Ru}(\text{bpy})_2(\text{DMCH})]^{2+}$ partitioned over Ru d orbitals and ligand C and N p orbitals.

Absorption Spectrum

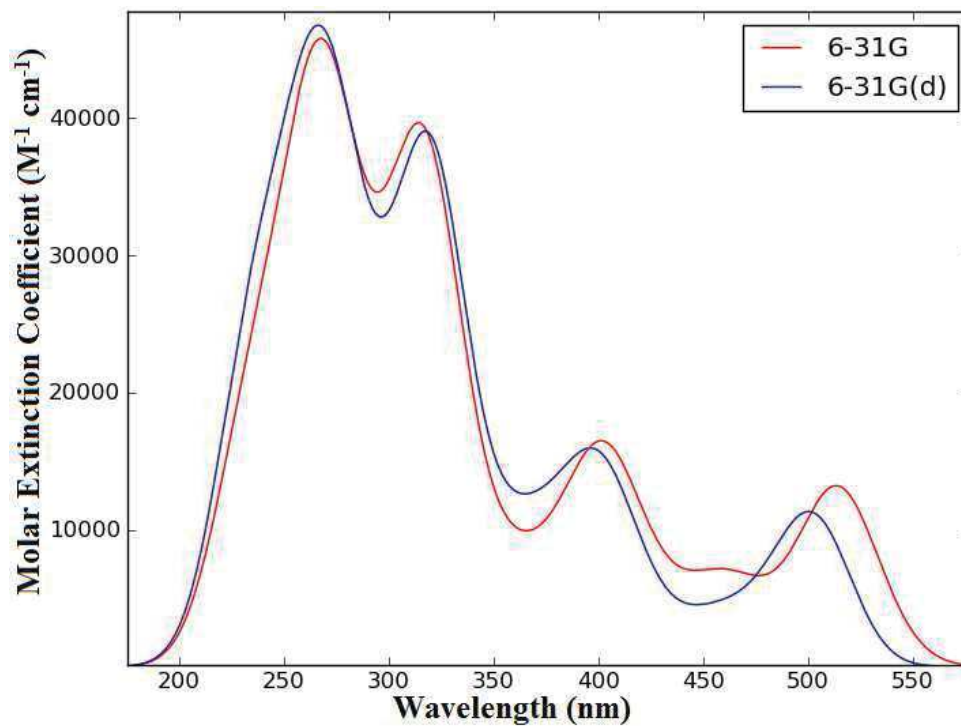


$[\text{Ru}(\text{bpy})_2(\text{DMCH})]^{2+}$ TD-B3LYP/6-31G and TD-B3LYP/6-31G(d) spectra.

36. Complex (38)[†]: [Ru(bpy)₂(OMCH)]²⁺

B3LYP/6-31G B3LYP/6-31G(d)
 $\epsilon_{\text{HOMO}} = -10.35 \text{ eV}$ $\epsilon_{\text{HOMO}} = -10.39 \text{ eV}$

Absorption Spectrum

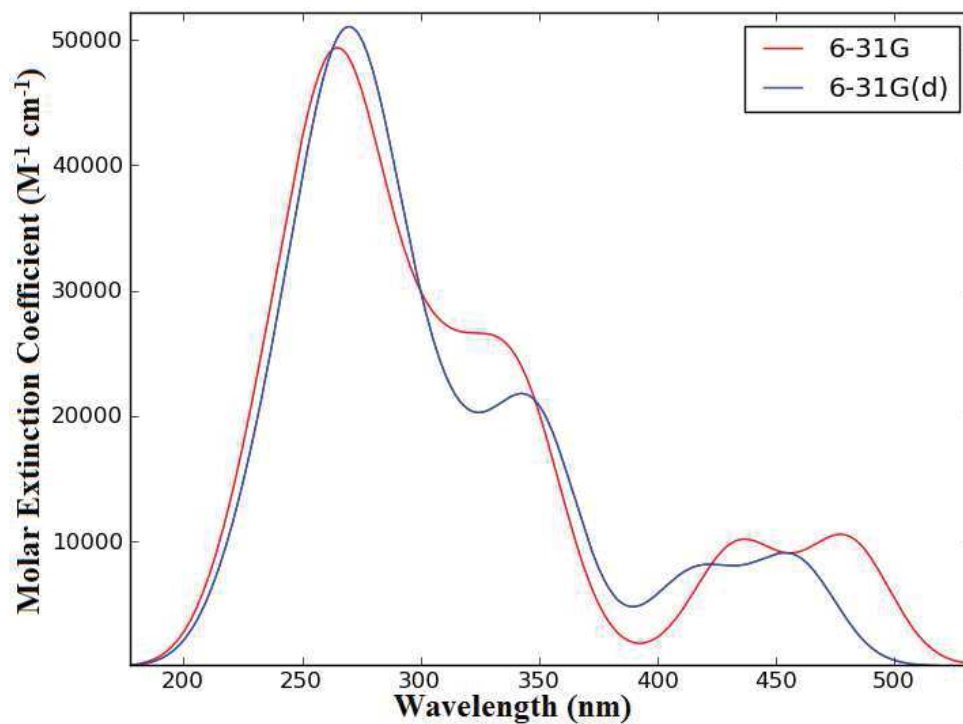


[Ru(bpy)₂(OMCH)]²⁺ TD-B3LYP/6-31G and TD-B3LYP/6-31G(d) spectra.

37. Complex (39)[†]: [Ru(bpy)₂(biq)]²⁺

Absorption Spectrum

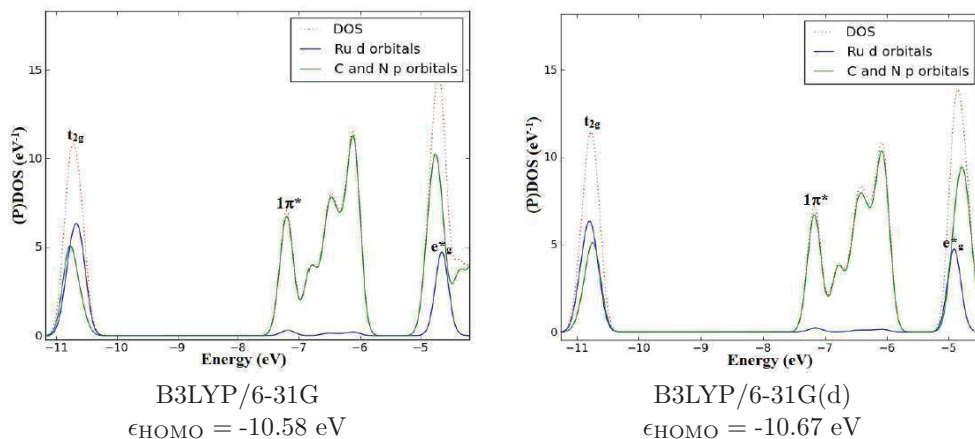
B3LYP/6-31G B3LYP/6-31G(d)
 $\epsilon_{\text{HOMO}} = -10.72 \text{ eV}$ $\epsilon_{\text{HOMO}} = -10.82 \text{ eV}$



[Ru(bpy)₂(biq)]²⁺ TD-B3LYP/6-31G and TD-B3LYP/6-31G(d) spectra.

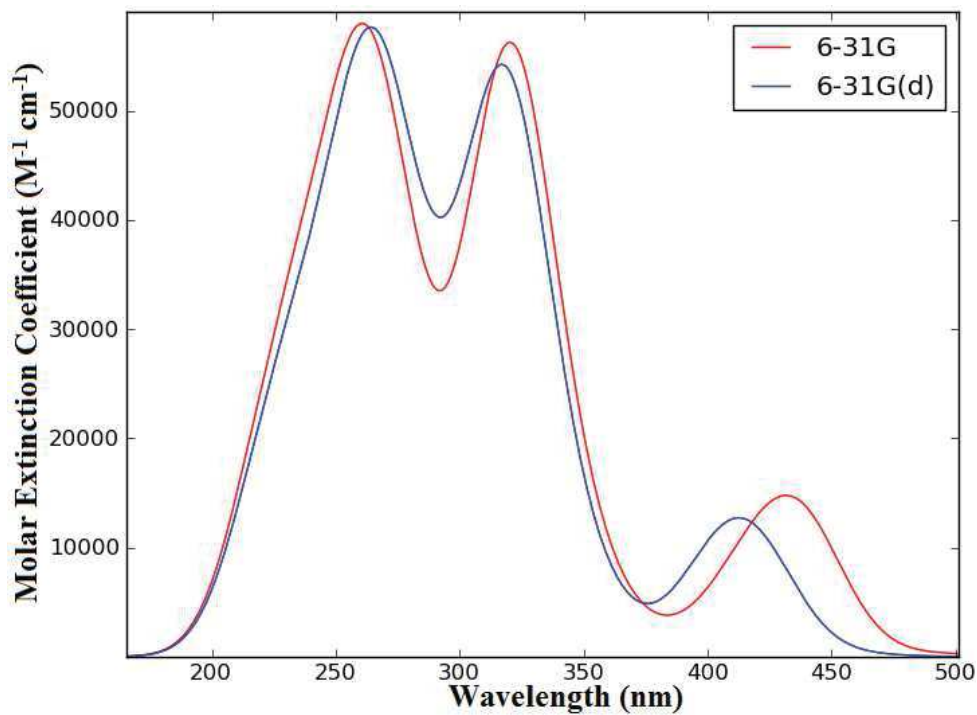
38. Complex (40): $[\text{Ru}(\text{bpy})_2(\text{i-biq})]^{2+}$

PDOS



Total and partial density of states of $[\text{Ru}(\text{bpy})_2(\text{i-biq})]^{2+}$ partitioned over Ru d orbitals and ligand C and N p orbitals.

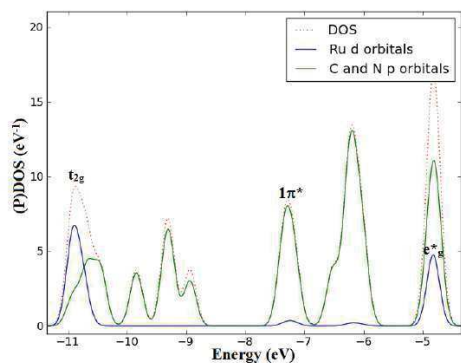
Absorption Spectrum



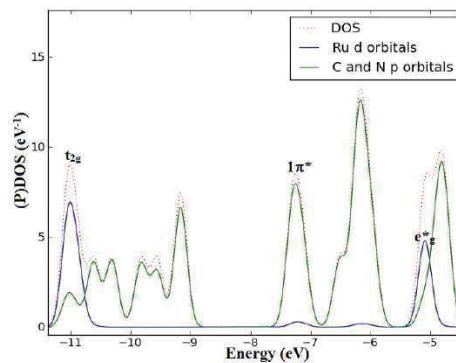
$[\text{Ru}(\text{bpy})_2(\text{i-biq})]^{2+}$ TD-B3LYP/6-31G and TD-B3LYP/6-31G(d) spectra.

39. Complex (41): $[\text{Ru}(\text{bpy})_2(\text{BL4})]^{2+}$

PDOS



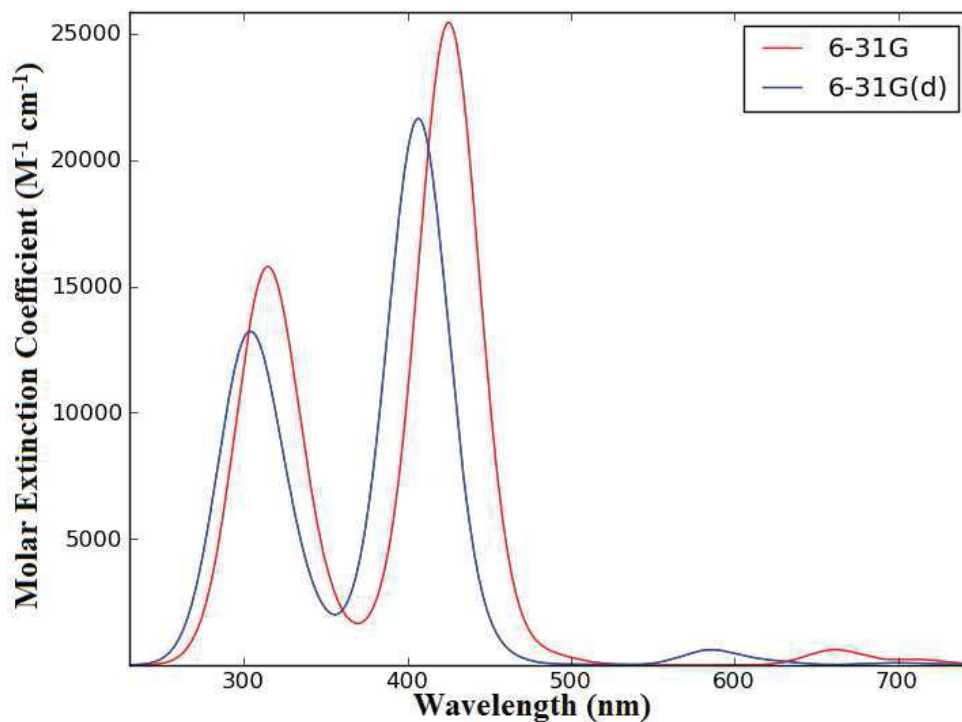
B3LYP/6-31G
 $\epsilon_{\text{HOMO}} = -8.94 \text{ eV}$



B3LYP/6-31G(d)
 $\epsilon_{\text{HOMO}} = -9.15 \text{ eV}$

Total and partial density of states of $[\text{Ru}(\text{bpy})_2(\text{BL4})]^{2+}$ partitioned over Ru d orbitals and ligand C and N p orbitals.

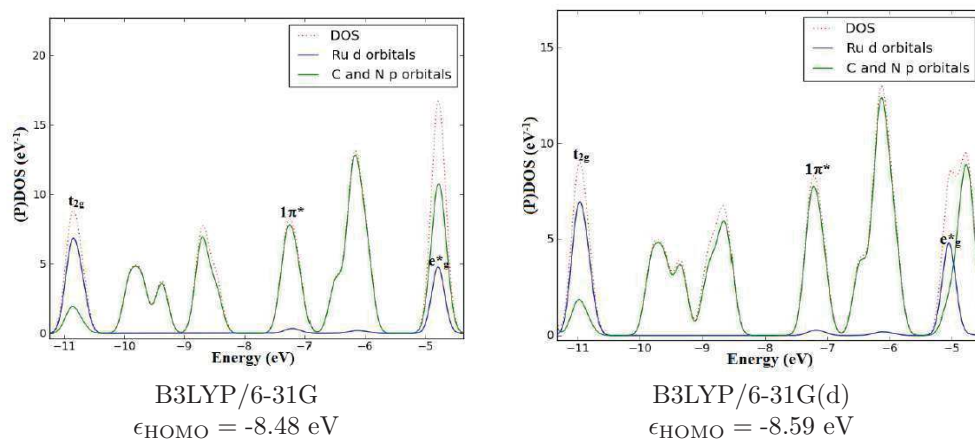
Absorption Spectrum



$[\text{Ru}(\text{bpy})_2(\text{BL4})]^{2+}$ TD-B3LYP/6-31G and TD-B3LYP/6-31G(d) spectra.

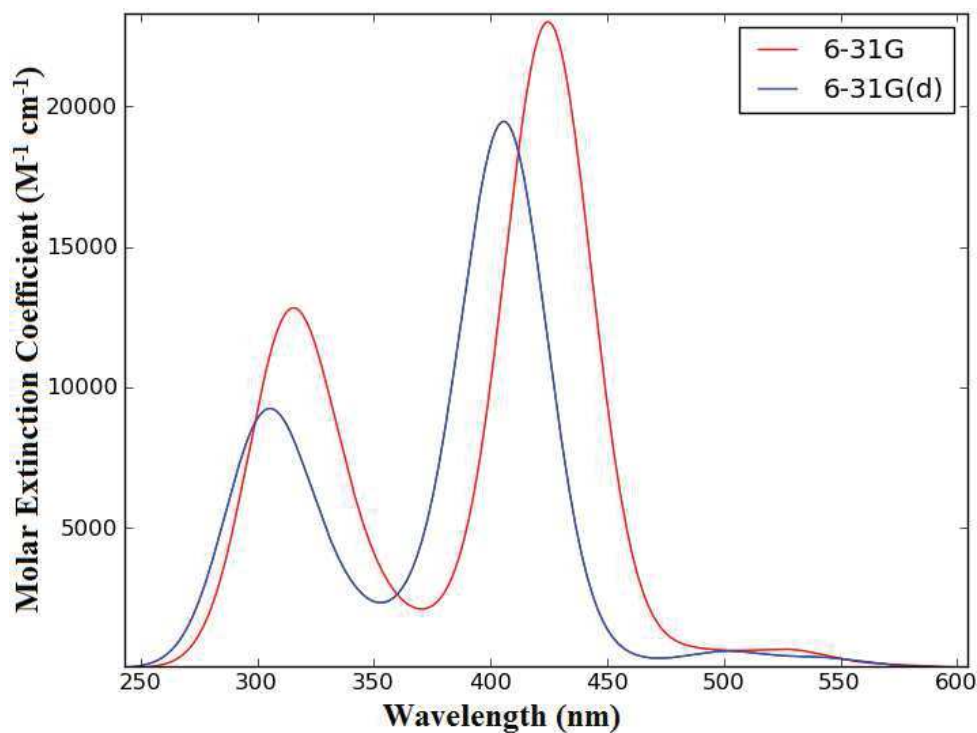
40. Complex (42): $[\text{Ru}(\text{bpy})_2(\text{BL5})]^{2+}$

PDOS



Total and partial density of states of $[\text{Ru}(\text{bpy})_2(\text{BL5})]^{2+}$ partitioned over Ru d orbitals and ligand C and N p orbitals.

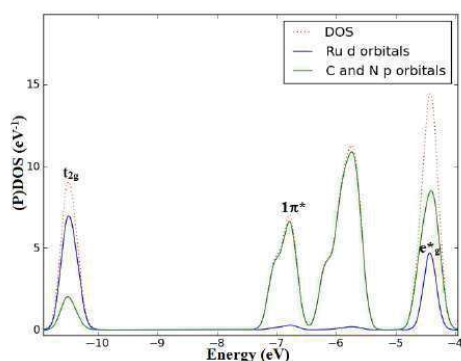
Absorption Spectrum



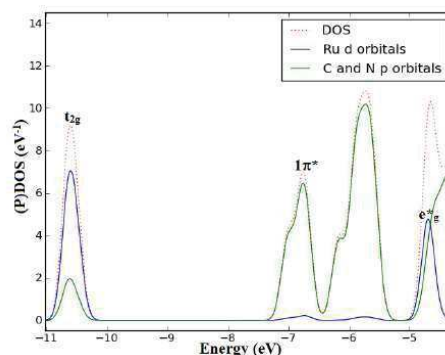
$[\text{Ru}(\text{bpy})_2(\text{BL5})]^{2+}$ TD-B3LYP/6-31G and TD-B3LYP/6-31G(d) spectra.

41. Complex (46): $[\text{Ru}(\text{bpy})(4,4'\text{-DTB-bpy})_2]^{2+}$

PDOS



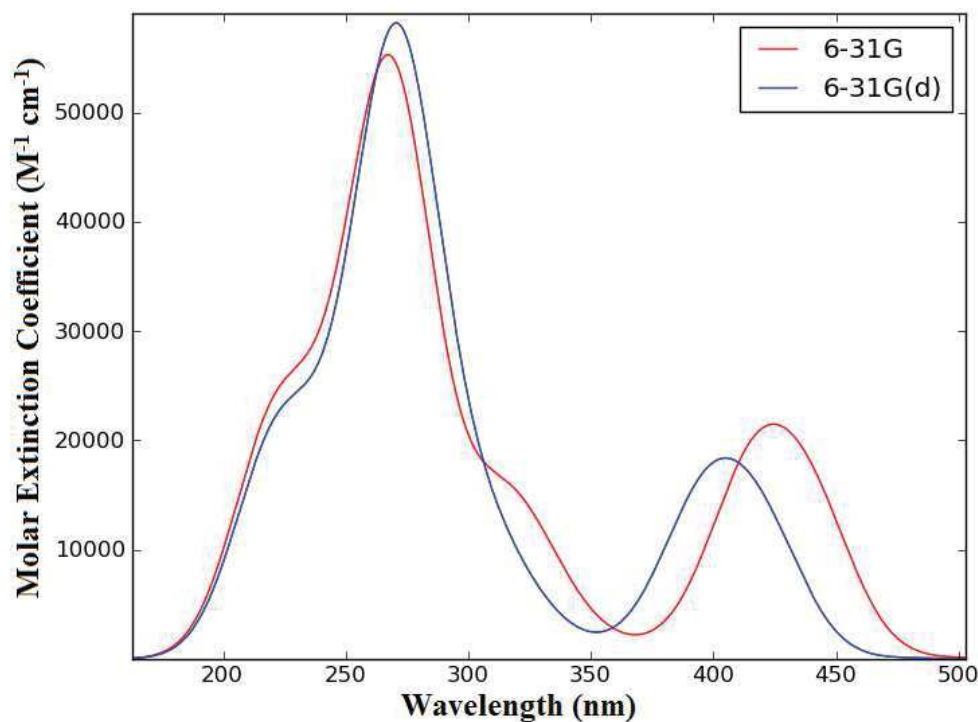
B3LYP/6-31G
 $\epsilon_{\text{HOMO}} = -10.36 \text{ eV}$



B3LYP/6-31G(d)
 $\epsilon_{\text{HOMO}} = -10.49 \text{ eV}$

Total and partial density of states of $[\text{Ru}(\text{bpy})(4,4'\text{-DTB-bpy})_2]^{2+}$ partitioned over Ru d orbitals and ligand C and N p orbitals.

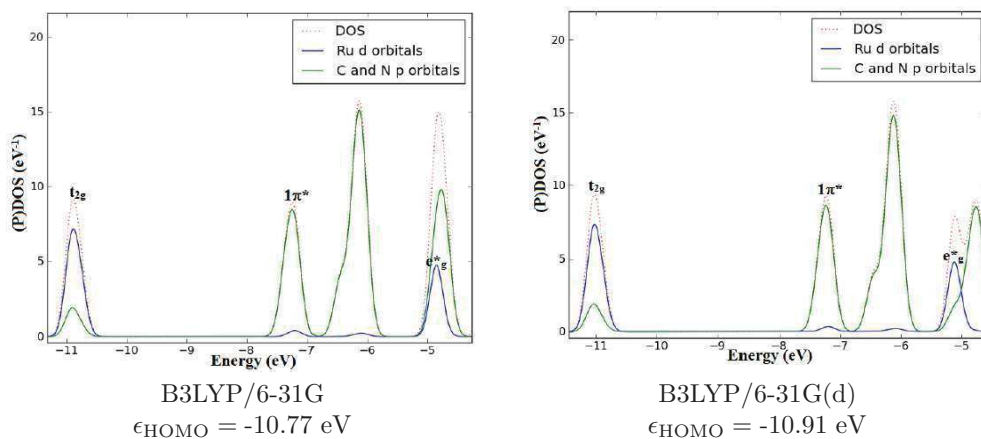
Absorption Spectrum



$[\text{Ru}(\text{bpy})(4,4'\text{-DTB-bpy})_2]^{2+}$ TD-B3LYP/6-31G and TD-B3LYP/6-31G(d) spectra.

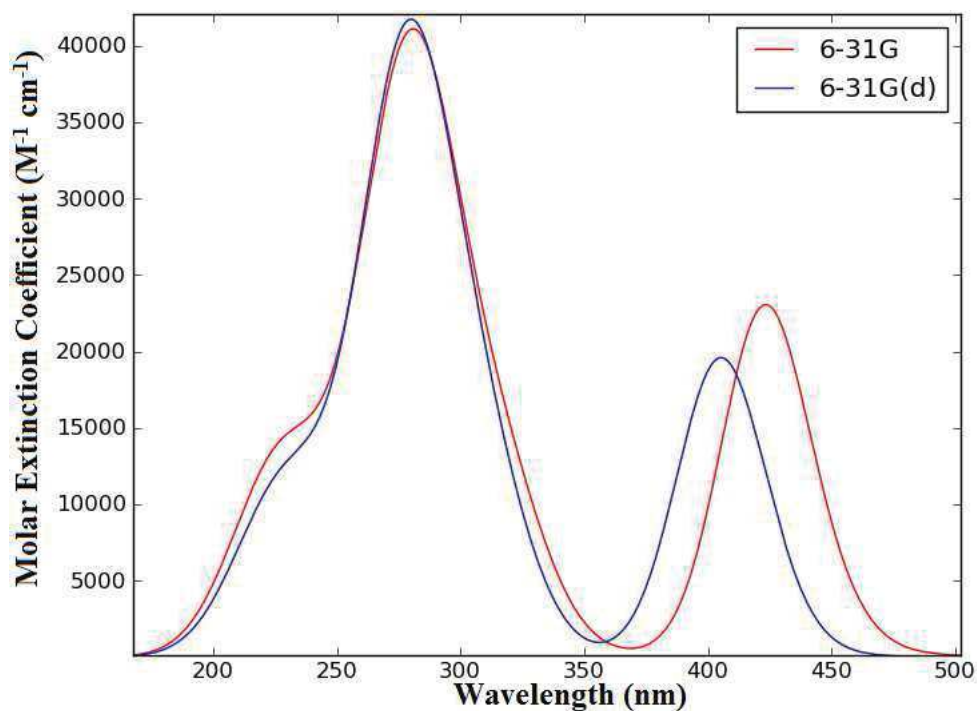
42. Complex (47): $[\text{Ru}(\text{bpy})(\text{h-phen})]^{2+}$

PDOS



Total and partial density of states of $[\text{Ru}(\text{bpy})(\text{h-phen})]^{2+}$ partitioned over Ru d orbitals and ligand C and N p orbitals.

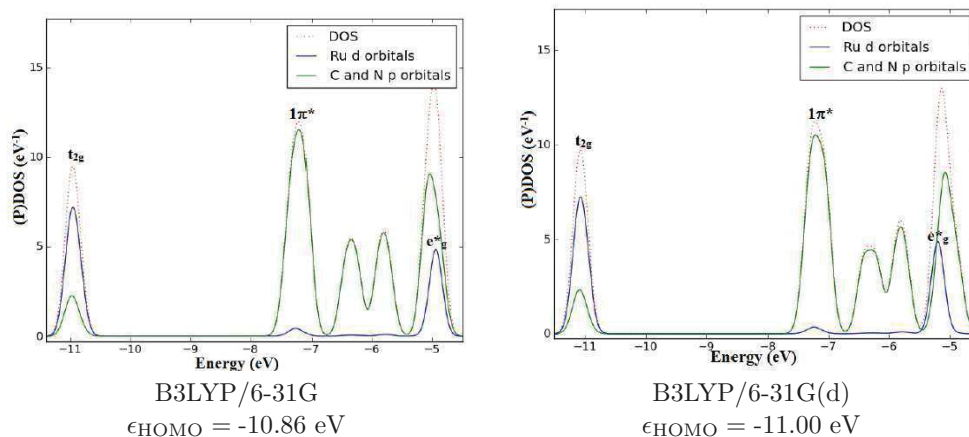
Absorption Spectrum



$[\text{Ru}(\text{bpy})(\text{h-phen})]^{2+}$ TD-B3LYP/6-31G and TD-B3LYP/6-31G(d) spectra.

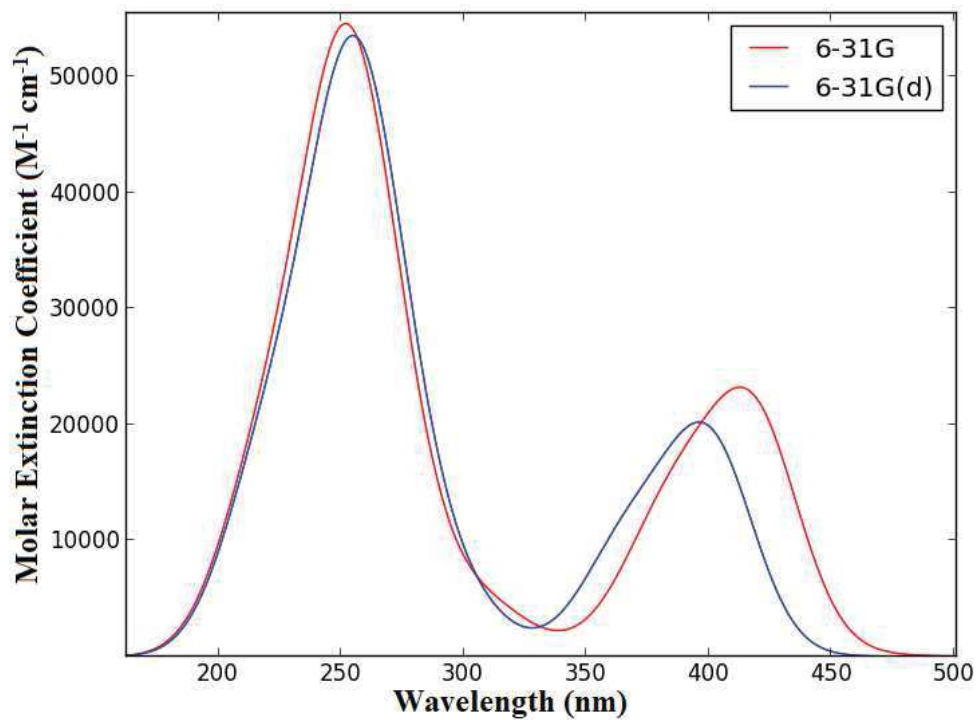
43. Complex (48): $[\text{Ru}(\text{bpy})(\text{phen})_2]^{2+}$

PDOS



Total and partial density of states of $[\text{Ru}(\text{bpy})(\text{phen})_2]^{2+}$ partitioned over Ru d orbitals and ligand C and N p orbitals.

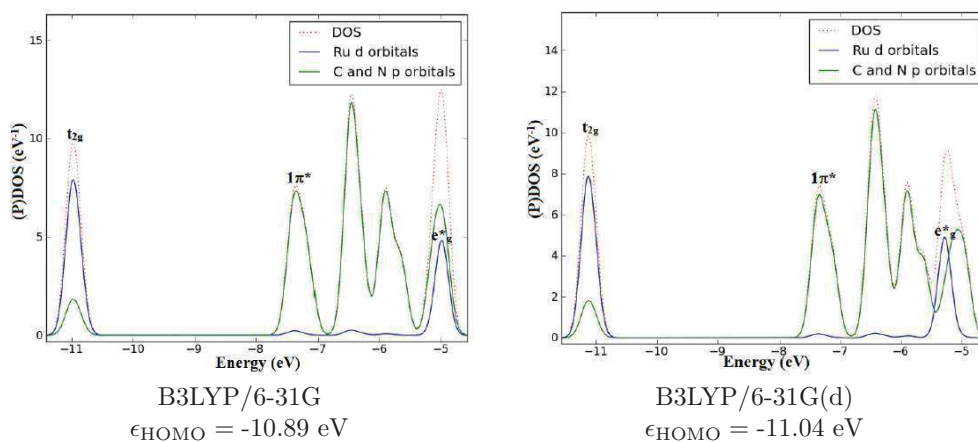
Absorption Spectrum



$[\text{Ru}(\text{bpy})(\text{phen})_2]^{2+}$ TD-B3LYP/6-31G and TD-B3LYP/6-31G(d) spectra.

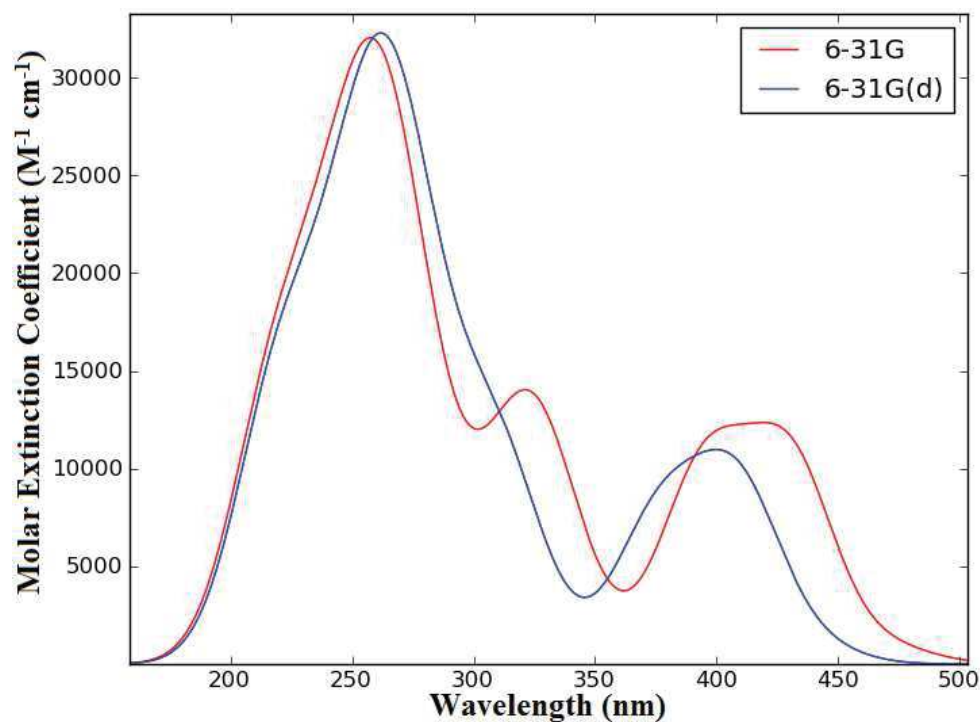
44. Complex (50): $trans\text{-}[\text{Ru}(\text{bpy})(\text{phen})(\text{py})_2]^{2+}$

PDOS



Total and partial density of states of $trans\text{-}[\text{Ru}(\text{bpy})(\text{phen})(\text{py})_2]^{2+}$ partitioned over Ru d orbitals and ligand C and N p orbitals.

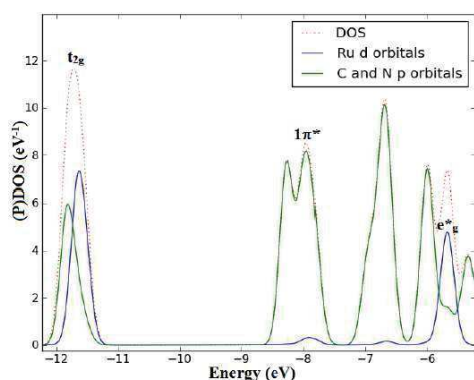
Absorption Spectrum



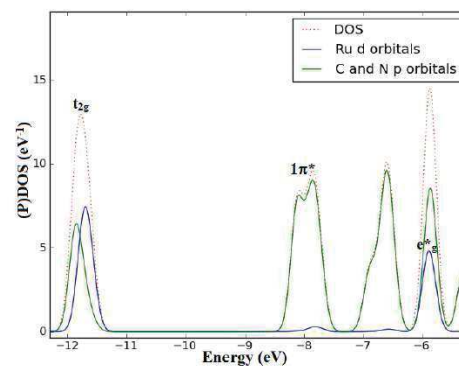
$Trans\text{-}[\text{Ru}(\text{bpy})(\text{phen})(\text{py})_2]^{2+}$ TD-B3LYP/6-31G and TD-B3LYP/6-31G(d) spectra.

45. Complex (52): $[\text{Ru}(\text{bpy})(\text{taphen})_2]^{2+}$

PDOS



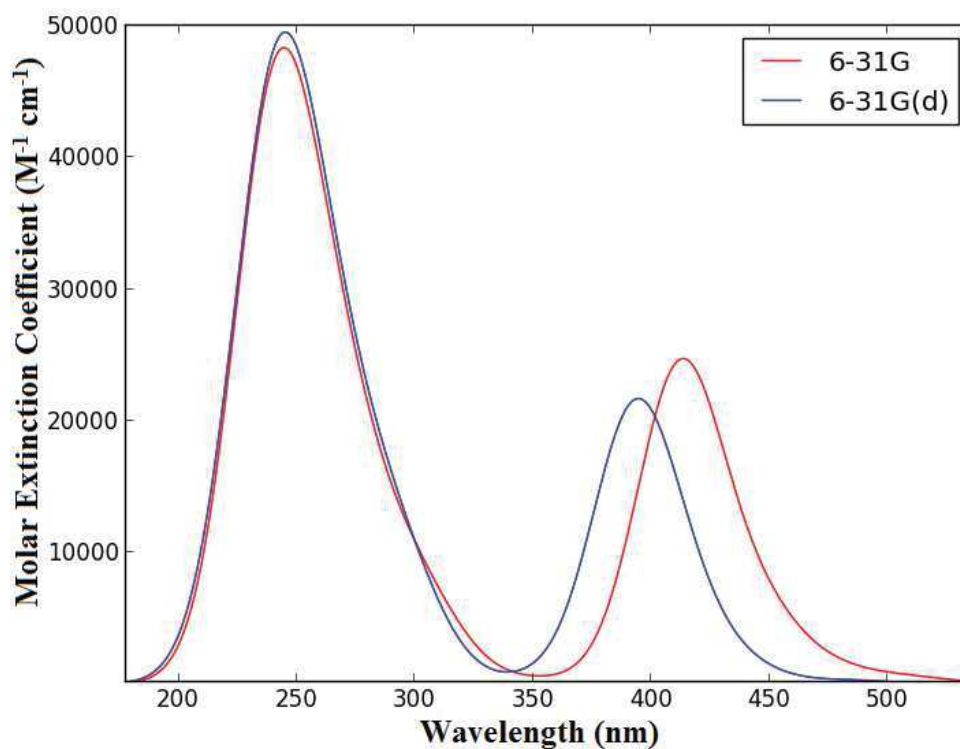
B3LYP/6-31G
 $\epsilon_{\text{HOMO}} = -11.53 \text{ eV}$



B3LYP/6-31G(d)
 $\epsilon_{\text{HOMO}} = -11.60 \text{ eV}$

Total and partial density of states of $[\text{Ru}(\text{bpy})(\text{taphen})_2]^{2+}$ partitioned over Ru d orbitals and ligand C and N p orbitals.

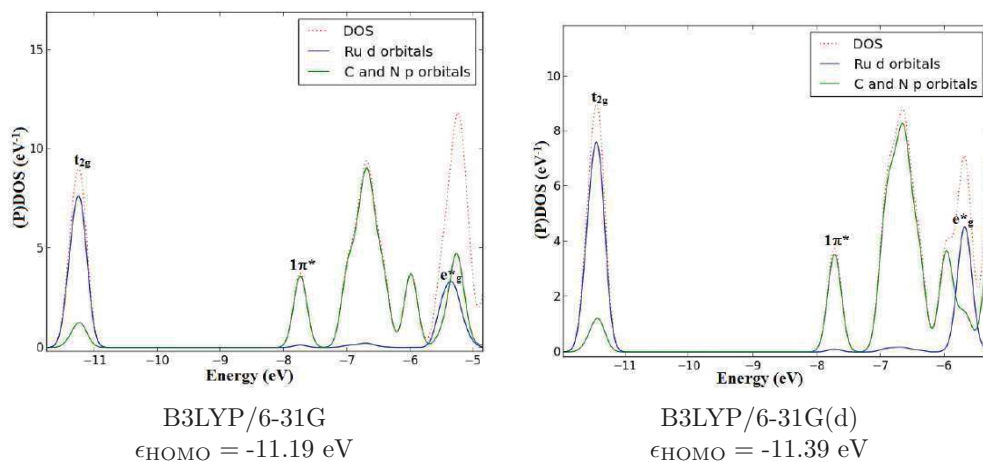
Absorption Spectrum



$[\text{Ru}(\text{bpy})(\text{taphen})_2]^{2+}$ TD-B3LYP/6-31G and TD-B3LYP/6-31G(d) spectra.

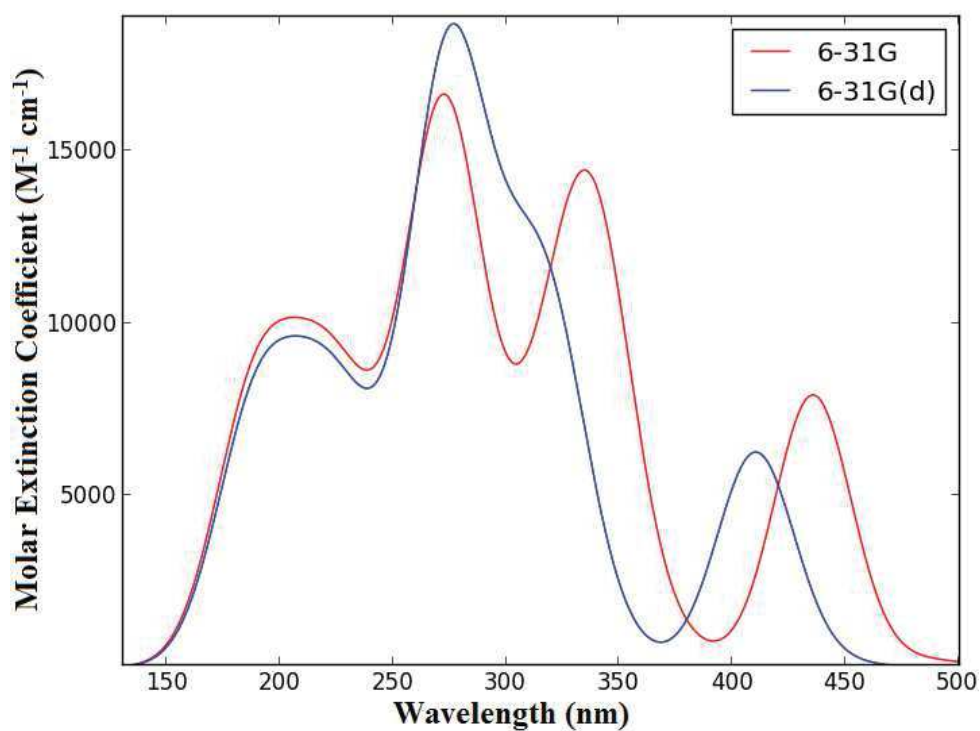
46. Complex (53): $[\text{Ru}(\text{bpy})(\text{py})_2(\text{en})]^{2+}$

PDOS



Total and partial density of states of $[\text{Ru}(\text{bpy})(\text{py})_2(\text{en})]^{2+}$ partitioned over Ru d orbitals and ligand C and N p orbitals.

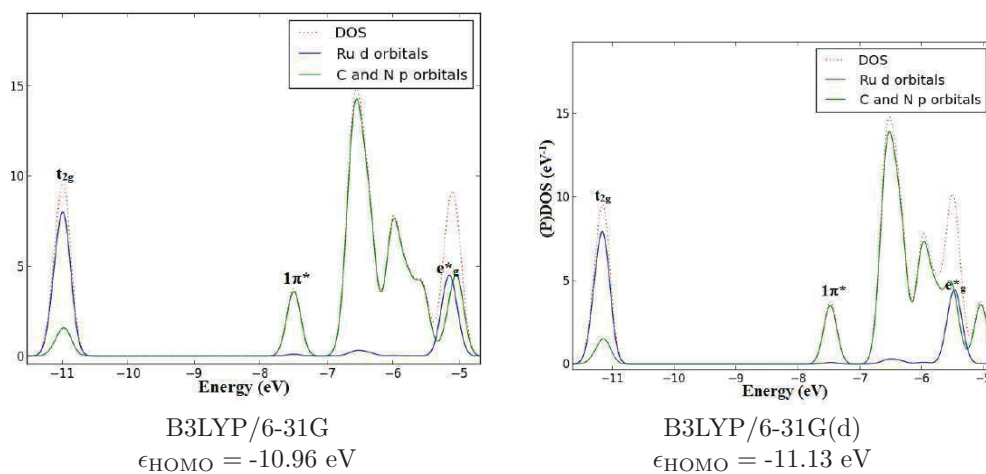
Absorption Spectrum



$[\text{Ru}(\text{bpy})(\text{py})_2(\text{en})]^{2+}$ TD-B3LYP/6-31G and TD-B3LYP/6-31G(d) spectra.

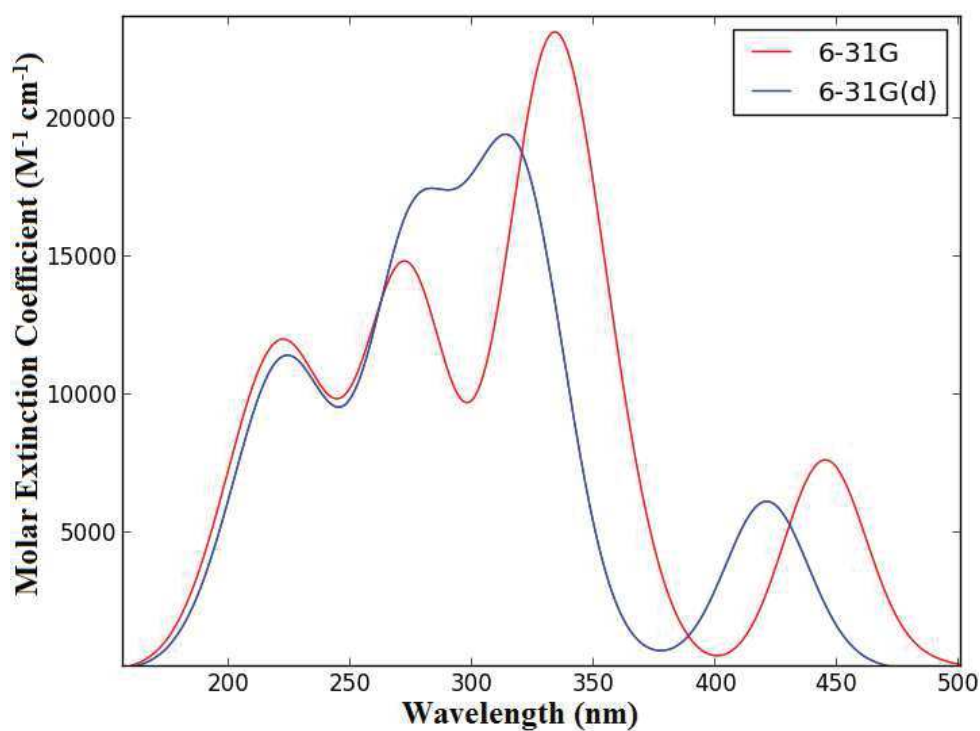
47. Complex (55): $[\text{Ru}(\text{bpy})(\text{py})_4]^{2+}$

PDOS



Total and partial density of states of $[\text{Ru}(\text{bpy})(\text{py})_4]^{2+}$ partitioned over Ru d orbitals and ligand C and N p orbitals.

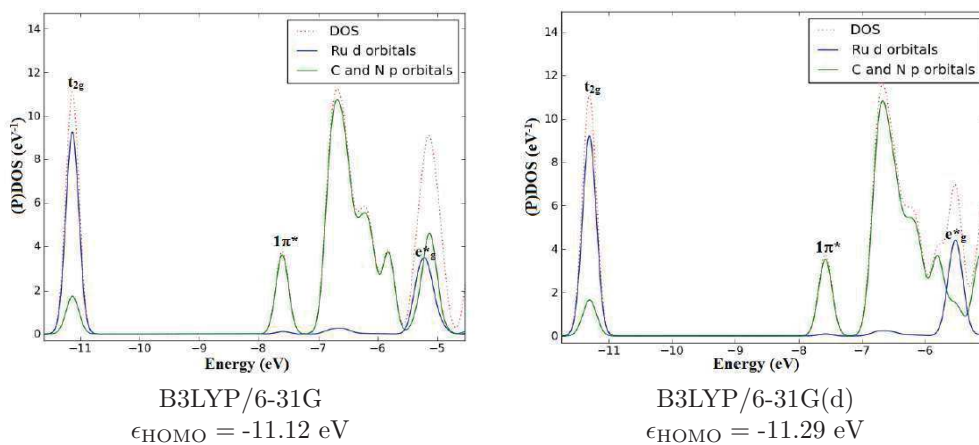
Absorption Spectrum



$[\text{Ru}(\text{bpy})(\text{py})_4]^{2+}$ TD-B3LYP/6-31G and TD-B3LYP/6-31G(d) spectra.

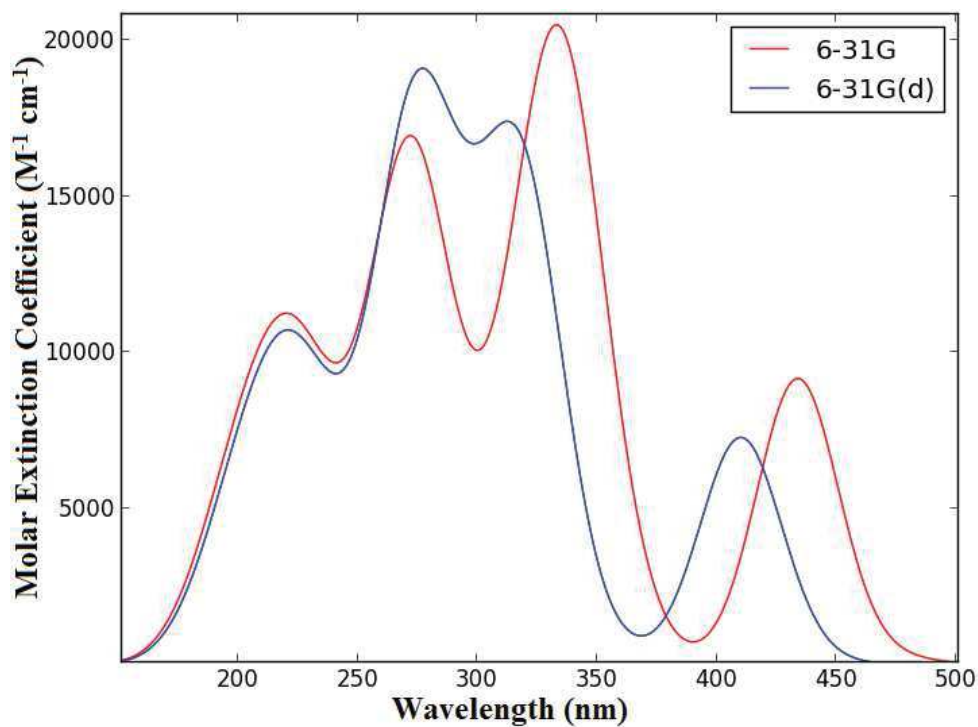
48. Complex (56): $[\text{Ru}(\text{bpy})(\text{py})_2(\text{PMA})]^{2+}$

PDOS



Total and partial density of states of $[\text{Ru}(\text{bpy})(\text{py})_2(\text{PMA})]^{2+}$ partitioned over Ru d orbitals and ligand C and N p orbitals.

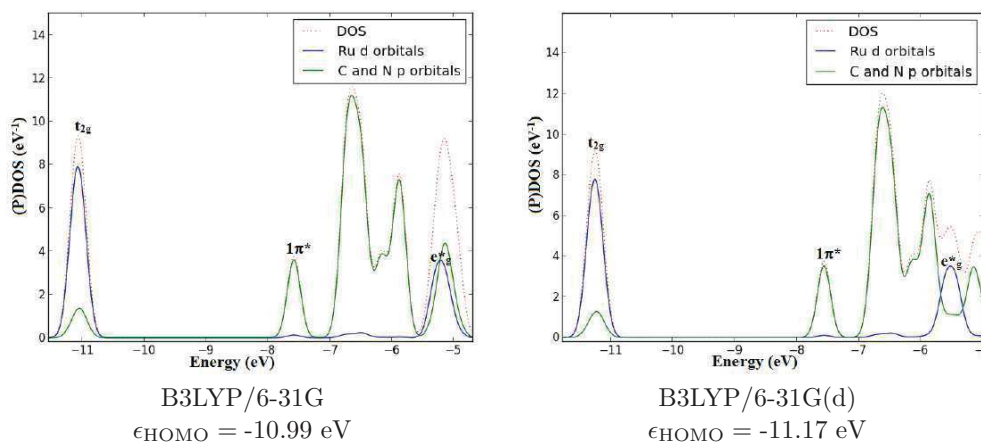
Absorption Spectrum



$[\text{Ru}(\text{bpy})(\text{py})_2(\text{PMA})]^{2+}$ TD-B3LYP/6-31G and TD-B3LYP/6-31G(d) spectra.

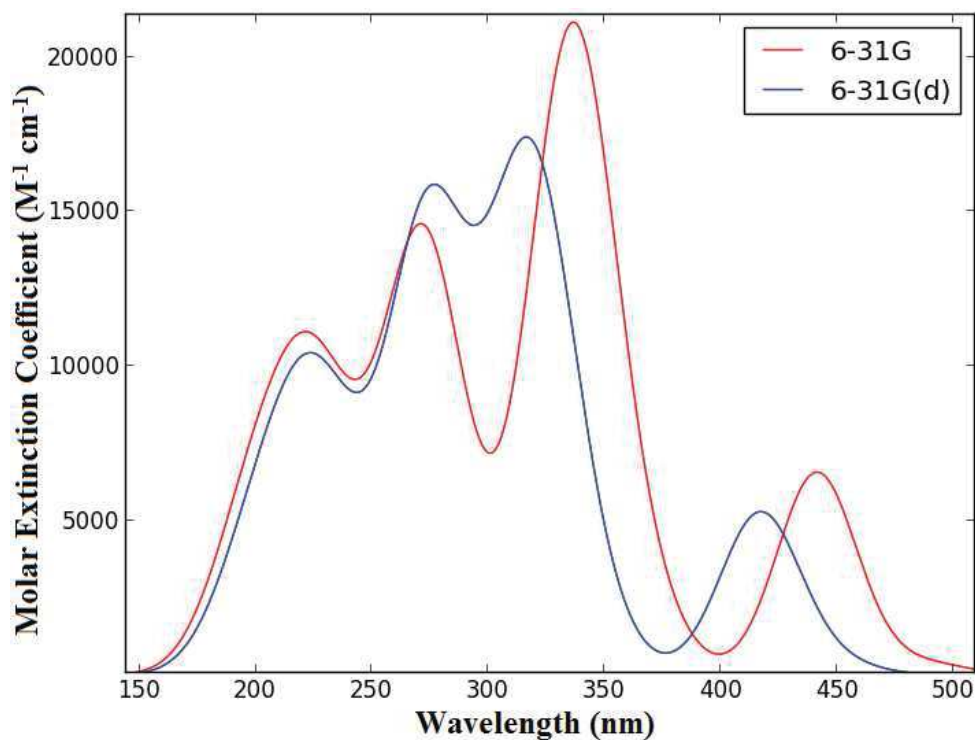
49. Complex (57): $[\text{Ru}(\text{bpy})(\text{py})_2(2\text{-AEP})]^{2+}$

PDOS



Total and partial density of states of $[\text{Ru}(\text{bpy})(\text{py})_2(2\text{-AEP})]^{2+}$ partitioned over Ru d orbitals and ligand C and N p orbitals.

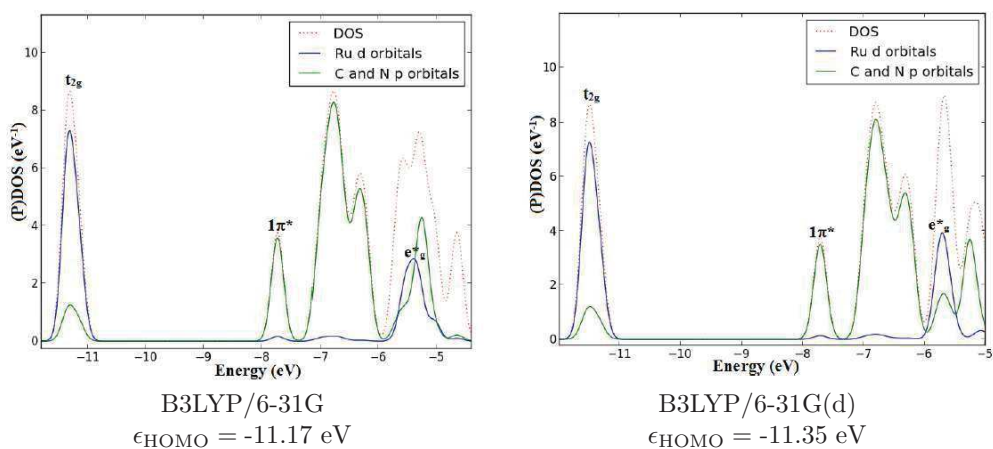
Absorption Spectrum



$[\text{Ru}(\text{bpy})(\text{py})_2(2\text{-AEP})]^{2+}$ TD-B3LYP/6-31G and TD-B3LYP/6-31G(d) spectra.

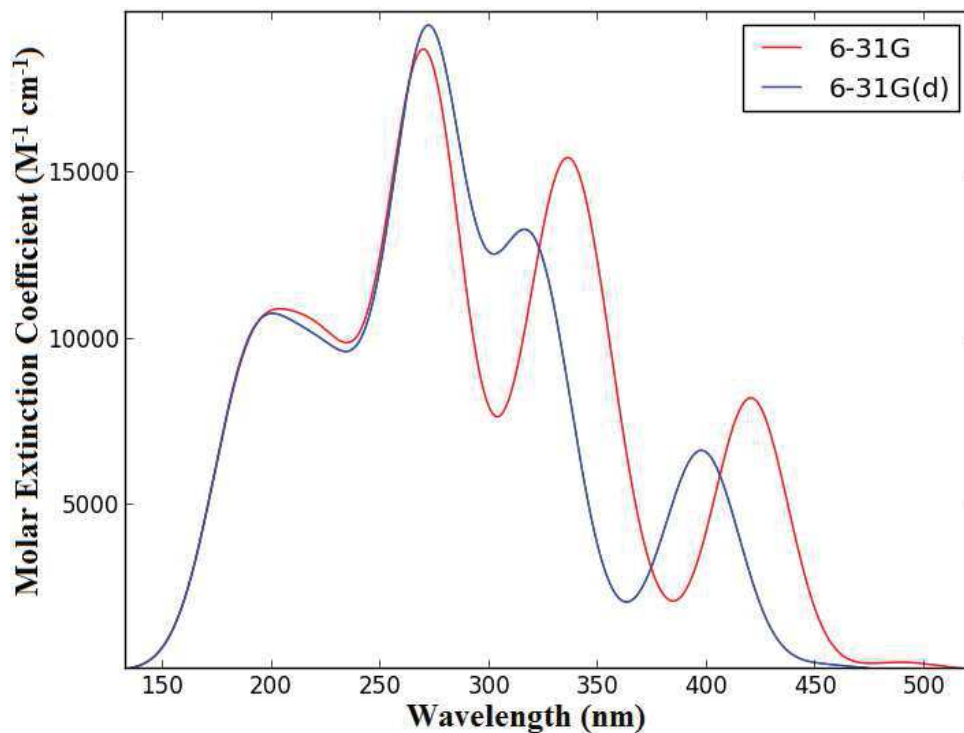
50. Complex (58): $[\text{Ru}(\text{bpy})(\text{PMA})_2]^{2+}$

PDOS



Total and partial density of states of $[\text{Ru}(\text{bpy})(\text{PMA})_2]^{2+}$ partitioned over Ru d orbitals and ligand C and N p orbitals.

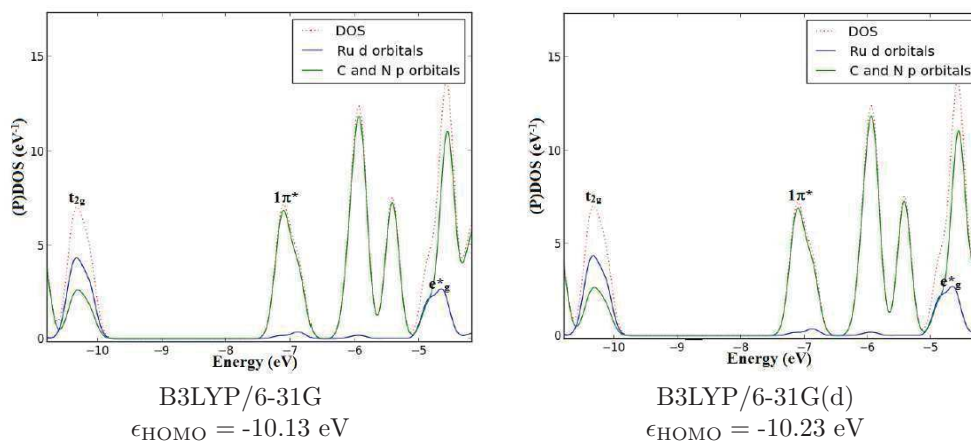
Absorption Spectrum



$[\text{Ru}(\text{bpy})(\text{PMA})_2]^{2+}$ TD-B3LYP/6-31G and TD-B3LYP/6-31G(d) spectra.

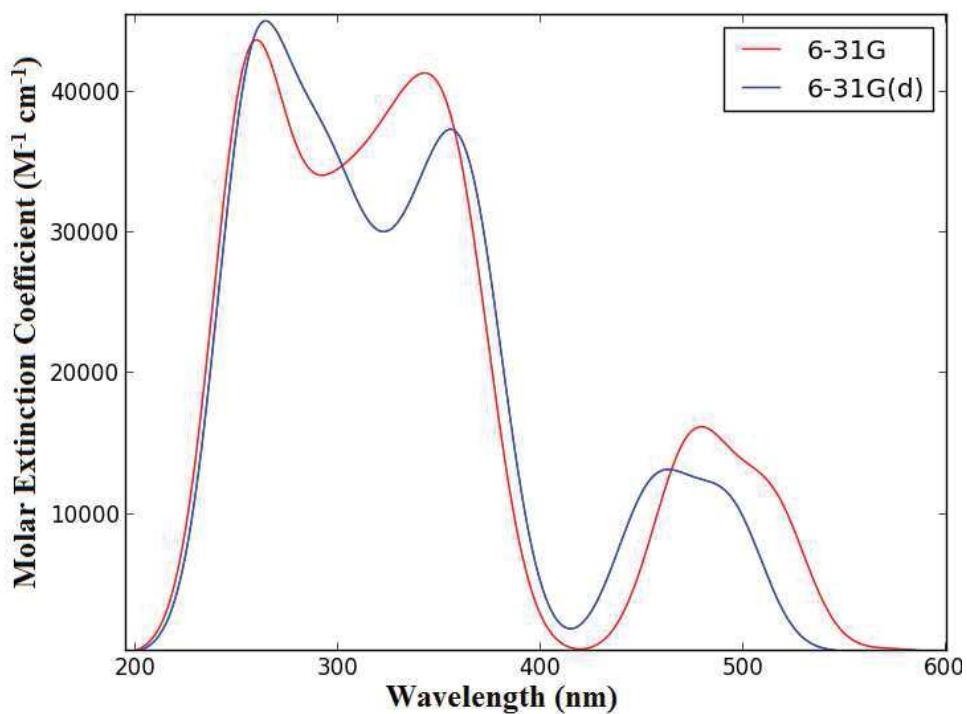
51. Complex (60): $[\text{Ru}(\text{bpy})(\text{DMCH})_2]^{2+}$

PDOS



Total and partial density of states of $[\text{Ru}(\text{bpy})(\text{DMCH})_2]^{2+}$ partitioned over Ru d orbitals and ligand C and N p orbitals.

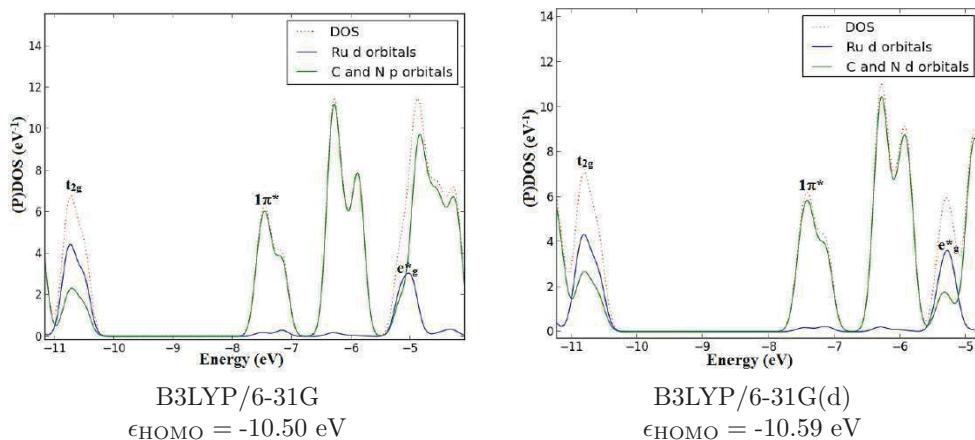
Absorption Spectrum



$[\text{Ru}(\text{bpy})(\text{DMCH})_2]^{2+}$ TD-B3LYP/6-31G and TD-B3LYP/6-31G(d) spectra.

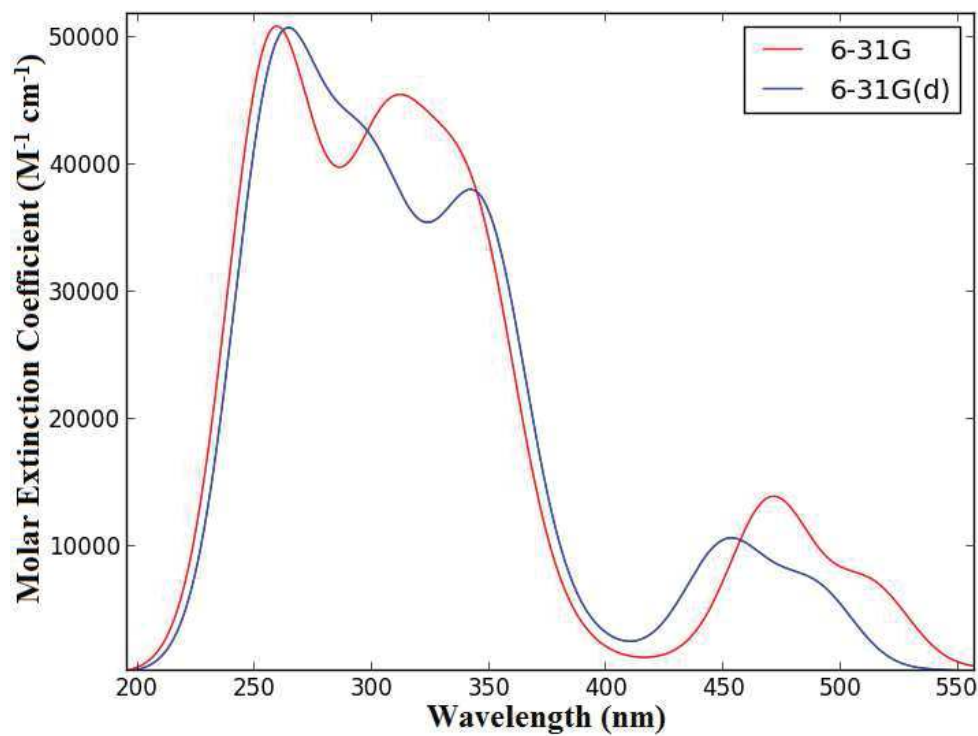
52. Complex (61): $[\text{Ru}(\text{bpy})(\text{biq})_2]^{2+}$

PDOS



Total and partial density of states of $[\text{Ru}(\text{bpy})(\text{biq})_2]^{2+}$ partitioned over Ru d orbitals and ligand C and N p orbitals.

Absorption Spectrum

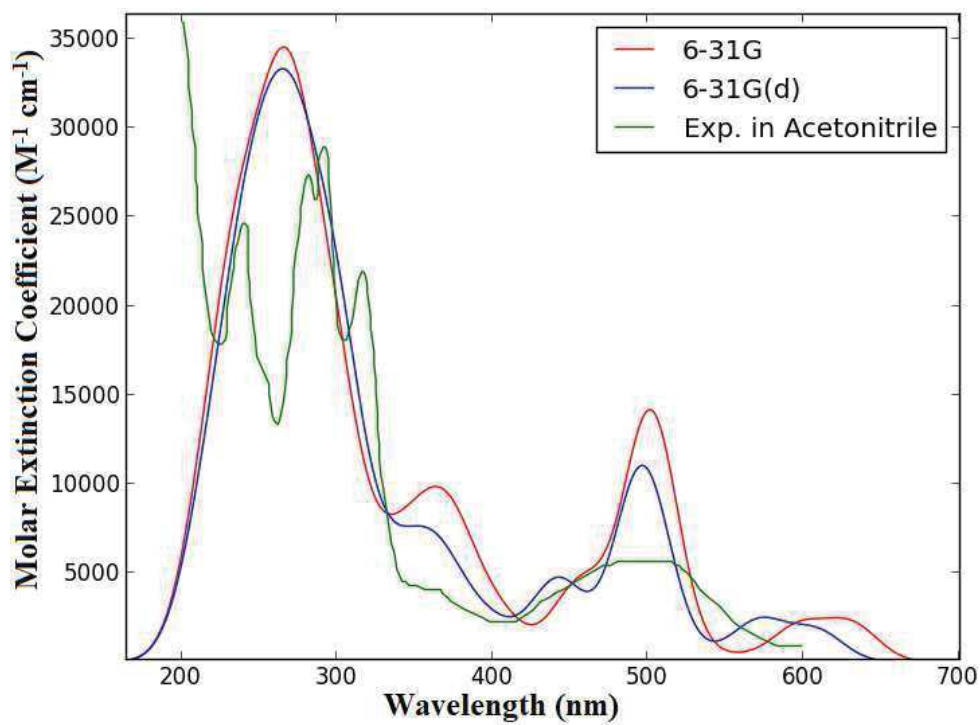


$[\text{Ru}(\text{bpy})(\text{biq})_2]^{2+}$ TD-B3LYP/6-31G and TD-B3LYP/6-31G(d) spectra.

53. Complex (63)[†]: [Ru(bpy)(trpy)Cl]⁺

B3LYP/6-31G B3LYP/6-31G(d)
 $\epsilon_{\text{HOMO}} = -7.76 \text{ eV}$ $\epsilon_{\text{HOMO}} = -7.78 \text{ eV}$

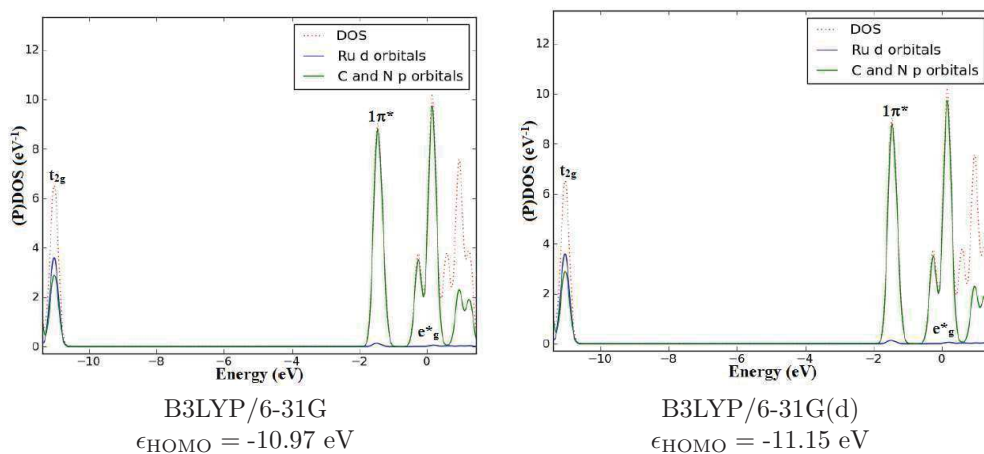
Absorption Spectrum



[Ru(bpy)(trpy)Cl]⁺ TD-B3LYP/6-31G, TD-B3LYP/6-31G(d), and experimental spectra. Experimental curve measured in acetonitrile at room temperature [9].

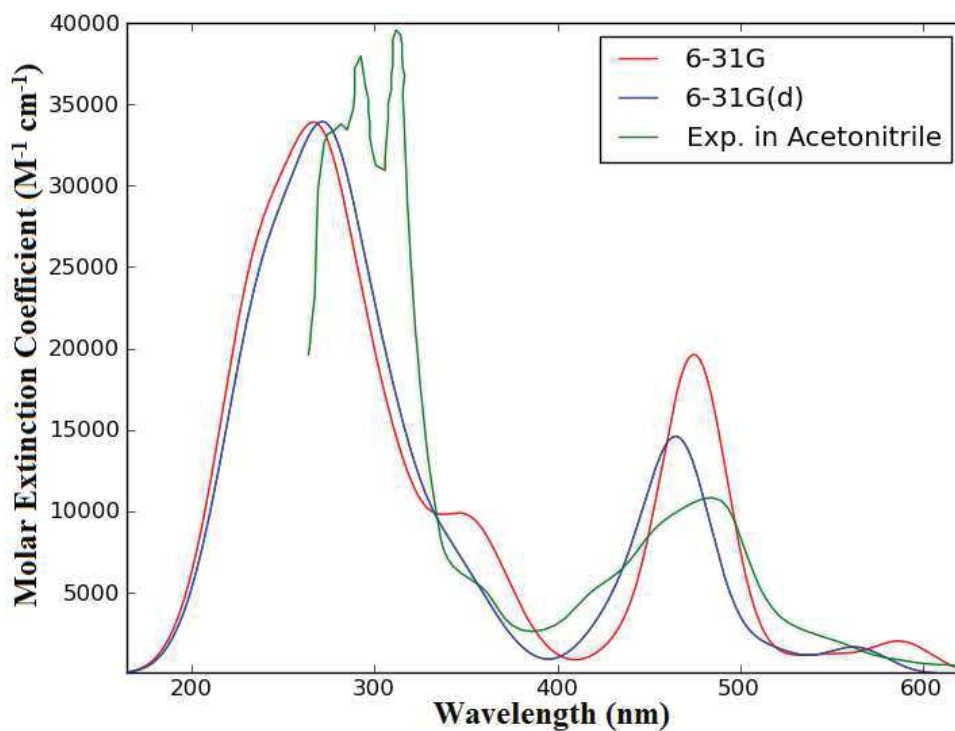
54. Complex (64)*: $[\text{Ru}(\text{bpy})(\text{trpy})(\text{CN})]^+$

PDOS



Total and partial density of states of $[\text{Ru}(\text{bpy})(\text{trpy})(\text{CN})]^+$ partitioned over Ru d orbitals and ligand C and N p orbitals.

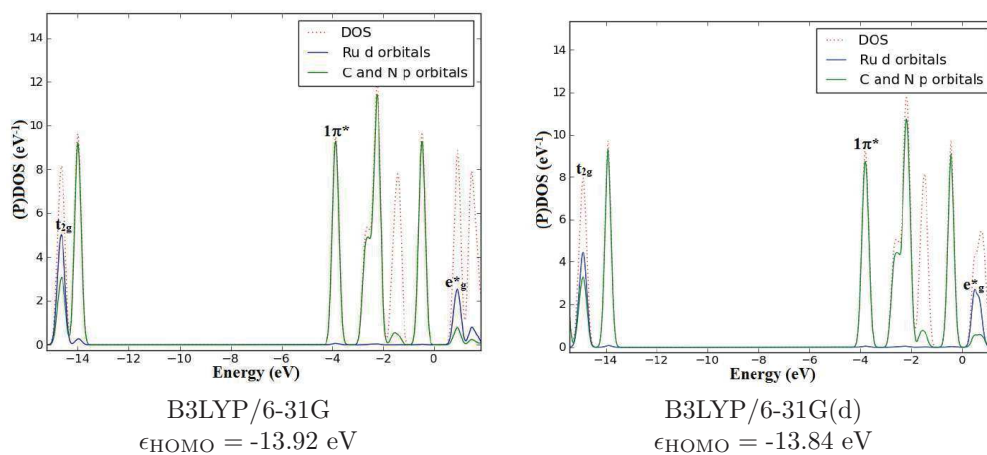
Absorption Spectrum



$[\text{Ru}(\text{bpy})(\text{trpy})(\text{CN})]^+$ TD-B3LYP/6-31G, TD-B3LYP/6-31G(d), and experimental spectra. Experiment in acetonitrile [11].

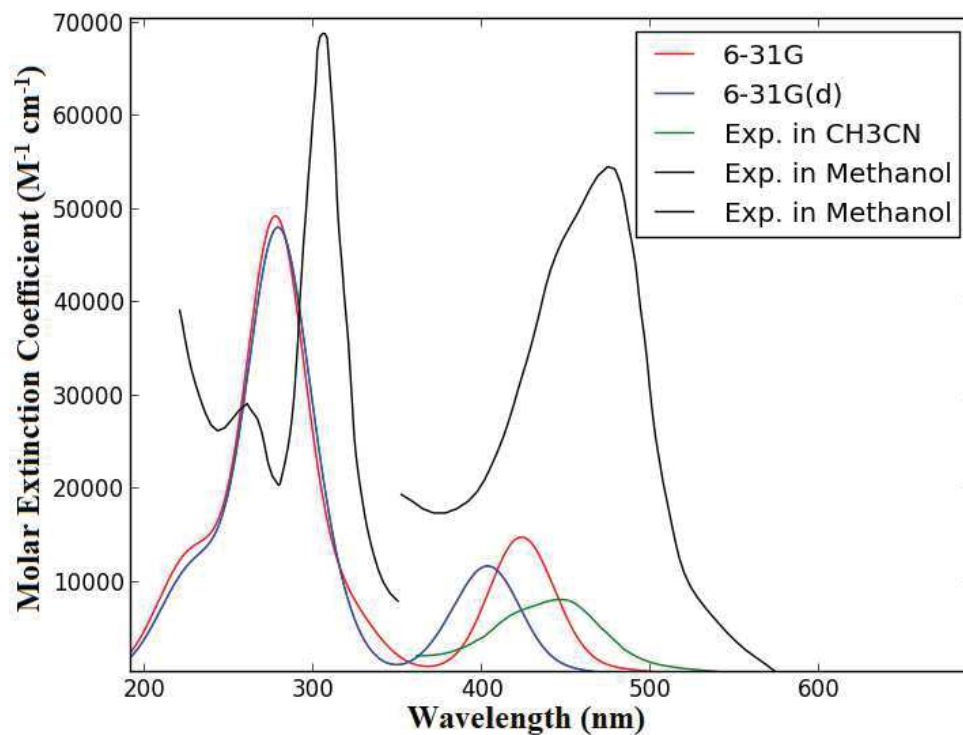
55. Complex (66)*: $[\text{Ru}(\text{6-m-bpy})_3]^{2+}$

PDOS



Total and partial density of states of $[\text{Ru}(\text{6-m-bpy})_3]^{2+}$ partitioned over Ru d orbitals and ligand C and N p orbitals.

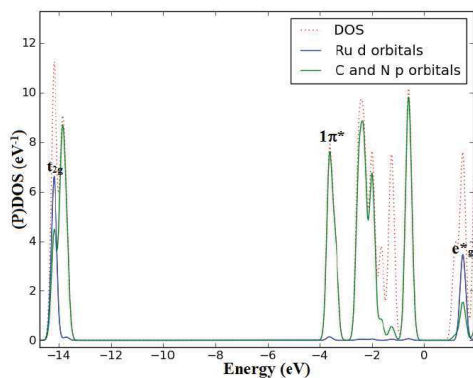
Absorption Spectrum



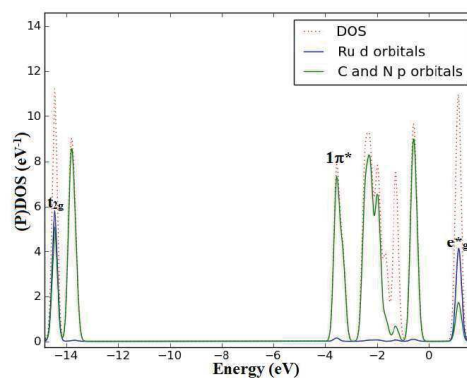
$[\text{Ru}(\text{6-m-bpy})_3]^{2+}$ TD-B3LYP/6-31G, TD-B3LYP/6-31G(d), and experimental spectra. Experimental curves measured in acetonitrile [12] and methanol [13], both at room temperature.

56. Complex (67)*: $[\text{Ru}(3,3'\text{-dm-bpy})_3]^{2+}$

PDOS



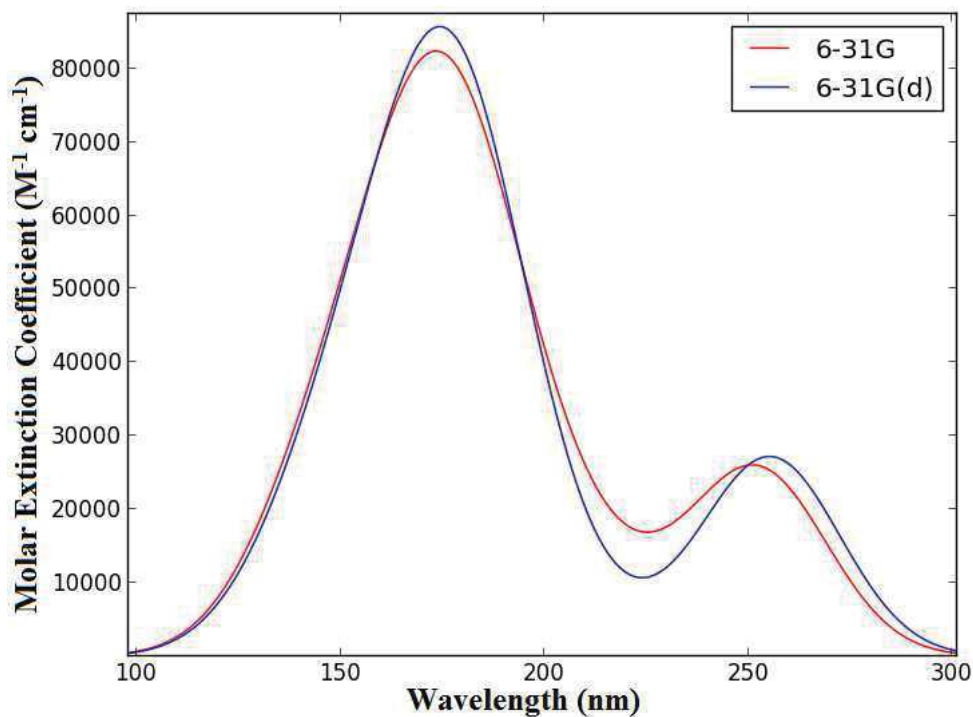
B3LYP/6-31G
 $\epsilon_{\text{HOMO}} = -13.72 \text{ eV}$



B3LYP/6-31G(d)
 $\epsilon_{\text{HOMO}} = -13.67 \text{ eV}$

Total and partial density of states of $[\text{Ru}(3,3'\text{-dm-bpy})_3]^{2+}$ partitioned over Ru d orbitals and ligand C and N p orbitals.

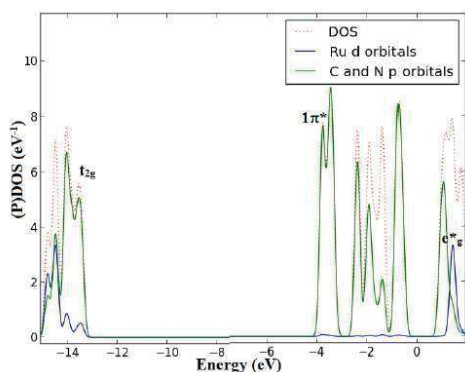
Absorption Spectrum



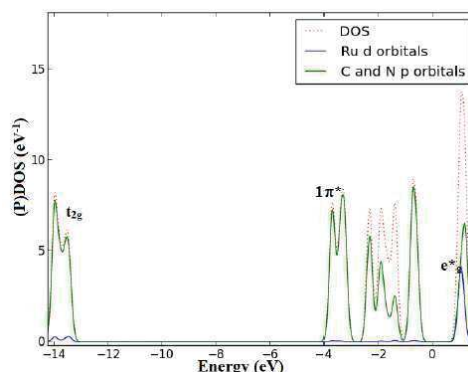
$[\text{Ru}(3,3'\text{-dm-bpy})_3]^{2+}$ TD-B3LYP/6-31G and TD-B3LYP/6-31G(d) spectra.

57. Complex (69): $[\text{Ru}(3,3'\text{-dm-bpy})(\text{phen})_2]^{2+}$

PDOS



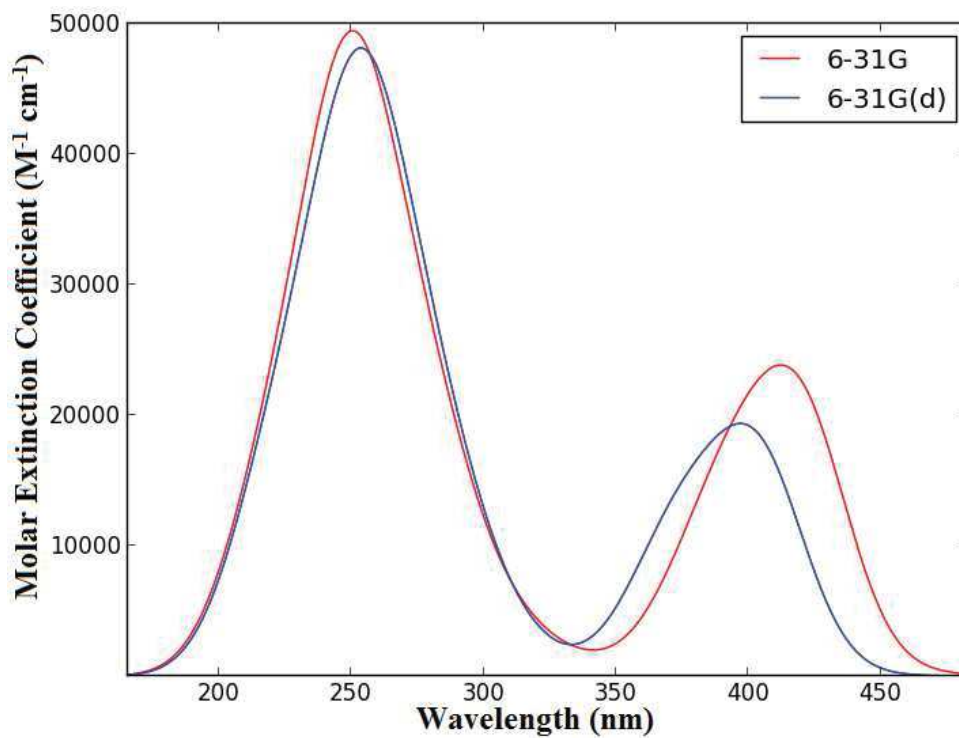
B3LYP/6-31G
 $\epsilon_{\text{HOMO}} = -13.45 \text{ eV}$



B3LYP/6-31G(d)
 $\epsilon_{\text{HOMO}} = -13.45 \text{ eV}$

Total and partial density of states of $[\text{Ru}(3,3'\text{-dm-bpy})(\text{phen})_2]^{2+}$ partitioned over Ru d orbitals and ligand C and N p orbitals.

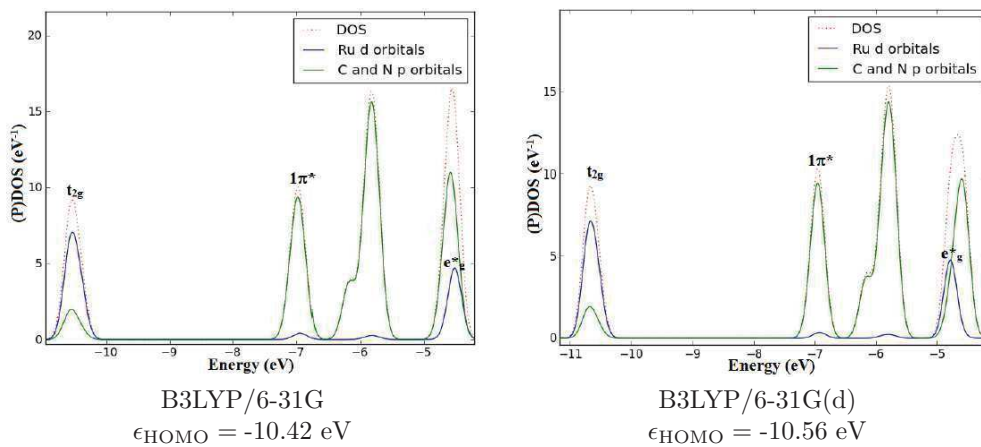
Absorption Spectrum



$[\text{Ru}(3,3'\text{-dm-bpy})(\text{phen})_2]^{2+}$ TD-B3LYP/6-31G and TD-B3LYP/6-31G(d) spectra.

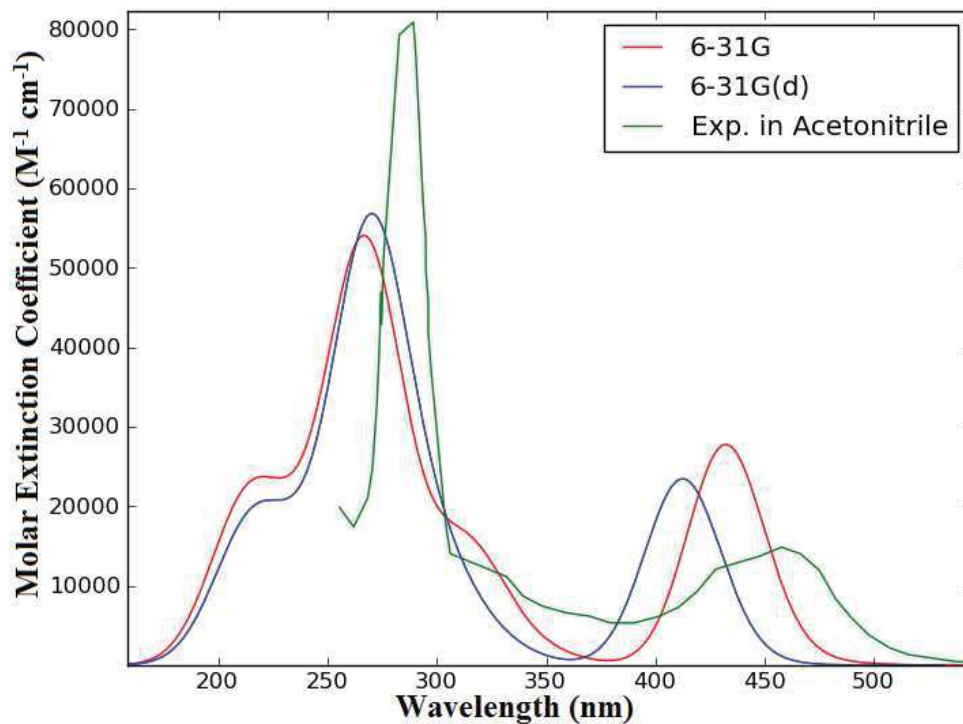
58. Complex (70): $[\text{Ru}(4,4'\text{-dm-bpy})_3]^{2+}$

PDOS



Total and partial density of states of $[\text{Ru}(3,3'\text{-dm-bpy})_3]^{2+}$ partitioned over Ru d orbitals and ligand C and N p orbitals.

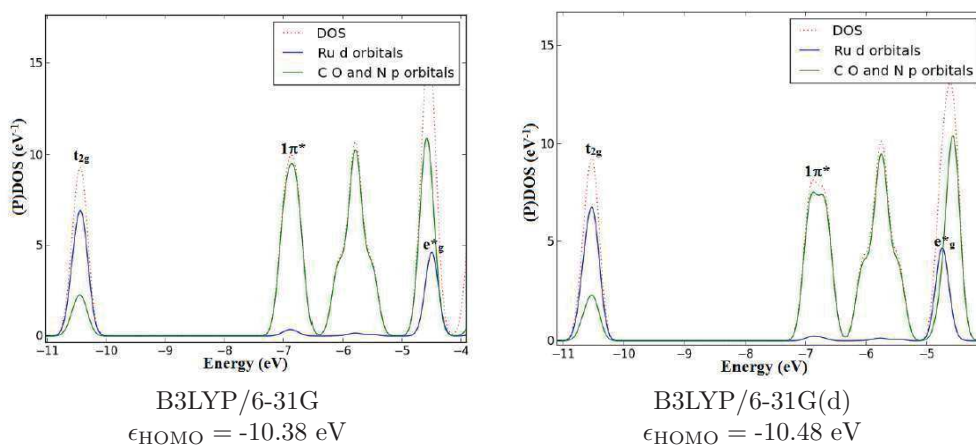
Absorption Spectrum



$[\text{Ru}(3,3'\text{-dm-bpy})_3]^{2+}$ TD-B3LYP/6-31G, TD-B3LYP/6-31G(d), and experimental spectra. Experimental spectrum measured in acetonitrile [14].

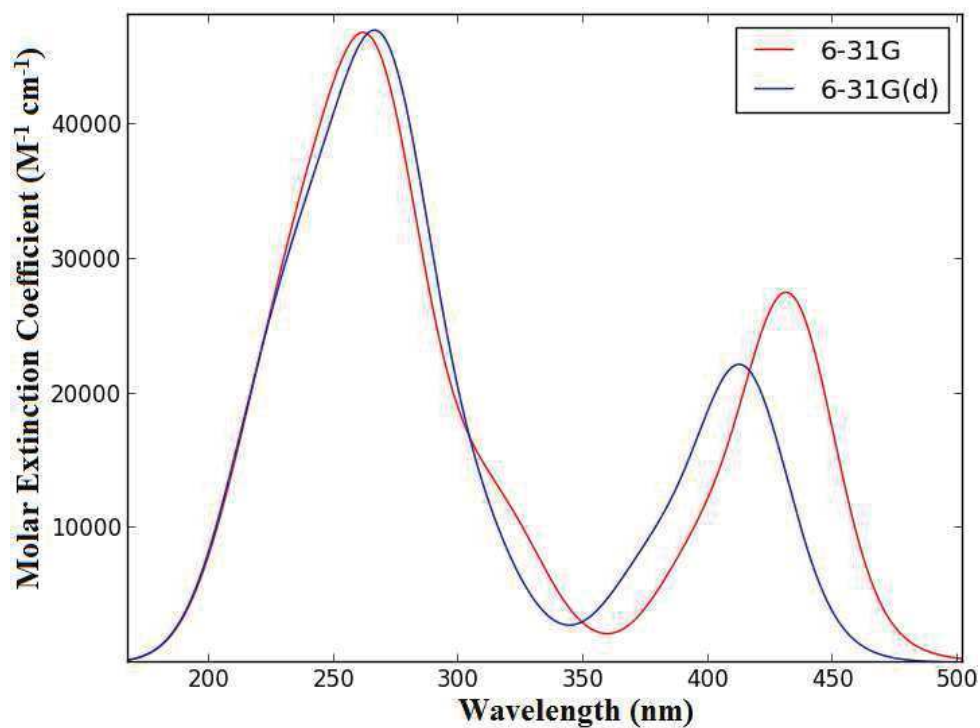
59. Complex (71): $[\text{Ru}(4,4'\text{-dm-bpy})_2(4,7\text{-dhy-phen})]^{2+}$

PDOS



Total and partial density of states of $[\text{Ru}(4,4'\text{-dm-bpy})_2(4,7\text{-dhy-phen})]^{2+}$ partitioned over Ru d orbitals and ligand C, O, and N p orbitals.

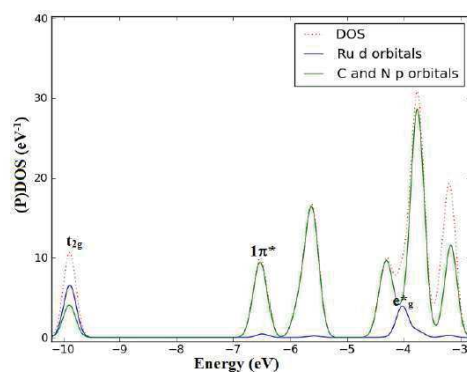
Absorption Spectrum



$[\text{Ru}(4,4'\text{-dm-bpy})_2(4,7\text{-dhy-phen})]^{2+}$ TD-B3LYP/6-31G and TD-B3LYP/6-31G(d) spectra.

60. Complex (73): $[\text{Ru}(4,4'\text{-dph-bpy})_3]^{2+}$

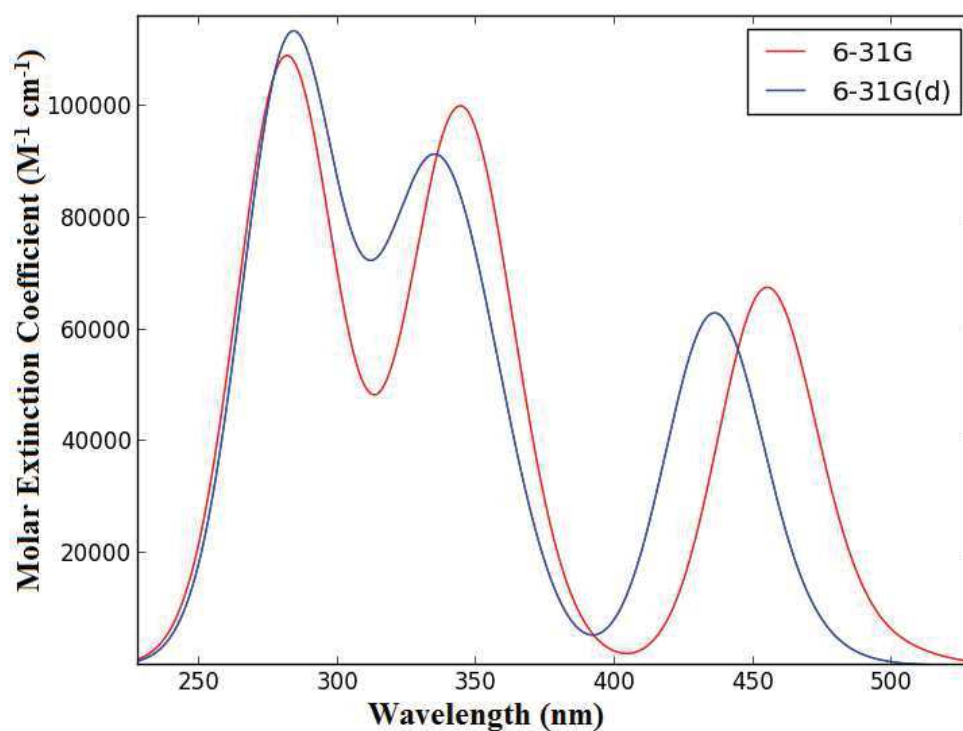
PDOS



B3LYP/6-31G
 $\epsilon_{\text{HOMO}} = -9.84 \text{ eV}$

Total and partial density of states of $[\text{Ru}(4,4'\text{-dph-bpy})_3]^{2+}$ partitioned over Ru d orbitals and ligand C and N p orbitals.

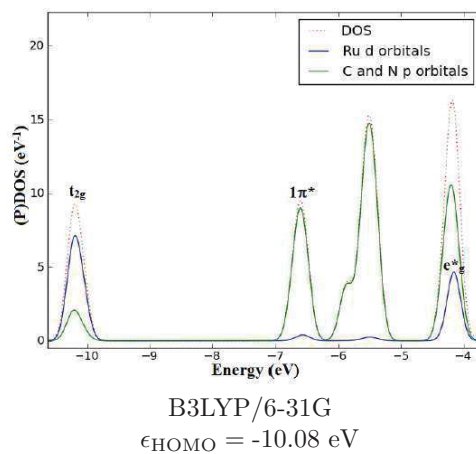
Absorption Spectrum



$[\text{Ru}(4,4'\text{-dph-bpy})_3]^{2+}$ TD-B3LYP/6-31G and TD-B3LYP/6-31G(d) spectra.

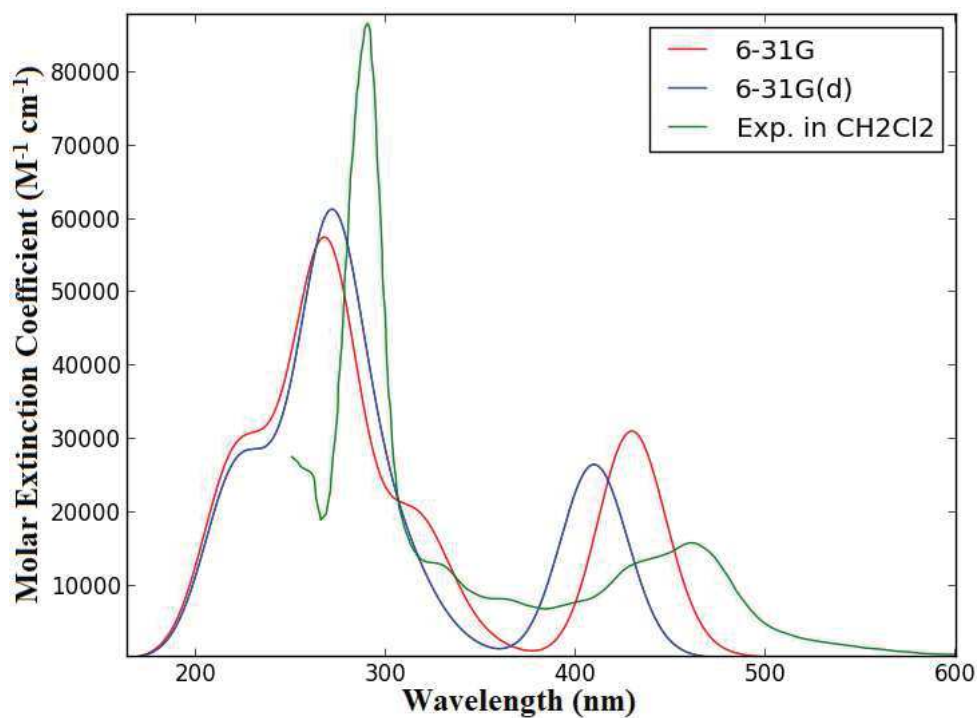
61. Complex (74): $[\text{Ru}(4,4'\text{-DTB-bpy})_3]^{2+}$

PDOS



Total and partial density of states of $[\text{Ru}(4,4'\text{-DTB-bpy})_3]^{2+}$ partitioned over Ru d orbitals and ligand C and N p orbitals.

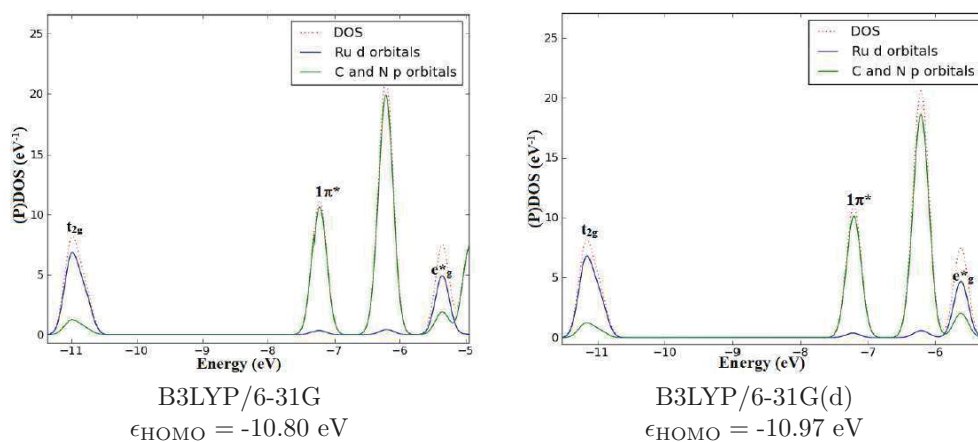
Absorption Spectrum



$[\text{Ru}(4,4'\text{-DTB-bpy})_3]^{2+}$ TD-B3LYP/6-31G, TD-B3LYP/6-31G(d), and experimental spectra. Experimental spectrum measured in dichloromethane at room temperature [15].

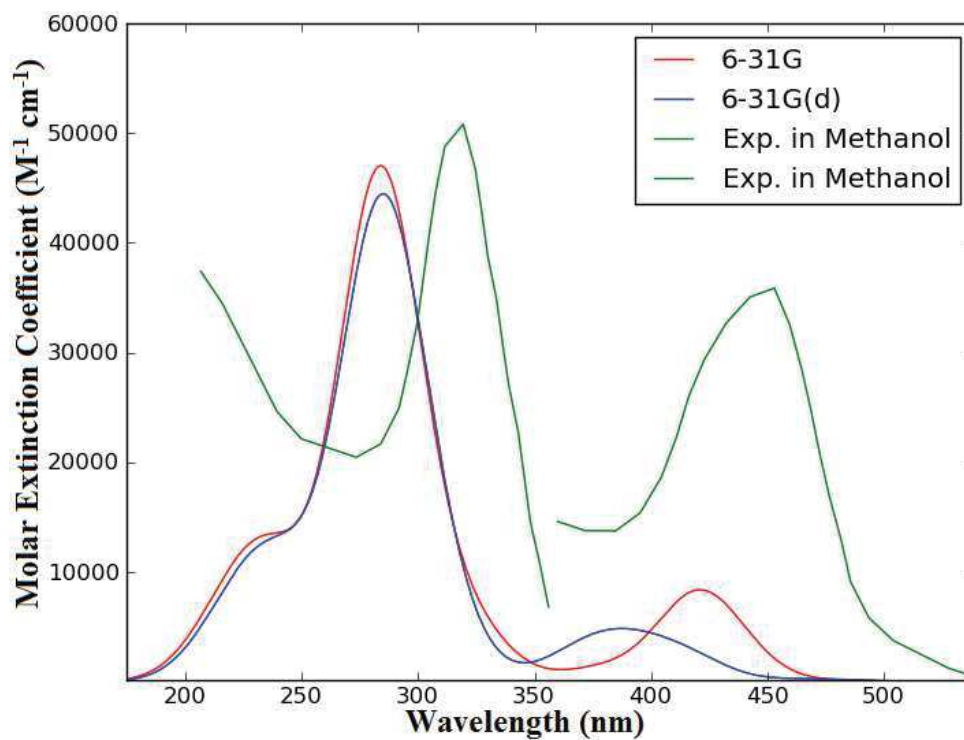
62. Complex (75): $[\text{Ru}(6,6'\text{-dm-bpy})_3]^{2+}$

PDOS



Total and partial density of states of $[\text{Ru}(6,6'\text{-dm-bpy})_3]^{2+}$ partitioned over Ru d orbitals and ligand C and N p orbitals.

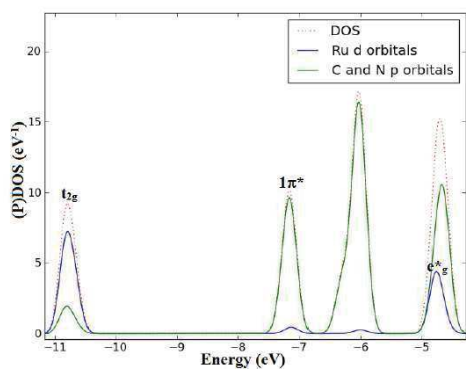
Absorption Spectrum



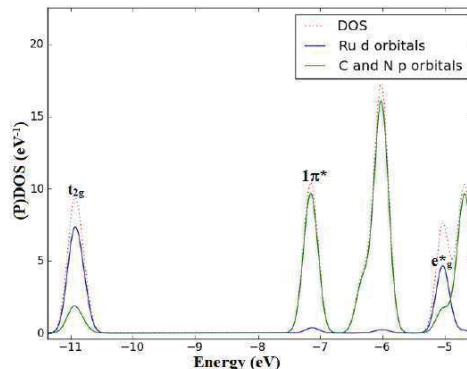
$[\text{Ru}(6,6'\text{-dm-bpy})_3]^{2+}$ TD-B3LYP/6-31G, TD-B3LYP/6-31G(d), and experimental spectra. Experimental spectrum measured in methanol [13].

63. Complex (76): $[\text{Ru}(\text{h-phen})_3]^{2+}$

PDOS



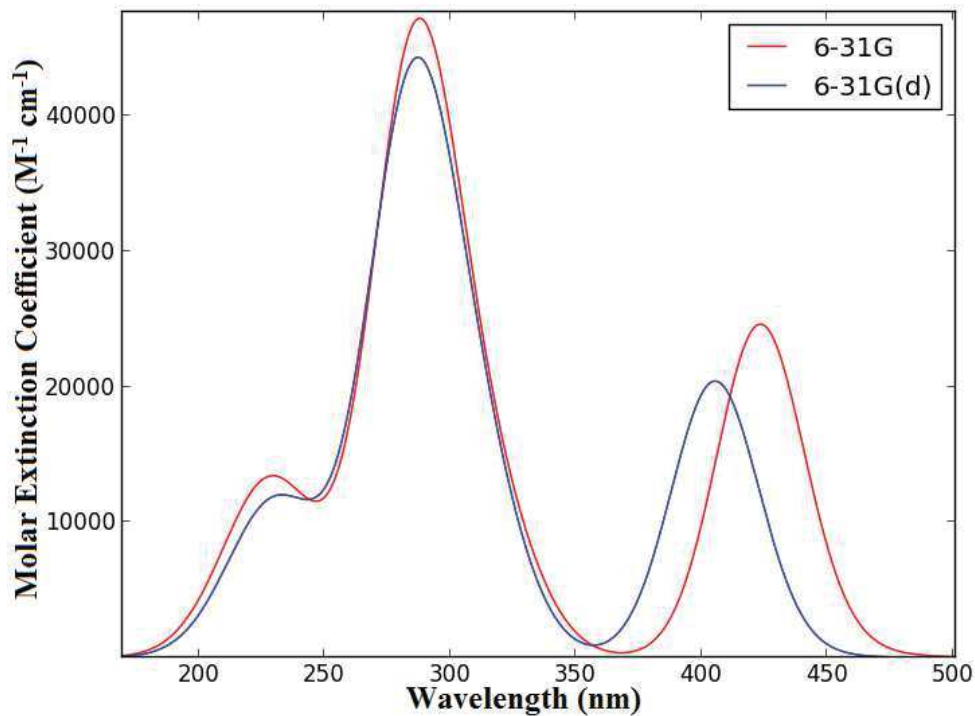
B3LYP/6-31G
 $\epsilon_{\text{HOMO}} = -10.68 \text{ eV}$



B3LYP/6-31G(d)
 $\epsilon_{\text{HOMO}} = -10.82 \text{ eV}$

Total and partial density of states of $[\text{Ru}(\text{h-phen})_3]^{2+}$ partitioned over Ru d orbitals and ligand C and N p orbitals.

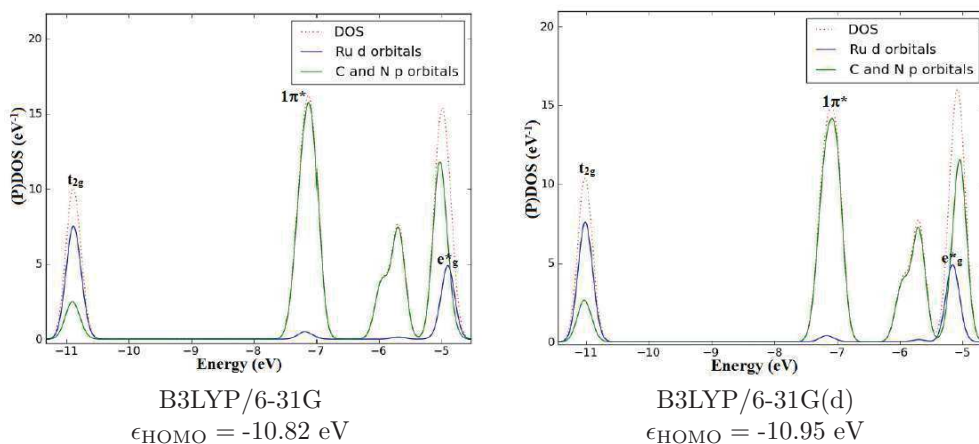
Absorption Spectrum



$[\text{Ru}(\text{h-phen})_3]^{2+}$ TD-B3LYP/6-31G and TD-B3LYP/6-31G(d) spectra.

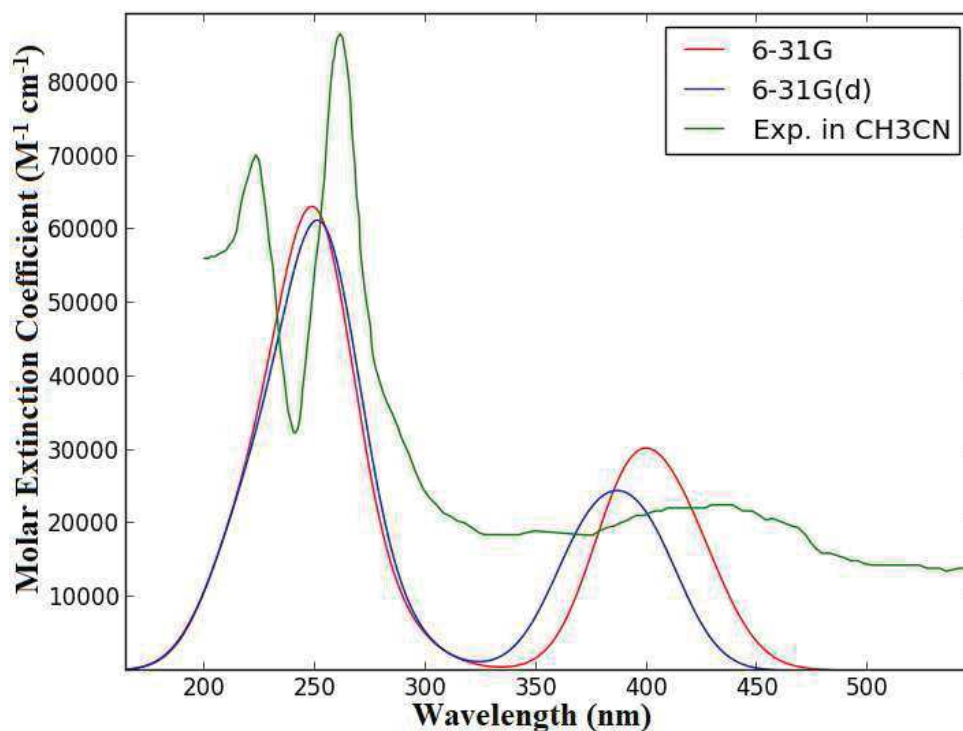
64. Complex (77): $[\text{Ru}(\text{phen})_3]^{2+}$

PDOS



Total and partial density of states of $[\text{Ru}(\text{phen})_3]^{2+}$ partitioned over Ru d orbitals and ligand C and N p orbitals.

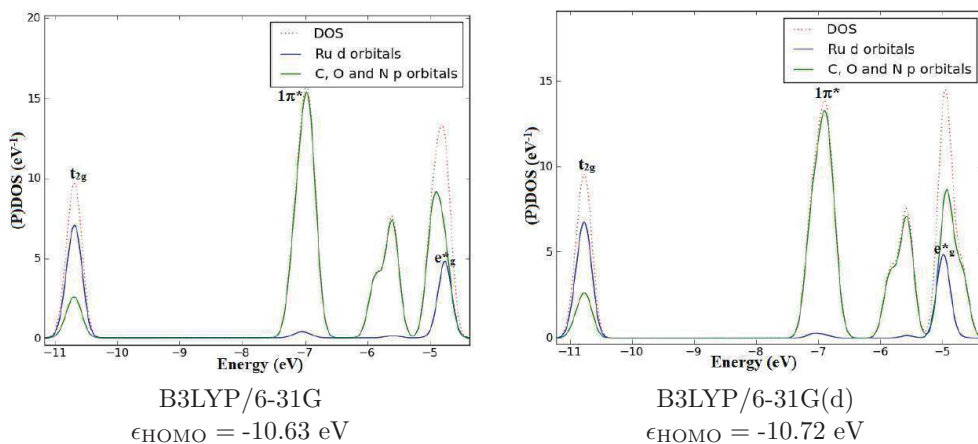
Absorption Spectrum



$[\text{Ru}(\text{phen})_3]^{2+}$ TD-B3LYP/6-31G, TD-B3LYP/6-31G(d), and experimental spectra. Experimental spectrum measured in acetonitrile [16].

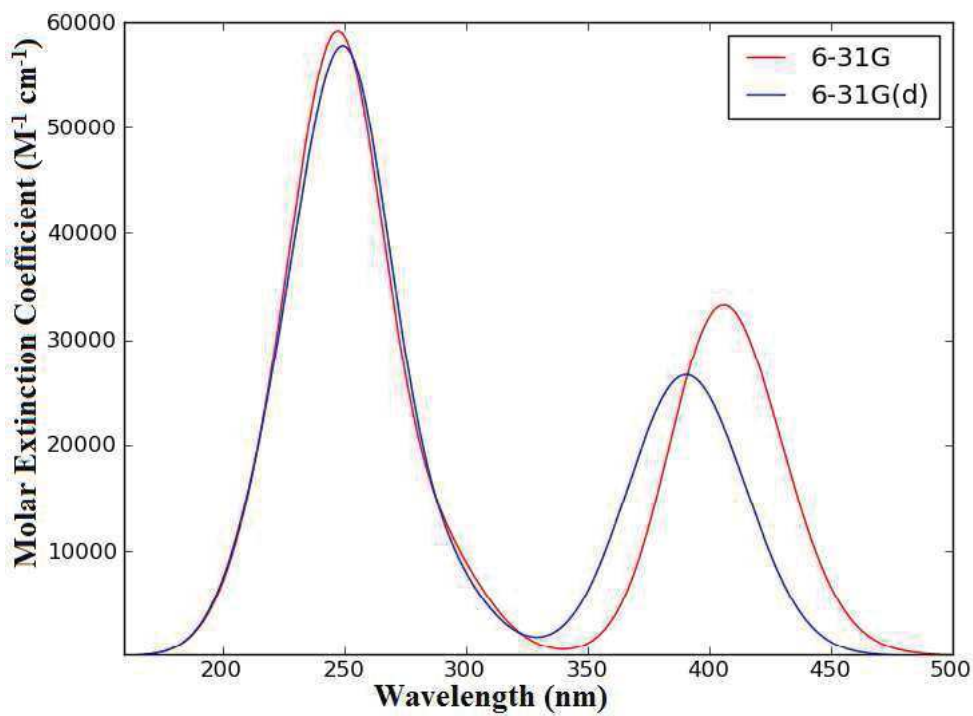
65. Complex (78): $[\text{Ru}(\text{phen})_2(4,7\text{-dhy-phen})]^{2+}$

PDOS



Total and partial density of states of $[\text{Ru}(\text{phen})_2(4,7\text{-dhy-phen})]^{2+}$ partitioned over Ru d orbitals and ligand C, O, and N p orbitals.

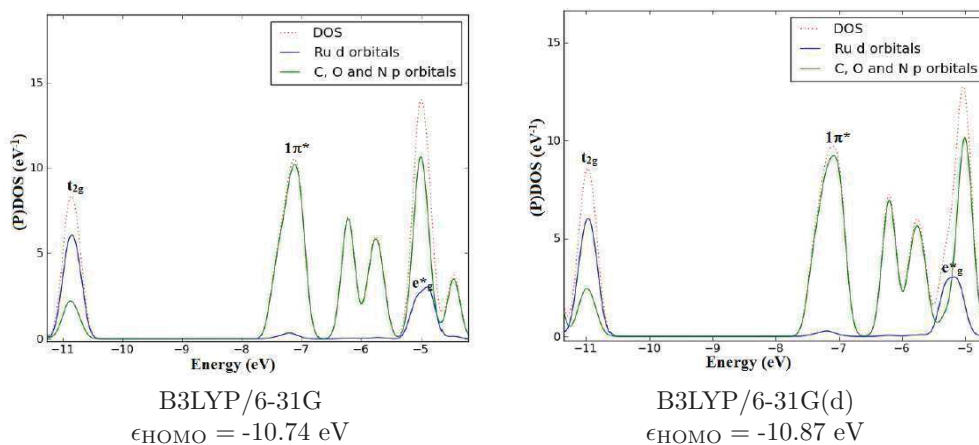
Absorption Spectrum



$[\text{Ru}(\text{phen})_2(4,7\text{-dhy-phen})]^{2+}$ TD-B3LYP/6-31G and TD-B3LYP/6-31G(d) spectra.

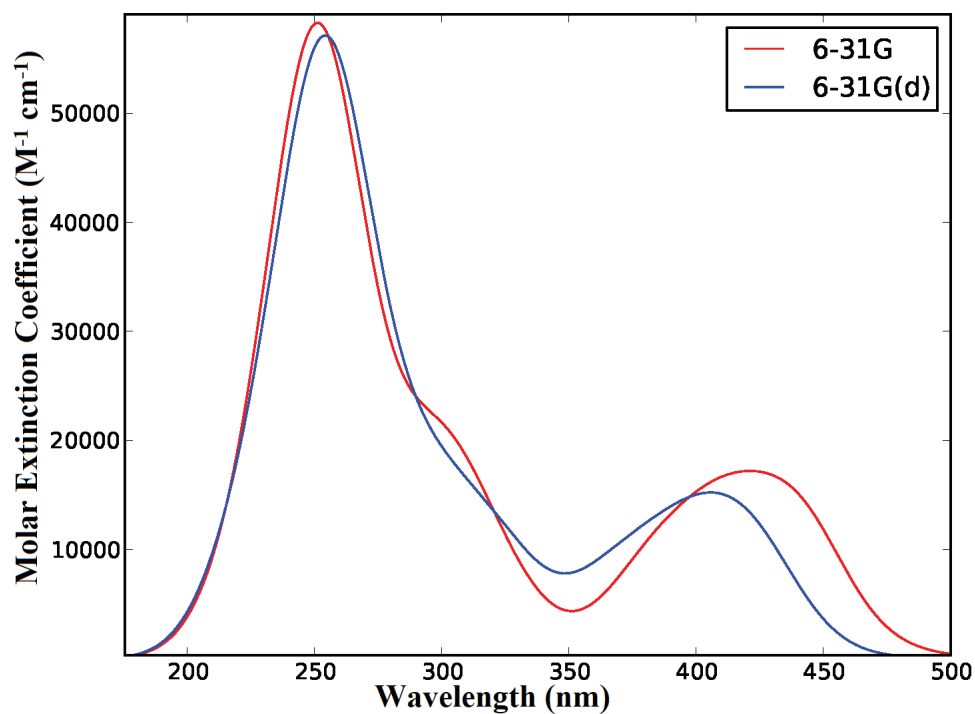
66. Complex (79): $[\text{Ru}(\text{phen})_2(\text{pq})]^{2+}$

PDOS



Total and partial density of states of $[\text{Ru}(\text{phen})_2(\text{pq})]^{2+}$ partitioned over Ru d orbitals and ligand C and N p orbitals.

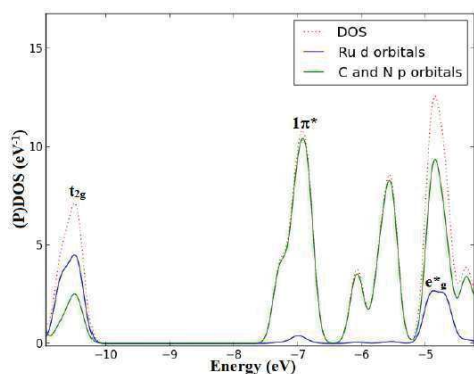
Absorption Spectrum



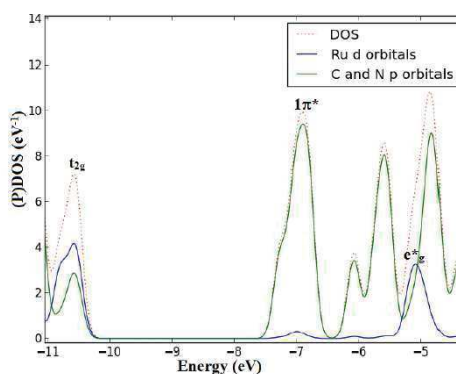
$[\text{Ru}(\text{phen})_2(\text{pq})]^{2+}$ TD-B3LYP/6-31G and TD-B3LYP/6-31G(d) spectra.

67. Complex (80): $[\text{Ru}(\text{phen})_2(\text{DMCH})]^{2+}$

PDOS



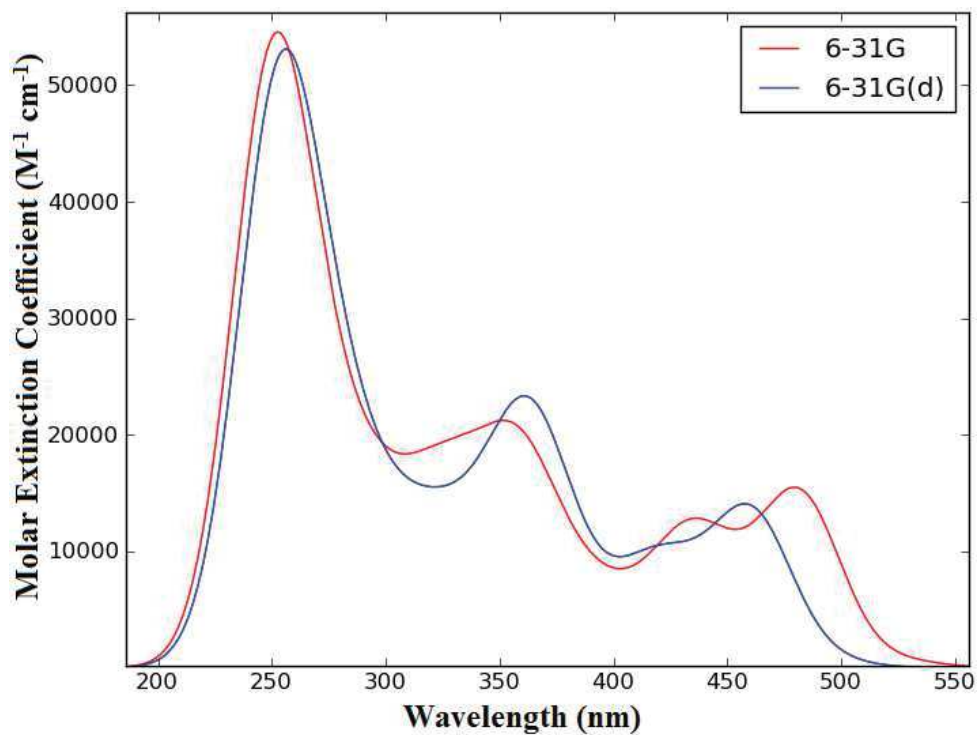
B3LYP/6-31G
 $\epsilon_{\text{HOMO}} = -10.42 \text{ eV}$



B3LYP/6-31G(d)
 $\epsilon_{\text{HOMO}} = -10.52 \text{ eV}$

Total and partial density of states of $[\text{Ru}(\text{phen})_2(\text{DMCH})]^{2+}$ partitioned over Ru d orbitals and ligand C and N p orbitals.

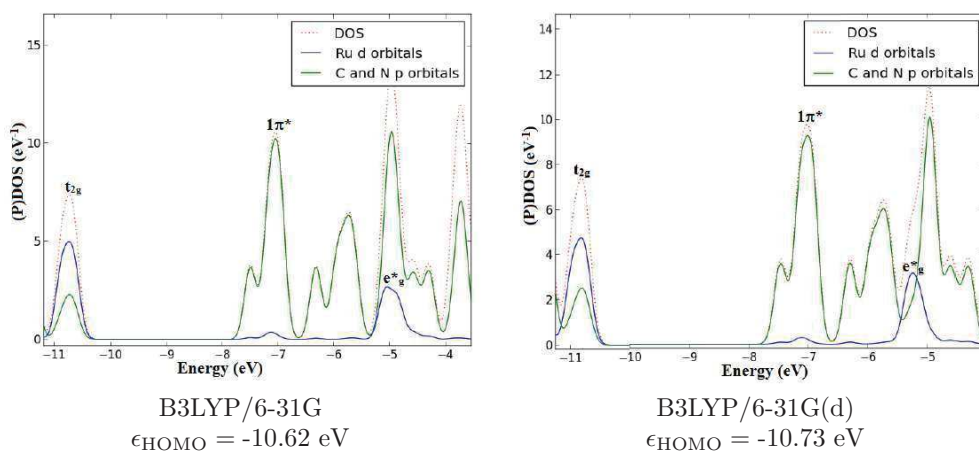
Absorption Spectrum



$[\text{Ru}(\text{phen})_2(\text{DMCH})]^{2+}$ TD-B3LYP/6-31G and TD-B3LYP/6-31G(d) spectra.

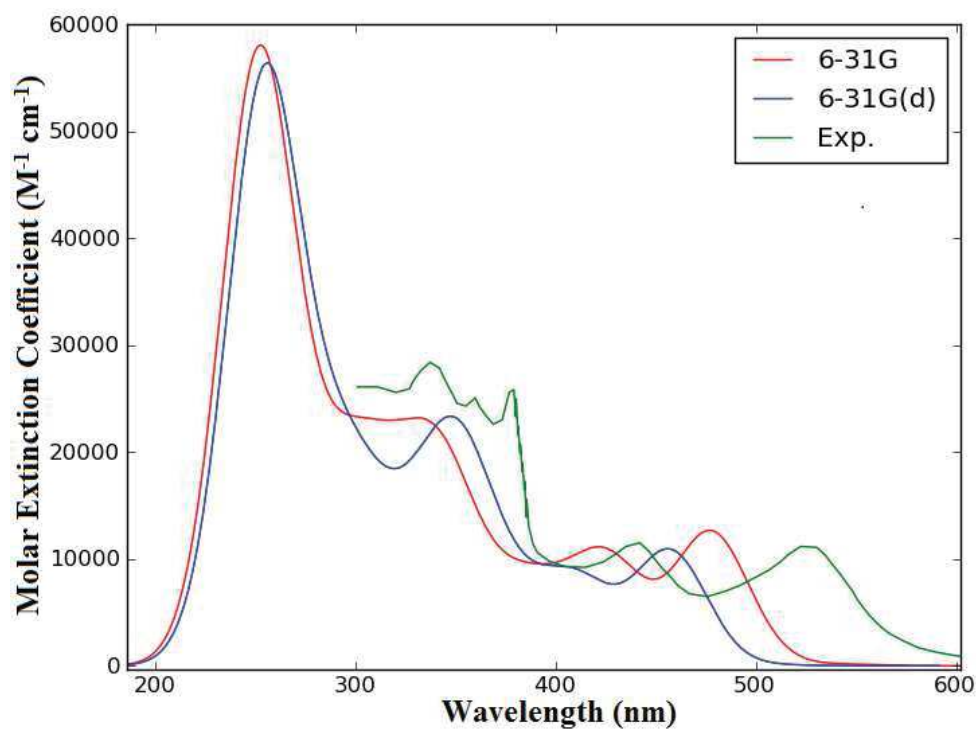
68. Complex (81): $[\text{Ru}(\text{phen})_2(\text{biq})]^{2+}$

PDOS



Total and partial density of states of $[\text{Ru}(\text{phen})_2(\text{biq})]^{2+}$ partitioned over Ru d orbitals and ligand C and N p orbitals.

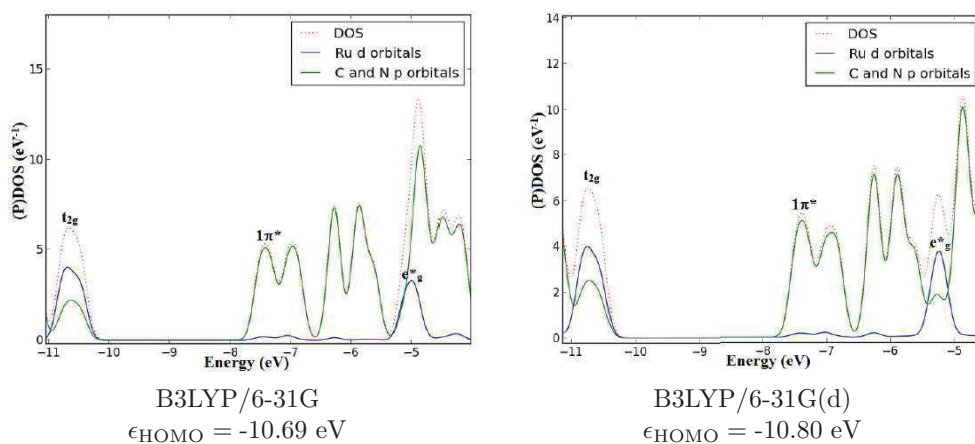
Absorption Spectrum



$[\text{Ru}(\text{phen})_2(\text{biq})]^{2+}$ TD-B3LYP/6-31G, TD-B3LYP/6-31G(d), and experimental spectra. The experimental spectrum is measured in water [17].

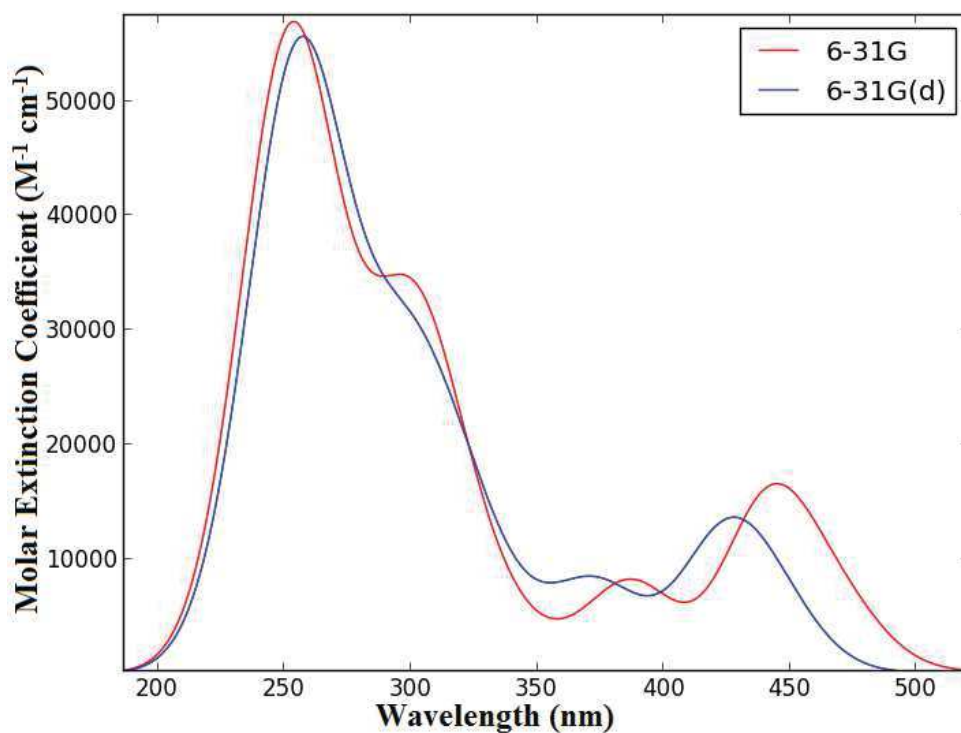
69. Complex (82): $[\text{Ru}(\text{phen})(\text{pq})_2]^{2+}$

PDOS



Total and partial density of states of $[\text{Ru}(\text{phen})(\text{pq})_2]^{2+}$ partitioned over Ru d orbitals and ligand C and N p orbitals.

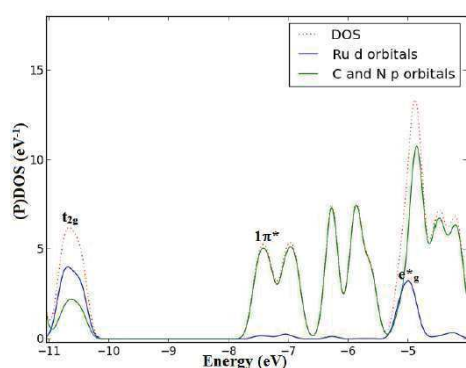
Absorption Spectrum



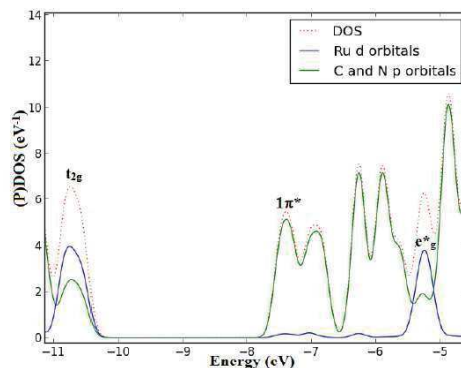
$[\text{Ru}(\text{phen})(\text{pq})_2]^{2+}$ TD-B3LYP/6-31G and TD-B3LYP/6-31G(d) spectra.

70. Complex (83): $[\text{Ru}(\text{phen})(\text{biq})_2]^{2+}$

PDOS



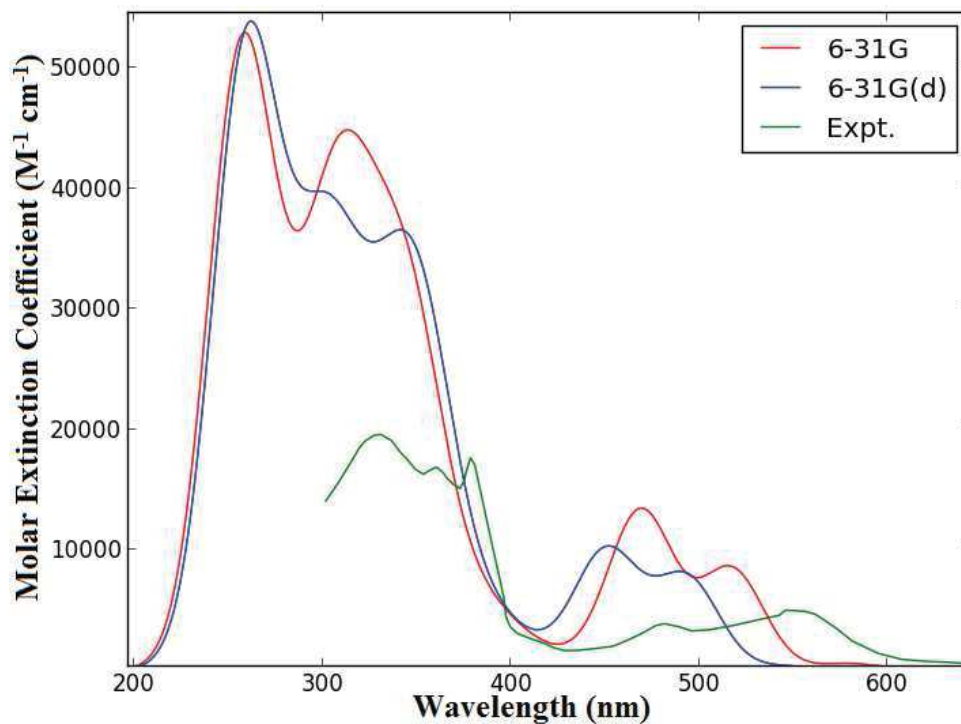
B3LYP/6-31G
 $\epsilon_{\text{HOMO}} = -10.46 \text{ eV}$



B3LYP/6-31G(d)
 $\epsilon_{\text{HOMO}} = -10.55 \text{ eV}$

Total and partial density of states of $[\text{Ru}(\text{phen})(\text{biq})_2]^{2+}$ partitioned over Ru d orbitals and ligand C and N p orbitals.

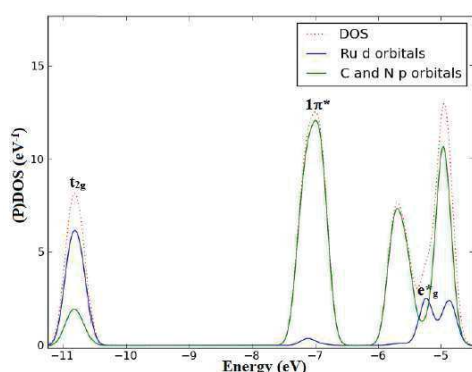
Absorption Spectrum



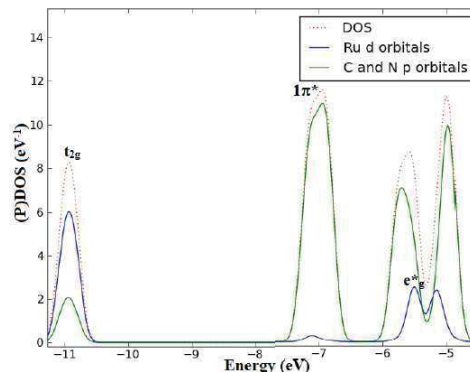
$[\text{Ru}(\text{phen})(\text{biq})_2]^{2+}$ TD-B3LYP/6-31G, TD-B3LYP/6-31G(d), and experimental spectra. Experimental spectrum measured in water [17].

71. Complex (84): $[\text{Ru}(\text{2-m-phen})_3]^{2+}$

PDOS



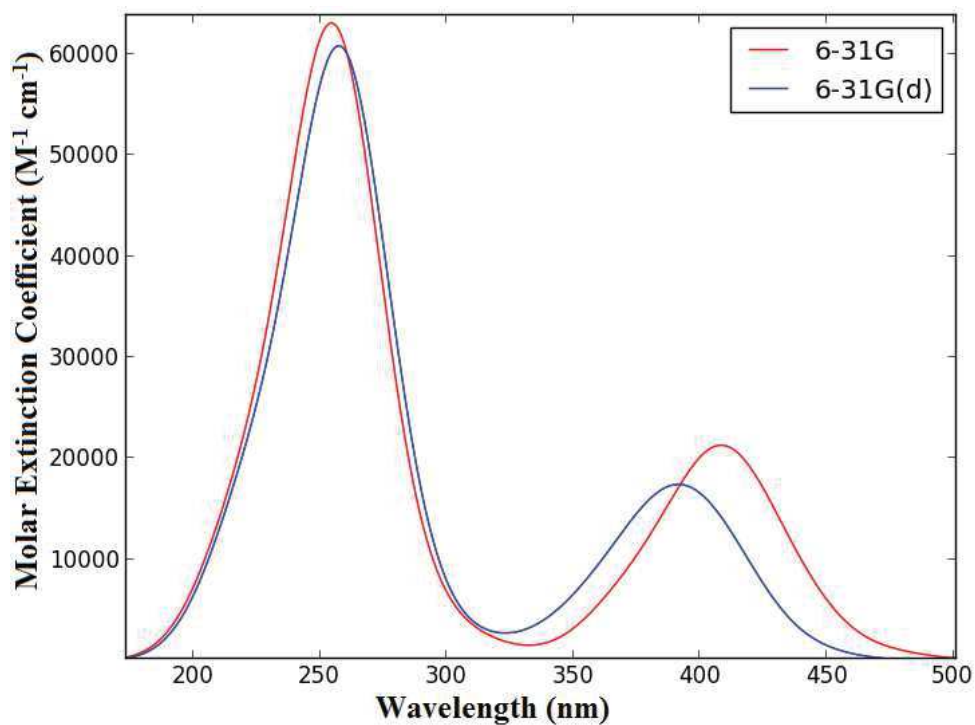
B3LYP/6-31G
 $\epsilon_{\text{HOMO}} = -10.68 \text{ eV}$



B3LYP/6-31G(d)
 $\epsilon_{\text{HOMO}} = -10.83 \text{ eV}$

Total and partial density of states of $[\text{Ru}(\text{2-m-phen})_3]^{2+}$ partitioned over Ru d orbitals and ligand C and N p orbitals.

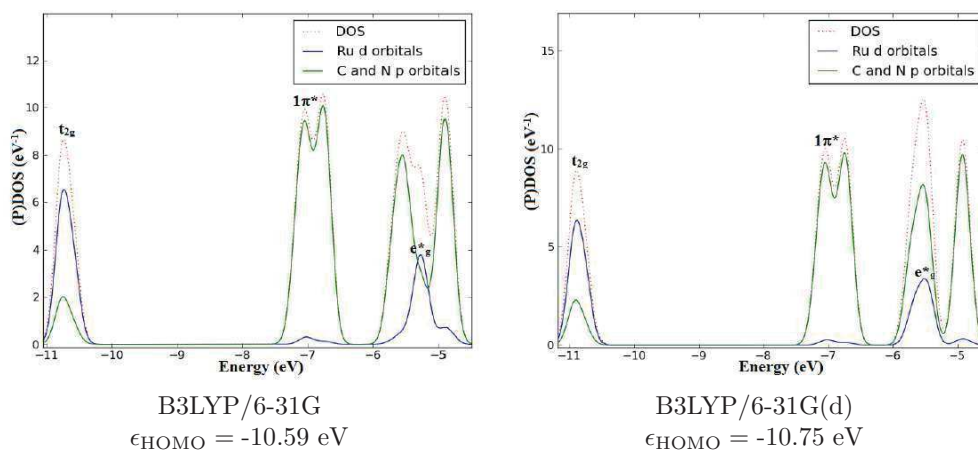
Absorption Spectrum



$[\text{Ru}(\text{2-m-phen})_3]^{2+}$ TD-B3LYP/6-31G and TD-B3LYP/6-31G(d) spectra.

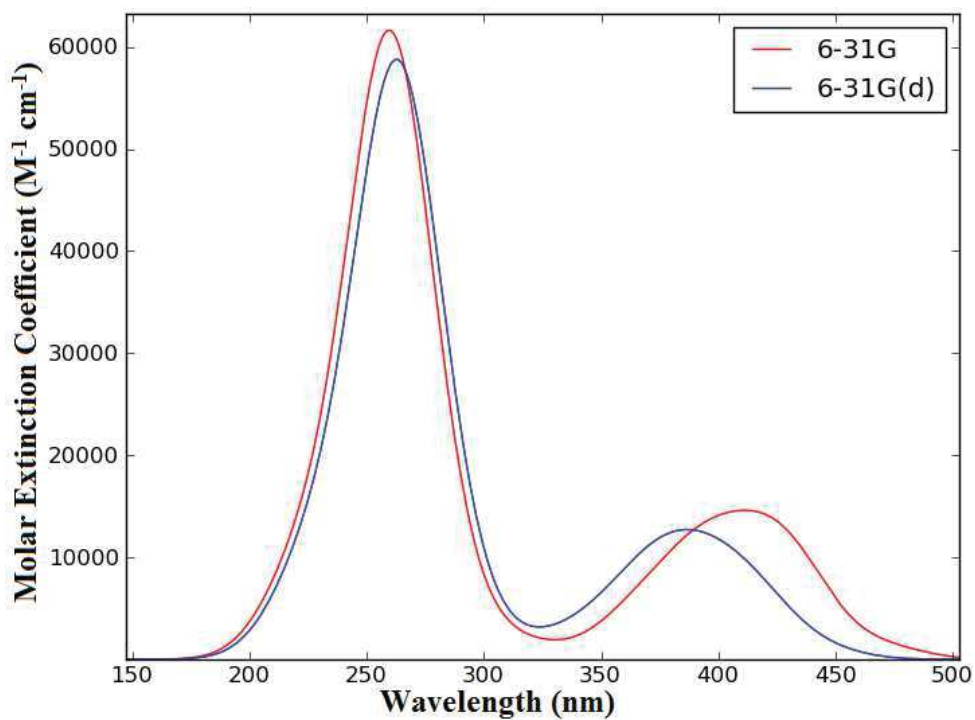
72. Complex (85): $[\text{Ru}(2,9\text{-dm-phen})_3]^{2+}$

PDOS



Total and partial density of states of $[\text{Ru}(2,9\text{-dm-phen})_3]^{2+}$ partitioned over Ru d orbitals and ligand C and N p orbitals.

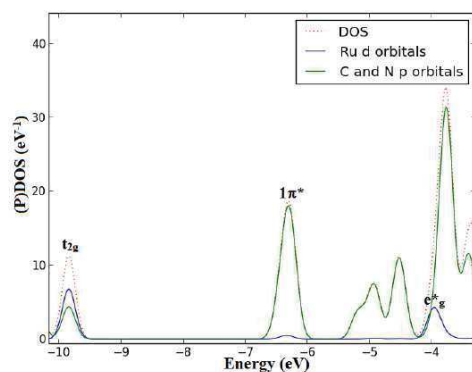
Absorption Spectrum



$[\text{Ru}(2,9\text{-dm-phen})_3]^{2+}$ TD-B3LYP/6-31G and TD-B3LYP/6-31G(d) spectra.

73. Complex (86): $[\text{Ru}(4,7\text{-Ph}_2\text{-phen})_3]^{2+}$

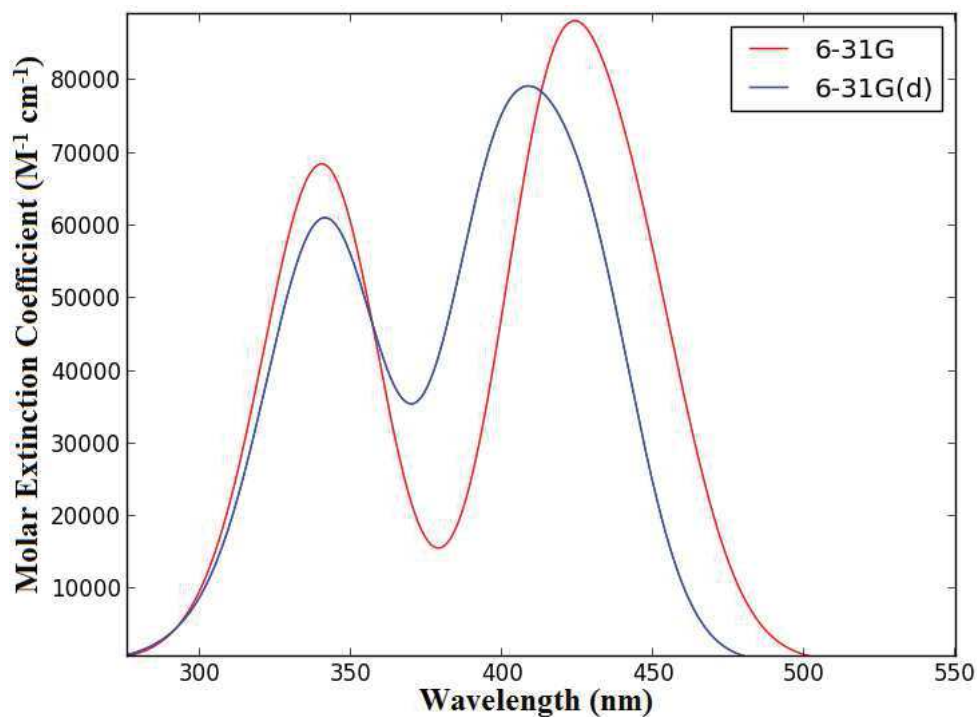
PDOS



B3LYP/6-31G
 $\epsilon_{\text{HOMO}} = -9.84 \text{ eV}$

Total and partial density of states of $[\text{Ru}(4,7\text{-Ph}_2\text{-phen})_3]^{2+}$ partitioned over Ru d orbitals and ligand C and N p orbitals.

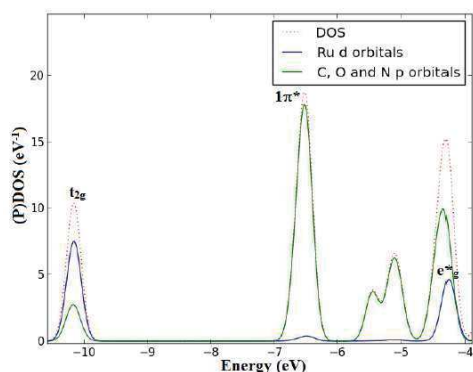
Absorption Spectrum



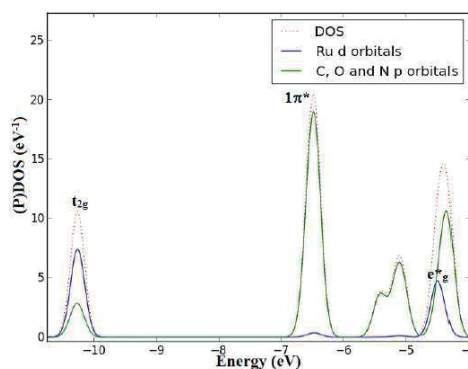
$[\text{Ru}(4,7\text{-Ph}_2\text{-phen})_3]^{2+}$ TD-B3LYP/6-31G and TD-B3LYP/6-31G(d) spectra.

74. Complex (87): $[\text{Ru}(4,7\text{-dhy-phen})(\text{tm1-phen})_2]^{2+}$

PDOS



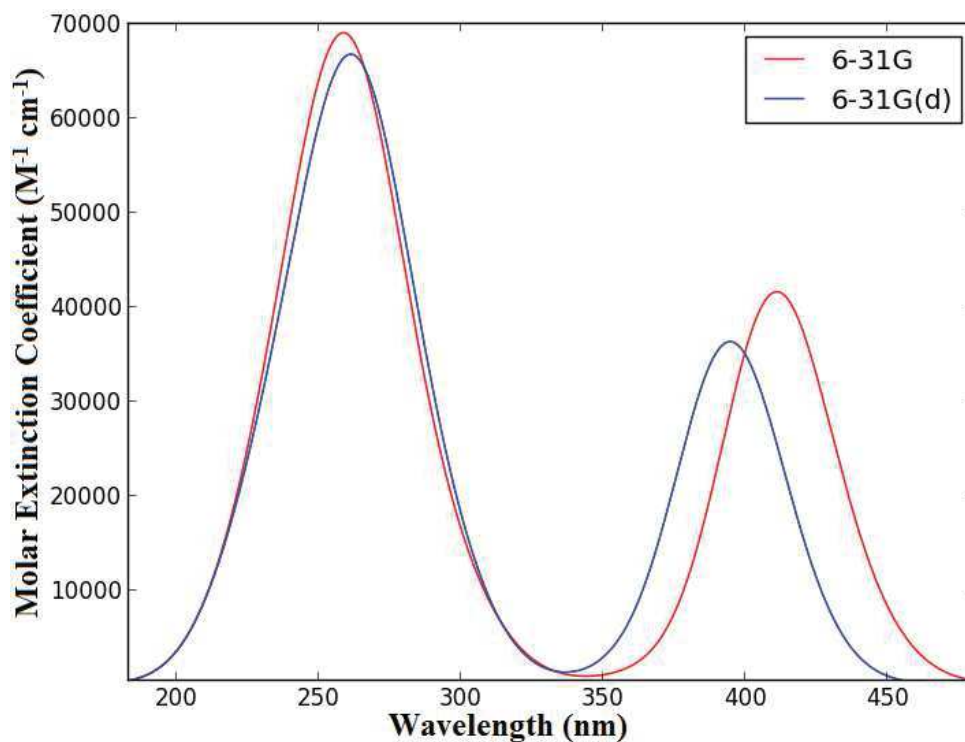
B3LYP/6-31G
 $\epsilon_{\text{HOMO}} = -10.11 \text{ eV}$



B3LYP/6-31G(d)
 $\epsilon_{\text{HOMO}} = -10.23 \text{ eV}$

Total and partial density of states of $[\text{Ru}(4,7\text{-dhy-phen})(\text{tm1-phen})_2]^{2+}$ partitioned over Ru d orbitals and ligand C, O, and N p orbitals.

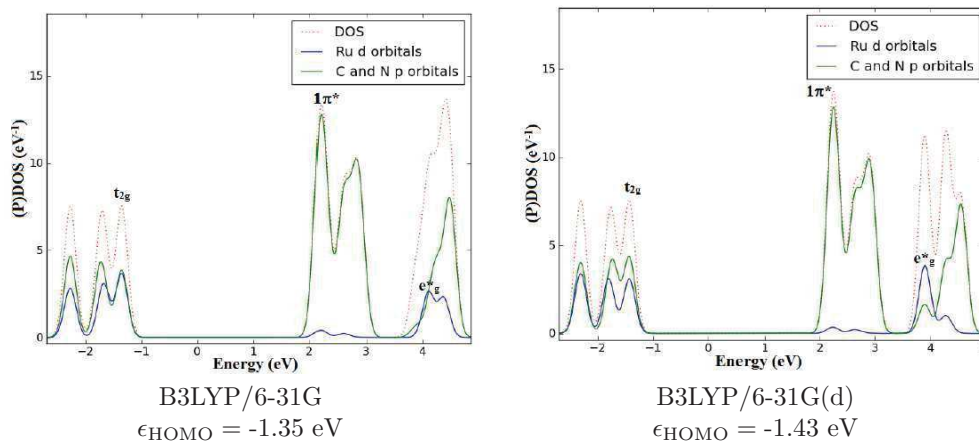
Absorption Spectrum



$[\text{Ru}(4,7\text{-dhy-phen})(\text{tm1-phen})_2]^{2+}$ TD-B3LYP/6-31G and TD-B3LYP/6-31G(d) spectra.

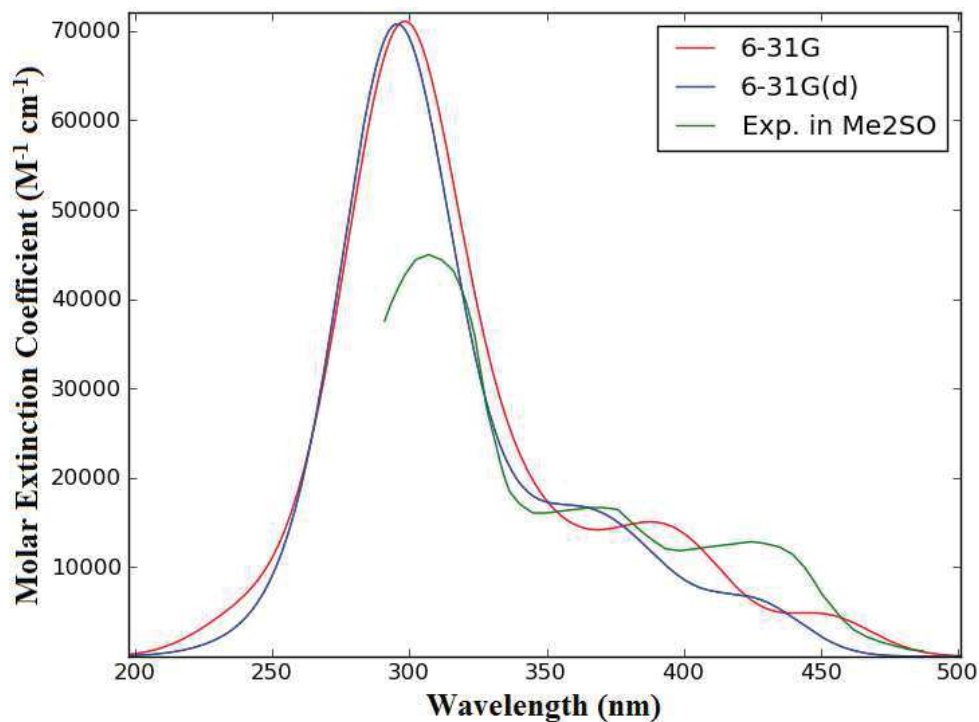
75. Complex (88)*: $[\text{Ru}(\text{DPA})_3]^-$

PDOS



Total and partial density of states of $[\text{Ru}(\text{DPA})_3]^-$ partitioned over Ru d orbitals and ligand C and N p orbitals.

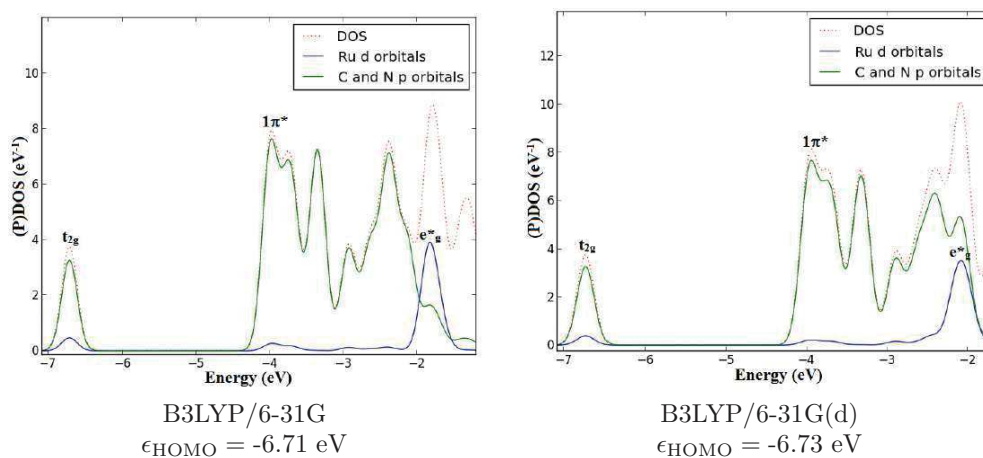
Absorption Spectrum



$[\text{Ru}(\text{DPA})_3]^-$ TD-B3LYP/6-31G, TD-B3LYP/6-31G(d), and experimental spectra. Experimental spectrum measured in dimethyl sulfoxide [18].

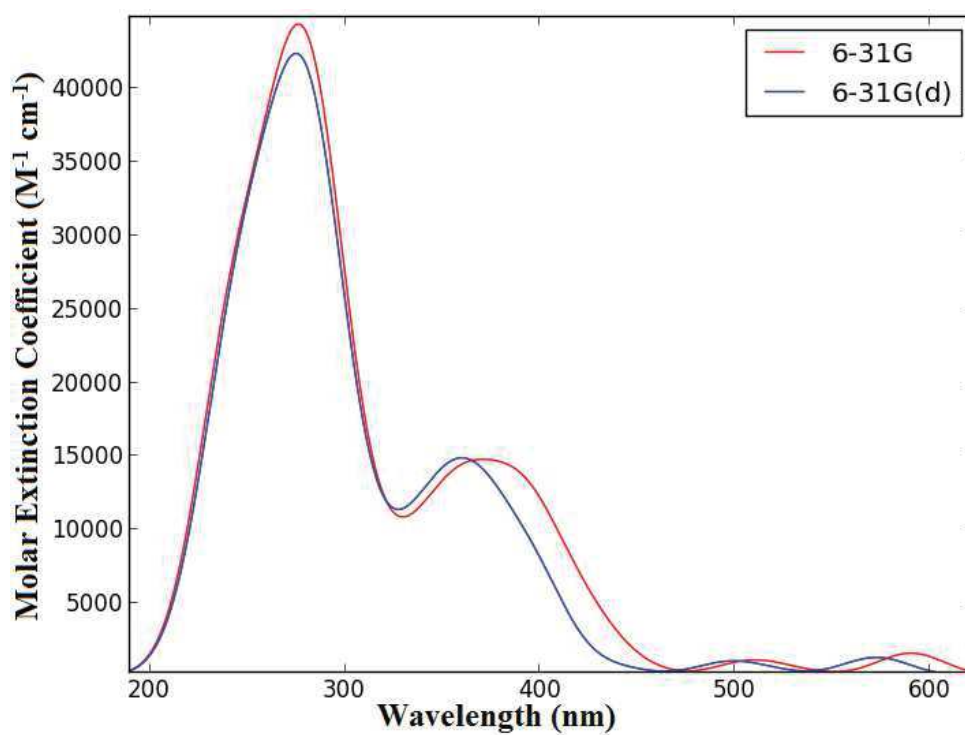
76. Complex (89): $[\text{Ru}(\text{DPA})(\text{DPAH})_2]^+$

PDOS



Total and partial density of states of $[\text{Ru}(\text{DPA})(\text{DPAH})_2]^+$ partitioned over Ru d orbitals and ligand C and N p orbitals.

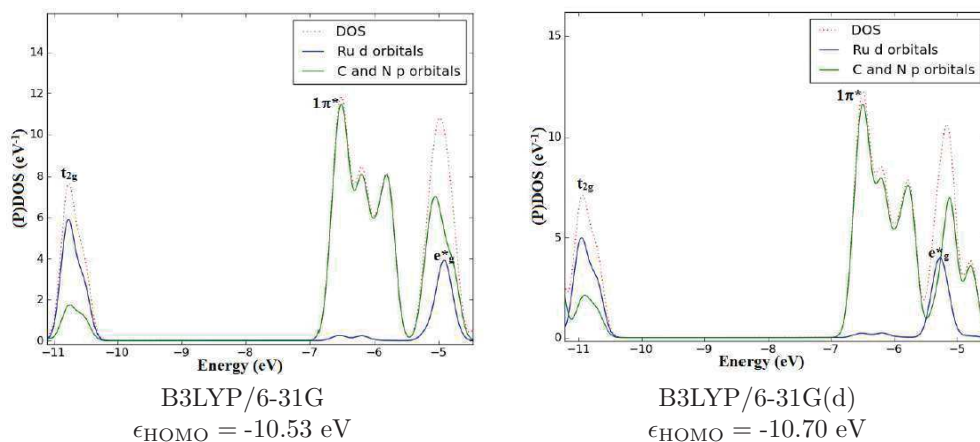
Absorption Spectrum



$[\text{Ru}(\text{DPA})(\text{DPAH})_2]^+$ TD-B3LYP/6-31G and TD-B3LYP/6-31G(d) spectra.

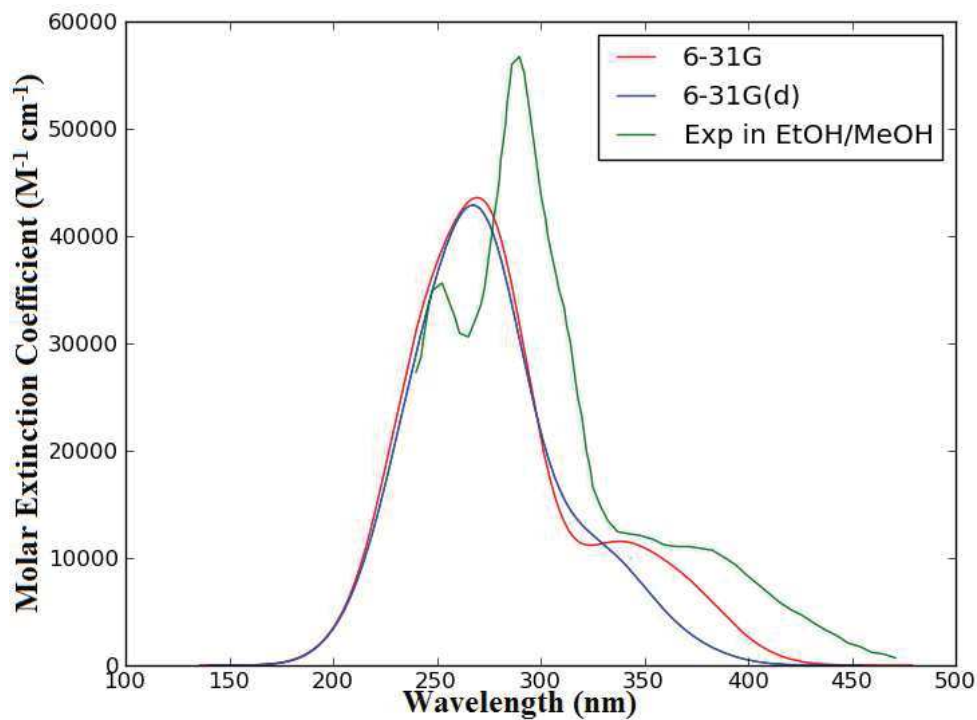
77. Complex (90): $[\text{Ru}(\text{DPAH})_3]^{2+}$

PDOS



Total and partial density of states of $[\text{Ru}(\text{DPAH})_3]^{2+}$ partitioned over Ru d orbitals and ligand C and N p orbitals.

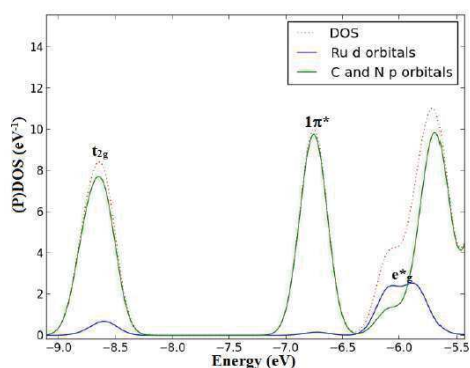
Absorption Spectrum



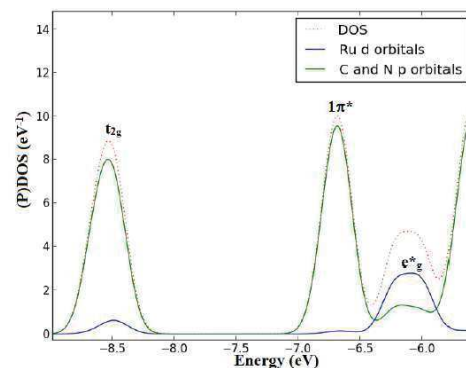
$[\text{Ru}(\text{DPAH})_3]^{2+}$ TD-B3LYP/6-31G, TD-B3LYP/6-31G(d), and experimental spectra. Experimental spectrum measured in a mixture of methanol and ethanol [18].

78. Complex (91): $[\text{Ru}(\text{Azpy})_3]^{2+}$

PDOS



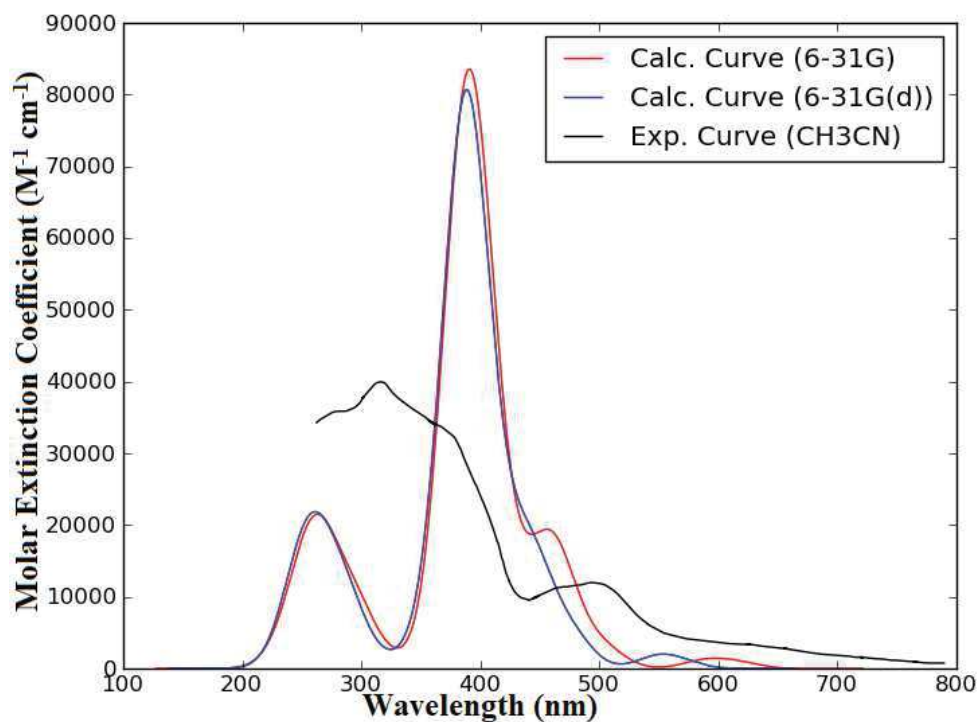
B3LYP/6-31G
 $\epsilon_{\text{HOMO}} = -11.66 \text{ eV}$



B3LYP/6-31G(d)
 $\epsilon_{\text{HOMO}} = -11.67 \text{ eV}$

Total and partial density of states of $[\text{Ru}(\text{Azpy})_3]^{2+}$ partitioned over Ru d orbitals and ligand C and N p orbitals.

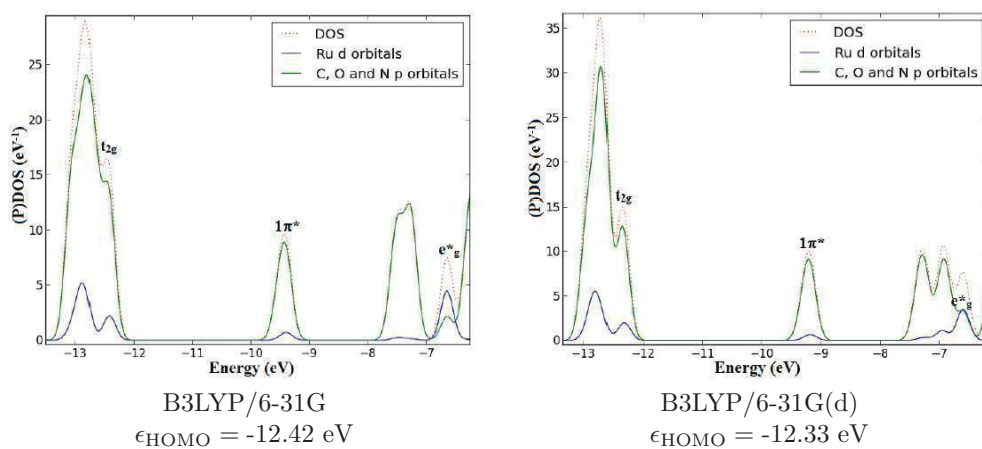
Absorption Spectrum



$[\text{Ru}(\text{Azpy})_3]^{2+}$ TD-B3LYP/6-31G, TD-B3LYP/6-31G(d), and experimental spectra. Experimental spectrum measured in acrylonitrile [16].

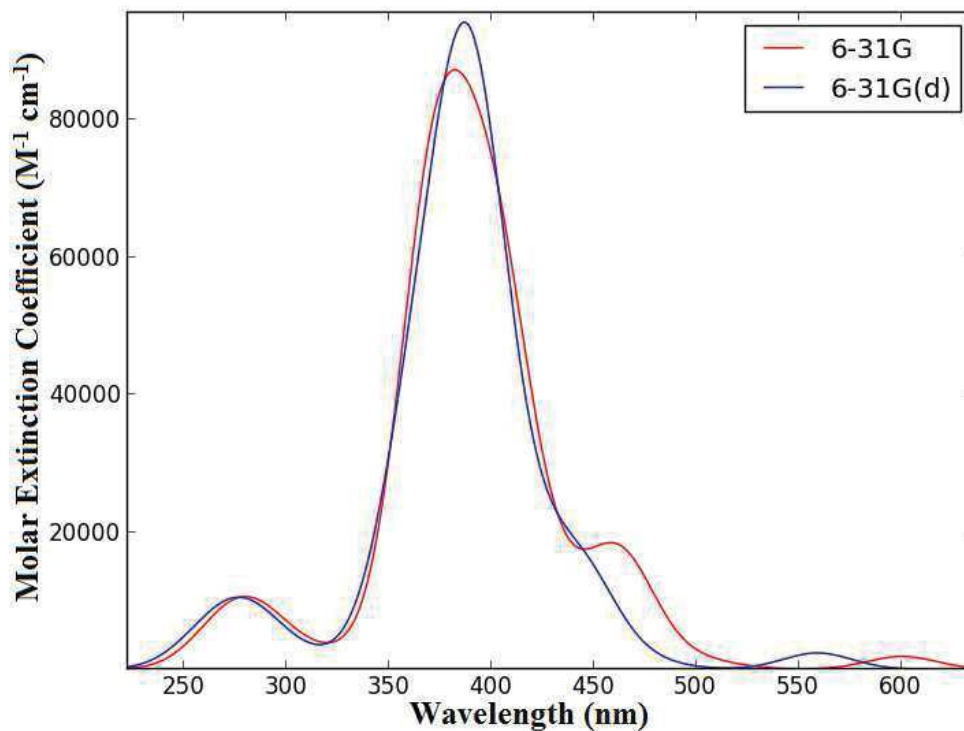
79. Complex (92): $[\text{Ru}(\text{NA})_3]^{2+}$

PDOS



Total and partial density of states of $[\text{Ru}(\text{NA})_3]^{2+}$ partitioned over Ru d orbitals and ligand C, O, and N p orbitals.

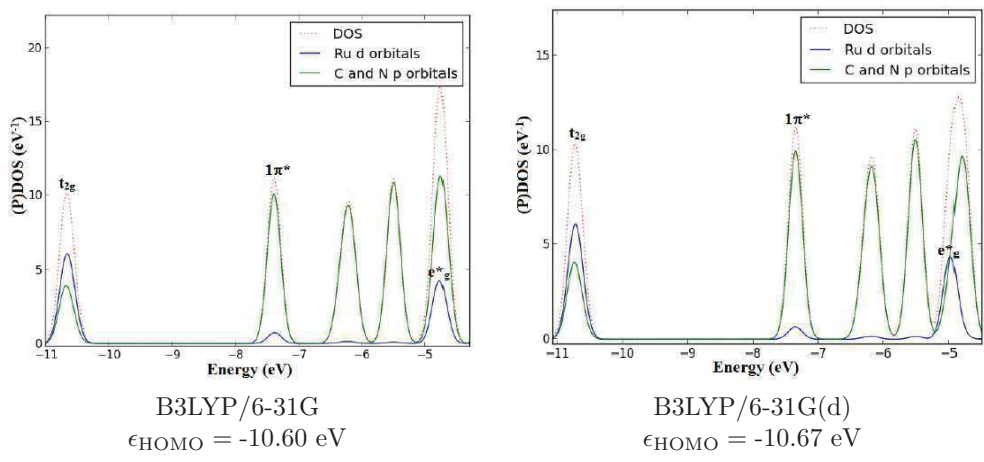
Absorption Spectrum



$[\text{Ru}(\text{NA})_3]^{2+}$ TD-B3LYP/6-31G and TD-B3LYP/6-31G(d) spectra.

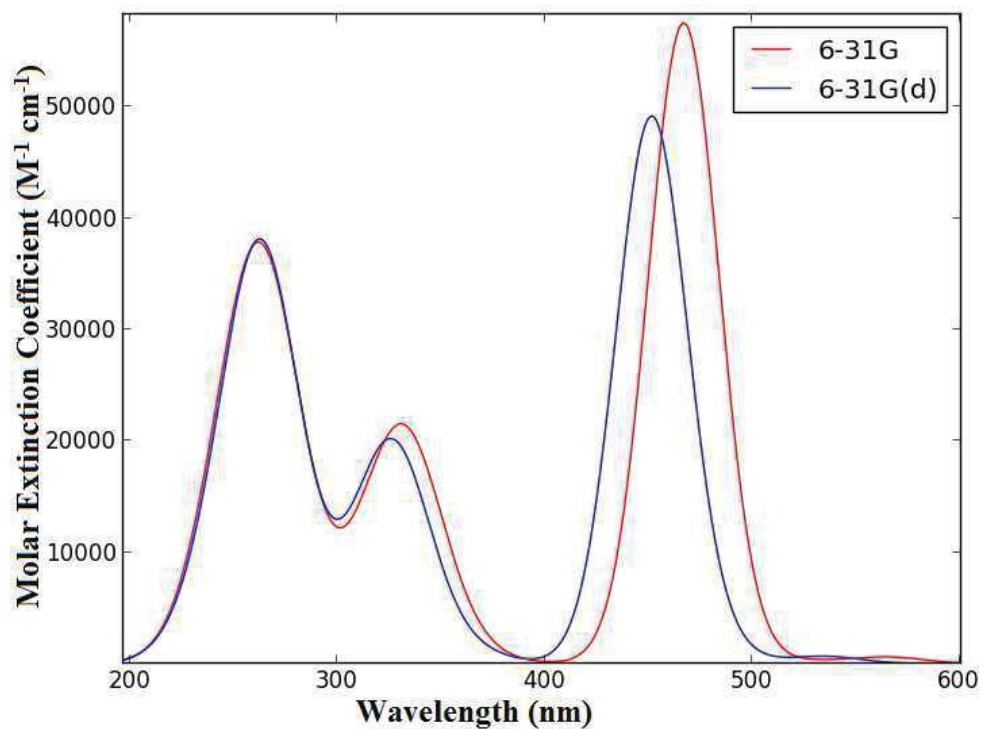
80. Complex (93): $[\text{Ru}(\text{hpiq})_3]^{2+}$

PDOS



Total and partial density of states of $[\text{Ru}(\text{hpiq})_3]^{2+}$ partitioned over Ru d orbitals and ligand C and N p orbitals.

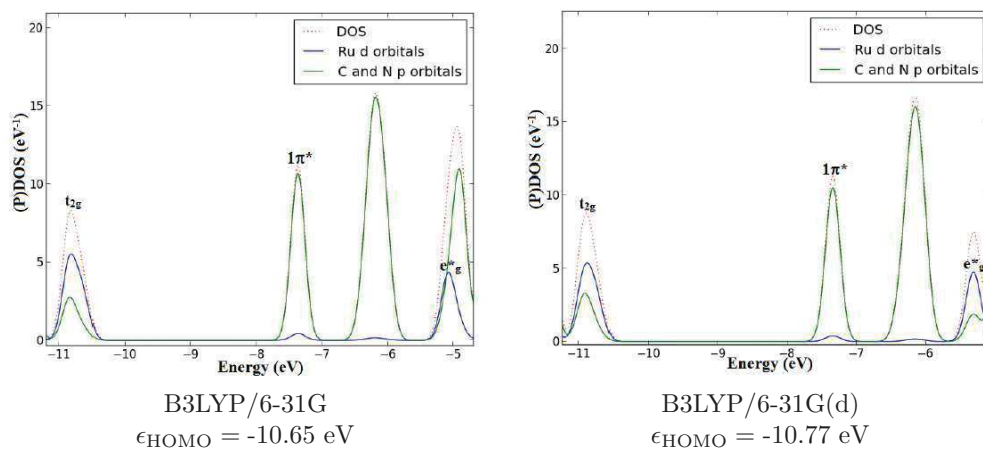
Absorption Spectrum



$[\text{Ru}(\text{hpiq})_3]^{2+}$ TD-B3LYP/6-31G and TD-B3LYP/6-31G(d) spectra.

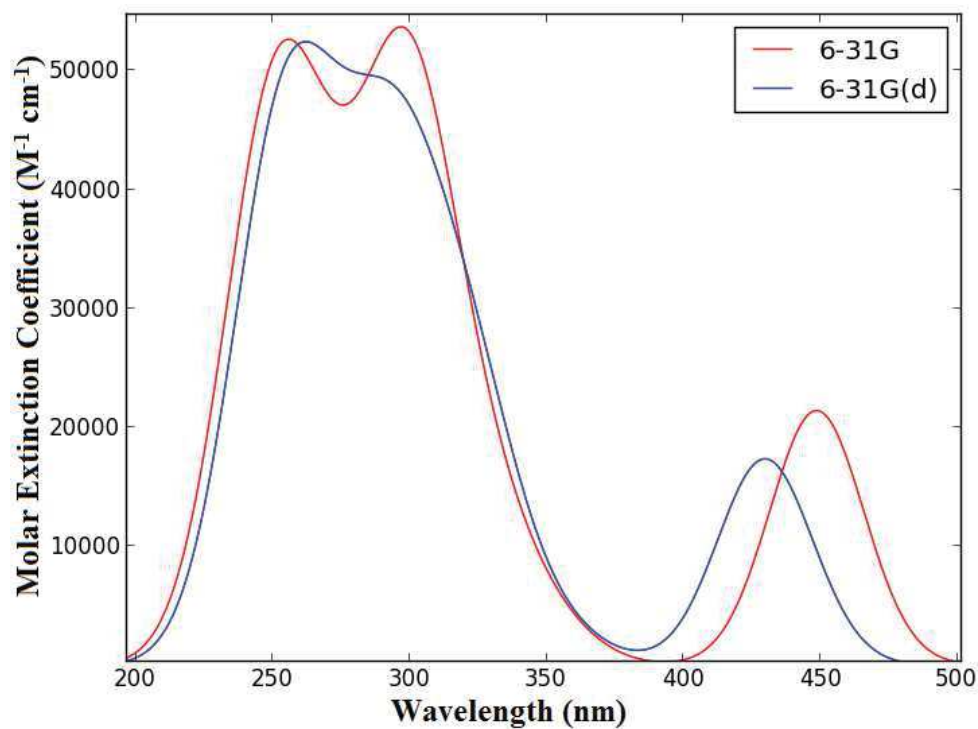
81. Complex (94): $[\text{Ru}(\text{pq})_3]^{2+}$

PDOS



Total and partial density of states of $[\text{Ru}(\text{pq})_3]^{2+}$ partitioned over Ru d orbitals and ligand C and N p orbitals.

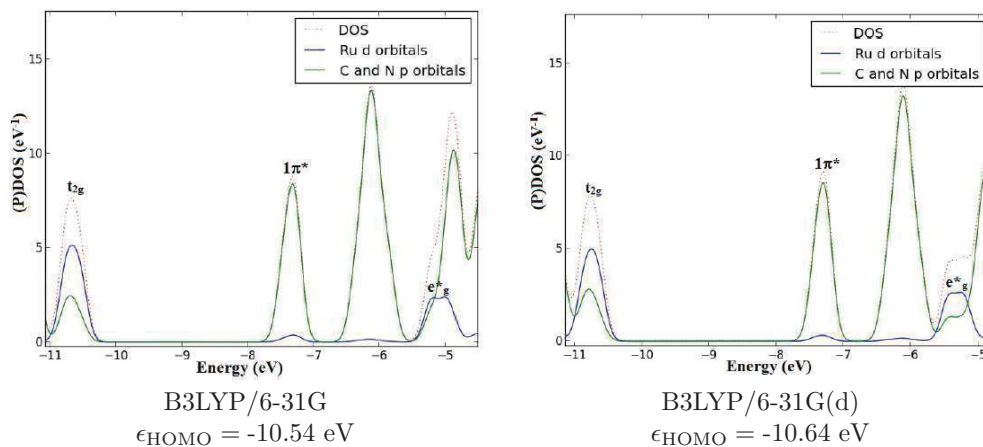
Absorption Spectrum



$[\text{Ru}(\text{pq})_3]^{2+}$ TD-B3LYP/6-31G and TD-B3LYP/6-31G(d) spectra.

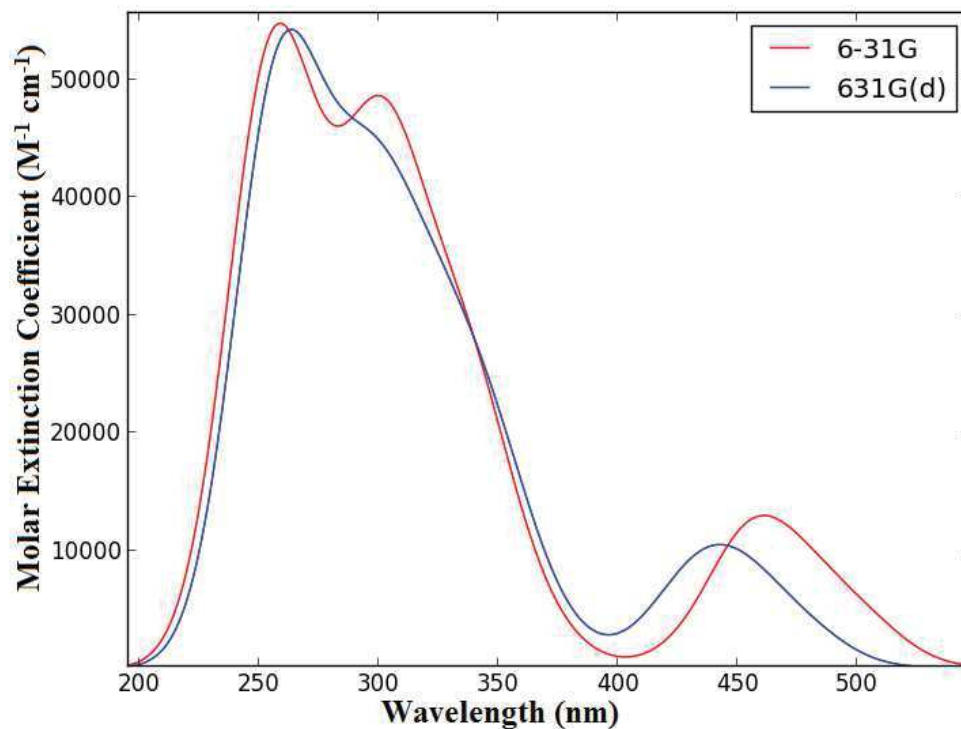
82. Complex (95): $[\text{Ru}(\text{pq})_2(\text{biq})]^{2+}$

PDOS



Total and partial density of states of $[\text{Ru}(\text{pq})_2(\text{biq})]^{2+}$ partitioned over Ru d orbitals and ligand C and N p orbitals.

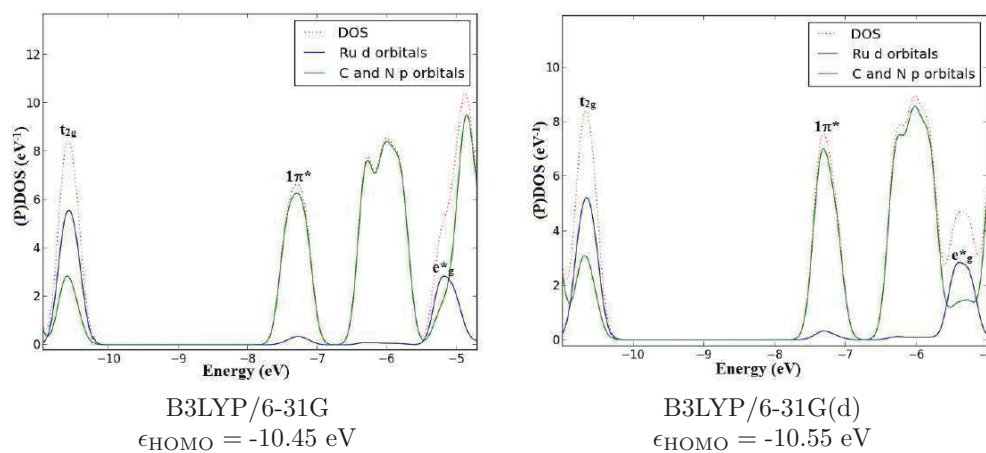
Absorption Spectrum



$[\text{Ru}(\text{pq})_2(\text{biq})]^{2+}$ TD-B3LYP/6-31G and TD-B3LYP/6-31G(d) spectra.

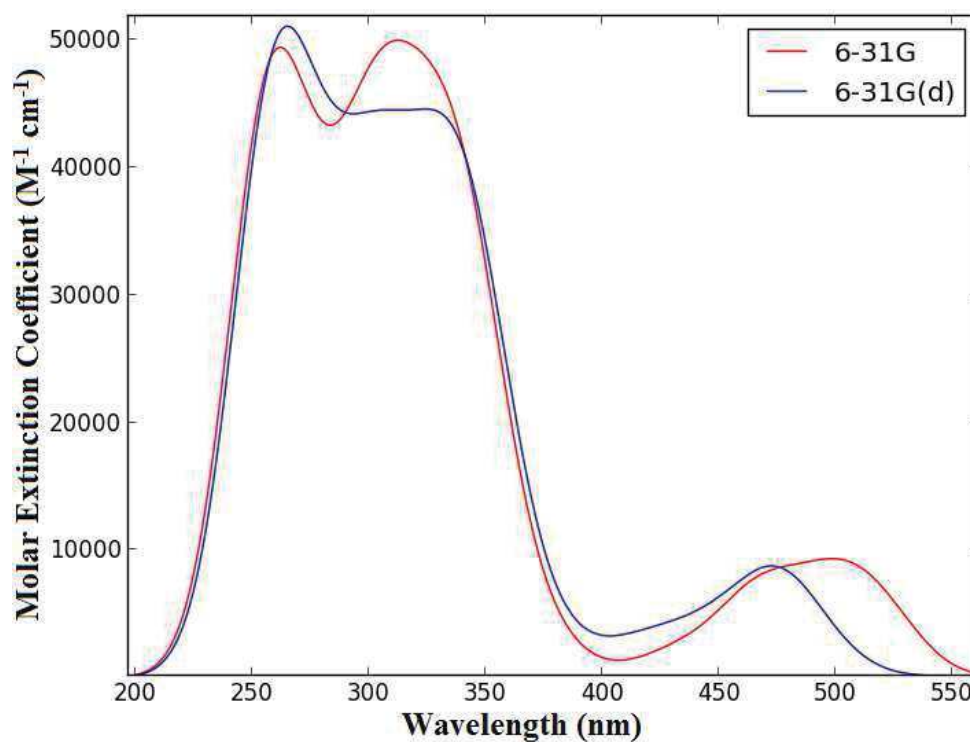
83. Complex (96): $[\text{Ru}(\text{pq})(\text{biq})_2]^{2+}$

PDOS



Total and partial density of states of $[\text{Ru}(\text{pq})(\text{biq})_2]^{2+}$ partitioned over Ru d orbitals and ligand C and N p orbitals.

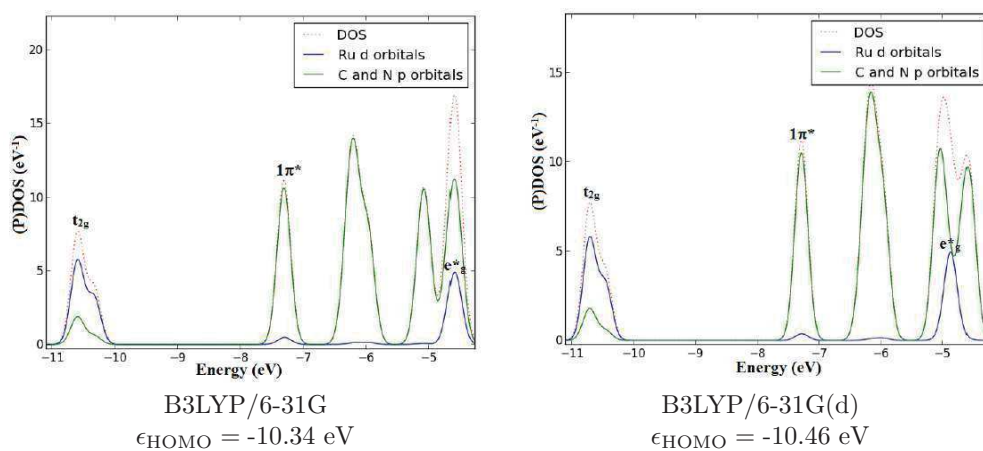
Absorption Spectrum



$[\text{Ru}(\text{pq})(\text{biq})_2]^{2+}$ TD-B3LYP/6-31G and TD-B3LYP/6-31G(d) spectra.

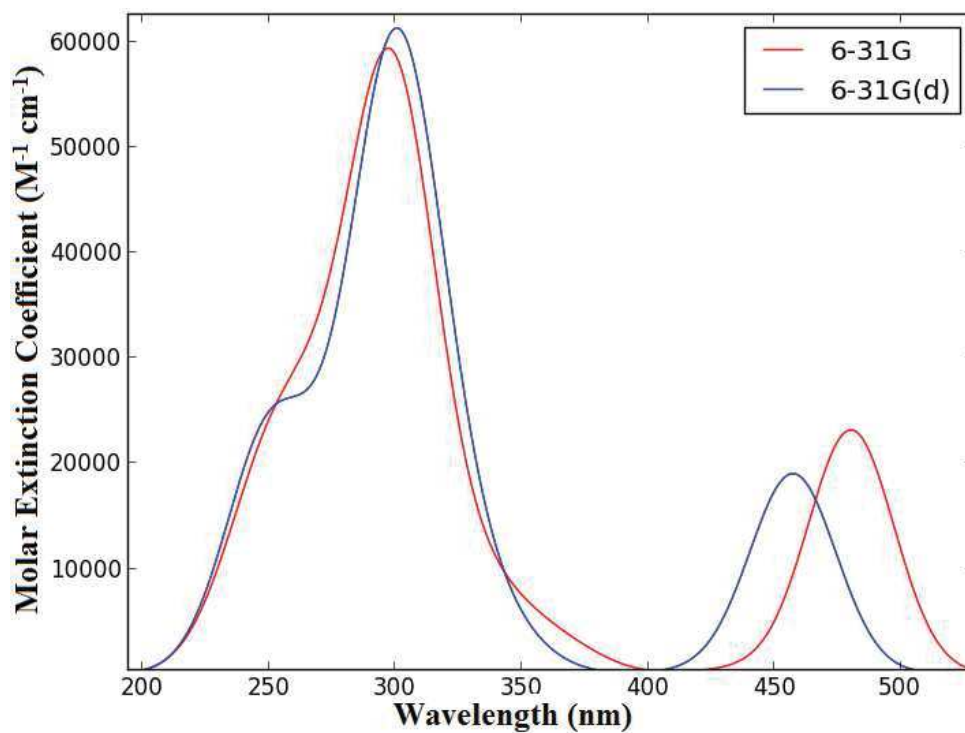
84. Complex (97): $[\text{Ru}(\text{pynapy})_3]^{2+}$

PDOS



Total and partial density of states of $[\text{Ru}(\text{pynapy})_3]^{2+}$ partitioned over Ru d orbitals and ligand C and N p orbitals.

Absorption Spectrum

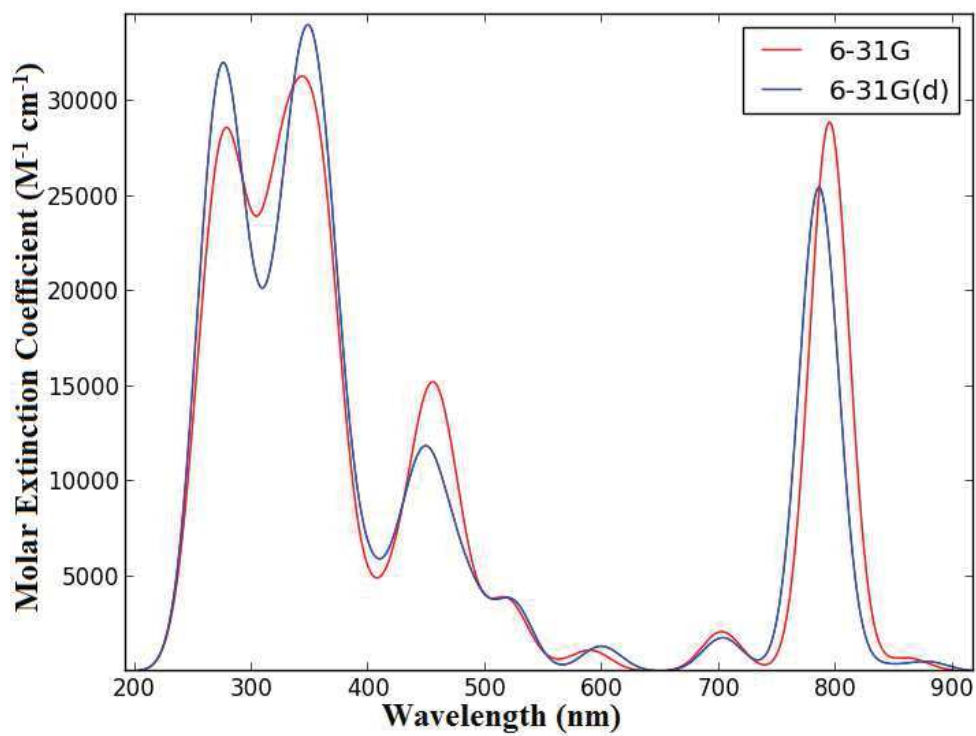


$[\text{Ru}(\text{pynapy})_3]^{2+}$ TD-B3LYP/6-31G and TD-B3LYP/6-31G(d) spectra.

85. Complex (98)[†]: [Ru(DMCH)₂Cl₂]

B3LYP/6-31G B3LYP/6-31G(d)
ε_{HOMO} = -4.36 eV ε_{HOMO} = -4.32 eV

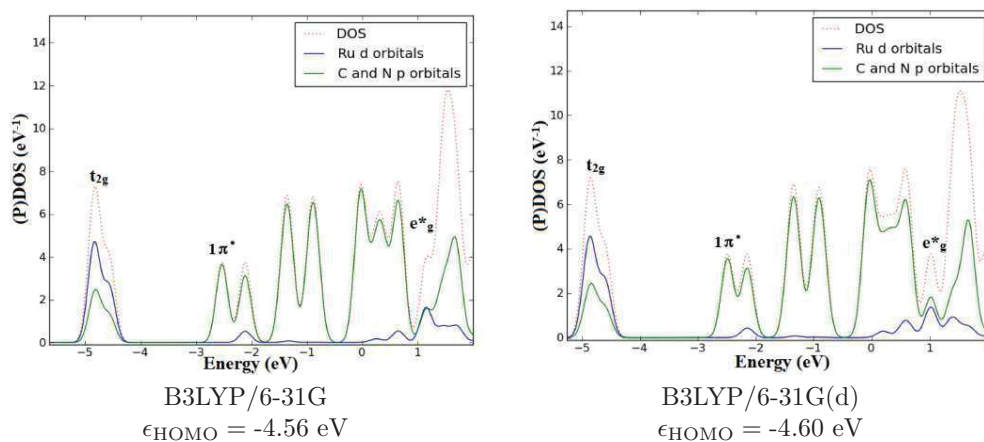
Absorption Spectrum



[Ru(DMCH)₂Cl₂] TD-B3LYP/6-31G and TD-B3LYP/6-31G(d) spectra.

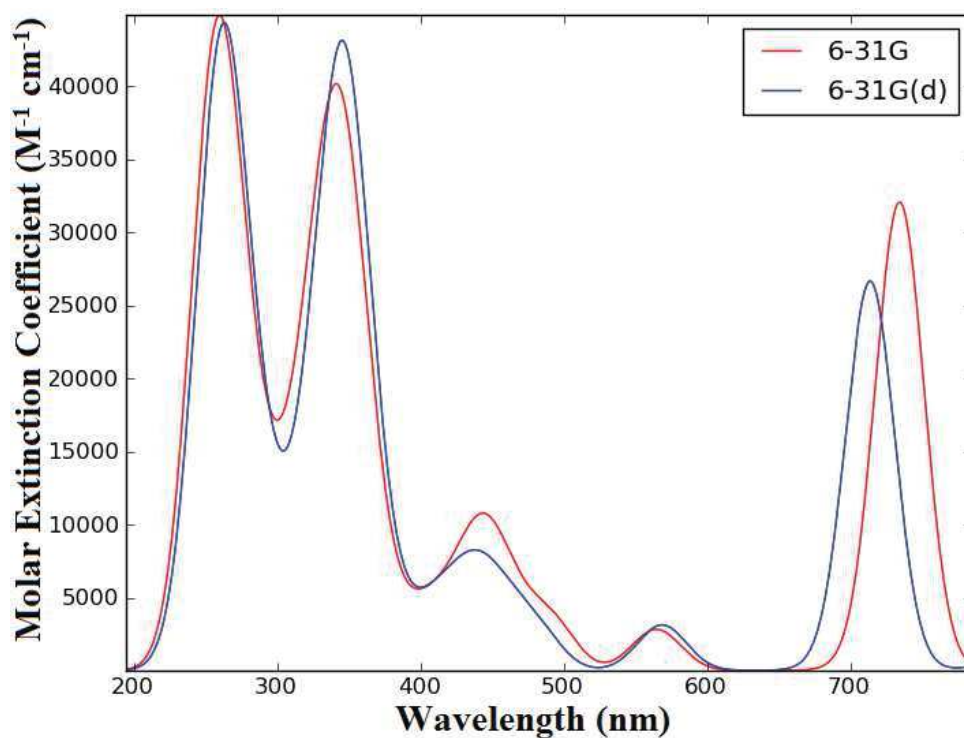
86. Complex (99)*: $[\text{Ru}(\text{DMCH})_2(\text{CN})_2]$

PDOS



Total and partial density of states of $[\text{Ru}(\text{DMCH})_2(\text{CN})_2]$ partitioned over Ru d orbitals and ligand C and N p orbitals.

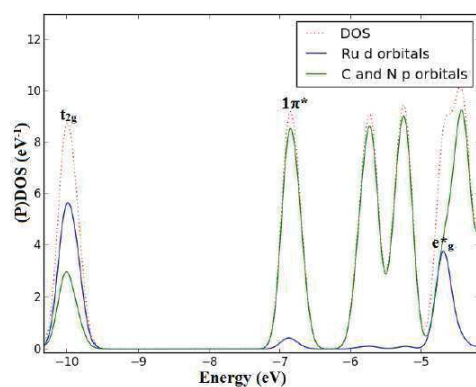
Absorption Spectrum



$[\text{Ru}(\text{DMCH})_2(\text{CN})_2]$ TD-B3LYP/6-31G and TD-B3LYP/6-31G(d) spectra.

87. Complex (100): $[\text{Ru}(\text{DMCH})_3]^{2+}$

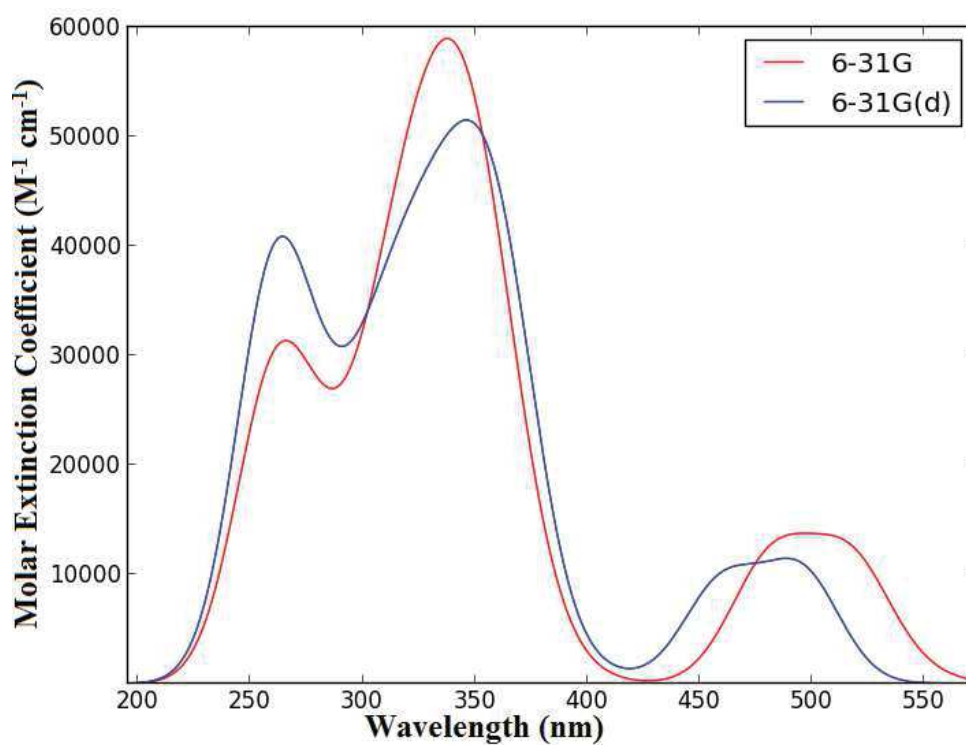
PDOS



6-31G
 $\epsilon_{\text{HOMO}} = -9.87 \text{ eV}$

Total and partial density of states of $[\text{Ru}(\text{DMCH})_3]^{2+}$ partitioned over Ru d orbitals and ligand C and N p orbitals.

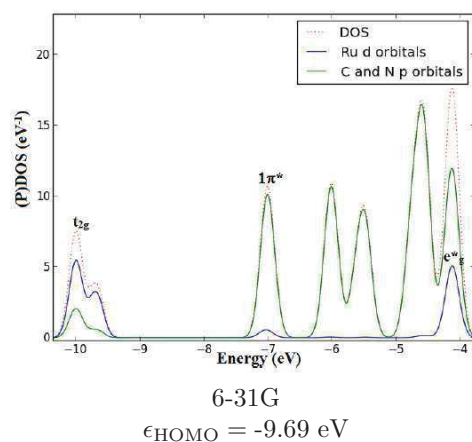
Absorption Spectrum



$[\text{Ru}(\text{DMCH})_3]^{2+}$ TD-B3LYP/6-31G and TD-B3LYP/6-31G(d) spectra.

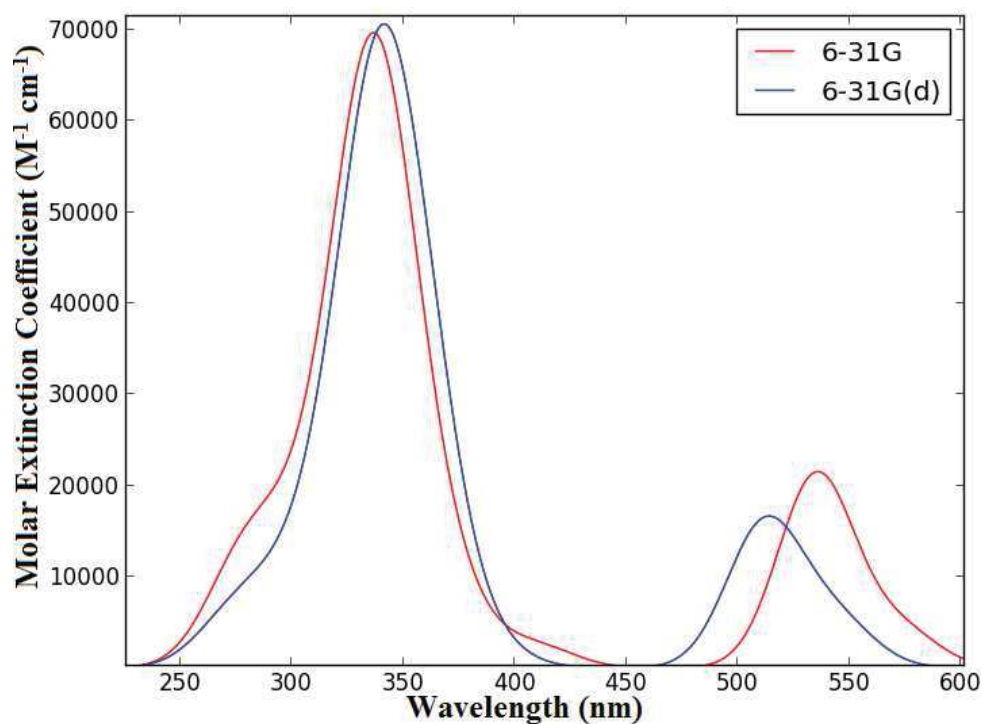
88. Complex (101): $[\text{Ru}(\text{dinapy})_3]^{2+}$

PDOS



Total and partial density of states of $[\text{Ru}(\text{dinapy})_3]^{2+}$ partitioned over Ru d orbitals and ligand C and N p orbitals.

Absorption Spectrum

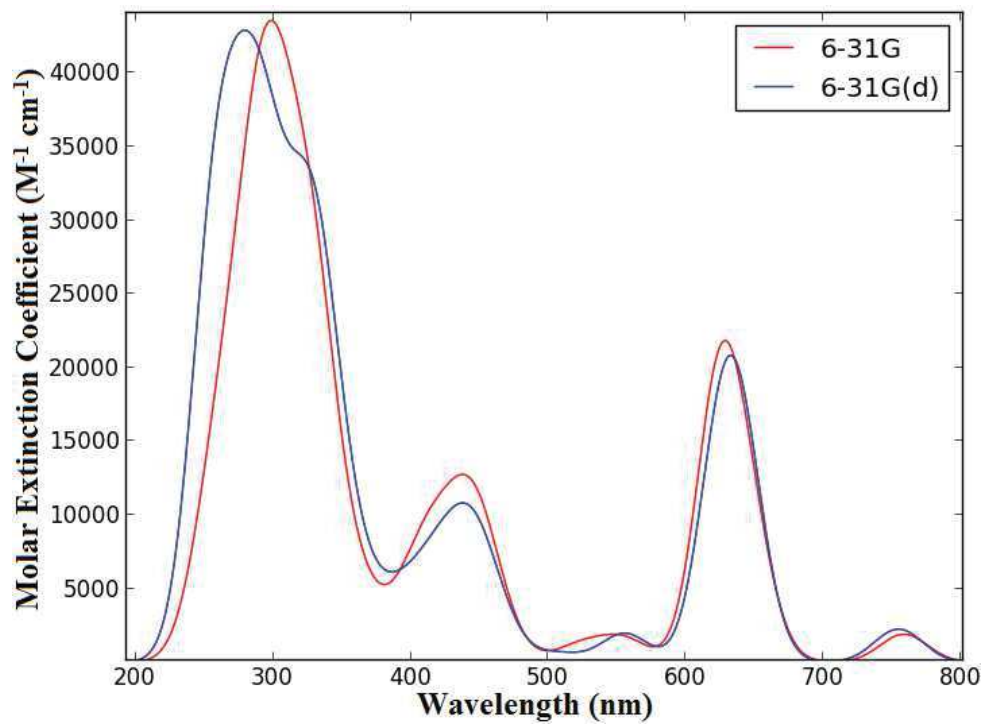


$[\text{Ru}(\text{dinapy})_3]^{2+}$ TD-B3LYP/6-31G and TD-B3LYP/6-31G(d) spectra.

89. Complex (102)[†]: [Ru(biq)₂Cl₂]

B3LYP/6-31G B3LYP/6-31G(d)
ε_{HOMO} = -4.80 eV ε_{HOMO} = -4.74 eV

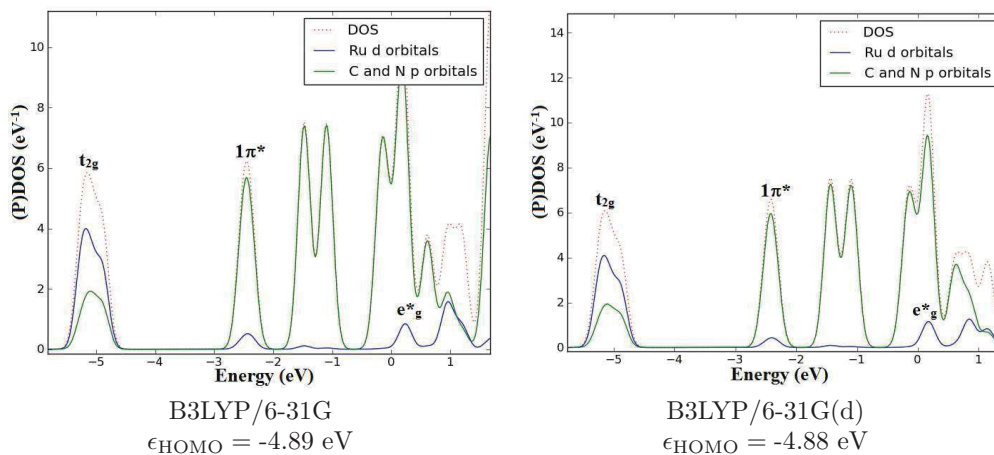
Absorption Spectrum



[Ru(biq)₂Cl₂] TD-B3LYP/6-31G and TD-B3LYP/6-31G(d) spectra.

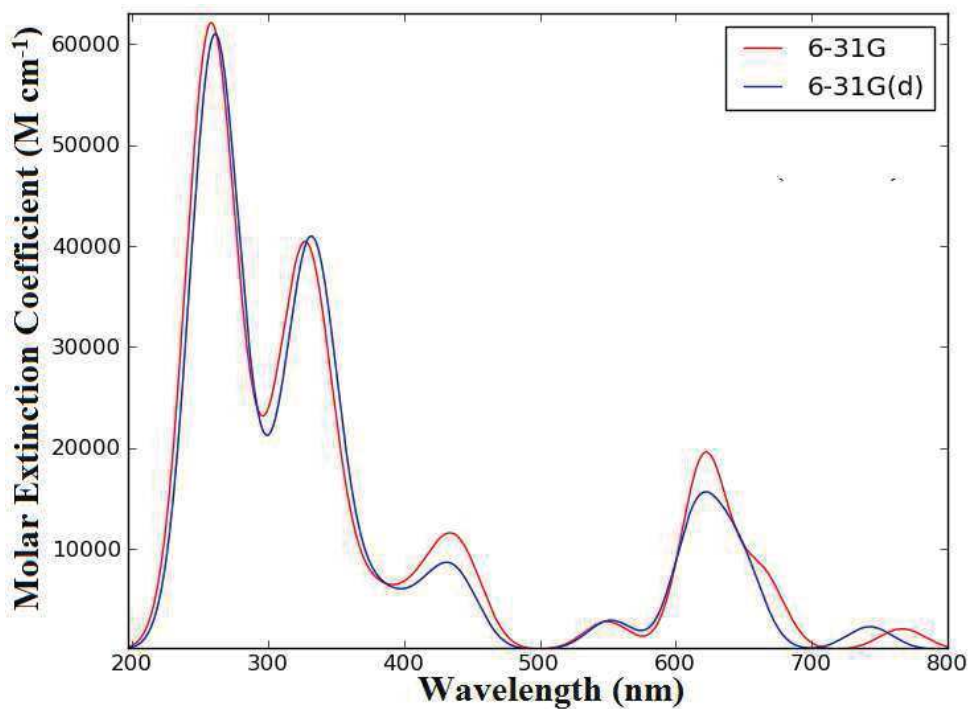
90. Complex (103)*: $[\text{Ru}(\text{biq})_2(\text{CN})_2]$

PDOS



Total and partial density of states of $[\text{Ru}(\text{biq})_2(\text{CN})_2]$ partitioned over Ru d orbitals and ligand C and N p orbitals.

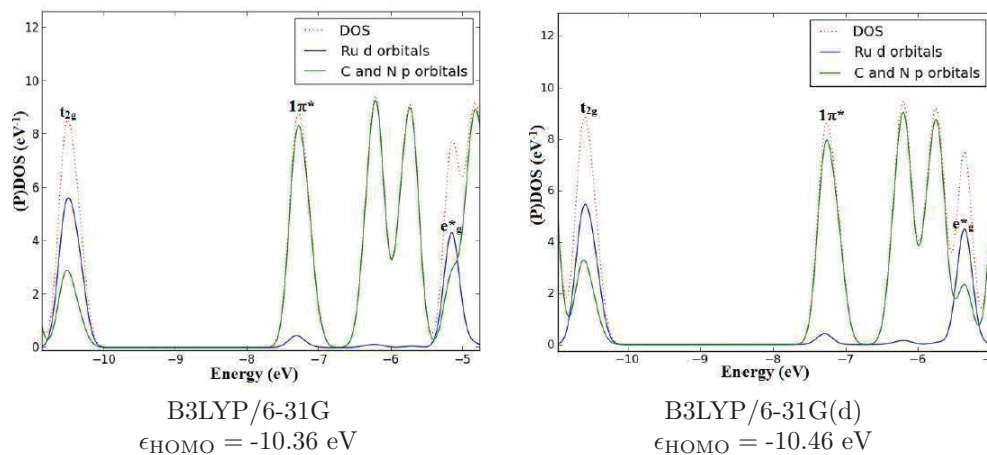
Absorption Spectrum



$[\text{Ru}(\text{biq})_2(\text{CN})_2]$ TD-B3LYP/6-31G and TD-B3LYP/6-31G(d) spectra.

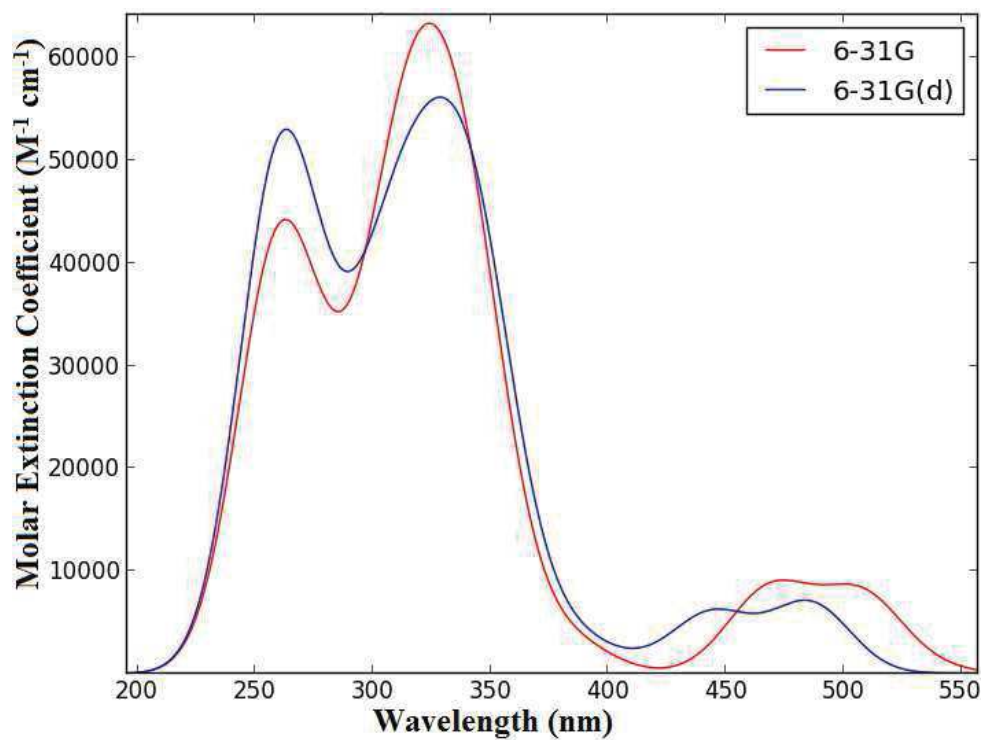
91. Complex (104): $[\text{Ru}(\text{biq})_3]^{2+}$

PDOS



Total and partial density of states of $[\text{Ru}(\text{biq})_3]^{2+}$ partitioned over Ru d orbitals and ligand C and N p orbitals.

Absorption Spectrum

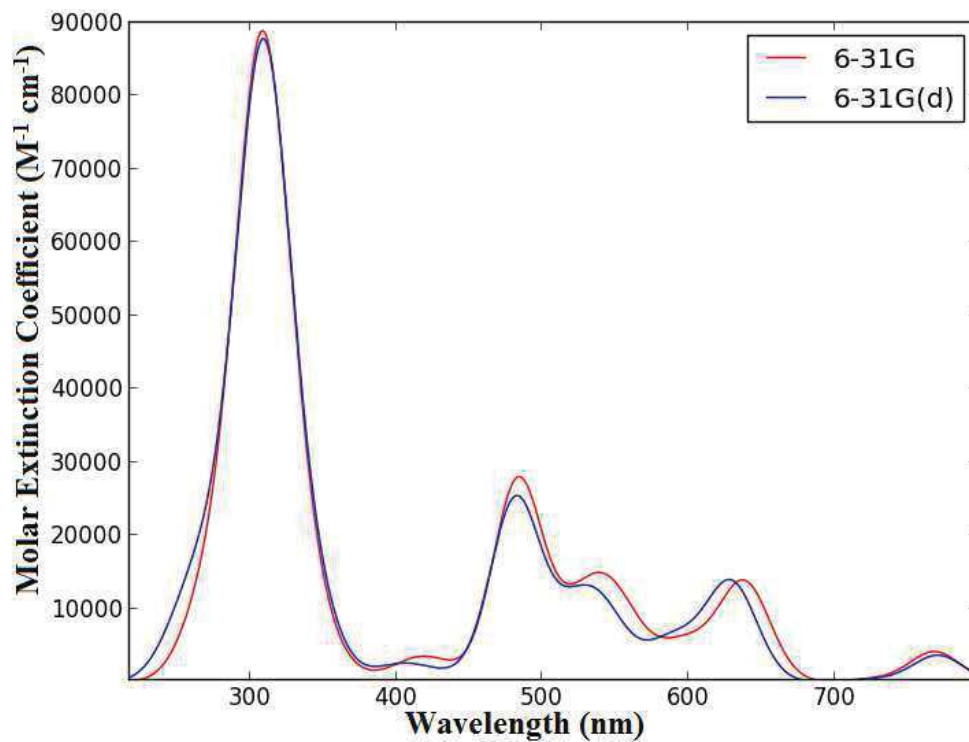


$[\text{Ru}(\text{biq})_3]^{2+}$ TD-B3LYP/6-31G and TD-B3LYP/6-31G(d) spectra.

92. Complex (105)[†]: [Ru(i-biq)₂Cl₂]

B3LYP/6-31G B3LYP/6-31G(d)
 $\epsilon_{\text{HOMO}} = -4.30 \text{ eV}$ $\epsilon_{\text{HOMO}} = -4.27 \text{ eV}$

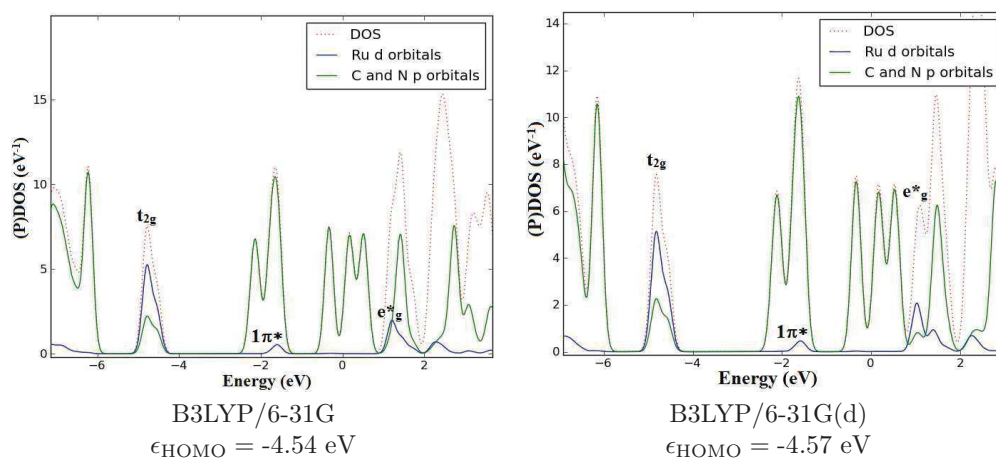
Absorption Spectrum



[Ru(i-biq)₂Cl₂] TD-B3LYP/6-31G and TD-B3LYP/6-31G(d) spectra.

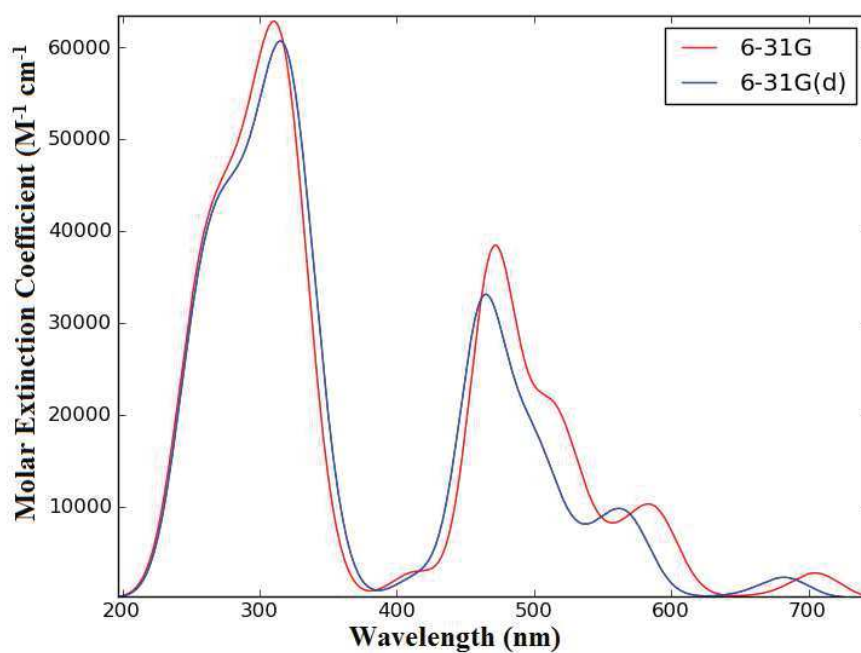
93. Complex (106)*: $[\text{Ru}(\text{i-biq})_2(\text{CN})_2]$

PDOS



Total and partial density of states of $[\text{Ru}(\text{i-biq})_2(\text{CN})_2]$ partitioned over Ru d orbitals and ligand C and N p orbitals.

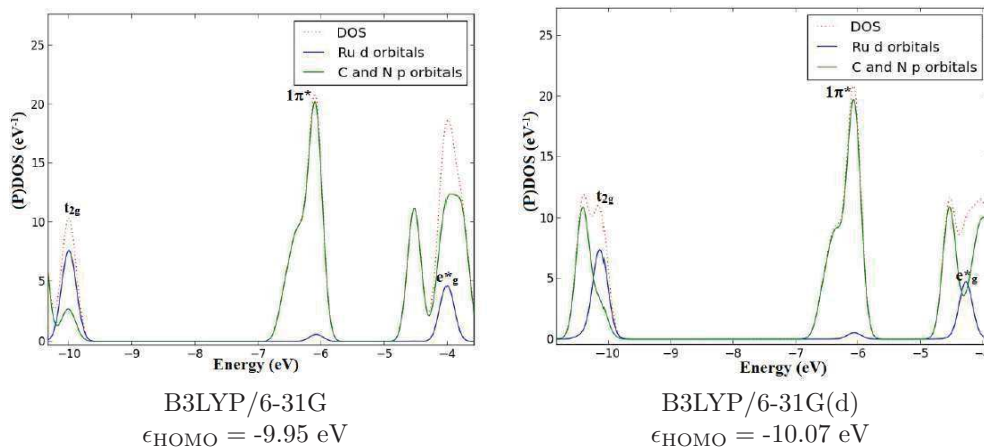
Absorption Spectrum



$[\text{Ru}(\text{i-biq})_2(\text{CN})_2]$ TD-B3LYP/6-31G and TD-B3LYP/6-31G(d) spectra.

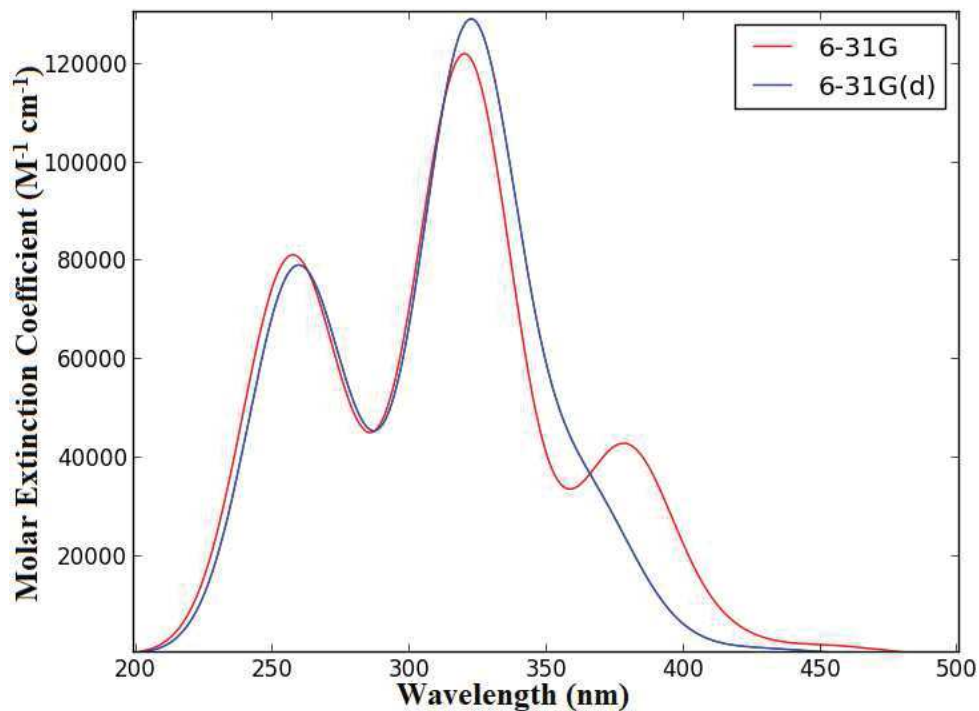
94. Complex (107): $[\text{Ru}(\text{i-biq})_3]^{2+}$

PDOS



Total and partial density of states of $[\text{Ru}(\text{i-biq})_3]^{2+}$ partitioned over Ru d orbitals and ligand C and N p orbitals.

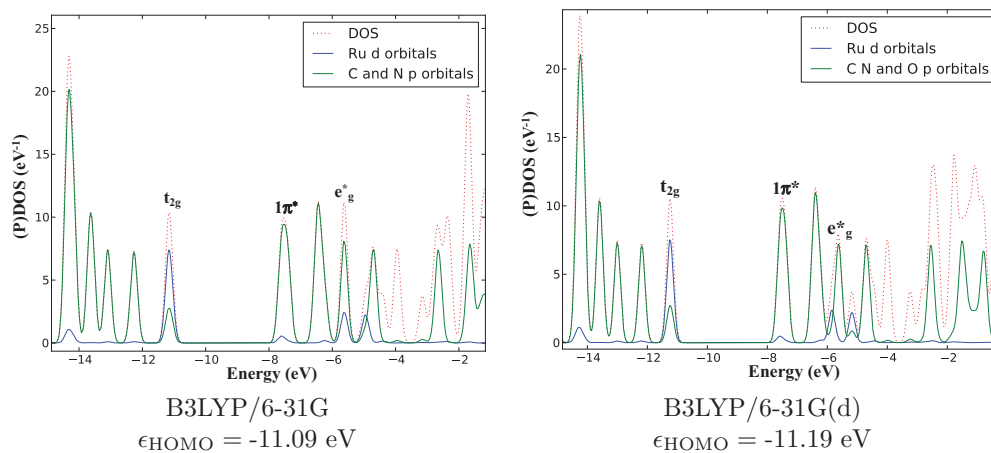
Absorption Spectrum



$[\text{Ru}(\text{i-biq})_3]^{2+}$ TD-B3LYP/6-31G and TD-B3LYP/6-31G(d) spectra.

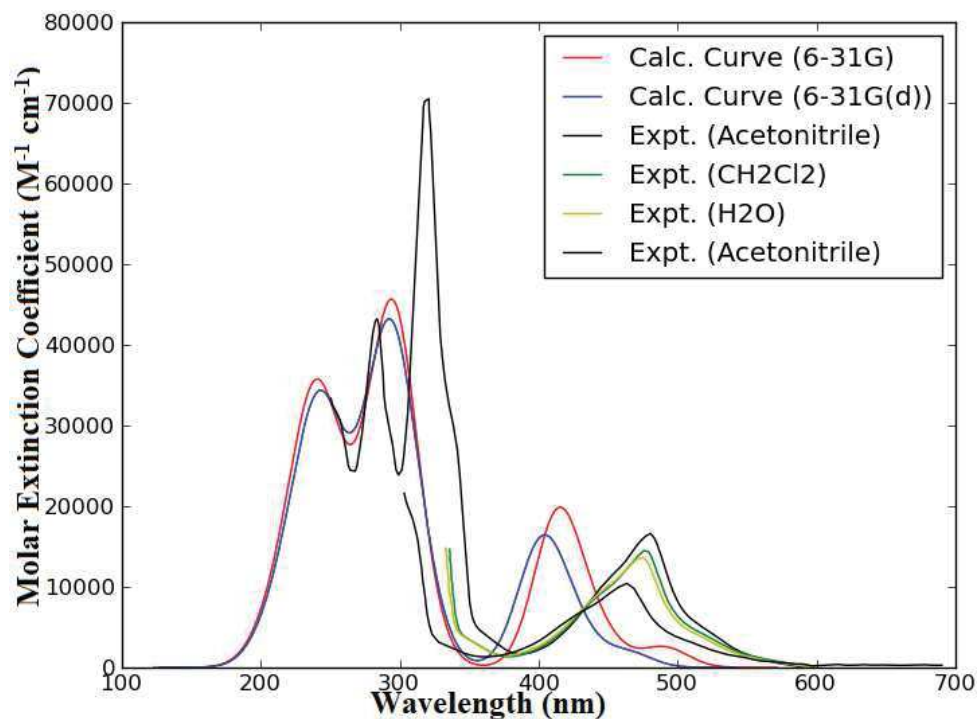
95. Complex (108): $[\text{Ru}(\text{trpy})_2]^{2+}$

PDOS



Total and partial density of states of $[\text{Ru}(\text{trpy})_2]^{2+}$ partitioned over Ru d orbitals and ligand C and N p orbitals.

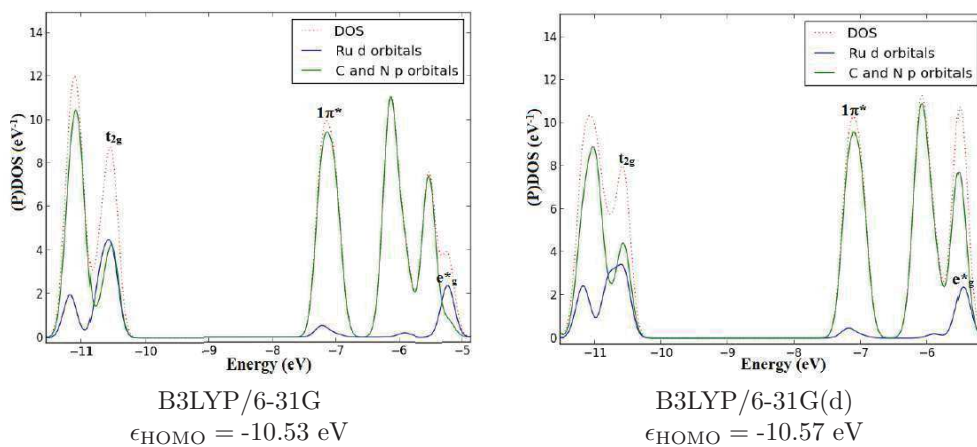
Absorption Spectrum



$[\text{Ru}(\text{trpy})_2]^{2+}$ TD-B3LYP/6-31G, TD-B3LYP/6-31G(d), and experimental spectra. Experimental spectra measured at 294K in acetone[19, 20] and at 298K in water (H_2O) and dichloromethane (CH_2Cl_2)[21].

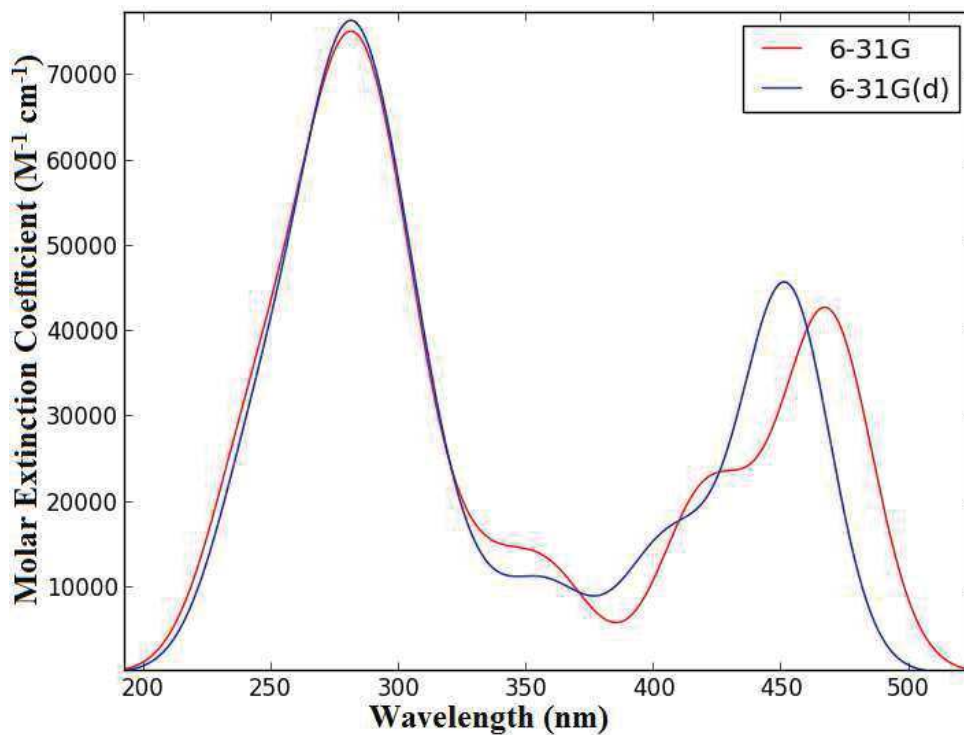
96. Complex (109): $[\text{Ru}(\text{tro})_2]^{2+}$

PDOS



Total and partial density of states of $[\text{Ru}(\text{tro})_2]^{2+}$ partitioned over Ru d orbitals and ligand C and N p orbitals.

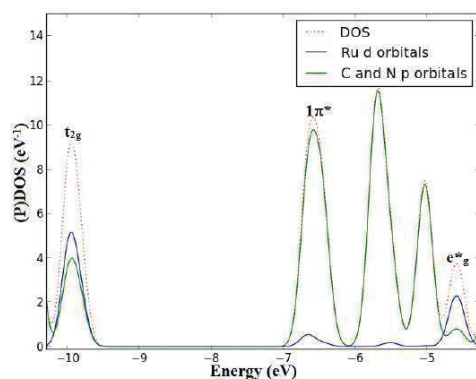
Absorption Spectrum



$[\text{Ru}(\text{tro})_2]^{2+}$ TD-B3LYP/6-31G and TD-B3LYP/6-31G(d) spectra.

97. Complex (110): $[\text{Ru}(\text{tsite})_2]^{2+}$

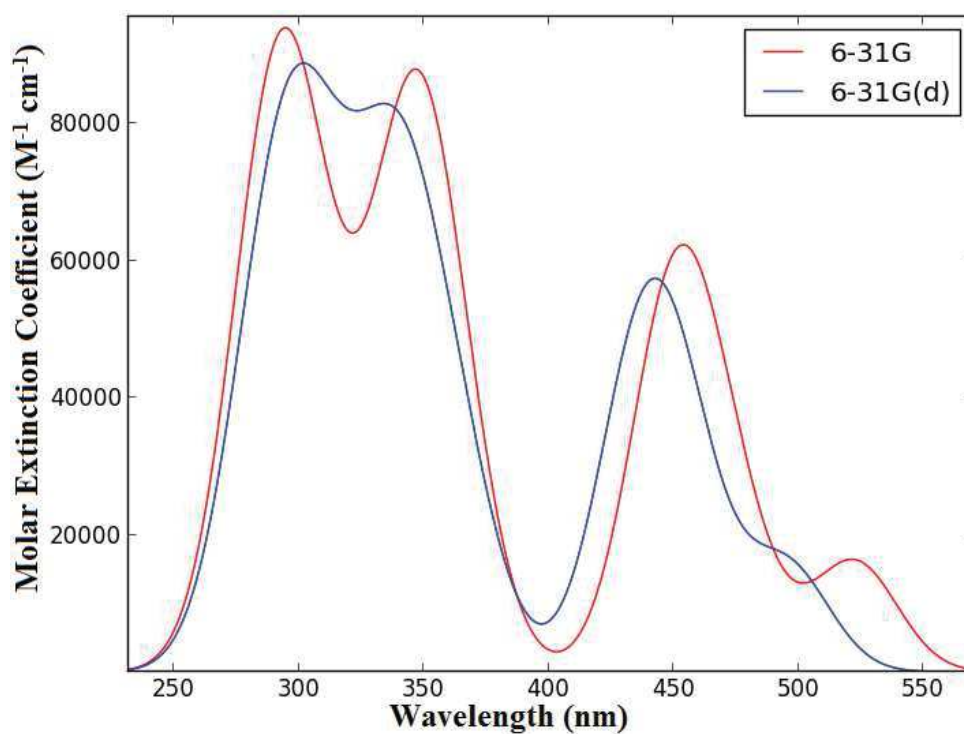
PDOS



6-31G
 $\epsilon_{\text{HOMO}} = -9.84 \text{ eV}$

Total and partial density of states of $[\text{Ru}(\text{tsite})_2]^{2+}$ partitioned over Ru d orbitals and ligand C and N p orbitals.

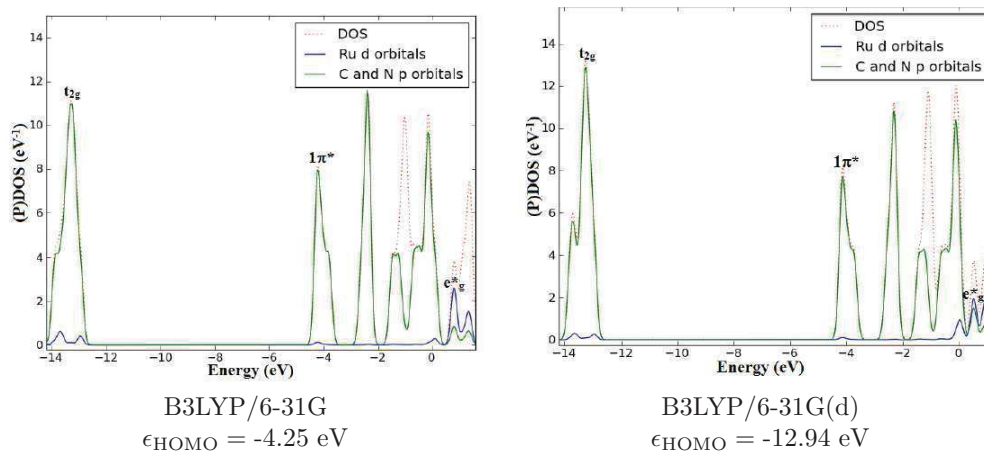
Absorption Spectrum



$[\text{Ru}(\text{tsite})_2]^{2+}$ TD-B3LYP/6-31G and TD-B3LYP/6-31G(d) spectra.

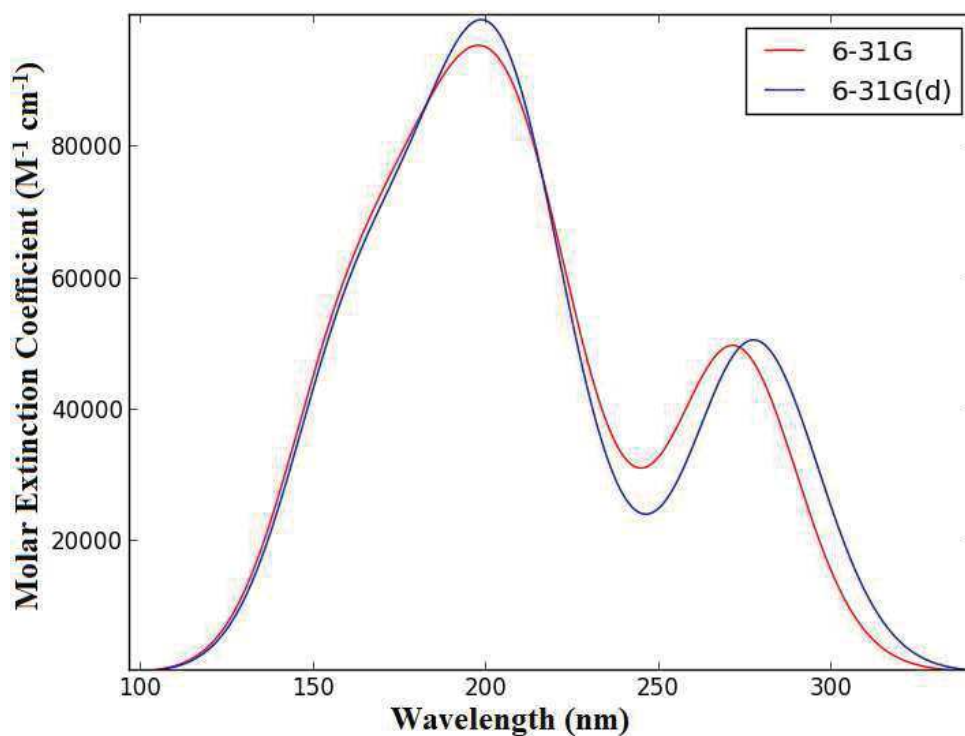
98. Complex (111)*: $[\text{Ru}(\text{dqp})_2]^{2+}$

PDOS



Total and partial density of states of $[\text{Ru}(\text{dqp})_2]^{2+}$ partitioned over Ru d orbitals and ligand C and N p orbitals.

Absorption Spectrum



$[\text{Ru}(\text{dqp})_2]^{2+}$ TD-B3LYP/6-31G and TD-B3LYP/6-31G(d) spectra.

REFERENCES

References

- [1] J. Gu, J. Chen, and R. H. Schmehl, Using intramolecular energy transfer to transform nonphotoactive, visible-light-absorbing chromophores into sensitizers for photoredox reactions, *J. Am. Chem. Soc.* **132**, 7338 (2010).
- [2] L. Fodor, G. Lendvai, and A. Horváth, Solvent Dependence of Absorption and Emission of Ru(bpy)₂(CN)₂: Experiment and Explanation Based on Electronic Structure Theory, *J. Phys. Chem. A* **111**, 12891 (2007).
- [3] H. Yersin, W. Humbs, and J. Strasser, Low-lying electronic states of [Rh(bpy)₃]³⁺, [Pt(bpy)₂]²⁺, and [Ru(bpy)₃]²⁺. A comparative study based on highly resolved and time-resolved spectra, *Coord. Chem. Rev.* **159**, 325 (1997).
- [4] B. Sullivan et al., Multiple emissions from charge transfer excited states of ruthenium (II) polypyridine complexes, *Chem. Phys. Lett.* **58**, 389 (1978).
- [5] D. P. Rillema, G. Allen, T. J. Meyer, and D. Conrad, Redox properties of ruthenium (II) tris chelate complexes containing the ligands 2, 2'-bipyrazine, 2, 2'-bipyridine, and 2, 2'-bipyrimidine, *Inorg. Chem.* **22**, 1617 (1983).
- [6] N. Yoshikawa et al., Transition states of the ³ MLCT to ³ MC conversion in Ru (bpy)₂(phen derivative)²⁺ complexes, *J. Mol. Struct.* **1094**, 98 (2015).
- [7] W. B. Heuer et al., Reaction of Ru^{II} Diazafluorenone Compound with Nanocrystalline TiO₂ Thin Film, *Inorg. Chem.* **49**, 7726 (2010).
- [8] E. Borfecchia et al., X-ray transient absorption structural characterization of the ³MLCT triplet excited state of *cis*-[Ru(bpy)₂(py)₂]²⁺, *Dalton Trans.* **42**, 6564 (2013).
- [9] Z. Z. Li, Y. L. Niu, H. Y. Zhou, H. Y. Chao, and B. H. Ye, Visible-Light-Induced Photooxidation of Ruthenium(II) Complex with 2,2-Biimidazole-like Ligand by Singlet Oxygen, *Inorg. Chem.* **52**, 10087 (2013).
- [10] C. D. Tait, T. M. Vess, M. K. McArmond, K. W. Hanck, and D. W. Wertz, Characterizations of the redox orbitals of mixed-ligand 2,2'-bipyridine-2-(2'-pyridyl)quinoline ruthenium(II) complexes, *J. Chem. Soc., Dalton Trans.* **1987**, 2467 (1987).
- [11] A. A. Cadranel, P. Albores, S. Yamazaki, V. D. Klieman, and L. M. Baraldo, Efficient energy transfer via the cyanide bridge in dinuclear complexes containing Ru(II) polypyridine moieties, *Dalton Trans.* **41**, 5343 (2012).
- [12] Q. Sun et al., Experimental Evidence of Ultrafast Quenching of the ³MLCT Luminescence in Ruthenium(II) Tris-bipyridyl Complexes via a ³dd State, *J. Am. Chem. Soc.* **135**, 13660 (2013).
- [13] R. H. Fabian, D. M. Klassen, and R. W. Sonntag, Synthesis and spectroscopic characterization of ruthenium and osmium complexes with sterically hindering ligands. 3. Tris complexes with methyl- and dimethyl-substituted 2,2'-bipyridine and 1,10-phenanthroline, *Inorg. Chem.* **19**, 1977 (1980).
- [14] B. Maubert, N. D. McClenaghan, M. T. Indelli, and S. Campagna, Absorption spectra and photophysical properties of a series of polypyridine ligands containing appended pyrenyl and anthryl chromophores and of their ruthenium(II) complexes, *J. Phys. Chem. A* **107**, 447 (2003).
- [15] M. Schwalbe et al., Synthesis and characterisation of poly(bipyridine)ruthenium complexes as building blocks for hetero-supramolecular arrays, *Euro. J. Inorg. Chem.* **2008**, 3310 (2008).
- [16] N. Leventis et al., Synthesis and Characterization of Ru(II) Tris(1,10-phenanthroline)-Electron Acceptor Dyads Incorporating the 4-Benzoyl-*N*-methylpyridinium Cation or *N*-Benzyl-*N*-methyl Viologen. Improving the Dynamic Range, Sensitivity, and Response Time of Sol-Gel-Based Optical Oxygen Sensors, *Chem. Mater.* **16**, 1493 (2004).
- [17] E. Wachter, D. K. Heidary, B. S. Howerton, S. Parkin, and E. C. Glazer, Light-activated ruthenium complexes photo bind DNA and are cytotoxic in the photodynamic therapy window, *Chem. Commun.* **48**, 9649 (2012).
- [18] D. P. Segers and M. K. DeArmond, Emission studies of transition-metal complexes of 2,2'-dipyridylamine. 2. Tris complexes of ruthenium(II), *J. Phys. Chem.* **86**, 3768 (1982).
- [19] J. T. Hewitt, P. J. Vallett, and N. H. Damrauer, Dynamics of the 3MLCT in Ru(II) Terpyridyl Complexes Probed by Ultrafast Spectroscopy: Evidence of Excited-State Equilibration and Interligand Electron Transfer, *J. Phys. Chem. A* **116**, 11536 (2012).
- [20] J. Sauvage et al., Ruthenium(II) and Osmium(II) bis(terpyridine) complexes in covalently-linked multicomponent systems: Synthesis, electrochemical behavior, absorption spectra, and photochemical and photophysical properties, *Chem. Rev.* **94**, 993 (1994).
- [21] E. Jakubikova et al., Electronic Structure and Spectroscopy of [Ru(tpy)₂]²⁺, [Ru(tpy)(bpy)(H₂O)]²⁺, and [Ru(tpy)(bpy)(Cl)]⁺, *Inorg. Chem.* **48**, 10720 (2009).

Appendix B

Curriculum Vitae

Denis MAGERO

PERSONAL DATA

PLACE AND DATE OF BIRTH: Kenya | 4 April 1986
ADDRESS: 152-30200, Kitale, Kenya
PHONE: +254 724737454
EMAIL: magerode@gmail.com

PROFILE

A self-driven, result oriented, time conscious and ambitious chemist with the ability to implement administrative management controls. Extensive knowledge of research methodologies and always ready to embrace and incorporate new ideas.

CAREER OBJECTIVE

To employ my skills in transforming my environment to be responsive to the everyday needs of our society through teamwork, innovation, and tenacity.

RESEARCH INTERESTS

Inorganic and Physical Chemistry (Computational Chemistry) as well as experimental work. Simulation and study of energy storage materials using *ab-initio* methods and other new materials that may contribute to the improvement of energy efficiency. Currently, material science is also an area of interest.

EDUCATION

AUG. 2014 to December 2017 **Ph.D (MOLECULAR AND STRUCTURAL CHEMISTRY) at Grenoble Alps University (France).**

Thesis: “Partial Density of States Ligand Field Theory (PDOS-LFT): Recovering a LFT-Like Picture and Application to Photoproperties of Ruthenium Polypyridine Complexes.”

| Thesis Directors: Prof. Mark E. Casida, Prof. Lusweti Kituyi, Prof. Amolo George and Dr. Makau Nicholas.

SEPT. 2010 to DEC. 2013 **Master of Science degree (M.Sc) in Chemistry (Physical Chemistry) at the University of Eldoret.**

Thesis: “ab-initio Studies of Magnesium Hydride and Lithium Hydride for Hydrogen Storage Applications: A Density Functional Theory Study.”

| Supervisors: Prof. Lusweti Kituyi, Prof. Amolo George, Dr. Makau Nicholas and Dr. Cleophas Wawire Muhavini.

- JULY 2009 **Environmental Impact Assessment and Environmental Audit Course at Moi University.**
Registered with National Environment Management Authority (NEMA) as an associate expert.
Expert in environmental impact assessment and auditing.
Have done several environmental impact assessments and environmental audits.
- AUG. 2005 to MAY 2009 **Bachelor of Science in Chemistry at Moi University.**
Final Grade: **Second Class Honors Upper Division.**
Project Title: “Study of Atmospheric Pollution Levels by Trace Elements: Analysis of Tree Bark, Roots and Leaves.” | Advisor: Prof. Pius Kipkemboi.
- FEB. 2000 to Nov. 2003 **Kenya Certificate of Secondary Education (K.C.S.E) at Friends’ School Kamusinga, Kimilili.**
Final Grade: **Mean Grade B+.**
- JAN. 1992 to Nov. 1999 **Kenya Certificate of Primary Education (K.C.P.E) at Nzoia Sugar Company Primary School, Bungoma.**
Final Grade: **548/700 Marks.**

WORK EXPERIENCE

Current
FROM SEP. 2017

Chemistry lecturer at ALUPE UNIVERSITY COLLEGE
School of Science, Department of Chemistry and Biochemistry

Current
FROM JAN. 2014

Part time lecturer at UNIVERSITY OF ELDORET
Taught in the School of Science in the Department of Chemistry and Biochemistry and in the School of Education in the Department of Center for teacher education. Courses taught are listed below:

ESC 100: Fundamentals of Chemistry

The purpose of this course is to introduce learners to the basic theories and concepts of atomic structure and discussion leading to the development of chemical bonding.

ESC 111: Introduction to Kinetics and Thermodynamics

This is a first year course that introduces learners to basic concepts of physical chemistry focusing on kinetics and thermodynamics.

CHEM 210: Atomic Structure and Bonding

The purpose of this course is to introduce learners to the basic principles and concepts of quantum numbers and bonding theories.

CHEM 213: Basic Thermodynamics and Chemical Kinetics

This course introduces learners to basis of thermodynamics including the 0th, 1st and 2nd laws of thermodynamics, thermodynamics, chemical equilibria and chemical kinetics.

ESC 313: Surface and Colloid Chemistry

The course deals with the 2nd law of thermodynamics, surface chemistry of solids, thermodynamics and equilibria and adsorption isotherms.

ESC 200: Bonding and Structure

	<p>The purpose of this course is to introduce learners to the basic principles and concepts of quantum numbers and bonding theories.</p> <p>ESC 301/CHEM 317: Electrochemistry The course introduces learners to the principles of electrochemistry.</p> <p>ANC 310: Computer Applications in Analytical Chemistry This course intends to introduce learners to the basic concepts of Computational Chemistry.</p> <p>ESC 211: Chemical Thermodynamics and Phase Equilibria The course builds up on basic thermodynamics and introduces the aspects of phase equilibria.</p> <p>ESC 414: Industrial Chemistry The course brings in fundamental ideas and implications of industry chemistry and the various processes involved in the industry.</p>
<p><i>Current</i> FROM AUG. 2010</p>	<p>Part time lecturer at ELDORET NATIONAL POLYTECHNIC Teaching in the department of health sciences pharmacy students; physical, inorganic and analytical chemistry. Administering and preparing students for various practical work including the Kenya National Examinations (KNEC). Achieved 100% pass in Chemistry practicals as well as an improved mean score in the successive years.</p>
<p>SEPT. - DEC. 2016</p>	<p>Tutorial Assistant - UNIVERSITÉ GRENOBLE ALPES, FRANCE CHI 131: Cristallographie https://sites.google.com/site/markcasida/home/chem-110 Taught and administered practicals in crystallography to the CHI 131 International students in France.</p>
<p>OCT. - DEC. 2015</p>	<p>Tutorial Assistant - UNIVERSITÉ GRENOBLE ALPES, FRANCE CHI 110: Crystal Structure https://sites.google.com/site/markcasida/home/chem-110 Taught and administered practicals in crystallography to the CHI 110 International students in France.</p>
<p>OCT. - NOV. 2013</p>	<p>Research Assistant - KENYA EDUCATION NETWORK (KENET) for University of Eldoret KENET Universities E-readiness project Conducted 37 interviews with members of staff of University of Eldoret. Recruited and supervised 10 students to collect data from students. Reviewed questionnaires for accuracy and completeness.</p>
<p>JAN. - AUG. 2010</p>	<p>Pharmaceutical representative at PAN PHARMACEUTICALS, NAIROBI Underwent a 1 month training of pharmaceutical products. Involved in sales and marketing in the Kisumu, Siaya, Kericho, Bondo and Kakamega region.</p>
<p>JUN. - DEC. 2009</p>	<p>Quality control analyst at MENENGAI OIL REFINERIES, NAKURU Analyzing of crude oil, analyzing of refined oil, water quality analysis and water treatment.</p>
<p>JUN. - AUG. 2008</p>	<p>Quality control analyst at INK PRINT AND COATINGS LIMITED, NAIROBI</p>

ORAL PRESENTATIONS

1. Fuzzy Molecular Orbital Theory: Luminescence in Ruthenium Polypyridine Complexes. Presented to the Special Interest Group (SIG) on Computational Modelling and Materials Science (CMMS) at the Masinde Muliro University of Science and Technology, Kakamega on 6th July, 2017.
2. Electrochemical and Photochemical Studies of Some Remarkable Ruthenium and Iridium Complexes. Presented to the comité de suivie de these at the Université Grenoble Alpes, France on 25th November, 2016.
3. Long lived excited lifetime or not? Molecular orbital indices for Ru complexes and other transition metal complexes. Presented at Andreas Hauser's group at the University of Geneva, Switzerland on 16th November, 2015.
4. Electrochemical and Photochemical Studies of Some Remarkable Ruthenium and Iron Complexes. Presented at the Laboratoire Chimie Théorique (LCT) meeting seminar in Grenoble, France on 25th September, 2015.
5. Electrochemical and Photochemical Studies of Some Remarkable Ruthenium and Iron Complexes. Presented to the Computational Material Science Group at the University of Eldoret on 30th April, 2015.
6. Electrochemical and Photochemical Studies of Some Remarkable Ruthenium and Iron Complexes. Presented at the 3rd African School on Electronic Structure Methods and Applications (ASESMA 2015) in Johannesburg, South Africa on 30th January, 2015.
7. Electrochemical and Photochemical Studies of Some Remarkable Ruthenium and Iron Complexes. Presented at the Laboratoire Chimie Théorique (LCT) meeting seminar in Grenoble, France on 5th December, 2014.
8. *ab-initio* studies of Magnesium hydride and Lithium hydride for hydrogen storage applications: A density functional study. Presented to the Chimie Théorique seminar in Grenoble, France on Friday 24th October, 2014.
9. Magero D., Makau N. W., Amolo G. O., Lutta S., Okoth M. D. O., Mwabora J. M., Musembi R. J., Maghanga, C. M., and Gateru R. Hydrogen as an alternative fuel: An *ab-initio* study of Lithium Hydride and Magnesium Hydride. 1st Young Scientist Material Science and Solar Energy Network for Eastern and Southern Africa (MSSEESA), Conference on Material Science and Solar Cell Technology. United Kenya Club, Nairobi, 28th to 29th November, 2013.
10. Magero Denis, Makau Nicholas, Amolo George and Lusweti Kituyi. Materials for the hydrogen storage economy: Lithium Hydride and Magnesium Hydride. The 2nd Science, Technology and Innovation week organized by the National Commission for Science, technology and innovation, Kenyatta International Conference Centre (K.I.C.C) Nairobi, 13th to 17th May, 2013.
11. Magero Denis, Makau Nicholas, Amolo George and Lusweti Kituyi. *ab-initio* studies of Lithium Hydride and Magnesium Hydride for hydrogen storage applications. The Nanotechnology and Materials Science Conference, Kenyatta University, 18th to 20th July, 2012.
12. Materials for the hydrogen storage economy: Lithium Hydride and Magnesium Hydride. Presented at the 2nd African School on Electronic Structure Methods and Applications

(ASESMA 2012) at the University of Eldoret, on 7th June, 2012.

CONFERENCES AND SCHOOLS ATTENDED

1. **Computational Modeling and Materials Science (CMMS) Workshop.**
Masinde Muliro University of Science and Technology, Kakamega. 6-7th July, 2017.
2. **The 4th African School on Electronic Structure Methods and Applications (ASESMA 2016).**
University of Ghana, Accra, GHANA. 13-24th June, 2016.
3. **The 3rd African School on Electronic Structure Methods and Applications (ASESMA 2015).**
University of the Witwatersrand, Johannesburg, SOUTH AFRICA. 19-30th Jan, 2015.
4. **The 2nd Science, Technology and Innovation week organized by the National Commission for Science, technology and innovation.**
Kenyatta International Conference Centre (K.I.C.C) Nairobi, 13th to 17th May, 2013.
5. **The 1st Young Scientist Material Science and Solar Energy Network for Eastern and Southern Africa (MSSEESA), Conference on Material Science and Solar Cell Technology.**
United Kenya Club, Nairobi, 28th to 29th November, 2013.
6. **Quantum Espresso and Quantum Monte Carlo Workshop.**
Chepkoilel University College (Moi University), KENYA. February, 2012.
7. **The 2nd African School on Electronic Structure Methods and Applications (ASESMA 2012).**
Chepkoilel University College (Moi University), KENYA. 28th May to 8th June, 2012.
8. **Nanotechnology and Materials Science Conference.**
Kenyatta University, KENYA. 18th July to 20th July, 2012.
9. **School on Numerical Methods for Materials Science Related to Renewable Energy Applications.**
International Centre for Theoretical Physics, Trieste, ITALY. 26th to 30th November, 2012.

PROFESSIONAL COURSES

Attended the FRENCH NATIONAL THEORETICAL CHEMISTRY LABEL COURSE in Lyon, France. These are additional courses offered to Masters students in Chemistry which allows them to add to their Master's diploma that they have taken courses in Theoretical Chemistry. For doctoral students, this is a convenient way to add breadth and fill in gaps.

Invited to attend the European Summer School in Quantum Chemistry (<http://www.esqc.org/>) in Sicily, Italy that covers a wide number of topics in quantum chemistry.

INVITED TALKS

Guest lecturer at the forth African School on Electronic Structure Methods and Applications (ASESMA2016) which was held from 13th to 24th June 2016 at the University of Ghana in Accra Ghana.

Guest lecturer at the third African School on Electronic Structure Methods and Applications (ASESMA2015) which was held from 18th to 31st January 2015 at the University of the Witwatersrand (Wits) in Johannesburg South Africa.

PUBLICATIONS

Magero Denis, Lusweti Kituyi, Makau Nicholas and Amolo George. Materials for the Hydrogen Energy Economy: Magnesium Hydride (MgH₂) and Lithium Hydride (LiH).

Kenya J. Sci. Tech. Inn. Vol 5(2015): 95-103.

Denis Magero, Mark E. Casida, George Amolo, Nicholas Makau and Lusweti Kituyi. Partial Density of States Ligand Field Theory (PDOS-LFT): Recovering a LFT-Like Picture and Application to Photoproperties of Ruthenium Polypyridine Complexes.

J. Photoch. Photobio. A, Volume 348, 2017, Pages 305-325, <https://doi.org/10.1016/j.jphotochem.2017.07.037>.

In Preparation

Mark. E Casida, Hemanadhan Myneni, Ala M. H. H. Aldin Darghouth and Denis Magero. Challenge of Time-dependent Density Functional Theory for Photochemistry. *Review Article*.

CONFERENCE PAPERS

1. Magero Denis, Makau Nicholas, Amolo George and Lusweti Kituyi. *ab-initio* studies of Lithium Hydride and Magnesium Hydride for hydrogen storage applications. The Nanotechnology and Materials Science Conference, Kenyatta University, 18th to 20th July, 2012.
2. Magero Denis, Lusweti Kituyi, Makau Nicholas and Amolo George. Materials for the Hydrogen Energy Economy: Magnesium Hydride (MgH₂) and Lithium Hydride (LiH). The Second National Science, Technology and Innovation Week, 13th -17th May 2013.
3. Magero D., Makau N. W., Amolo G. O., Lutta S., Okoth M. D. O., Mwabora J. M., Musembi R. J., Maghanga, C. M., and Gateru R. Hydrogen as an alternative fuel: An *ab-initio* study of Lithium Hydride and Magnesium Hydride. 1st Young Scientist Material Science and Solar Energy Network for Eastern and Southern Africa (MSSEESA), Conference on Material Science and Solar Cell Technology. United Kenya Club, Nairobi, 28th to 29th November, 2013.

AWARDS AND SCHOLARSHIPS

AUGUST 2014 French Embassy in Kenya scholarship for Doctoral studies in France.

APRIL 2012 National Commission for Science, Technology and Innovation (NACOSTI) grant for my masters research.
Grant number: NCST/ST&I/RCD/4th CALL M.Sc/149.

JUNE 2017 The African School on Electronic and Structure Methods (ASESMA) travel funds. Facilitated the attendance of the European Summer School in Quantum Chemistry in Sicily, Italy.

MEMBERSHIPS OF PROFESSIONAL AFFILIATIONS

National Environmental Management Authority (NEMA), registered as an associate expert.

Glob' Alps Association (France)- Association for Ph.D scholars in France.

LEADERSHIP AND SERVICE

- Current* | Coordinator, Department of Chemistry and Biochemistry at Alupe University College.
- Current* | Academic Advisor for Alupe University students at Alupe University College.
- Current* | Member, Strategic Planning Committee at Alupe University College.
- Current* | Member, Tendering and evaluation committee at Alupe University College.
- Current* | Member, Library advisory committee at Alupe University College.
- 2011/2012* | Finance Director, UNIVERSITY OF ELDORET GRADUATE STUDENTS' ORGANIZATION at University of Eldoret.
- 2008/2009* | Chairman, CHEMICAL ASSOCIATION OF MOI UNIVERSITY.
Treasurer, CATHOLIC STUDENTS ASSOCIATION.
- 2007/2008* | Project coordinator, CHEMICAL ASSOCIATION OF MOI UNIVERSITY.
Pioneers of the Green Chemistry Day (aimed towards environmental conservation).
- 2002-2003* | Senior Prefect (House Captain) at FRIENDS' SCHOOL KAMUSINGA

MEMBERSHIP

- February 2005 - 2009* | Member of Chemical Association of Moi University.
- August 2007 - 2009* | Member of Moi University student's Organization.
- August 2005 - 2009* | Member of Catholic Students Association.
- September 2014 to date* | Member of Glob' Alps Association (France).

LANGUAGE COMPETENCY

ENGLISH AND SWAHILI: Fluent, comfortable in reading and writing.
FRENCH: Basic Knowledge.

COMPUTER SKILLS

Basic Knowledge: HTML, python, C+, bash.
Advanced Knowledge: Excel, Word, PowerPoint, L^AT_EX, LINUX.
Advanced Knowledge: Electronic structure codes, QUANTUM ESPRESSO, GAUSSIAN and AMSTERDAM DENSITY FUNCTIONAL (ADF).

INTERESTS AND ACTIVITIES

Technology, Open-Source programming.
Reading, writing, cycling, making friends, travelling and watching sports.

REFEREES

1. Professor Casida Mark Earl,
Université Grenoble Alpes,
Laboratoire de Chimie Inorganique REdox (CIRE),
Département de Chimie Moléculaire (DCM, UMR CNRS/UJF 5250),
Institut de Chimie Moléculaire de Grenoble (ICMG, FR-2607),
301 rue de la Chimie, BP 53
F-38041 Grenoble Cedex 9
FRANCE.
Telephone : +33(0)4.76.63.56.28
e-mail: mark.casida@univ-grenoble-alpes.fr
web page: <http://sites.google.com/site/markcasida/home>
2. Professor Lusweti Kituyi,
University of Eldoret,
Department of Chemistry and Biochemistry,
P.O Box 1125-30100,
ELDORET, KENYA.
Telephone: +254 722584248
e-mail: joluki@yahoo.com
3. Professor George Amolo,
Technical University of Kenya,
School of Physical Sciences and Technology,
Department of Physics and Space Sciences,
P.O Box 52428-00200,
NAIROBI.
Telephone: +254 729401249
e-mail: georgeamolo862@gmail.com
4. Dr. Nicholas Makau,
University of Eldoret,
Department of Physics,
Computational Material Science Group,
P.O Box 1125-30100,
ELDORET.
Telephone: +254 727462626
e-mail: wanimak@yahoo.com